

Image Analysis of Vision Sensors 2022

Lead Guest Editor: Haibin Lv

Guest Editors: Minh-Son Dao and Cristiano Jacques Miosso

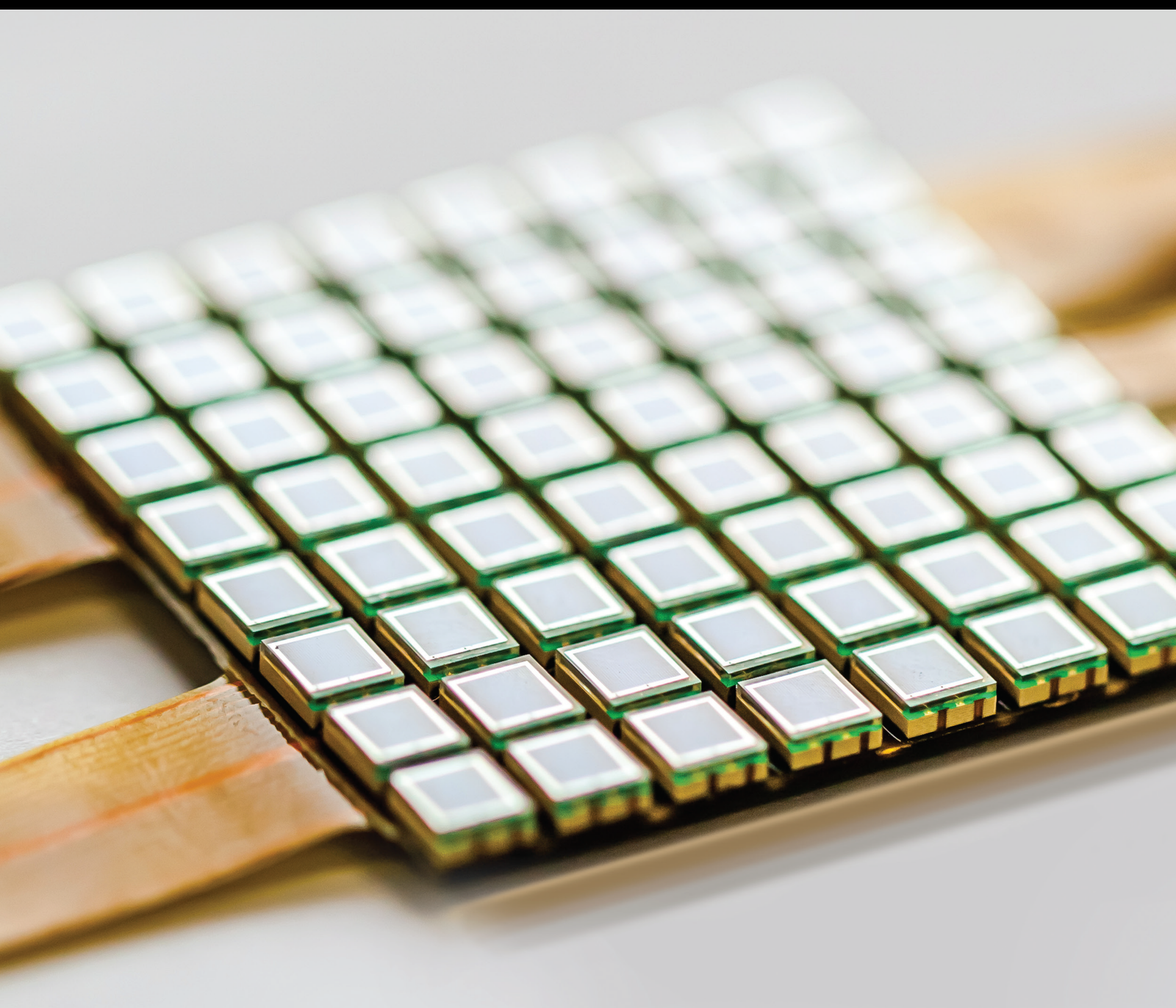




Image Analysis of Vision Sensors 2022

Journal of Sensors

Image Analysis of Vision Sensors 2022

Lead Guest Editor: Haibin Lv

Guest Editors: Minh-Son Dao and Cristiano
Jacques Miosso






Copyright © 2024 Hindawi Limited. All rights reserved.

This is a special issue published in "Journal of Sensors." All articles are open access articles distributed under the Creative Commons Attribution License, which permits unrestricted use, distribution, and reproduction in any medium, provided the original work is properly cited.

Chief Editor

Harith Ahmad , Malaysia

Associate Editors

Duo Lin , China
Fanli Meng , China
Pietro Siciliano , Italy
Guiyun Tian, United Kingdom

Academic Editors

Ghufran Ahmed , Pakistan
Constantin Apetrei, Romania
Shonak Bansal , India
Fernando Benito-Lopez , Spain
Romeo Bernini , Italy
Shekhar Bhansali, USA
Matthew Brodie, Australia
Ravikumar CV, India
Belén Calvo, Spain
Stefania Campopiano , Italy
Binghua Cao , China
Domenico Caputo, Italy
Sara Casciati, Italy
Gabriele Cazzulani , Italy
Chi Chiu Chan, Singapore
Sushank Chaudhary , Thailand
Edmon Chehura , United Kingdom
Marvin H Cheng , USA
Lei Chu , USA
Mario Collotta , Italy
Marco Consales , Italy
Jesus Corres , Spain
Andrea Cusano, Italy
Egidio De Benedetto , Italy
Luca De Stefano , Italy
Manel Del Valle , Spain
Franz L. Dickert, Austria
Giovanni Diraco, Italy
Maria de Fátima Domingues , Portugal
Nicola Donato , Italy
Sheng Du , China
Amir Elzawwy, Egypt
Mauro Epifani , Italy
Congbin Fan , China
Lihang Feng, China
Vittorio Ferrari , Italy
Luca Francioso, Italy

Libo Gao , China
Carmine Granata , Italy
Pramod Kumar Gupta , USA
Mohammad Haider , USA
Agustin Herrera-May , Mexico
María del Carmen Horrillo, Spain
Evangelos Hristoforou , Greece
Grazia Iadarola , Italy
Syed K. Islam , USA
Stephen James , United Kingdom
Sana Ullah Jan, United Kingdom
Bruno C. Janegitz , Brazil
Hai-Feng Ji , USA
Shouyong Jiang, United Kingdom
Roshan Prakash Joseph, USA
Niravkumar Joshi, USA
Rajesh Kaluri , India
Sang Sub Kim , Republic of Korea
Dr. Rajkishor Kumar, India
Rahul Kumar , India
Nageswara Lalam , USA
Antonio Lazaro , Spain
Chengkuo Lee , Singapore
Chenzong Li , USA
Zhi Lian , Australia
Rosalba Liguori , Italy
Sangsoon Lim , Republic of Korea
Huan Liu , China
Jin Liu , China
Eduard Llobet , Spain
Jaime Lloret , Spain
Mohamed Louzazni, Morocco
Jesús Lozano , Spain
Oleg Lupan , Moldova
Leandro Maio , Italy
Pawel Malinowski , Poland
Carlos Marques , Portugal
Eugenio Martinelli , Italy
Antonio Martinez-Olmos , Spain
Giuseppe Maruccio , Italy
Yasuko Y. Maruo, Japan
Zahid Mehmood , Pakistan
Carlos Michel , Mexico
Stephen. J. Mihailov , Canada
Bikash Nakarmi, China

Ehsan Namaziandost , Iran
Heinz C. Neitzert , Italy
Sing Kiong Nguang , New Zealand
Calogero M. Oddo , Italy
Tinghui Ouyang, Japan
SANDEEP KUMAR PALANISWAMY ,
India
Alberto J. Palma , Spain
Davide Palumbo , Italy
Abinash Panda , India
Roberto Paolesse , Italy
Akhilesh Pathak , Thailand
Giovanni Pau , Italy
Giorgio Pennazza , Italy
Michele Penza , Italy
Sivakumar Poruran, India
Stelios Potirakis , Greece
Biswajeet Pradhan , Malaysia
Giuseppe Quero , Italy
Linesh Raja , India
Maheswar Rajagopal , India
Valerie Renaudin , France
Armando Ricciardi , Italy
Christos Riziotis , Greece
Ruthber Rodriguez Serrezuela , Colombia
Maria Luz Rodriguez-Mendez , Spain
Jerome Rossignol , France
Maheswaran S, India
Ylias Sabri , Australia
Sourabh Sahu , India
José P. Santos , Spain
Sina Sareh, United Kingdom
Isabel Sayago , Spain
Andreas Schütze , Germany
Praveen K. Sekhar , USA
Sandra Sendra, Spain
Sandeep Sharma, India
Sunil Kumar Singh Singh , India
Yadvendra Singh , USA
Afaque Manzoor Soomro , Pakistan
Vincenzo Spagnolo, Italy
Kathiravan Srinivasan , India
Sachin K. Srivastava , India
Stefano Stassi , Italy

Danfeng Sun, China
Ashok Sundramoorthy, India
Salvatore Surdo , Italy
Roshan Thotagamuge , Sri Lanka
Guiyun Tian , United Kingdom
Sri Ramulu Torati , USA
Abdellah Touhafi , Belgium
Hoang Vinh Tran , Vietnam
Aitor Urrutia , Spain
Hana Vaisocherova - Lislalova , Czech
Republic
Everardo Vargas-Rodriguez , Mexico
Xavier Vilanova , Spain
Stanislav Vitek , Czech Republic
Luca Vollero , Italy
Tomasz Wandowski , Poland
Bohui Wang, China
Qihao Weng, USA
Penghai Wu , China
Qiang Wu, United Kingdom
Yuedong Xie , China
Chen Yang , China
Jiachen Yang , China
Nitesh Yelve , India
Aijun Yin, China
Chouki Zerrouki , France

Contents

Retracted: Motion Control Analysis of Tennis Robot Based on Ant Colony Algorithm

Journal of Sensors

Retraction (1 page), Article ID 9874180, Volume 2024 (2024)

Retracted: Sensor-Based Exercise Rehabilitation Robot Training Method

Journal of Sensors

Retraction (1 page), Article ID 9819425, Volume 2024 (2024)

Retracted: Application of Multisource Data Fusion Technology in the Construction of Land Ecological Index

Journal of Sensors

Retraction (1 page), Article ID 9815457, Volume 2024 (2024)

Retracted: Painting Color Editing System Based on Virtual Reality Sensor Technology

Journal of Sensors

Retraction (1 page), Article ID 9812412, Volume 2024 (2024)

Retracted: Motion Control and Tracking Control of UAV Based on Adaptive Sensor

Journal of Sensors

Retraction (1 page), Article ID 9757198, Volume 2024 (2024)

Retracted: Application of GIS and Multisensor Technology in Green Urban Garden Landscape Design

Journal of Sensors

Retraction (1 page), Article ID 9851593, Volume 2023 (2023)

Retracted: Research on Intelligent Pick-Up Route Planning of a Logistics Cycle Automatic Robot

Journal of Sensors

Retraction (1 page), Article ID 9842121, Volume 2023 (2023)

Retracted: New Energy Vehicle Electromagnetic Compatibility Test and Closed-Loop Simulation Analysis

Journal of Sensors

Retraction (1 page), Article ID 9801921, Volume 2023 (2023)

Retracted: Construction and Simulation of Deep Learning Algorithm for Robot Vision Tracking

Journal of Sensors

Retraction (1 page), Article ID 9790821, Volume 2023 (2023)

Retracted: Slope Topography Monitoring Based on UAV Tilt Photography Technology and Sensor Technology

Journal of Sensors

Retraction (1 page), Article ID 9753930, Volume 2023 (2023)

Retracted: Robot Target Localization and Visual Navigation Based on Neural Network

Journal of Sensors

Retraction (1 page), Article ID 9760397, Volume 2023 (2023)

Retracted: Construction of Tourism Area Capacity Early Warning System Based on Internet of Things Technology

Journal of Sensors

Retraction (1 page), Article ID 9846315, Volume 2023 (2023)

Retracted: Wearable Sensor and Its Application in Urban Landscape Design

Journal of Sensors

Retraction (1 page), Article ID 9764594, Volume 2023 (2023)

Retracted: A Training Method for a Sensor-Based Exercise Rehabilitation Robot

Journal of Sensors

Retraction (1 page), Article ID 9753429, Volume 2023 (2023)

Retracted: Application of BP Neural Network in Matching Algorithm of Network E-Commerce Platform

Journal of Sensors

Retraction (1 page), Article ID 9873759, Volume 2023 (2023)

Retracted: Design and Implementation of Multimedia Network Intelligent Control Robot Based on Software Definition

Journal of Sensors

Retraction (1 page), Article ID 9873149, Volume 2023 (2023)

Retracted: Optimization Strategy Analysis of Intelligent Product Service System Based on Computer Simulation Technology

Journal of Sensors

Retraction (1 page), Article ID 9869082, Volume 2023 (2023)

Retracted: Financing Efficiency Calculation of Energy Enterprises Based on Internet of Things

Journal of Sensors

Retraction (1 page), Article ID 9863630, Volume 2023 (2023)

Retracted: Design of Music Teaching System Based on Internet of Things Multimedia Intelligent Platform

Journal of Sensors

Retraction (1 page), Article ID 9863256, Volume 2023 (2023)

Retracted: Motion Rehabilitation Robot Control Based on Human Posture Information

Journal of Sensors

Retraction (1 page), Article ID 9859157, Volume 2023 (2023)

Retracted: Artificial Intelligence Optimization Design Analysis of Robot Control System

Journal of Sensors

Retraction (1 page), Article ID 9836123, Volume 2023 (2023)

Retracted: Intelligent Optimization Design of Automatic Sorting Robot Process

Journal of Sensors

Retraction (1 page), Article ID 9830576, Volume 2023 (2023)

Contents

Retracted: Dynamic Path Planning Analysis of Warehouse Handling Robot

Journal of Sensors

Retraction (1 page), Article ID 9829867, Volume 2023 (2023)

Retracted: The Function of Remote Monitoring System of a Robot Inverter Based on PLC and Cloud Platform

Journal of Sensors

Retraction (1 page), Article ID 9828713, Volume 2023 (2023)

Retracted: Development and Construction of Internet of Things Training Practice Platform for Employment Skills Assessment

Journal of Sensors

Retraction (1 page), Article ID 9828395, Volume 2023 (2023)

Retracted: Data Encryption Technology Analysis of Robot Computer Network Information

Journal of Sensors

Retraction (1 page), Article ID 9801202, Volume 2023 (2023)

Retracted: Navigation and Positioning Analysis of Electric Inspection Robot Based on Improved SVM Algorithm

Journal of Sensors

Retraction (1 page), Article ID 9784045, Volume 2023 (2023)

Retracted: Application of Internet of Things Technology in Mechanical Automation Control

Journal of Sensors

Retraction (1 page), Article ID 9871647, Volume 2023 (2023)

Retracted: Implementation of Personalized Information Recommendation Platform System Based on Deep Learning Tourism

Journal of Sensors

Retraction (1 page), Article ID 9857129, Volume 2023 (2023)

Retracted: Path Planning of Storage and Logistics Mobile Robot Based on ACA-E Algorithm

Journal of Sensors

Retraction (1 page), Article ID 9852801, Volume 2023 (2023)

Retracted: Mathematical Modeling Analysis of Data Attribute Encryption for Robot

Journal of Sensors

Retraction (1 page), Article ID 9836943, Volume 2023 (2023)

Retracted: Implementation of Network Data Mining Algorithm for Associated Users Based on Multi-Information Fusion

Journal of Sensors

Retraction (1 page), Article ID 9806432, Volume 2023 (2023)

Retracted: Design of the Vocal Music Feature Recognition System Based on the Internet of Things Technology

Journal of Sensors


Retraction (1 page), Article ID 9780698, Volume 2023 (2023)

Retracted: Automatic Modulation and Recognition of Robot Communication Signal Based on Deep Learning Neural Network

Journal of Sensors

Retraction (1 page), Article ID 9768304, Volume 2023 (2023)

[Retracted] Motion Control and Tracking Control of UAV Based on Adaptive Sensor

Xin Zhao, Zhihui Xu , Yifeng Fu, Shoupeng Xu, and Shasha Xiong

Research Article (7 pages), Article ID 7936019, Volume 2023 (2023)

[Retracted] Application of Multisource Data Fusion Technology in the Construction of Land Ecological Index

Juan Hao, Yang Yang , Haoyue Sun, Zhicheng Zhang, Zhanwu Kang, and Jianfang Zhang


Research Article (8 pages), Article ID 1804731, Volume 2023 (2023)

[Retracted] Painting Color Editing System Based on Virtual Reality Sensor Technology

Chunda Hu 



Research Article (6 pages), Article ID 6461843, Volume 2023 (2023)

[Retracted] Application of GIS and Multisensor Technology in Green Urban Garden Landscape Design

Dongli Shen 



Research Article (7 pages), Article ID 9730980, Volume 2023 (2023)

[Retracted] Sensor-Based Exercise Rehabilitation Robot Training Method

Shangsen Xie  and Jingru Zhang 


Research Article (9 pages), Article ID 7881084, Volume 2023 (2023)

[Retracted] Financing Efficiency Calculation of Energy Enterprises Based on Internet of Things

JingJing Wu  and YaJuan Zhang 


Research Article (8 pages), Article ID 7262788, Volume 2022 (2022)

[Retracted] Design of Music Teaching System Based on Internet of Things Multimedia Intelligent Platform

Bin Xie 

Research Article (7 pages), Article ID 6282581, Volume 2022 (2022)


[Retracted] Implementation of Network Data Mining Algorithm for Associated Users Based on Multi-Information Fusion

Hui Zhang 

Research Article (6 pages), Article ID 3350997, Volume 2022 (2022)


Contents

[Retracted] Implementation of Personalized Information Recommendation Platform System Based on Deep Learning Tourism

Xuejuan Wang 


Research Article (9 pages), Article ID 6221413, Volume 2022 (2022)

[Retracted] Application of BP Neural Network in Matching Algorithm of Network E-Commerce Platform

Jingcheng Zhang 

Research Article (8 pages), Article ID 2045811, Volume 2022 (2022)

[Retracted] Design of the Vocal Music Feature Recognition System Based on the Internet of Things Technology

Haifeng Huang 





Research Article (7 pages), Article ID 1164042, Volume 2022 (2022)

[Retracted] Optimization Strategy Analysis of Intelligent Product Service System Based on Computer Simulation Technology

Hang Liu , Yan Chu , Yongcheng Wang , and Zan Ren 

Research Article (8 pages), Article ID 1264655, Volume 2022 (2022)

[Retracted] Application of Internet of Things Technology in Mechanical Automation Control

Yonghui Xie , Haiqing Li , Qiushaung Jia , and Xiumin Nie 


Research Article (7 pages), Article ID 9388942, Volume 2022 (2022)

[Retracted] Slope Topography Monitoring Based on UAV Tilt Photography Technology and Sensor Technology

Jianfeng Cao , Yunfei Dai , Liqiang Hu , Yiju Liang , Yuan Liu , and Bo Yang 

Research Article (8 pages), Article ID 3531576, Volume 2022 (2022)

[Retracted] Construction of Tourism Area Capacity Early Warning System Based on Internet of Things Technology

Yanli Ma 


Research Article (8 pages), Article ID 8249032, Volume 2022 (2022)

[Retracted] Wearable Sensor and Its Application in Urban Landscape Design

Di Yao 


Research Article (7 pages), Article ID 7265038, Volume 2022 (2022)

[Retracted] Development and Construction of Internet of Things Training Practice Platform for Employment Skills Assessment

Xiaofeng Zhang 

Research Article (7 pages), Article ID 3014565, Volume 2022 (2022)

[Retracted] Design and Implementation of Multimedia Network Intelligent Control Robot Based on Software Definition

Hui Zhang 

Research Article (8 pages), Article ID 4894714, Volume 2022 (2022)

[Retracted] A Training Method for a Sensor-Based Exercise Rehabilitation Robot

Peng Suo , Xueqiang Zhu , Shu Wang , Mei Li , Ting Yu , Chunming Song , Haodi Ning , and Yi Xin 


Research Article (9 pages), Article ID 4336664, Volume 2022 (2022)

[Retracted] Artificial Intelligence Optimization Design Analysis of Robot Control System

Haifeng Guo , Yiyang Wang , Guangwei Wang , Zhongbo Du , Rui Chen , and He Sun 






Research Article (6 pages), Article ID 2235042, Volume 2022 (2022)

[Retracted] Dynamic Path Planning Analysis of Warehouse Handling Robot

Yue Zhao 

Research Article (7 pages), Article ID 4434971, Volume 2022 (2022)

[Retracted] Navigation and Positioning Analysis of Electric Inspection Robot Based on Improved SVM Algorithm

Yongfu Li , Yingkai Long , Mingming Du , Xiping Jiang , and Xianfu Liu 

Research Article (6 pages), Article ID 4613931, Volume 2022 (2022)

[Retracted] Automatic Modulation and Recognition of Robot Communication Signal Based on Deep Learning Neural Network

Xiaoguang Zou  and Xiaoyong Zou 


Research Article (7 pages), Article ID 3519010, Volume 2022 (2022)

[Retracted] Mathematical Modeling Analysis of Data Attribute Encryption for Robot

Jingyi Sun , Jie Yan , and Dingyi Yang 


Research Article (8 pages), Article ID 3976806, Volume 2022 (2022)

[Retracted] The Function of Remote Monitoring System of a Robot Inverter Based on PLC and Cloud Platform

Mengqi Yu 



Research Article (8 pages), Article ID 1178508, Volume 2022 (2022)

[Retracted] Motion Rehabilitation Robot Control Based on Human Posture Information

Guangfeng He 

Research Article (7 pages), Article ID 5067346, Volume 2022 (2022)

[Retracted] Construction and Simulation of Deep Learning Algorithm for Robot Vision Tracking

Siping Xu  and Lan Chen 

Research Article (6 pages), Article ID 1522657, Volume 2022 (2022)




Contents

[Retracted] Research on Intelligent Pick-Up Route Planning of a Logistics Cycle Automatic Robot

Qinlong Hu  and Yimin Fan 


Research Article (8 pages), Article ID 4268589, Volume 2022 (2022)

[Retracted] Intelligent Optimization Design of Automatic Sorting Robot Process

Jia Liu , JunFeng Wang , and Yuequn Xu 

Research Article (8 pages), Article ID 4860006, Volume 2022 (2022)

Construction of Robot Computer Image Segmentation Model Based on Partial Differential Equation

Quan Zhang 

Research Article (8 pages), Article ID 6216423, Volume 2022 (2022)

[Retracted] Motion Control Analysis of Tennis Robot Based on Ant Colony Algorithm

Feng Wang , Yujie Dong , Haobo Gao , and Lin Wu 

Research Article (8 pages), Article ID 6945310, Volume 2022 (2022)

Target Recognition, Localization, and Motion Control of Soccer Robot

Changsheng Zhu  and Min Gong 

Research Article (7 pages), Article ID 1145540, Volume 2022 (2022)

[Retracted] Data Encryption Technology Analysis of Robot Computer Network Information

Qiaolian Shi  and Yan Liu 


Research Article (7 pages), Article ID 5127989, Volume 2022 (2022)

[Retracted] Robot Target Localization and Visual Navigation Based on Neural Network

Haifeng Guo , Yiyang Wang , Guijun Yu , Xiang Li , Baoqi Yu , and Wenyi Li 



Research Article (8 pages), Article ID 6761879, Volume 2022 (2022)

[Retracted] Path Planning of Storage and Logistics Mobile Robot Based on ACA-E Algorithm

Yue Zhao 






Research Article (7 pages), Article ID 5757719, Volume 2022 (2022)

[Retracted] New Energy Vehicle Electromagnetic Compatibility Test and Closed-Loop Simulation Analysis

Ling Ma  and Yean Lu 

Research Article (7 pages), Article ID 3198944, Volume 2022 (2022)

Research on Navigation and Positioning of Electric Inspection Robot Based on Improved CNN Algorithm

Yingkai Long , Mingming Du , Xiaoxiao Luo , Siquan Li , and Yuqiu Liu 

Research Article (6 pages), Article ID 9369543, Volume 2022 (2022)

Retraction

Retracted: Motion Control Analysis of Tennis Robot Based on Ant Colony Algorithm

Journal of Sensors

Received 23 January 2024; Accepted 23 January 2024; Published 24 January 2024

Copyright © 2024 Journal of Sensors. This is an open access article distributed under the Creative Commons Attribution License, which permits unrestricted use, distribution, and reproduction in any medium, provided the original work is properly cited.

This article has been retracted by Hindawi following an investigation undertaken by the publisher [1]. This investigation has uncovered evidence of one or more of the following indicators of systematic manipulation of the publication process:

- (1) Discrepancies in scope
- (2) Discrepancies in the description of the research reported
- (3) Discrepancies between the availability of data and the research described
- (4) Inappropriate citations
- (5) Incoherent, meaningless and/or irrelevant content included in the article
- (6) Manipulated or compromised peer review

The presence of these indicators undermines our confidence in the integrity of the article's content and we cannot, therefore, vouch for its reliability. Please note that this notice is intended solely to alert readers that the content of this article is unreliable. We have not investigated whether authors were aware of or involved in the systematic manipulation of the publication process.

Wiley and Hindawi regrets that the usual quality checks did not identify these issues before publication and have since put additional measures in place to safeguard research integrity.

We wish to credit our own Research Integrity and Research Publishing teams and anonymous and named external researchers and research integrity experts for contributing to this investigation.

The corresponding author, as the representative of all authors, has been given the opportunity to register their agreement or disagreement to this retraction. We have kept a record of any response received.

References

- [1] F. Wang, Y. Dong, H. Gao, and L. Wu, "Motion Control Analysis of Tennis Robot Based on Ant Colony Algorithm," *Journal of Sensors*, vol. 2022, Article ID 6945310, 8 pages, 2022.

Retraction

Retracted: Sensor-Based Exercise Rehabilitation Robot Training Method

Journal of Sensors

Received 23 January 2024; Accepted 23 January 2024; Published 24 January 2024

Copyright © 2024 Journal of Sensors. This is an open access article distributed under the Creative Commons Attribution License, which permits unrestricted use, distribution, and reproduction in any medium, provided the original work is properly cited.

This article has been retracted by Hindawi following an investigation undertaken by the publisher [1]. This investigation has uncovered evidence of one or more of the following indicators of systematic manipulation of the publication process:

- (1) Discrepancies in scope
- (2) Discrepancies in the description of the research reported
- (3) Discrepancies between the availability of data and the research described
- (4) Inappropriate citations
- (5) Incoherent, meaningless and/or irrelevant content included in the article
- (6) Manipulated or compromised peer review

The presence of these indicators undermines our confidence in the integrity of the article's content and we cannot, therefore, vouch for its reliability. Please note that this notice is intended solely to alert readers that the content of this article is unreliable. We have not investigated whether authors were aware of or involved in the systematic manipulation of the publication process.

Wiley and Hindawi regrets that the usual quality checks did not identify these issues before publication and have since put additional measures in place to safeguard research integrity.

We wish to credit our own Research Integrity and Research Publishing teams and anonymous and named external researchers and research integrity experts for contributing to this investigation.

The corresponding author, as the representative of all authors, has been given the opportunity to register their agreement or disagreement to this retraction. We have kept a record of any response received.

References

- [1] S. Xie and J. Zhang, "Sensor-Based Exercise Rehabilitation Robot Training Method," *Journal of Sensors*, vol. 2023, Article ID 7881084, 9 pages, 2023.

Retraction

Retracted: Application of Multisource Data Fusion Technology in the Construction of Land Ecological Index

Journal of Sensors

Received 23 January 2024; Accepted 23 January 2024; Published 24 January 2024

Copyright © 2024 Journal of Sensors. This is an open access article distributed under the Creative Commons Attribution License, which permits unrestricted use, distribution, and reproduction in any medium, provided the original work is properly cited.

This article has been retracted by Hindawi following an investigation undertaken by the publisher [1]. This investigation has uncovered evidence of one or more of the following indicators of systematic manipulation of the publication process:

- (1) Discrepancies in scope
- (2) Discrepancies in the description of the research reported
- (3) Discrepancies between the availability of data and the research described
- (4) Inappropriate citations
- (5) Incoherent, meaningless and/or irrelevant content included in the article
- (6) Manipulated or compromised peer review

The presence of these indicators undermines our confidence in the integrity of the article's content and we cannot, therefore, vouch for its reliability. Please note that this notice is intended solely to alert readers that the content of this article is unreliable. We have not investigated whether authors were aware of or involved in the systematic manipulation of the publication process.

Wiley and Hindawi regrets that the usual quality checks did not identify these issues before publication and have since put additional measures in place to safeguard research integrity.

We wish to credit our own Research Integrity and Research Publishing teams and anonymous and named external researchers and research integrity experts for contributing to this investigation.

The corresponding author, as the representative of all authors, has been given the opportunity to register their agreement or disagreement to this retraction. We have kept a record of any response received.

References

- [1] J. Hao, Y. Yang, H. Sun, Z. Zhang, Z. Kang, and J. Zhang, "Application of Multisource Data Fusion Technology in the Construction of Land Ecological Index," *Journal of Sensors*, vol. 2023, Article ID 1804731, 8 pages, 2023.

Retraction

Retracted: Painting Color Editing System Based on Virtual Reality Sensor Technology

Journal of Sensors

Received 23 January 2024; Accepted 23 January 2024; Published 24 January 2024

Copyright © 2024 Journal of Sensors. This is an open access article distributed under the Creative Commons Attribution License, which permits unrestricted use, distribution, and reproduction in any medium, provided the original work is properly cited.

This article has been retracted by Hindawi following an investigation undertaken by the publisher [1]. This investigation has uncovered evidence of one or more of the following indicators of systematic manipulation of the publication process:

- (1) Discrepancies in scope
- (2) Discrepancies in the description of the research reported
- (3) Discrepancies between the availability of data and the research described
- (4) Inappropriate citations
- (5) Incoherent, meaningless and/or irrelevant content included in the article
- (6) Manipulated or compromised peer review

The presence of these indicators undermines our confidence in the integrity of the article's content and we cannot, therefore, vouch for its reliability. Please note that this notice is intended solely to alert readers that the content of this article is unreliable. We have not investigated whether authors were aware of or involved in the systematic manipulation of the publication process.

Wiley and Hindawi regrets that the usual quality checks did not identify these issues before publication and have since put additional measures in place to safeguard research integrity.

We wish to credit our own Research Integrity and Research Publishing teams and anonymous and named external researchers and research integrity experts for contributing to this investigation.

The corresponding author, as the representative of all authors, has been given the opportunity to register their agreement or disagreement to this retraction. We have kept a record of any response received.

References

- [1] C. Hu, "Painting Color Editing System Based on Virtual Reality Sensor Technology," *Journal of Sensors*, vol. 2023, Article ID 6461843, 6 pages, 2023.

Retraction

Retracted: Motion Control and Tracking Control of UAV Based on Adaptive Sensor

Journal of Sensors

Received 23 January 2024; Accepted 23 January 2024; Published 24 January 2024

Copyright © 2024 Journal of Sensors. This is an open access article distributed under the Creative Commons Attribution License, which permits unrestricted use, distribution, and reproduction in any medium, provided the original work is properly cited.

This article has been retracted by Hindawi following an investigation undertaken by the publisher [1]. This investigation has uncovered evidence of one or more of the following indicators of systematic manipulation of the publication process:

- (1) Discrepancies in scope
- (2) Discrepancies in the description of the research reported
- (3) Discrepancies between the availability of data and the research described
- (4) Inappropriate citations
- (5) Incoherent, meaningless and/or irrelevant content included in the article
- (6) Manipulated or compromised peer review

The presence of these indicators undermines our confidence in the integrity of the article's content and we cannot, therefore, vouch for its reliability. Please note that this notice is intended solely to alert readers that the content of this article is unreliable. We have not investigated whether authors were aware of or involved in the systematic manipulation of the publication process.

Wiley and Hindawi regrets that the usual quality checks did not identify these issues before publication and have since put additional measures in place to safeguard research integrity.

We wish to credit our own Research Integrity and Research Publishing teams and anonymous and named external researchers and research integrity experts for contributing to this investigation.

The corresponding author, as the representative of all authors, has been given the opportunity to register their agreement or disagreement to this retraction. We have kept a record of any response received.

References

- [1] X. Zhao, Z. Xu, Y. Fu, S. Xu, and S. Xiong, "Motion Control and Tracking Control of UAV Based on Adaptive Sensor," *Journal of Sensors*, vol. 2023, Article ID 7936019, 7 pages, 2023.

Retraction

Retracted: Application of GIS and Multisensor Technology in Green Urban Garden Landscape Design

Journal of Sensors

Received 19 December 2023; Accepted 19 December 2023; Published 20 December 2023

Copyright © 2023 Journal of Sensors. This is an open access article distributed under the Creative Commons Attribution License, which permits unrestricted use, distribution, and reproduction in any medium, provided the original work is properly cited.

This article has been retracted by Hindawi following an investigation undertaken by the publisher [1]. This investigation has uncovered evidence of one or more of the following indicators of systematic manipulation of the publication process:

- (1) Discrepancies in scope
- (2) Discrepancies in the description of the research reported
- (3) Discrepancies between the availability of data and the research described
- (4) Inappropriate citations
- (5) Incoherent, meaningless and/or irrelevant content included in the article
- (6) Manipulated or compromised peer review

The presence of these indicators undermines our confidence in the integrity of the article's content and we cannot, therefore, vouch for its reliability. Please note that this notice is intended solely to alert readers that the content of this article is unreliable. We have not investigated whether authors were aware of or involved in the systematic manipulation of the publication process.

Wiley and Hindawi regrets that the usual quality checks did not identify these issues before publication and have since put additional measures in place to safeguard research integrity.

We wish to credit our own Research Integrity and Research Publishing teams and anonymous and named external researchers and research integrity experts for contributing to this investigation.

The corresponding author, as the representative of all authors, has been given the opportunity to register their agreement or disagreement to this retraction. We have kept a record of any response received.

References

- [1] D. Shen, "Application of GIS and Multisensor Technology in Green Urban Garden Landscape Design," *Journal of Sensors*, vol. 2023, Article ID 9730980, 7 pages, 2023.

Retraction

Retracted: Research on Intelligent Pick-Up Route Planning of a Logistics Cycle Automatic Robot

Journal of Sensors

Received 19 December 2023; Accepted 19 December 2023; Published 20 December 2023

Copyright © 2023 Journal of Sensors. This is an open access article distributed under the Creative Commons Attribution License, which permits unrestricted use, distribution, and reproduction in any medium, provided the original work is properly cited.

This article has been retracted by Hindawi following an investigation undertaken by the publisher [1]. This investigation has uncovered evidence of one or more of the following indicators of systematic manipulation of the publication process:

- (1) Discrepancies in scope
- (2) Discrepancies in the description of the research reported
- (3) Discrepancies between the availability of data and the research described
- (4) Inappropriate citations
- (5) Incoherent, meaningless and/or irrelevant content included in the article
- (6) Manipulated or compromised peer review

The presence of these indicators undermines our confidence in the integrity of the article's content and we cannot, therefore, vouch for its reliability. Please note that this notice is intended solely to alert readers that the content of this article is unreliable. We have not investigated whether authors were aware of or involved in the systematic manipulation of the publication process.

Wiley and Hindawi regrets that the usual quality checks did not identify these issues before publication and have since put additional measures in place to safeguard research integrity.

We wish to credit our own Research Integrity and Research Publishing teams and anonymous and named external researchers and research integrity experts for contributing to this investigation.

The corresponding author, as the representative of all authors, has been given the opportunity to register their agreement or disagreement to this retraction. We have kept a record of any response received.

References

- [1] Q. Hu and Y. Fan, "Research on Intelligent Pick-Up Route Planning of a Logistics Cycle Automatic Robot," *Journal of Sensors*, vol. 2022, Article ID 4268589, 8 pages, 2022.

Retraction

Retracted: New Energy Vehicle Electromagnetic Compatibility Test and Closed-Loop Simulation Analysis

Journal of Sensors

Received 19 December 2023; Accepted 19 December 2023; Published 20 December 2023

Copyright © 2023 Journal of Sensors. This is an open access article distributed under the Creative Commons Attribution License, which permits unrestricted use, distribution, and reproduction in any medium, provided the original work is properly cited.

This article has been retracted by Hindawi following an investigation undertaken by the publisher [1]. This investigation has uncovered evidence of one or more of the following indicators of systematic manipulation of the publication process:

- (1) Discrepancies in scope
- (2) Discrepancies in the description of the research reported
- (3) Discrepancies between the availability of data and the research described
- (4) Inappropriate citations
- (5) Incoherent, meaningless and/or irrelevant content included in the article
- (6) Manipulated or compromised peer review

The presence of these indicators undermines our confidence in the integrity of the article's content and we cannot, therefore, vouch for its reliability. Please note that this notice is intended solely to alert readers that the content of this article is unreliable. We have not investigated whether authors were aware of or involved in the systematic manipulation of the publication process.

Wiley and Hindawi regrets that the usual quality checks did not identify these issues before publication and have since put additional measures in place to safeguard research integrity.

We wish to credit our own Research Integrity and Research Publishing teams and anonymous and named external researchers and research integrity experts for contributing to this investigation.

The corresponding author, as the representative of all authors, has been given the opportunity to register their agreement or disagreement to this retraction. We have kept a record of any response received.

References

- [1] L. Ma and Y. Lu, "New Energy Vehicle Electromagnetic Compatibility Test and Closed-Loop Simulation Analysis," *Journal of Sensors*, vol. 2022, Article ID 3198944, 7 pages, 2022.

Retraction

Retracted: Construction and Simulation of Deep Learning Algorithm for Robot Vision Tracking

Journal of Sensors

Received 17 October 2023; Accepted 17 October 2023; Published 18 October 2023

Copyright © 2023 Journal of Sensors. This is an open access article distributed under the Creative Commons Attribution License, which permits unrestricted use, distribution, and reproduction in any medium, provided the original work is properly cited.

This article has been retracted by Hindawi following an investigation undertaken by the publisher [1]. This investigation has uncovered evidence of one or more of the following indicators of systematic manipulation of the publication process:

- (1) Discrepancies in scope
- (2) Discrepancies in the description of the research reported
- (3) Discrepancies between the availability of data and the research described
- (4) Inappropriate citations
- (5) Incoherent, meaningless and/or irrelevant content included in the article
- (6) Peer-review manipulation

The presence of these indicators undermines our confidence in the integrity of the article's content and we cannot, therefore, vouch for its reliability. Please note that this notice is intended solely to alert readers that the content of this article is unreliable. We have not investigated whether authors were aware of or involved in the systematic manipulation of the publication process.

Wiley and Hindawi regrets that the usual quality checks did not identify these issues before publication and have since put additional measures in place to safeguard research integrity.

We wish to credit our own Research Integrity and Research Publishing teams and anonymous and named external researchers and research integrity experts for contributing to this investigation.

The corresponding author, as the representative of all authors, has been given the opportunity to register their agreement or disagreement to this retraction. We have kept a record of any response received.

References

- [1] S. Xu and L. Chen, "Construction and Simulation of Deep Learning Algorithm for Robot Vision Tracking," *Journal of Sensors*, vol. 2022, Article ID 1522657, 6 pages, 2022.

Retraction

Retracted: Slope Topography Monitoring Based on UAV Tilt Photography Technology and Sensor Technology

Journal of Sensors

Received 17 October 2023; Accepted 17 October 2023; Published 18 October 2023

Copyright © 2023 Journal of Sensors. This is an open access article distributed under the Creative Commons Attribution License, which permits unrestricted use, distribution, and reproduction in any medium, provided the original work is properly cited.

This article has been retracted by Hindawi following an investigation undertaken by the publisher [1]. This investigation has uncovered evidence of one or more of the following indicators of systematic manipulation of the publication process:

- (1) Discrepancies in scope
- (2) Discrepancies in the description of the research reported
- (3) Discrepancies between the availability of data and the research described
- (4) Inappropriate citations
- (5) Incoherent, meaningless and/or irrelevant content included in the article
- (6) Peer-review manipulation

The presence of these indicators undermines our confidence in the integrity of the article's content and we cannot, therefore, vouch for its reliability. Please note that this notice is intended solely to alert readers that the content of this article is unreliable. We have not investigated whether authors were aware of or involved in the systematic manipulation of the publication process.

Wiley and Hindawi regrets that the usual quality checks did not identify these issues before publication and have since put additional measures in place to safeguard research integrity.

We wish to credit our own Research Integrity and Research Publishing teams and anonymous and named external researchers and research integrity experts for contributing to this investigation.

The corresponding author, as the representative of all authors, has been given the opportunity to register their agreement or disagreement to this retraction. We have kept a record of any response received.

References

- [1] J. Cao, Y. Dai, L. Hu, Y. Liang, Y. Liu, and B. Yang, "Slope Topography Monitoring Based on UAV Tilt Photography Technology and Sensor Technology," *Journal of Sensors*, vol. 2022, Article ID 3531576, 8 pages, 2022.

Retraction

Retracted: Robot Target Localization and Visual Navigation Based on Neural Network

Journal of Sensors

Received 10 October 2023; Accepted 10 October 2023; Published 11 October 2023

Copyright © 2023 Journal of Sensors. This is an open access article distributed under the Creative Commons Attribution License, which permits unrestricted use, distribution, and reproduction in any medium, provided the original work is properly cited.

This article has been retracted by Hindawi following an investigation undertaken by the publisher [1]. This investigation has uncovered evidence of one or more of the following indicators of systematic manipulation of the publication process:

- (1) Discrepancies in scope
- (2) Discrepancies in the description of the research reported
- (3) Discrepancies between the availability of data and the research described
- (4) Inappropriate citations
- (5) Incoherent, meaningless and/or irrelevant content included in the article
- (6) Peer-review manipulation

The presence of these indicators undermines our confidence in the integrity of the article's content and we cannot, therefore, vouch for its reliability. Please note that this notice is intended solely to alert readers that the content of this article is unreliable. We have not investigated whether authors were aware of or involved in the systematic manipulation of the publication process.

Wiley and Hindawi regrets that the usual quality checks did not identify these issues before publication and have since put additional measures in place to safeguard research integrity.

We wish to credit our own Research Integrity and Research Publishing teams and anonymous and named external researchers and research integrity experts for contributing to this investigation.

The corresponding author, as the representative of all authors, has been given the opportunity to register their agreement or disagreement to this retraction. We have kept a record of any response received.

References

- [1] H. Guo, Y. Wang, G. Yu, X. Li, B. Yu, and W. Li, "Robot Target Localization and Visual Navigation Based on Neural Network," *Journal of Sensors*, vol. 2022, Article ID 6761879, 8 pages, 2022.

Retraction

Retracted: Construction of Tourism Area Capacity Early Warning System Based on Internet of Things Technology

Journal of Sensors

Received 3 October 2023; Accepted 3 October 2023; Published 4 October 2023

Copyright © 2023 Journal of Sensors. This is an open access article distributed under the Creative Commons Attribution License, which permits unrestricted use, distribution, and reproduction in any medium, provided the original work is properly cited.

This article has been retracted by Hindawi following an investigation undertaken by the publisher [1]. This investigation has uncovered evidence of one or more of the following indicators of systematic manipulation of the publication process:

- (1) Discrepancies in scope
- (2) Discrepancies in the description of the research reported
- (3) Discrepancies between the availability of data and the research described
- (4) Inappropriate citations
- (5) Incoherent, meaningless and/or irrelevant content included in the article
- (6) Peer-review manipulation

The presence of these indicators undermines our confidence in the integrity of the article's content and we cannot, therefore, vouch for its reliability. Please note that this notice is intended solely to alert readers that the content of this article is unreliable. We have not investigated whether authors were aware of or involved in the systematic manipulation of the publication process.

Wiley and Hindawi regrets that the usual quality checks did not identify these issues before publication and have since put additional measures in place to safeguard research integrity.

We wish to credit our own Research Integrity and Research Publishing teams and anonymous and named external researchers and research integrity experts for contributing to this investigation.

The corresponding author, as the representative of all authors, has been given the opportunity to register their agreement or disagreement to this retraction. We have kept a record of any response received.

References

- [1] Y. Ma, "Construction of Tourism Area Capacity Early Warning System Based on Internet of Things Technology," *Journal of Sensors*, vol. 2022, Article ID 8249032, 8 pages, 2022.

Retraction

Retracted: Wearable Sensor and Its Application in Urban Landscape Design

Journal of Sensors

Received 3 October 2023; Accepted 3 October 2023; Published 4 October 2023

Copyright © 2023 Journal of Sensors. This is an open access article distributed under the Creative Commons Attribution License, which permits unrestricted use, distribution, and reproduction in any medium, provided the original work is properly cited.

This article has been retracted by Hindawi following an investigation undertaken by the publisher [1]. This investigation has uncovered evidence of one or more of the following indicators of systematic manipulation of the publication process:

- (1) Discrepancies in scope
- (2) Discrepancies in the description of the research reported
- (3) Discrepancies between the availability of data and the research described
- (4) Inappropriate citations
- (5) Incoherent, meaningless and/or irrelevant content included in the article
- (6) Peer-review manipulation

The presence of these indicators undermines our confidence in the integrity of the article's content and we cannot, therefore, vouch for its reliability. Please note that this notice is intended solely to alert readers that the content of this article is unreliable. We have not investigated whether authors were aware of or involved in the systematic manipulation of the publication process.

In addition, our investigation has also shown that one or more of the following human-subject reporting requirements has not been met in this article: ethical approval by an Institutional Review Board (IRB) committee or equivalent, patient/participant consent to participate, and/or agreement to publish patient/participant details (where relevant).

Wiley and Hindawi regrets that the usual quality checks did not identify these issues before publication and have since put additional measures in place to safeguard research integrity.

We wish to credit our own Research Integrity and Research Publishing teams and anonymous and named external researchers and research integrity experts for contributing to this investigation.

The corresponding author, as the representative of all authors, has been given the opportunity to register their agreement or disagreement to this retraction. We have kept a record of any response received.

References

- [1] D. Yao, "Wearable Sensor and Its Application in Urban Landscape Design," *Journal of Sensors*, vol. 2022, Article ID 7265038, 7 pages, 2022.

Retraction

Retracted: A Training Method for a Sensor-Based Exercise Rehabilitation Robot

Journal of Sensors

Received 3 October 2023; Accepted 3 October 2023; Published 4 October 2023

Copyright © 2023 Journal of Sensors. This is an open access article distributed under the Creative Commons Attribution License, which permits unrestricted use, distribution, and reproduction in any medium, provided the original work is properly cited.

This article has been retracted by Hindawi following an investigation undertaken by the publisher [1]. This investigation has uncovered evidence of one or more of the following indicators of systematic manipulation of the publication process:

- (1) Discrepancies in scope
- (2) Discrepancies in the description of the research reported
- (3) Discrepancies between the availability of data and the research described
- (4) Inappropriate citations
- (5) Incoherent, meaningless and/or irrelevant content included in the article
- (6) Peer-review manipulation

The presence of these indicators undermines our confidence in the integrity of the article's content and we cannot, therefore, vouch for its reliability. Please note that this notice is intended solely to alert readers that the content of this article is unreliable. We have not investigated whether authors were aware of or involved in the systematic manipulation of the publication process.

Wiley and Hindawi regrets that the usual quality checks did not identify these issues before publication and have since put additional measures in place to safeguard research integrity.

We wish to credit our own Research Integrity and Research Publishing teams and anonymous and named external researchers and research integrity experts for contributing to this investigation.

The corresponding author, as the representative of all authors, has been given the opportunity to register their agreement or disagreement to this retraction. We have kept a record of any response received.

References

- [1] P. Suo, X. Zhu, S. Wang et al., "A Training Method for a Sensor-Based Exercise Rehabilitation Robot," *Journal of Sensors*, vol. 2022, Article ID 4336664, 9 pages, 2022.

Retraction

Retracted: Application of BP Neural Network in Matching Algorithm of Network E-Commerce Platform

Journal of Sensors

Received 13 September 2023; Accepted 13 September 2023; Published 14 September 2023

Copyright © 2023 Journal of Sensors. This is an open access article distributed under the Creative Commons Attribution License, which permits unrestricted use, distribution, and reproduction in any medium, provided the original work is properly cited.

This article has been retracted by Hindawi following an investigation undertaken by the publisher [1]. This investigation has uncovered evidence of one or more of the following indicators of systematic manipulation of the publication process:

- (1) Discrepancies in scope
- (2) Discrepancies in the description of the research reported
- (3) Discrepancies between the availability of data and the research described
- (4) Inappropriate citations
- (5) Incoherent, meaningless and/or irrelevant content included in the article
- (6) Peer-review manipulation

The presence of these indicators undermines our confidence in the integrity of the article's content and we cannot, therefore, vouch for its reliability. Please note that this notice is intended solely to alert readers that the content of this article is unreliable. We have not investigated whether authors were aware of or involved in the systematic manipulation of the publication process.

Wiley and Hindawi regrets that the usual quality checks did not identify these issues before publication and have since put additional measures in place to safeguard research integrity.

We wish to credit our own Research Integrity and Research Publishing teams and anonymous and named external researchers and research integrity experts for contributing to this investigation.

The corresponding author, as the representative of all authors, has been given the opportunity to register their agreement or disagreement to this retraction. We have kept a record of any response received.

References

- [1] J. Zhang, "Application of BP Neural Network in Matching Algorithm of Network E-Commerce Platform," *Journal of Sensors*, vol. 2022, Article ID 2045811, 8 pages, 2022.

Retraction

Retracted: Design and Implementation of Multimedia Network Intelligent Control Robot Based on Software Definition

Journal of Sensors

Received 13 September 2023; Accepted 13 September 2023; Published 14 September 2023

Copyright © 2023 Journal of Sensors. This is an open access article distributed under the Creative Commons Attribution License, which permits unrestricted use, distribution, and reproduction in any medium, provided the original work is properly cited.

This article has been retracted by Hindawi following an investigation undertaken by the publisher [1]. This investigation has uncovered evidence of one or more of the following indicators of systematic manipulation of the publication process:

- (1) Discrepancies in scope
- (2) Discrepancies in the description of the research reported
- (3) Discrepancies between the availability of data and the research described
- (4) Inappropriate citations
- (5) Incoherent, meaningless and/or irrelevant content included in the article
- (6) Peer-review manipulation

The presence of these indicators undermines our confidence in the integrity of the article's content and we cannot, therefore, vouch for its reliability. Please note that this notice is intended solely to alert readers that the content of this article is unreliable. We have not investigated whether authors were aware of or involved in the systematic manipulation of the publication process.

Wiley and Hindawi regrets that the usual quality checks did not identify these issues before publication and have since put additional measures in place to safeguard research integrity.

We wish to credit our own Research Integrity and Research Publishing teams and anonymous and named external researchers and research integrity experts for contributing to this investigation.

The corresponding author, as the representative of all authors, has been given the opportunity to register their agreement or disagreement to this retraction. We have kept a record of any response received.

References

- [1] H. Zhang, "Design and Implementation of Multimedia Network Intelligent Control Robot Based on Software Definition," *Journal of Sensors*, vol. 2022, Article ID 4894714, 8 pages, 2022.

Retraction

Retracted: Optimization Strategy Analysis of Intelligent Product Service System Based on Computer Simulation Technology

Journal of Sensors

Received 13 September 2023; Accepted 13 September 2023; Published 14 September 2023

Copyright © 2023 Journal of Sensors. This is an open access article distributed under the Creative Commons Attribution License, which permits unrestricted use, distribution, and reproduction in any medium, provided the original work is properly cited.

This article has been retracted by Hindawi following an investigation undertaken by the publisher [1]. This investigation has uncovered evidence of one or more of the following indicators of systematic manipulation of the publication process:

- (1) Discrepancies in scope
- (2) Discrepancies in the description of the research reported
- (3) Discrepancies between the availability of data and the research described
- (4) Inappropriate citations
- (5) Incoherent, meaningless and/or irrelevant content included in the article
- (6) Peer-review manipulation

The presence of these indicators undermines our confidence in the integrity of the article's content and we cannot, therefore, vouch for its reliability. Please note that this notice is intended solely to alert readers that the content of this article is unreliable. We have not investigated whether authors were aware of or involved in the systematic manipulation of the publication process.

Wiley and Hindawi regrets that the usual quality checks did not identify these issues before publication and have since put additional measures in place to safeguard research integrity.

We wish to credit our own Research Integrity and Research Publishing teams and anonymous and named external researchers and research integrity experts for contributing to this investigation.

The corresponding author, as the representative of all authors, has been given the opportunity to register their agreement or disagreement to this retraction. We have kept a record of any response received.

References

- [1] H. Liu, Y. Chu, Y. Wang, and Z. Ren, "Optimization Strategy Analysis of Intelligent Product Service System Based on Computer Simulation Technology," *Journal of Sensors*, vol. 2022, Article ID 1264655, 8 pages, 2022.

Retraction

Retracted: Financing Efficiency Calculation of Energy Enterprises Based on Internet of Things

Journal of Sensors

Received 13 September 2023; Accepted 13 September 2023; Published 14 September 2023

Copyright © 2023 Journal of Sensors. This is an open access article distributed under the Creative Commons Attribution License, which permits unrestricted use, distribution, and reproduction in any medium, provided the original work is properly cited.

This article has been retracted by Hindawi following an investigation undertaken by the publisher [1]. This investigation has uncovered evidence of one or more of the following indicators of systematic manipulation of the publication process:

- (1) Discrepancies in scope
- (2) Discrepancies in the description of the research reported
- (3) Discrepancies between the availability of data and the research described
- (4) Inappropriate citations
- (5) Incoherent, meaningless and/or irrelevant content included in the article
- (6) Peer-review manipulation

The presence of these indicators undermines our confidence in the integrity of the article's content and we cannot, therefore, vouch for its reliability. Please note that this notice is intended solely to alert readers that the content of this article is unreliable. We have not investigated whether authors were aware of or involved in the systematic manipulation of the publication process.

Wiley and Hindawi regrets that the usual quality checks did not identify these issues before publication and have since put additional measures in place to safeguard research integrity.

We wish to credit our own Research Integrity and Research Publishing teams and anonymous and named external researchers and research integrity experts for contributing to this investigation.

The corresponding author, as the representative of all authors, has been given the opportunity to register their agreement or disagreement to this retraction. We have kept a record of any response received.

References

- [1] J. Wu and Y. Zhang, "Financing Efficiency Calculation of Energy Enterprises Based on Internet of Things," *Journal of Sensors*, vol. 2022, Article ID 7262788, 8 pages, 2022.

Retraction

Retracted: Design of Music Teaching System Based on Internet of Things Multimedia Intelligent Platform

Journal of Sensors

Received 13 September 2023; Accepted 13 September 2023; Published 14 September 2023

Copyright © 2023 Journal of Sensors. This is an open access article distributed under the Creative Commons Attribution License, which permits unrestricted use, distribution, and reproduction in any medium, provided the original work is properly cited.

This article has been retracted by Hindawi following an investigation undertaken by the publisher [1]. This investigation has uncovered evidence of one or more of the following indicators of systematic manipulation of the publication process:

- (1) Discrepancies in scope
- (2) Discrepancies in the description of the research reported
- (3) Discrepancies between the availability of data and the research described
- (4) Inappropriate citations
- (5) Incoherent, meaningless and/or irrelevant content included in the article
- (6) Peer-review manipulation

The presence of these indicators undermines our confidence in the integrity of the article's content and we cannot, therefore, vouch for its reliability. Please note that this notice is intended solely to alert readers that the content of this article is unreliable. We have not investigated whether authors were aware of or involved in the systematic manipulation of the publication process.

Wiley and Hindawi regrets that the usual quality checks did not identify these issues before publication and have since put additional measures in place to safeguard research integrity.

We wish to credit our own Research Integrity and Research Publishing teams and anonymous and named external researchers and research integrity experts for contributing to this investigation.

The corresponding author, as the representative of all authors, has been given the opportunity to register their agreement or disagreement to this retraction. We have kept a record of any response received.

References

- [1] B. Xie, "Design of Music Teaching System Based on Internet of Things Multimedia Intelligent Platform," *Journal of Sensors*, vol. 2022, Article ID 6282581, 7 pages, 2022.

Retraction

Retracted: Motion Rehabilitation Robot Control Based on Human Posture Information

Journal of Sensors

Received 13 September 2023; Accepted 13 September 2023; Published 14 September 2023

Copyright © 2023 Journal of Sensors. This is an open access article distributed under the Creative Commons Attribution License, which permits unrestricted use, distribution, and reproduction in any medium, provided the original work is properly cited.

This article has been retracted by Hindawi following an investigation undertaken by the publisher [1]. This investigation has uncovered evidence of one or more of the following indicators of systematic manipulation of the publication process:

- (1) Discrepancies in scope
- (2) Discrepancies in the description of the research reported
- (3) Discrepancies between the availability of data and the research described
- (4) Inappropriate citations
- (5) Incoherent, meaningless and/or irrelevant content included in the article
- (6) Peer-review manipulation

The presence of these indicators undermines our confidence in the integrity of the article's content and we cannot, therefore, vouch for its reliability. Please note that this notice is intended solely to alert readers that the content of this article is unreliable. We have not investigated whether authors were aware of or involved in the systematic manipulation of the publication process.

Wiley and Hindawi regrets that the usual quality checks did not identify these issues before publication and have since put additional measures in place to safeguard research integrity.

We wish to credit our own Research Integrity and Research Publishing teams and anonymous and named external researchers and research integrity experts for contributing to this investigation.

The corresponding author, as the representative of all authors, has been given the opportunity to register their agreement or disagreement to this retraction. We have kept a record of any response received.

References

- [1] G. He, "Motion Rehabilitation Robot Control Based on Human Posture Information," *Journal of Sensors*, vol. 2022, Article ID 5067346, 7 pages, 2022.

Retraction

Retracted: Artificial Intelligence Optimization Design Analysis of Robot Control System

Journal of Sensors

Received 13 September 2023; Accepted 13 September 2023; Published 14 September 2023

Copyright © 2023 Journal of Sensors. This is an open access article distributed under the Creative Commons Attribution License, which permits unrestricted use, distribution, and reproduction in any medium, provided the original work is properly cited.

This article has been retracted by Hindawi following an investigation undertaken by the publisher [1]. This investigation has uncovered evidence of one or more of the following indicators of systematic manipulation of the publication process:

- (1) Discrepancies in scope
- (2) Discrepancies in the description of the research reported
- (3) Discrepancies between the availability of data and the research described
- (4) Inappropriate citations
- (5) Incoherent, meaningless and/or irrelevant content included in the article
- (6) Peer-review manipulation

The presence of these indicators undermines our confidence in the integrity of the article's content and we cannot, therefore, vouch for its reliability. Please note that this notice is intended solely to alert readers that the content of this article is unreliable. We have not investigated whether authors were aware of or involved in the systematic manipulation of the publication process.

Wiley and Hindawi regrets that the usual quality checks did not identify these issues before publication and have since put additional measures in place to safeguard research integrity.

We wish to credit our own Research Integrity and Research Publishing teams and anonymous and named external researchers and research integrity experts for contributing to this investigation.

The corresponding author, as the representative of all authors, has been given the opportunity to register their agreement or disagreement to this retraction. We have kept a record of any response received.

References

- [1] H. Guo, Y. Wang, G. Wang, Z. Du, R. Chen, and H. Sun, "Artificial Intelligence Optimization Design Analysis of Robot Control System," *Journal of Sensors*, vol. 2022, Article ID 2235042, 6 pages, 2022.

Retraction

Retracted: Intelligent Optimization Design of Automatic Sorting Robot Process

Journal of Sensors

Received 13 September 2023; Accepted 13 September 2023; Published 14 September 2023

Copyright © 2023 Journal of Sensors. This is an open access article distributed under the Creative Commons Attribution License, which permits unrestricted use, distribution, and reproduction in any medium, provided the original work is properly cited.

This article has been retracted by Hindawi following an investigation undertaken by the publisher [1]. This investigation has uncovered evidence of one or more of the following indicators of systematic manipulation of the publication process:

- (1) Discrepancies in scope
- (2) Discrepancies in the description of the research reported
- (3) Discrepancies between the availability of data and the research described
- (4) Inappropriate citations
- (5) Incoherent, meaningless and/or irrelevant content included in the article
- (6) Peer-review manipulation

The presence of these indicators undermines our confidence in the integrity of the article's content and we cannot, therefore, vouch for its reliability. Please note that this notice is intended solely to alert readers that the content of this article is unreliable. We have not investigated whether authors were aware of or involved in the systematic manipulation of the publication process.

Wiley and Hindawi regrets that the usual quality checks did not identify these issues before publication and have since put additional measures in place to safeguard research integrity.

We wish to credit our own Research Integrity and Research Publishing teams and anonymous and named external researchers and research integrity experts for contributing to this investigation.

The corresponding author, as the representative of all authors, has been given the opportunity to register their agreement or disagreement to this retraction. We have kept a record of any response received.

References

- [1] J. Liu, J. Wang, and Y. Xu, "Intelligent Optimization Design of Automatic Sorting Robot Process," *Journal of Sensors*, vol. 2022, Article ID 4860006, 8 pages, 2022.

Retraction

Retracted: Dynamic Path Planning Analysis of Warehouse Handling Robot

Journal of Sensors

Received 13 September 2023; Accepted 13 September 2023; Published 14 September 2023

Copyright © 2023 Journal of Sensors. This is an open access article distributed under the Creative Commons Attribution License, which permits unrestricted use, distribution, and reproduction in any medium, provided the original work is properly cited.

This article has been retracted by Hindawi following an investigation undertaken by the publisher [1]. This investigation has uncovered evidence of one or more of the following indicators of systematic manipulation of the publication process:

- (1) Discrepancies in scope
- (2) Discrepancies in the description of the research reported
- (3) Discrepancies between the availability of data and the research described
- (4) Inappropriate citations
- (5) Incoherent, meaningless and/or irrelevant content included in the article
- (6) Peer-review manipulation

The presence of these indicators undermines our confidence in the integrity of the article's content and we cannot, therefore, vouch for its reliability. Please note that this notice is intended solely to alert readers that the content of this article is unreliable. We have not investigated whether authors were aware of or involved in the systematic manipulation of the publication process.

Wiley and Hindawi regrets that the usual quality checks did not identify these issues before publication and have since put additional measures in place to safeguard research integrity.

We wish to credit our own Research Integrity and Research Publishing teams and anonymous and named external researchers and research integrity experts for contributing to this investigation.

The corresponding author, as the representative of all authors, has been given the opportunity to register their agreement or disagreement to this retraction. We have kept a record of any response received.

References

- [1] Y. Zhao, "Dynamic Path Planning Analysis of Warehouse Handling Robot," *Journal of Sensors*, vol. 2022, Article ID 4434971, 7 pages, 2022.

Retraction

Retracted: The Function of Remote Monitoring System of a Robot Inverter Based on PLC and Cloud Platform

Journal of Sensors

Received 13 September 2023; Accepted 13 September 2023; Published 14 September 2023

Copyright © 2023 Journal of Sensors. This is an open access article distributed under the Creative Commons Attribution License, which permits unrestricted use, distribution, and reproduction in any medium, provided the original work is properly cited.

This article has been retracted by Hindawi following an investigation undertaken by the publisher [1]. This investigation has uncovered evidence of one or more of the following indicators of systematic manipulation of the publication process:

- (1) Discrepancies in scope
- (2) Discrepancies in the description of the research reported
- (3) Discrepancies between the availability of data and the research described
- (4) Inappropriate citations
- (5) Incoherent, meaningless and/or irrelevant content included in the article
- (6) Peer-review manipulation

The presence of these indicators undermines our confidence in the integrity of the article's content and we cannot, therefore, vouch for its reliability. Please note that this notice is intended solely to alert readers that the content of this article is unreliable. We have not investigated whether authors were aware of or involved in the systematic manipulation of the publication process.

Wiley and Hindawi regrets that the usual quality checks did not identify these issues before publication and have since put additional measures in place to safeguard research integrity.

We wish to credit our own Research Integrity and Research Publishing teams and anonymous and named external researchers and research integrity experts for contributing to this investigation.

The corresponding author, as the representative of all authors, has been given the opportunity to register their agreement or disagreement to this retraction. We have kept a record of any response received.

References

- [1] M. Yu, "The Function of Remote Monitoring System of a Robot Inverter Based on PLC and Cloud Platform," *Journal of Sensors*, vol. 2022, Article ID 1178508, 8 pages, 2022.

Retraction

Retracted: Development and Construction of Internet of Things Training Practice Platform for Employment Skills Assessment

Journal of Sensors

Received 13 September 2023; Accepted 13 September 2023; Published 14 September 2023

Copyright © 2023 Journal of Sensors. This is an open access article distributed under the Creative Commons Attribution License, which permits unrestricted use, distribution, and reproduction in any medium, provided the original work is properly cited.

This article has been retracted by Hindawi following an investigation undertaken by the publisher [1]. This investigation has uncovered evidence of one or more of the following indicators of systematic manipulation of the publication process:

- (1) Discrepancies in scope
- (2) Discrepancies in the description of the research reported
- (3) Discrepancies between the availability of data and the research described
- (4) Inappropriate citations
- (5) Incoherent, meaningless and/or irrelevant content included in the article
- (6) Peer-review manipulation

The presence of these indicators undermines our confidence in the integrity of the article's content and we cannot, therefore, vouch for its reliability. Please note that this notice is intended solely to alert readers that the content of this article is unreliable. We have not investigated whether authors were aware of or involved in the systematic manipulation of the publication process.

Wiley and Hindawi regrets that the usual quality checks did not identify these issues before publication and have since put additional measures in place to safeguard research integrity.

We wish to credit our own Research Integrity and Research Publishing teams and anonymous and named external researchers and research integrity experts for contributing to this investigation.

The corresponding author, as the representative of all authors, has been given the opportunity to register their agreement or disagreement to this retraction. We have kept a record of any response received.

References

- [1] X. Zhang, "Development and Construction of Internet of Things Training Practice Platform for Employment Skills Assessment," *Journal of Sensors*, vol. 2022, Article ID 3014565, 7 pages, 2022.

Retraction

Retracted: Data Encryption Technology Analysis of Robot Computer Network Information

Journal of Sensors

Received 13 September 2023; Accepted 13 September 2023; Published 14 September 2023

Copyright © 2023 Journal of Sensors. This is an open access article distributed under the Creative Commons Attribution License, which permits unrestricted use, distribution, and reproduction in any medium, provided the original work is properly cited.

This article has been retracted by Hindawi following an investigation undertaken by the publisher [1]. This investigation has uncovered evidence of one or more of the following indicators of systematic manipulation of the publication process:

- (1) Discrepancies in scope
- (2) Discrepancies in the description of the research reported
- (3) Discrepancies between the availability of data and the research described
- (4) Inappropriate citations
- (5) Incoherent, meaningless and/or irrelevant content included in the article
- (6) Peer-review manipulation

The presence of these indicators undermines our confidence in the integrity of the article's content and we cannot, therefore, vouch for its reliability. Please note that this notice is intended solely to alert readers that the content of this article is unreliable. We have not investigated whether authors were aware of or involved in the systematic manipulation of the publication process.

Wiley and Hindawi regrets that the usual quality checks did not identify these issues before publication and have since put additional measures in place to safeguard research integrity.

We wish to credit our own Research Integrity and Research Publishing teams and anonymous and named external researchers and research integrity experts for contributing to this investigation.

The corresponding author, as the representative of all authors, has been given the opportunity to register their agreement or disagreement to this retraction. We have kept a record of any response received.

References

- [1] Q. Shi and Y. Liu, "Data Encryption Technology Analysis of Robot Computer Network Information," *Journal of Sensors*, vol. 2022, Article ID 5127989, 7 pages, 2022.

Retraction

Retracted: Navigation and Positioning Analysis of Electric Inspection Robot Based on Improved SVM Algorithm

Journal of Sensors

Received 13 September 2023; Accepted 13 September 2023; Published 14 September 2023

Copyright © 2023 Journal of Sensors. This is an open access article distributed under the Creative Commons Attribution License, which permits unrestricted use, distribution, and reproduction in any medium, provided the original work is properly cited.

This article has been retracted by Hindawi following an investigation undertaken by the publisher [1]. This investigation has uncovered evidence of one or more of the following indicators of systematic manipulation of the publication process:

- (1) Discrepancies in scope
- (2) Discrepancies in the description of the research reported
- (3) Discrepancies between the availability of data and the research described
- (4) Inappropriate citations
- (5) Incoherent, meaningless and/or irrelevant content included in the article
- (6) Peer-review manipulation

The presence of these indicators undermines our confidence in the integrity of the article's content and we cannot, therefore, vouch for its reliability. Please note that this notice is intended solely to alert readers that the content of this article is unreliable. We have not investigated whether authors were aware of or involved in the systematic manipulation of the publication process.

Wiley and Hindawi regrets that the usual quality checks did not identify these issues before publication and have since put additional measures in place to safeguard research integrity.

We wish to credit our own Research Integrity and Research Publishing teams and anonymous and named external researchers and research integrity experts for contributing to this investigation.

The corresponding author, as the representative of all authors, has been given the opportunity to register their agreement or disagreement to this retraction. We have kept a record of any response received.

References

- [1] Y. Li, Y. Long, M. Du, X. Jiang, and X. Liu, "Navigation and Positioning Analysis of Electric Inspection Robot Based on Improved SVM Algorithm," *Journal of Sensors*, vol. 2022, Article ID 4613931, 6 pages, 2022.

Retraction

Retracted: Application of Internet of Things Technology in Mechanical Automation Control

Journal of Sensors

Received 22 August 2023; Accepted 22 August 2023; Published 23 August 2023

Copyright © 2023 Journal of Sensors. This is an open access article distributed under the Creative Commons Attribution License, which permits unrestricted use, distribution, and reproduction in any medium, provided the original work is properly cited.

This article has been retracted by Hindawi following an investigation undertaken by the publisher [1]. This investigation has uncovered evidence of one or more of the following indicators of systematic manipulation of the publication process:

- (1) Discrepancies in scope
- (2) Discrepancies in the description of the research reported
- (3) Discrepancies between the availability of data and the research described
- (4) Inappropriate citations
- (5) Incoherent, meaningless and/or irrelevant content included in the article
- (6) Peer-review manipulation

The presence of these indicators undermines our confidence in the integrity of the article's content and we cannot, therefore, vouch for its reliability. Please note that this notice is intended solely to alert readers that the content of this article is unreliable. We have not investigated whether authors were aware of or involved in the systematic manipulation of the publication process.

Wiley and Hindawi regrets that the usual quality checks did not identify these issues before publication and have since put additional measures in place to safeguard research integrity.

We wish to credit our own Research Integrity and Research Publishing teams and anonymous and named external researchers and research integrity experts for contributing to this investigation.

The corresponding author, as the representative of all authors, has been given the opportunity to register their agreement or disagreement to this retraction. We have kept a record of any response received.

References

- [1] Y. Xie, H. Li, Q. Jia, and X. Nie, "Application of Internet of Things Technology in Mechanical Automation Control," *Journal of Sensors*, vol. 2022, Article ID 9388942, 7 pages, 2022.

Retraction

Retracted: Implementation of Personalized Information Recommendation Platform System Based on Deep Learning Tourism

Journal of Sensors

Received 22 August 2023; Accepted 22 August 2023; Published 23 August 2023

Copyright © 2023 Journal of Sensors. This is an open access article distributed under the Creative Commons Attribution License, which permits unrestricted use, distribution, and reproduction in any medium, provided the original work is properly cited.

This article has been retracted by Hindawi following an investigation undertaken by the publisher [1]. This investigation has uncovered evidence of one or more of the following indicators of systematic manipulation of the publication process:

- (1) Discrepancies in scope
- (2) Discrepancies in the description of the research reported
- (3) Discrepancies between the availability of data and the research described
- (4) Inappropriate citations
- (5) Incoherent, meaningless and/or irrelevant content included in the article
- (6) Peer-review manipulation

The presence of these indicators undermines our confidence in the integrity of the article's content and we cannot, therefore, vouch for its reliability. Please note that this notice is intended solely to alert readers that the content of this article is unreliable. We have not investigated whether authors were aware of or involved in the systematic manipulation of the publication process.

Wiley and Hindawi regrets that the usual quality checks did not identify these issues before publication and have since put additional measures in place to safeguard research integrity.

We wish to credit our own Research Integrity and Research Publishing teams and anonymous and named external researchers and research integrity experts for contributing to this investigation.

The corresponding author, as the representative of all authors, has been given the opportunity to register their agreement or disagreement to this retraction. We have kept a record of any response received.

References

- [1] X. Wang, "Implementation of Personalized Information Recommendation Platform System Based on Deep Learning Tourism," *Journal of Sensors*, vol. 2022, Article ID 6221413, 9 pages, 2022.

Retraction

Retracted: Path Planning of Storage and Logistics Mobile Robot Based on ACA-E Algorithm

Journal of Sensors

Received 22 August 2023; Accepted 22 August 2023; Published 23 August 2023

Copyright © 2023 Journal of Sensors. This is an open access article distributed under the Creative Commons Attribution License, which permits unrestricted use, distribution, and reproduction in any medium, provided the original work is properly cited.

This article has been retracted by Hindawi following an investigation undertaken by the publisher [1]. This investigation has uncovered evidence of one or more of the following indicators of systematic manipulation of the publication process:

- (1) Discrepancies in scope
- (2) Discrepancies in the description of the research reported
- (3) Discrepancies between the availability of data and the research described
- (4) Inappropriate citations
- (5) Incoherent, meaningless and/or irrelevant content included in the article
- (6) Peer-review manipulation

The presence of these indicators undermines our confidence in the integrity of the article's content and we cannot, therefore, vouch for its reliability. Please note that this notice is intended solely to alert readers that the content of this article is unreliable. We have not investigated whether authors were aware of or involved in the systematic manipulation of the publication process.

Wiley and Hindawi regrets that the usual quality checks did not identify these issues before publication and have since put additional measures in place to safeguard research integrity.

We wish to credit our own Research Integrity and Research Publishing teams and anonymous and named external researchers and research integrity experts for contributing to this investigation.

The corresponding author, as the representative of all authors, has been given the opportunity to register their agreement or disagreement to this retraction. We have kept a record of any response received.

References

- [1] Y. Zhao, "Path Planning of Storage and Logistics Mobile Robot Based on ACA-E Algorithm," *Journal of Sensors*, vol. 2022, Article ID 5757719, 7 pages, 2022.

Retraction

Retracted: Mathematical Modeling Analysis of Data Attribute Encryption for Robot

Journal of Sensors

Received 22 August 2023; Accepted 22 August 2023; Published 23 August 2023

Copyright © 2023 Journal of Sensors. This is an open access article distributed under the Creative Commons Attribution License, which permits unrestricted use, distribution, and reproduction in any medium, provided the original work is properly cited.

This article has been retracted by Hindawi following an investigation undertaken by the publisher [1]. This investigation has uncovered evidence of one or more of the following indicators of systematic manipulation of the publication process:

- (1) Discrepancies in scope
- (2) Discrepancies in the description of the research reported
- (3) Discrepancies between the availability of data and the research described
- (4) Inappropriate citations
- (5) Incoherent, meaningless and/or irrelevant content included in the article
- (6) Peer-review manipulation

The presence of these indicators undermines our confidence in the integrity of the article's content and we cannot, therefore, vouch for its reliability. Please note that this notice is intended solely to alert readers that the content of this article is unreliable. We have not investigated whether authors were aware of or involved in the systematic manipulation of the publication process.

Wiley and Hindawi regrets that the usual quality checks did not identify these issues before publication and have since put additional measures in place to safeguard research integrity.

We wish to credit our own Research Integrity and Research Publishing teams and anonymous and named external researchers and research integrity experts for contributing to this investigation.

The corresponding author, as the representative of all authors, has been given the opportunity to register their agreement or disagreement to this retraction. We have kept a record of any response received.

References

- [1] J. Sun, J. Yan, and D. Yang, "Mathematical Modeling Analysis of Data Attribute Encryption for Robot," *Journal of Sensors*, vol. 2022, Article ID 3976806, 8 pages, 2022.

Retraction

Retracted: Implementation of Network Data Mining Algorithm for Associated Users Based on Multi-Information Fusion

Journal of Sensors

Received 22 August 2023; Accepted 22 August 2023; Published 23 August 2023

Copyright © 2023 Journal of Sensors. This is an open access article distributed under the Creative Commons Attribution License, which permits unrestricted use, distribution, and reproduction in any medium, provided the original work is properly cited.

This article has been retracted by Hindawi following an investigation undertaken by the publisher [1]. This investigation has uncovered evidence of one or more of the following indicators of systematic manipulation of the publication process:

- (1) Discrepancies in scope
- (2) Discrepancies in the description of the research reported
- (3) Discrepancies between the availability of data and the research described
- (4) Inappropriate citations
- (5) Incoherent, meaningless and/or irrelevant content included in the article
- (6) Peer-review manipulation

The presence of these indicators undermines our confidence in the integrity of the article's content and we cannot, therefore, vouch for its reliability. Please note that this notice is intended solely to alert readers that the content of this article is unreliable. We have not investigated whether authors were aware of or involved in the systematic manipulation of the publication process.

Wiley and Hindawi regrets that the usual quality checks did not identify these issues before publication and have since put additional measures in place to safeguard research integrity.

We wish to credit our own Research Integrity and Research Publishing teams and anonymous and named external researchers and research integrity experts for contributing to this investigation.

The corresponding author, as the representative of all authors, has been given the opportunity to register their agreement or disagreement to this retraction. We have kept a record of any response received.

References

- [1] H. Zhang, "Implementation of Network Data Mining Algorithm for Associated Users Based on Multi-Information Fusion," *Journal of Sensors*, vol. 2022, Article ID 3350997, 6 pages, 2022.

Retraction

Retracted: Design of the Vocal Music Feature Recognition System Based on the Internet of Things Technology

Journal of Sensors

Received 22 August 2023; Accepted 22 August 2023; Published 23 August 2023

Copyright © 2023 Journal of Sensors. This is an open access article distributed under the Creative Commons Attribution License, which permits unrestricted use, distribution, and reproduction in any medium, provided the original work is properly cited.

This article has been retracted by Hindawi following an investigation undertaken by the publisher [1]. This investigation has uncovered evidence of one or more of the following indicators of systematic manipulation of the publication process:

- (1) Discrepancies in scope
- (2) Discrepancies in the description of the research reported
- (3) Discrepancies between the availability of data and the research described
- (4) Inappropriate citations
- (5) Incoherent, meaningless and/or irrelevant content included in the article
- (6) Peer-review manipulation

The presence of these indicators undermines our confidence in the integrity of the article's content and we cannot, therefore, vouch for its reliability. Please note that this notice is intended solely to alert readers that the content of this article is unreliable. We have not investigated whether authors were aware of or involved in the systematic manipulation of the publication process.

Wiley and Hindawi regrets that the usual quality checks did not identify these issues before publication and have since put additional measures in place to safeguard research integrity.

We wish to credit our own Research Integrity and Research Publishing teams and anonymous and named external researchers and research integrity experts for contributing to this investigation.

The corresponding author, as the representative of all authors, has been given the opportunity to register their agreement or disagreement to this retraction. We have kept a record of any response received.

References

- [1] H. Huang, "Design of the Vocal Music Feature Recognition System Based on the Internet of Things Technology," *Journal of Sensors*, vol. 2022, Article ID 1164042, 7 pages, 2022.

Retraction

Retracted: Automatic Modulation and Recognition of Robot Communication Signal Based on Deep Learning Neural Network

Journal of Sensors

Received 22 August 2023; Accepted 22 August 2023; Published 23 August 2023

Copyright © 2023 Journal of Sensors. This is an open access article distributed under the Creative Commons Attribution License, which permits unrestricted use, distribution, and reproduction in any medium, provided the original work is properly cited.

This article has been retracted by Hindawi following an investigation undertaken by the publisher [1]. This investigation has uncovered evidence of one or more of the following indicators of systematic manipulation of the publication process:

- (1) Discrepancies in scope
- (2) Discrepancies in the description of the research reported
- (3) Discrepancies between the availability of data and the research described
- (4) Inappropriate citations
- (5) Incoherent, meaningless and/or irrelevant content included in the article
- (6) Peer-review manipulation

The presence of these indicators undermines our confidence in the integrity of the article's content and we cannot, therefore, vouch for its reliability. Please note that this notice is intended solely to alert readers that the content of this article is unreliable. We have not investigated whether authors were aware of or involved in the systematic manipulation of the publication process.

Wiley and Hindawi regrets that the usual quality checks did not identify these issues before publication and have since put additional measures in place to safeguard research integrity.

We wish to credit our own Research Integrity and Research Publishing teams and anonymous and named external researchers and research integrity experts for contributing to this investigation.

The corresponding author, as the representative of all authors, has been given the opportunity to register their agreement or disagreement to this retraction. We have kept a record of any response received.

References

- [1] X. Zou and X. Zou, "Automatic Modulation and Recognition of Robot Communication Signal Based on Deep Learning Neural Network," *Journal of Sensors*, vol. 2022, Article ID 3519010, 7 pages, 2022.

Retraction

Retracted: Motion Control and Tracking Control of UAV Based on Adaptive Sensor

Journal of Sensors

Received 23 January 2024; Accepted 23 January 2024; Published 24 January 2024

Copyright © 2024 Journal of Sensors. This is an open access article distributed under the Creative Commons Attribution License, which permits unrestricted use, distribution, and reproduction in any medium, provided the original work is properly cited.

This article has been retracted by Hindawi following an investigation undertaken by the publisher [1]. This investigation has uncovered evidence of one or more of the following indicators of systematic manipulation of the publication process:

- (1) Discrepancies in scope
- (2) Discrepancies in the description of the research reported
- (3) Discrepancies between the availability of data and the research described
- (4) Inappropriate citations
- (5) Incoherent, meaningless and/or irrelevant content included in the article
- (6) Manipulated or compromised peer review

The presence of these indicators undermines our confidence in the integrity of the article's content and we cannot, therefore, vouch for its reliability. Please note that this notice is intended solely to alert readers that the content of this article is unreliable. We have not investigated whether authors were aware of or involved in the systematic manipulation of the publication process.

Wiley and Hindawi regrets that the usual quality checks did not identify these issues before publication and have since put additional measures in place to safeguard research integrity.

We wish to credit our own Research Integrity and Research Publishing teams and anonymous and named external researchers and research integrity experts for contributing to this investigation.


The corresponding author, as the representative of all authors, has been given the opportunity to register their agreement or disagreement to this retraction. We have kept a record of any response received.

References

- [1] X. Zhao, Z. Xu, Y. Fu, S. Xu, and S. Xiong, "Motion Control and Tracking Control of UAV Based on Adaptive Sensor," *Journal of Sensors*, vol. 2023, Article ID 7936019, 7 pages, 2023.

Research Article

Motion Control and Tracking Control of UAV Based on Adaptive Sensor

Xin Zhao, Zhihui Xu , Yifeng Fu, Shoupeng Xu, and Shasha Xiong

School of Aeronautics, Henan Mechanical and Electrical Vocational College, Zhengzhou, Henan 451191, China

Correspondence should be addressed to Zhihui Xu; 2010641112@hbut.edu.cn

Received 10 July 2022; Revised 26 August 2022; Accepted 31 August 2022; Published 25 April 2023

Academic Editor: Haibin Lv

Copyright © 2023 Xin Zhao et al. This is an open access article distributed under the Creative Commons Attribution License, which permits unrestricted use, distribution, and reproduction in any medium, provided the original work is properly cited.

In order to meet the requirements of UAV motion control and tracking control, an adaptive sensor-based technology is proposed. The main content of the technology is based on the mathematical model of the adaptive sensor, through the quaternion attitude update model, using nonlinear attitude SVDCK filtering and dynamic adaptive adjustment factors and other technologies, and finally through simulation experiments and analysis to build the research means of UAV motion control and tracking control system. The experimental results show that the roll Angle, pitch Angle, and yaw Angle of SVDCKF are 1.703, 1.972, and 1.928, respectively. By adjusting the dynamic adaptive factor, the attitude-filtering algorithm reduces the error of the attitude solution and improves the robustness of the attitude solution under high dynamic conditions. *Conclusion.* The technology research based on adaptive sensor can meet the requirements of UAV motion control and tracking control.

1. Introduction

In many application scenarios of UAV, target tracking is a very typical task. In the process of target tracking, UAV uses its mounted sensor to continuously observe the tracked target, which can obtain a lot of information about the target, and then realize the target identification and precise positioning. Therefore, UAV target tracking has great application value in battlefield reconnaissance, ground attack, city antiterrorism, and maritime search and rescue, and has received more and more attention [1]. Four-rotor UAVs are widely used in surveying, mapping, monitoring, and other fields due to their small appearance and easy concealment. In some specific scenarios, it is necessary to pay attention to the flight status of the UAV at all times, so the visual tracking of the UAV is particularly important, and the challenge of realizing efficient visual tracking lies in the reasonable appearance of the target and the selection of appropriate tracking strategy.

Due to the influence of UAV motion constrained sensor observation range and complex environmental conditions, a single UAV is usually not enough to achieve accurate and continuous target tracking. Therefore, multiple UAVs are needed to maintain the robustness of target tracking task

and obtain higher target positioning accuracy. Compared with single UAV target tracking, multi-UAV cooperative target tracking has two key problems. Collaborative fusion estimation of target state, that is, how to effectively fuse the target observations from different UAVs to obtain the optimal estimation of target state. Trajectory optimization decision of cooperative target tracking and observation by multiple UAVs, namely, how to coordinate the movement of these UAVs to obtain better observation of the target (to optimize the performance of target state estimation) [2]. Therefore, at present, domestic and foreign scholars have carried out a lot of research on these two key problems in cooperative target tracking of multiple UAVs. With the rapid development of UAV technology, it has gradually been applied to aerial photography, aerial detection, geographic mapping, power line inspection, personnel search, express delivery, maritime rescue, agricultural plant protection, environmental monitoring, and other fields. With the rapid development of UAV technology, autonomous tracking and landing of dynamic targets by UAV has become a key issue for many researchers.

With the rapid development of modern science and technology, UAV technology is widely used in surveying,

geology, meteorology, plant protection, inspection and monitoring, and other fields, and the application of UAV + industry is in the ascendant [3]. With the rapid development of UAV information technology, lightweight and miniaturized mission load technology, satellite communication technology, composite material structure technology, high efficiency aerodynamics technology, new energy and high efficiency power technology, integration technology of light and small sensors and data processing system, and take-off and landing technology, the performance of UAV is constantly improving. Functions continue to expand, various types of UAVs continue to emerge, and the application field is more and more extensive.

2. Literature Review

At present, UAV attitude calculation algorithms mainly include complementary filtering, Kalman filtering, and so on. Among them, complementary filtering relies on the frequency complementary characteristics between sensors and fuses sensor data to calculate the heading. UAV technology is widely used in today's society. UAV has the characteristics of low-cost, high efficiency, maneuver, flexibility, real-time, high resolution, simple operation, high image resolution, and little influence by terrain factors. It can adapt to a complex environment outside, and has good controllability of flight routes during aerial survey, which can be set according to actual needs. As an aerial IoT device, UAV has many different characteristics from low-orbit satellites and ground networks. UAV has lower path loss and is very beneficial to wireless transmission in the Internet of Things because of its on-demand deployment in hover mode [4]. However, the excessive dependence of the cellular Internet of Things on ground infrastructure is not conducive to the deployment of the Internet of Things in remote areas and disaster areas. In contrast, UAVs have the flexibility to respond quickly to remote operations and control, can deploy IoT quickly without ground infrastructure, and UAVs have air superiority and access to better line-of-sight links, conducive to sending information sufficiently close to IoT devices. As a result, UAVs can quickly meet a variety of business needs, such as providing data offloading wireless coverage communications relays and edge computing for hot spot disasters and remote areas as well as military operations. UAV aerial photography is a combination of visible light camera, infrared thermal imager, hyperspectral imager, laser radar and image transmission equipment carried by UAV, and aircraft with image transmission technology to transmit high-definition pictures in real-time and complete image information processing of the control area. Unmanned aerial vehicle (UAV) with the aid of wireless control technology and process control devices to operate applications, use of prior planning process to realize the automatic operation intelligent vehicle has the most advanced visual system and sensor system, can be in a stable hover flight, with automatic returning obstacles perception and auxiliary function, and can carry specified parts to adapt to different scenarios [5].

To solve the above problems, in order to meet the requirements of UAV motion control and tracking control, an adaptive sensor-based technology is proposed. The main content of the technology is based on the mathematical model of the adaptive sensor, through the quaternion attitude update model, using nonlinear attitude SVDC filtering and dynamic adaptive adjustment factors and other technologies, and finally through simulation experiments and analysis to build the research means of UAV motion control and tracking control system. For small unmanned aerial vehicle (UAV) under the condition of complex flight navigation position of calculating precision and robustness problem, this paper proposes a dynamic adaptive adjustment of the singular value volume navigation pose estimation of the Kalman filter algorithm, considering the low-cost airlines posture sensor random, the problem of large deviation, the navigation position sensor random deviation as to estimate parameters and to eliminate the influence of stochastic error sensor [6].

3. Research Method

3.1. Adaptive Sensor Mathematical Model

3.1.1. Quaternion Attitude Update Model. In the attitude representation method of UAV strapdown, unit quaternion is usually used for fast calculation of attitude update and rigid body transformation, as shown in the following:

$$q = q_w + q_x i + q_y j + q_z k = \begin{bmatrix} q_w \\ q_v \end{bmatrix} = \begin{bmatrix} \cos(\theta/2) \\ e_x \sin(\theta/2) \\ e_y \sin(\theta/2) \\ e_z \sin(\theta/2) \end{bmatrix}. \quad (1)$$

In the formula, q_w is the real part of a quaternion, q_v is the imaginary part of a quaternion, and e is the rotation axis. Quaternion continuous multiplication operation can be defined by the following:

$$p \otimes q = \begin{bmatrix} P_w q_w - P_v^T q_v \\ P_w q_v + q_w P_v + P_v \times q_v \end{bmatrix}, \quad (2)$$

$$q \otimes q^{-1} = [1, 0, 0, 0]^T. \quad (3)$$

In formulas (2) and (3), the quaternion multiplication operator is a reversible quaternion of q , and the quaternion must satisfy the orthogonal principle of

$$|q| = \sqrt{q \otimes q^{-1}} = \sqrt{q_w^2 + q_x^2 + q_y^2 + q_z^2} = 1. \quad (4)$$

In this paper, the unit quaternion is used to update the UAV attitude, the quaternion attitude differential equation is solved by the first-order Picard's substitution method, and the discrete model is given [7, 8].

Attitude calculation is dependent on measurements from attitude sensors using low-cost attitude sensors, mainly

including gyroscopes, accelerometers, and magnetometers. These sensors are attached to the center of gravity of the small UAV body, and the three axes of the sensor are orthogonal to each other under ideal conditions [9].

UAV attitude model is a nonlinear system in practice. Therefore, this paper establishes the nonlinear system model of UAV attitude in the Gaussian discrete state, as shown in the following:

$$\begin{cases} x_k = f(x_{k-1}, v_{k-1}) + m_{k-1}, \\ z_k = h(x_k) + n_k. \end{cases} \quad (5)$$

In the formula x_k is the attitude state estimation parameters, $f(\cdot)$ is the nonlinear dynamic function, v_{k-1} is the attitude sensor input parameters, z_k is the attitude observation parameters, and $h(\cdot)$ is the nonlinear observation function. Among them, m_{k-1} and n_k are system dynamic noise and observation noise, respectively. It is assumed that both of them are zero-mean Gaussian white noise and unrelated.

3.1.2. Nonlinear Attitude SVDCK Filtering. For nonlinear pose filtering, CKF filtering method is adopted in this paper, which has better solution accuracy than EKF and UKF. The Cholesky decomposition state covariance matrix P and $P = U^T U$, U is the triangular matrix [10]. However, there are some problems with using the Cholesky decomposition.

- (1) When Cholesky decompose the state covariance matrix P , P must satisfy the property of positive definite or symmetric positive definite, which limits the value range of P and leads to unstable attitude solution
- (2) The state covariance matrix may become a sparse matrix during the operation of the attitude-filtering algorithm, which destroys the requirement of Cholesky's decomposition for P

Therefore, this paper uses Singular Value Decomposition (SVD) to replace Cholesky's decomposition, so that the state covariance matrix P can overcome the above problems as shown in Figure 1.

3.1.3. Dynamic Adaptive Regulatory Factor. Under different flight conditions of UAV, the triaxial acceleration of the accelerometer will change greatly, especially some harmful acceleration or abnormal measurement values may affect the value of acceleration [11]. Also, during the drone flight, body jitter and turbulence will also make the acceleration value uncertain. Therefore, based on the adaptive adjustment of the noise variance of the sensor, a dynamic adaptive adjustment factor is designed to improve the noise variance of the accelerometer. And, the flight conditions of UAV are divided into static conditions, low dynamic conditions, and high dynamic conditions. Figure 2 is the block diagram of dynamic adaptive SVDCKF filter, in which the dynamic

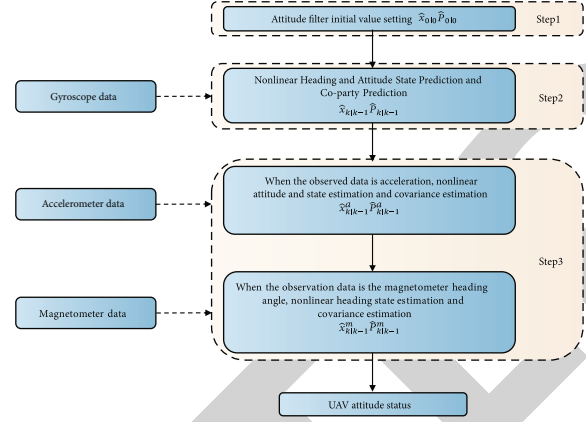


FIGURE 1: Block diagram of nonlinear attitude filtering.

acceleration factor can be defined by the following:

$$\partial = \left| \sqrt{a_{fx}^2 + a_{fy}^2 + a_{fz}^2} - g \right|. \quad (6)$$

- (1) Static condition: before the UAV takes off, the flight state on the horizontal ground can be assumed to be in static condition. At this time, the triaxial acceleration is only affected by the local gravitational acceleration and slight shake of the body. Due to the use of low-cost inertial devices, the device itself has great sensor noise [12]
- (2) Under low dynamic conditions: the UAV is affected by body jitter and airflow disturbance in the flight process, which is transmitted to the accelerometer and produces harmful accelerations. These harmful accelerations will pollute the triaxial acceleration value and then lead to the failure of UAV attitude calculation [13]
- (3) In high dynamic conditions, the UAV can be disturbed by some bad factors during flight, such as strong winds, turbulence, and birds. These sudden and dramatic changes will all cause triaxial acceleration to be unusable

3.1.4. Key Technology. The key technology of UAV full-flight self-optimizing control in complex environment integrates advanced information technology, communication technology, control technology, sensor technology, and system integration technology. The intelligent control of traditional PID flight control system is optimized by using the modern control technology of artificial intelligence and the analysis and fusion of a large number of flight case data [14].

Complex environment refers to complex geographical environment, complex meteorological environment, complex electromagnetic environment, complex scenes, and a variety of complex UAV platform models.

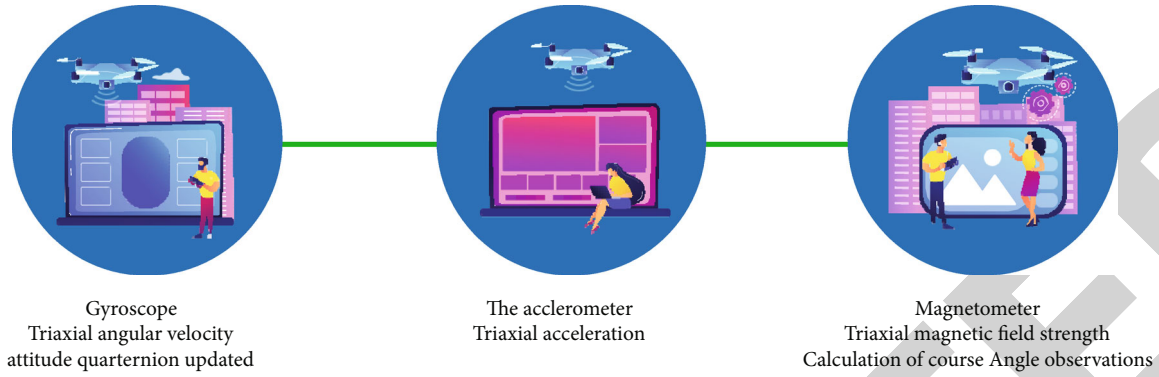


FIGURE 2: Adaptive filtering block diagram of SVDCKF.

- (1) The nonlinear adaptive variable parameter control algorithm, fault self-diagnosis, and control law reconstruction are proposed to solve the problem of accurate control of UAV trajectory and navigation point in complex environment. The whole process control strategy control process and control algorithm of UAV from takeoff to landing are proposed to realize intelligent and accurate autonomous control of UAV in complex environment [15]
- (2) Based on the pilot following method, artificial potential field method, virtual structure method, and behavior-based method, the optimal estimation filter and vertical high-order control loop were constructed by integrating multisensor information under different mission requirements and aircraft type conditions. The problem of precise cooperative control and collision avoidance of multiple aircraft formations is solved, and the cooperative formation flight of UAVs in wide airspace with long distance and large speed is realized [16]

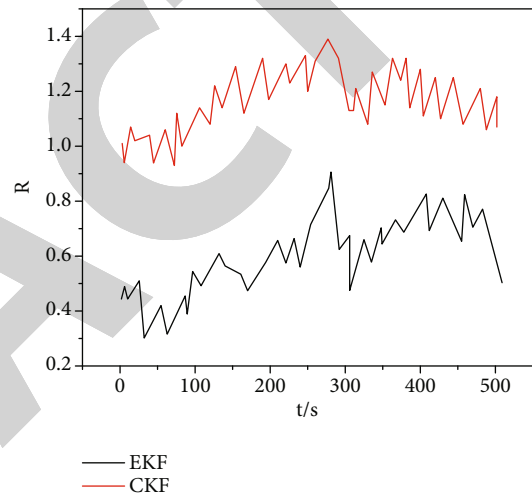


FIGURE 3: Roll Angle, pitch Angle, and yaw Angle error diagram under static condition.

3.2. Simulation Experiment

3.2.1. Experimental Platform and Analysis. In this paper, the experimental platform is used to collect UAV attitude sensor data, including MPU6500 inertial measurement unit and HMC5893 magnetometer. During the experiment, rotor UAV was used to collect attitude sensor data under static and low dynamic conditions, and fixed wing UAV was used to collect attitude sensor data under high dynamic conditions [17].

In order to better verify the performance of the proposed attitude-filtering algorithm, the collected attitude sensor data is used to analyze the algorithm on the simulation software, and the algorithm is compared with EKF and CKF attitude filtering [18].

Figure 3 describes the variation of UAV's triaxial acceleration under static conditions. Compared with EKF and CKF, the attitude error of the proposed aeropose-filtering algorithm is the smallest. Since the variation of triaxial acceleration under static conditions is relatively stable, the measurement noise has little influence on the accuracy of aeropose. In this case, the accurate nonlinear attitude model

and the high-dimensional nonlinear attitude-filtering algorithm will affect the solution of the attitude accuracy [19]. In this paper, a 13-dimensional attitude estimation model and high-dimensional singular value volumetric Kalman filter are designed to improve the accuracy of attitude filtering and reduce the interference of some uncertain factors.

Figure 4 describes the variation of UAV's triaxial acceleration under low dynamic conditions. Under low dynamic conditions, EKF's attitude filtering attitude error is the largest, mainly because EKF introduces rounding error to the first-order truncation description of nonlinear attitude model, which is then transmitted to the attitude solution and amplifies the error of attitude solution [20]. Although the attitude calculation error of CKF is smaller than that of EKF, the measured value of triaxial acceleration will be interfered by some uncertain factors during low dynamic flight. At this time, the acceleration noise will be constantly changing. CKF cannot eliminate the influence brought by these disturbances because the constant acceleration noise variance is set. Therefore, a dynamic adaptive adjustment factor is designed in this paper, through which the acceleration noise variance is constantly adjusted to reduce the attitude error.

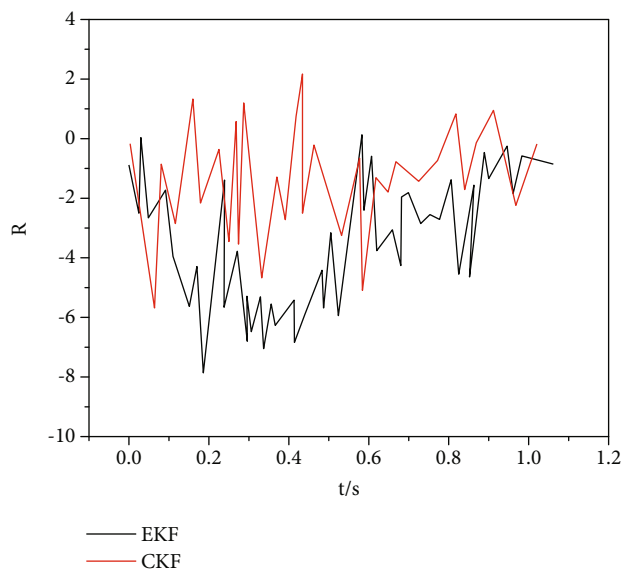


FIGURE 4: Error diagram of roll Angle, pitch Angle, and yaw Angle under low dynamic condition.

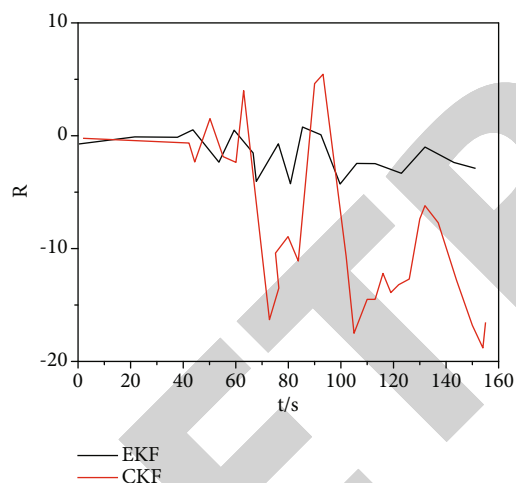


FIGURE 5: Roll Angle, pitch Angle, and yaw Angle error diagram under high dynamic condition.

Figure 5 describes the variation of UAV's triaxial acceleration under high dynamic conditions. In low dynamic conditions, fixed-wing UAV is used in this paper to collect attitude sensor data under high dynamic flight conditions. Compared with rotor-wing UAV, fixed-wing UAV has faster flight speed and more flexible maneuvering. The attitude error of EKF attitude filter changes sharply after 40s. This is because, under high dynamic conditions, the nonlinear degree of the sailing attitude model is enhanced, which leads to an increasingly large rounding error caused by EKF first-order truncation. Under high dynamic conditions, SVDCKF with dynamic adaptive adjustment factor has better processing effect on the acceleration measurement noise than CKF, which eliminates the influence of nonacceleration on the attitude calculation and improves the calculation accuracy.

TABLE 1: Comparison of attitude accuracy among EKF, CKF, and SVDCKF.

Method	The attitude angle/(°)			
	Roll angle R	Angle of pitch P	Yaw angle Y	
EKF	MAE	3.294/7	5.147/8	6.011/5
	STD	6.007/5	9.869/7	12.594/0
	RMSE	9.037/3	14.801/0	22.694/0
CKF	MAE	2.712/3	3.714/3	4.014/3
	STD	5.057/0	6.510/5	6.380/4
	RMSE	6.786/8	7.608/6	10.264/0
SVDCKF	MAE	1.703/6	1.972/3	1.928/0
	STD	3.548/2	4.396/8	4.467/2
	RMSE	3.335/1	3.436/3	4.136/2

4. Interpretation of Result

In this paper, a SVDCKF nonlinear attitude-filtering algorithm with dynamic adaptive adjustment factor is proposed. Taking small unmanned aerial vehicle (UAV) as the research object, the attitude calculation requirements of UAV during flight are analyzed and designed, which improves the accuracy and robustness of UAV attitude calculation. Compared with other attitude algorithms, the proposed attitude algorithm has the following advantages:

- (1) A nonlinear attitude system model of the attitude state was designed, and the random errors of the gyroscope accelerometer and magnetometer were used as state estimation parameters to eliminate the influence of the random errors of the attitude sensor on the accuracy of the attitude solution
- (2) In view of the nonlinear problem of UAV attitude model and matrix nonpositive definite problem of state covariance in the filtering process, singular value decomposition was used to replace Cholesky's decomposition, and then combined with volume Kalman filter, the nonlinear attitude model was processed to improve the accuracy of attitude solution [21].
- (3) A dynamic adaptive adjustment factor was designed to deal with the variance of acceleration measurement noise, which improved the robustness and immunity of the attitude filtering

Table 1 provides the mean absolute error standard deviation and root mean square error of EKF, CKF, and SVDCKF attitude accuracy of UAV under high dynamic conditions. As can be seen from Table 1, the value of SVDCKF roll Angle is 1.703, pitch Angle is 1.972, and yaw Angle is 1.928. By adjusting the dynamic adaptive factor, the proposed algorithm can reduce the error of attitude calculation and improve the robustness of attitude calculation under high dynamic conditions.

5. Conclusion

To solve the above problems, in order to meet the requirements of UAV motion control and tracking control, an adaptive sensor-based technology is proposed. The main content of the technology is based on the mathematical model of the adaptive sensor, through the quaternion attitude update model, using nonlinear attitude SVCK filtering and dynamic adaptive adjustment factors and other technologies, and finally through simulation experiments and analysis to build the research means of UAV motion control and tracking control system. Considering the influence of the triaxial acceleration in the attitude sensor on UAV attitude calculation under different flight conditions, a dynamic adaptive factor was proposed based on the idea of adaptive filtering to continuously adjust the noise variance of the acceleration measurement, which improved the robustness of the attitude filtering under complex conditions. Aiming at the nonlinear problem of the UAV's attitude model and the matrix nonpositive definite problem of the state covariance in the filtering process, the singular value decomposition is used to replace the Cholesky decomposition, and then combined with the volumetric Kalman filter, the nonlinear attitude model is analyzed. Processing to improve the accuracy of the attitude calculation, experimental results show that the proposed algorithm not only effectively improves the accuracy of the nonlinear attitude model and meets the flight requirements of small UAVs but also eliminates the influence of the random deviation of the attitude sensor and the noise of the triaxial acceleration measurement on the attitude solution, and improves the robustness and immunity of the algorithm.

Data Availability

The data used to support the findings of this study are available from the corresponding author upon request.

Conflicts of Interest

The authors declare that they have no conflicts of interest.

References

- [1] L. Hou, F. Lian, S. Tan, C. Xu, and G. Abreu, "Robust generalized labeled multi-bernoulli filter for multitarget tracking with unknown non-stationary heavy-tailed measurement noise," *IEEE Access*, vol. 9, pp. 94438–94453, 2021.
- [2] M. Beauchamp, R. Fablet, C. Ubelmann, M. Ballarotta, and B. Chapron, "Intercomparison of data-driven and learning-based interpolations of along-track nadir and wide-swath swot altimetry observations," *Remote Sensing*, vol. 12, no. 22, p. 3806, 2020.
- [3] P. B. Holden, A. J. Rebelo, and M. G. New, "Mapping invasive alien trees in water towers: a combined approach using satellite data fusion, drone technology and expert engagement," *Remote Sensing Applications Society and Environment*, vol. 21, no. 1, article 100448, 2021.
- [4] B. Rohman, M. B. Andra, and M. Nishimoto, "Through-the-wall human respiration detection using uwb impulse radar on hovering drone," *IEEE Journal of Selected Topics in Applied Earth Observations and Remote Sensing*, vol. 14, pp. 6572–6584, 2021.
- [5] I. F. Ammarprawira, M. S. Fauzi, A. Jabbaar, and N. Syafitri, "Implementasi automatic waypoint untuk return trip pada autonomous robot dengan titik acuan potensi korban bencana," *ELKOMIKA Jurnal Teknik Energi Elektrik Teknik Telekomunikasi & Teknik Elektronika*, vol. 8, no. 1, p. 203, 2020.
- [6] L. Su and V. Lau, "Data and channel-adaptive sensor scheduling for federated edge learning via over-the-air gradient aggregation," *IEEE Internet of Things Journal*, vol. 9, no. 3, pp. 1640–1654, 2022.
- [7] Z. Wang, K. M. Schmalbach, R. L. Penn, D. Poerschke, and A. Stein, "3d periodic and interpenetrating tungsten-silicon oxycarbide nanocomposites designed for mechanical robustness," *ACS Applied Materials & Interfaces*, vol. 13, no. 27, pp. 32126–32135, 2021.
- [8] M. Roelfs, D. Dudal, and D. Huybrechs, "Quaternionic step derivative: machine precision differentiation of holomorphic functions using complex quaternions," *Journal of Computational and Applied Mathematics*, vol. 398, no. 3, article 113699, 2021.
- [9] R.-F. Li, X.-X. Wang, L. Wu et al., "Xanthomonas campestris sensor kinase hpas co-opts the orphan response regulator vemr to form a branched two-component system that regulates motility," *Molecular Plant Pathology*, vol. 21, no. 3, pp. 360–375, 2020.
- [10] S. Chen, Y. Shen, Y. Yan, D. Wang, and S. Zhu, "Cholesky decomposition-based metric learning for video-based human action recognition," *Access*, vol. 8, pp. 36313–36321, 2020.
- [11] S. Yang, X. Hu, X. Wang, and D. Li, "A structure scheme to reduce the influence of the accelerometer inner lever-arm effect on tri-axis inertial navigation systems," *Measurement Science and Technology*, vol. 32, no. 5, article 055103, 2021.
- [12] C. Dang, J. Li, and J. Tang, "Systematic research on measuring acceleration of gravity by laser interferometry," *Journal of Physics: Conference Series*, vol. 1982, no. 1, article 012146, 2021.
- [13] M. Albacha, L. Rambault, A. Sakout, K. A. Meraim, and S. Cauet, "Software sensor for airflow modulation and noise detection by cyclostationary tools," *Sensors*, vol. 20, no. 8, p. 2414, 2020.
- [14] C. N. Umstead, K. M. Unertl, N. M. Lorenzi, and N. L. Lovett, "Enabling adoption and use of new health information technology during implementation: roles and strategies for internal and external support personnel," *Medical Informatics*, vol. 28, no. 7, pp. 1543–1547, 2021.
- [15] A. Bakushinsky and A. Smirnova, "A study of frozen iteratively regularized gauss-newton algorithm for nonlinear ill-posed problems under generalized normal solvability condition," *Journal of Inverse and Ill-Posed Problems*, vol. 28, no. 2, pp. 275–286, 2020.
- [16] X. Yan, D. Jiang, R. Miao, and Y. Li, "Formation control and obstacle avoidance algorithm of a multi-usv system based on virtual structure and artificial potential field," *Journal of Marine Science and Engineering*, vol. 9, no. 2, p. 161, 2021.
- [17] A. Sharma and R. Kumar, "Performance comparison and detailed study of AODV, DSDV, DSR, TORA and OLSR routing protocols in ad hoc networks," in *2016 Fourth International Conference on Parallel, Distributed and Grid Computing*, pp. 732–736, Wagnaghat, India, 2016.

Retraction

Retracted: Application of Multisource Data Fusion Technology in the Construction of Land Ecological Index

Journal of Sensors

Received 23 January 2024; Accepted 23 January 2024; Published 24 January 2024

Copyright © 2024 Journal of Sensors. This is an open access article distributed under the Creative Commons Attribution License, which permits unrestricted use, distribution, and reproduction in any medium, provided the original work is properly cited.

This article has been retracted by Hindawi following an investigation undertaken by the publisher [1]. This investigation has uncovered evidence of one or more of the following indicators of systematic manipulation of the publication process:

- (1) Discrepancies in scope
- (2) Discrepancies in the description of the research reported
- (3) Discrepancies between the availability of data and the research described
- (4) Inappropriate citations
- (5) Incoherent, meaningless and/or irrelevant content included in the article
- (6) Manipulated or compromised peer review

The presence of these indicators undermines our confidence in the integrity of the article's content and we cannot, therefore, vouch for its reliability. Please note that this notice is intended solely to alert readers that the content of this article is unreliable. We have not investigated whether authors were aware of or involved in the systematic manipulation of the publication process.

Wiley and Hindawi regrets that the usual quality checks did not identify these issues before publication and have since put additional measures in place to safeguard research integrity.

We wish to credit our own Research Integrity and Research Publishing teams and anonymous and named external researchers and research integrity experts for contributing to this investigation.

The corresponding author, as the representative of all authors, has been given the opportunity to register their agreement or disagreement to this retraction. We have kept a record of any response received.

References

- [1] J. Hao, Y. Yang, H. Sun, Z. Zhang, Z. Kang, and J. Zhang, "Application of Multisource Data Fusion Technology in the Construction of Land Ecological Index," *Journal of Sensors*, vol. 2023, Article ID 1804731, 8 pages, 2023.

Research Article

Application of Multisource Data Fusion Technology in the Construction of Land Ecological Index

Juan Hao,¹ Yang Yang ,¹ Haoyue Sun,¹ Zhicheng Zhang,² Zhanwu Kang,² and Jianfang Zhang¹

¹Hebei University of Architecture, College of Information Engineering, Zhangjiakou, Hebei 075000, China

²Hebei Technical College of Mechanical and Electrical Engineering, Department of Modern Manufacturing, Zhangjiakou, Hebei 075000, China

Correspondence should be addressed to Yang Yang; 20151180067@m.scnu.edu.cn

Received 15 July 2022; Revised 10 August 2022; Accepted 24 August 2022; Published 3 April 2023

Academic Editor: Haibin Lv

Copyright © 2023 Juan Hao et al. This is an open access article distributed under the Creative Commons Attribution License, which permits unrestricted use, distribution, and reproduction in any medium, provided the original work is properly cited.

In order to control the grassland ecological environment, an application method of multisource data fusion technology in the construction of land ecological index is proposed. Due to the high requirements for grassland environmental monitoring, the use of traditional technologies to monitor grassland environmental conditions lacks certain effectiveness, has high investment costs, and consumes a lot of manpower and material resources. The use of sensors to dynamically monitor the grassland environment is conducive to monitoring the environment from a scientific and technological level. By understanding the fusion principle and process of three fusion methods, adaptive weighted average, BP neural network, and D-S evidence theory, the construction of Bashang grassland ecological energy big data platform based on multisource data fusion is proposed. A two-level data fusion model based on grassland environmental monitoring is proposed. Several environmental parameters in the experimental environment were monitored, and the validity of the two-level fusion model was verified by two evaluation indicators, the mean absolute percentage error and the corrosion error. This suggests that a combination of BP neural network and D-S proof theory improves system performance. It provides the possibility for more comprehensive monitoring of grassland ecological environment in the future.

1. Introduction

In recent years, data fusion technology is widely used in both military and civil fields. With the continuous development of informatization in China, scholars began to apply multisource data fusion technology to environmental monitoring. In the earth's ecological environment, grassland ecology, as an important part, has laid a solid foundation for the development of animal husbandry. The study of multisource data integration technology in the background of pastureland monitoring helps to effectively manage the pasture environment and is a valuable scientific guide to pastureland protection [1, 2]. After the reform and opening up, some achievements have been made in the development of animal husbandry economy, but behind its remarkable achievements, it is obtained at the expense of grassland ecology. The main reasons for the destruction of grassland ecosystem

are as follows. (1) Global warming: the chief culprit of the rapid degradation of grassland environment is the continuous drought of grassland. Most of the annual rainfall in the grassland ecological area is less than the annual evaporation, which increases the risk of grassland desertification and degradation and significantly reduces the vegetation coverage. (2) Unreasonable utilization of grassland: with the increase of population, driven by their own interests, it is common to turn natural pastures into grain fields. However, due to wind erosion and the reduction of soil fertility, it is very different from the expected economic benefits. As a result, most of the reclaimed land is abandoned, and the area of grassland is gradually decreasing.

However, it is gratifying that the seriousness of the problem has attracted people's attention. In order to implement the restoration of grassland ecology, a series of countermeasures are formulated, of which the most important is to

monitor the grassland environment. Traditional grassland environmental monitoring uses a single sensor to collect the data of various environmental factors, but due to its instability, if the sensor fails, the data is likely to be lost, resulting in the paralysis of the whole system. Now, people use multiple sensors to receive these data. Using multiple sensors to collect information obviously enhances the survivability of the system, but the redundancy between the measured information is high, so these data need to be processed [3]. Considering comprehensively, this topic introduces multisource data fusion technology into grassland environment monitoring and deeply studies the relevant theories and key technologies of multisource data fusion in grassland environment monitoring. The final results can accurately reflect the situation of grassland environment; this is a reference to pastureland science management and governance measures [4].

2. Literature Review

Data fusion technology began to develop gradually in recent 30 years, and there is still no exact concept up to now. The definition proposed by JDL (joint) in 1991 is widely used today. It gives the definition of data fusion, from a multifaceted and multilevel perspective, so as to improve the accuracy of characteristic estimation and completely evaluate the battlefield situation and threat [5]. In 1973, research institutions in the United States began to study sonar signals. This study is regarded as the earliest research related to information fusion [6]. In the future, relevant fusion technologies came into being. Until the late 1970s, the concept of multisource information fusion appeared in the published literature. In 1988, information fusion technology was listed by the US Department of Defense as one of the key technologies for development and research in the 1990s [7]. The C3 Technical Committee (TPC3) under JDL has established a professional group to organize and guide relevant work. In 1991, the United States used data fusion technology in military electronic systems. As early as 1973, relevant institutions began to study sonar signal system. In 1984, the United States established an expert group to do research on it. In 1988, data fusion was included in the plan of accelerating development and research by the United States [8]. The research on this aspect started relatively late. Until the late 1980s, the research on related technologies began to be reported one after another, and there were different opinions on its understanding. The main formulations were data synthesis, compilation, collection, and fusion. Although China started late, its development is relatively fast. In the early 1990s, it caused heated debate in China, prompting colleges and universities and scientific research institutes to start research. Until the mid-21st century, the technology was further valued by the state, so various popular studies followed [9]. Although China started late, in recent years, its application and improved algorithm have made remarkable achievements. Some researchers have explored the hierarchical fusion model of coal mine safety monitoring, determined the hierarchical fusion model, determined the membership degree and corresponding weight by using the analytic hier-

archy process, fused the feature layer by using the fuzzy evaluation method, and then fused by using the D-S evidence theory, so as to select the appropriate algorithm for calculation and processing according to the types of different input data. In addition, aiming at the problem of bridge health monitoring, using the advantages of BP neural network in data recognition, a three-tiered BP neural network model was developed. In order to prevent falling into local minimum, the method of additional momentum is used to train the function. Finally, the simulation experiment compares the data of multisensor and single sensor to analyze the fusion results [10, 11].

3. Research Methods

3.1. Multidata Fusion. Multisource data fusion (multisource data fusion), also known as multisensor data fusion, refers to the comprehensive processing of data from multiple sensors for a certain purpose, in order to obtain both accurate and reliable estimation or reasoning decisions. According to this definition, we can further clarify that this technology uses computer technology to coordinate and manage the information monitored by sensors according to the expected objectives and tasks and build the corresponding model. Then, the collected information is unified, selected and eliminated, and classified and fused, so as to achieve the effect of comprehensively and accurately judging the object. For the process of multisensor data fusion technology, see Figure 1 [12].

Data fusion organically combines old and new technologies. In data fusion technology, scholars will generally use probability theory methods, mathematical methods, and so on. If the fusion methods are divided, they can be roughly divided into two kinds: one is based on probability theory, which includes Bayesian estimation and Kalman filter. The other is based on nonprobabilistic methods, such as D-S evidence theory, neural network, and fuzzy set theory. Neural network is a fusion method that can realize a certain function based on human's understanding and understanding of its brain neural network [13]. It simulates the brain neural structure and function. At present, neural networks are classified from different angles. The common ones are single-layer feedforward, multilayer feedforward, and Hopfield feedback networks. The simplest network structure can construct a nonlinear structure with multiple inputs but only one output [14].

In data fusion, neural network is widely used. Its use can be roughly divided into the following two types: one is to apply BP neural network as a calculation tool to the existing fusion model; the other is to apply the data fusion method to the neural network structure. When using a BP neural network to aggregate data, the aggregation process can be divided into the following three stages. The first step is to build an appropriate BP neural network model according to the fusion requirements and data characteristics and fully consider the characteristics of neurons and some learning rules. The second step is to establish the corresponding relationship between all levels and determine the weight to facilitate the efficient completion of network training. The third

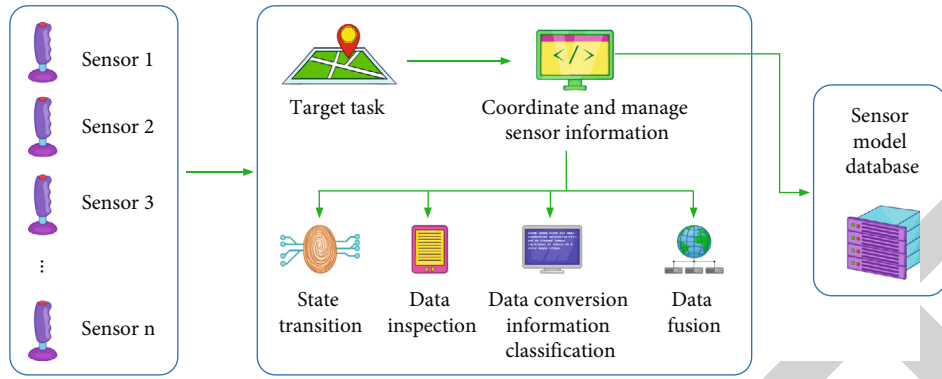


FIGURE 1: Technical process of multisensor data fusion.

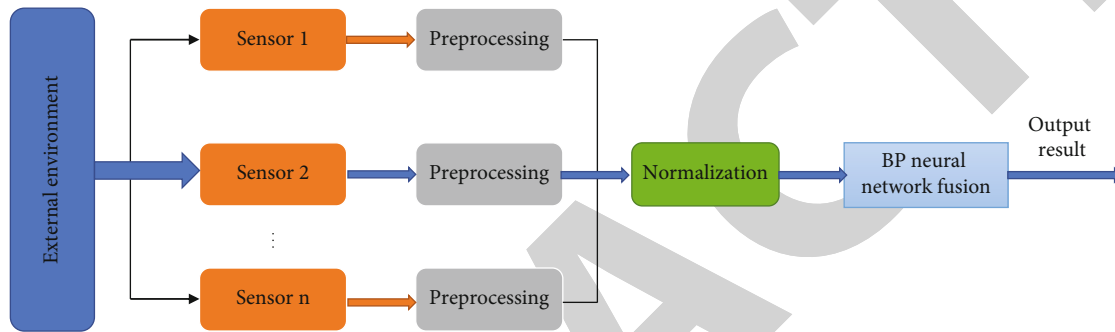


FIGURE 2: Data fusion process of BP neural network.

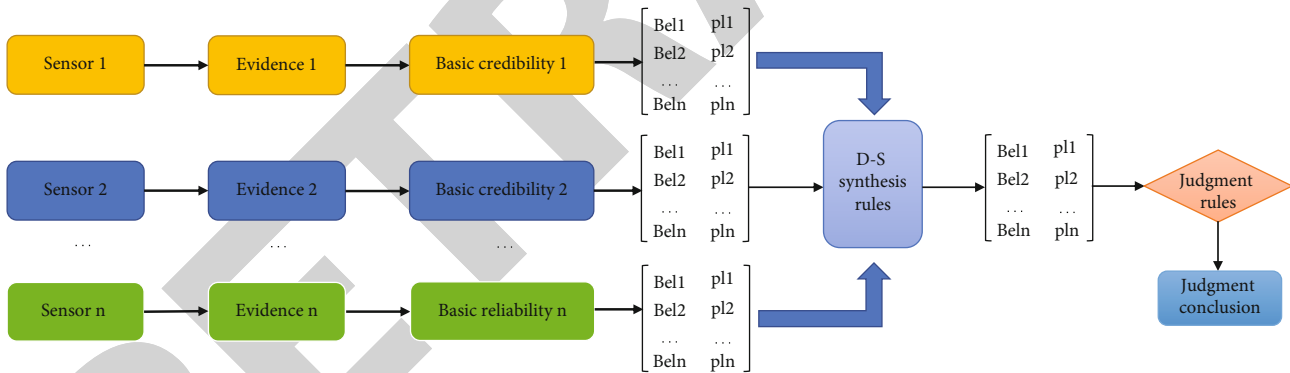


FIGURE 3: Data fusion model of D-S evidence theory.

step is to fuse the data with the help of the trained neural network, as shown in Figure 2.

The operation of D-S evidence theory is based on a trust function that is more adaptable to different situations than probability theory. In addition, it has strong flexibility, which is reflected in distinguishing uncertainty and accurately showing the evidence collection process [15]. For the data fusion model of D-S evidence theory, see Figure 3.

For processing of data collected by multiple sensors through a combination of D-S proof theory, its basic process is, firstly, preprocess the data from each sensor (i.e., evidence). Then, calculate the basic probability distribution value, trust degree, and likelihood of the evidence, and then, recalculate the basic probability distribution assignment, reliability, and likelihood of all the evidence under the joint

action by the DS synthesis rule. Finally, select the hypothesis with the maximum reliability and likelihood according to the decision rules, and regard this as the fusion result [16].

3.2. Two-Level Data Fusion Model for Grassland Environmental Monitoring. In grassland environment monitoring, due to the large monitored area and the large number of sensor nodes, reducing node energy consumption is also one of the important purposes of data fusion. The two-level data fusion model proposed in this study fuses the data at the cluster head node and the gateway node, respectively. Several sensor nodes are arranged in each region, and then, a cluster head node is selected in each region according to certain rules according to LEACH protocol to form a clustering structure [17]. In the topology of

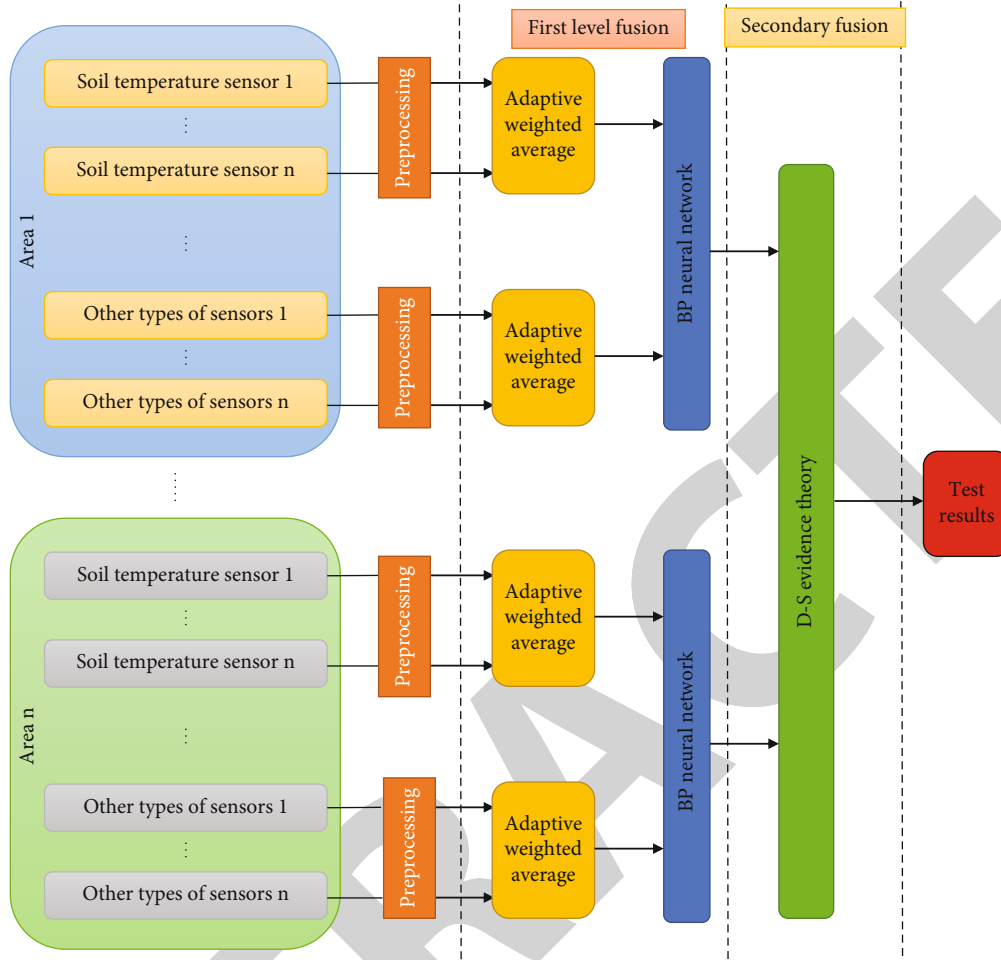


FIGURE 4: Schematic diagram of multisource data fusion model for grassland environmental monitoring.

grassland environment monitoring network, the sensor nodes collect the environmental parameter data, and the cluster head node is responsible for receiving data from each sensor node in the region. After receiving data from each sensor node, the cluster head node performs the first level of melting and then transmits it to the output node after the first level of melting. The output node is responsible for receiving data from different regions and performs secondary melting after receiving data from each region and obtaining the final environmental status through the comprehensive analysis of the fusion results [18].

There are many indicators that can evaluate grassland environmental conditions. In this paper, the environmental monitoring indicators are determined as soil temperature, soil humidity, light intensity, carbon dioxide concentration, and wind speed, so as to effectively solve the problem of lack of systematic decision-making credibility caused by a single monitoring index. The complexity of grassland environment leads to the complex reasons for the healthy growth of vegetation. If only a single fusion structure is used, it will bring great challenges to obtain comprehensive and accurate information [19]. This paper designs a two-level data fusion model, as shown in Figure 4. Once the cluster head nodes of each site receive the data collected from each sensor in the

region, they first use the weighted average method of adaptation to melt the data from the same sensor in the region and then aggregate it locally using the BP neural network method. This is the aggregation of nonhomogeneous sensor data in each region [20]. The first-level smelting result is then sent to the second-level smelting output node. Filter the entire pasture environment [21].

3.3. Decision-Level Integration Process of Grassland Environmental Monitoring. To make the results of pastureland monitoring more accurate, the D-S proof theory is used in global smelting. The results of local aggregation obtained through the BP neural network are uncertain, and the D-S evidence theory provides an effective way to address uncertainty in data aggregation. After the first level of melting, local conclusions can be obtained for each region. The D-S proof theory is then used to normalize the local judgment results for each region and to consolidate the decision levels. In this paper, the specific method of smelting process based on D-S proof theory is as follows.

Suppose that the grassland is divided into n regions, in which the result of region 1 after BP local fusion is recorded as L_1 , the result of region 2 after BP local fusion is recorded as L_2 , and so on; the result of region n after BP local fusion is

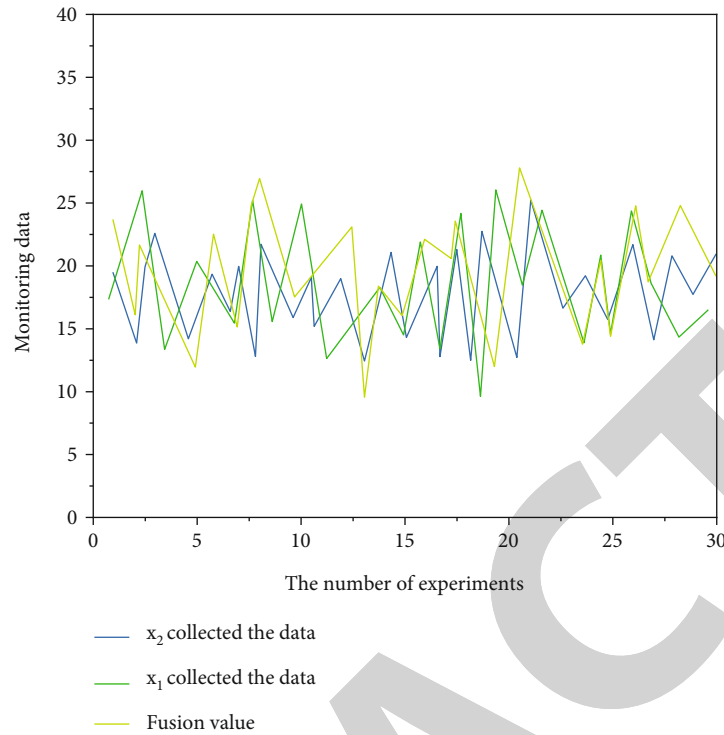


FIGURE 5: Data collected by three soil temperature sensors in area A.

recorded as L_n , and the focus element of each trust function corresponds to the local judgment result of each region. All local judgment results form the recognition framework and then normalize the output of BP neural network in each region to obtain m of each focus element. Finally, the D-S synthesis rule is applied for fusion to obtain the condition of grassland environment [22, 23].

In the problem domain, any proposition A belongs to power set 2^Ω . The basic probability assignment function m is defined on $2^\Omega \rightarrow [0, 1]$, and m satisfies

$$m(\phi) = 0, \sum_{A \in \Omega} m(A) = 1, \quad (1)$$

where ϕ is called an empty set, which also refers to impossible events, m is the assignment of basic probability distribution on 2^Ω , and $m(A)$ is the basic probability value of A .

In the formula, all subsets A satisfying $m(A) > 0$ are called focal elements of m . The confidence function and probability function Pl in the D-S evidence theory are defined in

$$\text{Bel}(A) = \sum_{B \subseteq A} m(B), \quad (2)$$

$$\text{Pl}(A) = 1 - \text{Bel}(A) = \sum_{B \cap A \neq \emptyset} m(B). \quad (3)$$

For all A satisfying condition $A \subseteq \Omega$, there are $\text{Bel}(A) \leq \text{Pl}(A)$. Please provide evidence that can be derived from multiple sources of evidence according to the above D-S proof theory formula [24, 25].

4. Result Analysis

To test the effectiveness of a two-level smelting model, a lawn was selected and divided into five areas, labeled C1, C2, C3, C4, and C0, respectively. In each area, thousands of soil temperature, soil humidity, light intensity, wind speed, and carbon dioxide concentration sensor nodes and a cluster head node were arranged. The MATLAB simulation tool is selected for the simulation experiment. The collected data is used for the experiment. In order to make the experiment universal, 180 samples are randomly selected from the data collected by various sensors for simulation in each simulation experiment, and the remaining 20 samples are used as a model test package. Using a two-level smelting model, the data are aggregated on a preprocessed sample data into a first-tier compound; the fusion values of environmental parameters in each region are obtained by using the adaptive weighted average method. For example, the data collected by two soil temperature sensors in area A are tested, and the two sensor nodes are marked as x_1 and x_2 . Measured in an experiment, $x_1=28.6^\circ\text{C}$ and $x_2=27.79^\circ\text{C}$. The node variance obtained is $\sigma_1^2=0.02$ and $\sigma_2^2=0.13$; the corresponding weight is $w_1=0.34$ and $w_2=0.47$. At this time, the fusion result $X=28.059^\circ\text{C}$. After 30 experiments, the results are shown in Figure 5.

It can be seen from the above experiments that the data collected by some nodes fluctuate greatly, but after the data fusion of similar sensors by adaptive weighted average method, the data with large fluctuation does not have a great impact on the experimental results. It shows that the data after adaptive weighted average fusion is more authentic and effectively improves the accuracy of environmental

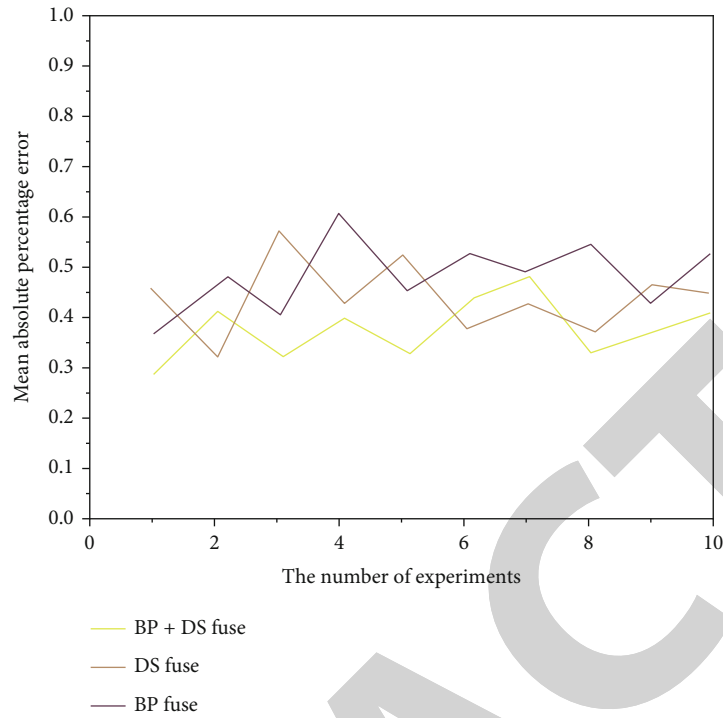


FIGURE 6: Comparison of average absolute percentage error.

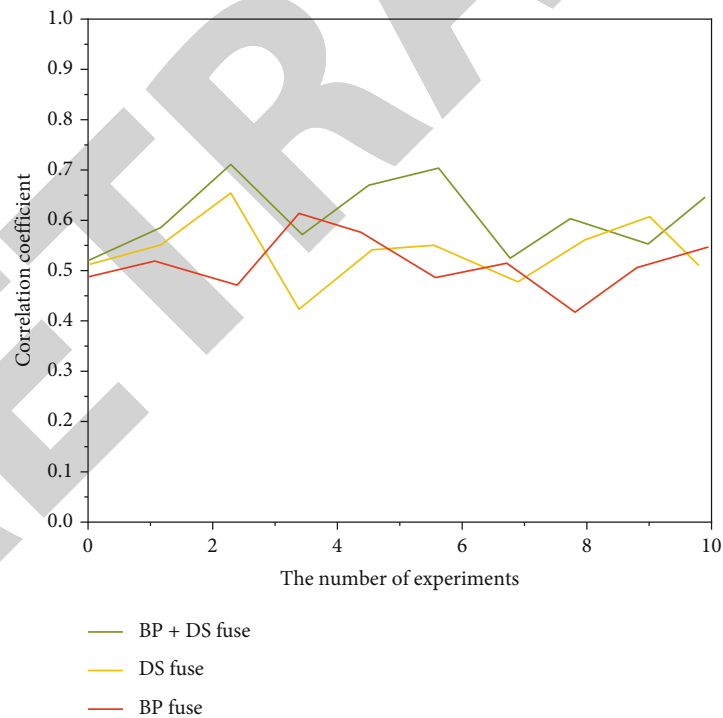


FIGURE 7: Correlation coefficient comparison.

parameters. Each region gets the fusion value of each environmental parameter through primary fusion, inputs the environmental parameters into the neural network for training, obtains the basic probability distribution value of each region, and then makes fusion judgment by using the D-S evidence theory.

According to the functional structure of the two-level fusion model and the form of experimental data collected, the average absolute percentage error and correlation coefficient are selected to comprehensively evaluate the performance of the two-level fusion model. The calculation formula is shown in formulas (4) and (5).

Average absolute percentage error:

$$\text{MAPE} = \frac{1}{n} \sum_{i=1}^n \frac{|f(x_i) - y_i|}{y_i}. \quad (4)$$

Correlation coefficient:

$$\lambda = \frac{(n \sum_{i=1}^n f(x_i) y_i - \sum_{i=1}^n f(x_i) \sum_{i=1}^n y_i)^2}{\left(n \sum_{i=1}^n f(x_i)^2 - (\sum_{i=1}^n f(x_i))^2 \right) \left(n \sum_{i=1}^n y_i^2 - (\sum_{i=1}^n y_i)^2 \right)}, \quad (5)$$

where $f(x_i)$ is the fusion value, y_i is the true value (the data collected by each sensor), and n is the total value. The better the performance of the model, the smaller the absolute value of MAPE, and vice versa: if the correlation coefficient is within $[0, 1]$, the better the performance of the model, and the closer the coefficient is to 1. BP neural network, D-S evidence theory, and their combination are used for fusion, respectively. After 10 experiments, the average absolute percentage error and correlation coefficient are obtained. The comparison is shown in Figures 6 and 7.

As shown in Figure 6, the absolute mean error of using a BP neural network unit alone is generally greater than using a theoretical combination of D-S proofs alone. However, the combination of the two is much smaller than the average error for using the BP neural network or D-S proof theory alone. In the analysis of the results shown in Figure 7, the correlation coefficients used in combination with the BP neural network and the D-S proof theory are close to 1, most of which are greater than 0.5. This suggests that a combination of BP neural network and D-S proof theory improves system performance. This test confirms the accuracy of the two-level smelting design, and the design improves the accuracy of the system, indicating that the results of the multi-sensor data aggregation are more consistent with the real situation.

5. Conclusion

Based on grassland environmental monitoring, this paper studies the model and related fusion methods of multisource data fusion. The main research work is as follows. (1) Firstly, this paper introduces the research status of data fusion at home and abroad, as well as the basic concept and structure level of multisource data fusion. (2) This paper introduces the data fusion algorithms and summarizes the advantages and disadvantages of the data fusion algorithms used by domestic researchers in various fields. (3) For the subjective problem of the basic probability distribution function in D-S evidence theory, which is often obtained from expert experience, this paper is used to normalize the output of the neural network of BP to calculate the basic function of probability distribution. At present, it can solve the uncertainty in the local aggregation of the BP neural network, as well as solve the subjective error of the DS evidence theory in the basic function of probability distribution through the BP neural network and reduce the influence of uncertainties. (4) This

document conducts validation tests on a two-tier multisensor data supply model. The validity of the data preprocessing is examined, and the effectiveness of the two-level smelting model is evaluated. The rationality of data preprocessing is verified, and the effectiveness of the two-level fusion model is evaluated. Then, the fusion method after the improved algorithm is verified.

Data Availability

The data used to support the findings of this study are available from the corresponding author upon request.

Conflicts of Interest

The authors declare that they have no conflicts of interest.

Acknowledgments

This study is funded by the Basic Scientific Research Business Fund Project of Universities in Hebei Province, Research on construction strategy of Bashang grassland ecological big data platform (2021QNJS12); the Basic Scientific Research Business Fund Project of Universities in Hebei Province, Research on Automatic Monitoring of Traffic Road Anomalies Based on Computer Vision (2022QNJS11); and the Basic Scientific Research Business Fund Project of Universities in Hebei Province, Research on noninvasive detection of electrical equipment in office building based on machine learning (2022CXTD09).

References

- [1] E. Mcglynn, S. Li, M. F. Berger, M. Amend, and K. L. Harper, "Addressing uncertainty and bias in land use, land use change, and forestry greenhouse gas inventories," *Climatic Change*, vol. 170, no. 1-2, 2022.
- [2] D. Kim, J. Yu, J. Yoon, S. Jeon, and S. Son, "Comparison of accuracy of surface temperature images from unmanned aerial vehicle and satellite for precise thermal environment monitoring of urban parks using in situ data," *Remote Sensing*, vol. 13, no. 10, p. 1977, 2021.
- [3] S. Chang, H. Chen, B. Wu, E. Nasanbat, and B. Davdai, "A practical satellite-derived vegetation drought index for arid and semi-arid grassland drought monitoring," *Remote Sensing*, vol. 13, no. 3, p. 414, 2021.
- [4] J. Umhuoza, G. Jiapaer, H. Yin, R. Mind'Je, and E. D. Umwali, "The analysis of grassland carrying capacity and its impact factors in typical mountain areas in Central Asia—a case of Kyrgyzstan and Tajikistan," *Ecological Indicators*, vol. 131, no. 1, article 108129, 2021.
- [5] M. Ahmadipari, A. Yavari, and M. Ghobadi, "Ecological monitoring and assessment of habitat suitability for brown bear species in the oshtorankoo protected area, Iran," *Ecological Indicators*, vol. 126, no. 11, article 107606, 2021.
- [6] A. C. Bellido and B. C. Rundquist, "Semi-automatic fractional snow cover monitoring from near-surface remote sensing in grassland," *Remote Sensing*, vol. 13, no. 11, p. 2045, 2021.
- [7] J. L. Steiner, J. Wetter, S. Robertson, S. Teet, and X. Xiao, "Grassland wildfires in the southern great plains: monitoring

Retraction

Retracted: Painting Color Editing System Based on Virtual Reality Sensor Technology

Journal of Sensors

Received 23 January 2024; Accepted 23 January 2024; Published 24 January 2024

Copyright © 2024 Journal of Sensors. This is an open access article distributed under the Creative Commons Attribution License, which permits unrestricted use, distribution, and reproduction in any medium, provided the original work is properly cited.

This article has been retracted by Hindawi following an investigation undertaken by the publisher [1]. This investigation has uncovered evidence of one or more of the following indicators of systematic manipulation of the publication process:

- (1) Discrepancies in scope
- (2) Discrepancies in the description of the research reported
- (3) Discrepancies between the availability of data and the research described
- (4) Inappropriate citations
- (5) Incoherent, meaningless and/or irrelevant content included in the article
- (6) Manipulated or compromised peer review

The presence of these indicators undermines our confidence in the integrity of the article's content and we cannot, therefore, vouch for its reliability. Please note that this notice is intended solely to alert readers that the content of this article is unreliable. We have not investigated whether authors were aware of or involved in the systematic manipulation of the publication process.

Wiley and Hindawi regrets that the usual quality checks did not identify these issues before publication and have since put additional measures in place to safeguard research integrity.

We wish to credit our own Research Integrity and Research Publishing teams and anonymous and named external researchers and research integrity experts for contributing to this investigation.

The corresponding author, as the representative of all authors, has been given the opportunity to register their agreement or disagreement to this retraction. We have kept a record of any response received.

References

- [1] C. Hu, "Painting Color Editing System Based on Virtual Reality Sensor Technology," *Journal of Sensors*, vol. 2023, Article ID 6461843, 6 pages, 2023.

Research Article

Painting Color Editing System Based on Virtual Reality Sensor Technology

Chunda Hu 

Tonghua Normal College of Fine Arts, Tonghua, Jilin 400072, China

Correspondence should be addressed to Chunda Hu; 202006000305@hceb.edu.cn

Received 14 July 2022; Revised 9 August 2022; Accepted 20 August 2022; Published 3 April 2023

Academic Editor: Haibin Lv

Copyright © 2023 Chunda Hu. This is an open access article distributed under the Creative Commons Attribution License, which permits unrestricted use, distribution, and reproduction in any medium, provided the original work is properly cited.

In order to solve the problem of large color matching error in color matching system, this paper proposes a painting color editing system based on virtual reality sensing technology. Apply virtual reality technology (technology) to the proposed system design, and design the system framework based on the three-tier architecture, which includes data access layer, business logic layer, and presentation layer. The hardware includes spectrophotometer, central processing unit, storage device, and virtual reality somatosensory interaction device. The software part takes BP neural network algorithm as the core, trains and processes the three color values, constructs the automatic matching model of painting colors according to the training results, and realizes the logical operation and analysis of the system software. The experimental results show that although there is still a certain error between the painting color matching output by the system and the actual color matching of the test samples, the maximum absolute error of the matching is relatively small, which is less than 0.05. The error between 6 groups of actual matching samples and predicted matching samples is <1.5 . Although the designed system has some errors with the expected color matching, the error is small, so the color difference does not affect the visual presentation effect.

1. Introduction

Virtual reality takes immersion, interactivity and creativity as the most basic and important attributes. For this young medium, the continuous development and change and the exploration of content are the current situation of Virtual Reality Art [1]. The arrival of 5G communication technology provides an important foundation for the popularization of virtual reality technology. The rapid development of technology and hardware rewrites and expands the possibility of virtual reality art design expression at any time. From the perspective of technology, everything in life cannot be separated from interaction. Interaction design has affected the development of technology and human life, just as smartphones, WeChat, and Alipay have brought changes to modern life. Many previously impossible connections, behaviors and habits have become the basic elements of modern life, bringing the evolution from thinking mode to behavior logic. Virtual reality interactive art design involves a lot of disciplinary knowledge and thinking of different majors. From the perspective of designers and creators, it is an inevitable choice

to structure and promote works through the method of art design in the process of interactive design, whether to improve the quality of works and the user's experience, or to obtain new and charming creative works. Excellent works do not come out of thin air. This study explores the space for improvement of works through thinking and combing while experiencing and designing various works of virtual reality. With the rapid development of hardware and technology, the discussion of immersive virtual reality interaction and its artistic design is an important process to promote the generation of truly excellent virtual reality interactive works [2, 3].

2. Literature Review

Zhao and Ma mentioned that "virtual reality will enhance the power of transforming real art. Picture frames, stages and cinemas restrict art by blocking art as a part of reality. However, virtual reality can strengthen reality and allow a smoother and orderly transition between virtual and real. This ability is enough to scare psychologists, but it provides artists with an unprecedented power to change society" [4].

His remarks affirmed the social value of virtual reality art, which has the ability to strengthen reality in comparison with traditional art. Li et al. created the first interactive VR work of traditional scroll painting, using VR to realize the reconstruction of the court scene in the scroll of court life of Qiu Ying, a painter in the Ming Dynasty, “Han palace spring dawn.” The work was exhibited in the main exhibition hall of the fourth World Internet Conference, attracting many visitors to visit and experience. Dunhuang Cultural Heritage digitalization research results, virtual reality Museum, using VR to restore the high-precision virtual cave built based on the current situation of cave 159 of Mogao Grottoes, to show the exquisite mural art [5]. Dimov first added artistic creation to the field of virtual reality cultural application. VR artist Zhang Xiao has created many VR paintings and painted on site in conjunction with Google art and culture and the Palace Museum at China’s first International Import Expo [6]. Zhang et al. created the classic scenes of the Hero League game. The novel comic painting style of this work has attracted the attention of young groups. Mutual movement and immersion are conducive to the audience to have a good resonance [7]. Xu and Wang’s works show that virtual reality technology and three-dimensional models combine human’s own breathing balance and sound wave activities to make people feel free from gravity in a special space, in a weightless state, and roaming in the original state of human creation. The artist did not simulate the real scene, let people perceive the philosophy in nature, and explore the special connection between the environment and sensory, psychological and emotional [8]. Chatham et al. created a groundbreaking interactive art installation. The experimenter rode a fixed bicycle through a simulated city composed of computer-generated three-dimensional letters. The letters formed words and sentences on both sides of the street according to the road chosen by people. The physical labor in reality was transferred to the virtual environment, allowing people to form an interactive connection on their limbs with the virtual environment [9]. The works of Dong et al. show that the audience can fly freely on the rotating 3D Earth, stretch their arms, adjust the inclination of their bodies to the left and right sides to change the flight direction, and determine the flight speed according to the degree of forward tilt. The audience can get the experience of flying in the valley by controlling their bodies [10].

Although there are many color matching systems that have been developed, there is no system specifically for painting color matching. Therefore, there is a certain color difference in the matched colors, resulting in a large gap between the designed painting and the ideal, and losing a certain cultural heritage. In this context, in order to meet the design needs and apply virtual reality technology (VR technology) to the system design, this paper designs a professional painting color automatic matching system. The system design includes four parts: framework design, hardware design, software design, and system testing.

3. Research Methods

The key point in painting design is how to integrate traditional culture into products. To achieve the above purpose,

the use of color is essential. Vision is the most sensitive to color, and different color combinations give products different emotions and connotations. Take porcelain products as an example: porcelain is composed of white and blue, and white symbolizes purity and cleanliness; green symbolizes spring and vitality in Han culture and is the color of auspiciousness. White glazed porcelain is mainly monochromatic white, and there are many kinds of white, and the higher the whiteness, the stronger the meaning of sweetness and purity. Therefore, once there is a problem with the matching white, the soul of white glazed porcelain will be lost. Different colors can play different visual effects together, and once they are mismatched, there will be nondescript phenomena [11]. Therefore, in order to design a good painting, the virtual reality technology is applied to the color matching, so as to help designers “immersively” appreciate the effect of color matching and adjust the design scheme in time, so that the painting design can achieve the expected goal.

3.1. System Framework Design. The framework of automatic painting color matching system based on virtual reality technology is designed with reference to the b/s three-tier framework mode, including data access layer, business logic layer, and presentation layer.

3.1.1. Data Access Layer. Be responsible for directly operating the database and adding, deleting, modifying, and searching data resources. The access layer in this system mainly stores a large number of painting samples, color matching schemes, and various operation program codes [12].

3.1.2. Business Logic Layer. Operation for specific problems, which can also be said to be the operation of the data layer, is the core layer of the whole system. In the system, it is mainly composed of integrated circuit chips, which are responsible for color matching operation.

3.1.3. Presentation Layer. Generally speaking, it is the interface presented to users, which is responsible for the successful display of color matching to users. In the past, the achievements of color matching system are mostly two-dimensional images, which lack intuitive three-dimensional sense. In the designed system, the display results are mainly displayed through VR technology, which is more intuitive.

3.2. System Hardware Design. The main hardware used in the automatic matching system of painting color based on virtual reality technology includes spectrophotometer, central processing unit, storage device, virtual reality somatosensory interaction device, etc. The following is a specific analysis.

3.2.1. Spectrophotometer. The function of spectrophotometer is to measure the color composition of samples, which is the key to color matching and adjustment [13]. The spectrophotometer in this system is CS-580. The features of the equipment are as follows:

- (i) LED color display, TFT true color 2.8 inch, and resolution 320 × 480

- (ii) There are two kinds of measuring calibers of $\Phi 8/4$ mm, which are suitable for measuring in a variety of scenes
- (iii) The interface can use the power adapter for direct charging operation
- (iv) Soft rubber buttons are measured at the back of the fuselage, which conforms to ergonomic design
- (v) The storage capacity of the instrument is 100 standard samples and 20000 samples. It is automatically saved during measurement, and the record can be cleared

The central processing unit is responsible for the overall control and all operations of the system, and it is the core part of the system. In this system, STM32 f429/f439 microcontroller based on ARM® Cortex™ M4 is selected as the central processor. The technical parameters of the controller are shown in Table 1.

3.2.2. Virtual Reality Somatosensory Interaction Device. Virtual reality somatosensory interaction device is the key to the automatic color matching effect of users' reading paintings. The device is mainly composed of helmet-mounted display and data sensing gloves.

The function of HMD is to provide users with three-dimensional scenes in virtual reality. The helmet-mounted display selected in the system is 3Glasses S2 display [14]. The display is characterized by driveless installation, plug and play, and inside Ou positioning system; mainstream computers can access massive content and Cortana voice interaction. The main function of data sensing gloves is to accurately and real-time transmit the posture of the human hand to the virtual environment, so that users can naturally interact with the establishment of three-dimensional images through gestures, such as using simple gestures to open applications, selecting and adjusting the size of targets, and dragging and dropping holograms, which greatly enhances the interactivity and immersion. The data sensing glove in this system is cyberglove II data glove [15]. The device can measure up to 22 joint angles with high accuracy, and adopts advanced anti-bending induction technology, which can accurately convert the actions of hands and fingers into digital real-time joint angle data.

3.2.3. Storage Devices. The main function of storage device is to store programs and various data. Because a large amount of sample data is required to ensure the accuracy of color matching; it is insufficient to rely only on the memory capacity of the central processor of the system, and a storage expansion device is also required in the system. The storage expansion device model in the system is BBA-364.

3.3. System Software Program Design. The total working process of the software of the painting color automatic matching system based on virtual reality technology is shown in Figure 1.

TABLE 1: Technical parameters of STM32 f429/f439 microcontroller.

Technical indicators	Parameter
Pin number	176
Device core	ARM cortex M4
Data bus width (bit)	32
Program memory size (Mb)	1.024
Maximum frequency (MHz)	168
Memory size (kb)	256
USB channel	2
Number of PWM units	2
ADC channel	24
Number of SPI channels	3
Typical working power supply voltage (v)	3.6
Number of PCI channels	0
Number of timers	12
Number of UART channels	2
Number of USART channels	4
PWM resolution (bit)	16
Program memory type	Flash memory
Pulse width modulation	2 (16 bits)
Number of Lin channels	0
Number of Ethernet channels	1
Number of ADC units	3
Minimum operating temperature (°C)	-40~85

In the whole system color matching process, the key algorithm is the application of BP neural network algorithm. For this system, the input value of RGB three color value of sample color, and the output value is the proportion of various colors of painting, that is, color scheme. The basic process of building an automatic painting color matching model based on BP neural network algorithm is as follows.

Step 1 (sample preparation). The training of BP neural network model needs a lot of sample data support, so the first step to establish an automatic color matching model of painting based on BP neural network algorithm is to build a sample library, and the sample content in the sample library needs to be selected according to the target painting [16].

Step 2 (sample data collection). RGB color characteristic values are collected by spectrophotometer.

Step 3 (standardize RGB color characteristic values). The RGB color characteristic values collected by spectrophotometer can not only be directly input into neural network but also need to be standardized. The method used is premmx function in MATLAB.

Step 4 (neural network model construction). The problem to be solved by the designed system is the prediction of painting color matching.

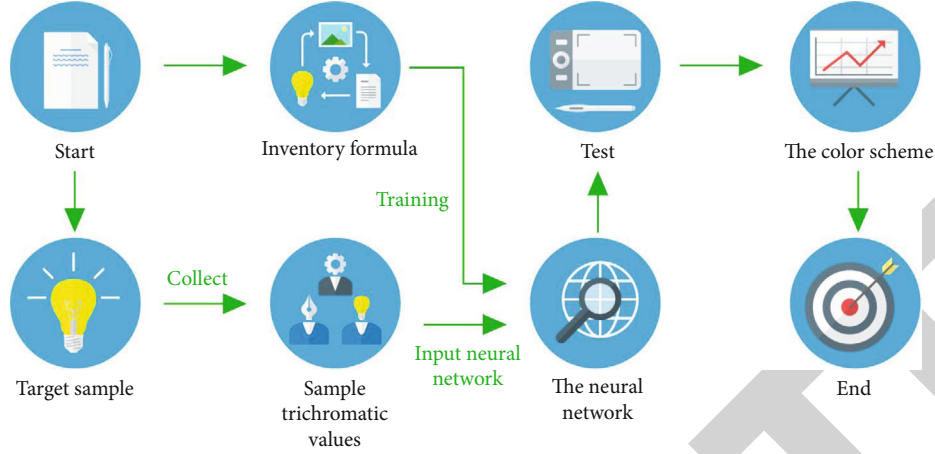


FIGURE 1: Basic process of system color matching.

TABLE 2: System test environment.

Name	Parameter
Development language	VRML, HTML, and C++
Web application service	Visual Studio 2005
Database	Microsoft SQL Server 2000
Modeling tools	Microsoft Office Visio 2003
Image processing tools	Adobe Photoshop 6.0
Virtual reality software	Pano2VR
Simulation software	MATLAB 2.0

The construction of BP neural network model is mainly divided into two parts: training and testing. The collected sample data is generally divided into two groups, the more part will be used as the training sample set, and the less part will be used as the test sample set.

Training: input the training sample set into the BP neural network model, and reach the output layer after being processed by the hidden layer transfer function. Finally, through the output layer transfer function operation, the painting color matching scheme is obtained. At this time, it is necessary to judge whether the difference between the actual painting color matching scheme and the expected painting color matching scheme is less than the preset threshold [17, 18]. If the difference is less than the preset threshold, the training of BP neural network model is completed. If the difference value is greater than the preset threshold value, the difference value needs to be used as the input value for reverse propagation, and the weights of each layer need to be continuously adjusted until the adjusted weights affect, and the actual painting color matching scheme is output to meet the expectation.

Test: input the test sample set into the trained BP neural network model structure and output the painting color matching scheme.

The input quantity of BP neural network input layer is shown in

$$o_j^{(1)} = x(j), j = 1, 2, 3, 4. \quad (1)$$

TABLE 3: Parameter setting table of BP neural network.

Parameter	Value
Network layers	3
Number of nodes in each layer	3
Transfer function	Tansig
Output transfer function	Purelin
Learning rule function	Traingdx
Training error	0.07
Maximum steps of training	2000

The input and output of BP neural network hidden layer are shown in

$$\text{net}_i^{(2)}(k) = \sum_{j=0}^m w_{ij}^{(2)} O_j^{(1)}(k), \quad (2)$$

$$o_i^{(2)}(k) = f[\text{net}_i^{(2)}(k)], i = 1, 2, \dots, 5, \quad (3)$$

where $w_{ij}^{(2)}$ is the weighting coefficient from the input layer to the hidden layer of BP neural network, and the input layer, hidden layer, and output layer correspond to the above marks (1), (2), and (3), respectively; M is the input number of neurons. The hyperbolic tangent function of hidden layer neurons is the excitation function, as shown in

$$f(x) = \frac{e^x - e^{-x}}{e^x + e^{-x}}. \quad (4)$$

4. Result Analysis

In order to test the automatic color matching performance of the system, a silk fabric is taken as the object to study the color matching, and the color difference of the color matching is taken as the inspection standard.

4.1. System Test Environment. The system test environment is shown in Table 2.

TABLE 4: System color matching results (part).

Sample serial number	Actual proportion			Network output ratio			Maximum absolute error of proportioning
	Brown	White	Red	Brown	White	Red	
31	5	3	2	5.262	2.767	1.764	0.0458
32	4	4	2	4.192	3.501	1.919	0.0196
33	3	5	2	2.530	5.535	2.175	0.0372
34	3	4	3	3.157	3.772	3.071	0.0238
35	3	3	4	3.244	2.813	3.873	0.0304
36	4	3	3	4.141	2.845	3.053	0.0155

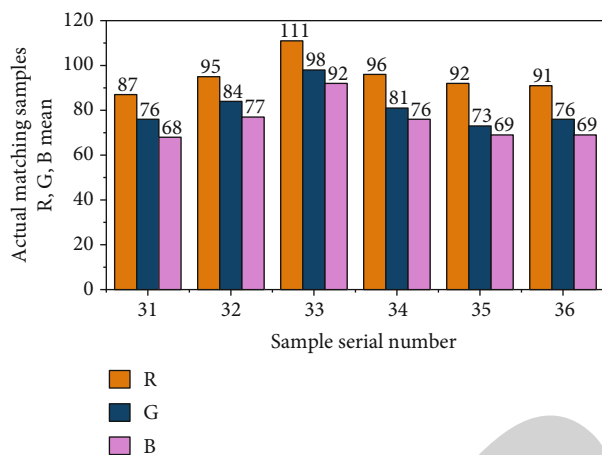


FIGURE 2: Average values of R, G, and B of actual matching samples.

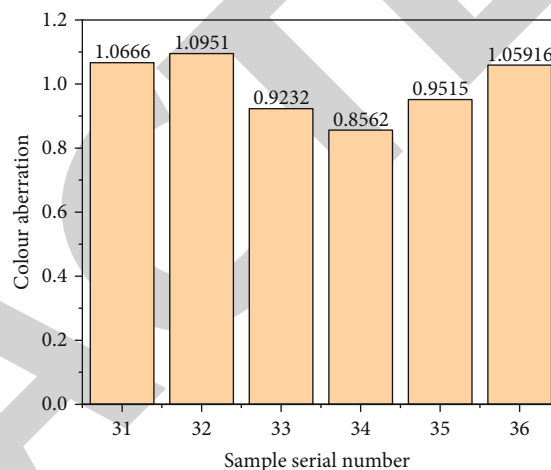


FIGURE 4: Chromatic aberration of R, G, and B mean values of actual matching samples and predicted matching samples.

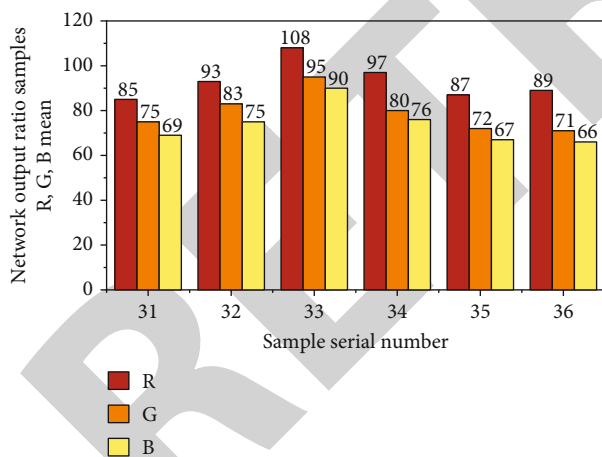


FIGURE 3: Average value of R, G, and B of network output matching samples.

4.2. *Test Samples.* In this paper, 150 kinds of silk fabrics are selected as objects to build a sample library.

The RGB color characteristic values are collected by spectrophotometer, and 150 groups of original sample data sets are obtained. After standardization, the training sample set and inspection sample set are obtained. Among them, 80% of the data is used as the training sample set, and the remaining 20% is used as the test sample set [19, 20].

4.3. *BP Neural Network Parameter Setting.* The parameter settings of BP neural network are shown in Table 3.

4.4. *System Color Matching Results.* The calculation results of the automatic color matching model of painting based on BP neural network algorithm are shown in Table 4 (the last six groups are selected for explanation).

It can be seen from Table 4 that although there is still a certain error between the painting color matching output by the system and the actual color matching of the test samples, the maximum absolute error of the matching is relatively small, both less than 0.05, which proves the effectiveness of the study to a certain extent.

4.5. *Color Difference Statistical Results.* The above research results are not intuitive and have little practical reference significance. Therefore, in order to further test the color matching effect of the system, the color difference is taken as an index for further testing. Color difference detection refers to the analysis of color difference after extracting the color characteristic value of the image [21, 22].

The color difference detection results are shown in Figures 2–4.

It can be seen from Figures 2–4 that the error between the six groups of actual matching samples and the predicted matching samples R, G, and B is $\Delta E < 1.5$, which proves that

Retraction

Retracted: Application of GIS and Multisensor Technology in Green Urban Garden Landscape Design

Journal of Sensors

Received 19 December 2023; Accepted 19 December 2023; Published 20 December 2023

Copyright © 2023 Journal of Sensors. This is an open access article distributed under the Creative Commons Attribution License, which permits unrestricted use, distribution, and reproduction in any medium, provided the original work is properly cited.

This article has been retracted by Hindawi following an investigation undertaken by the publisher [1]. This investigation has uncovered evidence of one or more of the following indicators of systematic manipulation of the publication process:

- (1) Discrepancies in scope
- (2) Discrepancies in the description of the research reported
- (3) Discrepancies between the availability of data and the research described
- (4) Inappropriate citations
- (5) Incoherent, meaningless and/or irrelevant content included in the article
- (6) Manipulated or compromised peer review

The presence of these indicators undermines our confidence in the integrity of the article's content and we cannot, therefore, vouch for its reliability. Please note that this notice is intended solely to alert readers that the content of this article is unreliable. We have not investigated whether authors were aware of or involved in the systematic manipulation of the publication process.

Wiley and Hindawi regrets that the usual quality checks did not identify these issues before publication and have since put additional measures in place to safeguard research integrity.

We wish to credit our own Research Integrity and Research Publishing teams and anonymous and named external researchers and research integrity experts for contributing to this investigation.

The corresponding author, as the representative of all authors, has been given the opportunity to register their agreement or disagreement to this retraction. We have kept a record of any response received.

References

- [1] D. Shen, "Application of GIS and Multisensor Technology in Green Urban Garden Landscape Design," *Journal of Sensors*, vol. 2023, Article ID 9730980, 7 pages, 2023.

Research Article

Application of GIS and Multisensor Technology in Green Urban Garden Landscape Design

Dongli Shen 

Department of Art and Design, Dongchang College of Liaocheng University, Liaocheng, Shandong 252000, China

Correspondence should be addressed to Dongli Shen; 20141209@stu.sicau.edu.cn

Received 14 July 2022; Revised 9 August 2022; Accepted 16 August 2022; Published 27 March 2023

Academic Editor: Haibin Lv

Copyright © 2023 Dongli Shen. This is an open access article distributed under the Creative Commons Attribution License, which permits unrestricted use, distribution, and reproduction in any medium, provided the original work is properly cited.

In order to solve the problem of low definition of the original 3D virtual imaging system, the author proposes the application method of GIS and multisensor technology in green urban garden landscape design. By formulating a hardware design framework, an image collector is selected for image acquisition according to the framework, the image is filtered and denoised by a computer, the processed image is output through laser refraction, and a photoreceptor and a transparent transmission module are used for virtual imaging. Formulate a software design framework, perform noise reduction processing on the collected image through convolutional neural network calculation, and use pixel grayscale calculation to obtain the feature points of the original image, and use C language to set and output the virtual imaging, thus completing the software design. Combined with the above hardware and software design, the design of 3D virtual imaging system in garden landscape design is completed. Construct a comparative experiment to compare with the original system. The results showed the following: The designed system has a significant improvement in the clarity, the original system clarity is 82%~85%, and the image clarity of this system is 85%~90%. In conclusion, the author designed the method to be more effective.

1. Introduction

With the continuous improvement of people's material and living water quality and the change of the main contradictions in Chinese society, people's appreciation level has also been continuously enhanced, and higher requirements have been put forward for aesthetic appreciation, leisure health care and health recuperation. As the artery of the city, the road is the most frequent place for urban people to move and use and the most user-involved environmental space in urban garden landscape design [1]. Under the current social situation, urban residents are under great pressure in life and work, and they are eager for some places where their lives and work can be satisfied; the second road environment is the place where urban residents have the most contact and stay for the longest time in their life and work. At present, in the public leisure space in most cities in China, including parks and green spaces in major cities, most urban landscape road designs are mainly reflected in the user's visual perception level, when users are in such a visually colorful garden landscape environment for a long time middle, the sur-

rounding environment will become monotonous and boring, and the user and the environment lack emotional communication and cannot feel from other senses. With the improvement of residents' living standards, people are more urgently in need of a garden landscape environment that is pleasing from multiple senses; therefore, garden landscape design from the five senses design and people's multiple senses is a modern social situation to meet the living needs of urban residents. Inevitable development trend [2]. Design is a purposeful creative act that serves people, and the design of garden landscape is to make urban residents meet the real-life problems at the same time, it can make the road users more pleasing to the eyes, and through the five senses, design can build a bridge of communication between the garden landscape and the subjective feelings of the human body. The author mainly studies the concepts and ideas of predecessors in the design of five senses and innovatively applies them to landscape design [3]. By summarizing and summarizing the principles of garden landscape design, the concept of five senses design can be added to the process of garden landscape design, so that

garden landscape design can be reflected in people's daily life in a more delicate and diverse manner in real life.

2. Literature Review

Meerakker focuses on the introduction of parametric software, especially modeling and the use of visualization software. The parametric software is mainly involved in the construction of terrain models, the creation of prototypes, and the parametric generation of landscape systems. Use laser scanner, Google Earth, and computer numerical control technology to build digital model and numerical control model, use numerical control machining model to simulate the environment for testing, and finally use digital model and numerical control model to express accurately. This method not only focuses on "parametric design" but also needs to integrate "parametric construction" [4]. Lyver and O'Neal pointed out that elements such as the center of the city, walls, squares, and parks can no longer be defined rigidly as the representatives of contemporary cities. The city should be regarded as a nonstatic process of continuous development, it is the combination of various spaces, the construction of logic, and the self-circulation of the system, it is a complicated flow network, rather than various rigid spatial layouts and functional divisions, the process is called fluid urbanism, and this concept is also used in subsequent projects [5]. Kola and Liarakapis use parametric tools to understand the structure and function of organisms and to simulate the operation of biological systems; this method is related to the design of landscape architecture; that is, the flow of elements and energy in the design site, and the Energy transfer and supply in living organisms, as well as physicochemical reactions, converting the specific problems of the site into ecological related theories and establishing a "special" landscape system can be called "biomimetic" design in the field of landscape architecture [6]. Bergues-Pupo et al. used parametric tools (peg office of landscape+architecture) to conduct a research project called "Edaphic Effects" (Edaphic Effects); the simulations then form "unit prototypes" and build them; eventually, it becomes a landscape system with parametric logical aesthetic form. It can be seen that foreign designers have begun to try to apply the concept of "parametric design" to specific practical projects from different perspectives, and the field of parametric landscape architecture planning and design has also made progress [7].

In order to solve the problems of low-resolution images and traditional artworks, the author created a three-dimensional virtual landscape rendering system. Using these methods to display the garden landscape makes it easier to plan the garden landscape, improves the technological process of the garden landscape, and provides more support for future construction.

3. Research Methods

3.1. GIS Technology. GIS (geographic information system) is a computer system based on geospatial databases that was slowly developed in the middle and late 20th century; it is

an interdisciplinary subject interspersed in earth science, information science, and space science, based on geospatial database; use computer systems to collect, manage, store, process, analyze, and build geographic models of spatial data; provide dynamic geographic information based on space; and provide technical support for geographic research and decision-making services.

Nowadays, GIS has gradually penetrated into various industries, such as surveying and mapping, agriculture, environmental protection, transportation, urban construction, and public security. When GIS conducts spatial analysis, it associates its spatial position with attribute relationship, and the final result also shows the three-dimensional relationship of space. GIS software can process the data obtained by remote sensing technology and GPS and build a corresponding database; the processed data are all geocoded, which is also the difference between GIS and other computer systems. Geographic information system is a tool discipline. In landscape architecture planning and design, GIS software can be introduced into the design, and the advantages of GIS can be fully utilized to conduct data query analysis, location analysis, topographic and landform analysis, hydrological analysis, trend analysis, simulation analysis, etc.

GIS software is essentially the work of data processing and at the same time has the ability to centrally process scattered data; the existing data of some large urban landscape sites are relatively complex and scattered; the integration, management, maintenance, storage, database construction, and data analysis and processing of scattered data through GIS software greatly improve the work efficiency of designers.

GIS can draw models for existing data in three-dimensional space; in the past landscape architecture planning and design, designers need to familiarize themselves with local landscapes and collect data through on-site exploration methods; when the volume of the landscape site is large, it will inevitably greatly reduce the work efficiency of the designers. The generation of GIS solves this problem very well; the site data stored in the computer can be reflected by means of surface effects and scene display; the modeling method in GIS technology can be combined with virtual reality technology at the same time and visually and diversely express the scenes to be designed or evaluated, and then designers can generate 3D models through GIS for further analysis, and then they can carry out related planning and follow-up management and maintenance work. Later, using the GIS database, it is also possible to analyze and integrate relevant data in a small area and finally build a data model of the entire urban landscape through the method of data connection, so as to classify, query, and manage the data in the future.

3.2. Hardware Design of 3D Virtual Imaging System

3.2.1. Hardware Framework Design. According to the understanding of virtual imaging technology, the hardware of 3D virtual imaging system in garden landscape design is designed; the specific design framework is shown in Figure 1.

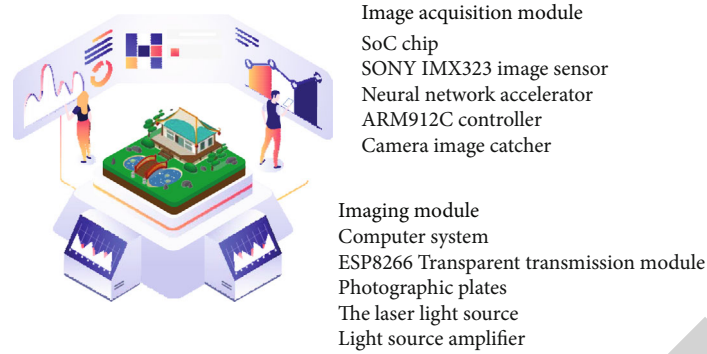


FIGURE 1: Hardware frame diagram of 3D virtual imaging system.

The hardware of the system is set as an image acquisition device and a virtual imaging device. Image collectors include camera capturers, microcontrollers, image sensors, image controllers, and neural network accelerators [8, 9]. The virtual imaging device consists of a computer, a projection device, a photoreceptor, a laser amplifier, and an ESP8266 transparent transmission module.

3.2.2. Image Grabber Design. When printing large images, most of them use a single-chip computer as the main source of image printing. The device detects the presence of a 3D virtual imaging system in the landscape design select SoC chip as the first image capture [10]. To support graphics, select the SONYIMX323 image sensor, camera device, ARM912C controller, neural network accelerator, and database driven controller. The image sensor was configured and designed using the SCCB protocol. A schematic part of the imaging equipment is shown in Figure 2.

The picture in the garden design is collected by a circuit consisting of an amplifier and some resistors. All current is set to 3.7 V, and the standard current is used to control the graphics, which can ensure that the high current does not affect the graphics. To increase the voltage safety, an electric stabilizer is added to the original circuit, and this function ensures the safety of the image capture.

3.2.3. Design of Virtual Imaging Equipment. Using three-dimensional light to convey the details of the garden landscape design requires air and light design and control room design.

The benefits of garden design are integrated and computer-generated, and the finished image is made using holographic projection technology. The laser is used to illuminate virtual images, and the light emitted by the laser beam is divided into two segments: one part is directed directly at the photosensitive film; the other is refracted by photosensitive film by light amplifier, and light is led by photosensitive film.

In a virtual video, ESP8266 is used to control the transparent transmission, and by using this technology, the finished image is sent to the transparent transmission by the computer; the module operates the secondary and then operates the simulated transmission; the emitted image is

sent by the laser to a photosensitive form, completing the virtual image.

3.3. 3D Virtual Imaging System Software Design Software. The developer includes an original image search module, an image generation module, and a virtual rendering module.

3.3.1. Detection Module. When creating virtual images of a garden landscape, it is necessary to take pictures first, and unlike the first shot, 3D virtual imaging technology requires the use of camera design images to describe about virtual objects, and get simulation images based on drawings [11].

In order to ensure the clarity of the image, noise reduction processing is performed on the image. Set the image acquisition sample; the specific formula is as follows:

$$Y = X + N. \quad (1)$$

In the formula, X is the first figure; Y represents the tone of the sample after collection; N is the approximate volume of the output layer. Graphic models are arranged in a matrix using a convolutional neural network [12]. Let the popular image be matrix f and the main matrix be g . The graphics have been processed to prevent scattering in the network. The drawing is done by rotation patterns, and the special patterns are as follows:

$$(f^* g)(1, 1) = \sum_{k=0}^m \sum_{h=0}^n f(h, k)h(n-h, m-k). \quad (2)$$

By using inactivated neurons and parameters for image reconstruction and outputting the residual image, the output image data is reproduced.

3.3.2. The Image Making Module. The image making module collects images through the above parts and processes the collected images uniformly [13]. Through the Moravec algorithm, the image is subjected to the pixel point grayscale change operation, and the depth calculation is performed, and the pixel point is set to (x, y) ; then the

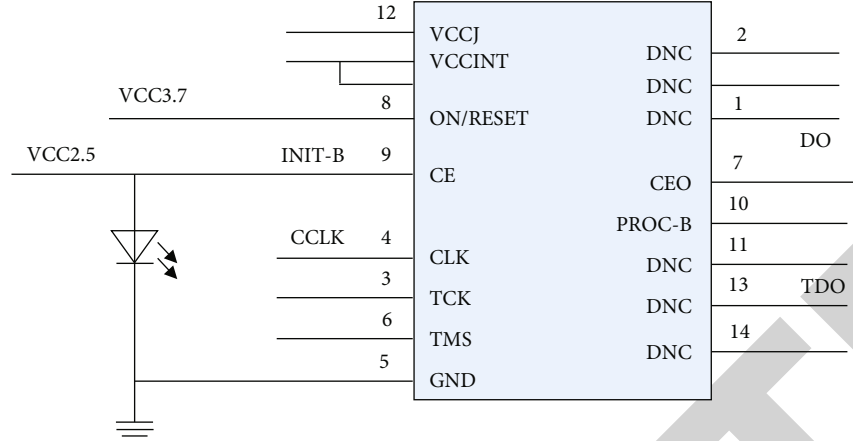


FIGURE 2: Part of the circuit of the acquisition hardware device.

square sum of the grayscale differences in the four directions is as follows:

$$\left\{ \begin{array}{l} Q_1 = \sum_{i=-k}^{k-1} (g_{x+i} - g_{x+i+1,y})^2, \\ Q_2 = \sum_{i=-k}^{k-1} (g_{x,y+i} - g_{x,y+i+1})^2, \\ Q_3 = \sum_{i=-k}^{k-1} (g_{x,y+i} - g_{x,y+i+1})^2, \\ Q_4 = \sum_{i=-k}^{k-1} (g_{x+i,y-i} - g_{x+i+1,y-i-1})^2. \end{array} \right. \quad (3)$$

The high value of the point measurement is used as the main point, the window frame is set, and the highest value of the equations of the squares of the different grayscale is obtained. The image collection by deleting the content feature was achieved, and the images were taken as special to ensure the accuracy of the image.

3.3.3. Virtual Imaging Module. Based on the above model, the images are printed and processed, and the finished images are passed through virtual work to become a three-dimensional virtual representation. Based on the hardware design of 3D virtual imaging, the computer is used to control the final image displayed during the virtual image processing, and the virtual language can be used [14, 15]. The output image is passed through a combination of photoreceptors and amplifiers to realize the virtual image. Currently, the design of a 3D virtual vision system in the landscape design of the park has been completed.

4. Results Analysis

In order to ensure the scientificity of the 3D virtual imaging system in the garden landscape design, a comparison test was carried out with the original virtual imaging system to test the image clarity of the 3D virtual imaging system [16].

TABLE 1: Parameters of simulation experiment equipment.

Equipment	Configure	Parameter
Server	Intel Xeon ES-2620 2.0 GHz	20 GB RAM
Database	SQL Server 2019 database	—
Interface control	DIV+CSS	2 GB RAM
Operating system	Windows Server 2018	—
Use the web	IE8.0 browser	—
Internet speed	8 M Ethernet	—
Host	Windows 10 system	—

4.1. Experiment Preparation Process. To ensure the accuracy of the experiment, some landscape design images have been selected for visualization, and virtual visualization and design techniques have been used in virtual visualization, and the sharpness of the image arose. The test equipment was set up as shown in Table 1 [17]. With the help of the above parameters, a virtual representation of the garden landscape is made. In the experiment, a total of 20 landscape parks were selected, a total of 3 virtual images were taken, and the brilliance was counted and analyzed.

4.2. Analysis of Experimental Results. The author's design is represented by system 1, and the original system is represented by system 2 in Tables 2–4 [18]. The data in the table show that the resolution of the virtual imaging system developed by the author is usually between 85% and 90%, and the resolution of the original imaging system is usually between 82% and 85%. It is obvious that the actual virtual images created by the author are higher than the original virtual imaging system. It can be seen that the author model of the virtual imaging system has achieved the benefits of visual acuity. Based on the above results, after using the virtual measuring machine developed by the author in the landscape design, its visibility is much higher than the industry average [19]. The virtual rendering system developed by the author can show the landscape of the garden in a simple and direct way. The three-dimensional virtual visualization system designed by the author is perfect for garden design.

TABLE 2: Comparison table between the original system and the system clarity of the first test.

Picture label	Sharpness of the first trial (%)	
	System 1	System 2
1	89.3	82.6
2	89.7	83.6
3	89.1	82.5
4	89	84.9
5	90.3	83.3
6	88.1	82.9
7	90	83.1
8	88.3	82
9	88.4	82
10	89.7	83.9
11	89.3	83.9
12	88	82.3
13	89.6	84.6
14	89.4	82.7
15	88.3	82.9
16	90.6	83.2
17	90.8	84.6
18	90.6	83.9
19	89.3	82.6
20	89.5	84.2

TABLE 4: The comparison table of the original system and the system clarity of the third test.

Picture label	3rd trial clarity (%)	
	System 1	System 2
1	90.2	83.9
2	88.7	83.6
3	88	82.1
4	88.5	83.3
5	90.2	83.2
6	90.6	84.1
7	90.1	85
8	90.5	82.4
9	89.6	83.9
10	88.3	82.5
11	90.4	84.9
12	90.9	83.1
13	90.3	84.6
14	90.3	83.4
15	90.5	82.7
16	88.9	83
17	90.5	84
18	90.2	83
19	88.2	82.2
20	90.2	84.5

TABLE 3: Comparison table between the original system and the system clarity of the second test.

Picture label	Second trial clarity (%)	
	System 1	System 2
1	89.3	82.8
2	85	83.4
3	88.6	83
4	87.1	83.7
5	89	83.7
6	89.1	84
7	87.5	85
8	89.4	84.1
9	85	84.5
10	88.5	85
11	85.3	83.5
12	89.8	83.4
13	88.9	83.8
14	86.4	83.4
15	88.3	82.6
16	89.3	83.7
17	89.7	83.6
18	85.4	82.2
19	86.3	82.6
20	85	82.2

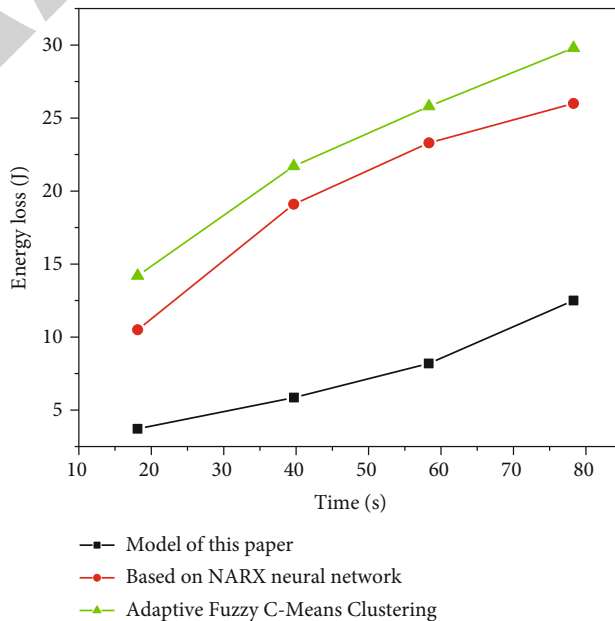


FIGURE 3: Comparison of energy consumption of three methods.

4.3. *Energy Consumption Analysis.* For data storage and processing, the author uses a real-world number to reduce the cost of data retention and communication costs between nodes. The different groups of data are represented by a combination of components, which makes data sharing more efficient [20]. In this experiment, the remote sensing

sensor network of the landscape area consisted of 110 nodes, and the nodes were divided into an area of 110 m × 110 m. Figure 3 shows a comparison of the data transmissions used between the three different models.

From the analysis of Figure 3, it can be seen that the energy consumption of the fusion process material of the sample is higher than that of the sample. This is because there are always two heads sending data in each model group, which makes data transmission and processing more efficient [21]. By using a genetic algorithm, the model cannot only improve the accuracy of data integration and storage but also reduce data retrieval, reduce the use of fire electricity, and improve the performance of data integration in the landscape design process [22–26].

5. Conclusion

With the continuous popularization of 3D virtual imaging technology in China, this technology is applied in all walks of life, through 3D virtual imaging of garden landscapes, deficiencies in garden design can be discovered in time and corrected. By using this technology to visualize the virtual landscape, it is guaranteed that people can fully perceive the designer's feeling. Based on the current virtual imaging technology, the research on imaging technology should be continuously strengthened, and the scientificity and feasibility of the equipment should be continuously improved, so as to apply this technology more proficiently.

Data Availability

The data used to support the findings of this study are available from the corresponding author upon request.

Conflicts of Interest

The author declares that there are no conflicts of interest.

References

- [1] I. Ralaj, M. Donlic, and D. Sersic, "Dual imaging – can virtual be better than real?," *IEEE Access*, vol. 8, no. 1, pp. 40246–40260, 2020.
- [2] H. Deng, Y. Mi, B. Lu, and P. Xu, "Application of virtual touch tissue imaging quantification in diagnosis of supraspinatus tendon injury," *Journal of X-Ray Science and Technology*, vol. 29, no. 5, pp. 881–890, 2021.
- [3] X. Li, Z. Li, J. Li, J. Song, and B. Liu, "Optimize non-contrast head ct imaging tasks using multiple virtual monochromatic image sets in dual-energy spectral ct," *Journal of X-Ray Science and Technology*, vol. 28, no. 2, pp. 345–356, 2020.
- [4] T. Meerakker, "Section Meetings," *SMPTE Motion Imaging Journal*, vol. 129, no. 4, pp. 8–9, 2020.
- [5] K. Lyver and J. E. O'Neal, "Section Meetings," *SMPTE Motion Imaging Journal*, vol. 129, no. 2, pp. 10–13, 2020.
- [6] F. Kola and F. Liarokapis, "Study of full-body virtual embodiment using noninvasive brain stimulation and imaging," *International Journal of Human-Computer Interaction*, vol. 37, no. 1, pp. 1–14, 2021.
- [7] A. E. Bergues-Pupo, R. Lipowsky, and A. V. Verde, "Unfolding mechanism and free energy landscape of single, stable, alpha helices at low pull speeds," *Soft Matter*, vol. 16, no. 43, pp. 9917–9928, 2020.
- [8] R. Ali, "Looking to the future of the cyber security landscape," *Network Security*, vol. 2021, no. 3, pp. 8–10, 2021.
- [9] Z. Li, X. Han, L. Wang, T. Zhu, and F. Yuan, "Feature extraction and image retrieval of landscape images based on image processing," *Traitement du Signal*, vol. 37, no. 6, pp. 1009–1018, 2020.
- [10] C. Yi and X. Feng, "Home interactive elderly care two-way video healthcare system design," *Journal of Healthcare Engineering*, vol. 2021, Article ID 6693617, 11 pages, 2021.
- [11] C. Latsou, J. A. Erkoyuncu, and M. Farsi, "A multi-objective approach for resilience-based system design optimisation of complex manufacturing systems," *Procedia CIRP*, vol. 100, no. 19, pp. 536–541, 2021.
- [12] T. Breckle, J. Kiefer, C. Schlüter, and N. Gro, "Multi-criteria evaluation within concept planning phase of assembly system design," *Procedia CIRP*, vol. 97, no. 2, pp. 296–301, 2021.
- [13] T. Breckle, M. Manns, and J. Kiefer, "Assembly system design using interval-based customer demand," *Journal of Manufacturing Systems*, vol. 60, no. 2, pp. 239–251, 2021.
- [14] W. Ajayi and J. O. Erihri, "Design concerns in system architecture," *Technology Reports of Kansai University*, vol. 63, no. 2, pp. 7137–7146, 2021.
- [15] Y. Yang, L. Deng, Q. Wang, and W. Zhou, "Zone fare system design in a rail transit line," *Journal of Advanced Transportation*, vol. 2020, Article ID 2470579, 10 pages, 2020.
- [16] N. Meekel, D. Vughs, F. Been, and A. M. Brunner, "Online prioritization of toxic compounds in water samples through intelligent HRMS data acquisition," *Analytical Chemistry*, vol. 93, no. 12, pp. 5071–5080, 2021.
- [17] J. Lin, S. Zhao, and Q. Yuan, "A novel technology for separating live earthworm from vermicompost: experiment, mechanism analysis, and simulation," *Waste Management*, vol. 131, no. 4, pp. 50–60, 2021.
- [18] O. Jahanmahin, D. J. Kirby, B. D. Smith et al., "Assembly of gold nanowires on gold nanostripe arrays: simulation and experiment," *The Journal of Physical Chemistry C*, vol. 124, no. 17, pp. 9559–9571, 2020.
- [19] R. T. McDonald, M. Condino, M. A. Neumann, and C. A. Kitts, "Navigation of scalar fronts with multirobot clusters in simulation and experiment," *IEEE Systems Journal*, vol. 14, no. 3, pp. 3755–3766, 2020.
- [20] D. E. Artemov, O. E. Nanii, A. P. Smirnov, and A. I. Fedoseev, "Dynamics of a q-switched bismuth-doped fibre laser: simulation and comparison with experiment," *Quantum Electronics*, vol. 51, no. 4, pp. 299–305, 2021.
- [21] G. Liu, J. Yu, C. Chen, and W. Wen, "Evaluating cognitive task result through heart rate pattern analysis," *Healthcare Technology Letters*, vol. 7, no. 2, pp. 41–44, 2020.
- [22] A. Sharma and R. Kumar, "Performance comparison and detailed study of AODV, DSDV, DSR, TORA and OLSR routing protocols in ad hoc networks," in *2016 Fourth International Conference on Parallel, Distributed and Grid Computing (PDGC)*, pp. 732–736, Wagnaghat, India, 2016.
- [23] M. Raj, P. Manimegalai, P. Ajay, and J. Amose, "Lipid data acquisition for devices treatment of coronary diseases health stuff on the internet of medical things," *Journal of Physics: Conference Series*, vol. 1937, article 012038, 2021.

Retraction

Retracted: Sensor-Based Exercise Rehabilitation Robot Training Method

Journal of Sensors

Received 23 January 2024; Accepted 23 January 2024; Published 24 January 2024

Copyright © 2024 Journal of Sensors. This is an open access article distributed under the Creative Commons Attribution License, which permits unrestricted use, distribution, and reproduction in any medium, provided the original work is properly cited.

This article has been retracted by Hindawi following an investigation undertaken by the publisher [1]. This investigation has uncovered evidence of one or more of the following indicators of systematic manipulation of the publication process:

- (1) Discrepancies in scope
- (2) Discrepancies in the description of the research reported
- (3) Discrepancies between the availability of data and the research described
- (4) Inappropriate citations
- (5) Incoherent, meaningless and/or irrelevant content included in the article
- (6) Manipulated or compromised peer review

The presence of these indicators undermines our confidence in the integrity of the article's content and we cannot, therefore, vouch for its reliability. Please note that this notice is intended solely to alert readers that the content of this article is unreliable. We have not investigated whether authors were aware of or involved in the systematic manipulation of the publication process.

Wiley and Hindawi regrets that the usual quality checks did not identify these issues before publication and have since put additional measures in place to safeguard research integrity.

We wish to credit our own Research Integrity and Research Publishing teams and anonymous and named external researchers and research integrity experts for contributing to this investigation.

The corresponding author, as the representative of all authors, has been given the opportunity to register their agreement or disagreement to this retraction. We have kept a record of any response received.

References

- [1] S. Xie and J. Zhang, "Sensor-Based Exercise Rehabilitation Robot Training Method," *Journal of Sensors*, vol. 2023, Article ID 7881084, 9 pages, 2023.

Research Article

Sensor-Based Exercise Rehabilitation Robot Training Method

Shangsen Xie ¹ and Jingru Zhang ²

¹*School of Physical Education, Fuyang Normal University, Fuyang, Anhui 236037, China*

²*School of Information Engineering, Fuyang Normal University, Fuyang, Anhui 236037, China*

Correspondence should be addressed to Jingru Zhang; 11231518@stu.wxica.edu.cn

Received 10 July 2022; Revised 6 August 2022; Accepted 22 August 2022; Published 24 March 2023

Academic Editor: Haibin Lv

Copyright © 2023 Shangsen Xie and Jingru Zhang. This is an open access article distributed under the Creative Commons Attribution License, which permits unrestricted use, distribution, and reproduction in any medium, provided the original work is properly cited.

In order to provide convenience for rehabilitation doctors to formulate rehabilitation plans for patients, this paper proposes a training method for exercise rehabilitation robots based on sensors. In this research, the customized wearable sensor and universal mobile terminal are used as the hardware. Based on the sensor, the motion capture algorithm and motion reconstruction algorithm are developed. The table of experimental results shows that the cost can be saved by using the sensor, and the data can be captured accurately, which can meet the needs of rehabilitation medicine for motor function evaluation and training guidance. The range of motion of the joint and the manual measurement value are within 5°, which can meet the needs of rehabilitation medicine for motor function evaluation and training guidance. The system delay is less than 0.5 s, which has good real-time performance and can respond quickly to emergencies, ensuring the safety of patients' out-of-hospital rehabilitation. The training method of motion rehabilitation robot based on sensor is helpful for rehabilitation doctors to carry out statistical data of functional evaluation and is of great significance for rehabilitation doctors to make training plans for patients and carry out rehabilitation training.

1. Introduction

With the rapid development of information technology, traditional medical equipment is constantly developing in the direction of intelligence, while rehabilitation robots are combined with the development results of multiple disciplines and are widely used in medical diagnosis and treatment, clinical surgery, rehabilitation medicine, and other related medical fields [1].

Sensor technology is one of the important basic technologies of modern information technology. With the development of modern detection, control, and automation technology, sensor technology is becoming more and more mature. People pay more and more attention to it, and it is widely used in various fields [2]. The application of sensor technology in the field of rehabilitation medicine provides a new impetus for the development of rehabilitation evaluation and treatment technology [3].

As a medical robot used in the field of rehabilitation medicine, rehabilitation robot can help patients with exer-

cise or cognitive function training and to some extent solve the problems of fatigue and differences in multiple training in artificial rehabilitation training [4]. According to their different functional training, rehabilitation robots can be divided into motion disability rehabilitation robots and cognitive disability rehabilitation robots. According to the difference of the trained limbs, the rehabilitation robot for movement disorders can be divided into upper limb rehabilitation robot and lower limb rehabilitation robot. The upper limb rehabilitation robot mainly assists the exercise training of the patient's shoulder, elbow, hand, and other upper limb joints. Through the active and passive rehabilitation training, the strength of the patient's muscle tissue and the flexibility of the hand to do fine movements are strengthened, and the force, torque, and other sensors are installed to evaluate the process and results of the rehabilitation training. The lower limb rehabilitation robot is mainly the lower limb exoskeleton robot, which focuses on the rehabilitation training of patients such as auxiliary standing, balance and walking. If the patient's rehabilitation training can be captured by

the sensor for a long time to form statistical data and then evaluated by the rehabilitation doctor according to the statistical value, the results are of great significance for the development of rehabilitation medicine and the evaluation of interventional treatment effect. Therefore, the rehabilitation training robot has become one of the research hotspots in medical robots in recent years. Figure 1 shows the interaction method in the rehabilitation training robot.

2. Literature Review

With the development of science and technology, sports rehabilitation robot has achieved unprecedented development in recent years. By making use of the characteristics of robots such as high precision, high repeatability, and customization and combining with the basic idea of sports rehabilitation therapy, robots are applied to sports rehabilitation, resulting in a large number of sports rehabilitation robots, including robots for rehabilitation training of upper limbs, lower limbs, ankles, and feet. Among them, sports rehabilitation robots based on wearable exoskeletons have been widely studied and applied in recent years, as shown in Table 1.

Dionisio and others analyzed and compared the monitoring data of 10 parts of the manikin measured by Kinect sensor and the most advanced markable 3D camera (MBC) by using the principal component analysis method and found that Kinect sensor has high accuracy in identifying the whole body movement mode, and the price is low, which is more suitable for promotion and application in clinical rehabilitation training [5]. Chen and others designed a knee flexion angle measurement system based on resistance sensor. The system records the resistance changes during movement through the resistance sensor installed in the wearable knee pad and then calculates the knee flexion angle. It can be used by rehabilitation professionals and patients with knee dysfunction to monitor the knee flexion angle in real time during training, so as to improve the process of rehabilitation evaluation and rehabilitation training [6]. Jang and others developed an integrated sensor shoe composed of pressure and bending sensors. This shoe can send the gait information collected during walking to the server so that doctors can visually observe the changes of foot weight and ankle angle when patients walk [7]. Duan and others monitored the daily energy consumption of hemiplegic patients by placing a swp2a system composed of 2 accelerometers, 1 skin electric response sensor, heat sensor, skin temperature sensor, and 1 ambient temperature sensor at the midpoint of the healthy triceps brachii. Combined with the individual conditions of the patients, such as height, body mass, and other information, the intensity of each exercise of the subjects is calculated through a unique formula, so as to achieve the purpose of monitoring the energy consumption of hemiplegic patients [8]. Yu and others used inertia and air pressure sensors to make a device similar to a wrist watch. After the patient wears this device on the wrist, the metabolic equivalent of the patient's activities of daily living can be monitored in real time according to the information received by the sensor. Compared with the previous equip-

ment for monitoring the amount of metabolism, it is simpler and will not affect the patient's activities [9].

In view of the above problems, considering that the optical tracking equipment is difficult to play a role in various complex environmental conditions, in this paper, we developed a MEMS device and motion capture algorithm based on Magnetometer and inertial sensor to realize the research on the training method of motion rehabilitation robot.

3. Method

3.1. Research Scheme

3.1.1. Equipment Composition. The core component of the wearable sensor device described in this paper is the yd122 sensor, which is a MEMS sensor [10]. Each sensor is integrated with a 9-axis mpu9250 chip, which can measure the acceleration, angular velocity, and magnetic field strength of three axes [11]. The STM32 microprocessor inside the sensor filters the measured acceleration, angular velocity, and magnetic force values into four elements or Euler angles representing the current attitude. In addition, the yd122 master sensor has its own battery and Bluetooth module, which can be used alone or in cascade with a yd122 slave sensor. When in use, a single master sensor is fixed to the chest of the subject through a strap, and 4 sets of master + Slave sensors are, respectively, bound to the outside of the left and right thighs, the outside of the left and right lower legs, the outside of the left and right upper arms, and the outside of the left and right forearms, a total of 9. In addition to the sensors, the device also includes a general-purpose mobile terminal, which is used to obtain the data of 9 sensors and reconstruct the motion state.

In order to minimize the quality of the exoskeleton and improve the response speed of start and stop, 6061 aluminum alloy is selected as the part material of the exoskeleton manipulator [12]. At the same time, in order to improve the wearing comfort, the shoulder structure is installed on the rack, and the patient does not have to bear the quality of any part after wearing. According to the weight of exoskeleton, combined with adult weight statistics and clinical rehabilitation training experience, the dynamic parameters required for each degree of freedom are selected, as shown in Table 2.

3.1.2. Motion Capture Algorithm. The posture change of human body can be decomposed into the roll angle, heading angle, and pitch angle of trunk, head, and limbs. After wearing the sensor device, the sensor is synchronized with human motion, and the measured changes of magnetic field, acceleration, and angular velocity can be used to reconstruct the motion state. In this experiment, the movements of both sides of the trunk and limb joints of the subjects were mainly tracked (usually the limbs on both sides of the joints have obvious movement pattern differences), while the movements of the head and the ends of the limbs were ignored. In addition, the trunk is also assumed as a whole, regardless of the flexion and extension of the spine.

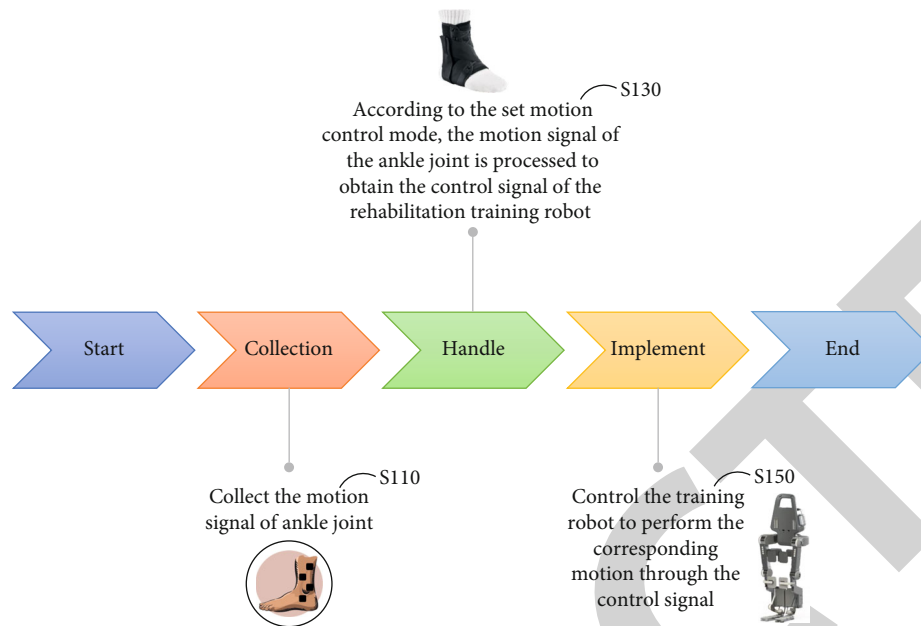


FIGURE 1: Interaction method in rehabilitation training robot.

TABLE 1: Some common exercise rehabilitation training robots and their functions.

Robot name	Configuration type	Applicable parts	Freedom	Active training	Passive training	Impedance training	Seme	Game interaction
MT-MANUS	End pull type	Shoulder, elbow	3	√	√			√
ARMin	Exoskeleton type	Shoulder, elbow, wrist	6		√	√		√
Harmon	Exoskeleton type	Simultaneous training of both upper limbs	12	√	√			
Co-Exos	Exoskeleton type	Upper limb	6	√	√		√	
Lokomat	Exoskeleton type	The legs	4	√	√	√		√
Ekso	Exoskeleton type	The legs	4		√			
Indego	Exoskeleton type	The legs	4		√			
HAL	Exoskeleton type	The legs	6	√	√		√	
AIDER	Exoskeleton type	The legs	6	√	√		√	
HemiGo	Exoskeleton type	The legs	6	√	√	√		√
GEMS-HI	Exoskeleton type	Hip joint	1	√				
GEMS-K1	Exoskeleton type	Knee joint	1	√				
GEMS-A1	Exoskeleton type	Ankle joint	1	√				
RutgersAnkle	End pull type	Ankle joint	1	√	√			√
PAFO	Exoskeleton type	Ankle joint	1		√			
ReStore	Exoskeleton type	Ankle joint	1	√	√	√		

TABLE 2: Dynamic parameters of two degrees of freedom.

Freedom	Torque (N.m)	Maximum speed (r/min)	Motor power (W)
Elbow flexion/extension	23	30	100
Shoulder flexion/extension	35	30	200
Shoulder abduction/adduction	41	30	200

In the motion capture algorithm of multisensor data fusion, the wearing position of the sensor has a great impact on the algorithm design. The forearm and upper arm can change freely in three degrees of freedom, and the speed is fast, and the direction cannot be predicted. The movement of thigh and calf is mainly the change of flexion and extension direction and orientation, and the deflection (roll) to both sides is less, and the range is small. The trunk part is mainly translational, with less large forward tilt, backward tilt, and lateral bending, and the movement is slow. Here, taking the sensor placed on the thigh as an example, the motion capture algorithm implemented in this device is introduced.

The thigh flexion and extension angle θ is defined as the angle between the y -axis and the opposite direction of gravity, and the thigh swing velocity (angular velocity) is $v = d\theta/dt$ [13, 14]. Considering that the swinging speed of the thigh is slow, the sampling rate of the sensor is 25 Hz, the angular velocity changes very little within the sampling interval (the change value can be simulated by the system noise), and the filter uses the constant angular velocity model to deduce. The state update equation is

$$\begin{bmatrix} \theta_k \\ v_k \\ a_k \\ c_k \end{bmatrix} = \begin{bmatrix} 1 & t_s & 0 & 0 \\ 0 & 1 & 0 & 0 \\ 0 & 0 & 1 & 0 \\ 0 & 0 & 0 & 1 \end{bmatrix} \cdot \begin{bmatrix} \theta_{k-1} \\ v_{k-1} \\ a_{k-1} \\ c_{k-1} \end{bmatrix} + \begin{bmatrix} w_\theta \\ w_v \\ w_a \\ w_c \end{bmatrix}, \quad (1)$$

where the subscript represents time k and time $k-1$, T_s is the sampling interval, and w_θ , w_v , w_a and w_c are the system noise of each state variable, respectively [15]. It can be assumed that they are independent 0-means Gaussian noise, and their distribution function is

$$P(w_\theta, w_v, w_a, w_c) \sim N(0, Q). \quad (2)$$

The calculation method of Q is

$$Q = \begin{bmatrix} Q_\theta & t_s & 0 & 0 \\ 0 & Q_v & 0 & 0 \\ 0 & 0 & Q_a & 0 \\ 0 & 0 & 0 & Q_c \end{bmatrix}. \quad (3)$$

Q_θ , Q_v , Q_a , and Q_c are the variances of each state variable [16]. The measured value of the sensor is the acceleration D in the x -axis direction and the acceleration B in the y -axis direction. The relationship between the observed value and the state variable (observation equation) is

$$\begin{cases} d_k = -g \sin \theta_k + a_k \sin \theta_k + c_k \cos \theta_k + w_d, \\ b_k = -g \cos \theta_k + a_k \cos \theta_k - c_k \sin \theta_k - rv_k^2 + w_b, \end{cases} \quad (4)$$

where w_d and w_b are the observation noise and R is the distance from the hip joint to the sensor. Similarly, it is

assumed that the observation noise is Gaussian noise with independent 0-means [17]:

$$P(w_d, w_b) \sim N(0, R), \quad (5)$$

where $R = \begin{bmatrix} R_d & 0 \\ 0 & R_b \end{bmatrix}$ is the covariance matrix of the observation noise, and R_b and R_d are the variances of the measured values. Equation (4) is written into a matrix format as shown in the following formula [18]:

$$\begin{bmatrix} d_k \\ b_k \end{bmatrix} = h(\theta_k, v_k, a_k, c_k) + \begin{bmatrix} w_d \\ w_b \end{bmatrix}. \quad (6)$$

The observation equation in Equations (4) and (5) is not linear, so the Kalman equation cannot be derived directly. It needs to be locally linearized, and the partial derivative of function h to each state variable is obtained, that is, $H = \partial h / (\partial (\theta_k, v_k, a_k, c_k))$ obtains the following equation:

$$H = \begin{bmatrix} -g \cos \theta_k + a_k \cos \theta_k - c_k \sin \theta_k & 0 & \sin \theta_k & \cos \theta_k \\ -g \cos \theta_k - a_k \sin \theta_k - c_k \cos \theta_k & -2rv_k & \cos \theta_k & -\sin \theta_k \end{bmatrix}. \quad (7)$$

Local linearization shall be carried out according to the following equation:

$$\begin{bmatrix} d_k \\ b_k \end{bmatrix} = \begin{bmatrix} \tilde{d}_k \\ \tilde{b}_k \end{bmatrix} + H \cdot \begin{bmatrix} \theta_k - \tilde{\theta}_k \\ v_k - \tilde{v}_k \\ a_k - \tilde{a}_k \\ c_k - \tilde{c}_k \end{bmatrix} + \begin{bmatrix} w_d \\ w_b \end{bmatrix}, \quad (8)$$

where \tilde{d}_k and \tilde{b}_k are the estimated values of d_k and b_k and $\tilde{\theta}_k$, \tilde{v}_k , \tilde{a}_k , and \tilde{c}_k are the estimated values of θ_k , v_k , a_k , and c_k , respectively. After obtaining the posterior predicted value of the state variable, update the covariance matrix of the estimated value of the state variable according to the following equation:

$$P_k = \begin{bmatrix} P_\theta & t_s & 0 & 0 \\ 0 & P_v & 0 & 0 \\ 0 & 0 & P_a & 0 \\ 0 & 0 & 0 & P_c \end{bmatrix} = E \left\{ \begin{bmatrix} \theta_k - \tilde{\theta}_k \\ v_k - \tilde{v}_k \\ a_k - \tilde{a}_k \\ c_k - \tilde{c}_k \end{bmatrix} \cdot \left[\theta_k - \tilde{\theta}_k v_k - \tilde{v}_k a_k - \tilde{a}_k c_k - \tilde{c}_k \right] \right\}. \quad (9)$$

The above steps are recursive derivation of Kalman filter. In actual use, it is necessary to estimate the state variables, system

noise, observation noise, and covariance matrix (see initialization parameter settings and recursive calculation examples). Taking time $k-1$ as an example, the prior prediction of time k according to the state equation is shown in Equation (10), the parameter with wave line on the right side of the equation is the filter estimation value of time $k-1$, and the subscript $(k|k-1)$ represents the one-step prediction from time $k-1$ to time k :

$$\begin{bmatrix} \theta_{(k|k-1)} \\ v_{(k|k-1)} \\ a_{(k|k-1)} \\ c_{(k|k-1)} \end{bmatrix} = \begin{bmatrix} 1 & t_s & 0 & 0 \\ 0 & 1 & 0 & 0 \\ 0 & 0 & 1 & 0 \\ 0 & 0 & 0 & 1 \end{bmatrix} \cdot \begin{bmatrix} \tilde{\theta}_{k-1} \\ \tilde{v}_{k-1} \\ \tilde{a}_{k-1} \\ \tilde{c}_{k-1} \end{bmatrix}. \quad (10)$$

At the same time, the covariance matrix is predicted in one step, as shown in the following equation:

$$P_{(kk-1)} = A\tilde{P}_{k-1}A^T + Q, \quad (11)$$

where $A = \begin{bmatrix} 1 & t_s & 0 & 0 \\ 0 & 1 & 0 & 0 \\ 0 & 0 & 1 & 0 \\ 0 & 0 & 0 & 1 \end{bmatrix}$ is the state transition matrix of Equation (1). Single step prediction of observed values is

$$\begin{cases} d_{(k|k-1)} = -g \sin \theta_{(k|k-1)} + a_{(k|k-1)} \sin \theta_{(k|k-1)} + c_{(k|k-1)} \cos \theta_{(k|k-1)} \\ b_{(k|k-1)} = -g \cos \theta_{(k|k-1)} + a_{(k|k-1)} \cos \theta_{(k|k-1)} - c_{(k|k-1)} \sin \theta_{(k|k-1)} - rv_{(k|k-1)}^2 \end{cases}. \quad (12)$$

The Kalman gain is derived from multiple covariance matrices and locally linearized observation functions, as shown in the following equation [19]:

$$K_k = P_{(k|k-1)}H^T (HP_{(k|k-1)}H^T + R)^{-1}. \quad (13)$$

As shown in Equation (14), the estimated value of the state variable at time k is obtained by weighting the two estimated values by the Kalman gain.

$$\begin{bmatrix} \tilde{\theta}_k \\ \tilde{v}_k \\ \tilde{a}_k \\ \tilde{c}_k \end{bmatrix} = \begin{bmatrix} \theta_{(k|k-1)} \\ v_{(k|k-1)} \\ a_{(k|k-1)} \\ c_{(k|k-1)} \end{bmatrix} + K_k \begin{bmatrix} d_k - d_{(\wedge|k-1)} \\ b_k - b_{(\wedge|k-1)} \end{bmatrix} \quad (14)$$

Finally, the covariance matrix of the estimated value of the state variable is updated to prepare for filtering at $k+1$, as shown in the following equation:

$$P_k = [1 - K_kH]P_{(k\mu-1)}. \quad (15)$$

The above is the algorithm for tracking the pitch angle of the thigh. This algorithm is also applicable to the legs with similar motion modes. According to the suggestion of the rehabilitation doctor, the pitching and rolling motions of the trunk are small and change slowly. The system obtains them by triangulation according to the components of the gravity component on each axis, and the azimuth of the trunk is also obtained by triangulation of the magnetometer component. The actions of the forearm and upper arm are relatively complex. The Kalman filter similar to the above

is used in the equipment for tracking. The principle is the same, but the dimensions of variables and matrices in the state update equation and observation equation are greatly increased. The Kalman filter used in the tracking algorithm is a filtering algorithm without system delay. The filtering value of the current state parameter can be obtained after the new measured value is obtained at time k . For the microprocessor with strong computing power, the data filtering can be completed within a sampling interval.

3.2. Joint Control Experiment. Since the mirror control and synchronous control are only different in motion control mode, and the process of upper limb motion data processing and transformation is basically similar, only the single joint somatosensory mirror control is experimentally analyzed here. The experimenter's right arm (affected limb) wears an exoskeleton mechanical arm, stands at a distance of 2.0~2.5 m from Kinect, and faces Kinect. The left arm (healthy limb) performs slow shoulder abduction, forward flexion, and elbow flexion single joint movements. Kinect collects the joint angle of the left arm, which is converted into control signals through the upper computer processing program, and the somatosensory control exoskeleton mechanical arm drives the right arm to perform mirror motion [20].

In order to further study the "follow-up" performance of each axis in the mirror mode, extract the upper limb motion data and the actual position of the motor within 15 s (the extraction frequency is 30 Hz), and draw the change curve, as shown in Figures 2(a), 2(b), and 2(c). At the beginning of the movement, there is a large error between the joint angle of the control arm and the joint angle of the exoskeleton manipulator. This is because the first group of angles calculated from the somatosensory data obtained by Kinect are

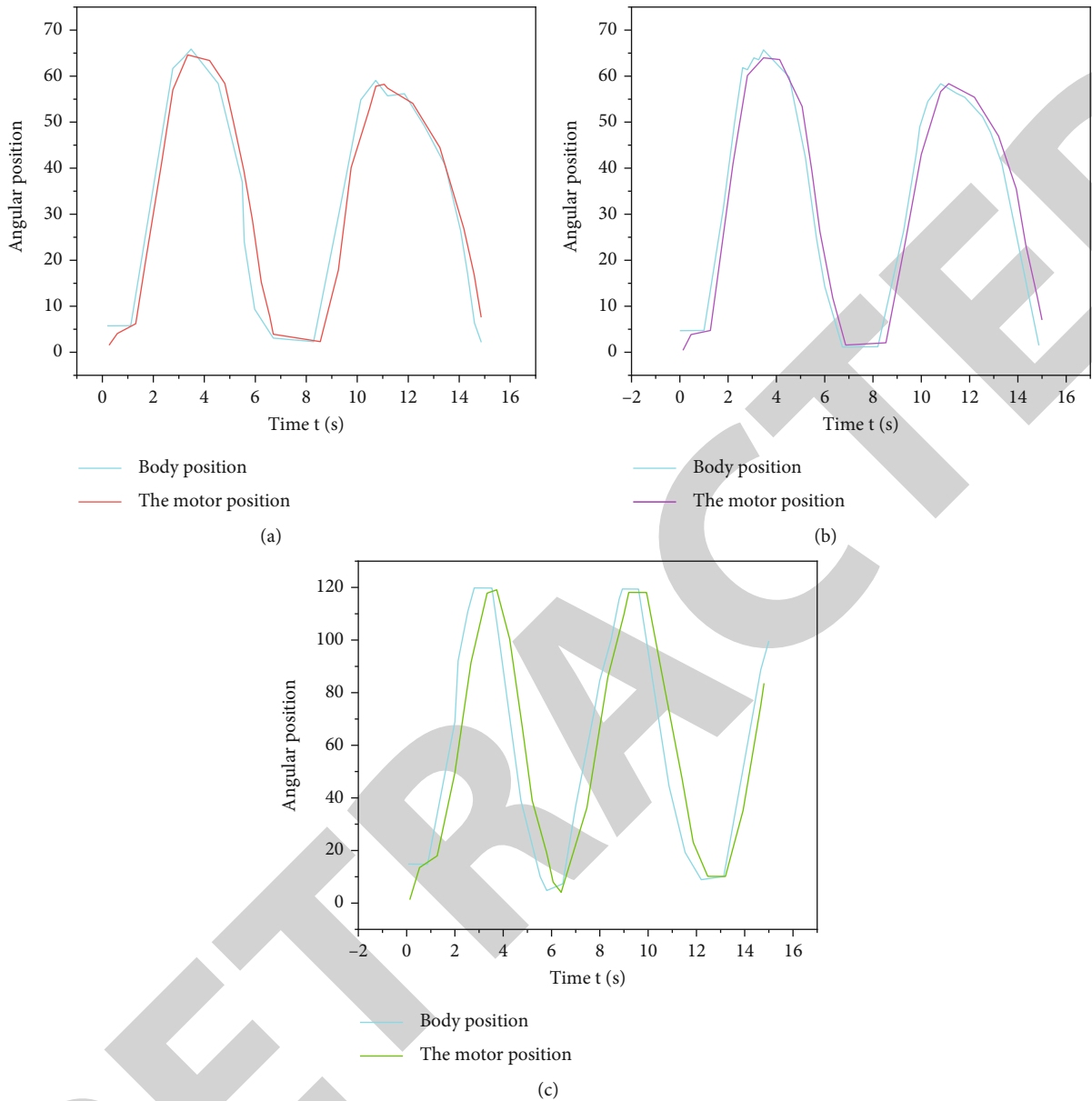


FIGURE 2: (a) Shoulder abduction/adduction angle curve. (b) Shoulder flexion/extension angle curve. (c) Elbow flexion/extension angle curve.

often not zero, and the drive motors of each axis are at the initial zero position [21]. After a period of exercise, the difference between the two decreased gradually. The horizontal straight line generated by the crest or trough of the curve is due to the limitation of the range of joint movement during data processing, so as to ensure the safe operation of the system. Table 3 shows the average angular velocity of each joint, the average angular error of each joint in a single flexion and extension, and the maximum action delay within a certain period of time.

It can be seen from Table 3 that the greater the angular velocity of the healthy limb joint movement, the greater the error between the angle obtained by the somatosensory and the actual position of the exoskeleton robot arm joint. This is because the refresh rate of the joint angle obtained

by Kinect is 30 frames per second, while the position update speed of the motor lags behind under load. With the decrease of joint velocity, the position error and maximum delay decrease, and the follow-up performance is improved. Generally, the joint angular velocity of rehabilitation training is carried out at a low speed below $30^\circ/\text{s}$. The follow-up performance of each axis of the upper limb exoskeleton rehabilitation robot basically meets the requirements of rehabilitation training.

4. Result Analysis

Considering that the equipment is a kind of monitoring equipment, not a treatment or diagnostic equipment, and the equipment will not exert auxiliary movement effect on

TABLE 3: Follow-up performance of each joint.

	Average angular velocity ($^{\circ}/s$)	Mean value of angle error ($^{\circ}$)	Maximum delay (s)
Elbow flexion/extension	34.3	12.3	0.80
Shoulder abduction/adduction	25.6	6.8	0.41
Shoulder flexion/extension	17.3	3.1	0.37

patients, the selection of cases is mainly based on the following two points: ① Patients need to have good movement ability and perform large range of movement in the monitoring process, and ② patients have good compliance and cognitive ability and can wear equipment for a long time to complete monitoring. Disease type, drug treatment, and other factors are not taken as the basis for case selection. Based on the above considerations, three home-based rehabilitation patients with normal cognitive ability were selected for the preliminary experiment. The Brunnstrom stages of upper and lower limbs of the three patients were more than 4 when they left the hospital. They had similar transfer and daily living abilities and were able to wear and use the equipment as required. After the system is deployed in the patient's home, each patient will wear sensors in the morning and afternoon for 2h of motion capture. During the experiment, the patients received a total of 1H rehabilitation training according to the doctor's requirements, including 20 min treadmill walking training, and could freely move indoors at other times. The experiment lasted for 4 weeks. To ensure the repeatability of the experiment, we selected the walking training with high similarity for the test. When the patient was walking, the speed of the treadmill was set at 3 km/h. In addition to wearing sensors for monitoring, the optical tracking method described in previous studies is also used as a reference, and the walking video is synchronously recorded at a frame rate of 25 Hz. The included angle between the thigh centerline and the vertical direction is measured frame by frame for the obtained video, forming a pitching angle curve as shown by the dotted line in Figure 3 [22]. At the same time, according to the Kalman filter algorithm, the pitch angle curve of the thigh during walking is drawn as a solid line in Figure 3.

The two curves in Figure 3 show the same change trend. The average deviation of the maximum value of the thigh pitch angle monitored by the two methods is 0.063 radians ($\approx 3.6^{\circ}$), the average deviation of the minimum value is 0.067 radians ($\approx 3.8^{\circ}$), and the average difference of the angles of the two curves is 0.072 radians ($\approx 4.1^{\circ}$). In addition to the above clips, after the statistics of the 4-week walking test results of 3 patients, the average difference of thigh pitch angle obtained by the optical and Kalman filtering algorithms is 3.7° , 4.3° , and 4.0° , respectively, with an average of 4.0° [23]. In this study, the maximum delay of the equipment in data transmission is 80 ms, while the TD is 320 ms. The increase of delay is related to the filtering algorithm. The Kalman filter described in this paper adopts the constant angular velocity model. When the angular velocity changes sud-

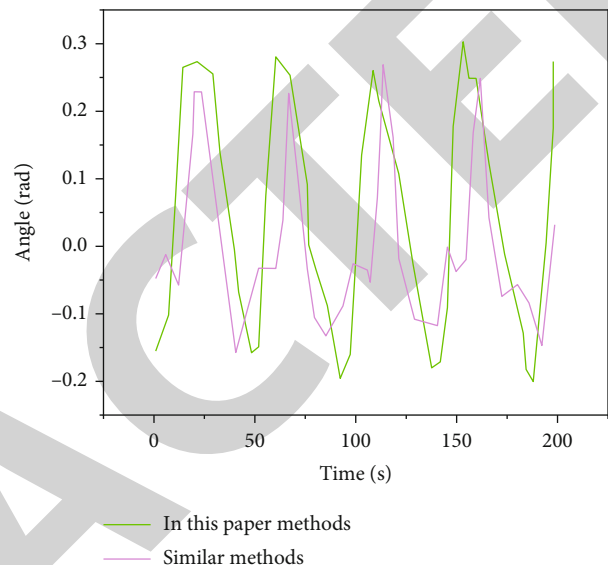


FIGURE 3: Thigh pitch angle curve during walking.

denly, the swing velocity of the thigh in this example suddenly increases or decreases, and the angular velocity value and the corresponding covariance matrix need several iterations to match the current motion. The filtering result is expressed as a lag period of time, which also leads to the difference between the measurement and calculation of the angle value at the same time by the above optical and Kalman filtering algorithms [24]. After the statistics of the walking test results of three patients, the maximum delay of the system was 480 ms, with an average of 297 ms.

The rehabilitation doctor's evaluation on the use of the device is also a part of the experiment. The rehabilitation doctor observes the actual action and the model action displayed by the mobile terminal when the patient uses the device. The evaluation conclusions are as follows: ① The model action has a high degree of reduction relative to the actual action of the patient, and the action is accurate and continuous, which can replace manual monitoring, and does not use cameras, and does not infringe on the privacy of the patient; ② the range of motion displayed by the motion reconstruction app is within 5° of the manual measured value, meeting the needs of rehabilitation medicine for motor function evaluation and training guidance; and ③ the system delay is less than 0.5 s, which has good real-time performance and can respond quickly to emergencies, ensuring the safety of patients' out-of-hospital rehabilitation [25].

5. Conclusion

In this research, the customized wearable sensor and universal mobile terminal are used as the hardware. Based on the sensor, the motion capture algorithm and motion reconstruction algorithm are developed. In the initial experimental application, it has been proved that this device can provide stable and accurate real-time motion capture results, provide statistical data that can help rehabilitation doctors conduct functional evaluation, and is of great significance for rehabilitation doctors to formulate training plans and carry out rehabilitation training for patients. It is a crucial attempt in the field of "Internet of things + rehabilitation medicine."

Data Availability

The data used to support the findings of this study are available from the corresponding author upon request.

Conflicts of Interest

The authors declare that they have no conflicts of interest.

Acknowledgments

The study was supported by the Anhui Province Philosophy and Social Science Planning project "Research on the Institutional Guarantee and Policy Support of Mass Sports Development in Anhui Province under the Prerequisite of Comprehensive Well-off society" (AHSKQ2020D108); Key Projects of Humanities and Social Sciences Research in Universities in Anhui Province: Research on high-quality Integrated Development of Sports Industry in the Yangtze River Delta region under the new pattern of "double cycle" (SK2021A0411); Fuyang Normal University 2021 Key Youth Talent Project "Research on the Development Path of Ecological Sports in Anhui Province under the New Normal" (rcxm202115); and Anhui Province Quality Engineering Project: New Liberal Arts, New Medical Research and Reform Practice Project (2020wyxm134).

References

- [1] X. Li, Z. Zhu, N. Shen, W. Dai, and Y. Hu, "Deeply feature learning by cmac network for manipulating rehabilitation robots," *Future Generation Computer Systems*, vol. 121, no. 1, pp. 19–24, 2021.
- [2] M. Wang, R. Ou, and Y. Wang, "Multiplicatively weighted voronoi-based sensor collaborative redeployment in software-defined wireless sensor networks," *International Journal of Distributed Sensor Networks*, vol. 18, no. 3, article 155014772114057, 2022.
- [3] N. D. Silverberg and G. L. Iverson, "Reply to letter to the editor: expert panel survey to update the American congress of rehabilitation medicine definition of mild traumatic brain injury," *Archives of Physical Medicine and Rehabilitation*, vol. 102, no. 6, p. 1239, 2021.
- [4] H. Y. Zhao, J. Q. Han, H. T. Liu, Q. Wang, and D. Hu, "Effects of hand continuous passive motion system combined with functional training and pressure gloves in treating early scar contracture after burn on the back of the hand," *Chinese journal of burns*, vol. 37, no. 4, pp. 1–8, 2021.
- [5] R. Dionisio, P. Torres, A. Ramalho, and R. Ferreira, "Magneto-resistive sensors and piezoresistive accelerometers for vibration measurements: a comparative study," *Journal of Sensor and Actuator Networks*, vol. 10, no. 1, p. 22, 2021.
- [6] D. Chen, Q. Liu, Z. Han et al., "Sensor-actuators: 4D printing strain self-sensing and temperature self-sensing integrated sensor-actuator with bioinspired gradient gaps (Adv. Sci. 13/2020)," *Advanced Science*, vol. 7, no. 13, p. 2070075, 2020.
- [7] D. Jang, G. Jung, Y. Jeong, S. Hong, and J. H. Lee, "Barometric pressure sensor with air pocket integrated with mosfets on the same substrate," *Journal of Semiconductor Technology and Science*, vol. 20, no. 3, pp. 305–310, 2020.
- [8] Q. Duan, Y. Mao, H. Zhang, and W. Xue, "Add-on integration module-based proportional-integration-derivative control for higher precision electro-optical tracking system," *Transactions of the Institute of Measurement and Control*, vol. 43, no. 6, pp. 1347–1362, 2021.
- [9] Y. Yu, R. Chen, L. Chen, W. Li, and H. Zhou, "H-WPS: hybrid wireless positioning system using an enhanced WI-FI FTM/RSSI/MEMS sensors integration approach," *IEEE Internet of Things Journal*, vol. 99, pp. 1–1, 2021.
- [10] Y. Bouteraa, I. B. Abdallah, and A. Elmogy, "Design and control of an exoskeleton robot with emg-driven electrical stimulation for upper limb rehabilitation," *Industrial Robot: the international journal of robotics research and application*, vol. 47, no. 4, pp. 489–501, 2020.
- [11] X. Chen and Z. Feng, "Order spectrum analysis enhanced by surrogate test and Vold-Kalman filtering for rotating machinery fault diagnosis under time-varying speed conditions," *Mechanical Systems and Signal Processing*, vol. 154, no. 331, p. 107585, 2021.
- [12] G. Sonowal and K. S. Kuppusamy, "PhiDMA - a phishing detection model with multi-filter approach," *Journal of King Saud University - Computer and Information Sciences*, vol. 32, no. 1, pp. 99–112, 2020.
- [13] G. Kim, S. Y. Lee, J. S. Oh, and S. Lee, "Deep learning-based estimation of the unknown road profile and state variables for the vehicle suspension system," *IEEE Access*, vol. 9, pp. 13878–13890, 2021.
- [14] N. Sai, T. Zhang, J. Wu, and W. J. Han, "Noise-induced blood-labyrinth-barrier trauma of guinea pig and the protective effect of matrix metalloproteinase inhibitors," *Chinese journal of otorhinolaryngology head and neck surgery*, vol. 55, no. 4, pp. 363–370, 2020.
- [15] S. Elsheikh, A. Fish, and D. Zhou, "Exploiting spatial information to enhance DTI segmentations via spatial fuzzy c-means with covariance matrix data and non-Euclidean metrics," *Applied Sciences*, vol. 11, no. 15, p. 7003, 2021.
- [16] G. Gao, S. Gao, G. Hu, and X. Peng, "Spectral redshift observation-based sins/srs/cns integration with an adaptive fault-tolerant cubature Kalman filter," *Measurement Science and Technology*, vol. 32, no. 9, p. 095103, 2021.
- [17] E. Angelakis, A. Andreopoulou, and A. Georgaki, "Multisensory biofeedback: promoting the recessive somatosensory control in operatic singing pedagogy," *Biomedical Signal Processing and Control*, vol. 66, no. 3, article 102400, 2021.
- [18] G. Dhiman, V. Kumar, A. Kaur, and A. Sharma, "Don: deep learning and optimization-based framework for detection of novel coronavirus disease using x-ray images,"

Retraction

Retracted: Financing Efficiency Calculation of Energy Enterprises Based on Internet of Things

Journal of Sensors

Received 13 September 2023; Accepted 13 September 2023; Published 14 September 2023

Copyright © 2023 Journal of Sensors. This is an open access article distributed under the Creative Commons Attribution License, which permits unrestricted use, distribution, and reproduction in any medium, provided the original work is properly cited.

This article has been retracted by Hindawi following an investigation undertaken by the publisher [1]. This investigation has uncovered evidence of one or more of the following indicators of systematic manipulation of the publication process:

- (1) Discrepancies in scope
- (2) Discrepancies in the description of the research reported
- (3) Discrepancies between the availability of data and the research described
- (4) Inappropriate citations
- (5) Incoherent, meaningless and/or irrelevant content included in the article
- (6) Peer-review manipulation

The presence of these indicators undermines our confidence in the integrity of the article's content and we cannot, therefore, vouch for its reliability. Please note that this notice is intended solely to alert readers that the content of this article is unreliable. We have not investigated whether authors were aware of or involved in the systematic manipulation of the publication process.

Wiley and Hindawi regrets that the usual quality checks did not identify these issues before publication and have since put additional measures in place to safeguard research integrity.

We wish to credit our own Research Integrity and Research Publishing teams and anonymous and named external researchers and research integrity experts for contributing to this investigation.

The corresponding author, as the representative of all authors, has been given the opportunity to register their agreement or disagreement to this retraction. We have kept a record of any response received.

References

- [1] J. Wu and Y. Zhang, "Financing Efficiency Calculation of Energy Enterprises Based on Internet of Things," *Journal of Sensors*, vol. 2022, Article ID 7262788, 8 pages, 2022.

Research Article

Financing Efficiency Calculation of Energy Enterprises Based on Internet of Things

JingJing Wu¹ and YaJuan Zhang²

¹College of Information Engineering, Fuyang Normal University, Fuyang, Anhui 236000, China

²Business College, Fuyang Normal University, Fuyang, Anhui 236000, China

Correspondence should be addressed to JingJing Wu; 2020020551@stu.cdut.edu.cn

Received 14 July 2022; Revised 9 August 2022; Accepted 16 August 2022; Published 27 August 2022

Academic Editor: Haibin Lv

Copyright © 2022 JingJing Wu and YaJuan Zhang. This is an open access article distributed under the Creative Commons Attribution License, which permits unrestricted use, distribution, and reproduction in any medium, provided the original work is properly cited.

In order to conduct a special study on the financing efficiency of a certain industry, the authors propose a method for calculating the financing efficiency of energy enterprises based on the Internet of Things. Combining the DEA method with the Bootstrap method, taking the IoT data of 30 SME boards and 30 energy companies listed on the ChiNext listed in 2010 as a research sample, and using R language and Deap2.1 software, the financing efficiency from 2011 to 2015 is calculated. Experimental results show that from 2011 to 2015, only 28.3% of the enterprises reached the effective state of technical efficiency on average, and the financing efficiency of energy enterprises was generally inefficient. The pure technical efficiency value of the whole enterprise decreases year by year, and its technical efficiency value lower than its scale efficiency is the main reason that its technical efficiency is generally not high.

1. Introduction

Affected by the financial crisis, the world situation is complex and volatile, and economic growth lacks impetus [1]. Although the financial crisis occurred in the United States, with the intensification of the European sovereign debt crisis, the global financial crisis also shifted to Europe. In the past few decades, Asian economies, especially East Asian economies, have been the most dynamic in global economic growth. Looking at the overall situation, although the international situation is turbulent and my country is also hit by the financial crisis, the development environment facing my country is generally good. The first 20 years of the 21st century or even longer is a period of strategic opportunities that my country needs to seize and make full use of, and it is also a period of overcoming difficulties in the adjustment of my country's economic structure.

After more than 30 years of development, China has grown into a big manufacturing country. The manufacturing industry has played an important role in supporting economic and social development and meeting people's living

needs; the prosperity and development of the manufacturing industry have driven the rise of China's GDP [2]. However, with the development of economy, some enterprises in our country have the problem of overcapacity. In terms of quantitative standards, the capacity utilization rate of traditional industries such as steel, cement, electrolytic aluminum, flat glass, and coke is between 70% and 75%. Internationally, the capacity utilization rate of a normal competitive market should exceed 80%-85%.

In order to solve the problem of overcapacity of enterprises, we should first start with improving the quality of enterprises. Secondly, the excess production capacity of a group of enterprises can be digested through mergers and reorganizations, and a group of backward production capacity can be eliminated through the survival of the fittest. Finally, companies can also go overseas to develop and transfer production capacity. In the market economy environment, the product has a moderate surplus, which can stimulate market competition and can also promote the improvement and progress of enterprise management level. However, overcapacity will not only cause waste of resources

and labor but also be detrimental to the long-term development of enterprises and even affect the healthy operation of the economy. Enterprises in the industrial industry have difficulties in their own development and low profits, and a considerable number of enterprises are in a state of loss. Some companies still need to produce even knowing that they are losing money; in order to sell their products, they fight a “price war”; this leads to vicious competition among enterprises [3]. Figure 1 shows the financing processing system and method. Vicious competition among enterprises will lead to protectionism in some places, resulting in market segmentation. If this happens, it is very unfavorable for our country to change the mode of economic development and adjust the economic structure. Therefore, resolving the problem of overcapacity in enterprises has become one of the priorities for adjusting the economic structure and transforming the mode of economic development at present and in the future.

2. Literature Review

Chau and others believe that, without taking corporate tax into account, first of all, the size of an enterprise’s debt will not affect the value of the enterprise; that is, the financing structure of the enterprise has nothing to do with the value of the enterprise. Secondly, the cost of equity of a debt-burdened company is the sum of the cost of equity of a non-debt-burdened company with the same risk and the risk premium, and the risk premium is also determined by the cost of equity, debt financing cost, and risk premium of a non-debt-burdened company; the proportion of property rights of the enterprise is determined [4]. Jwo et al. believe that if personal income tax is taken into account, the interest expenses incurred by enterprises due to debt financing will be deducted from the total tax payment, and the effect of the increase in enterprise value will be reduced, and the tax shield of debt will be reduced; the effect is not so obvious [5]. Zhang et al. proposed that enterprises should not only consider the tax saving effect brought by interest deduction when choosing debt financing methods but should also consider the increase in financial costs caused by interest expenses and the agency cost pressure on company managers because of growing conflicts between creditors and the company’s original shareholders. Bankruptcy is inevitable if the financial burden and agency costs faced by the business are large enough that the business itself cannot bear it. Therefore, it is concluded that the optimal debt financing structure of an enterprise should be when its debt burden is equal to the marginal cost of agency problems and the marginal benefit brought by its tax savings [6]. Sidloski and Diab considered the contradiction between corporate shareholders and creditors caused by the increase in the proportion of debt financing and also took into account the issue of entrustment and agency within the company; that is, because the principal is the shareholder of the company, the agency cost problem is caused by the unequal information held by the managers of the agency companies and the agency companies [7]. Modisane and Jokonya believe that information asymmetry exists not only within share-

holders and managers but also between companies and external investors. When a company chooses equity or debt financing, investors will have a positive or negative impression of the value of the company, so that the actual value of the company is overvalued or undervalued to varying degrees. Specifically, investors believe that stocks will only be issued when the operating conditions of the company are not ideal; of course, investors will not buy shares at this time, and the value of the company is undervalued [8]. Gao and others believe that the financing efficiency of an enterprise should be the ability of the enterprise to obtain funds, and the size of the financing ability determines the financing efficiency of the enterprise. Before China entered the market economy, the financing efficiency of enterprises could not be reflected independently, and it was integrated with the overall economic efficiency of the country; in modern economic society, the level of corporate financing ability is an important manifestation of the efficiency of economic development [9].

From the above review, it can be seen that the existing research literature rarely conducts special research on the financing efficiency of a certain industry, and there is not much improvement in research methods. Based on this, the authors select the energy industry that has received high attention in recent years and add the Bootstrap method to evaluate the financing efficiency of enterprises on the basis of using the DEA method.

3. Research Methods

3.1. Research Method Design of Financing Efficiency of Energy Enterprises

(1) Model establishment

The DEA (Data Envelope Analysis) method, namely, the data envelopment analysis method, is based on the concept of relative efficiency and is a method of evaluating the relative effectiveness or benefit of similar decision-making units (DMU) according to multi-indicator input and multi-indicator output; this method can divide the efficiency of the evaluation unit into technical efficiency (TE), pure technical efficiency (PTE), and scale efficiency (SE), and the relationship between the three efficiencies is $PTE = TE/SE$; therefore, it has an absolute advantage in processing multi-input-multioutput effectiveness evaluation [10]. The basic evaluation principle of the DEA method is as follows: take each enterprise as an efficiency evaluation unit (DMU), evaluate the efficiency of each DMU according to the input and output indicators, and determine an efficiency after comprehensively considering the efficiency of all DMUs, the frontier surface, and then according to the distance between each DMU and the efficiency frontier surface; it is determined whether the efficiency of the evaluation unit is DEA effective.

Although the DEA method has many advantages in efficiency evaluation, because what it measures is only a kind of “relative efficiency,” an upper limit of “absolute efficiency,” and a biased and inconsistent estimator, the true value of efficiency should be below this “relative efficiency” [11].

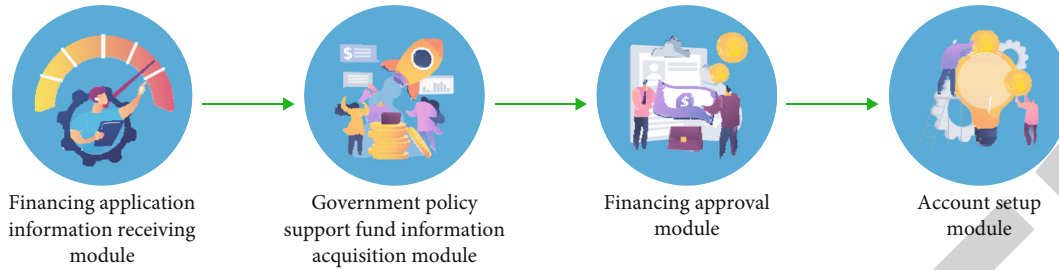


FIGURE 1: Financing processing system and method.

The Bootstrap-DEA method solves the defects of the DEA method; the main steps of the method are as follows:

- (1) Measure the efficiency values $\hat{\theta}_j$ and $j = 1, 2, \dots, n$ of each decision-making unit under the DEA method
- (2) Using the Bootstrap method, repeated sampling with replacement in the original efficiency value $\hat{\theta}_j$ produces a sample $(\theta^*_{1b}, \dots, \theta^*_{nb})$ of size n , where b represents the number of iterations of Bootstrap and $b = 1, \dots, B$
- (3) Calculate the simulated sample (X^*_{jb}, X_j) , where $X^*_{jb} = \hat{\theta}_j / (\theta^*_{jb}) \cdot X_j, j = 1, \dots, n$
- (4) Using such a simulated sample, calculate the efficiency values θ^*_j and $j = 1, \dots, n$ using the DEA method
- (5) Repeat steps (2) to (4) times for each decision-making unit (take = 2000) to generate a series of efficiency values θ^*_{jb} and $b = 1, \dots, B$
- (6) Correct the estimated deviation of DEA efficiency value: $\text{bias}(\hat{\theta}_j) = E(\hat{\theta}_j) - \hat{\theta}_j$
- (7) $\widehat{\text{Bias}}(\hat{\theta}_j) = B - 1 \sum_{b=1}^B \hat{\theta}^*_{jb} - \hat{\theta}_j$, the corrected efficiency value is $\bar{\theta}_j = \hat{\theta}_j - \widehat{\text{Bias}}(\hat{\theta}_j) = 2\hat{\theta}_j - B - 1 \sum_{b=1}^B \hat{\theta}^*_{jb}$ [12, 13]
- (2) Construction of evaluation index system

The DEA model belongs to the multi-input-multioutput relative efficiency evaluation model; whether the selection of model input and output indicators is reasonable will directly affect the evaluation effect of the model. According to the characteristics of the energy industry and the experience of previous index selection, the authors constructed the following input and output index system, as shown in Table 1.

- (3) Data source and processing

The authors take energy companies as research objects and, on the basis of ensuring the integrity and continuity of corporate financial data, selected 30 SME board and 30 ChiNext energy companies listed in 2010 as research sam-

ples [14, 15]. The study interval span was selected from 2011 to 2015. The financial index data of the sample companies involved in the research all come from wind information financial terminal. Since the values of the input and output indicators cannot be negative values when using the DEA method, the authors perform dimensionless processing on all the indicator data; the specific processing method is as follows (1):

$$x^*_{ij} = \frac{x_{ij} - \min_{ij}}{\max_{ij} - \min_{ij}} \times 0.9 + 0.1. \quad (1)$$

Among them, x_{ij} represents the i input or output index of the j th decision-making unit; \max_{ij} and \min_{ij} , respectively, represent the maximum or minimum value of the i input or output indicators of the j th decision-making unit [16].

4. Result Analysis

4.1. Bootstrap-DEA of Overall Financing Efficiency

- (1) Analysis of the overall financing efficiency under the DEA model

First, through the rDEA package and Deap2.1 software in R language, the input and output data of 30 SME boards and 30 GEM energy companies from 2011 to 2015 were analyzed and processed by the DEA method; finally, the calculation results of technical efficiency (TE), pure technical efficiency (PTE), and scale efficiency (SE) of 60 enterprises are obtained, as shown in Tables 2 and 3 below.

According to the calculation results of the DEA model in Tables 2 and 3, it can be seen from the average from 2011 to 2015 that the financing technical efficiency of the sample energy enterprises on the small and medium-sized board and the ChiNext board reached 1; that is to say, the number of companies that achieved DEA is 8 and 9, respectively, and the two together account for 28.3% of the total number of samples; this shows that less than 1/3 of the sample companies' financing behavior has reached a "relatively efficient" state with no redundancy in input and maximizing output; for most companies, the financing efficiency is not ideal, and its input and output still have room for further improvement. In addition, we can see from the average efficiency that whether it is a small and medium-sized board or a

TABLE 1: Input and output index system of financing efficiency of energy enterprises.

Indicator category	Indicator name	Indicator meaning
Input indicator	Total assets (X_1)	It reflects the size of the overall asset size of the enterprise and reflects the level of the enterprise's financing ability
	Assets and liabilities (X_2)	Equal to the total assets divided by the total liabilities, is a comprehensive evaluation index to measure the structure of an enterprise's assets and liabilities
	Financial expenses (X_3)	It reflects the interest expense caused by financing in the business process of the enterprise, that is, the cost of using funds
	Return on net assets (Y_1)	Net profit divided by total net assets reflects the company's ability to use assets to obtain income and also measures the income of shareholders' equity
Output indicator	Total asset turnover (Y_2)	It reflects the utilization efficiency of all the assets owned by the enterprise and measures the capital operation ability and management level of the enterprise
	Main business income growth rate (Y_3)	It reflects the growth and development ability of the enterprise; the larger the index, the stronger the profitability of the enterprise
	Growth rate of intangible assets (Y_4)	The growth rate of intangible assets of energy enterprises, which shows the transformation efficiency of their research and development investment

TABLE 2: Calculation results of DEA financing efficiency of small and medium-sized energy enterprises.

Years	Number of SMEs with DEA valid (percentage)		
	TE	PTE	SE
2011	9 (15.0%)	12 (20.0%)	9 (15.0%)
2012	8 (13.3%)	14 (23.3%)	8 (13.3%)
2013	6 (10.0%)	10 (16.7%)	6 (10.0%)
2014	9 (15.0%)	10 (16.7%)	11 (18.3%)
2015	9 (15.0%)	12 (20.0%)	11 (18.3%)
Average number of homes	8 (13.7%)	12 (19.3%)	9 (15.0%)
Efficiency mean	0.787	0.841	0.935

TABLE 3: Calculation results of DEA financing efficiency of GEM energy companies.

Years	Number of effective DEA companies on the Growth Enterprise Market (proportion)		
	TE	PTE	SE
2011	8 (13.3%)	12 (20.0%)	8 (13.3%)
2012	9 (15.0%)	11 (18.3%)	9 (15.0%)
2013	9 (15.0%)	13 (21.7%)	10 (16.7%)
2014	1 (18.3%)	17 (28.3%)	12 (20.0%)
2015	7 (11.7%)	14 (23.3%)	7 (11.7%)
Average number of homes	9 (14.6%)	13 (22.3%)	9 (15.3%)
Efficiency mean	0.837	0.904	0.926

ChiNext board, the main reason for the low technical efficiency is that the pure technical efficiency is lower than the scale efficiency [17].

(2) Analysis of overall financing efficiency after modification by the Bootstrap method

As mentioned above, in order to reduce the negative impact of the DEA model due to its defects in the efficiency measurement and make the results more reliable, the authors use the Benchmarking package in the R language,

set the number of Bootstrap iterations to 2000, set the confidence interval to 95%, and then correct the original DEA efficiency value. According to the revised efficiency value, as shown in Table 4 (due to limited space, only the average efficiency of all sample companies in each year is listed here), we found that the financing efficiency originally reached a "relatively efficient" state under the DEA method enterprise [18]. At this time, each efficiency value did not reach 1, and the efficiency values of all enterprises after Bootstrap correction were lower than the efficiency values under the DEA method, which indicated that the overall financing efficiency

TABLE 4: Bootstrap-DEA method revised financing efficiency calculation results.

Years	Annual average technical efficiency of SMEs					Annual average technical efficiency of GEM companies				
	Original TE value	Correction value	Difference	Lower boundary	Upper boundary	Original TE value	Correction value	Difference	Lower boundary	Upper boundary
2011	0.797	0.707	0.09	0.646	0.781	0.802	0.71	0.092	0.643	0.786
2012	0.841	0.769	0.071	0.713	0.831	0.839	0.768	0.071	0.712	0.827
2013	0.769	0.695	0.074	0.641	0.757	0.862	0.773	0.089	0.706	0.848
2014	0.776	0.702	0.075	0.646	0.765	0.881	0.789	0.093	0.720	0.867
2015	0.753	0.654	0.098	0.593	0.736	0.800	0.703	0.097	0.640	0.783
Mean	0.787	0.705	0.082	0.647	0.772	0.837	0.749	0.088	0.695	0.831

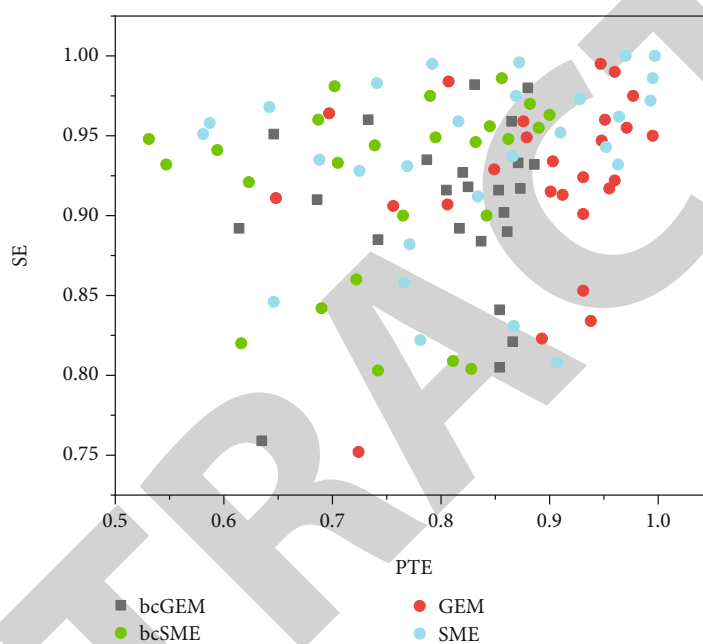


FIGURE 2: The mean scatter plot of pure technical efficiency and scale efficiency from 2011 to 2015.

of the sample enterprises after the correction was better than the calculation results of the DEA method.

4.2. Analysis of Pure Technical Efficiency and Scale Efficiency.

By decomposing technical efficiency, we can specifically analyze the pure technical efficiency and scale efficiency of enterprises [19]. As shown in Figure 2 (GEM is the ChiNext board, SME is the small and medium-sized board, and the black and white dots are the values before and after correction), from the distribution of the average pure technical efficiency value and the average scale efficiency value of each sample enterprise from 2011 to 2015, the following features can be found:

- (1) Scale efficiency (SE) is significantly better than pure technical efficiency (PTE)

It can be clearly seen from the distribution shape of the scatter points that almost all sample points are concentrated in the upper half of the graph, whether before correction (solid black points) or after correction (open white points),

that is, the scale efficiency value (0.75, 1.0) range, and there is almost no sample point distribution below 0.75; although the sample points in the (0.75, 1.0) interval are more densely distributed than the (0.5, 0.75) interval for pure technical efficiency, it is still not as good as the overall distribution of scale efficiency [20]. This further illustrates that the financing efficiency of most energy companies is mainly limited by their lower pure technical efficiency. Therefore, when the scale of financing reaches a relatively ideal state, how to improve their pure technical efficiency and effectively manage and make good use of funds is the key point that energy companies should pay attention to in the future.

- (2) The Bootstrap correction efficiency value is lower than the original efficiency value

As shown in Figure 2, before the original financing efficiency value is revised, most of the black solid sample points are concentrated in the upper right area, that is, closer to the two "effective frontiers" with an efficiency value of 1, and some sample points just fall on the "effective frontier." After

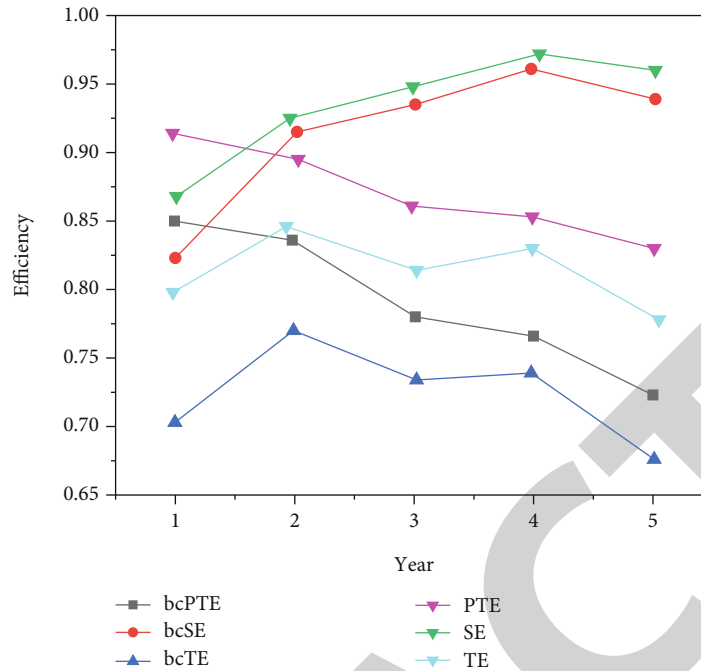


FIGURE 3: Trends in the overall financing efficiency of energy companies from 2011 to 2015.

correcting the efficiency value, it can be found that there is no white hollow sample point distribution on the “effective frontier” and its overall left shift, but the downward shift is not obvious [21]. The corrected efficiency value provides a more accurate measurement result and the change in the distribution shape before and after the scatter; it also confirms the previous finding that the contribution of scale efficiency to technical efficiency is greater than that of pure technical efficiency [22].

4.3. Trend Analysis of Overall Financing Efficiency. The financing efficiency trend of all 60 SME and ChiNext energy sample companies before and after the revision is shown in Figure 3 [23]. As can be seen from the figure, the revised technical efficiency (bcTE) values from 2011 to 2015 were 0.708, 0.768, 0.732, 0.740, and 0.675, showing a slight and slow decreasing trend in the fluctuating state as a whole [24]. As far as the revised pure technical efficiency (bcPTE) is concerned, from 0.856 in 2011 to 0.726 in 2015, it shows a significant decline in technical efficiency. Comparatively speaking, the scale efficiency showed a different increasing trend year by year from 2011 to 2014, but it showed a downward trend in 2015 [25].

In addition, we can notice that compared with the original efficiency values, the three efficiency values after the Bootstrap method correction have not changed in trend, and compared to the technical efficiency and pure technical efficiency, the correction of scale efficiency is the slightest. Therefore, for energy companies, reversing the declining trend of pure technical efficiency and maintaining the growth trend of scale efficiency are the key to improving the overall financing efficiency, and the former is more important.

5. Conclusion

By using the DEA method, the authors measured the financing efficiency of 30 SME board and 30 ChiNext energy companies listed in 2010 from 2011 to 2015 and introduced the Bootstrap method to improve the technical efficiency and pure technology of enterprises, the measurement accuracy of efficiency, and scale efficiency; on this basis, the following research conclusions are drawn: first, the overall financing efficiency of my country’s energy enterprises is in a state of inefficiency, more than 70% of the enterprises’ financing behavior cannot reach the effective level of DEA, and the financing efficiency after the Bootstrap method is revised. Second, the financing inefficiency of energy companies is mostly caused by their pure technical inefficiency; therefore, the capital management and application technology of enterprises need to be improved urgently. Third, from the perspective of the vertical time trend, although the scale efficiency shows an increasing trend as a whole, the pure technical efficiency is decreasing year by year.

Energy is a key industry that the world pays attention to at present; under the background of “mass entrepreneurship and innovation,” China has also given policy support in many aspects of the energy industry; however, based on the above research, it can be seen that the financing efficiency of energy companies is generally low, which will undoubtedly bring difficulties to their future development, which is a small hindrance. In view of this, the authors provide the following policy suggestions: first, enterprises should use funds reasonably and effectively, increase their own R&D investment, and use the raised funds more for technological innovation. Secondly, clarify the purpose of

financing, correct the motivation of financing, and avoid blind expansion of enterprise scale in the capital market. Finally, while improving the issuance mechanism and strengthening postevent supervision, the state still strives to improve the construction of a multilevel capital market system; a capital market with a complete structure and rich levels is the demand for corporate financing and development; at the same time, it is also a powerful guarantee for enterprises to have a good financing environment.

Data Availability

The data used to support the findings of this study are available from the corresponding author upon request.

Conflicts of Interest

The authors declare that they have no conflicts of interest.

Acknowledgments

This work was supported by University Excellent Talents Support Program in Anhui Province, Research on the practical path of protecting the interests of small and medium investors under the registration system of stock issuance (Project No. gxyq2021078).

References

- [1] G. Li, F. Liu, A. Sharma et al., "Research on the natural language recognition method based on cluster analysis using neural network," *Mathematical Problems in Engineering*, vol. 2021, Article ID 9982305, 13 pages, 2021.
- [2] D. Selva, D. Pelusi, A. Rajendran, and A. Nair, "Intelligent network intrusion prevention feature collection and classification algorithms," *Algorithms*, vol. 14, no. 8, p. 224, 2021.
- [3] J. Chen, J. Liu, X. Liu, X. Xu, and F. Zhong, "Decomposition of toluene with a combined plasma photolysis (CPP) reactor: influence of UV irradiation and byproduct analysis," *Plasma Chemistry and Plasma Processing*, vol. 41, no. 1, pp. 409–420, 2020.
- [4] N. T. Chau, H. Deng, and R. Tay, "A perception-based model for mobile commerce adoption in vietnamese small and medium-sized enterprises," *Journal of Global Information Management*, vol. 29, no. 1, pp. 44–67, 2021.
- [5] J. S. Jwo, C. S. Lin, and C. H. Lee, "An interactive dashboard using a virtual assistant for visualizing smart manufacturing," *Mobile Information Systems*, vol. 2021, no. 1, 9 pages, 2021.
- [6] C. Zhang, J. He, C. Bai, X. Yan, and H. Zhang, "How to use advanced fleet management system to promote energy saving in transportation: a survey of drivers' awareness of fuel-saving factors," *Journal of Advanced Transportation*, vol. 2021, no. 3, 19 pages, 2021.
- [7] M. Sidloski and E. Diab, "Understanding the effectiveness of bus rapid transit systems in small and medium-sized cities in North America," *Transportation Research Record*, vol. 2674, no. 10, pp. 831–845, 2020.
- [8] P. Modisane and O. Jokonya, "Evaluating the benefits of cloud computing in small, medium and micro-sized enterprises (SMMEs)," *Procedia Computer Science*, vol. 181, no. 1, pp. 784–792, 2021.
- [9] L. G. Gao, D. G. Fleming, D. G. Truhlar, and X. Xu, "Large anharmonic effects on tunneling and kinetics: reaction of propane with muonium," *Journal of Physical Chemistry Letters*, vol. 12, no. 17, pp. 4154–4159, 2021.
- [10] T. Duerinck, G. Verberkmoes, C. Fritz, M. Leman, and W. V. Paepegem, "Listener evaluations of violins made from composites," *The Journal of the Acoustical Society of America*, vol. 147, no. 4, pp. 2647–2655, 2020.
- [11] F. Dillinger, F. Formann, and G. Reinhart, "Lean production und Industrie 4.0 in der Produktion," *ZWF Zeitschrift fuer Wirtschaftlichen Fabrikbetrieb*, vol. 115, no. 10, pp. 738–741, 2020.
- [12] L. Li, J. Huang, L. Hui, F. Guan, and Y. Chen, "Two lathyrane diterpenoid stereoisomers containing an unusualtrans-gem-dimethylcyclopropane from the seeds of *Euphorbia lathyris*," *RSC Advances*, vol. 11, no. 5, pp. 3183–3189, 2021.
- [13] V. Yaghoubi, L. Cheng, W. V. Paepegem, and M. Kersemans, "A novel multi-classifier information fusion based on Dempster–Shafer theory: application to vibration-based fault detection," *Structural Health Monitoring*, vol. 21, no. 2, pp. 596–612, 2022.
- [14] H. Ahmadi, M. Hajikazemi, and W. V. Paepegem, "A computational study about the effects of ply cracking and delamination on the stiffness reduction of damaged lamina and laminate," *International Journal of Damage Mechanics*, vol. 31, no. 3, pp. 325–347, 2022.
- [15] M. Kaabar, V. Kalvandi, N. Eghbali, M. Samei, Z. Siri, and F. Martínez, "A generalized ML-Hyers-Ulam stability of quadratic fractional integral equation," *Nonlinear Engineering*, vol. 10, no. 1, pp. 414–427, 2021.
- [16] A. Y. Astapov, I. P. Krivolapov, D. V. Akishin, A. S. Gordeev, and A. A. Naydenov, "Improvement of energy efficiency of agricultural enterprises through the survey of high-voltage transmission lines using unmanned aerial vehicles," *IOP Conference Series: Earth and Environmental Science*, vol. 845, no. 1, article 012156, 2021.
- [17] D. Wang and C. Tellambura, "Performance analysis of energy beamforming WPCN links with channel estimation errors," *Communications Society*, vol. 1, pp. 1153–1170, 2020.
- [18] N. P. Lisa, Z. Zuraihan, R. Fernand, and D. Siska, "Estimation of energy consumption efficiency in office rooms cooling systems to create thermal comfort for the user," *IOP Conference Series: Earth and Environmental Science*, vol. 738, no. 1, article 012016, 2021.
- [19] W. Shao, K. Yang, and X. Bai, "Impact of financial subsidies on the R&D intensity of new energy vehicles: a case study of 88 listed enterprises in China," *Energy Strategy Reviews*, vol. 33, no. 4, article 100580, 2021.
- [20] K. V. Osintsev and A. N. Shishkov, "Increasing the energy efficiency of the industrial enterprise technological and mechanical equipment due to the use of converter steam," *IOP Conference Series: Materials Science and Engineering*, vol. 1064, no. 1, p. 012033, 2021.
- [21] I. V. Dolotovskiy, E. A. Larin, and B. A. Semyonov, "Polygeneration plants in the energy complex of oil and gas enterprises: the concept of synthesis and a method for assessing efficiency," *Journal of Physics: Conference Series*, vol. 1652, no. 1, article 012035, 2020.
- [22] Y. Swami, N. Singh, and U. Soni, "Performance measurement of various ai techniques for energy estimation and its optimisation using sensitivity analysis," *Intelligent Enterprise*, vol. 9, no. 2, p. 181, 2022.

Retraction

Retracted: Design of Music Teaching System Based on Internet of Things Multimedia Intelligent Platform

Journal of Sensors

Received 13 September 2023; Accepted 13 September 2023; Published 14 September 2023

Copyright © 2023 Journal of Sensors. This is an open access article distributed under the Creative Commons Attribution License, which permits unrestricted use, distribution, and reproduction in any medium, provided the original work is properly cited.

This article has been retracted by Hindawi following an investigation undertaken by the publisher [1]. This investigation has uncovered evidence of one or more of the following indicators of systematic manipulation of the publication process:

- (1) Discrepancies in scope
- (2) Discrepancies in the description of the research reported
- (3) Discrepancies between the availability of data and the research described
- (4) Inappropriate citations
- (5) Incoherent, meaningless and/or irrelevant content included in the article
- (6) Peer-review manipulation

The presence of these indicators undermines our confidence in the integrity of the article's content and we cannot, therefore, vouch for its reliability. Please note that this notice is intended solely to alert readers that the content of this article is unreliable. We have not investigated whether authors were aware of or involved in the systematic manipulation of the publication process.

Wiley and Hindawi regrets that the usual quality checks did not identify these issues before publication and have since put additional measures in place to safeguard research integrity.

We wish to credit our own Research Integrity and Research Publishing teams and anonymous and named external researchers and research integrity experts for contributing to this investigation.

The corresponding author, as the representative of all authors, has been given the opportunity to register their agreement or disagreement to this retraction. We have kept a record of any response received.

References

- [1] B. Xie, "Design of Music Teaching System Based on Internet of Things Multimedia Intelligent Platform," *Journal of Sensors*, vol. 2022, Article ID 6282581, 7 pages, 2022.

Research Article

Design of Music Teaching System Based on Internet of Things Multimedia Intelligent Platform

Bin Xie 

Guangxi Arts University, Nanning, Guangxi 530000, China

Correspondence should be addressed to Bin Xie; 201903506@stu.ncwu.edu.cn

Received 10 July 2022; Revised 5 August 2022; Accepted 10 August 2022; Published 27 August 2022

Academic Editor: Haibin Lv

Copyright © 2022 Bin Xie. This is an open access article distributed under the Creative Commons Attribution License, which permits unrestricted use, distribution, and reproduction in any medium, provided the original work is properly cited.

In order to improve the practical and popularization value of the multimedia vocal music teaching system, the author proposes a teaching system based on the Internet of Things multimedia intelligent platform. Mainly use Visual C++ to realize the acquisition, playback, and display of audio and realize the real-time modification of the sound wave waveform on the computer and also add the function of vocal score. Experimental results show that in the pitch comparison, the standard fundamental frequency average value of the fundamental frequency track of the two pieces of music is obtained by the cepstral method: $\text{avgF0} = 143.12\text{HZ}$ and the average fundamental frequency of the trial singing: $\text{avgF0} = 142.05\text{HZ}$. The average distance and score of each parameter of the testers are $\text{mindisv} = 726.126$ for pitch intensity, $\text{path length} = 144$; $\text{mindisp} = 4.51987$, $\text{path length} = 163$ for pitch, $\text{breath smoothness} = 484.20$. *Conclusion.* This method not only improves the intuitiveness and interaction of vocal music teaching, but also increases the interest of vocal music teaching.

1. Introduction

Since entering the twenty-first century, the popularization of computer technology has reached an unprecedented speed, and people's life has gradually become inseparable from computer technology. The information technology and digital technology it brings have fully covered our work and life. The same is true in the field of music; digital technology to assist music production and music editing has become a very common phenomenon in the music industry, and several famous software companies in the world have launched very practical music production software; the CD we hear now, MP3, and other music are produced through these software [1]. Music production software can help music producers set and edit various timbres, volume, pitch, rhythm, etc., and finally produce excellent musical sounds. In China's digital multimedia technology-assisted music teaching, in recent years, it has also achieved considerable development; all kinds of large, medium, and small schools in China have also started to use multimedia technology to assist the classroom teaching of music. The courses of music appreciation, music theory,

music composition, and music production are the most common places to use multimedia teaching; after the use of multimedia-assisted teaching, these courses have achieved good teaching results. It improves the quality and efficiency of music teaching, expands the popularization of music teaching, and is loved by the taught group. However, the introduction of digital technology into music teaching has also encountered many problems; the most important ones are focusing only on the use of multimedia technology while ignoring the use of other advantages of digital technology. The status quo of music teaching is that most schools in China focus on using multimedia digital technology to teach music appreciation courses and basic theory courses [2, 3]. Convenient and convenient multimedia technology is only a technical means in digital technology, and it can only be undertaken in music teaching, the teaching work of this part of popularizing music and improving the efficiency of music teaching, its use does not maximize the advantages of digital technology-assisted music teaching, and it does not well reflect the scientific, intuitive, interactive, and visual advantages of digital technology. In view of the current situation of

music education in China, this subject wants to conduct in-depth research on digital technology to assist music teaching research and contribute to the modernization of music teaching. Because the scope of music education is relatively broad, the author can only make breakthroughs from a small aspect, hoping to help digital technology gradually, introduced to all aspects of music education.

2. Literature Review

Guo and Liu discussed the new connotation and new characteristics of online learning resources, focusing on what kind of learning resources Internet + education needs and how to realize the sharing of high-quality resources in the Internet + era [4]; finally, China's Internet + resource strategy and its implementation path are proposed, which have certain theoretical value and strong practical guiding significance. Pradhan et al. have successively discussed the quality requirements of vocal music teachers and the exertion of students' subjectivity, the language of vocal music classroom teaching and its normative application, the core content of vocal music teaching—the teaching of key professional skills, and the teaching of vocal music singing skills; research and analysis are carried out in turn in terms of thinking about contradictions [5]. Zhang et al. advocated teaching design at different levels according to the different characteristics of different students and stratified teaching according to their aptitude, and reforming and innovating education and teaching, reflecting the development direction of art education in the new era [6]. Liu enumerated the landmark achievements in the use and development of new media software. Try to use the mobile Internet analysis chart to interpret the development process of new media, explore the internal driving force of new media development, and have positive guiding significance for the application of new media [7]. Wang et al., through case studies and comparative research methods, mainly discussed the reform methods of traditional teaching such as “learning by listening,” “learning by doing,” and “learning by feeling,” and different online learning and teaching methods, etc. [8] enable teachers to help students develop the knowledge and skills they need in the digital age; the purpose is to guide students to cultivate and improve their thinking ability and knowledge level towards success. It aims to promote the transformation of teaching paradigms, implement effective teaching and learning, and improve the level of support services for teachers and the overall teaching quality. Zhao et al. provide a very procedural and unified teaching method that compromises the combination of scientific, mechanical, and holistic [9].

The author proposes a design method for multimedia vocal music teaching and develops an interactive multimedia vocal music teaching system, which enables vocal music teaching to achieve more independent choices and human-computer interaction functions and lays the foundation for the autonomy of vocal music teaching [10]. At the same time, it also provides a new way for the realization of multimedia vocal music teaching.

3. Research Methods

3.1. Implementation of Interactive Multimedia Vocal Music Teaching System. The key to realizing the multimedia vocal music teaching system is the establishment of the vocal music teaching module. The vocal music teaching module is mainly based on professional vocal practice, and users can modify the singing results in real time and form the correct pronunciation, so as to realize the real interactive teaching mode [11]. At the same time, a vocal score function is also added. First, a singing model is established through the original singing audio, and the comparison parameters of volume, pitch, and breath are selected, and then the extracted singing audio parameters are compared with the original singing model parameters, and finally, the corresponding evaluation and opinions are given according to the matching degree of the two.

3.2. Establishment of Interactive Multimedia Vocal Music Teaching System. In order to realize the systematic multimedia teaching of vocal music, it is very important to establish a complete library of vocal music. Considering the wide adaptability of teaching content, the music library firstly divides the parts and vocal types, and users can choose the corresponding vocal music library for practice according to their own needs. The content of the music library refers to professional vocal music theory textbooks and practical guidance materials, and a vocal music practice tutorial is designed in a targeted manner. For example, the bel canto baritone course mainly includes breathing exercises, humming exercises (open and closed mouth), 5 vowel exercises (a, e, i, o, u), and scale exercises of changing voice areas, a total of 9 exercises. Another example, the national female voice course mainly focuses on breathing exercises and various humming exercises [12].

The use of digital means should give full play to its advantages to make vocal music teaching more intuitive. Its approach is to record the audio passages sung by students in a targeted manner and help students find a good voice state by revising and comparing the results of several times of singing, so that students can feel how to mobilize their singing state is correct. For this purpose, the teaching interaction module established by the author has the following two functions: (1) audio collection and playback and (2) audio editing [13].

In vocal music teaching, in order to let students sing a good voice, first of all, let students know their own voice. Let the students know what the voice they usually sing is like and is this kind of sound beautiful [14]. Only when students know their own voice can they find out their shortcomings and make improvements. In the vocal music teaching in multimedia mode, the function of audio capture and playback is very important and very practical, mainly using low-level audio functions to achieve.

Low-level audio services can deal directly with audio drivers, operate on audio data, and perform special sound effects, including waveform audio and MIDI low-level functions. Figure 1 illustrates the Windows audio services hierarchy.

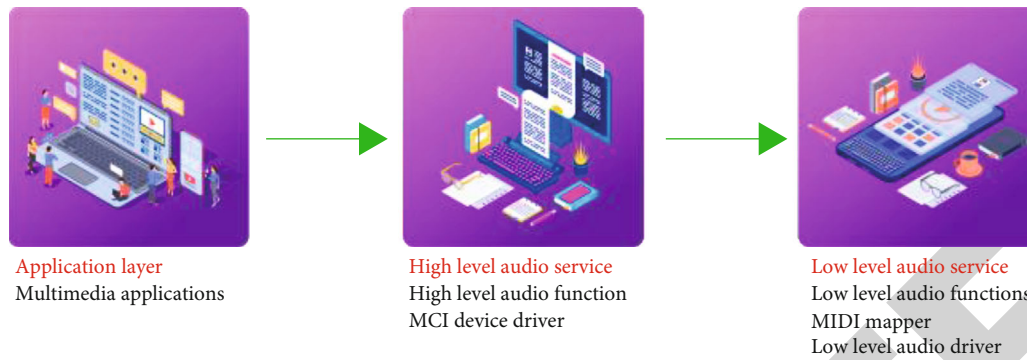


FIGURE 1: Hierarchical relationship of Windows audio services.

The basic process of waveform audio acquisition is as follows:

- (1) Use the functions `waveInGetNumDevs()` and `waveInGetDevCps()` to query whether the system has a device for recording sound, and check its performance
- (2) Call the following function to open the sound input device, and return the `hwi` of the waveform input device for later use:

```
MMRESULT waveInOpen(LPHWAVEIN phwi, UINT DeviceID, LPWAVEFORMATEX pwx, DWORD dwCallback, DWORD dwCallbackInstance, DWORD fdwOpen).
```

`Pwfx` points to the `WAVEFORMATEX` data structure for waveform audio, which determines the format of the acquired waveform data. `DwCallback` points to a callback function that handles audio input.

- (3) Before entering the audio record, a memory area needs to be defined to store the data [15]. Then call the function:

```
MMRESULT waveInPrepareHeader(HWAVEIN hwi, LPWAVEHDR pwh, UINT cbwh).
```

Where `pwh` points to a `WAVEHDR` structure, the data storage area location, size, and other fields in this structure must be copied and specified in advance. Then, call the function again:

- (4) After the above function is called successfully, you can start recording sound and call the function: `MMRESULT waveInStart(HWAVEIN hwi)`
- (5) After completing the route, call the following functions in turn to clear the waveform audio data structure `WAVEHDR`, release the allocated resources, and close the waveform audio input device:

```
MMRESULT waveInUnprepareHeader(HWAVEIN hwi, LPWAVEHDR pwh, UINT cbwh), MMRESULT waveInStop(HWAVEIN hwi), MMRESULT waveInClose(HWAVEIN hwi).
```

The function called by using the low-level audio function to play the waveform sound is similar to the function called

by the waveform audio acquisition, and the implementation process is also similar [16].

In order to realize the interactive characteristics of digital vocal music teaching, this module adds an audio editing function. Students can modify the sound waveform and pitch parameters in real time and compare the sound effects before and after the modification through audio playback; in this way, students have a more intuitive and specific understanding of the singing state. The implementation method is as follows:

- (1) Graphical display of sound. Set the time interval, and periodically take out the collected sound signal from the memory, the signal is a function of time, and a waveform curve is drawn
- (2) Volume editing. The volume editor on the program interface, the program mainly uses the function `Envelope` to modify the amplitude envelope, where `lpWaveData` is the waveform audio data block pointer, `factor` is the editing factor, and the waveform amplitude can be changed by changing the value of `factor`

$$\begin{aligned} & ((\text{short} *)\text{Wave.lpWaveData})[i] \\ & = (\text{short})(((\text{short} *)\text{Wave.lpWaveData})[i] * \text{factor}) \end{aligned} \quad (1)$$

- (3) Pitch editing. Vocal singing often encounters such a problem: In a specific sound area, the singer often causes intonation problems due to the position and breath of the voice [17]. This problem is difficult to solve, especially for students who have not yet been able to use their singing skills proficiently, and it is even more difficult to solve the intonation problem at this time, because in this state, the inner pitch of the singer is accurate and the immature singing technology causes the pitch difference. Without a reference, the singer is difficult to detect; in response to this situation, the teacher can cut out the waveform with inaccurate pitch, point out the problem first,

then correct the pitch to establish the accuracy of hearing, and then tell the students that they should make subtle adjustments to the singing state, such as insufficient breath and open pharynx, not enough, and the sound position is low; this allows students to reach the pitch in a good singing state rather than a blunt “pitch enough.” This function mainly adopts the pitch shifter plug-in in Opensource’s FMODProgrammers API Win32, which realizes the real-time pitch modification and audio playback functions

After students practice vocal music, the system can give an objective evaluation based on the singing results. The key to the singing instruction module is to establish the corresponding vocal measurement method and scoring mechanism.

Vocal scoring is different from previous voice scoring methods. Voice scoring generally uses a factor evaluation method; this system uses a vocal measurement method based on the comparison of audio feature parameters, by analyzing the sound wave parameters of the user’s audition voice and the original singing model; the characteristics of breath, sound intensity, and pitch are extracted; matching and comparison are carried out; and then the scoring mechanism gives objective evaluation scores according to the degree of similarity.

Breath is an important aspect of the basic skills of singing; the quality of breath control during singing will directly affect the effect of vocalization and the performance of emotions. If you cannot master your breathing, you cannot sing a good voice and even damage your voice [18]. The key technique for singing breath is the length and smoothness of the breath. The system measures the continuity and smoothness of breath by calculating the standard deviation of the test sound waveform. Standard deviation is a measure of how far apart a set of values is from the mean. For a vector X , the function $\text{std}(X)$ of its standard deviation is the following formula:

$$\text{std}(X) = \left(\frac{1}{n-1} \sum_{i=1}^n (x_i - \bar{x})^2 \right)^{1/2}. \quad (2)$$

Among them, n represents the number of sampling points, and \bar{x} represents the average amplitude.

The larger the calculated standard deviation, the less stable the breath; otherwise, the better the user’s grasp of the breath.

The sound intensity indicates the volume of singing, and in vocal singing, it reflects the opening and closing amplitude of the vocal cords when they vibrate and the impact force of the breath. This system performs short-duration processing on the acoustic signal, the volume parameters are extracted by the frame-by-frame method, and the volume intensity curve is obtained. It is assumed that each frame of signal is represented by $S_n(m)$, where $m = 0, 1, \dots, M-1$, $n = 0, 1, \dots, N-1$ and N are the total number of frames, that is, the length of the volume intensity curve, and M is the size of the sound frame. The volume intensity

curve is defined as the following formula:

$$\text{Mag}(n) = \frac{1}{M} \sum_{m=0}^{M-1} |S_n(m)|, n = 0, 1, \dots, N-1. \quad (3)$$

In the process of singing, the singer’s grasp of the pitch is reflected in the accuracy of the singing pitch; this accuracy can not only measure the singer’s vocal skills, but also reflect his innate musical hearing and sense of music. The system measures the pitch accuracy by comparing the audition results with the spectrum of the original singing model, the specific implementation method is to first extract the short time frame of the signal to be compared, then extract the fundamental frequency parameters by the cepstrum (CEP-cepstrum) method, and finally use the dynamic time warping (DTW) method to perform data comparison; since DTW continuously calculates the distance between the two vectors to find the optimal matching path, the obtained matching between the two vectors is a regular function with the smallest cumulative distance; this ensures that there is a maximum acoustic similarity between them. Assuming that the test sound signal parameters share I frame vector, and the reference template share J frame vector, and $I \neq J$, then dynamic time warping is to find a time warping function $j = w(i)$, which nonlinearly maps the time axis i of the test vector to the time of the template on the axis j , and make the function w satisfy, as shown in the following formula:

$$D = \min_{x(i)} \sum_{i=1}^I d[T(i), R(w(i))]. \quad (4)$$

Among them, $d[T(i), R(w(i))]$ is the distance measure between the test vector $T(i)$ of the i th frame and the template vector $R(i)$ of the j th frame, and D is the distance between the two vectors in the case of optimal time warping.

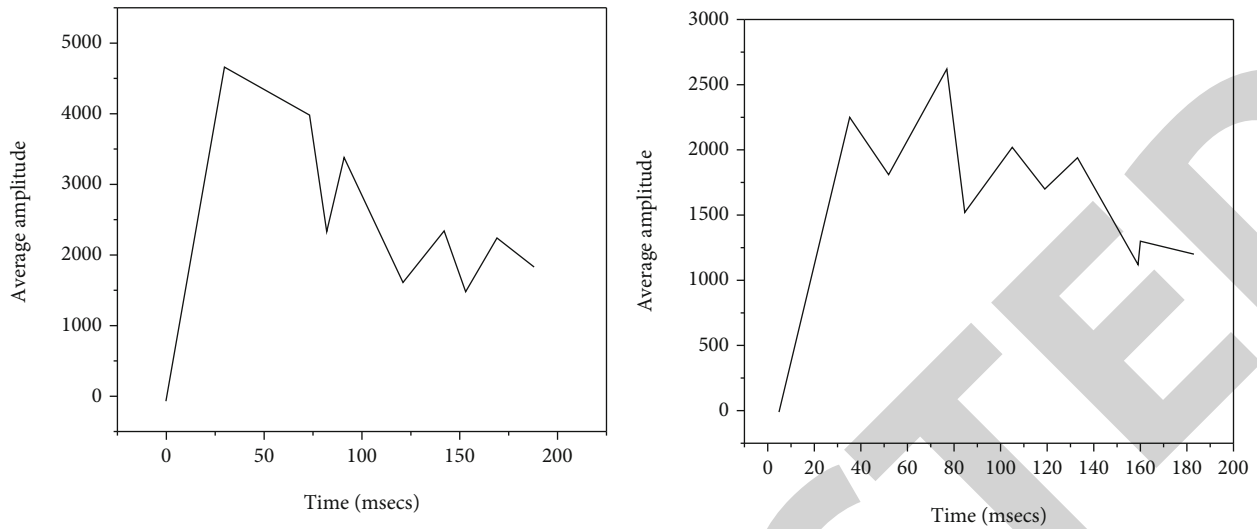
By transforming the sound intensity parameter and the pitch parameter through DTW, respectively, two minimum correction path paths and corresponding DTW distances can be obtained, these two distances reflect the difference in volume and melody of the two songs, respectively. The smaller the difference, the more similar the two are.

4. Analysis of Results

4.1. Scoring Test Results. The scoring mechanism of the singing scoring system is based on the comparison of the above-mentioned breath, sound intensity, and pitch characteristics; the auditioner can see not only the scores in real time, but also the final total score of the audition. The system scoring formula is shown in the following:

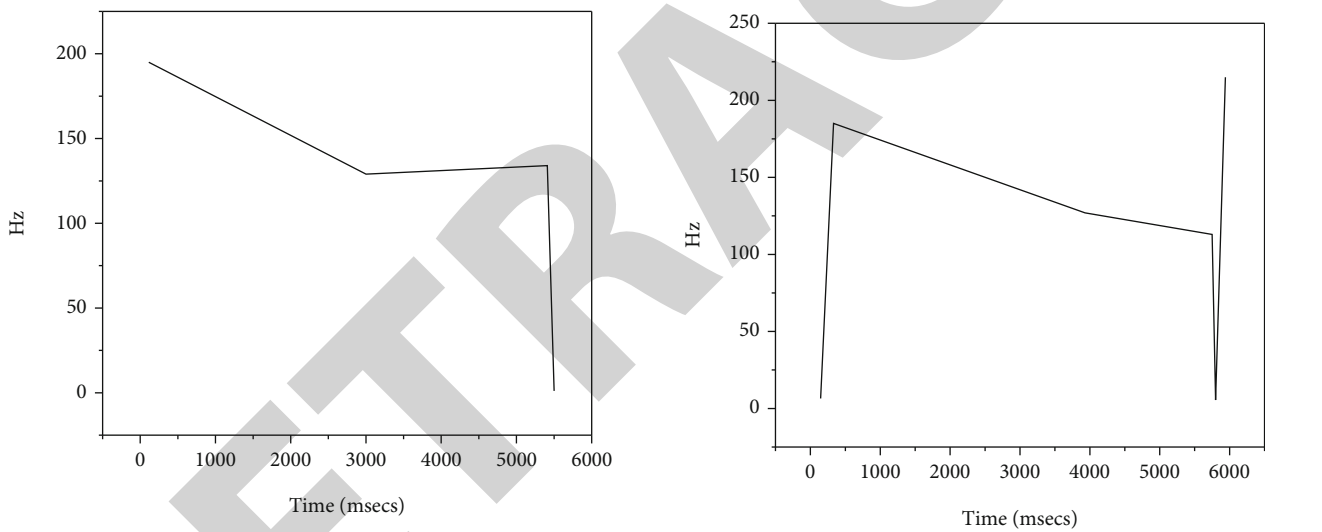
$$\text{score} = k_1 \frac{100}{1 + a_1(\text{mindisi})^{b_1}} + k_2 \frac{100}{1 + a_2(\text{mindisp})^{b_2}} + k_3 \frac{100}{1 + a_3(\text{st})^{b_3}}. \quad (5)$$

Among them, $a_1, a_2, a_3, b_1, b_2, b_3 > 0$, $k_1 + k_2 + k_3 = 1$, and k_1, k_2, k_3 are the weights of each scoring parameter in the scoring mechanism, and mindisv and mindisp are the



(a) Schematic diagram of the standard volume intensity curve (b) Schematic diagram of the tester's volume intensity curve

FIGURE 2: Schematic diagram of volume intensity curve.



(a) Schematic diagram of standard fundamental frequency trace (b) Schematic diagram of the fundamental frequency track of the trial singing

FIGURE 3: Schematic diagram of fundamental frequency trace.

distances calculated by the sound intensity and pitch parameters, respectively. st represents the breath stability parameter; through repeated experiments of machine scoring and manual scoring, the weights reflect the best mapping relationship between the two, so that the computer can better simulate the expert scoring. The following is an example of a simulation experiment conducted with the male voice etude:

The measurement of breath is a process of self-comparison. In the experiment, the smoothness of breath is measured by calculating the standard deviation of the test sound waveform. In the sound intensity comparison, the volume intensity curves were drawn for the standard and audition music, respectively. Figure 2 is a schematic diagram of a standard volume intensity curve (a) and a tester's volume intensity curve (b).

In the pitch comparison, the fundamental frequency traces of the two pieces of music are obtained by the cepstrum method, respectively, as shown in Figure 3; (a) is the standard fundamental frequency trace, and (b) is the trial singing fundamental frequency trace [19]. At the same time, the average value of the standard fundamental frequency can be obtained: $avgF0 = 143.12\text{HZ}$, and the average value of the fundamental frequency of the trial singing is $avgF0 = 142.05\text{HZ}$.

Table 1 shows the average distance and score of each parameter of the test singers. Among them, $mindisv = 726.126$ of pitch, $path\ length = 144$; $mindisp = 4.51987$, $path\ length = 163$ of pitch, $breath\ smoothness = 484.20$. It can be seen from Table 1 that the scoring system is more sensitive to pitch and breath stability, but not very sensitive to sound intensity. It can be seen that the fundamental

TABLE 1: The average distance and score of each parameter of the auditioners.

Characteristic parameters	Sound intensity	Pitch	Breath stability	Final score	Error
Machine scoring	0.01	77.46	87.65	75.12	2.442%
Human scoring	5	80	85	77	

frequency trace represents the highest importance, followed by the breath smoothness, and finally the volume intensity curve.

Etude library evaluation results. In the machine scoring, through experiments we set the weights of the three feature parameters to be 5%, 80%, and 15%, respectively.

5. Conclusion

The challenges of the information society to various fields of music education are obvious, the introduction of advanced science and technology and the use of advanced methods and means for vocal music teaching are an inevitable trend for the improvement and development of the discipline. The author proposes a vocal music teaching method based on VC++, applies multimedia technology to traditional vocal music teaching, and develops a set of simple interactive multimedia vocal music teaching system [20]. This method breaks through the limitations of traditional vocal music teaching and can provide students with an interactive teaching and self-study platform with skill guidance and correction functions. This will change the dull and single status quo of vocal music teaching and greatly improve the intuition, effectiveness, interactivity, and learnability of the vocal music teaching process. It is not only original, but also has high practical value.

Data Availability

The data used to support the findings of this study are available from the corresponding author upon request.

Conflicts of Interest

The author declares that there are no conflicts of interest.

Acknowledgments

The study was supported by 2020 Guangxi Higher Education Undergraduate Teaching Reform Project: Curriculum Construction and Reform of College Vocal Music from Cultural Integration Perspective of Traditional Chinese Culture Relating to 24 Solar Terms (2020)GA255).

References

- [1] S. Billa, S. Dixit, and S. Pavan, "Analysis and design of an audio continuous-time 1-x fir-mash delta-sigma modulator," *IEEE Journal of Solid-State Circuits*, vol. 55, no. 10, pp. 2649–2659, 2020.
- [2] Y. Liu, "Intelligent analysis platform of agricultural sustainable development based on the internet of things and machine learning," *Acta Agriculturae Scandinavica, Section B-Soil & Plant*, vol. 71, no. 8, pp. 718–731, 2021.
- [3] L. Liu and S. B. Tsai, "Intelligent recognition and teaching of English fuzzy texts based on fuzzy computing and big data," *Wireless Communications and Mobile Computing*, vol. 2021, no. 1, Article ID 1170622, p. 10, 2021.
- [4] J. Guo and J. Liu, "Optimal system design of language training strategy based on artificial intelligence," *Journal of Intelligent and Fuzzy Systems*, vol. 40, no. 4, pp. 1–11, 2020.
- [5] J. Pradhan, S. Kumar, A. K. Pal, and H. Banka, "Texture and colour region separation based image retrieval using probability annular histogram and weighted similarity matching scheme," *IET Image Processing*, vol. 14, no. 7, pp. 1303–1315, 2020.
- [6] H. Zhang, X. Yang, and J. Ma, "Diffraction imaging using the two-way imaging condition," *Geophysics*, vol. 85, no. 2, pp. H1–H11, 2020.
- [7] Y. Liu, "Interactive system design of entrepreneurship education based on internet of things and machine learning," *Journal of Intelligent and Fuzzy Systems*, vol. 39, no. 4, pp. 5761–5772, 2020.
- [8] W. Wang, Y. Zhang, S. Sun, and G. Xiao, "Gray image segmentation algorithm based on one-dimensional image complexity," *Journal of Intelligent and Fuzzy Systems*, vol. 40, no. 10, pp. 1–10, 2020.
- [9] Z. Y. Zhao, W. Z. Huang, J. Pan, Y. A. Huang, and C. Q. Yu, "A sparse feature extraction method with elastic net for drug-target interaction identification," *Scientific Programming*, vol. 2021, no. 44, Article ID 6686409, p. 10, 2021.
- [10] A. Sadeghzadeh and H. Ebrahimzadeh, "Pose-invariant face recognition based on matching the occlusion free regions aligned by 3D generic model," *IET Computer Vision*, vol. 14, no. 5, pp. 268–277, 2020.
- [11] C. Zhang and X. Zhang, "Multimedia system and database simulation based on internet of things and cloud service platform," *Journal of Intelligent and Fuzzy Systems*, vol. 40, no. 2, pp. 2613–2624, 2021.
- [12] S. Chen, Y. Liu, and C. Zhang, "Water-body segmentation for multi-spectral remote sensing images by feature pyramid enhancement and pixel pair matching," *International Journal of Remote Sensing*, vol. 42, no. 13, pp. 5025–5043, 2021.
- [13] H. A. Khattak, M. A. Khan, A. Almogren, and I. U. Din, "Doodle-based authentication technique using augmented reality," *IEEE Access*, vol. 8, no. 1, pp. 4022–4034, 2020.
- [14] D. Zhang and P. Tan, "Internet of things and intelligent transportation system," *Journal of Physics: Conference Series*, vol. 2066, no. 1, p. 012066, 2021.
- [15] G. Veselov, A. Tselykh, A. Sharma, and R. Huang, "Applications of artificial intelligence in evolution of smart cities and societies," *Informatica (Slovenia)*, vol. 45, no. 5, p. 603, 2021.
- [16] S. Shriram, J. Jaya, S. Shankar, and P. Ajay, "Deep learning-based real-time AI virtual mouse system using computer vision to avoid COVID-19 spread," *Journal of healthcare engineering*, vol. 2021, Article ID 8133076, 8 pages, 2021.
- [17] Q. Liu, X. Liu, T. Liu, Y. Kang, and H. Zhang, "Seasonal variation in particle contribution and aerosol types in shanghai based on satellite data from MODIS and CALIOP," *Particuology*, vol. 51, pp. 18–25, 2020.

Retraction

Retracted: Implementation of Network Data Mining Algorithm for Associated Users Based on Multi-Information Fusion

Journal of Sensors

Received 22 August 2023; Accepted 22 August 2023; Published 23 August 2023

Copyright © 2023 Journal of Sensors. This is an open access article distributed under the Creative Commons Attribution License, which permits unrestricted use, distribution, and reproduction in any medium, provided the original work is properly cited.

This article has been retracted by Hindawi following an investigation undertaken by the publisher [1]. This investigation has uncovered evidence of one or more of the following indicators of systematic manipulation of the publication process:

- (1) Discrepancies in scope
- (2) Discrepancies in the description of the research reported
- (3) Discrepancies between the availability of data and the research described
- (4) Inappropriate citations
- (5) Incoherent, meaningless and/or irrelevant content included in the article
- (6) Peer-review manipulation

The presence of these indicators undermines our confidence in the integrity of the article's content and we cannot, therefore, vouch for its reliability. Please note that this notice is intended solely to alert readers that the content of this article is unreliable. We have not investigated whether authors were aware of or involved in the systematic manipulation of the publication process.

Wiley and Hindawi regrets that the usual quality checks did not identify these issues before publication and have since put additional measures in place to safeguard research integrity.

We wish to credit our own Research Integrity and Research Publishing teams and anonymous and named external researchers and research integrity experts for contributing to this investigation.

The corresponding author, as the representative of all authors, has been given the opportunity to register their agreement or disagreement to this retraction. We have kept a record of any response received.

References

- [1] H. Zhang, "Implementation of Network Data Mining Algorithm for Associated Users Based on Multi-Information Fusion," *Journal of Sensors*, vol. 2022, Article ID 3350997, 6 pages, 2022.

Research Article

Implementation of Network Data Mining Algorithm for Associated Users Based on Multi-Information Fusion

Hui Zhang 

Yancheng Teachers University, Yancheng, Jiangsu 224002, China

Correspondence should be addressed to Hui Zhang; 1710711225@hbut.edu.cn

Received 29 June 2022; Revised 23 July 2022; Accepted 8 August 2022; Published 27 August 2022

Academic Editor: Haibin Lv

Copyright © 2022 Hui Zhang. This is an open access article distributed under the Creative Commons Attribution License, which permits unrestricted use, distribution, and reproduction in any medium, provided the original work is properly cited.

In order to accurately and effectively mine relevant users in social networks, we can stop false information and illegal activities in the network, thereby ensuring the safety and integrity of the network environment. A method is proposed for the implementation of a data mining algorithm of a user network based on the fusion of several data. AUMA-MRL (associated user mining algorithm based on multi-information representation learning) proposes an associated user mining algorithm based on node characteristics, neighborhood information, and global network structure information. The steps of the algorithm are as follows: combining each user of the social network into a node using a method where each node is installed separately and combining network user characteristics and user relationship information. A user pair is a network similarity vector that represents the similarity of users in different dimensions. Based on these similarity vectors, a corresponding user separation algorithm is formed. It examines the feasibility and efficiency of the AUMA-MRL algorithm for researching relevant users. The proportion of associated users in the network to be fused is lower than that of nonassociated users, and the prediction has little effect on improving the recall rate of nonassociated users, so the recall rate is slightly lower than the accuracy. This algorithm can quickly get the embedding of new nodes and the similarity vector between new nodes and other nodes in the network, so as to quickly mine the associated users of new nodes in the network and enhance the robustness of the network associated user mining algorithm.

1. Introduction

Social network is a virtual community composed of interaction and connection between different members of society. With the rapid development of the Internet, various social networking platforms are gradually penetrating into all aspects of people's life and work, such as Twitter and Douban. These social networks play an important role in the human world, but they hide some security issues and threats in the process of sharing information [1]. In social networks, the same user organization registers different accounts on different social networks. These different virtual accounts are called vest or related users. Relying on users is the driving force of public hotspot communication and brings many security risks, such as jacket fraud and naval rumors. How to effectively identify connected users has become one of the important issues in social media content security research. Most traditional related user mining methods iden-

tify related users by measuring the similarity of user profile information in the same social network [2]. However, the similarity, falsity, and inconsistency of user characteristics in social networks can only be analyzed by user characteristic information vulnerable to malicious users. It is very difficult to create complete and accurate user extraction by using various dimensions such as user behavior, user characteristics, and network structure information. Figure 1 shows the framework of data fusion. Most relevant user extraction methods are based on solving the "anonymity" problem on social media, which is somewhat similar to the user extraction problem, but there are significant differences in practical application options. The two networks involved in "anonymization" are similar to some subnetworks, while the user duplication and user interaction between the two networks involved in extracting relevant users are very small, about 60%. Therefore, most anonymous methods cannot perform the related user extraction tasks well [3].

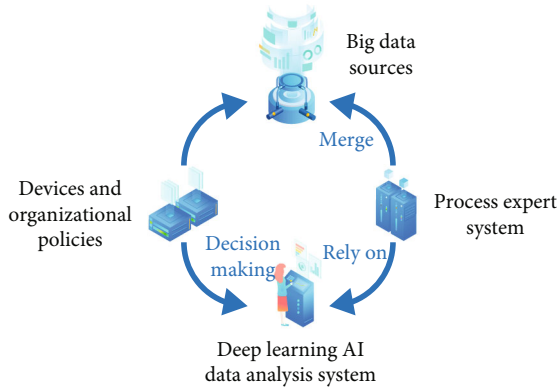


FIGURE 1: Data fusion framework.

TABLE 1: Data set information.

Data set	Number of nodes	Number of sides	Clustering coefficient
PPI	14744	222111	0.1768
Flickr	80522	5899878	0.1648
Facebook	4041	88241	0.6049

TABLE 2: Algorithm recovery rate comparison when overlap is 60%.

Algorithm	PPI	Flickr	Facebook
NS	0.3134	0.3249	0.2311
Grh	0.3989	0.1189	0.1161
AUMA-MRL	0.4187	0.3941	0.42899

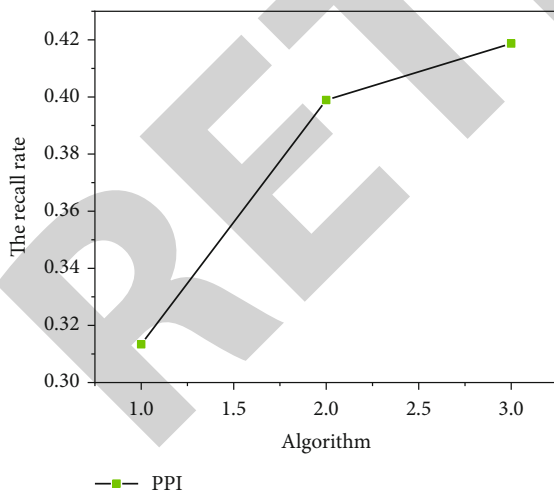


FIGURE 2: Recall rate of associated user mining in PPI to be fused network.

A network information retrieval system can only solve simple targets in the form of keywords and cannot solve complex fuzzy targets in the form of samples provided by users. Network data mining technology follows the great achievements in network data search, such as robotics and full-text search, and

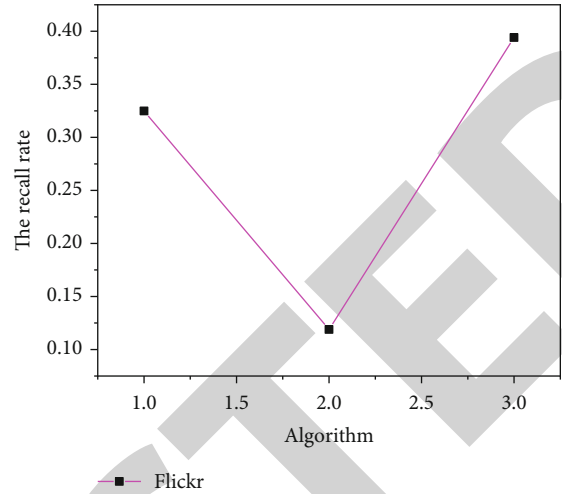


FIGURE 3: Recall rate of associated user mining in Flickr to be fused network.

comprehensively uses various technologies such as artificial intelligence and pattern recognition. It is possible to perform a purposeful information search in a network or database according to user-defined requirements and target attribute information.

The update speed of information has increased, and the problem of information overload has arisen due to the explosion of network data. Academia and industry have struggled to accurately identify consumer needs and preferences and filter out content that is not useful or interesting to consumers. Integrating multiple data is the primary method for making personalized recommendations. It selects the most similar people by finding similarities between different people.

Because of the increasing amount of data and the improvement of users' requirements for personalized recommendations, many multi-information fusion methods cannot provide excellent results. This paper is aimed at improving the accuracy of recommendation, combining multiclass information and matrix decomposition technology to improve the data sparsity and cold start problems faced by the recommendation system, and improving the accuracy of the recommendation results.

2. Literature Review

To solve this research problem, Ma and Zhang mined users' preferences from users' comments on items and used them in recommendation tasks [4]. Pouyap et al. use the topic model to model the text content and mine the influence of the above factors on the score from the text information [5]. Xue et al. proposed a method combining the dimension of potential score and the subject of potential comment. This method can obtain better performance than using single score information or text information [6]. Du and Zhao proposed CTR (collaborative topic regression) model. CTR realizes the effective combination of implicit Dirichlet allocation (LDA) and probability matrix decomposition PMF in a tightly coupled manner [7]. Ren and Li used the deep

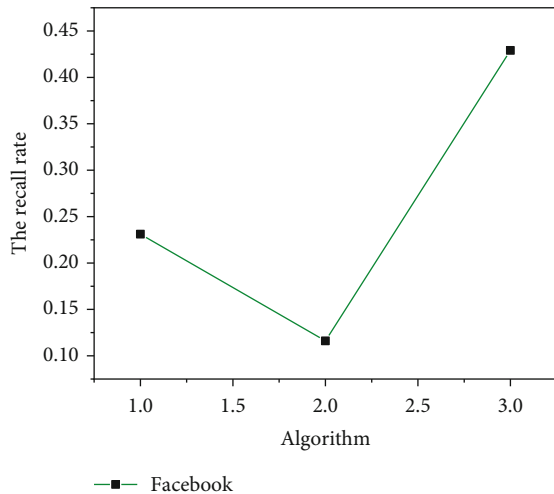


FIGURE 4: Recall rate of associated user mining in Facebook to be integrated network.

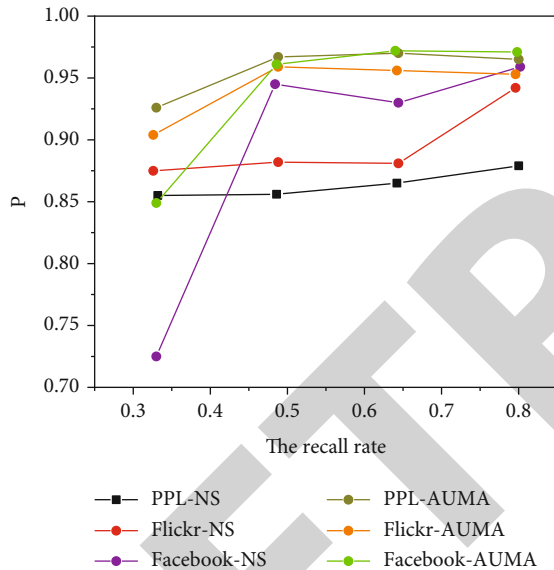


FIGURE 5: Comparison of accuracy between AUMA-MRL and NS under different network overlap.

convolution neural network CNN to extract the features of pictures, combined the interactive information between users and pictures at the last full connection layer, and then output the sorting of labels [8]. Huang et al. first used the recurrent neural network (RNN) to model the user's historical click records and then used the feedback neural network (FNN) to simulate multi-information fusion and finally produce the recommendation results [9]. Ji et al. proposed an algorithm that can combine structured data and unstructured data for recommendation. For structured data, TRANSR is used to obtain the vector features of entities. For text data and image data, stacked denoising autoencoders (sdae) and stacked convolutional autoencoders are used to propose vector features, respectively. A variety of vectors are spliced as the vector features of the article [10]. Liu first applied the self-encoder model to the recom-

mendation system and proposed the self-encoder based collaborative filter (ACF) [11]. Xiao et al. proposed collaborative deep learning (CDL), which combines stacked denoising autoencoder (sdae) with probability matrix decomposition in a tightly coupled manner [12]. Zheng et al. constructed an unsupervised associated user mining method by calculating the rarity of word segmentation through user name word segmentation and n-gram probability [13].

Based on the existing research, a user extraction algorithm AUMA-MRL (user extraction algorithm based on multidata unified representation) is introduced based on the node behavior model, public data, and international data. The steps of the algorithm are as follows: integrate each user in the social network into a node, use the input method for each node, and integrate user behavior and user relationship information. Similarity vector between pairs of network users represents the similarity of different users. Based on the similarity vector, a user interference extraction algorithm was established. When the network overlap is 60%, the recall rates of associated user mining by different algorithms in the three groups of networks to be fused are compared. The AUMA-MRL algorithm achieves the best results on our data set, confirming that combining user attributes and technical knowledge relationships is more effective than using user relationships alone to extract affected users. The AUMA-MRL algorithm works well for my web users.

Web usage mining is mainly used to understand the meaning of users' online behavior data. Network content mining objects and network structure mining objects are the core data of the Internet, while network usage mining deals with peripheral data extracted when users interact with the network, such as web server usage logs and proxy server logs.

Recommendation system has always been focused on how to improve the real-time performance and accuracy of key algorithms, and its advantages and disadvantages directly affect the quality of recommendation services. Today, these algorithms are roughly classified as content-based recommendation, multi-information fusion recommendation, and, of course, some other popular research methods, such as social network-based recommendation, time-aware recommendation, label-based recommendation, context-based recommendation, and matrix decomposition-based recommendation. Content-based recommendations are predicted directly based on the content information of the item, without requiring relevant evaluation information, but it becomes slightly difficult when the content information of the item is not easily interpreted.

It can be noted that the diversification of various user behaviors on the website can reflect users' preferences in a sense and can be very well applied in the recommendation methods. However, when users have many different behaviors, selecting only one of behavioral information to understand user preferences is not comprehensive. In other words, we need to comprehensively consider the multifaceted personalized information of users to help us get more real and effective preference information and make more accurate recommendations for users.

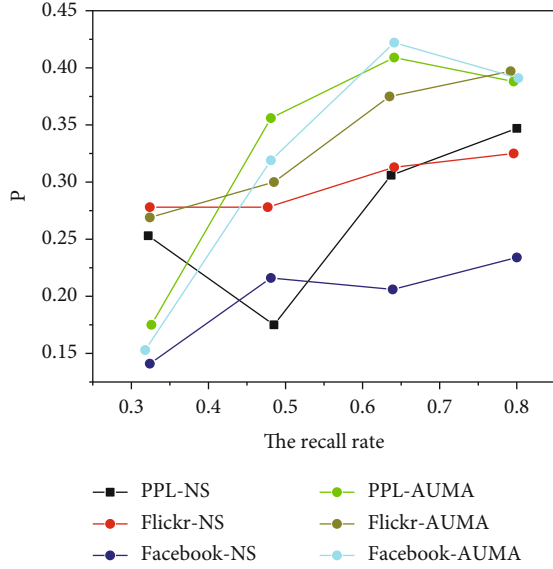


FIGURE 6: Comparison of recall rates of AUMA-MRL and NS under different network overlap.

3. Associated User Mining Algorithm Integrating User Attributes and User Relationships

The goal of user engagement is to find the most accurate and useful user experience in two overlapping domains [14]. AUMA-MRL algorithm for user mining is introduced to combine various information according to node characteristics, public information, and international information standards.

In general, a recommendation system often only serves a specific type of item, where the “item” refers to the general term of recommended content for users (such as movies and news). Therefore, in the whole recommendation system, both the initial requirement design and the most core recommendation algorithm are designed to push the application-based and valuable recommendation results to a specific scene. In order to conquer the most core algorithm link, the recommendation system analyzes different preferences by acquiring user behavior or preferences, which can be roughly divided into explicit preferences and implicit preferences. Explicit preferences often mean direct feedback on items, such as scoring a product; implicit preferences include browsing the profile page of a movie, buying an item, etc. Based on these two preferences and several other limitations, the system enables predictions and provides the most accurate recommended items and services.

In general, nodes with more neighbors in a network are more similar. In this paper, the local topology of the network is obtained by sampling the neighborhood of network nodes. AUMA-MRL first uniformly samples the k -order neighborhood of the target node and sets the sampling window size to ω .

To combine the neighbor information of the nodes, we choose the aggregation function [15]. If the neighborhood depth of the target node is k , the aggregation of its neighborhood information can be expressed as $h_{N(v)}^k = \max(\{\sigma(W_{\text{pool}} h_u^{k-1} + b), \forall u \in N(v)\})$. In order to effectively integrate the embedding of user attributes and user relationships and make the nodes with similar attributes and structures have similar embedded representations, this paper uses graph-based loss function and gradient descent method to learn the parameters in the fusion function. The graph-based loss function is shown in Equation (1), where adjacent node embeddings are similar and disjoint nodes are less similar.

$$L(Z_v) = -\log(\sigma(z_v^T Z_u)) - Q \cdot E_{u_n \sim P_n}(u) \log(\sigma(-z_v^T Z_{u_n})). \quad (1)$$

Personalization-based recommendations are based on “best efforts” based on user experience and historical settings of different users. It is the most suitable way to give recommendations with good accuracy, but it is expensive.

The core idea of content-based recommendation is to calculate the degree of internal correlation based on the item metadata provided to the user and then to record the user history preferences stored in the system database and search for the closest correlation degree of the items stored in the system database. It is also widely used in many social networking sites due to provide better results.

Because the above node neighborhood information fusion process only samples the k -order neighborhood of the target node, and the sampling window is fixed; the process indirectly saves the local structure information of the node while learning the node attribute information. However, this process does not save the global topology information of nodes in the network, that is, the complete user relationship. In order to fully and effectively combine the characteristics and relationships between consumers, this paper introduces an adjacency matrix A to the unemployment problem. This matrix stores the complete information of the network, i.e., the user relationships [16], as shown in

$$L(z_v) = -\log(\sigma(z_v^T z_u)) - Q \cdot E_{u_n \sim P_n(u)} \log(\sigma(z_v^T z_{u_n})) - \text{corr}(f_1(A; \theta_1), f_2(z_v; \theta_2)). \quad (2)$$

In Equation (2), $f(x) = \theta x + b$. Aggregating user behavior data and user interaction data in social networks and representing these data as low-dimensional density vectors provide a good basis for mining user problems [17].

Because the social relations and attribute information of the same natural person have certain similarities in different social network platforms, this paper judges whether the node pairs are related users through the similarity of node pairs between networks, as shown in

$$\text{Sin}_{ij} = \sqrt{(R_i^A - R_j^B)(R_i^A - R_j^B)^T}. \quad (3)$$

This paper marks the similarity vectors of nodes in the network using the joint information of low-income users

of the network. A pair of labeled nodes is taken as a model, and after training parameters, a corresponding user discrimination model is created, which is used to judge whether a pair of unlabeled nodes is a corresponding user. Given a set of n , where n is the data $\{(x_{ij}, y_{ij})\}$ with real label extracted from N_t , x_{ij} represents the d -dimensional similarity vector between user i and user j , and $y_{ij} \in \{1, -1\}$, as shown in

$$f(x) = w^T x + b, \quad (4)$$

$$L_{(w,b)} = \frac{\gamma_L}{2} \|w\|^2 + C \sum \xi_{ij} \quad (5)$$

$$\text{s.t. } y_{ij}(w^T x_{ij} + b) \geq 1 - \xi_{ij}, \quad \xi_{ij} \geq 0.$$

Since there may be some users who lack tag information in reality, the hybridcf algorithm is difficult to guarantee the accuracy of the final results. In this case, the hybridcf algorithm combines the current user's friend data to find the top 10 most common tags that all its friends add to fill in the current user's tag matrix. Because the supplement for tag data can effectively help current users to fill in their own preferences from their friends, it can help the cold start problem to be alleviated to some extent. If, after the label expansion, some users still have insufficient TopN list items obtained, then follow the UserCF algorithm mechanism to help supplement [18].

Recommender systems, which provide users with personalized recommendations based on their hobbies and needs, have gained increasing attention and acceptance over the past decade and are now a hot research area in both academia and industry. In general, the topics of the recommendation strategy usually include historical user data, semantic content, and associations between items. Find the preferences of similar users other than the target user to predict interest or demand by finding similar items. Today, social networks have become an integral part of the Web 2.0 environment.

Web data mining techniques mainly deal with the combination of semistructured data source models and semistructured data models. This requires a model that clearly represents the network data, and finding a semistructured data model is key to solving this problem. In addition, semistructured model extraction techniques are also needed, i.e., techniques for automatically extracting semistructured models from existing data.

Clients can choose and implement different programs to process the data according to their needs, and the server only needs to send the same XML file. The initiative to process the data is handed over to the client, and what the server does is to insert the data into the XML file as completely and accurately as possible. XML's self-descriptive capabilities allow clients to understand the logical structure and meaning of the data when they receive it, thus enabling widespread and general distributed computing. It is more suitable for solving the problem of personal needs of users highlighted by data mining of network information.

4. Results and Analysis

In order to verify the applicability and effectiveness of AUMA-MRL algorithm in association user mining task, association user mining experiments are carried out on three real public data sets. The statistics of our data are shown in Table 1. A PPI is a protein complex that contains information and demographic information. Facebook data is collected through survey participants using Facebook app and contains a variety of attribute information of users.

The overlaps of different groups were extracted from our network with overlapping ratios of 33%, 45%, 60%, and 80%.

In the experiment, we extracted 20% of the network node pairs and created a test set based on some records related to user-provided data, in order to evaluate the appropriate model [19, 20]. As shown in Table 2, Figures 2–4 compare the recovery rates of different algorithms for mining users when the three sets of fusion networks overlap at 60%. It can be seen that AUMA-MRL algorithm has achieved the best results on three data sets, which proves that the effect of fusing user attributes and user relationship information is better than mining associated users only using user relationship. AUMA-MRL algorithm can effectively mine associated users in the network.

To verify the robustness of the power generation system, the overlaps of the experimentally generated networks are 33%, 45%, 60%, and 80%. Figure 5 compares the accuracy of two user mining algorithms under different network overlap conditions. Because the increase of network overlap makes the node embedding contain more similar information, the accuracy of associated users will increase with the increase of network overlap. Figure 6 shows the recovery speed of the two algorithms in different parts of the network [21, 22]. The proportion of associated users in the network to be fused is lower than that of nonassociated users, and the prediction has little effect on improving the recall rate of nonassociated users, so the recall rate is slightly lower than the accuracy.

AUMA-MRL user extraction algorithm proposed in this paper can be implemented well when different networks overlap [23, 24]. User interactions between new network nodes improve the power of network user interaction mining algorithms [25]. Trust matrix also has the problem of sparse data. First, we need to fill in the missing values of the corresponding position and realize the decomposition and dimension reduction with the help of SVD matrix decomposition method. Consider that the original trust model calculates the similarity for the trust relationship and does not involve the possible deviation of the trust individual. For example, some individuals lack independent thinking and are more likely to blindly trust others; then, their trust data may be generally high.

5. Conclusion

This paper proposes multi-information fusion representation learning (AUMA-MRL) based on associated user mining algorithm. In the first mock exam, the learning information is used to learn the same size information (user

Retraction

Retracted: Implementation of Personalized Information Recommendation Platform System Based on Deep Learning Tourism

Journal of Sensors

Received 22 August 2023; Accepted 22 August 2023; Published 23 August 2023

Copyright © 2023 Journal of Sensors. This is an open access article distributed under the Creative Commons Attribution License, which permits unrestricted use, distribution, and reproduction in any medium, provided the original work is properly cited.

This article has been retracted by Hindawi following an investigation undertaken by the publisher [1]. This investigation has uncovered evidence of one or more of the following indicators of systematic manipulation of the publication process:

- (1) Discrepancies in scope
- (2) Discrepancies in the description of the research reported
- (3) Discrepancies between the availability of data and the research described
- (4) Inappropriate citations
- (5) Incoherent, meaningless and/or irrelevant content included in the article
- (6) Peer-review manipulation

The presence of these indicators undermines our confidence in the integrity of the article's content and we cannot, therefore, vouch for its reliability. Please note that this notice is intended solely to alert readers that the content of this article is unreliable. We have not investigated whether authors were aware of or involved in the systematic manipulation of the publication process.

Wiley and Hindawi regrets that the usual quality checks did not identify these issues before publication and have since put additional measures in place to safeguard research integrity.

We wish to credit our own Research Integrity and Research Publishing teams and anonymous and named external researchers and research integrity experts for contributing to this investigation.

The corresponding author, as the representative of all authors, has been given the opportunity to register their agreement or disagreement to this retraction. We have kept a record of any response received.

References

- [1] X. Wang, "Implementation of Personalized Information Recommendation Platform System Based on Deep Learning Tourism," *Journal of Sensors*, vol. 2022, Article ID 6221413, 9 pages, 2022.

Research Article

Implementation of Personalized Information Recommendation Platform System Based on Deep Learning Tourism

Xuejuan Wang 

Department of Culture and Tourism, Shanxi Vocational and Technical College of Finance and Trade, Taiyuan, Shanxi 030031, China

Correspondence should be addressed to Xuejuan Wang; 11231513@stu.wxjc.edu.cn

Received 9 July 2022; Revised 10 August 2022; Accepted 11 August 2022; Published 26 August 2022

Academic Editor: Haibin Lv

Copyright © 2022 Xuejuan Wang. This is an open access article distributed under the Creative Commons Attribution License, which permits unrestricted use, distribution, and reproduction in any medium, provided the original work is properly cited.

In order to provide tourists with better tourism services, a system method of personal information recommendation platform based on deep learning tourism is proposed. The system includes noise reduction autoencoder, feature extraction module, data preprocessing module, recommendation calculation module, expert evaluation module, recommendation result output module, customer feedback module, and storage module. The personal information recommendation platform system based on deep learning tourism of the present invention enables tourists to obtain tourism information conveniently and quickly through scientific information organization and presentation form and helps tourists to better arrange tourism plans and form tourism decisions. By effectively aggregating multiple neighborhoods of nodes, embedding high-order collaboration information into the node embedding vector, obtaining the potential preferences of users, solving the problems of user data sparse and cold start, and finally through experimental analysis, a research method is proposed. It is used to build the model of tourist attraction recommendation system. Experimental results show that the proposed method for cold-start user recommendation has the best performance in terms of accuracy, recall, and normalized loss cumulative gain, and it is 17.9% higher than BPR in recall rate $\text{Recall}@5$ and 11.8% higher in accuracy rate. It is proved that the system has a significant impact on the diversity and novelty of tourist attraction recommendation.

1. Introduction

In recent years, the tourism industry has developed rapidly, and the number of tourist attractions and tourism information on the Internet has become more and more numerous [1]. The process for users to decide on attractions is complicated and inefficient. A good tourist attraction recommendation service can recommend scenic spots that meet their interests and preferences, so as to improve the efficiency of users' decision of scenic spots and also improve the user's travel satisfaction. The types of attractions are easy to distinguish, and users of similar types will show very similar preferences for tourist attractions. Therefore, an intuitive idea to implement attraction recommendation is to make full use of user preferences and attractions based on the "similarity" between user groups and attractions, and the intrinsic association of attractions implements the recommendation model. Aiming at the problems of sparse data, insufficient

tourism factors, and low recommendation accuracy in the existing tourism recommendation research, this paper takes advantage of the characteristics of microblog data, such as personalized expression, strong current situation, and the intelligent prediction function of machine learning, and proposes a new model based on microblog data. The scenic spot recommendation method based on blog data and machine learning realizes accurate and personalized recommendation of tourist attractions.

In the planning of travel itinerary, it is compared with the elements of accommodation, transportation, and restaurants [2]. As the ultimate goal of tourists' travel itinerary, scenic spots are undoubtedly the most important part of itinerary planning; therefore, the choice of tourist attractions will greatly affect tourists' travel satisfaction and obtain the required scenic spot information from travel websites; at the time, tourists mainly rely on information retrieval and recommendation systems. A typical example of information

retrieval is a search engine, that is, a travel website returns the attractions related to the keywords according to the keywords provided by tourists [3]. The recommendation system is a travel website that pushes relevant attractions based on the prediction of tourists' preferences. In the face of the massive amount of scenic spot information on the website, it is often difficult for tourists or it takes a lot of time and energy to obtain the required information, which leads to the problem of information overload. Although search engines can alleviate the problem of information overload to a certain extent, tourists are required to choose appropriate keywords to describe their needs; however, some studies have found that a large number of tourists cannot clearly express their travel needs. Therefore, since tourists cannot accurately input keywords, search engines are powerless to alleviate the problem of information overload for tourists when choosing scenic spots [4].

Different from search engines, the recommendation system does not require the active input of tourists; through the analysis of historical data of tourists, it realizes the mining of tourists' preferences, so as to provide tourists with personalized scenic spot recommendation services, which not only meets the needs of tourists but also improves the tourists' preference, and website loyalty has now become an important part of major travel websites [5]. It is a new type of machine learning and a new type of deep learning. Through scientific information organization and presentation, it allows tourists to easily and quickly obtain tourism information, helping tourists to better arrange tourism plans and form tourism decisions. The brand-new service experience brought by smart tourism can be felt during the decision-making process of tourism planning and tourism planning.

2. Literature Review

Kumar et al. said that with the development of technology and the performance breakthrough of computer hardware equipment, big data analysis methods have become a handy tool for researchers [6]. Based on the paper of Al-Garadi et al., the application of data mining to the tourism market is an important technological breakthrough in the field of tourism research, in which tourism route planning is an indispensable part of smart tourism research and tourism recommendation system development [7]. Relying on the vigorous development of deep learning and the Internet of Things and its supporting technologies and hardware, the mining and prediction accuracy of tourists' interests through models has been greatly improved, which will bring great importance to the rapid development and progress of smart tourism and tourism economy; it also provides a core competitiveness for the development of local tourism. The core of the system is tourists, so the starting point of the system and algorithm design should be in line with the interests and motivations of tourists. Tourists' satisfaction with the route planned by the system will directly affect tourists' subjective evaluation of the tourist city attractions and thus indirectly affect the tourists. Tourists make travel plans and affect users' stickiness to the system. In order to further opti-

mize the efficiency of route planning, this paper proposes several optimization strategies, which greatly accelerate the speed of route finding through fast pruning. Through a large number of experiments, applying the method proposed in this paper can effectively perform scenic spot extraction and travel route planning and compare the effects of multiple optimization strategies. On the basis of taking tourists as the center, the optimal route is planned around the interest, time, budget, experience, and other factors of tourists; a personalized travel route can bring tourists the best travel experience.

Kumoro and Hasanah said that at present, by studying several professional travel websites in China, it is found that the current recommendation method is mainly based on the recommendation of a single tourist attraction [5]. If tourists want to make overall planning for the travel route, there are mainly two ways; the first one is that tourists can obtain letters through social platforms such as strategies, magazines, and friend recommendations and then make travel plans according to their own time, budget, etc. The second way is to design the routes according to the most popular tourist cities, the most visited cities, and the highest star ratings, by the travel platform (usually including travel agencies and travel websites, etc.), but these routes are fixed. It is the same for all mass tourists and ordinary consumers. In the past, this kind of planning met the basic needs of mass tourists, but in today's highly developed information, tourists are more eager to obtain a personalized travel experience. At the same time, this planning method also ignores some scenic spots with high quality, which is not conducive to the development of these scenic spots. In addition, it is impossible for travel agencies to designate exclusive travel routes for every ordinary tourist. Therefore, not all the scenic spots in the routes formulated by the travel platform are of interest to tourists. For these attractions, tourists can only passively accept them, and these methods have different drawbacks. At the same time, if tourists choose the method to plan the route by themselves, they may develop an inappropriate route due to information asymmetry, unreliable information, and other factors; therefore, there are some shortcomings in these two methods.

Hu et al. said that according to the problem background and data type, the graph convolutional network in deep learning and IoT technology is used to capture useful information in user and scenic spot data, in order to expect better scenic spot recommendation effect, and provide users with intelligent recommendation services that can meet their interests and preferences [8]. The recommended comprehensive processing module removes the tourist attractions that the target user has traveled and forms a final recommendation set to recommend to the target user. At this point, the module design is completed. The test results show that, for the same target user, compared with the traditional recommendation model, tourism-based recommendation, there is some new information in the recommended results of the scenic spot recommendation model, and the recommended content is more comprehensive, and the recommendation model is better than the traditional recommendation model.

(1) Radio frequency identification technology

Radio frequency identification technology, also known as RFID technology, emerged in the 1990s and is an automatic identification technology. Radio frequency identification technology is based on the basic principle of radio frequency signal and its spatial combination and transmission characteristics, which can realize the automatic identification of stationary and moving objects. Radio frequency identification technology does not require mechanical contact or optical contact between the identification system and the identification target but identifies specific targets and completes the reading and writing of related data through radio signals. From the perspective of the operation mode of radio frequency identification technology, the basic components of radio frequency identification system mainly include the following three types, and tags are mainly used for communication with radio frequency antennas, which are divided into two categories: active and passive. The tags include coupling elements, chips, and built-in antennas. Each tag has a unique electronic code, which is attached to the object and identifies the target object. RFID readers can read the target object's data stored in the tag. The reader is the information control and processing center of the RFID system, it is composed of a radio frequency module and a digital signal processing unit, the main function is to read and write the tag and read and write the data information in the tag, and it can be fixed. It can also be hand-carried. The application of radio frequency identification technology is inseparable from the spatial propagation of radio frequency signals and wireless communication connections. The function of the antenna is to realize the spatial propagation of frequency signals between the tag and the reader and establish a wireless communication connection, which is the medium between the tag and the reader. Not only that, the identification range of the RFID system is affected by the antenna design parameters, and the higher the antenna performance, the greater the identification range of the RFID technology, which requires the antenna to have superior impedance matching characteristics. The application range of RFID technology is extremely wide, and it can be used to track and manage almost all physical objects, such as electronic tickets in scenic spots, and automatic road tolls [9].

(2) Sensing technology

Sensing technology includes two parts: sensors and wireless sensor networks; first, as far as sensors are concerned, a sensor is an information detection device that can not only detect information but also transmit the detected information in electrical signals or other forms. In the Internet of Things, sensors are mainly responsible for information collection, which is a prerequisite for automatic detection and automatic control and occupies a fundamental position. The application value of sensors is significant, and with the continuous upgrading of technical means, the application fields of sensors are also expanding, becoming important equipment in industrial production, energy development, aerospace, and national defense. Secondly, as far as the wireless sensor network is concerned, the wireless sensor network is a multihop self-organizing network formed by

wireless communication, which is composed of many micro sensor nodes in a specific area. As a brand-new information acquisition platform, the wireless sensor network can dynamically monitor and collect the information of the detected objects in the area and send the acquired information to each gateway node. In addition to micro sensor nodes, the constituent elements of wireless sensor networks also include receivers and transmitters, communication satellites, and task management nodes. Micro sensor node is not only the constituent unit of wireless sensor network, but also a completed sensor unit, including sensor unit, processing unit, communication unit, and power supply, and it has the advantages of rapid development and strong invulnerability. It plays an important role in the construction of smart scenic spots [10].

(3) Network and communication technology

The Internet of Things technology is the product of the development of network information technology. Network and communication technology is the most basic content of the Internet of Things technology, and it is also the precondition for the emergence of the Internet of Things technology. Network and communication technology includes two parts: network technology and computer communication technology. First of all, in terms of network technology, network technology is the combination of computer technology and communication technology, which can connect computers in different areas through communication equipment and lines, so as to achieve the goals of information transmission and resource sharing. The network system is the external manifestation of network technology, including the communication network and network resources. The main equipment includes network management, network bridges, routers, switches, repeaters, and hubs. Barrier-free communication can be achieved between each node in the network system; secondly, in terms of computer communication technology, computer communication refers to the process of information exchange and transmission between devices and computers and between computers. From the perspective of the development process of communication technology, it is mainly divided into three stages: the era of analog communication, the era of digital communication, and the era of data traffic. The Internet of Things technology was born in the era of data communication, and the so-called data communication refers to the data signal sent by the information source as the carrier. The specific exchange methods are divided into three types: message exchange, circuit exchange, and packet exchange. The information sharing and transmission between computers mainly rely on network protocols, and the network protocols are not fixed and need to be selected according to the actual situation [11].

(4) Data mining and fusion technology

Data mining technology is the fusion of artificial intelligence and database technology, also known as knowledge discovery in database, and the main function is to dig out an information resource that can meet people's data usage needs from massive, random, and noisy data. The combination of

questionnaire survey and automatic capture is used to collect user information, user ratings, and other tourism data, and stratified sampling of the data is used to generate a “smart tourism” data set containing user travel preference information. Based on this dataset, the user ratings are preprocessed, and a collaborative filtering algorithm is carried out based on user clustering to calculate the similarity between the target user and the cluster center. Combined with the travel preference information generated by the stratified sampling model, a mixed recommendation list is output. Data mining includes three stages of data preparation, data mining, and result expression, which can extract valuable information from the database. Data mining is realized through data analysis, and with the help of the analysis of massive data, valuable information can be mined from it. Data analysis methods mainly include association analysis, classification analysis, cluster analysis, anomaly analysis, evolution analysis, and specific group analysis. Each analysis method can dig out a type of valuable information; for example, with the help of correlation analysis, the relevant information in the massive information can be presented; for example, with the help of evolution analysis, the evolution process of a set of data can be displayed. Data mining technology has greatly improved the application value of data information and has very significant value in many fields such as market planning, business decision-making, and financial forecasting. Information fusion is the development trend of data mining technology, and data mining and fusion technology, one of the key technologies of the Internet of Things, is the product of the connection between data mining and information fusion. Data mining and fusion technology is based on the information resources obtained by data mining, uses existing knowledge and experience to process information in different fields, and uses this information to identify, estimate, and judge targets [12].

(5) Convolutional neural network model

In deep learning, convolutional neural networks (CNN or ConvNet) are a class of deep neural networks [13]. Convolutional neural network is a shared weight architecture based on convolution kernel, and features were used to scan hidden layers. Its network structure usually consists of multiple convolutional layers and fully connected layers, and a pooling layer is usually inserted into the convolutional layers. The convolution operation can be viewed as a process in which one function performs a linear transformation on another function to map to a new value. We can think of it as a sliding window function applied to the matrix; as shown in Figure 1 below, the convolution kernel slides on the feature matrix by a specified step size, multiplies the convolution kernel matrix value and the feature matrix value in turn, and then finds and gets a full convolution. Use the convolution kernel to slide on the feature matrix to get different feature layers. The pooling layer reduces the amount of data computation by combining the outputs of a layer of neurons, the usual pooling types are max pooling or average pooling, and a smaller feature matrix is obtained through pooling and then connected to the next layer. Fully connected layer is an important part of convolutional neural network (CNN), the convolutional neural network process starts with convolu-

tion and pooling, decomposes the matrix into features, and then analyzes them independently, the result of the process will be passed into a fully connected neural network structure, and the optimal result from this structure is the final classification decision. Finally, the fully connected layer is connected to the output layer, and finally, the probability prediction values of different classifications are obtained to form an interest vector. The number of layers of the convolutional network can be increased according to requirements and accuracy.

(6) Activation function

The activation function is also an important concept in convolutional neural networks, so it is explained as a single concept [14]. Biologically, whether a neuron is activated depends on whether the signal value is greater than a certain threshold. In the artificial neural network, the activation function is to judge whether the feature strength of a certain area reaches a threshold. The activation function determines the output of the deep learning model, its accuracy, and the computational efficiency of training the model. Commonly used activation functions help to normalize the output of each neuron to a range of 1 to 0 or -1 to 1. If the trigger condition is not met, the function indicates that the convolution kernel has no features extracted in this area, or the features are very weak; common activation sigmoid function, tanh function, the popular ReLU function, leaky ReLU function in recent years, and Softmax function.

2.1. Tourist Attraction Recommendation Method Based on Graph Convolutional Network. This section will introduce the proposed personalized travel recommendation method based on graph convolutional network, and the overall structure includes four parts: embedding layer, information dissemination aggregation layer, information self-encoding layer, and prediction layer.

(1) Embedding layer

Like the mainstream recommendation system, the latent vectors x_u and $x_i \in R^d$ of the Euclidean space are used to represent the user u and the scenic spot i , respectively, and d represents the dimension of the embedding vector, thus establishing a lookup table X as the initial value of users and attractions, which is randomly initialized through normal distribution, as shown in the following formula:

$$X = [x_{u_1}, x_{u_2}, \dots, x_{u_N}, x_{i_1}, x_{i_2}, \dots, x_{i_N}], \quad (1)$$

where N and M represent the number of users and attractions, respectively. In the traditional recommendation model, the initial embedding vectors of users and attractions are directly input into the interaction layer for end-to-end optimization, but users and attractions in real scenes are not isolated, and there is a certain connection between them. When the feedback records of users are sparse, simple splicing or nonlinear interaction cannot well extract the associations between users and users, users and attractions, and

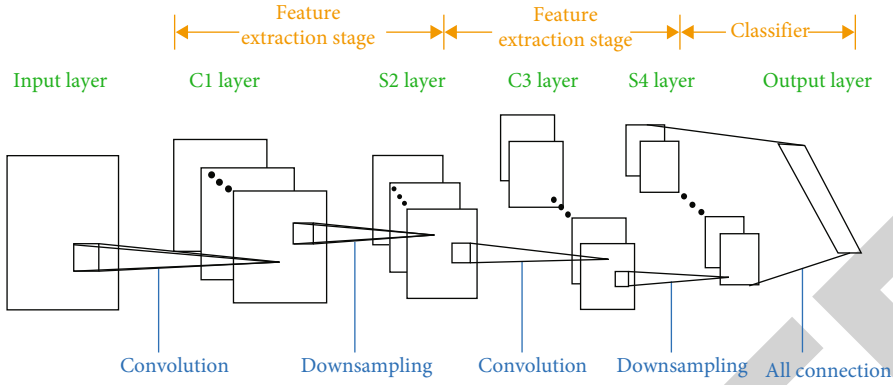


FIGURE 1: Principle of convolutional neural network.

attractions and attractions. All users and attractions are regarded as each node in the graph, so that preference information is propagated in the user-attraction interaction graph, so that nodes not only focus on local neighbors but also obtain higher-order relationships between users and attractions through information diffusion, and contacts get effective collaborative information embedding into user and sight embedding vectors to alleviate the data sparsity problem.

(2) PageRank-based graph convolutional network information propagation and aggregation layer

In the user-spot interaction, each user or scenic spot is not isolated but related to each other, and the user's direct interactive scenic spot is defined as the user's local neighbor, for example, scenic spot i_1, i_2, i_4 in Figure 2 is the local neighbors of user u_1 , they reflect the user's direct preference evidence, and the user's potential preference is also affected by the local neighbors. Attraction i_2, i_4 is visited by user u_2 to establish a connection, so u_1 is the second-order neighbor of u_2 , and u_2 reflects the second-order potential preference of user u_1 . However, the farther the neighbor nodes are from user u_1 , the smaller the preference and influence on user u_1 's node is, which is a decay process, similar to water waves. The user's preference information can be regarded as the diffusion of personalization on the interaction graph. Therefore, when the user has only a few sparse interactions, this connection and preference propagation relationship can be used to spread the user's preference to higher-order neighborhoods to obtain the user's higher-order latent preference, as shown in Figure 2.

Existing research shows that graph convolution can effectively process data with graph structure, and some progress has also been made in the field of recommendation; using graph convolution to mine collaborative signals from graph structure to obtain user preferences can improve recommendation performance [15]. Studies have shown that GCN will oversmooth as the number of layers increases, all nodes will tend to a value, and as the number of layers increases, the amount of parameters will also increase exponentially. And some studies have shown that the number of GCN layers generally needs to reach 4-5 layers to cover all

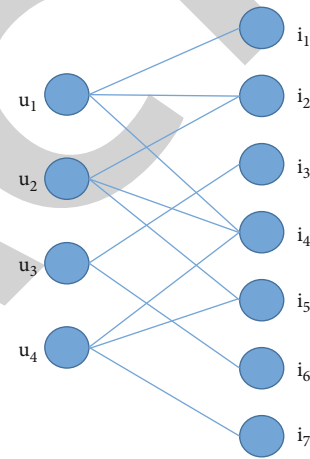


FIGURE 2: User-attraction interaction diagram.

nodes in the graph, the traditional graph convolution method has very limited expandable neighborhoods, and the effect on the problem of user cold start is not ideal. Differentiated numerical similarity calculation methods are designed for different types of users to alleviate the deficiencies of traditional numerical similarity when faced with sparse data. Finally, numerical similarity and structural similarity are combined to form sparse cosine similarity. Inspired by the literature, we utilize a graph convolutional network with personalized PageRank propagation to model the process of user preference propagation on the user-spot interaction graph, the algorithm increases the opportunity to transmit back to the root node and does not have to be limited by the size of the node neighborhood, it can effectively aggregate an infinite number of neighborhoods to obtain user and scenic spot information into the node embedding vector, and there will be no node smoothing.

Embedding vector for each user and attraction node, the information of its neighbor nodes and the embedded information of the node itself are combined through the neural network. For a user node x_u reaches the scenic spot node x_i in a random walk, the preference information of node x_u is also propagated to node x_i , then node x_i carries the preference information of user node x_u , and node x_u is

adjusted through personalized PageRank propagation, such as the following formula:

$$m(x_u) = \alpha \left(I_n - (1 - \alpha) \hat{A} \right)^{-1} x_u \quad (2)$$

m represents the message embedding (that is, the information to be propagated), $\alpha \in (0, 1]$ is the transmission probability, $I(u, i)$ is the influence score of node x_i on node x_u , the influence of node x_i on node x_u is equal to the influence of node x_u on node x_i , and this value is different for each root node. The preference influence reduction from the root node can be adjusted by α . The matrix-form propagation equations of the propagation rules of each layer of the graph convolution of personalized PageRank propagation are as follows:

$$Z^0 = H = X, \quad (3)$$

$$Z^{l+1} = (1 - \alpha) \hat{A} Z^{(l)} + \alpha H, \quad (4)$$

where $Z^l \in R^{(N+M) \times d_l}$ is the embedding vector of users and attractions obtained after l -step propagation. X^0 is set to X during the initial message passing iteration; I represents an identity matrix, $\hat{A} \sim D^{-1/2} A \sim D^{-1/2}$ is a symmetric normalized adjacency matrix with self-circular sum, and A represents the Laplacian matrix of the user-item graph, expressed as the following equation:

$$A = \begin{pmatrix} 0 & R \\ R^T & 0 \end{pmatrix}, \quad (5)$$

where $R \in R^{N \times M}$ is the user-item interaction matrix, 0 is the matrix with all 0s, A is the adjacency matrix, and D is the opposite angle matrix. Personalized PageRank Propagation Graph Convolutional Networks can efficiently use even infinitely many neighbor aggregation layers, so higher-order connectivity information can be explored by stacking more embedding propagation layers. As shown in Figure 3, a small number of user access records can be extended to all nodes to obtain the user's potential preference information.

(3) Information autoencoder

For the embedding vector of each layer of users and scenic spots obtained through the graph convolutional network propagated by personalized PageRank, an autoencoder is used to filter the encoded information to obtain the effective embedding vector of each layer of users and scenic spots, and for the final model prediction, the calculation formula is shown in the following equation:

$$E^l = W_1^l Z^{(l)}. \quad (6)$$

$W_1^{(l)} \in R^{d \times d'}$ is a learnable parameter for each layer, which is used to extract useful information in the embedding vectors of users and attractions obtained by each propagation layer for message aggregation.

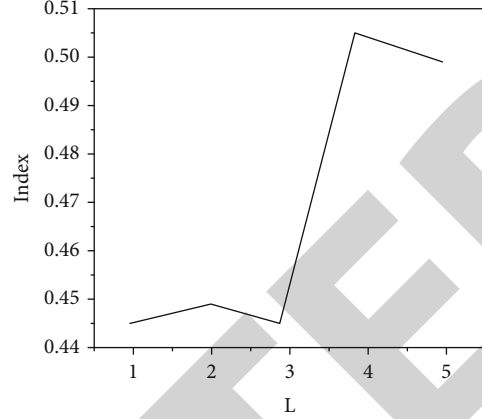


FIGURE 3: The result of the influence of the number of propagation layers L on the Recall@10 indicator of cold-start users.

2.2. Experimental Setup. The author uses two datasets, MFW and UbiComp, to verify the effectiveness of the proposed method, MFW is a self-built tourism dataset, and UbiComp is a widely used public restaurant recommendation dataset; it is used to verify the universality of the algorithm, and the details are as follows:

MFW: the dataset used for the experiment contains 9157 users who have visited at least two destinations and 1407 attractions that have been visited by at least 10 users, and we choose a destination that users recently visited as a test and travel records of other destinations visited as training. Users who visit less than 4 attractions in the training set are cold-start users, and other users are hot-start users [16].

UbiComp: this dataset includes New York City restaurant check-in and labeling data collected from Foursquare from October 2019 to February 2020, including 3112 users, 3298 sites, and 27149 access records. The users who visit less than 4 attractions in the training set are cold-start users, and other users are hot-start users [17]. The traditional neuron classification method based on geometric morphology relies on the extraction and selection of neuron spatial structure features, which will lose a lot of useful neuron classification information. The adaptive projection algorithm is used to convert three-dimensional neurons without extracting the neuron's characteristics.

3. Results and Analysis

3.1. Performance Comparison Experiment of Different Recommendation Methods on MFW Dataset. In order to verify the effectiveness of the model, we compare the proposed method with several mainstream recommendation methods, which are introduced below, and the BPR method optimizes the MF model using pairwise Bayesian personalized ranking loss [18]. The PTRMJL method is a personalized travel recommendation method based on multiview joint learning [19]. PTRMJL is a travel package recommendation method based on multiview attention mechanism. It learns the unified representation of travel packages with the help of deep learning technology and

TABLE 1: Comparison of algorithm recommendation performance for different types of users on MFW dataset.

Type	Method	Recall@5	Precision@5	NDCG@5	Recall@10	Precision@10	NDCG@10
Warm user	BPRMF	0.239	0.284	0.267	0.346	0.243	0.367
	PERMJL	0.320	0.351	0.450	0.478	0.295	0.482
	NGCF	0.279	0.284	0.362	0.390	0.251	0.387
	GCMC	0.339	0.341	0.441	0.469	0.299	0.468
	PTRGCN	0.347	0.339	0.440	0.459	0.291	0.462
Cold user	BPRMF	0.214	0.230	0.373	0.314	0.205	0.304
	MRPTR	0.292	0.333	0.399	0.442	0.272	0.440
	NGCF	0.270	0.259	0.329	0.382	0.226	0.362
	GCMC	0.325	0.306	0.392	0.444	0.265	0.427
	PTRGCN	0.393	0.357	0.464	0.496	0.291	0.490

learns the user’s interest representation based on the long-term and short-term clickstream data of online travel users to generate recommendations. The method consists of tourism package encoding and user interest encoding. In the tourism package encoding module, a unified tourism package representation is learned by using word-level and view-level attention networks to select important words and views from the attributes of the tourism package. The GCMC method employs a GCN encoder to generate representation vectors for users and items, considering only the nearest neighbors [20]. The NGCF method propagates user and item embeddings on the user-item graph data structure and then comprehensively utilizes each layer of propagated embeddings combined with CF for recommendation [21]. In order to evaluate the performance of recommendations, we provide a list of Top-N recommendations for each user in the test set.

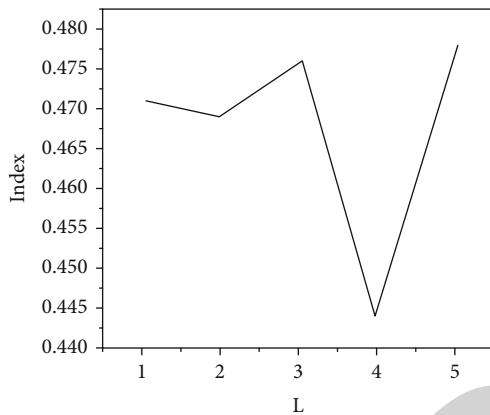
Table 1 presents the comparison of the two types of recommendation performance between the proposed method and other recommendation methods on the MFW dataset. It can be seen from the table that PTRGCN outperforms several other comparison methods in the user cold-start scenario of the MFW dataset. For hot-start users, the PTRMJL method has the best recommendation performance, and the method proposed by the author is second only to the PTRMJL method and the GCMG method, but it is 5.7% more accurate than the BPR method, 9.7% improvement in recall rate. In the recommendation for cold-start users, the method proposed by the author has the best performance in terms of precision rate, recall rate, and normalized loss cumulative gain, and the recall rate Recall@5 is 17.9% higher than BPR, and the accuracy is improved by 11.8%. The method proposed by the author has better travel recommendation performance for cold-start users than hot-start users, because the algorithm utilizes the deep potential connections between nodes; since hot-start users are directly connected to more scenic spots than cold-start users, there are many local neighbors, during the training process. Overfitting may lead to performance degradation; therefore, the method proposed by the author is more suitable for cold-start users, as shown in Table 1.

3.2. Performance Comparison of Different Recommendation Methods on UbiComp Dataset. In order to verify the universality of the proposed method, the author verified the effectiveness of the method on the UbiComp dataset, and the experimental results are shown in Table 2. From the experimental results, it can be seen that the PTRGCN method proposed by the author improves the accuracy of Precision@5 by 15.8%, the recall rate of Reach@10 by 7.4%, and the improvement of NDCG@10 by 14.5% for hot-start users. The recommendation performance accuracy rate, recall rate, and normalized ranking index of cold-start users are higher than those of warm-start users. For cold-start users, the accuracy rate of Precision@5 is increased by 13.1%, and the recall rate of Recall@10 is increased by 17.1%. Because cold-start user access records are sparse, methods such as BPR and GCMG are limited by data sparsity and have low accuracy. Therefore, the method proposed by the author effectively improves the recommendation performance for cold-start users on the basis of maintaining the recommendation performance of hot-start users, as shown in Table 2.

3.3. The Effect of the Number of Propagation Layers. The number of layers of graph propagation plays a key role in the method proposed in this chapter, and the method proposed by the author does not make nodes smooth as the number of layers deepens. The author discusses the impact of changing the depth of graph model propagation on recommendation performance, and Figures 3 and 4 show the results of experiments on the dataset MFW. From the experimental results, it can be seen that the PTRGCN method achieves the best performance when the number of layers in the recommendation for cold-start users is $L = 4$, and the performance when $L = 5$ is similar to that when $L = 4$, and the algorithm successfully avoids the oversmoothing problem; with the increase of the number of layers, the recommendation recall rate and accuracy rate of cold-start users increase, and the recommendation performance improves more significantly than that of hot-start users. Since hot-start users have more local neighbors to represent their preferences, and cold-start users have few access records, they

TABLE 2: Algorithm recommendation performance comparison for different types of users on UbiComp dataset.

Type	Method	Recall@5	Precision@5	NDCG@5	Recall@10	Precision@10	NDCG@10
Warm user	BPRMF	0.002	0.003	0.003	0.004	0.003	0.004
	NGCF	0.053	0.139	0.172	0.068	0.107	0.142
	GCMC	0.070	0.024	0.070	0.035	0.058	0.063
	PTRGCN	0.062	0.161	0.176	0.080	0.126	0.149
Cold user	BPRMF	0.001	0.002	0.005	0.001	0.001	0.002
	NGCF	0.117	0.118	0.170	0.143	0.086	0.170
	GCMC	0.044	0.043	0.049	0.062	0.039	0.057
	PTRGCN	0.132	0.131	0.166	0.172	0.103	0.174

FIGURE 4: The effect of the number of propagation layers L on the recommendation index of the hot-start user Recall@10.

need to mine users and scenic spots that have deep connections with users through the expansion of layers; therefore, cold-start users are more than hot-start users, and users are more sensitive to an increase in the number of layers. Cold-start users need higher-level expansion, so that users' potential preferences can be propagated to more nodes to mine users' deep-level preferences, as shown in Figures 3 and 4.

4. Conclusion

The author proposes a tourist attraction recommendation method based on deep learning and Internet of Things research, using graph convolutional network architecture to provide tourist attraction recommendation mainly for cold-start users. From the experimental results, it can be seen that the PTRGCN method improves the accuracy by 15.8% on the hot-start user, on the Reach@10 by 7.4%, and on the NDCG@10 by 14.5%. The recommendation performance accuracy rate, recall rate, and normalized ranking index of cold-start users are higher than those of warm-start users. For cold-start users, the accuracy rate of Precision@5 is increased by 13.1%, and the recall rate of Recall@10 is increased by 17.1%. Because cold-start user access records are sparse, methods such as BPR and GCMG are limited by data sparsity and have low accuracy. Through experimental deduction, it is proved that deep

learning and Internet of Things technology can effectively meet the needs of tourist attractions recommendation.

Data Availability

The data used to support the findings of this study are available from the corresponding author upon request.

Conflicts of Interest

The author declares no conflicts of interest.

References

- [1] Q. Zhang, Y. Liu, L. Liu, S. Lu, and X. Yu, "Location identification and personalized recommendation of tourist attractions based on image processing," *Traitement du Signal*, vol. 38, no. 1, pp. 197–205, 2021.
- [2] Y. M. Arif, S. Harini, S. Nugroho, and M. Hariadi, "An automatic scenario control in serious game to visualize tourism destinations recommendation," *IEEE Access*, vol. 9, pp. 89941–89957, 2021.
- [3] K. A. Alattas and A. Mardani, "A novel extended internet of things (iot) cybersecurity protection based on adaptive deep learning prediction for industrial manufacturing applications," *Environment, Development and Sustainability*, vol. 24, no. 7, pp. 9464–9480, 2022.
- [4] C. T. Guo, D. A. Polasky, F. Yu, and A. I. Nesvizhskii, "Fast deisotoping algorithm and its implementation in the MSFragger search engine," *Journal of Proteome Research*, vol. 20, no. 1, pp. 498–505, 2021.
- [5] D. T. Kumoro and U. Hasanah, "Tinjauan desain interface website E-commerce wisata Mototravel.id menggunakan evaluasi heuristik," *JTIM Jurnal Teknologi Informasi dan Multimedia*, vol. 2, no. 1, pp. 43–49, 2020.
- [6] A. Kumar, K. Abhishek, C. Chakraborty, and N. Kryvinska, "Deep learning and internet of things based lung ailment recognition through coughing spectrograms. IEEE," *Access*, vol. 9, pp. 95938–95948, 2021.
- [7] M. A. Al-Garadi, A. Mohamed, A. Al-Ali, X. Du, and M. Guizani, "A survey of machine and deep learning methods for Internet of Things (IoT) security," *IEEE Communications Surveys & Tutorials*, vol. 22, no. 3, pp. 1646–1685, 2020.
- [8] Y. Hu, H. Shen, W. Liu, F. Min, and K. Jin, "A graph convolutional network with multiple dependency representations for relation extraction. IEEE," *IEEE Access*, vol. 9, pp. 81575–81587, 2021.

Retraction

Retracted: Application of BP Neural Network in Matching Algorithm of Network E-Commerce Platform

Journal of Sensors

Received 13 September 2023; Accepted 13 September 2023; Published 14 September 2023

Copyright © 2023 Journal of Sensors. This is an open access article distributed under the Creative Commons Attribution License, which permits unrestricted use, distribution, and reproduction in any medium, provided the original work is properly cited.

This article has been retracted by Hindawi following an investigation undertaken by the publisher [1]. This investigation has uncovered evidence of one or more of the following indicators of systematic manipulation of the publication process:

- (1) Discrepancies in scope
- (2) Discrepancies in the description of the research reported
- (3) Discrepancies between the availability of data and the research described
- (4) Inappropriate citations
- (5) Incoherent, meaningless and/or irrelevant content included in the article
- (6) Peer-review manipulation

The presence of these indicators undermines our confidence in the integrity of the article's content and we cannot, therefore, vouch for its reliability. Please note that this notice is intended solely to alert readers that the content of this article is unreliable. We have not investigated whether authors were aware of or involved in the systematic manipulation of the publication process.

Wiley and Hindawi regrets that the usual quality checks did not identify these issues before publication and have since put additional measures in place to safeguard research integrity.

We wish to credit our own Research Integrity and Research Publishing teams and anonymous and named external researchers and research integrity experts for contributing to this investigation.

The corresponding author, as the representative of all authors, has been given the opportunity to register their agreement or disagreement to this retraction. We have kept a record of any response received.

References

- [1] J. Zhang, "Application of BP Neural Network in Matching Algorithm of Network E-Commerce Platform," *Journal of Sensors*, vol. 2022, Article ID 2045811, 8 pages, 2022.

Research Article

Application of BP Neural Network in Matching Algorithm of Network E-Commerce Platform

Jingcheng Zhang 

Rey Juan Carlos University, Center for Higher Education for Business, Innovation and Technology (IUNIT), Madrid 28002, Spain

Correspondence should be addressed to Jingcheng Zhang; 202003332@stu.ncwu.edu.cn

Received 29 June 2022; Revised 24 July 2022; Accepted 16 August 2022; Published 26 August 2022

Academic Editor: Haibin Lv

Copyright © 2022 Jingcheng Zhang. This is an open access article distributed under the Creative Commons Attribution License, which permits unrestricted use, distribution, and reproduction in any medium, provided the original work is properly cited.

In order to solve the matching algorithm problem of network e-commerce platform, a method of applying BP neural network in the network e-commerce platform matching algorithm is proposed. First of all, combined with the actual situation of the platform, select 9 factors that are most in line with the company's actual business model to influence the selection for analysis; secondly, import 60 sets of data into MATLAB software, measure the input and output data uniformly, and divide the sample data matrix into training set and test. Finally, after multiple factor combinations and verifications, it is concluded that in the training model of the five main factors, the prediction results of the model are compared with the real values. The feasibility of establishing the selection model based on BP neural network is proved. Online e-commerce platforms can refer to this model to build a product selection model that meets the needs of the platform, helping enterprises to achieve more efficient product selection work. Since the parameter initialization of the neural network is random, although the output results are different after the program runs for many times, the R^2 is still stable between 0.7 and 1.0, which proves that the predicted value made by the system is highly approximate to the real value and can achieve the predicted effect.

1. Introduction

Back propagation neural network (BP network) is one of the most mature and widely used artificial neural networks. Its basic network is three-layer feedforward network, including input layer, hidden layer, and output layer. For the input signal, it is necessary to propagate forward to the hidden node. After the function, the output information of the hidden node is transmitted to the output node, and finally, the output variable result is obtained. The neuron node function is usually taken as the S-type function. BP network can realize any complex nonlinear mapping relationship from input to output and has good generalization ability. It can complete the task of complex pattern recognition, as shown in Figure 1 [1].

With the development of national economy and Internet technology, network e-commerce platform has developed more and more rapidly in recent years. Among many cross-border e-commerce models, the buyer platform reduces the selection cost of consumers, improves consumers' trust, and is favored by consumers by directly participating in

the source organization, commodity selection, logistics, warehousing, and sales process. But at the same time, under this mode, the capital occupation is high, which requires enterprises to accurately perceive the needs of consumers. Platform buyers need to have high selection ability to improve the dynamic sales rate and ensure the healthy operation of the platform. At present, platform buyers rely more on personal experience and traditional data processing methods for product selection. Buyers often fail to make the choice of maximizing benefits due to the deviation of personal subjective judgment.

2. Literature Review

In the face of this problem, most of the existing studies give reasonable suggestions to guide the selection of products on the network e-commerce platform by analyzing many factors affecting the selection of products on the network e-commerce platform, such as using technical selection method, trial and error selection method, and market selection method. However, most of the existing studies give

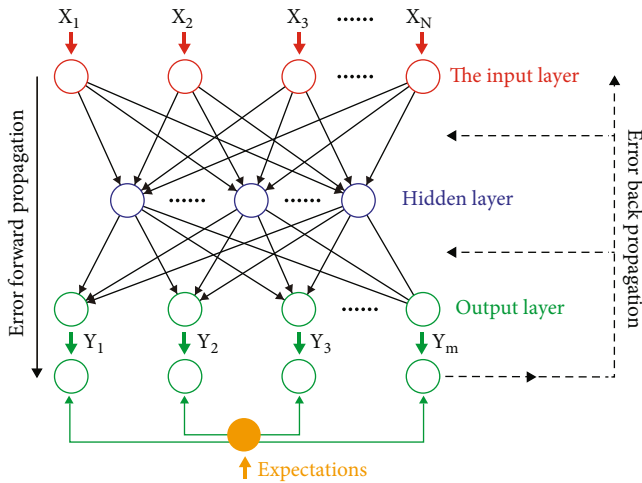


FIGURE 1: Structure of BP neural network.

selection suggestions from the perspective of qualitative analysis and lack of selection model after quantitative analysis, and the accuracy of selection is difficult to verify. On the basis of previous studies, this paper studies the selection process and related influencing factors of online e-commerce platform, selects the optimal combination of influencing factors through quantitative analysis, and verifies it. At present, artificial intelligence technology has been applied to all aspects of human life, and the fashion retail industry has also begun to explore the use of artificial intelligence and big data technology to change the traditional operation mode and help enterprises achieve more accurate market prediction and style development. This paper uses the artificial intelligence algorithm (BP neural network) to find the combination of factors that can output the best prediction results, so as to build a selection model that can help platform buyers reduce personal subjective judgment deviation and improve the accuracy of selection, so as to realize the accurate prediction of commodity selection.

Lu et al. presented an entity matching method based on distance. The main task of this method is to give appropriate weights to the attributes of each describing entity [2]. Liu stated that based on the idea of reducing the solution space of the genetic algorithm by constructing the feature ellipse of feature point set and the parallel mechanism of genetic algorithm, a feature point matching algorithm based on genetic algorithm search strategy under affine transformation is proposed [3]. Murthy et al. introduced the concept of matching matrix while using the relaxation algorithm. They adopted the idea of two-way matching [4]. Wu et al. proposed a point feature matching algorithm based on the crosscorrelation function. Firstly, crosscorrelation is used to obtain the initial matching between feature point sets, and then epipolar geometric constraints are used to screen the patterns of matching point pairs to obtain accurate feature point matching point pairs [5]. Moholkar and Patil studied the fast point pattern matching algorithm, which uses the clustering method to determine the rotation of two point sets to be matched θ , and the algorithm has high efficiency [6]. Du designed a new feature point matching algorithm. The search strategy of this

method adopts the deterministic annealing algorithm, which shows good robustness to false points, high proportion of missing points, and noise [7]. Kung proposed a matching algorithm similar to the iterative matching nearest point (ICP) method. The idea of the algorithm is to select the nearest set of feature points at each step of the iteration to determine the corresponding relationship and then obtain the spatial transformation according to the corresponding relationship [8]. Jin regards platform enterprises as modules based on the business ecosystem, and enterprises can provide users with complementary products or services through the platform [9]. Wang et al. focused on the differences between industrial platforms and product platforms and proposed that the realization of user value by industrial platforms is mainly through the provision of complementary products and services. These enterprises complement each other through the technical platform with common reuse basis provided by industrial platforms [10]. Yiyue et al. pointed out that customs clearance is the biggest barrier restricting the service quality of crossborder e-commerce, and the uncontrollability of its process greatly affects the convenience of transaction [11].

On the basis of current research, a matching algorithm optimization for network e-commerce platform based on BP neural network is proposed. By studying the main factors affecting the selection decision of online crossborder e-commerce buyer platform, 15 influencing factors in five categories are summarized. Combined with practical cases and using BP neural network, a three-layer neural network model is finally constructed, which takes price competitiveness, brand popularity, product popularity, design creativity, and product sales as five inputs and the probability of successful sales of goods as a single output. Since the parameter initialization of the neural network is random, although the output results of the program run many times are different, R2 is still stable between 0.7 and 1.0, which proves that the predicted value made by the system has a high approximation to the real value and can achieve the prediction effect [12].

3. Optimization of Matching Algorithm of Network e-Commerce Platform Based on BP Neural Network

3.1. BP Neural Network

3.1.1. Theoretical Basis. Artificial neural network is an important content in the field of artificial intelligence. Its structure and working principle are designed according to the organizational structure and activity rules of the human brain, but it is not a true restoration of the human brain. It only reflects some characteristics of the human brain and is a simplification, abstraction, or imitation of it. With the prominence of the advantages of neural network and the deepening of its theoretical research, neural network theory has been gradually applied to the automatic matching technology of feature points. BP neural network is one of the most classical and mature networks in the neural network theory system. It was proposed by the team of scientists led by Rumelhart and McClelland in 1986. It is a multilayer feedforward neural network trained according to the error

back propagation algorithm. BP neural network can learn and store a large number of input-output mode mapping relationships without knowing the mathematical equations describing this mapping relationship in advance. This self-learning, self-organization, and self-mapping ability of BP neural network makes it more and more widely used [13].

3.1.2. Working Principle of BP Neural Network Algorithm.

The learning rule of BP neural network uses the steepest descent method. The basic BP algorithm includes two aspects: forward propagation of signal and back propagation of error. That is, the actual output is calculated in the direction from input to output, while the correction of weight and threshold is carried out in the direction from output to input. The weight and threshold of the network are continuously adjusted through back propagation to minimize the sum of squares of the error of the network. BP neural network works by several neurons through certain connections. Each neuron has a general model, and its general model is shown in Figure 2 [14].

x_i is the input of neurons, w_i is the connection weight between neurons, b is the threshold of neurons, or bias, f is the transfer function of neurons, or excitation function, and y is the output of neurons. y is calculated by formula (1).

$$y = f\left(\sum_{i=1}^R x_i w_i + b\right). \quad (1)$$

The topological structure of the BP neural network model includes three parts: input layer, hidden layer, and output layer. Theoretically, due to the introduction of hidden layer neurons, a three-layer BP neural network can realize the mapping of multidimensional space R^M to R^N with arbitrary accuracy.

3.1.3. BP Neural Network Design. Because the specific application fields of BP neural network are different, it is necessary to design a practical and reliable BP neural network model for specific problems. Usually, the design of BP neural network needs to consider the number of layers of the network, the number of neurons in each layer, the selection of initial weight and threshold, and learning rate, and relevant experts and scholars have summarized some design experience and guiding principles. The details are as follows:

(1) *Number of Layers of the Network.* It has been proved that the three-layer BP neural network can realize the accurate mapping of multidimensional space R^M to R^N . Although increasing the number of layers can further improve the accuracy and reduce the error, it also increases the complexity of the network, thus increasing the training time of the network [15]. Therefore, unless special circumstances, priority can be given to reducing network error and improving accuracy by appropriately increasing the number of hidden layer neurons on the basis of three-layer BP neural network.

(2) *Number of Neurons in Hidden Layer.* In terms of improving the accuracy of network training, although only one hid-

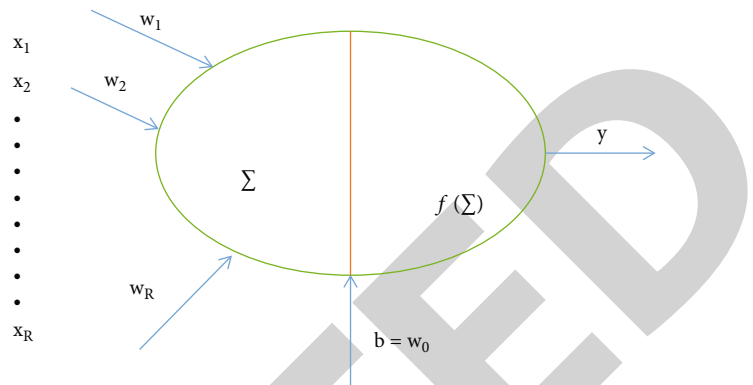


FIGURE 2: The single neuron structure model of BP neural network.

den layer is used, the method of increasing the number of neurons is much simpler than increasing the number of hidden layers. However, the number of hidden layers is not the more the better. Practice has proved that with the increase of the number of hidden layers, the training error of the network continues to decrease. At the same time, there will be the phenomenon of network training overfitting, which will reduce the generalization ability of the network.

(3) *Selection of Initial Weight and Threshold.* Because the BP neural network algorithm system is nonlinear, the selection of the initial weight and threshold of the network determines which point of the error surface the network training starts from. This not only directly affects the training time of the network but also relates to whether the training results of the network can get the global optimal solution. For example, if the initial weight and threshold are too large, the input falls into the saturation region of the S-type transfer function after the network weighting calculation, resulting in a very small gradient, which makes the adjustment process difficult to continue. Therefore, it is generally expected that after the initial weighting calculation of the network, the output of neurons will approach zero as much as possible, so that the weight of each neuron can be adjusted at the place where their S-type activation function changes the most [16]. Therefore, it generally takes the random number with the initial weight between $[-1, 1]$. The initial weight and threshold of traditional BP neural network are selected by random initialization in the $[-1, 1]$ interval. At this point, the algorithm with global optimization characteristics can be used to assist in selecting the initial weight and threshold of the network.

(4) *Transmission Function, Learning Rate, and Learning Function of Network.* In general, the transmission function of the network hidden layer adopts the S-type function, while the output layer adopts linear function. If the learning rate is too high, it will lead to the global optimal solution, and it is easy to enter the global optimal solution. There are many ways to design the learning function, among which the Levenberg-Marquardt back propagation learning algorithm, which is commonly used and has better performance and training speed, is selected.

To sum up, although the neural network with hidden layer can realize the mapping of multidimensional space RM to RN, if some parameters are selected appropriately in the training process, the training time of neural network can be shortened, and satisfactory training results can be obtained. Among them, the selection of network initial weight and threshold has a great impact on the training process. BP neural network has high nonlinearity and strong generalization ability, but the standard BP algorithm has some disadvantages, such as easy to fall into local minimum solution, slow convergence speed, and oscillation effect. At present, there is no complete theory to guide the design process of BP neural network. At present, its design mainly focuses on the design and optimization of network structure and the adjustment algorithm of network weight and threshold. In this regard, relevant experts have summarized many optimization methods on the basis of a large number of research [17]. In the optimization of network structure design, based on the strategy of traditional optimization theory, algorithms such as waterfall correlation construction method, crosstest method, and neural center surgery optimization are proposed. The gradient descent algorithm is usually used in BP neural network. The gradient descent algorithm has an obvious advantage. It only follows one direction in local optimization; so, the search speed is very fast. However, the gradient descent algorithm is easy to fall into the local optimal solution. Therefore, other algorithms are often needed to optimize it in practical application.

3.2. Proposal of BP Neural Network Matching Method

3.2.1. Starting Point of Method Proposal. Feature point matching is to find the corresponding matching relationship and spatial mapping relationship between two feature point sets. The mapping relationship between image points obtained by the same spatial point on different images is determined to exist, and its mapping relationship is shown in Figure 3.

Although the mapping relationship between spatial points and image points and between image points on different images becomes complex due to the influence of shooting angle and environment, if the influence of external noise is not considered, the mapping relationship of all feature point sets of the image is basically the same. Therefore, if the corresponding relationship of a certain number of feature points is determined in advance by some method, the matching of the remaining feature points can be completed in theory. Generally, the matching method based on the position of platform feature points often needs to establish its accurate mathematical model. If the mathematical model is not accurate enough, it will directly reduce the correctness of the matching results and even lead to matching failure. BP neural network has the ability of self-learning and self-mapping. Its input and output relationship itself can be regarded as a mapping relationship. Users only need to provide some a priori samples for network learning without knowing the specific mapping relationship between sample input and output [18]. Therefore, when the matching relationship of some feature points in the feature point set of the platform is known, the matching of the remaining fea-

ture points can be completed by establishing the BP neural network mapping model. The feature point matching method based on BP neural network is actually equivalent to using BP neural network to fit an inherent and exact mapping relationship. Generally, BP neural network has two pre-conditions in fitting application:

(1) There are enough known samples for network training and self-learning. (2) There is an exact but unknown or functional relationship between the input and output of samples. As mentioned earlier, there is a certain mapping relationship between images taken from different angles of the same space object, and when some matching points are obtained by some method, it meets the premise of using BP neural network.

3.2.2. Idea of BP Neural Network Matching Method. Taking the matching of the platform as an example, this paper takes the characteristic points of the known matching relationship on the platform as the training samples of the network, trains the network, obtains the mapping relationship of the platform simulated by the network, and uses the mapping model to predict the corresponding relationship between the point sets to be matched. That is, the feature points in the left figure are successively input into the trained network model, and the predicted position of the matching points of these feature points in the right figure can be obtained through the calculation of the network model. Due to certain errors in network prediction, it is impossible for the predicted position to coincide with the actual position; that is, there is a certain distance. However, as long as the error is within the allowable range, it can be considered that there are corresponding matching points in these feature points in the figure. Otherwise, it is considered that there are no matching points in the graph. If the corresponding matching point exists, the feature point closest to the predicted position is selected as the correct matching point within the allowable error range according to the principle of maximum similarity. The flow chart of the whole process is shown in Figure 4 [19].

In fact, in the feature point matching method based on BP neural network, the most important work in the early stage is to establish the BP neural network model. It can be said that after the network model is established, the mapping relationship between feature points will be known, and then the feature point matching will be completed.

3.3. Establishment of BP Neural Network Matching Method Model. As mentioned above, the most important and core task of using BP neural network for feature point matching is to establish an ideal network model that can correctly reflect the mapping relationship between platform feature point sets [20]. The matching method based on BP neural network includes three parts: sample classification and processing, the design of BP neural network topology, and the design of matching constraint criteria.

3.3.1. Sample Classification and Processing. To complete the matching process of feature points to be matched, we must first analyze and process the sample data. The analysis and

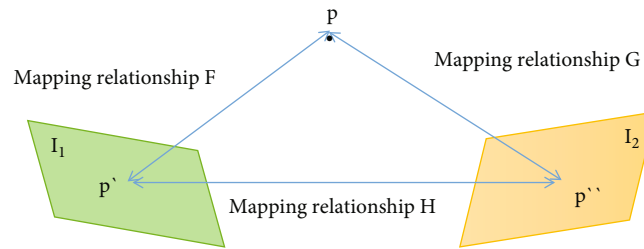


FIGURE 3: Schematic diagram of mapping relationship between image points obtained by the same spatial point on different images.

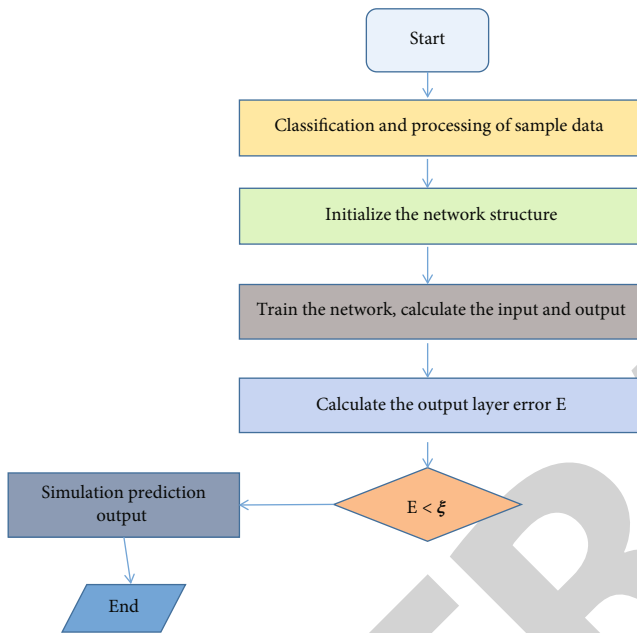


FIGURE 4: Flow chart of the BP neural network matching method.

processing of sample data in this subject mainly include the normalization of samples and the division of samples.

(1) *Sample Normalization*. Normalization is to limit the data to be processed to a certain range after being processed by some algorithm. Firstly, normalization is for the convenience of later data processing. Secondly, it speeds up the convergence when the correction program is running and can convert the dimensional data into dimensionless data, so as to eliminate the phenomenon that some attributes of the sample cannot play a practical role due to the large difference between the data [21]. Although normalization cannot be carried out, because the transfer function used by BP neural network is the Sigmoid function, its value is between 0 and 1, it is often sensitive to the number between [0, 1], and the output function of neuron is the most sensitive between [0, 1] ([-1, 1]). Therefore, in order to improve the efficiency of training, the sample data should be normalized before the network training.

(2) *Sample Division*. After the network model is established, it is necessary to analyze its approximation ability to the laws contained in the samples. Its approximation ability, that is,

generalization ability, should be evaluated by the error size of nontraining samples. The most direct and objective criterion to judge whether the established network model can effectively reflect the real law is that the error of other samples other than training samples is as small as possible and close to the error of training samples [22]. Through repeated experiments, it is found that the trend law of training sample error and sample error to be tested is inconsistent, and sometimes, there is an opposite trend, while the trend of verification sample training error and sample error to be tested is basically the same. This shows that the network training may enter the state of over fitting, resulting in a small error of the training samples and a large error of the samples to be tested. Therefore, we cannot use all the known samples for network training but reserve a small number of samples to evaluate the network performance and finally determine the optimal network result. Therefore, before network training, all training samples are divided into training samples and nontraining samples. In this paper, the result of the minimum training error of the verification sample is retained as the final network result, and the network is used to match the feature points to be matched. In this paper, this method is called the method of using validation samples to determine the final network results [23].

3.4. *Development History of Online Crossborder e-Commerce Platform Industry*. Online crossborder e-commerce activity refers to an international business activity in which trading entities across different customs territories complete commodity transactions through e-commerce platform, and the third party makes payment and settlement and delivers commodities with the help of crossborder logistics system to perform transactions. The crossborder e-commerce mentioned in this paper mainly refers to the individuals engaged in this activity; that is, crossborder e-commerce enterprises, which aims to summarize the business model innovation as an individual enterprise through the analysis of the general environment of the industry. At present, the development of online crossborder e-commerce can be roughly divided into three stages, realizing the industrial upgrading from information services to online transactions, and then to the whole industrial chain services.

- (1) Crossborder e-commerce phase 1.0: at this stage, China's crossborder e-commerce is fledgling. As a tentative complementary channel with traditional international trade, the focus is on channel development and marketing promotion. Using the Internet

as a channel to open up the market reduces the operating costs of small and medium-sized enterprises participating in international trade and makes them have more advantages in international competition. At the same time, the effectiveness of marketing promotion is also particularly critical. Most of the companies involved in providing such services are large-scale, represented by Alibaba International Station and Global Tesco

- (2) Crossborder e-commerce phase 2.0: after creating the crossborder e-commerce trade mode, foreign trade enterprises at this stage began to use e-commerce platforms providing various services more skillfully and began to integrate resources and establish their own crossborder e-commerce companies with the help of seller's platform, payment platform, and logistics platform, and the proportion of online transactions gradually increased
- (3) Cross border e-commerce phase 3.0: at this stage, foreign trade enterprises use the platform of crossborder e-commerce more deeply and make full use of various tools. Some foreign trade enterprises began to establish their own overseas warehouses and overseas teams and received more feedback from overseas consumers through the Internet, producing corresponding products for sale [24]

3.5. Development Status of Online Crossborder e-Commerce Platform Industry. Online crossborder e-commerce has developed against the background of the shrinkage of the traditional international trade market. The global financial crisis in 2008 pushed the international trade competition to a white hot stage. With the deepening of trade friction, the appreciation of RMB, and the increasing cost of means of production such as labor and land, the traditional import and export trade has been hit hard. In this context, the development of crossborder e-commerce has sprung up. The total amount of crossborder e-commerce transactions in 2010 was 1.3 trillion yuan, which had doubled to 290 million yuan by 2013.

4. Design and Application of Selection Model Based on BP Neural Network

4.1. Data Set Establishment. Select an online crossborder e-commerce buyer platform for empirical research. The enterprise is a crossborder e-commerce mainly engaged in apparel goods of overseas luxury brands, and its goods suppliers are mainly Italian luxury dealers. Based on the factors affecting the selection in Table 1, the person in charge of the buyer of the platform and several professional buyers engaged in the selection work in the enterprise were interviewed. Combined with the actual situation of the platform, 9 factors affecting the selection that most accord with the actual business model of the company were selected, which are price competitiveness, brand popularity, product popularity, design creativity, fabrics and materials, compatibility, wearability, natural environment, and past sales of products (similar or similar). At the same time, according to the

degree or subjective evaluation, from low to high, a 5-level scale is adopted to formulate quantitative scoring standards for each factor. For example, among the price competitiveness factors, "1" means that the product price competitiveness is very low, "5" means that the product price competitiveness is very high; In terms of fabric and material factors, "1" means that the product fabric and material are very poor, and "5" means that the product fabric and material are very good. Then, with the permission of the crossborder e-commerce buyer platform, the commodities with a selling out rate of more than 80% and a selling out rate of less than 20% in 2019 were randomly selected, and a total of 60 commodities were collected, of which the commodities with good sales and poor sales accounted for half, respectively. The distribution of goods by category is shown in Table 2. Commodity data includes brand item number, commodity name, purchase price, category, color, commodity picture, and historical sales data.

Finally, the commodity data of the 60 pieces (sets) of commodities are made into a table, and the person in charge of the buyer of the platform evaluates each commodity according to the 9 factors affecting the selection. The scores of each influencing factor of each commodity are summarized into the selection model input vector $x = (x_1, x_2, \dots, x_{60})^t$. In the output vector o , the goods with a sold out rate of more than 80% are assigned as "1," and the goods with a sold out rate of less than 20% are assigned as "0."

4.2. Establishment of Neural Network. First, import 60 groups of data into MATLAB software. Secondly, in order to unify the measurement of input and output data, normalize the data to make the final data fall between [0, 1]. Treatment formula (2) is as follows:

$$x_i = \frac{x_i - x_{\min}}{x_{\max} - x_{\min}} \quad (2)$$

Then, the sample data matrix is divided into training set and test set. The training set contains 40 groups of sample data, and the remaining 20 groups of sample data are test sets, which are used to detect the accuracy of the prediction results of the trained neural network. The goods with good sales and poor sales in training set and test set are randomly selected according to the ratio of 1:1. Then, the BP neural network program is written in MATLAB. The number of input layer and output layer nodes of neural network is determined by the training samples. If there are 9 input variables (i.e., factors affecting selection) and 1 output variable (i.e., commodity selection or not), the number of input layer nodes is 9, and the number of output layer nodes is 1. The BP neural network with single hidden layer can map all continuous functions; so, the selection system model adopts the neural network with single hidden layer for training. Hidden layer nodes can be continuously adjusted and determined according to the empirical formula $L \leq m + N + A$, where L represents the number of hidden layer nodes, M represents the number of input layer nodes, n is the number of output layer nodes, and a is a constant of 0~10. In practice, a can be set as 1 first, and the number of nodes corresponding to

TABLE 1: Factors affecting selection.

Factors affecting selection	Factor segmentation	Examples of evaluation methods
Product attributes	Color/pattern	Does it attract buyers' attention
	Fabric/material	Whether there is good performance
Matching degree of fashion trend	Product popularity	Matching degree between attributes and popular trends
Environmental factor	Natural factors	Is it suitable for this season
Sales and inventory	Procurement budget	Whether the purchase budget is met
Supplier situation	Supplier contract conditions	Are the contract details reasonable

TABLE 2: Quantity distribution of collected commodities.

Product category	Sold out rate is higher than 80%	Sold out rate is less than 20%
Blouse	15	6
Women's skirt	4	4
Men's coat	12	16

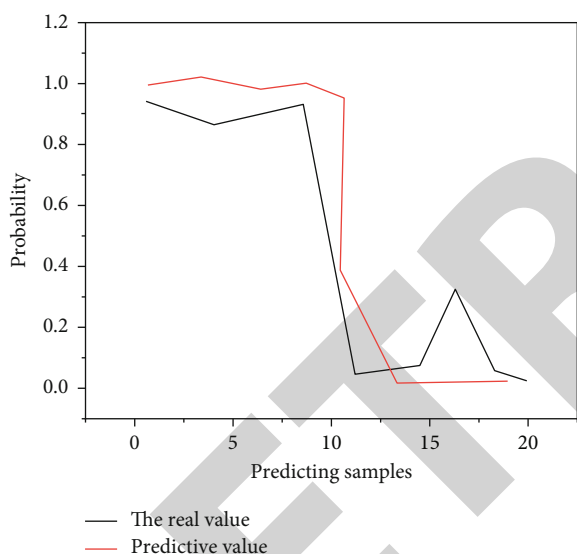


FIGURE 5: Comparison diagram of prediction error of the selection model.

the smallest error can be determined through repeated tests. The activation functions of the hidden layer and the output layer adopt the continuous differentiable unipolar Sigmoid function of nonlinear transformation. The calculation formula (3) is as follows:

$$\text{logsig}(x) = \frac{1}{1 + e^{-x}}. \quad (3)$$

The learning rate is set as 0.001, and the maximum number of training steps is 5000. After the training, the trained neural network is tested with 20 groups of data from the test set, the prediction results are output, and the error is compared with the real value.

4.3. Result Collection and Analysis. After many factor combinations and verification, it is finally concluded that the accuracy of the output prediction result is the best in the training model that retains the five main factors of price competitiveness, brand popularity, product popularity, design creativity, and product sales. The number of input layer nodes is 5, the number of hidden layer nodes is 11, the number of output layer nodes is 1, the learning rate is 0.001, and the maximum number of training steps is 5000 [25]. The comparison between the predicted results of the model and the real value is shown in Figure 5. The ordinate in the figure is the probability of successful sales of goods, "0" represents poor sales of goods (the selling out rate is lower than 20%), and "1" represents good sales (the selling out rate is higher than 80%). Correspondingly, in the selection forecast, "0" means that the buyer platform should not select this commodity in the selection process, and "1" means that this commodity should be selected in the selection process. The circle points in the figure represent the real sales of goods, and the solid points represent the predicted values given by the selection model. It can be seen from the figure that the predicted value of the model is basically consistent with the real value. R2 is the tracking of the predicted value to the real value during the training process. The closer R2 is to 1, the stronger the explanatory ability of the variables in the model to the output variables and the better the prediction accuracy. R2 shown in the figure is 0.95, indicating high prediction accuracy. At the same time, because the parameter initialization of the neural network is random, although the output results of running the program for many times are different, R2 is still stable between 0.7 and 1.0, which proves that the predicted value made by the system is highly approximate to the real value and can achieve the prediction effect.

5. Conclusion

By studying the main factors affecting the selection decision of online crossborder e-commerce buyer platform, this paper summarizes 15 influencing factors in five categories. At the same time, combined with practical cases and using BP neural network, a three-layer neural network model is finally constructed, which takes price competitiveness, brand popularity, product popularity, design creativity, and product sales as five inputs and the probability of successful sales of goods as a single output. The prediction results of the model are relatively stable and accurate. The model verifies the feasibility of constructing the selection model based on

Retraction

Retracted: Design of the Vocal Music Feature Recognition System Based on the Internet of Things Technology

Journal of Sensors

Received 22 August 2023; Accepted 22 August 2023; Published 23 August 2023

Copyright © 2023 Journal of Sensors. This is an open access article distributed under the Creative Commons Attribution License, which permits unrestricted use, distribution, and reproduction in any medium, provided the original work is properly cited.

This article has been retracted by Hindawi following an investigation undertaken by the publisher [1]. This investigation has uncovered evidence of one or more of the following indicators of systematic manipulation of the publication process:

- (1) Discrepancies in scope
- (2) Discrepancies in the description of the research reported
- (3) Discrepancies between the availability of data and the research described
- (4) Inappropriate citations
- (5) Incoherent, meaningless and/or irrelevant content included in the article
- (6) Peer-review manipulation

The presence of these indicators undermines our confidence in the integrity of the article's content and we cannot, therefore, vouch for its reliability. Please note that this notice is intended solely to alert readers that the content of this article is unreliable. We have not investigated whether authors were aware of or involved in the systematic manipulation of the publication process.

Wiley and Hindawi regrets that the usual quality checks did not identify these issues before publication and have since put additional measures in place to safeguard research integrity.

We wish to credit our own Research Integrity and Research Publishing teams and anonymous and named external researchers and research integrity experts for contributing to this investigation.

The corresponding author, as the representative of all authors, has been given the opportunity to register their agreement or disagreement to this retraction. We have kept a record of any response received.

References

- [1] H. Huang, "Design of the Vocal Music Feature Recognition System Based on the Internet of Things Technology," *Journal of Sensors*, vol. 2022, Article ID 1164042, 7 pages, 2022.

Research Article

Design of the Vocal Music Feature Recognition System Based on the Internet of Things Technology

Haifeng Huang 

Nantong Normal College, Nantong, Jiangsu 226000, China

Correspondence should be addressed to Haifeng Huang; 202003000134@hceb.edu.cn

Received 7 July 2022; Accepted 8 August 2022; Published 25 August 2022

Academic Editor: Haibin Lv

Copyright © 2022 Haifeng Huang. This is an open access article distributed under the Creative Commons Attribution License, which permits unrestricted use, distribution, and reproduction in any medium, provided the original work is properly cited.

In order to meet the needs of vocal feature recognition, the author proposes a system design based on the Internet of things technology. The principle of the method is that the body sensory layer of the body puts the sound sensors in different positions, records the primary sound signal, and monitors and makes the sound signal using the TMS320VC5402 light red processor. The network transport layer audio signal processes and sends the voice signal database in the process layer. The sound characteristic analysis module in the application layer uses a real-time dynamic change algorithm to obtain the best similarity between the experimental model and the design, identify the characteristics of the sound set red, and identify the content of the voice feature, the music, and the emotional results of the song. Experiments have shown that the system is capable of recognizing speech in a noisy environment, with an accuracy of approximately 95%, resulting in better sound control and the ability to switch switches and remote control. The system, developed with the Internet of things technology, has been proven to improve voice recognition.

1. Introduction

The history of the development of modern science proves that “computer music,” which appeared in the 1970s, is the intersection of the art of music, research of literature, and the intersection of different disciplines. For the past thirty years, computer music has achieved a wide range of performance and the rapid development of electronic instruments, digital encoding of music, digital compression, and digital storage. It promotes the popularization and application of CD, DVD, digital broadcasting and multimedia, and shows a broad market prospect. However, computer vocal music as a new discipline, its fundamental goal is to use computers to simulate people's cognition and creative intelligence of vocal music. It is very difficult to deal with such subjects as vocal theory, cognitive science, artificial intelligence, information processing, pattern recognition, intelligent control and automation. It should be noted that research in this area has only just begun.

The characteristics of vocal music can be divided into basic characteristics, complex characteristics, and overall characteristics. Correspondingly, the identification of vocal features can also be divided into three levels: firstly, the basic features of vocal music are extracted, the second is to analyze the complex features on this basis, and the last is to identify the overall features of the music according to the basic and complex features of vocal music, including the musical structure, style, and emotional connotation of vocal music.

Recognition of sound features depends on the development of the art of speech recognition, the acquisition of the sound content through music, and the acquisition of sounds such as sound style and feelings. The study of sound features covers a wide range of topics, including the study of psychoacoustics, the analysis of musical instruments, and the study of music theory. Currently, voice recognition technology is not widely used due to the lack of design capabilities to help improve data performance. With the advent of the Internet of things technology, it has become a voice recognition tool.

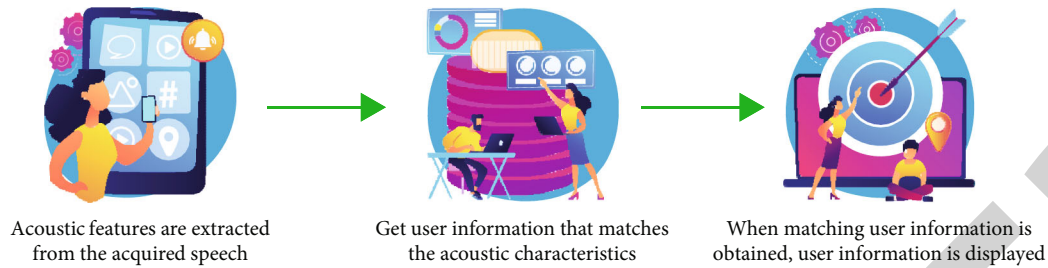


FIGURE 1: User recognition method based on sound features.

Figure 1 shows the user experience based on the characteristics of the sound. Internet of things technology enables intelligent detection, operation, and monitoring of audio signals by transmitting data over wired and wireless networks in real time, with improved accessibility, high quality, good delivery, convenience, and speed. Create an Internet of things that recognizes sound based on Internet technology, and use the Internet of things technology to receive, transmit, and recognize music [1].

2. Literature Review

The advent of computers and communication has led to many interdisciplinary disciplines that provide science and art. In the search for music, music has gradually shifted to digital literature and technology as an art form that interacts with everyday life and learning. In recent years, the development of modern musical instruments, including the use of electronic music, has led scientists to pay more attention to the recognition, production, and integration of computer music [2].

At present, the research on vocal music information is mainly divided into three aspects: vocal music cognition, vocal music creation, and vocal music database retrieval. In terms of vocal music cognition, it includes not only the analysis and recognition of complex features such as rhythm and harmony but also a computer system that can analyze vocal music style, feel vocal music like a human, and perform vocal music like a performer. In terms of vocal music creation, it includes the following two aspects: one is to recombine some vocal pieces according to a certain style. The other is to combine vocal music with visual art and produce different graphics and animations according to vocal music. In terms of vocal music database retrieval, according to a short melody, the corresponding songs are found in the vocal music database, which will be of great significance for the search of vocal music data [3]. Because vocal music information contains a lot of fuzziness and uncertainty, lack of strict mathematical description and mathematical model, can not be solved by traditional information processing methods. So most of the research uses fuzzy system neural network expert system genetic algorithm and other intelligent information analysis and processing methods.

With the rapid development and widespread popularization of computer technology, the Internet of things technology provides great convenience for vocal music recognition and has become a hot spot in the research and development

of vocal music recognition today. From the perspective of the needs of vocal music recognition, multimedia technology represented by sound spectrum analysis technology, MIDI technology, and audio workstation technology can reach a considerable level in terms of sound wave display, pitch measurement, and voice part determination; however, in actual vocal music recognition middle, the use of these techniques is rare. The reason is that, first, vocal musicians often have professional theoretical knowledge and practical experience of vocal music but lack systematic computer theoretical knowledge, so they cannot master various computer operation techniques in time. Second, many IoT technologies are scattered on their respective software and hardware platforms and can only be used for the analysis of a certain segment or several segments of voice and cannot be used as a systematic vocal recognition software. Aiming at the above problems, research and develop an intuitive and easy-to-operate vocal music recognition system, which has high practical and popularization value [4].

Based on the current research, the author presents models of voice recognition based on IoT technology. The author's design addresses the inadequacy of the existing voice recognition capability to eliminate noise and provides the MIC with a special antinoise function using the BU8332KV-M signal processing IC combined with the V290pub speaker recognition module, effective to reduce noise, voice recognition, and finally achieve the purpose of voice control terminal.

3. Research Methods

3.1. Identification Method of Vocal Features

3.1.1. Rhythm Recognition. In music, it is only when the repetition of the texts is set up that the music becomes more closely related to their relationships (e.g., percussion, atherosclerosis, and steady atherosclerosis) that it becomes important. Thus, the concept of atherosclerosis is a narrow reversal of the sequence of sounds and the main purpose of cognition is to find similar rhythms that are separated by the difference of the assembly. Because rhythm patterns have nothing to do with sound, rhythmic studies are usually included, So the rhythm can be represented by a set of numbers. How to show in [5]. Although this method is simple, it does not affect the force of the form, so some studies use graphs to show the time of the horizontal axis and the speed and force of the vertical line [6].

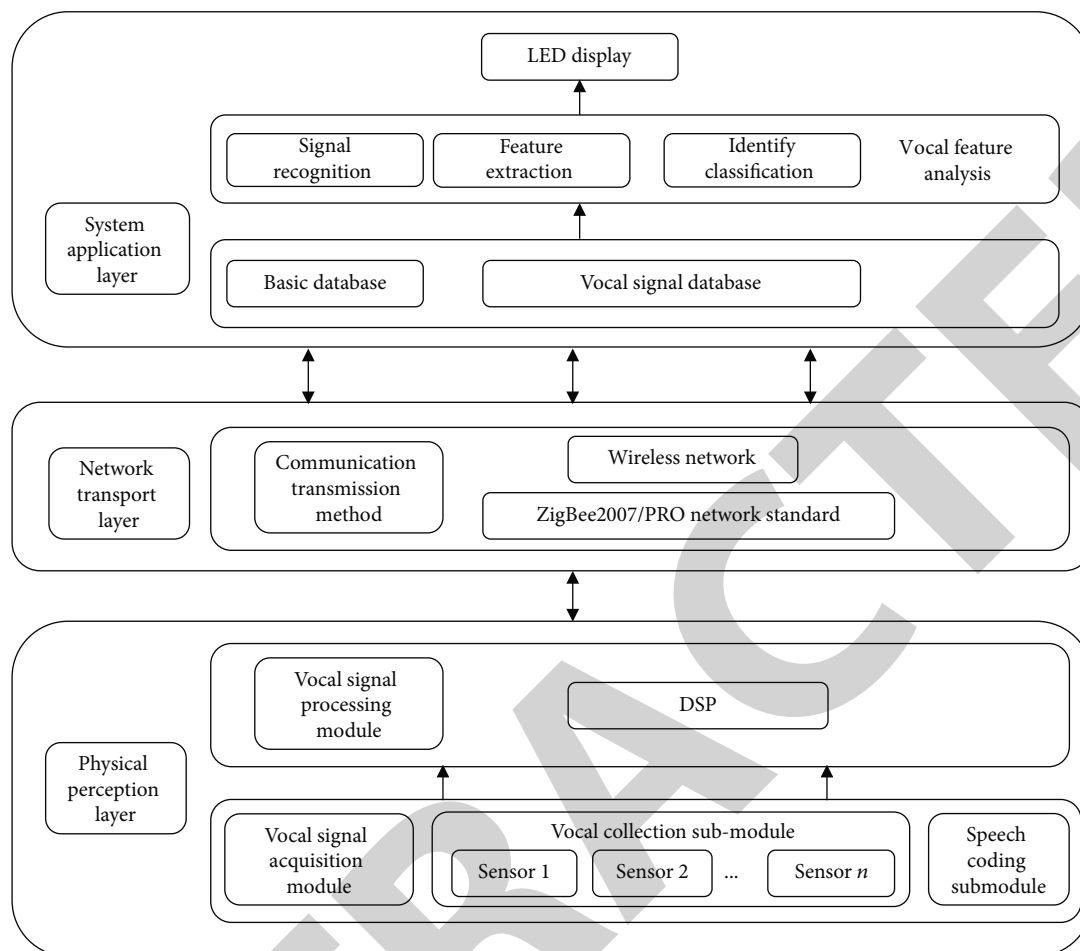


FIGURE 2: Block diagram of the overall structure of the system.

In order to be familiar with music, it is first necessary to design a traditional assembly pattern in a stable assembly [7]. The patterns of sound and percussion patterns are intertwined and together represent the structure of the period. In Western music, this type of continuity is usually multilayered, so the assembly pattern must be multilayered. One way to identify music is to compare the music that has been identified to the original melody patterns, which is difficult because the music is constantly changing [8]. So now, the experience of the ensemble is focused on the stable and the special music, especially the dance music.

3.1.2. Identification of Melody. The main factors that affect the melody are pitch and length. Since the melody perceived by people is only a meaningful outline, it is far more than the perception of pure pitch, so the method of recording the relative pitch is often used (for example, the minor second is "1") [9, 10]. There are roughly three ways to describe the melody: the first method is based on the first note of the studied piece, as a standard note to record the pitch difference of other notes from the standard note. The second method is to record the pitch difference of two adjacent notes. The advantage of these two methods is to save storage space, and it avoids the influence of transposition on the melody

itself; the disadvantage is that it is not imagery enough and it is not suitable for recording harmony. The third method is extended on the basis of the above two methods, and the relative pitch value is represented by two-dimensional coordinates; this method is more intuitive and solves the problem of recording harmony. The fourth method is to use a tree-like structure, which can not only record the outline of the melody but also reflect the structural characteristics of the melody. In addition, some scholars have adopted the fuzzy set method [11].

A piece of music is often played by many kinds of instruments, including melody, harmony, and rhythm parts, so the main content of melody recognition is to find the main melody of the piece [12, 13]. Since a piece of music or a movement of a piece of music will have a theme, such as Beethoven's "Fate" and Tchaikovsky's "Sadness," these themes are mostly repeated through the main melody, so the main melody can be used in the whole piece (movement) to search for the number of repetitions of a certain melody and locate the one with the highest number of repetitions as the main melody. The difficulty is that these main themes are often rewritten in six ways: imitation, canon, inversion, increment, depreciation, and retrograde, rather than simply repeating [14]. Therefore, the key to determining the main melody is to determine

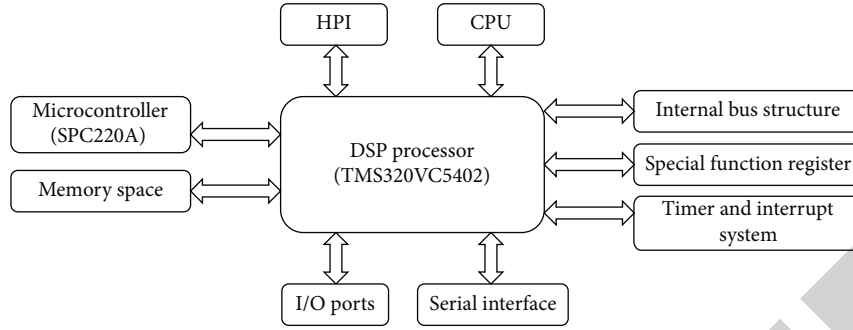


FIGURE 3: TMS320VC5402 functional structure diagram.

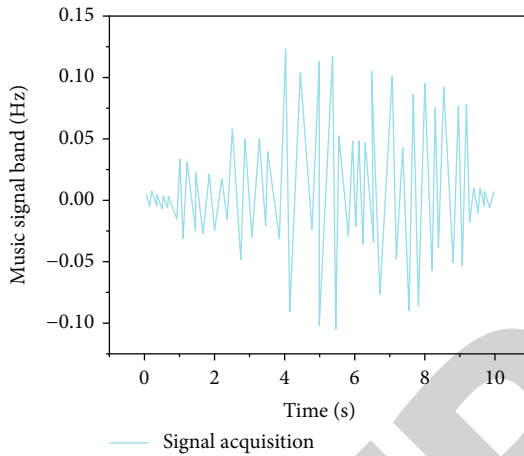


FIGURE 4: Vocal signal acquisition results (location 1).

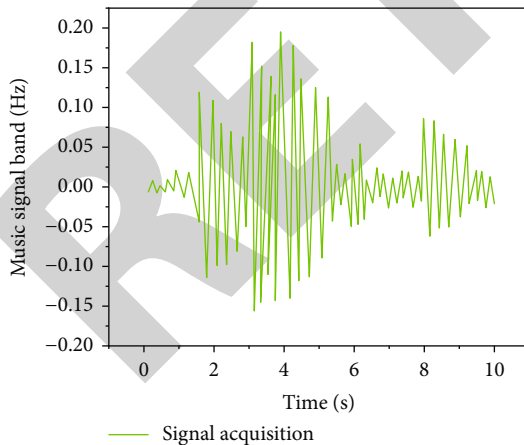


FIGURE 5: Vocal signal acquisition results (location 2).

whether the two melodies are essentially similar, such as whether there are ornamental sounds, additional sounds, missing sounds, etc. At the same time, for Western classical music, the melody part has the following characteristics compared with the rhythm and harmony parts:

- (1) The melody should be the loudest sequence
- (2) There should be no more than two octave changes in pitch between adjacent notes, and the number of large pitch changes should not be too many
- (3) A complete phrase should be played by the same timbre
- (4) The melody is coherent, usually lasting several bars

3.1.3. Harmony Recognition. Harmony analysis requires a comprehensive knowledge of harmony theory. The difficulty and key point of harmony analysis in music feature recognition system lies in how to embed this knowledge into the whole system in a reasonable way. Some research teams have successfully designed fuzzy systems that automatically analyze sound. [15]. However, because there are too many individual elements in music, it is difficult to fully explain it with the existing music theory, so the analysis of harmony is only limited to the category of music works of a certain style or a certain era.

3.2. Overall Structure of the Vocal Feature Recognition System. The system for recognizing the characteristics of music based on the Internet of things technology is usually a layer of physical understanding, a layer of network connections, and a layer of technology [16]. A block diagram of the entire structure of the system is shown in Figure 2.

The process of understanding the body usually includes patterns for receiving sounds and patterns for making sounds [17]. Among them, the audio signal receiver module determines the signal demand from the sound sensor receiver system in various locations and sends the audio signal to the signal processing module, which uses the DSP processor. This module uses DSP processor to process vocal signal. The network transport layer transmits the data collected and processed by the physical perception layer to the system application layer through wireless network communication. The network transmission layer records the level of physical understanding through the wireless network communication and sends the completed data to the process layer. The application layer of the system records the music and creates a record of the characters [18].

3.2.1. The Design of the Vocal Signal Acquisition Module. The audio signal receiving module includes the audio receiving

equipment and speech encoding submodule. The audio receiver submodule has sound sensors installed in different locations and is responsible for receiving the noise. The voice sensor has a voice-sensitive built-in capacitor power microphone, which is converted by an A/D converter and sent to a speech-encoding submodule. The speech-encoding submodule is responsible for compressing the main signal with high accuracy without loss, converting the signal into the input file, and then transmitting it to the audio signal processing module.

3.2.2. Design of the Vocal Signal Processing Module. The audio signal processing module is designed for the DSP processor [19]. The module uses a stable DSP chip TMS320VC5402DSP suitable for voice signal operation, and DSP chip has low power consumption, is fast, can carry 2 MCBSPS (multichannel non-stop port), and is connected to CODEC (codec) with audio input, 8-bit upgraded host parallel port (HPI8), 4KBROM, and 16KBDARAM. Its structure is shown in Figure 3.

The internal cabinets of TMS320VC5402 are as follows:

The interior design of the bus consists of 4 bus and 4 software/bus data which design 8 16-bit bus. The specialized >function file contains 26 specialized operational files for tracking, managing, and accessing each office. The timer and trigger itself include a 4-bit preset 16-bit timer. The main memory space of TMS320VC5402DSP is 192 KB, and all the storage space, data space, and input and output space are 1/3, and the application storage space can be up to 1 MB. The TMS320VC5402DSP has two general inputs and ports, BIO and XF. In addition, access to the input and output allows for input and output port expansion and the HPI and MCBSP of the TMS320VC54XDSP can be configured according to the general purpose owners. The MCBSP of the TMS320VC5402 is capable of operating in the SPI mode, which is effective for serial A/D and serial E2PROM connections. The host port provides a single connection for the DSP connection and the external process, which is ideal for exchanging data between the DSP and the external process.

3.3. Identification of Vocal Features

3.3.1. Feature Recognition of Vocal Signal. The voice characteristic analysis module in the system application layer uses the dynamic time (DTW) algorithm to determine the sound signal characteristics by comparing the Euclidean distance of the sound characteristics test models and designs [20]. Follow the research of the DTW algorithm to develop sound measurement models, use conversation patterns, and sound similarity. Assume that the design and test samples are represented as follows:

$$\begin{aligned} S &= \{S(1), S(2), S(m), S(M)\}, \\ P &= \{P(1), P(2), P(n), P(N)\}. \end{aligned} \quad (1)$$

In the model, all the word frames are included in the design and test model; m and n are arbitrary multiple numbers of S and P . The method of calculating the Euclidean distance is

shown in equation (2):

$$l[P(n), S(m)] = \frac{1}{k} \sum_{r=1}^K (H_r - H'_r)^2. \quad (2)$$

The DTW algorithm searches and marks the optimal local path, accumulates the local distance along this path to obtain the global cumulative distance, obtains the optimal template matching similarity, and takes this path as the optimal path. Assuming that the grid points that the path passes through in turn are $(n1, m1), \dots, (ni, mi), (nN, mM)$, according to the endpoint constraints, we can get $(n1, m1) = (1, 1)$ and $(nN, mM) = (N, M)$, in order to meet the slope constraint; the slope selection interval is $0.5 \sim 2.5$.

From the perspective of local search, it is assumed that the last lattice point of the lattice point (ni, mi) passed by the best path is one of the three $(ni - 1, mi)$, $(ni - 1, mi - 1)$, and $(ni - 1, mi - 2)$; assume that the partial cumulative distances from the origin to these three grid points are $L[(ni - 1, mi)]$, $L[(ni - 1, mi - 1)]$, and $L[(ni - 1, mi - 2, respectively)]$; then, (ni, mi) selects some grid points with the smallest cumulative distance to move forward and so on. The cumulative distance of the final path is shown in formula (3):

$$L[(ni, mi)] = l[T(n_i, R(m_i))] + L[(ni - 1, mi - 1)]. \quad (3)$$

Therefore, the minimum cumulative distance is the maximum similarity between the test template and the reference template, that is, the vocal signal feature recognition result.

3.4. Vocal Feature Content Recognition

3.4.1. Feature Extraction of Vocal Music. The melody of vocal music usually includes two similar phrases. In order to analyze the structure of vocal music form, the method of searching similar melody is adopted. The search efficiency and accuracy are improved through the three-step identification method of preliminary identification, key identification and supplementary identification, while taking into account the rhythm and harmony characteristics of vocal music form. [21]:

- (1) Preliminary identification according to rhythm and tonality preliminarily divides the entire vocal music according to vocal rhythm and tonality characteristics, narrows the scope, provides a basis for key identification, and increases search efficiency
- (2) Through the identification of key points of melody search, according to the characteristics of vocal music, the 3-step hypothesis is adopted to further increase the search efficiency of similar melody

Assumption 1. 16 measures make up a phrase. This hypothesis is widely used in vocal structure research and has been tested to be correct.

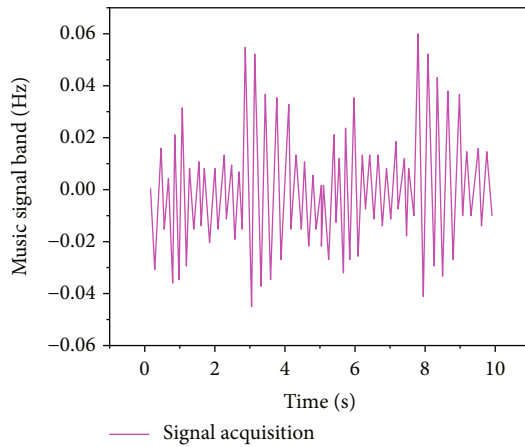


FIGURE 6: Vocal signal acquisition results (location 3).

TABLE 1: Music feature recognition results.

Place	Curved features	Emotional characteristics	Recognition accuracy (%)
1	One piece	Solemnly	100
2	Variation	Enthusiastic	100
3	Rondo	Lyrical	100

Assumption 2. The key part of the phrase is the first 4 bars. This hypothesis uses a small number of notes to characterize the phrase, and the hypothesis is correct.

Hypothesis 3. The clarinet, violin, and flute are the most likely instruments to play the main melody among many instruments. This assumption is conducive to quickly finding the main melody tone, which is the premise of key recognition through melody search.

Based on the 3-step hypothesis, a tree structure is used to record the overall outline of the melody and the search for similar melody is completed. The tree structure includes 4 layers: the first layer is a melody consisting of 16 bars. The 2nd layer is the first 4 bars of the melody. The 3rd layer is the 3 upbeats of each measure. The 4th layer is the upbeat and half beats of each measure. The rhythm of the tree structure is 34 beats, and the main function is to record the relative pitch of the vocal music.

- (3) Based on the harmonic characteristics and supplementary identification of vocal music, after preliminary identification and key identification, vocal-style features can be extracted but there are exceptions [22]. Therefore, by terminating a vocal structure and the harmonic complement of a musical idea to identify the musical structure, improve search accuracy

3.4.2. Vocal Emotion Feature Extraction. After the music feature was released, the song was divided into several smaller

tunes. The speed, music, sound, and other characteristics of each section are assessed, and the characteristics of the mind are obtained by the use of ambiguous materials. Finally, the notion of music is necessarily explained according to thought patterns [23].

4. Results Analysis

Using VisualC++ to simulate the system prototype on the Windows2010 platform, verify the validity of the system. The vocal signals of three different locations in a monitoring area collected by the system sound sensor are shown in Figures 4–6 [24]. It can be seen from the figure that the curve of the vocal signal collected by the system is smooth, there is no burr, and no signal interruption occurs, indicating that the system is running stably and the sound quality of the collected vocal signal is good [25]. According to the vocal signal collected, the results of using the system to identify the vocal characteristics are shown in Table 1.

From the analysis of Table 1, it can be seen that the system accurately identifies the characteristics of music and the perception of music and the level of knowledge of music in intelligence up to 100%. The experimental results show that the system is capable of detecting speech in a loud environment, with an accuracy of approximately 95%.

5. Conclusion

The author has developed voice recognition based on IoT technology output; the audio signal receiving system can receive music from multiple sources, set up speech-encoding submodules, get high-precision, lossless compressed original music signal, etc., can improve and reduce power consumption, and improve the accuracy of music feature recognition. The author provides the software and hardware design of each system modules, the choice of hardware equipment is reasonable, the design performance is perfect, the system certification is high, security is good, and integration is easy. Experiments have shown that the system is capable of recognizing speech in a noisy environment, with an accuracy of approximately 95%, which achieves sound control and can switch keyboards and switches remote control. As a result, the Internet-based system of any technology can improve the perception of sound quality.

Data Availability

The data used to support the findings of this study are available from the corresponding author upon request.

Conflicts of Interest

The authors declare that they have no competing interests.

References

- [1] G. Dhiman, V. Kumar, A. Kaur, and A. Sharma, "Don: deep learning and optimization-based framework for detection of novel coronavirus disease using x-ray images," *Interdisciplinary*

Retraction

Retracted: Optimization Strategy Analysis of Intelligent Product Service System Based on Computer Simulation Technology

Journal of Sensors

Received 13 September 2023; Accepted 13 September 2023; Published 14 September 2023

Copyright © 2023 Journal of Sensors. This is an open access article distributed under the Creative Commons Attribution License, which permits unrestricted use, distribution, and reproduction in any medium, provided the original work is properly cited.

This article has been retracted by Hindawi following an investigation undertaken by the publisher [1]. This investigation has uncovered evidence of one or more of the following indicators of systematic manipulation of the publication process:

- (1) Discrepancies in scope
- (2) Discrepancies in the description of the research reported
- (3) Discrepancies between the availability of data and the research described
- (4) Inappropriate citations
- (5) Incoherent, meaningless and/or irrelevant content included in the article
- (6) Peer-review manipulation

The presence of these indicators undermines our confidence in the integrity of the article's content and we cannot, therefore, vouch for its reliability. Please note that this notice is intended solely to alert readers that the content of this article is unreliable. We have not investigated whether authors were aware of or involved in the systematic manipulation of the publication process.

Wiley and Hindawi regrets that the usual quality checks did not identify these issues before publication and have since put additional measures in place to safeguard research integrity.

We wish to credit our own Research Integrity and Research Publishing teams and anonymous and named external researchers and research integrity experts for contributing to this investigation.

The corresponding author, as the representative of all authors, has been given the opportunity to register their agreement or disagreement to this retraction. We have kept a record of any response received.

References

- [1] H. Liu, Y. Chu, Y. Wang, and Z. Ren, "Optimization Strategy Analysis of Intelligent Product Service System Based on Computer Simulation Technology," *Journal of Sensors*, vol. 2022, Article ID 1264655, 8 pages, 2022.

Research Article

Optimization Strategy Analysis of Intelligent Product Service System Based on Computer Simulation Technology

Hang Liu ¹, Yan Chu ², Yongcheng Wang ¹ and Zan Ren ¹

¹School of Management Engineering, Zhengzhou University of Aeronautics, Zhengzhou, Henan, China 450000

²Department of Internal Audit, The First Affiliated Hospital of Zhengzhou University, Zhengzhou, Henan, China 450000

Correspondence should be addressed to Hang Liu; 1710122128@hbut.edu.cn

Received 30 June 2022; Revised 26 July 2022; Accepted 4 August 2022; Published 17 August 2022

Academic Editor: Haibin Lv

Copyright © 2022 Hang Liu et al. This is an open access article distributed under the Creative Commons Attribution License, which permits unrestricted use, distribution, and reproduction in any medium, provided the original work is properly cited.

In order to solve the needs of a large number of users and the efficiency of user service requirements, an optimization strategy analysis method of intelligent product service system based on computer simulation technology is proposed. Aiming at the two challenges of massive requests and efficient service in the network intelligent service system, the characteristics of the network intelligent service system are analyzed, and the network intelligent service system is formally modeled as an agent system. The performance modeling, performance evaluation, and performance optimization methods of the network intelligent service system are proposed. In order to solve this massive demand, the performance modeling of the network intelligent service system is carried out based on queuing theory. This paper proposes a task assignment algorithm for the network intelligent service system. Through the application of these results, the processing efficiency of the entire medical insurance application system has been greatly improved, and the average completion time of all businesses has been shortened by 59%, providing new ideas for optimizing service methods and improving service quality.

1. Introduction

The use of computer simulation technology to complete the automation system planning, taking informatization as the support for the construction of the simulation model, promotes the improvement of the operational efficiency and operation ability of the logistics system and creates more profits for the enterprise [1]. In the actual analysis, it is necessary to use computer simulation technology to monitor and evaluate the operation status of the system equipment, logistics flow, etc., and find out the existing problems in order to propose optimization suggestions. Using dynamic simulation technology for modeling, the system operation can be modeled and drilled. In the system, by virtualizing the actions and behaviors of the workpieces in each link, the random variables that affect the operation of the logistics system can be obtained, which can be used to complete the model construction. Combined with the degree of influence of variables on the operating efficiency of the system, the simulation data can be modified, and finally, the best system optimization scheme can be obtained [2].

With the development and popularization of the Internet and mobile terminal technology, the application mode of the traditional management information system oriented to business handling and functional modules has undergone great changes. This system has changed from a closed-based internal modular circulation system to a system with networked, process-based, and intelligent functions [3]. The application system based on the network, process, and intelligent service mode is called the network intelligent service system. Networking means that anyone can conduct business transactions at any time and anywhere in an open network through network terminals, mobile phones, and other devices [4]. For example, in the early days, people could only go to the office hall to handle medical insurance reimbursement through various approval windows; now, you can not only handle the medical insurance reimbursement business as before but also apply for the medical insurance reimbursement business on the corresponding network terminal or mobile terminal; two methods are used to meet the needs of different Medicare reimbursement applicants. Process-based means that for the business organization that handles

it, after a task is completed, the process of transferring to the next task is automatically judged by the workflow drive. For example, after the medical insurance reimbursement business application is accepted, according to the workflow predetermined rules, the audit business is automatically transferred to the next audit node as in [5]. Intelligence means that the system becomes more and more intelligent, and the entire management information system serves the complex requests of users like an agent. For example, in order to complete the audit task, the system first makes necessary judgments, adopts reasonable scheduling, and allocates the most appropriate resources in the system [6].

As people's business demands for network applications continue to increase and their expectations for system service efficiency are getting higher and higher, networked intelligent service systems need to face two major challenges in order to have networked, process-based, and intelligent service capabilities. One is the quantification of user requests; that is, since each service terminal of the system is open based on the Internet and oriented to the public, this will bring a large number of requests, and the system will also have complex load changes. Another challenge is service efficiency; that is, people's expectations for service efficiency are significantly improved; it is required that the system can respond to requests on time, and the efficiency of request processing is also getting higher and higher, so the system needs to improve service efficiency to meet more requests in order to serve the public [7, 8].

In order to solve the above two challenges, improving the throughput capacity and service efficiency of the networked intelligent service system is the key problem to be solved by the networked intelligent service system.

2. Literature Review

Because the content of the authors' research is relatively new, the traditional research is not completely directly related to the authors' research, in order to solve the two major challenges of request massization and service efficiency. The agent-based modeling method provides an idea for the author to formalize the networked intelligent service system. Service software and systems for traditional business processes can provide a reference for this study to solve the massive requests of the networked intelligent service system. System modeling and analysis methods based on business processes and related methods of system performance modeling and analysis provide references and ideas for solving the challenges of massive requests [9]. At present, Morales et al. believe that there are still some emerging websites that have built their platform into a crowdsourcing service platform. In crowdsourcing, resources are people. For the research on task allocation and scheduling in crowdsourcing, this research also focuses on how to improve the system's performance. Service efficiency provides a method [10]. Workflow and business process based on agent systems were studied. By modeling and analyzing the agent system, we can better understand the composition of the system, find problems, and make improvements to the system [11]. Martin et al. believe that the modeling of business process-

oriented service software and systems not only records the existing service system and determines the requirements of personnel, systems, and facilities but also lays the foundation for the planning and modification, performance evaluation, and optimization of the existing system. In recent years, researchers have been researching and exploring the life cycle of business processes, modeling methods and improvements, and performance evaluation [12]. In the modeling of business processes, Miraglia et al. proposed an efficient and formalized process design method; the rules of this process allow the generation of BPMN models integrated with rules from semantic knowledge engineering methods. Such a model can be viewed as a structured rule base; it provides an explicit inference flow dictated by process control flow. Studying the fundamentals of intelligent business process management, a framework business process management that distinguishes three levels needs to be introduced: multi-process management, process model management, and process instance management, and expanded the understanding of intelligent business process management [13]. In the performance evaluation of service systems such as business processes, Liu et al.'s research is mainly divided into two steps: the first step is to select performance indicators for performance evaluation, and the second step is to perform performance evaluation of business processes. When selecting performance indicators for business process performance evaluation, one of the most important indicators is time [14]. Jain and Jain believe that the time performance of business instances is an important basis for real-time management and scheduling of business processes and propose an equivalent model of time performance for activities in execution and waiting; the concept of instance attribution subatlas is proposed to track the dynamic change of the reachable subnetwork of the instance and solve the complex instance time performance problem, converted to a simpler performance-solving problem of attribution subgraphs; an example is used to demonstrate the performance evaluation process of business instances [15]. Yang et al. proposed new performance metrics for performance evaluation of business processes. There are researchers investing heavily information technology and the relevance of business process reengineering to improve enterprise productivity and performance by integrating individual tasks into complete cross-functional processes [16]. Moradi et al. use fixed effects and first differences to analyze firm-level panel data covering the period 1987-2008 and found that in the project launch year, return on assets has dropped significantly. According to the fixed effects results, performance and productivity measures improved after the project started; it shows that BPR does have a positive effect on corporate performance on average. Besides, enterprise-wide business process reengineering projects during project initiation compared to functionally focused projects have more negative returns [17].

To sum up, the modeling and performance evaluation of business processes are the basis and premise of business process optimization, and these modeling, performance evaluation, and optimization methods are used for reference in the study of networked intelligent service systems. However, there are few researches on the modeling of business

processes under networked conditions, and the performance indicators for performance evaluation are mostly time-based, the selection of performance indicators is relatively simple, and in the process of optimization, because only the business process under a certain condition is considered, the optimization target is relatively simple; these are problems that need to be improved and further studied.

3. Research Methods

3.1. Formal Modeling of Networked Intelligent Service System. In view of the two major challenges of request massization and service efficiency of the networked intelligent service system, by analyzing the similarity between the networked intelligent service system and the agent system's service capabilities, the authors formalize the modeling of the networked intelligent service system into an agent system; the agent system has the functions of processing massive user requests and improving service efficiency. The entire system acts like an agent in the face of complex requests from users. By quickly accepting requests from system users and completing tasks in real time, it solves the challenge of massive requests and at the same time assigns tasks to the most suitable people or positions to complete, solving the challenge of service efficiency. The four elements of the agent system are environment, state, action, and reward. The environment faced mainly refers to the user's request. The agent system makes decisions on the allocation of tasks and resources by perceiving the environment, improving service efficiency, and optimizing the environment feedback of the agent system as incentives and rewards [18].

The authors formalize the modeling of the networked intelligent service system based on the agent system, the networked intelligent service system is similar to the agent system, but it is different from the agent system. The four elements of the agent system in artificial intelligence are environment, state, action, and reward; these four elements are mapped into different categories under the networked intelligent service system [19].

The networked intelligent service system model can be represented by a four-tuple $\langle N_E, N_S, N_A, N_R \rangle$, where N_E is the environment of the networked intelligent service system, N_S is the state of the networked intelligent service system, N_A is the action of the networked intelligent service system, and N_R is the reward of the networked intelligent service system.

The formal modeling of the networked intelligent service system as an agent system mainly solves two problems: one is to respond to and resolve massive requests, and the other is to raise people's expectations for service efficiency. According to the above analysis of the similarity of the service capabilities of the networked intelligent service system and the agent system, the analysis of the four elements of the agent, and the corresponding relationship of the four elements in the networked intelligent service system, a formal model of the agent-based networked intelligent service system is obtained, as shown in Figure 1 [20].

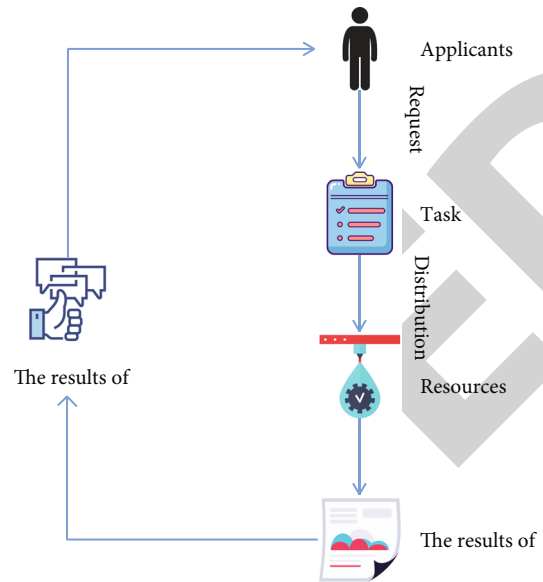


FIGURE 1: Schematic diagram of the formal model of the agent-based networked intelligent service system.

3.2. Performance Evaluation and Optimization of Networked Intelligent Service System. Aiming at the massive request challenge of the networked intelligent service system, in order to deal with the massive requests in real time, it is necessary to evaluate the performance of the networked intelligent service system. First, the idea of queuing theory is adopted to model the performance of the networked intelligent service system based on the formal modeling of the agent system; after that, the performance indicators used for performance evaluation were selected, and the formulas of these performance indicators were interpreted under the queuing theory model $M/M/c$; a method for performance evaluation of networked intelligent service systems is presented [21].

In the networked intelligent service system, assuming that the arrival of a task is random and independent and has no long-term correlation, the arrival process can be described as a Poisson process. For a task, the length of service time to complete it is also random and independent of the arrival of the task, so the service time can be characterized by a negative exponential distribution. In this way, the queuing network can be used to describe the networked intelligent service system. From a single point of view, such a task service relationship between task arrival and service window can be represented by the block diagram shown in Figure 2 [22].

When applying the $M/M/c$ model of queuing theory to analyze the networked intelligent service system, all the performance indicators of queues in queuing theory, such as performance indicators such as average queue length, average job residence time, and queue throughput, can all be used to describe the modeled networked intelligent service system. There are many kinds of performance evaluation indicators for the networked intelligent service system. Here, the following four indicators are mainly selected and used.

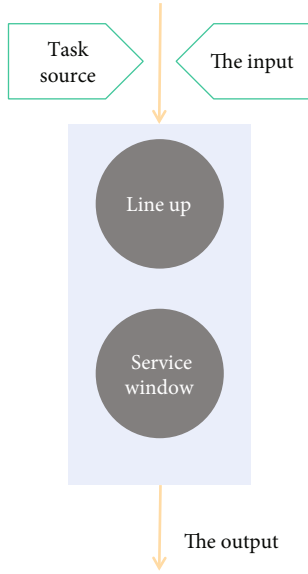


FIGURE 2: Basic block diagram of queuing model.

3.2.1. Average Queue Length. The queue length distribution describes the number of jobs arriving at a node in the same time interval. If the queue length is large, there may be an overload situation in the entire process; that is, the nodes cannot complete the work on time, and these jobs will accumulate more and more at the nodes. Contrary to the above situation is “underwork,” which describes the situation that the node can complete the work quickly, and the work does not accumulate at the node. According to the characteristics of the $M/M/c$ model, the definition of work reaching intensity is

$$\rho = \frac{\lambda}{\mu}, \quad (1)$$

where ρ is the average rate of customer arrivals, that is, the average number of customers arriving per minute. μ is the average service rate of the system, which is the number of customers the service desk can serve per minute. Then, the average queue length L_q is obtained, which is expressed as

$$L_q = \sum_{i=C}^{\infty} (i-C)P_i = \frac{\rho^{C+1}P_0}{(C-1)!(C-\rho)^2}, \quad (2)$$

where P_i is the queue length distribution calculated from the number of customers in the queue system and the number of service desks and P_0 is the initial value of P_i . C is the number of service desks.

3.2.2. Average Work Stay Time. The evaluation of service processes is different from that of industrial processes, because it is difficult to have a clear input or output of a visual standard; it is difficult to measure and compare. Many studies have shown that only the time parameter is the most important for evaluation and comparison. Let W_s denote the average residence time of the job; in its formula, W_q is the average waiting time, such as

$$W_s = W_q + \frac{1}{\mu} = \frac{\mu(\lambda/\mu)^C P_0}{(C-1)!(C\mu - \lambda)^2} + \frac{1}{\mu}, \quad (3)$$

$$W_q = \frac{L_q}{\lambda} = \frac{\mu(\lambda/\mu)^C}{(C-1)!(C\mu - \lambda)^2} P_0, \quad (4)$$

$$L_s = \lambda W_s, \quad (5)$$

where L_s is the average number of people in the system.

3.2.3. Working Intensity. The job arrival strength p represents the current service strength of the node when a job arrives at the node. It is used to describe the free and idle states of a node. If the intensity is high, the node has been busy. Conversely, if it is low-intensity, the node is in an “underworked” state.

3.2.4. Throughput. Throughput is the maximum efficiency of a node’s work or the maximum rate of a transaction process, represented by H . If a networked intelligent service system has a large throughput, it means that the networked intelligent service system has good service capability and high utilization rate. Throughput can also be characterized by throughput rate, which is the number of tasks completed by a node per unit of time.

Extending this analysis method from the first node to other nodes, the $M/M/c$ or $M/M/1$ queue model can be used to solve this problem for all nodes in the system. Likewise, each node has to consider external incoming traffic and fall-back phenomena.

According to the above calculation results, it can be obtained that under the current situation, there are relevant performance indicators of the entire networked intelligent service system.

The average service intensity $\bar{\rho}$ of the networked intelligent service system is

$$\bar{\rho} = \frac{\rho_1 + \rho_2 + \dots + \rho_n}{n}. \quad (6)$$

The average waiting leader \bar{L}_q of the queue is

$$\bar{L}_q = \frac{L_{q1} + L_{q2} + \dots + L_{qn}}{n}. \quad (7)$$

For applicants, the total time W_{sum} required to complete the entire process is

$$W_{\text{sum}} = W_{s1} + W_{s2} + \dots + W_{sn}. \quad (8)$$

The average stay time \bar{W} for a node is

$$\bar{W} = W_{s1} + W_{s2} + \dots + W_{sn}. \quad (9)$$

Using formulas (5) to (9), the quantitative data is calculated, and the performance evaluation of each node is obtained based on these data, and then, the judgment of the node whose service efficiency needs to be improved is obtained.

In the networked intelligent service system, when a node is full of business, and the node cannot process the business, the work of the node cannot be transmitted to the next node normally, and such a node is called a bottleneck node. The bottleneck node affects the efficiency of the entire system, so only by improving the service efficiency of the bottleneck node can the efficiency of the entire system be improved. Whether a node is a bottleneck node is also affected by the workload. It is a bottleneck node when the workload is saturated, but it may not be a bottleneck node when the workload is insufficient. The case of insufficient workload is not considered here, and only the general case is discussed.

In a system, there may be multiple nodes that affect the efficiency. Using the calculation formulas (5) to (9), the performance index values of each node are calculated. By analyzing and comparing these index values, the most efficient efficiency can be obtained, poor bottleneck node.

- (1) *The Bottleneck Node with the Worst Queue Length Index Value.* Calculate the maximum queue length of each node

$$L_{qk} = \max \{L_{q1}, L_{q2}, \dots, L_{qn}\}. \quad (10)$$

Then, the node S_k is the bottleneck node with the worst queue length index value.

- (2) *The Bottleneck Node with the Worst Average Job Stay Time Indicator Value.* Calculate the maximum value of the average job stay time of each node

$$W_{sj} = \max \{W_{s1} + W_{s2} + \dots + W_{sn}\}. \quad (11)$$

Then, node S_j is the bottleneck node with the worst average job residence time.

- (3) *The Bottleneck Node with the Largest Job Arrival Intensity Index Value.* Calculate the maximum value of the job arrival intensity of each node

$$\rho_l = \max \{\rho_1, \rho_2, \dots, \rho_n\}. \quad (12)$$

Then, the node S_l is the bottleneck node with the largest job arrival intensity.

- (4) *The Bottleneck Node with the Smallest Throughput.* Calculate the minimum throughput of each node

$$H_{Sr} = \min \{H_{S1}, H_{S2}, \dots, H_{Sn}\}. \quad (13)$$

Then, the node S_r is the bottleneck node with the smallest throughput.

3.3. Task Allocation Algorithm of Networked Intelligent Service System. In view of the challenge of service efficiency of the networked intelligent service system, in order to

assign tasks to the most suitable people and positions, the authors propose a task assignment algorithm for the networked intelligent service system. In the case of massive data, because the tasks accepted by the system are different, the resources allocated by the agent system are also different. At the same time, many tasks are no longer performed only by the fixed staff in the system; these tasks can be outsourced by using crowdsourcing platforms to improve service efficiency and save work costs. In order to make task allocation and resource allocation more efficient and orderly, the task assignment algorithm of the networked intelligent service system proposed by the authors optimizes the service efficiency of the networked intelligent service system, reduces the operating cost of the system, and satisfies people's expectations for system service efficiency.

Aiming at the second challenge faced by the networked intelligent service system, namely, service efficiency, the authors propose a task allocation algorithm; the algorithm is based on a crowdsourced task assignment method that assigns tasks to the most appropriate resources to complete. The task allocation algorithm is divided into two parts: the first part is the generation of a personalized task list, and the second part is the allocation of resources [23].

The generation of the personalized task list is to generate different task lists for different requests. There are many different types of tasks in the entire task set of the entire networked intelligent service system; for an applicant, he may need to start from the first step of the system process; then, the system needs to extract the task subset that completes the task from the entire task set to complete his application. If the applicant has already done the first step of the system process, then his application only needs to start from the second step of the system process, and there is no need to perform the first step. The generation process is shown in Figure 3.

The allocation of resources is to assign tasks to the right people to handle. When the networked intelligent service system faces a request, the agent system first generates a personalized task list, then, in all resource sets, select the resources that match the requested personalized task list, make decisions, and allocate appropriate resources to the corresponding tasks. The resource allocation process is shown in Figure 4.

4. Analysis of Results

4.1. Intelligent Artificial Resource Allocation Algorithm. After completing the generation of the personalized task list mentioned above, the design agent system will allocate appropriate resources for the tasks to be completed; this is the second part of the task allocation algorithm—the intelligent artificial resource allocation algorithm.

The resources to complete this task have a total of m workers, and each worker has a work queue; the reason why the task queue is used is to realize the principle of first-come, first-served. The work queue of the i th worker is $Wqi - 1$, and $Wi - 1(t)$ is the number of tasks in the work queue at time t . All task queues can be assigned to tasks, and

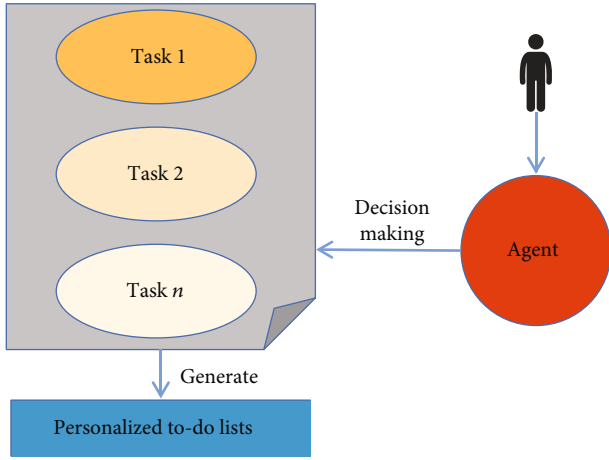


FIGURE 3: Schematic diagram of the generation process of the personalized task list.

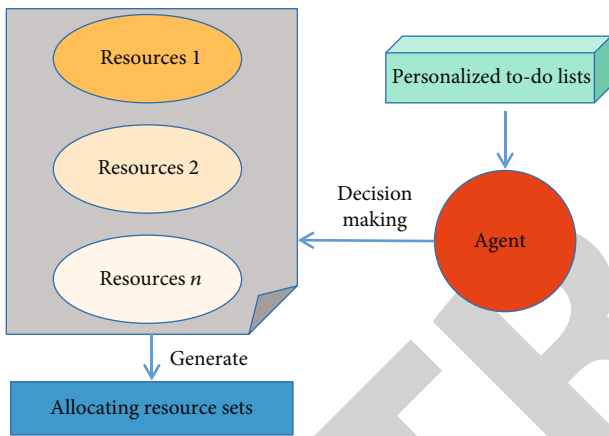


FIGURE 4: Schematic diagram of resource allocation process.

finally, the algorithm results will allocate tasks to appropriate resources [24].

4.2. Practical Application Verification. The author’s research results are applied in the medical insurance reimbursement business process for application verification and experimental analysis. By collecting practical application data, the performance modeling of the medical insurance reimbursement business process based on queuing theory is carried out, the performance index values related to the current process are calculated through the data, and then, the performance of the process is evaluated. The whole process is optimized, and finally, the task allocation algorithm is applied to the process to optimize.

Then, the task allocation optimization algorithm is applied to social insurance, and the completion time of the top ten most frequently requested services in social insurance is calculated. Figure 5 shows the 10 most commonly used services in social insurance and a comparison of the average completion time before applying the task assignment optimization algorithm and after applying the task assignment optimization algorithm. The results show that after applying the task allocation optimization algorithm,

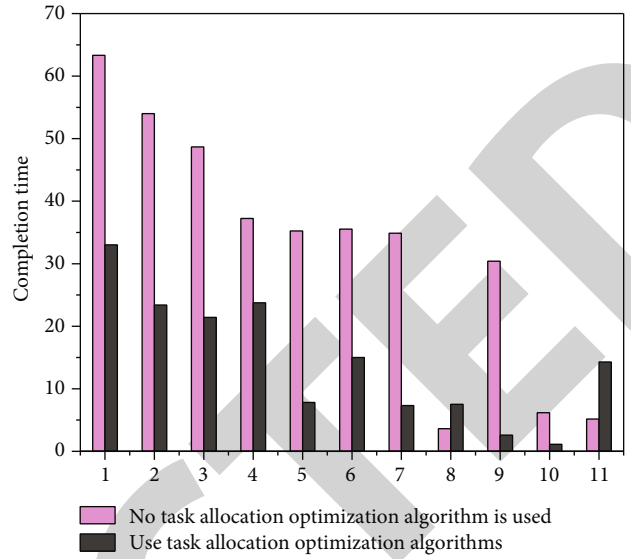


FIGURE 5: The average completion time (days) of the top ten most commonly used services before and after applying the task allocation optimization algorithm.

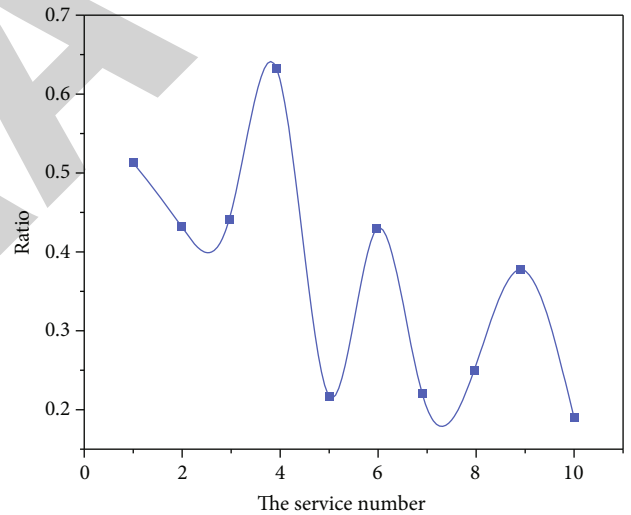


FIGURE 6: The average completion time ratio of the top ten most frequent requests.

the average completion time of the top 10 most frequently requested services is greatly reduced, and the average completion time is shortened by $1-14.29/34.76 = 58.9\% \approx 59\%$.

In the government department’s social insurance reimbursement business process, after using the task allocation algorithm, the ratio of the average completion time required by ordinary software systems to the top ten most frequently requested social insurance reimbursement business services is shown in Figure 6. These ten services are arranged in order of decreasing average completion time under common software systems. It can be seen that after using the task allocation optimization algorithm, the task completion time of the entire process is greatly reduced, and the service efficiency of the process is improved [25].

5. Conclusion

With the wide application of the networked intelligent service system, its related research has attracted more and more attention, and its modeling, performance evaluation, and performance optimization have become one of the important research topics. The authors study the modeling, resource allocation, and key technologies of the networked intelligent service system and prove the correctness of the research results through experiments. The work done in the full text is summarized as follows:

- (1) The authors propose a formal modeling method for networked intelligent service systems. Aiming at the two major challenges of massive request and efficient service of networked intelligent service system, the characteristics of networked intelligent service systems are analyzed, and it is found that it has many similar service capabilities to the agent. Therefore, the networked intelligent service system is formally modeled as an agent system
- (2) The authors propose methods for performance modeling, performance evaluation, and performance optimization of networked intelligent service systems. In order to solve the massive request, the performance modeling of the networked intelligent service system is carried out based on queuing theory
- (3) The authors propose a task assignment algorithm for the networked intelligent service system. Aiming at the challenge of efficient service of networked intelligent service systems, the system needs to be able to assign different tasks to appropriate people to improve service efficiency. In order to this end, the author applies the idea of the crowdsourcing task assignment method to generate different task lists for different users; appropriate tasks are then assigned to appropriate people, so that task assignment can be carried out in a more efficient and orderly manner, which improves the service efficiency of the networked intelligent service system and reduces the operating cost of the system
- (4) Using data from medical insurance reimbursement business processes, the main content of the study is experimentally validated. Based on queuing theory, the performance modeling and performance evaluation of the process are carried out, and the process is optimized through the task allocation algorithm. Experiments have proved that, through the application of the results, the processing efficiency of the entire medical insurance application system has been greatly improved, and the average completion time of all businesses has been shortened by 59%

Data Availability

The data used to support the findings of this study are available from the corresponding author upon request.

Conflicts of Interest

The authors declare that they have no conflicts of interest.

Acknowledgments

The study was supported by the (1) Foundation for Youth Scholars of Higher Institution of Henan Province (2019GGJS179) and (2) Key Scientific and Technological Project of Henan Province (202102310311).

References

- [1] H. Sun, S. Wang, F. Zhou, L. Yin, and M. Liu, "Dynamic deployment and scheduling strategy for dual-service pooling based hierarchical cloud service system in intelligent buildings," *Computing*, vol. PP (99), pp. 1–1, 2021.
- [2] C. Yi and X. Feng, "Home interactive elderly care two-way video healthcare system design," *Journal of Healthcare Engineering*, vol. 2021, Article ID 6693617, 11 pages, 2021.
- [3] F. Matoui, B. Boussaid, B. Metoui, and M. N. Abdelkrim, "Contribution to the path planning of a multi-robot system: centralized architecture," *Intelligent Service Robotics*, vol. 13, no. 1, pp. 147–158, 2020.
- [4] A. P. Murdan, V. Bucktowar, V. Oree, and M. P. Enoch, "Low-cost bus seating information technology system," *IET Intelligent Transport Systems*, vol. 14, no. 10, pp. 1303–1310, 2020.
- [5] Z. Ye, H. Ni, Z. Xu, and D. Zhang, "Sensor fault estimation of networked vehicle suspension system with deny-of-service attack," *IET Intelligent Transport Systems*, vol. 14, no. 5, pp. 455–462, 2020.
- [6] T. Qin, Y. Yang, B. Wen et al., "Research on human gait prediction and recognition algorithm of lower limb-assisted exoskeleton robot," *Intelligent Service Robotics*, vol. 14, no. 3, pp. 445–457, 2021.
- [7] R. E. Bavili, A. Akbari, and R. M. Esfanjani, "Passivity-based control of nonlinear teleoperation systems with non-passive interaction forces," *Intelligent Service Robotics*, vol. 13, no. 3, pp. 419–437, 2020.
- [8] L. Xing, B. Jiao, Y. Du, X. Tan, and R. Wang, "Intelligent energy-saving supervision system of urban buildings based on the internet of things: a case study," *IEEE Systems Journal*, vol. 14, no. 3, pp. 4252–4261, 2020.
- [9] N. Wang, K. Zhong, X. Shi, X. Zhang, and L. Zhang, "Fuzzy-pi double-layer stability control of an online vision-based tracking system," *Intelligent Service Robotics*, vol. 14, no. 2, pp. 187–197, 2021.
- [10] E. F. Morales, R. Murrieta-Cid, I. Becerra, and M. A. Esquivel-Basaldua, "A survey on deep learning and deep reinforcement learning in robotics with a tutorial on deep reinforcement learning," *Intelligent Service Robotics*, vol. 14, no. 5, pp. 773–805, 2021.
- [11] A. Barth, Y. Sun, L. Zhang, and O. Ma, "Genetic fuzzy-based method for training two independent robots to perform a cooperative task," *Intelligent Service Robotics*, vol. 14, no. 4, pp. 535–548, 2021.
- [12] J. G. Martin, J. Frejo, R. A. García, and E. F. Camacho, "Multi-robot task allocation problem with multiple nonlinear criteria using branch and bound and genetic algorithms," *Intelligent Service Robotics*, vol. 14, no. 5, pp. 707–727, 2021.

Retraction

Retracted: Application of Internet of Things Technology in Mechanical Automation Control

Journal of Sensors

Received 22 August 2023; Accepted 22 August 2023; Published 23 August 2023

Copyright © 2023 Journal of Sensors. This is an open access article distributed under the Creative Commons Attribution License, which permits unrestricted use, distribution, and reproduction in any medium, provided the original work is properly cited.

This article has been retracted by Hindawi following an investigation undertaken by the publisher [1]. This investigation has uncovered evidence of one or more of the following indicators of systematic manipulation of the publication process:

- (1) Discrepancies in scope
- (2) Discrepancies in the description of the research reported
- (3) Discrepancies between the availability of data and the research described
- (4) Inappropriate citations
- (5) Incoherent, meaningless and/or irrelevant content included in the article
- (6) Peer-review manipulation

The presence of these indicators undermines our confidence in the integrity of the article's content and we cannot, therefore, vouch for its reliability. Please note that this notice is intended solely to alert readers that the content of this article is unreliable. We have not investigated whether authors were aware of or involved in the systematic manipulation of the publication process.

Wiley and Hindawi regrets that the usual quality checks did not identify these issues before publication and have since put additional measures in place to safeguard research integrity.

We wish to credit our own Research Integrity and Research Publishing teams and anonymous and named external researchers and research integrity experts for contributing to this investigation.

The corresponding author, as the representative of all authors, has been given the opportunity to register their agreement or disagreement to this retraction. We have kept a record of any response received.

References

- [1] Y. Xie, H. Li, Q. Jia, and X. Nie, "Application of Internet of Things Technology in Mechanical Automation Control," *Journal of Sensors*, vol. 2022, Article ID 9388942, 7 pages, 2022.

Research Article

Application of Internet of Things Technology in Mechanical Automation Control

Yonghui Xie ¹, Haiqing Li ¹, Qiushaung Jia ¹ and Xiumin Nie ²

¹Department of Mechanical and Electrical Engineering, Weifang Vocational College, Weifang, Shandong 262737, China

²Shandong Key Research Center Precision Manufacturing for Magnetic Equipment, Weifang, Shandong 262737, China

Correspondence should be addressed to Yonghui Xie; 1711231128@hbut.edu.cn

Received 30 June 2022; Revised 27 July 2022; Accepted 4 August 2022; Published 16 August 2022

Academic Editor: Haibin Lv

Copyright © 2022 Yonghui Xie et al. This is an open access article distributed under the Creative Commons Attribution License, which permits unrestricted use, distribution, and reproduction in any medium, provided the original work is properly cited.

In order to solve the problem of low production efficiency of the mechanical electromechanical automatic control system, this paper proposes a manufacturing mechanical automatic detection system based on Internet of things technology. Automatic detection of manufacturing machinery is realized by setting data module monitoring, which includes the data monitoring module and signal detection module. The experimental results show that compared with the traditional computer vision system, the detection system designed in this paper has a higher level of basic data and better detection accuracy. The detection accuracy can be improved by about 10% in different detection times. *Conclusion.* The mechanical and electrical automation control system based on the Internet of things can effectively improve the production efficiency and control accuracy of the mechanical and electrical automation control system.

1. Introduction

With the continuous development of the Internet of things technology, the Internet of things has been gradually applied in various fields as an emerging industry in the new era, changing the face of world economic development. The numerical control technology of the Internet of things can solve many problems in mechanical control, bring opportunities and challenges to mechanical and electrical automation control, and create a good numerical control foundation for the mechanical and electrical automation control system to adapt to modern development [1].

With the development of the Internet, many Internet-related technologies have also been innovated and developed. All emerging Internet technologies are affecting people's real life [2]. People begin to try to set up an ID card for all objects in real life, so that they can connect all objects to the network, and use the convenience of the Internet to control all objects in real life. The purpose of the Internet of things is to connect all objects in real life. Gradually, the industrial sector has begun to introduce and apply the Internet of things technol-

ogy, which is based on the characteristics that the Internet of things can accurately control production, which is beyond the reach of human beings, especially the actual production of precision mechanical automation engineering projects [3].

Due to the high demand for initial data in the design process of the manufacturing machinery automatic detection system, it is necessary to collect machinery automatic data with high accuracy in the preliminary stage of design, so as to improve the design of the overall detection system [4]. The traditional automatic inspection system for manufacturing machinery based on computer vision is designed to query the image of the internal part structure of the machinery, adjust the internal operation structure of the inspection system, and obtain accurate inspection results [5]. The traditional manufacturing machinery automatic detection system based on node detection is designed to analyze the detection network of the detection system, build a detection platform, and strengthen the control of the detection platform according to the network analysis content, so as to achieve better detection results [6]. However, the traditional system design has a small grasp of the mechanical automation data of the

manufacturing industry, which does not meet the requirements of the sustainable development of the system, and the detection accuracy is low [7].

2. Literature Review

The application of the mechanical electromechanical automatic control system is mostly realized in complex and harsh environment. Therefore, it is necessary for the staff to remotely control the equipment and operation procedures on the automatic production site and monitor the parameters of the equipment operation status and system production status on the site. The staff at the monitoring point under the Internet of things numerical control technology can generally skillfully control the software and hardware resources in the system, so as to achieve the purpose of system fault elimination and maintenance and reduce the human resources of the system on site. At the same time, Internet of things numerical control can also be used to analyze and process on-site data, with preventive troubleshooting of potential faults in the system. It can also provide a more reliable data execution basis for mechanical and electrical automation technology through Internet of things numerical control technology and improve the efficiency of mechanical and electrical automation [8]. The following requirements must be met in the overall framework design of the CNC mechanical and electrical automation control system based on the Internet of things:

- (1) IOT CNC can fully control and manage the mechanical and electromechanical automatic machining program [9]. The production program data in the mechanical electromechanical automation system can be systematized through the Internet of things numerical control technology, and relevant management personnel can retrieve the mechanical electromechanical automation production program parameters at any time, which is conducive to timely maintenance of hardware equipment and improvement of automation level [10]
- (2) The Internet of things numerical control technology is applied to ensure the safety of mechanical electromechanical automation parameters. During the implementation of the system, the operating parameters of the machine tool will change due to the operator's control error, increasing the material loss of mechanical electromechanical automation. Therefore, it is necessary to monitor the parameters in the system in real time through the Internet of things numerical control technology to avoid parameter changes [11]
- (3) Mechanical and electrical automatic production equipment pays more attention to the production quantity of equipment, and operators often ignore the maintenance of production equipment. Therefore, it is necessary to apply the Internet of things NC to monitor the automatic machine tools, reduce

the faults of automatic production equipment, and extend the service life of the machine tools

- (4) In the process of mechanical, electromechanical, and automatic production, no artificial mechanical control is involved, but professional personnel are required to monitor the production data in real time to meet the safety and manufacturing stability in the production process, and then, the Internet of things numerical control technology is applied to maintain or expand the wireless communication function of the machine tool, so as to increase the efficiency of mechanical [12], electromechanical, and automatic production
- (5) The key technology of Internet of things numerical control is wireless sensor communication technology, which can be applied to the production communication of mechanical and electrical automation [13]. The potential resources in the network topology development system such as Ethernet gateway and data format frame number are designed in the numerical control mechanical and electrical automation equipment. With the increase of the flexibility of Internet of things, the monitoring, data acquisition, and analysis in the mechanical and electrical automation control system are reflected

Therefore, in view of the above problems, this paper proposes a new design of the manufacturing machinery automatic detection system based on Internet of things technology to analyze and solve the above problems [14].

3. Research Methods

3.1. Hardware Design of Manufacturing Machinery Automatic Detection System Based on Internet of Things Technology. As a convenient and intuitive intelligent operation technology, Internet of things can communicate and exchange goods and networks in an open environment, providing a corresponding shortcut for the development of different industries [15]. This paper uses the sensing node information of the Internet of things to adjust the system hardware, track the data operation space in the system hardware component structure, and construct the network node sensing diagram, as shown in Figure 1. Different operation modules are set for data processing to improve the effectiveness of the overall hardware design. Automatic detection of manufacturing machinery is realized by setting data module monitoring, which includes data monitoring module and signal detection module [16].

3.1.1. Data Monitoring Module. The data monitoring module selects the industrial digital camera and connects the camera status. The module has high receiving sensitivity and strong anti-interference performance and can be easily embedded into the system. It has half duplex communication function, is ism multiband, does not need to apply for frequency free use, and has multiple frequency options. It has a variety of transmission rates and ISSI channel

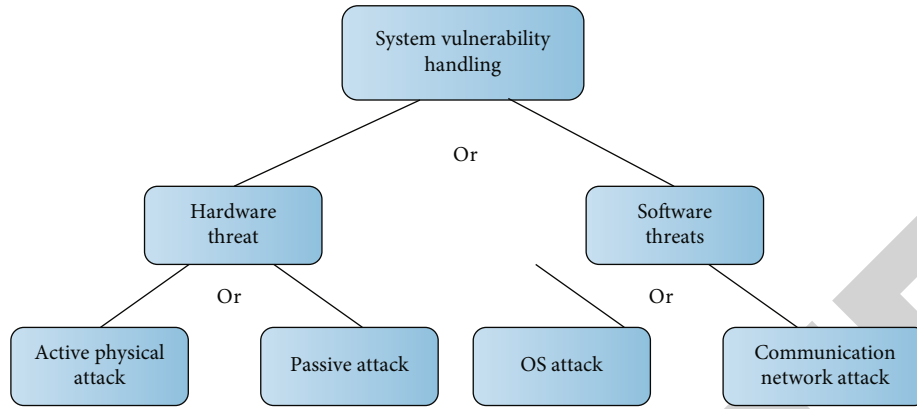


FIGURE 1: Network node perception diagram.

detection functions and can provide a relatively good monitoring environment for the system with strong monitoring performance [17].

3.1.2. Signal Detection Module. The signal detection module selects the TL signal transmission cable to enhance the transmission system theoretically and selects pro-w10gx broadband digital RF detector to optimize the system detection mode and increase the dominant ability of the system [18]. The detector has unparalleled sensitivity in the RF frequency range of 0~10 GHz. It can display most digital frequencies and unprecedented analog signals up to 6 GHz to ensure the accuracy of signal detection. When used in the secret mode, the detector can monitor the signal strength in beep mode or silent mode to fully display the different states of the signal [19]. Equipped with semirigid multiband whip antenna and directional high gain antenna, the input frequency range is 1 MHz~10000 MHz, and the audio frequency response is 400 Hz~5 kHz ± 2 db, with high data processing capacity, built-in 3.7v1500 Ma rechargeable lithium battery, which can work for eight hours under full power, facilitating system research and realizing overall signal inspection operation. There is a detector in the detection module, which is responsible for the modular detection of automatic data and the analysis of the detection structure of different detection spaces. Due to the complexity of the internal detection circuit of the detection module, it is necessary to set up multiple MCU for microcontrol of the detection circuit while performing the detection, assist the detection circuit to execute the detection instructions, protect the circuit, improve the security of the detection, set the image of the detection circuit, adjust the detection strength of the module detection, optimize the internal detection switch of the detector, and connect the detection switch with the detection data interface. Realize accurate detection of data. Thus, the overall system hardware design is completed.

3.2. Software Design of Manufacturing Machinery Automatic Detection System Based on Internet of Things Technology. The system software is designed based on the designed hardware detection data, and the data transmission network of Internet of things technology is used for the rapid transmission of mechanical automation data, and the system

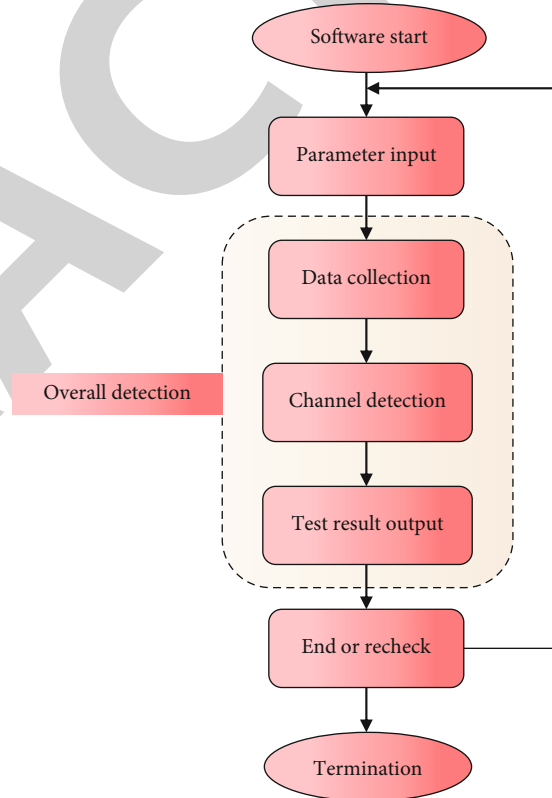


FIGURE 2: Software detection flow chart.

detection software platform is built [20]. The set internal detection flow chart is shown in Figure 2.

Input the data to be tested into the software platform, integrate the mechanical automation images in the working process of the manufacturing industry according to the relevant platform software execution instructions, strengthen the marking of the automation data, and conduct basic management on the marked data. The management formula is as follows:

$$N = \sqrt{A - P^3}. \tag{1}$$

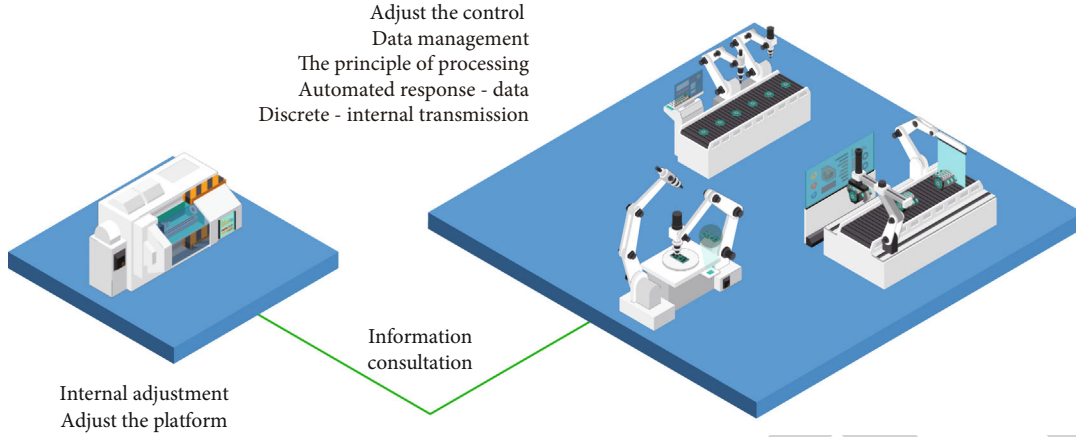


FIGURE 3: Information adjustment diagram.

In equation (1), N represents management data, A represents automatic data marking information, and P represents relevant collation principle parameters. After completing the above management operations, adjust the automation information. The build information adjustment diagram is shown in Figure 3.

The image display device is selected to display the detection data image in real time, adjust the automatic data content in different spaces, allocate the storage location of the automatic data, and store the automatic data belonging to the same storage mechanism for centralized management. Relieve the internal pressure of the detection platform and set the software platform detection formula as follows:

$$T = \frac{s + \sqrt{k}}{n} - q. \quad (2)$$

T is the detection result parameter, s is the internal storage mechanism data, k is the corresponding storage location parameter, n is the number of data detected, and q is the internal automatic data transmission direction data. According to the above detection operations, enhance the detection accuracy of the overall software, and take protection measures for the software platform at the same time of detection, so as to prevent data leakage within the software platform, thereby affecting the detection result data. Match the protection mechanism of the software platform, manage the basic contents of different protection mechanisms, connect the protection mechanism with the detection data transmission channel, execute protection instructions during data transmission, ensure data transmission security, and set the data protection instruction formula:

$$P = \int A \cdot h + c^2. \quad (3)$$

In the above formula, P represents the protection instruction data, A represents the internal data of the transmission channel, h represents the corresponding transmission rule, and c represents the transmission parameters generated in

the transmission process. Thus, the design of the overall detection system software is realized [21].

4. Result Analysis

After the above system design is realized, the data results of the designed system are compared, and the corresponding comparison experiments are set up. The comparison indicators are as follows:

- (1) Master degree of mechanical automation data in manufacturing industry
- (2) Detection accuracy of the detection system. According to the above two indicators, the setting of comparative experiment is carried out, and the experimental parameter table is designed

In Table 1, different operating parameters are used to analyze the degree of mastering the mechanical automation data of the initial manufacturing industry of the detection system, so as to strengthen the internal management of the detection system and improve the efficiency of the overall detection. Put the manufacturing machinery automation data in the initial storage space of the detection system and analyze whether there is data missing in the automation data in the space. Timely supplement missing data and strengthen the data filtering mechanism of the detection system to prevent detection errors caused by the intrusion of external data. Monitor the data flow direction of the system for detection and analysis at all times, adjust the direction appropriately, and combine the automatic parameters with the detection algorithm. Carry out automatic data inspection of the system according to the inspection process [22]. Strengthen the internal control over the detection information of the detection system to prevent the degradation of the detection function of the detection system due to data leakage. Match the information of the system experiment platform and the software detection platform at this time, compare the different platform information with the internal detection data, enter the comparison result data into the

TABLE 1: Experimental parameters.

Project	Parameter
Number of sensors	5
Number of detection mechanism systems	6
Fixed value setting	k
Experiment data operation	Information entry
Algorithmic mechanism	System detection algorithm
Software platform	Network platform
System state	Normal

platform detection algorithm to wait for the system algorithm detection, and realize the overall detection operation. Execute the detection management instructions to avoid the detection commands being intercepted by the system during the issuing process. At the same time, cooperate with the independent data cleaning operation of the detection software platform to clean up the data consistent with the cleaning principle as a whole, so as to ensure the smooth development of the experimental research. Sort out the obtained result data, and set the data comparison diagram as shown in Figure 4.

As can be seen in Figure 4, the degree of mastering manufacturing machinery automation data designed by the manufacturing machinery automation detection system based on Internet of things technology in this paper is higher than that designed by the other two traditional manufacturing machinery automation detection systems [23]. After the first experimental study is realized, the secondary experimental research operation is carried out by using the research data, the experimental indicators are analyzed, and the experimental parameter table is constructed as shown in Table 2.

In Table 2, connect the internal management platform with the monitoring elements of the detection system, classify and process the detection data of different structures, divide the relevant module space, and compare and store the divided data. Select the internal monitoring device to conduct real-time monitoring operation on the stored information, and strengthen the detection strength of the detection system. Based on the collected data, perform the data detection task under the standard mode [24]. In the process of detection, the amount of detection data is allocated, so as to avoid the redundancy of detection data caused by excessive concentration of detection data, which affects the detection effect of the detection system. Input all the results detected by different detection systems into the result comparison space for data comparison, and set the result comparison table as shown in Tables 3 and 4.

The detection accuracy of the automatic manufacturing machinery detection system designed in this paper based on the Internet of things technology is higher than that of the other two traditional automatic manufacturing machinery detection systems. The main reason for this difference is that the detection system in this paper uses the internal detection criteria for data detection, executes internal

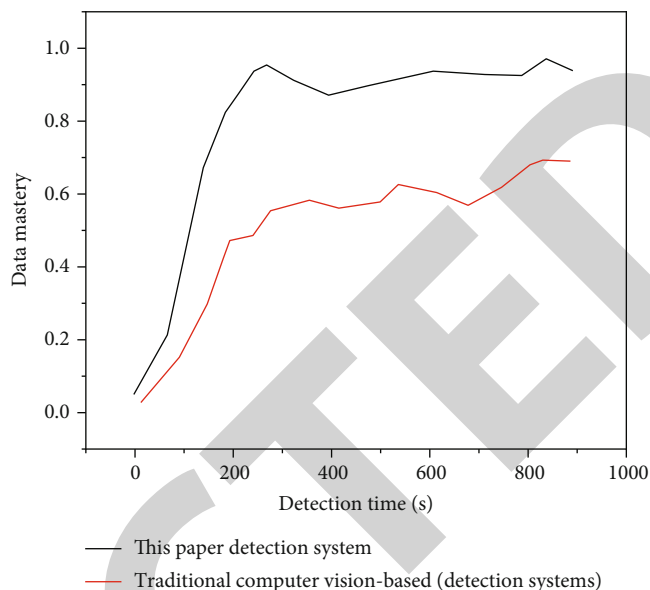


FIGURE 4: Comparison of data mastery.

TABLE 2: Experimental parameters.

Project	Parameter
System architecture	C/S
Processing module	Data processing module
Detection mechanism	Data detection mechanism
Mode adjustment	Detection monitoring mode
System protocol	TCP protocol
Number of hosts	2
Number of sensing nodes	50

TABLE 3: Test accuracy results of this system design.

Test time (d)	Detection accuracy (%)
10	89
20	92
30	94
40	96
50	97
60	99

TABLE 4: Test accuracy results of traditional computer vision-based system design.

Test time (d)	Detection accuracy (%)
10	76
20	78
30	82
40	84
50	87
60	91

control instructions in the initial stage of detection, and configures a monitoring system with high monitoring integrity to ensure the integrity of data monitoring [25]. To sum up, the manufacturing machinery automatic detection system based on the Internet of things technology in this paper has a high level of basic data and better detection accuracy. It can conduct experimental operations in different scenarios, meets the needs of system detection, better provides relevant services for users, and has a broader space for development.

5. Conclusion

Based on the design of the traditional manufacturing machinery automatic detection system, this paper presents a design of the manufacturing machinery automatic detection system based on Internet of things technology. In this paper, the internal mechanical operation structure of mechanical automation in the manufacturing industry is used to adjust the overall detection system, strengthen the integration and management of the system, realize the accurate analysis and information search of the detection data, obtain more accurate mechanical automation data, and achieve the purpose of data collection of the detection system. At the same time, this paper executes the detection instructions on the basis of data collection, constructs the software platform under the premise of hardware component transformation, obtains a more reliable detection information source, and then improves the detection accuracy and efficiency of the overall detection system. The experimental results show that the testing effect of the automatic testing system for manufacturing machinery based on the Internet of things technology is significantly better than that of the traditional automatic testing system for manufacturing machinery and can better provide solid testing services for the development of manufacturing machinery automation. Apply the Internet of things numerical control technology to improve the stability and accuracy of the mechanical electromechanical automatic control system, and effectively integrate the advantages of the Internet of things numerical control into the mechanical electromechanical automatic control system.

Data Availability

The data used to support the findings of this study are available from the corresponding author upon request.

Conflicts of Interest

The authors declare that they have no conflicts of interest.

References

- [1] C. Chen and X. Zhu, "Application research on information security of aerobics information digital system based on internet of things technology," *Journal of Intelligent and Fuzzy Systems*, vol. 1, no. 1, pp. 1–8, 2021.
- [2] W. Xu, C. Zhao, and X. Wang, "The role of the internet technology in the employment structural transformation under background of "internet plus" in China," *Theoretical Economics Letters*, vol. 11, no. 5, pp. 1020–1037, 2021.
- [3] N. Georgeva and P. Tsankov, "Analysis of energy consumption in the industrial sector in the European Union," *IOP Conference Series: Materials Science and Engineering*, vol. 1032, no. 1, article 012026, 2021.
- [4] J. Lee, "Integration of digital twin and deep learning in cyber-physical systems: towards smart manufacturing," vol. 38, no. 8, pp. 901–910, 2020.
- [5] H. Supriyono and A. Akhara, "Design, building and performance testing of gps and computer vision combination for increasing landing precision of quad-copter drone," *Journal of Physics: Conference Series*, vol. 1858, no. 1, article 012074, 2021.
- [6] T. Han and Y. Xu, "Mechanical automation design and manufacturing based on artificial intelligence technology," *Journal of Physics Conference Series*, vol. 1852, no. 2, article 022034, 2021.
- [7] R. Millington, A. R. Giles, N. V. Luijk, and L. Hayhurst, "Sport for sustainability? The extractives industry, sport, and sustainable development," *Journal of Sport & Social Issues*, vol. 46, no. 3, pp. 293–317, 2022.
- [8] Z. Koruba and P. Szmidi, "The remote control of the artillery rocket set as a strongly nonlinear system subject to random loads," *Electronics*, vol. 10, no. 13, p. 1507, 2021.
- [9] J. Fang, F. Ouyang, S. Lu, K. Wang, X. Min, and B. Xiao, "Variation of elastic modulus of high strength 21-6-9 tube and its influences on forming quality in numerical control rotary draw bending," *Proceedings of the Institution of Mechanical Engineers, Part C: Journal of Mechanical Engineering Science*, vol. 235, no. 21, pp. 5684–5694, 2021.
- [10] E. Bakan and N. Bakan, "Prevention of extra-analytical phase errors by non-analytical automation in clinical laboratory," *Turkish Journal of Biochemistry*, vol. 46, no. 3, pp. 235–243, 2021.
- [11] K. Bi and Y. Bi, "Research on real time monitoring of operation status of large data platform for energy conservation supervision based on computer," *Journal of Physics: Conference Series*, vol. 1744, no. 2, article 022052, 2021.
- [12] X. Huang, F. Zhao, Z. Sun, Z. Zhu, and X. Mei, "A novel condition monitoring signal analysis method of numerical control machine tools in varying duty operation1," *IEEE Access*, vol. 8, pp. 72577–72584, 2020.
- [13] W. An, L. Hong, Y. Luo, K. Ma, and X. Huang, "A wideband dual-function solar cell dipole antenna for both energy harvesting and wireless communications," *IEEE Transactions on Antennas and Propagation*, vol. 69, no. 1, pp. 544–549, 2020.
- [14] V. T. Truong, A. Nayyar, and S. A. Lone, "System performance of wireless sensor network using lora-zigbee hybrid communication," *Computers, Materials & Continua*, vol. 68, no. 2, pp. 1615–1635, 2021.
- [15] A. Riyaz, P. K. Sadhu, A. Iqbal, and M. Tariq, "Power quality enhancement of a hybrid energy source powered packed e-cell inverter using an intelligent optimization technique," *Journal of Intelligent & Fuzzy Systems*, vol. 42, no. 2, pp. 817–825, 2021.
- [16] D. B. Hertanto, R. Asnawi, F. Surwi, and N. Setiawan, "Prototype development of distance detection system based on the internet of things using esp 8266 wifi nodemcu module," *Journal of Physics: Conference Series*, vol. 2111, no. 1, article 012049, 2021.

Retraction

Retracted: Slope Topography Monitoring Based on UAV Tilt Photography Technology and Sensor Technology

Journal of Sensors

Received 17 October 2023; Accepted 17 October 2023; Published 18 October 2023

Copyright © 2023 Journal of Sensors. This is an open access article distributed under the Creative Commons Attribution License, which permits unrestricted use, distribution, and reproduction in any medium, provided the original work is properly cited.

This article has been retracted by Hindawi following an investigation undertaken by the publisher [1]. This investigation has uncovered evidence of one or more of the following indicators of systematic manipulation of the publication process:

- (1) Discrepancies in scope
- (2) Discrepancies in the description of the research reported
- (3) Discrepancies between the availability of data and the research described
- (4) Inappropriate citations
- (5) Incoherent, meaningless and/or irrelevant content included in the article
- (6) Peer-review manipulation

The presence of these indicators undermines our confidence in the integrity of the article's content and we cannot, therefore, vouch for its reliability. Please note that this notice is intended solely to alert readers that the content of this article is unreliable. We have not investigated whether authors were aware of or involved in the systematic manipulation of the publication process.

Wiley and Hindawi regrets that the usual quality checks did not identify these issues before publication and have since put additional measures in place to safeguard research integrity.

We wish to credit our own Research Integrity and Research Publishing teams and anonymous and named external researchers and research integrity experts for contributing to this investigation.

The corresponding author, as the representative of all authors, has been given the opportunity to register their agreement or disagreement to this retraction. We have kept a record of any response received.

References

- [1] J. Cao, Y. Dai, L. Hu, Y. Liang, Y. Liu, and B. Yang, "Slope Topography Monitoring Based on UAV Tilt Photography Technology and Sensor Technology," *Journal of Sensors*, vol. 2022, Article ID 3531576, 8 pages, 2022.

Research Article

Slope Topography Monitoring Based on UAV Tilt Photography Technology and Sensor Technology

Jianfeng Cao ¹, Yunfei Dai ¹, Liqiang Hu ¹, Yiju Liang ², Yuan Liu ², and Bo Yang ²

¹Guangxi Xinfazhan Communications Group Co, Ltd, Nanning, Guangxi 530000, China

²Guangxi Road and Bridge Engineering Group Co., Ltd., Nanning, Guangxi 530000, China

Correspondence should be addressed to Liqiang Hu; 1430407203@post.usts.edu.cn

Received 25 June 2022; Revised 18 July 2022; Accepted 26 July 2022; Published 16 August 2022

Academic Editor: Haibin Lv

Copyright © 2022 Jianfeng Cao et al. This is an open access article distributed under the Creative Commons Attribution License, which permits unrestricted use, distribution, and reproduction in any medium, provided the original work is properly cited.

In order to solve the problems of high risk and low efficiency of the traditional rock mass structure logging method of open-pit mine slope, this paper proposes a method to improve the geological logging of traditional open-pit mine slope by using UAV tilt photography technology. Taking the slope of an open-pit quarry as an example, this method expounds the application method and work flow of UAV photography technology in geological logging. The experimental results show that the maximum and minimum absolute errors in the X direction of UAV test are 5.1 cm and 1.1 cm, respectively; MAE value is 2.90 cm; and RMSE value is 3.17 cm. The maximum and minimum absolute errors in Y direction are 3.3 cm and 0.9 cm, respectively; MAE value is 2.36 cm; and RMSE value is 2.498 cm. Vertical error refers to the error in elevation. The maximum and minimum absolute errors in Z direction are 9.6 cm and 5.7 cm, respectively; MAE value is 7.44 cm; and RMSE value is 7.54 cm. *Conclusion.* The reliability of this technology is verified by comparing the occurrence measured by compass and that calculated by point cloud. On this basis, the dominant occurrence of structural plane is divided, which provides basic data support for the analysis of mine slope stability.

1. Introduction

The occurrence of geological disasters is the inevitable product of the evolution of geological bodies to a certain stage. In essence, the prevention and control of geological disasters are to restore the geological body in an unbalanced or critical equilibrium state to a new equilibrium state through artificial means. Due to the rapid development of economy, the tourism development of complex landforms such as Qifeng and Junling, as well as large-scale engineering construction and resource development, and the collapse disasters of high and steep slopes occur frequently. However, for high and steep slopes and high-level dangerous rocks, due to the lack of close contact, it is difficult to accurately obtain the physical characteristics such as the size of dangerous rocks and the distribution and development of rock mass structural planes, so it is impossible to accurately grasp the evolution state of geological bodies, which is extremely harmful and greatly increases the difficulty of treatment [1]. In order to

effectively control the collapse disaster of high and steep slope, geological survey and rock mass stability evaluation are very necessary, but the survey of high and steep slope and the acquisition of geological and topographic information have always been engineering problems [2]. The stability evaluation from the perspective of geology mechanics also needs to establish corresponding physical and mechanical models supplemented by simulation calculation and analysis. For high and steep slopes, effective and accurate terrain data is more difficult to obtain.

2. Literature Review

Due to the advantages of multisensor data fusion, all countries attach great importance to the research on the theory and application of multisensor data fusion system and have obtained rich research results. Azizi, M. A. use Ku band GB-INSAR to detect the complex earth rock landslide in an urban area and monitor the landslide area in near real

time [3]. It is pointed out that GB-INSAR is not applicable to all types of landslides, mainly for landslides with slow change and medium speed range, but GB-INSAR cannot effectively observe the phenomena of debris flow and rock falling from slope, indicating that the single monitoring of GB-INSAR has limitations. Kocharyan, G. G. placed a metal disc equipped with a worm gear engine at the monitoring station to produce a controllable displacement (0.01 mm) of 120 meters [4]. They tried to estimate GB-INSAR measurements, but they were limited by DEM matching accuracy. The metal disk is not clear on the topographic point cloud, which is the difference in the scale of remote sensing data, resulting in the limited evaluation of deformation mapping results. Nizametdinov, N. F. set up a station at the same position by using slope radar and total station at the same time to monitor the deformation of the slope of an open-pit mine in China. Several radar monitoring targets are set in the scene, and the reflection prism of total station is installed next to the target. The total station uses the automatic looking prism mode to collect deformation, which is consistent with the time interval of deformation obtained by slope radar. At the same time, it realizes the matching between slope data and total station data in its own coordinate system [5]. However, there was no significant displacement in the selected scene. Since the target shape variables were less than 1 mm, the fusion result was also the trend comparison of the two sensor data. Abramov, A. V. according to the relationship model between slope radar system and SAR image and the relationship model between slope radar system and terrain data, this paper analyzes the geometric mapping three-dimensional matching method based on range and azimuth conditions, which has achieved good results [6]. Ding, W. and others analyzed the geometric mapping 3D matching method based on range and azimuth conditions according to the relationship model between slope radar system and SAR image and the relationship model between slope radar system and terrain data. This method achieved good results [7]. In a landslide monitoring operation, Zhang, D. and others fused high-precision laser scanning point cloud and slope radar results for data fusion. Although there is no detailed description of how to obtain higher interference phase quality, the most critical area is localization relative to work activities, and the displacement detected by GB in SAR is visualized in three dimensions by merging with the three-dimensional model [8].

Jiangling, L. I. and others use the data obtained by laser scanning technology as the main support of external elevation information. According to the geometric projection principle of radar imaging, they realize the registration between point cloud data and radar pixels on the projection plane, so as to promote the conversion from the coordinates of ground radar image to local three-dimensional coordinates. The research results are used to explain and analyze the three-dimensional deformation in the monitoring application of practical slope radar system [9]. Foo, Y. L. and others believe that in general, all types of slope radar systems have not significantly improved the accuracy of deformation measurement. The adjustment of mechanical structure and the difference of radar system have introduced new (uncon-

ventional) processing links, resulting in inconsistency within the system, which will increase the cumulative error and affect the accuracy of deformation calculation.

From the research results of many scholars at home and abroad, it can be seen that photogrammetry technology can realize rapid and accurate three-dimensional reconstruction of geological bodies [10]. However, at present, UAV photogrammetry is mainly used in the monitoring and investigation of geological disasters, and there is less research on rock mass structure interpretation and logging. Studying the application of UAV in this field will help to analyze the stability of slope. Based on the analysis and summary of the application status of this technology at home and abroad, this paper forms a set of UAV tilt photography workflow suitable for geological logging of open-pit mines. Taking a rock slope in an open-pit quarry in province as an example, the point cloud model is used to extract the occurrence information of structural plane, and the reliability of this method is verified by comparing the manual measurement results.

3. Research Methods

3.1. UAV Photographic Observation System and Work Flow.

The UAV photography and observation system is mainly composed of two parts: air flight part and ground control part. The air flight part includes unmanned aerial vehicle, PTZ and photographic equipment, and the ground control part includes ground controller, digital image display, and flight control system. The flight control system is the core of the whole observation system, so that the UAV can fly autonomously in varying degrees between manual control and automatic control.

The research of this paper adopts a certain type of UAV, which is divided into light UAV. This type of UAV has the advantages of light weight, low cost, flexibility, portability, and speed [11] (see Table 1 for specific parameters).

According to the technical code for slope engineering of noncoal open-pit mines (Ministry of Housing and Urban Rural Development, 2014) and the code for investigation of landslide, collapse, and debris flow disasters (1:50000) (Ministry of Land and Resources, 2014), on the basis of making full use of the advantages of UAV photography and observation system, the geological investigation of open-pit mines that can be carried out includes the following: (1) investigating the distribution range of adverse geological processes such as landslide and collapse in the site; (2) finding out the type, occurrence, and distribution of structural plane; and (3) establishing three-dimensional point cloud model, orthophoto map (DOM), and digital surface model (DSM) of geological hazard body as permanent records of slope at a certain time.

The geological survey of open-pit slope based on UAV photographic observation system is mainly composed of three parts: mining area data preparation, field aerial photography data acquisition and indoor aerial photography data processing and analysis [12]. The task of data preparation of the mining area is to collect satellite photos and topographic data of the working mining area, preliminarily plan

TABLE 1: Specific parameters of UAV.

Camera model	FC6310S
Image sensor	1 inch CMOS
Camera pixel	20 million (5472 × 3648)
Field angle (FOV)	84°
Maximum altitude	500 m
Maximum horizontal flight speed	20 m/s
Maximum flight time	About 30 min
Working ambient temperature	0~40°C
Satellite positioning module	GPS /GLONASS dual mode

the route, and check the UAV equipment in advance. Field aerial photography data acquisition mainly includes site survey, route design, ground control point layout, and UAV aerial photography [13]. Indoor aerial photography data processing and analysis is to use the photos obtained by UAV aerial photography to reconstruct the rock mass in three dimensions; generate three-dimensional point cloud, DOM, and DSM; and digitally interpret the rock mass to obtain the occurrence information of rock mass and establish the spatial data file of rock mass. According to the above contents, the working process of geological logging and investigation of open-pit slope based on UAV photography is shown in Figure 1.

3.2. 3D Reconstruction and Occurrence Extraction of Rock Mass. Due to the limitation of the picture frame of the UAV equipped with photography equipment, a large number of photos need to be collected according to a certain sequence and interval to realize the three-dimensional reconstruction of rock mass. Based on the principle of stereo vision, each feature point should correspond to at least three pictures. In order to better reconstruct the sparse geometry of the target scene from the two-dimensional image, the navigation overlap rate and side overlap rate should be more than 70%. As a three-dimensional reconstruction method of monocular vision, structure from motion (SFM) has the characteristics of strong robustness, wide applicability, and large reconstruction scene. For rock mass, which does not have regular texture, regular contour, large reconstruction scene, and uneven natural illumination intensity, the reconstruction effect of SFM method can better meet the needs of all aspects. The research shows that the accuracy of terrain data using SFM method can reach centimeter level.

3.2.1. 3D Reconstruction of Rock Mass Based on SFM Method. SFM method is a method to estimate the camera parameters of the motion state through the homonymous feature points between different pictures and recover the 3D scene by using the epipolar geometric relationship between the camera parameters and the homonymous feature points. Like the human eye perceives the three-dimensional state of the object through movement or perspective change, SFM method observes the points in real space from different perspectives to obtain the depth infor-

mation of the scene, so as to realize the matching of feature points with the same name and restore the sparse three-dimensional structure of the scene. In this paper, the open source library VisualSFM developed by Wu (2013) of the University of Washington is used to realize the three-dimensional reconstruction of rock mass. The specific process includes feature point extraction and matching, sparse reconstruction, and dense reconstruction.

Feature point extraction and matching. Because the scale and rotation angle of the picture will inevitably change when shooting with UAV, the ambient light intensity will not change much in one shooting process, and the ambiguity can also be controlled manually. Therefore, the scale invariant feature transform (SIFT) algorithm is used to extract the features of the pictures taken by the UAV. When extracting the feature points, the SIFT algorithm has the invariance of image rotation, translation, scaling, and affine and has certain anti illumination interference and viewing angle change ability. The specific operation steps of SIFT algorithm ① use Gaussian convolution function to transform the scale of UAV aerial photos, so as to obtain the expression sequence of the image in different scale spaces. ② The equation form of difference of Gaussian (DoG) in scale space is used to convolute with the image to obtain the extreme values. The extreme points corresponding to these extreme values are the feature points of the image. After the feature points are extracted, the topological structure between the images is established by combining the GPS coordinate information and the pose angle information of inertial measurement unit (IMU) when the UAV collects the image, and the corresponding relationship between the feature points between the image and the image is calculated by using the nearest neighbor NN algorithm to complete the matching work.

Sparse reconstruction. Sparse reconstruction is to use the matched feature point set of the same name to incrementally reconstruct the scene and obtain a “rough” three-dimensional point cloud model. The basic idea is (1) to reconstruct the three-dimensional coordinate information of a point from two-dimensional images, at least know the position of the point in the two images and the internal and external parameters of the corresponding image. Since the whole process is taken with the same camera, the internal parameters of the image have been determined when the camera leaves the factory. Only the external parameters of the image, i.e., the rotation matrix and translation vector between the images, need to be taken. (2) After knowing all the internal and external parameters of the two pictures, the three-dimensional coordinates of the spatial points can be calculated according to triangulation; that is, the three-dimensional spatial coordinates corresponding to the matching points can be restored by using the projection relationship. (3) Because the feature point matching is not absolutely accurate, the calculated three-dimensional point coordinates also have errors. In order to obtain more accurate results, it is necessary to use the bundle adjustment (BA) step by step iteration to continuously minimize the re projection error between the projection points and the observed image points and calculate the best camera pose and the three-dimensional point cloud coordinates of the

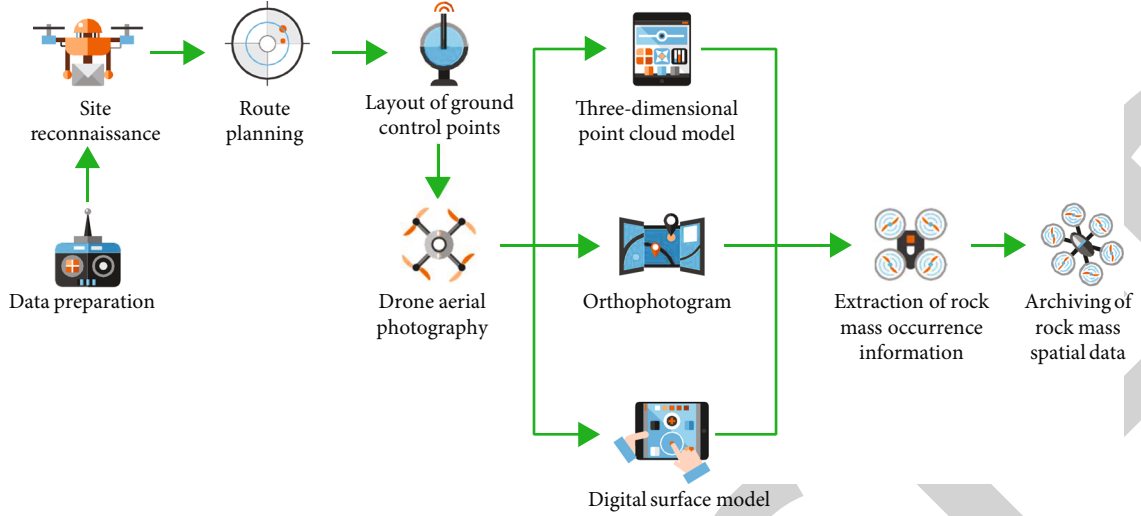


FIGURE 1: Flow chart of geological logging based on UAV photography.

scene. However, according to the research, when the picture quality is high and the GPS coordinate information is accurate, the ability of Ba method as an optimization algorithm to reduce the error is very limited.

Intensive refactoring. For irregular objects such as rock mass, the “rough” point cloud model restored by sparse reconstruction is not enough to describe it finely. Therefore, it is necessary to increase the density of point cloud and improve the fineness of the model. According to the previous research results, CMVS-PMVS (cluster multiview stereo patch-based multiview stereo) method is used to cluster and classify the images, remove the redundant images in the original image, and then generate a series of sparse patches and corresponding image regions from the sparse matching points with high reliability, and repeatedly diffuse and filter these regions, so as to obtain a relatively fine rock mass point cloud model.

3.2.2. Extraction of Rock Mass Structure Occurrence. The 3D point cloud model obtained by 3D reconstruction can be understood as describing a rock mass with tens of millions of 3D coordinate points, and all structural information of the rock mass is contained in these “points.” Since the topological structure of the whole point cloud model is based on the GPS sensor and IMU sensor machine carried on the UAV, the point cloud coordinates generated by three-dimensional reconstruction are the coordinates under WGS84 geodetic coordinate system, and their coordinate position relationship is the same as the objective world. The relatively stable occurrence of rock mass structural plane can be calculated directly by extracting the coordinates of points on the exposed surface of rock mass structure. Referring to the research results [14], the geometric relationship of structural plane occurrence is shown in Figure 2. Assuming that there is a structural plane J in the space, and the occurrence is expressed by inclination ($0^\circ \sim 360^\circ$) \angle inclination ($0^\circ \sim 90^\circ$), the occurrence of the structural plane is $\alpha \angle \beta$. Pick the coordinates $J_1(x_1, y_1, z_1)$, $J_2(x_2, y_2, z_2)$, and $J_3(x_3, y_3, z_3)$ of three points that are not collinear

on the structural plane, and then, the unit normal vector $n(x_n, n_y, n_z)$ of structural plane J can be expressed as follows [15]:

$$\begin{cases} n_x = \frac{A}{\sqrt{A^2 + B^2 + C^2}} \\ n_y = \frac{B}{\sqrt{A^2 + B^2 + C^2}} \\ n_z = \frac{C}{\sqrt{A^2 + B^2 + C^2}} \end{cases}, \quad (1)$$

where

$$\begin{cases} A = (y_2 - y_1)(z_3 - z_1) - (y_3 - y_1)(z_2 - z_1) \\ B = (x_3 - x_1)(z_2 - z_1) - (x_2 - x_1)(z_3 - z_1) \\ C = (x_2 - x_1)(y_3 - y_1) - (x_3 - x_1)(y_2 - y_1) \end{cases}. \quad (2)$$

According to the geometric relationship between n and β in Figure 2 [16], the included angle of the unit vector $(0, 0, 1)$ in the direction of n and z is the inclination β of the structural plane.

$$\beta = \arccos \left| \frac{n_z}{\sqrt{n_x^2 + n_y^2 + n_z^2}} \right|. \quad (3)$$

And because $n_x^2 + n_y^2 + n_z^2 = 1$, then

$$\beta = \arccos |n_z|. \quad (4)$$

To calculate the tendency of the structural plane, it is necessary to determine the quadrant of the projection n' of the unit normal vector n of the structural plane in the $X - Y$ plane [17]; then,

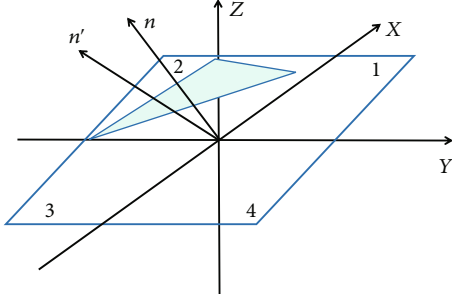


FIGURE 2: Schematic diagram of geometric relationship of occurrence of structural plane.

when $n_z^2 > 0$,

$$\alpha = \begin{cases} \arccos \frac{n_y}{\sqrt{n_x^2 + n_y^2}} \left(n_x^2 > 0, n' \text{ in quadrant } \textcircled{1} \textcircled{2} \right) \\ 2\pi - \arccos \frac{n_y}{\sqrt{n_x^2 + n_y^2}} \left(n_x^2 < 0, n' \text{ in quadrant } \textcircled{3} \textcircled{4} \right) \end{cases} \quad (5)$$

When $n_z^2 < 0$,

$$\alpha = \begin{cases} \arccos \frac{-n_y}{\sqrt{n_x^2 + n_y^2}} \left(n_x^2 < 0, n' \text{ in quadrant } \textcircled{3} \textcircled{4} \right) \\ 2\pi - \arccos \frac{-n_y}{\sqrt{n_x^2 + n_y^2}} \left(n_x^2 > 0, n' \text{ in quadrant } \textcircled{1} \textcircled{2} \right) \end{cases} \quad (6)$$

- (1) When $n_z = 0$, it means that the structural plane is upright and the tendency does not exist. Its occurrence is generally described by strike

According to the above principles, CloudCompare plugin can be used to extract the stable occurrence of rock mass structural plane based on three-dimensional point cloud data [18, 19].

4. Result Analysis

4.1. Field Data Acquisition. Taking an open-pit quarry as an example, the total area of the mining area is about $101,510 \text{ m}^2$, the maximum elevation of the top of the slope on the slope surface is about $+85.0 \text{ m}$, and the elevation of the bottom varies from $+5.0 \text{ m}$ to $+20.0 \text{ m}$. After the field survey, it is found that the natural slope of the mountain in the mining area is about $15^\circ \sim 25^\circ$, the overall field of vision is wide, and the GPS satellite signal is stable, which is suitable for UAV flight. Therefore, the shooting process adopts the airborne computer automatic control mode. According to the size of the mining area, plan the route, set the navigation height of 140 m , and the overlap rate of heading and

TABLE 2: Coordinates of ground control points.

Number	Ground control point coordinates/M		
	X	Y	Z
G1	305835.837	3127230.082	15.014
G2	305830.566	3227096.412	11.332
G3	303848.825	3028034.090	11.078
G4	301004.015	3327157.308	13.315
G5	301050.258	3326985.668	13.245
G6	301205.034	3326984.380	20.428
G7	300875.022	3326967.954	21.324
G8	301233.966	3327165.605	15.239

side direction is 80%. At the same time, 8 ground control points are arranged within the mining area and the three-dimensional coordinates are measured with RTK (Table 2). A total of 217 photos were taken during this flight, which took 13 minutes, and the orthophoto map and digital surface model with ground resolution of 3.9 cm/PX were generated.

4.2. Horizontal and Vertical Errors. The accuracy of point cloud model reconstruction is evaluated by using the coordinates of 8 ground control points measured by RTK. Pick up the center of the ground control point target in the point cloud model, read the coordinates, and compare with the data in Table 2. The results are shown in Figure 3.

The accuracy is evaluated by mean absolute error (MAE) and relative root mean square error (RMSE). Horizontal error refers to the deviation between the measured value and the true value of UAV on the X-Y plane [20], which is divided into x and Y directions. The maximum and minimum absolute errors in the X direction of this test are 5.1 cm and 1.1 cm , respectively; MAE value is 2.90 cm ; and RMSE value is 3.17 cm . The maximum and minimum absolute errors in Y direction are 3.3 cm and 0.9 cm , respectively; MAE value is 2.36 cm ; and RMSE value is 2.498 cm . Vertical error refers to the error in elevation. The maximum and minimum absolute errors in Z direction are 9.6 cm and 5.7 cm , respectively; MAE value is 7.44 cm ; and RMSE value is 7.54 cm [21, 22].

From the above calculation results, it can be seen that the vertical accuracy of UAV measurement data is significantly lower than the horizontal measurement accuracy by about three times. The reason may be that the vertical accuracy of GPS itself is lower than the horizontal accuracy. In general, the maximum value, minimum value, MAE, and RMSE are kept within the accuracy of centimeter level [23], which is basically sufficient for the occurrence logging of rock mass structural plane and ensures the reliability of occurrence extraction to a certain extent.

4.3. Extraction and Accuracy Verification of Rock Mass Occurrence. As the rock mass of nantao slope is well exposed, the structural plane is obviously developed, and the slope toe is gently inclined, which is suitable for manual measurement, and this section of slope is selected to extract and verify the occurrence information of rock mass

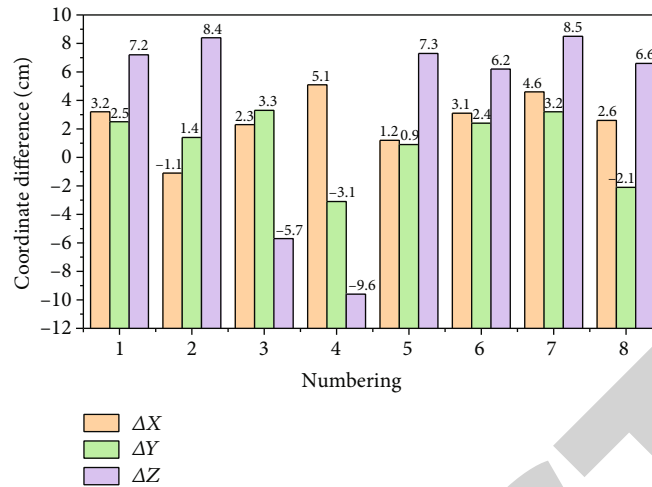


FIGURE 3: Comparison and verification results of ground control points.

TABLE 3: Calculation results of structural plane occurrence.

Number	Compass measurement tendency/(°)	Compass measuring inclination/(°)	Point cloud computing tendency/(°)	Inclination of point cloud calculation/(°)	Absolute difference of tendency error/(°)	Absolute difference of inclination error/(°)
1	45	80	40.15	78.32	4.85	1.68
2	331	67	339.23	65.61	8.23	1.39
3	345	74	349.12	76.89	4.12	2.89
4	246	57	250.83	55.52	4.83	1.48
5	306	76	310.43	80.98	4.43	4.98
6	148	80	145.31	80.94	2.69	0.94
7	317	80	320.74	77.24	3.74	2.76
8	340	67	342.34	62.38	2.34	4.62
9	139	66	140.98	65.22	1.98	0.78
10	130	85	128.03	81.12	1.97	3.88
11	93	61	91.66	58.74	1.34	2.26
12	310	55	312.87	59.44	2.87	4.44
13	345	30	350.45	32.46	5.45	2.46
14	320	50	327.94	51.89	7.94	1.89
15	335	60	331.35	58.47	3.65	1.53
16	290	60	284.78	60.23	5.22	0.23
17	356	25	351.56	22.74	4.44	2.26
18	75	33	72.84	30.14	2.16	2.86
19	320	70	324.62	71.69	4.62	1.69
20	315	69	312.04	68.21	2.96	0.79
Mean absolute error					4.00	2.29

structural plane. Use geological compass to measure the structural plane with stable occurrence, and record the position of the structural plane. Cut out the Nandang part from the dense reconstructed point cloud model, circle three non-collinear points with the mouse according to the manually measured and marked structural plane position, record their coordinate information, and calculate the occurrence of the structural plane according to the method described in the previous section. The results are shown in Table 3.

Through the comparison between the attitude measured by 20 compasses and the attitude calculated according to the point cloud coordinates [24, 25], it can be found that the average absolute error of inclination is 4.00° , and the average absolute error of inclination is 2.29° . The attitude results obtained by the two measurement methods are basically the same, so the attitude calculated by reconstructing the point cloud by UAV photography is reliable. All 106 occurrence stereograms are projected onto the isodensity network

to draw the occurrence isocratic map and pole map, analyze the isocratic map and pole map, and divide the dominant occurrence of nantao slope rock mass into 5 groups. The ranges of dominant occurrence are: ① $139^{\circ}\sim 177^{\circ}\angle 54^{\circ}\sim 83^{\circ}$, ② $203^{\circ}\sim 221^{\circ}\angle 64^{\circ}\sim 85^{\circ}$, ③ $220^{\circ}\sim 247^{\circ}\angle 10^{\circ}\sim 43^{\circ}$, ④ $228^{\circ}\sim 247^{\circ}\angle 66^{\circ}\sim 82^{\circ}$, and ⑤ $326^{\circ}\sim 352^{\circ}\angle 48^{\circ}\sim 77^{\circ}$; among them, group ③ is relatively slow, and the other four groups are relatively steep.

5. Conclusion

This paper expounds the technical principle and work flow of UAV photography technology in mine slope geological logging and applies this technology to the structural plane logging of a mine slope in. The following conclusions are drawn:

- (1) Compared with the traditional structural plane occurrence logging method of compass + tape, UAV photography technology overcomes the limitations of rock mass structural plane statistics, avoids the danger of high and steep slope survey, improves the work efficiency of geological logging, and makes it easier to obtain the basic data of geological survey
- (2) Combined with the motion recovery structure (SFM) algorithm, the two-dimensional photos obtained by UAV photography can recover the three-dimensional point cloud data with rock mass structure under complex terrain conditions, and the occurrence of rock mass structural plane can be interpreted by extracting the point cloud coordinates. In addition, the point cloud model also records all rock mass structures of the slope in a certain period, which can provide data support for the study of the impact of mining on slope stability in the future
- (3) Compared with the RTK measurement results, the horizontal and vertical errors of the UAV tilt photogrammetry in this test are within the centimeter accuracy, which ensures the reliability of occurrence extraction to a certain extent
- (4) Comparing the attitude measured by compass with that calculated by point cloud coordinates, it is found that the absolute average error of inclination is 4.00° , and the absolute average error of inclination is 2.29° , which proves the reliability of reconstructing point cloud attitude by UAV photography. All the acquired occurrences are drawn in the stereographic projection of chipping, and the dominant occurrences of five groups of structural planes are obtained, which are, respectively: ① $139^{\circ}\sim 177^{\circ}\angle 54^{\circ}\sim 83^{\circ}$, ② $203^{\circ}\sim 221^{\circ}\angle 64^{\circ}\sim 85^{\circ}$, ③ $220^{\circ}\sim 247^{\circ}\angle 10^{\circ}\sim 43^{\circ}$, ④ $228^{\circ}\sim 247^{\circ}\angle 66^{\circ}\sim 82^{\circ}$, and ⑤ $326^{\circ}\sim 352^{\circ}\angle 48^{\circ}\sim 77^{\circ}$, which can reflect the spatial position relationship of rock mass structural plane in the measured area

At present, the interpretation of rock mass structure using UAV tilt photography technology is only aimed at the interpretation of the occurrence of structural plane. In

the future, the research in this field will be further extended to the acquisition of trace length, spacing, gap width, and other information of rock mass structural plane. On this basis, the automatic recording of all parameters of structural plane can be realized.

Data Availability

The data used to support the findings of this study are available from the corresponding author upon request.

Conflicts of Interest

The authors declare that they have no conflicts of interest.

Acknowledgments

The study was supported by the Ningbo Transportation Technology Plan (Project No: 202110) and the Science and Technology Program of Zhejiang Provincial Communications Department (Project No: 2019040).

References

- [1] A. Zd, B. Lw, C. Wl, D. Zw, and E. Qe, "Mathematical modeling and fuzzy approach for disaster analysis on geo-spatial rock mass in open-pit mining," *Computer Communications*, vol. 150, pp. 384–392, 2020.
- [2] F. K. Nizametdinov, V. D. Baryshnikov, E. Zhanatuly et al., "Selection and justification of design variables for strength properties of rocks in slope stability analysis for open pits," *Journal of Mining Science*, vol. 57, no. 3, pp. 386–392, 2021.
- [3] M. A. Azizi, I. Marwanza, M. K. Ghifari, and U. Trisakti, "Low-wall slope stability analysis using planar surface and 3d simplified janbu method," *Technology Reports of Kansai University*, vol. 62, no. 3, pp. 569–580, 2020.
- [4] G. G. Kocharyan, S. B. Kishkina, and Z. Z. Sharafiev, "Laboratory research of slope stability under impacts," *Journal of Mining Science*, vol. 57, no. 6, pp. 965–977, 2021.
- [5] N. F. Nizametdinov, R. F. Nizametdinova, A. A. Nagibin, and A. R. Estaeva, "Slope stability in open pit mines in clayey rock mass," *Journal of Mining Science*, vol. 56, no. 2, pp. 196–202, 2020.
- [6] A. V. Abramov, A. P. Beketov, G. N. Rykovanov, A. N. Khrule, and A. O. Chernyavskii, "Influence of acting factors on the thermal and stress state of the geological structure of a deep burial site for radwaste," *Atomic Energy*, vol. 130, no. 3, pp. 174–179, 2021.
- [7] W. Ding, Z. Wang, X. Huang, L. Chen, and Y. Zheng, "Influence of corrosion on anchoring bond behavior of jointed rock mass," *KSCE Journal of Civil Engineering*, vol. 26, no. 4, pp. 1914–1928, 2022.
- [8] D. Zhang, J. Wei, and X. Fang, "Study on the variation of rock pore structure after polymer gel flooding," *E-Polymers*, vol. 20, no. 1, pp. 32–38, 2020.
- [9] L. I. Jiangling, K. Chou, and Q. Shu, "Structure and viscosity of $\text{CaO-Al}_2\text{O}_3\text{-B}_2\text{O}_3$ based mould fluxes with varying $\text{CaO/Al}_2\text{O}_3$ mass ratios," *ISIJ International*, vol. 60, no. 1, pp. 51–57, 2020.

Retraction

Retracted: Construction of Tourism Area Capacity Early Warning System Based on Internet of Things Technology

Journal of Sensors

Received 3 October 2023; Accepted 3 October 2023; Published 4 October 2023

Copyright © 2023 Journal of Sensors. This is an open access article distributed under the Creative Commons Attribution License, which permits unrestricted use, distribution, and reproduction in any medium, provided the original work is properly cited.

This article has been retracted by Hindawi following an investigation undertaken by the publisher [1]. This investigation has uncovered evidence of one or more of the following indicators of systematic manipulation of the publication process:

- (1) Discrepancies in scope
- (2) Discrepancies in the description of the research reported
- (3) Discrepancies between the availability of data and the research described
- (4) Inappropriate citations
- (5) Incoherent, meaningless and/or irrelevant content included in the article
- (6) Peer-review manipulation

The presence of these indicators undermines our confidence in the integrity of the article's content and we cannot, therefore, vouch for its reliability. Please note that this notice is intended solely to alert readers that the content of this article is unreliable. We have not investigated whether authors were aware of or involved in the systematic manipulation of the publication process.

Wiley and Hindawi regrets that the usual quality checks did not identify these issues before publication and have since put additional measures in place to safeguard research integrity.

We wish to credit our own Research Integrity and Research Publishing teams and anonymous and named external researchers and research integrity experts for contributing to this investigation.

The corresponding author, as the representative of all authors, has been given the opportunity to register their agreement or disagreement to this retraction. We have kept a record of any response received.

References

- [1] Y. Ma, "Construction of Tourism Area Capacity Early Warning System Based on Internet of Things Technology," *Journal of Sensors*, vol. 2022, Article ID 8249032, 8 pages, 2022.

Research Article

Construction of Tourism Area Capacity Early Warning System Based on Internet of Things Technology

Yanli Ma 

Shanxi Art Vocational College, Taiyuan, Shanxi 030002, China

Correspondence should be addressed to Yanli Ma; 31115423@njau.edu.cn

Received 28 June 2022; Revised 28 July 2022; Accepted 4 August 2022; Published 16 August 2022

Academic Editor: Haibin Lv

Copyright © 2022 Yanli Ma. This is an open access article distributed under the Creative Commons Attribution License, which permits unrestricted use, distribution, and reproduction in any medium, provided the original work is properly cited.

In order to make up for the shortage of smart tourism construction highlighted by public tourism safety accidents due to the bearing capacity of scenic spots, this paper proposes a tourism area capacity early warning system based on the Internet of Things technology. By combining the main characteristics of a park and a place, this paper determines the composition of its tourism capacity and the corresponding calculation methods. At the same time, in order to control the number of tourists in peak hours within a reasonable range, the peak constraint method is proposed to improve the traditional algorithm of daily space capacity; then this paper calculates the tourism capacity of a park and a place by combining the relevant data obtained by investigation and observation methods. The experimental results show that according to the given number, the instantaneous tourism capacity of a park can be accurately calculated as 11841 person times/day and the daily tourism capacity as 21313 person times/day. The instantaneous tourism capacity of a certain place is 1066 person times/day, and the daily tourism capacity is 9594 person times/day. The construction of the early warning system of the tourism area based on the Internet of Things can effectively solve the problems such as public tourism safety accidents caused by the problem of carrying capacity. It will play an important role in the customized services of tourists, the innovation of scenic spot business processes, and the integration of tourism enterprise resources and provide data support for the early warning system.

1. Introduction

With the continuous improvement of people's living standards, people are pursuing high-quality spiritual life while meeting material needs. As a service-oriented industry, tourism has become an urgent need for people to pursue self-realization [1]. People's requirements for the service level of tourism have become higher and higher, which has prompted the transformation of tourism to meet the needs of the market. With the rapid development of tourism, the number of tourists has increased dramatically. Many scenic spots are often overcrowded and crowded in the peak tourism season, which not only greatly reduces the quality of tourists' experience, but also poses a great threat to the ecological environment and sustainable development of the tourism destination [2].

Tourism is an information intensive industry. With the continuous innovation and development of cloud computing, the Internet of Things, artificial intelligence, and other new technologies, tourism has a new demand for information construction [3]. From the perspective of tourism destination, it is necessary to realize the integrated marketing of tourism resources with the help of information management platform to provide comprehensive and intelligent services for tourists; from the perspective of tourists, personalized and intelligent services are needed to achieve a smooth tour of the scenic spot [4]. As the core combination of tourism, how to improve the management level of tourists in scenic spots has become one of the urgent problems to be solved in the information construction of scenic spots [5, 6]. In view of the existing problems, the concept of smart tourism is introduced to build a more modern progressiveness smart

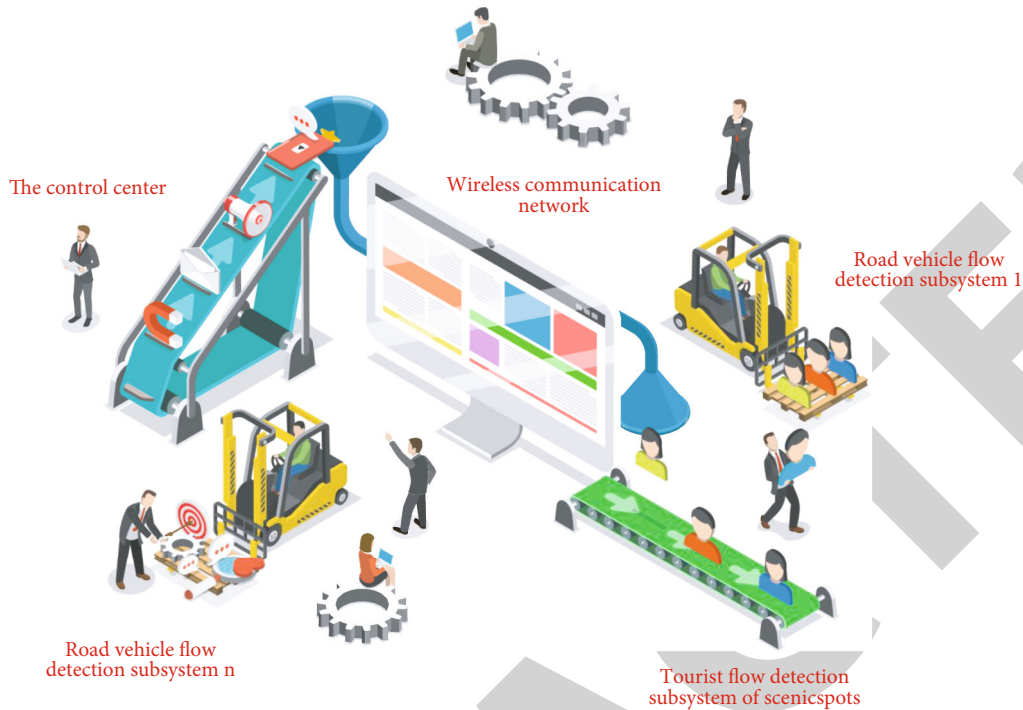


FIGURE 1: Tourist flow warning platform of tourist attractions.

regional tourism early warning system, in order to provide reference for the construction of smart tourism. Figure 1 shows the tourist flow warning platform of tourist attractions.

2. Literature Review

As an important part of scenic spot management, the level of tourist management directly affects the satisfaction of tourists and then affects the image building of scenic spots. Due to the different emphases of the research, scholars' understanding of tourist management is also different. Hu and Hou believe that tourist management is a process in which tourist destination managers use modern management means to achieve tourist satisfaction and tourist destination satisfaction through tourist responsibility management and tourist experience management [7]. Soroka and Wojciechowska-Solis believe that tourist management is the organization and management of the whole process of tourists' activities in the scenic spot, taking tourists as the management object. It is a part of scenic spot management [8]. Suklabaidya and Aggarwal believe that tourist management is the organization and management of the whole process of tourist behavior by tourism management departments or institutions using information, technology, education, and other means. Through the regulation and management of tourist capacity, behavior, safety, etc., the attraction of tourism resources and environment is strengthened, so as to improve the quality of tourist experience and satisfaction and achieve the sustainable development of tourism destinations [9]. Rivera believes that tourist management means that the scenic spot managers take tourists as the management object to organize and man-

age the activities of tourists in the scenic spot in the whole process, so as to ensure the long-term and stable development of tourism activities in the scenic spot [5]. According to the concept of tourist management, it can be seen that tourist management in scenic spots is a management activity with tourists as the management object, tourist behavior and its influencing factors as the management content, and the maximization of comprehensive benefits of tourist destinations as the management objective [10, 11]. According to different emphases of tourist management, tourist management modes can be divided into three types: environment oriented, tourist oriented, and environment tourist oriented. The main goal of environmental orientation is to protect the environment of tourism destination by controlling the number of tourists and standardizing the behavior of tourists [12]; the tourist-oriented management mode is to take tourists as the center and improve tourist satisfaction as the goal; the environment tourist-oriented management mode is to meet the needs of tourists to the greatest extent on the premise of protecting resources and environment, so as to achieve the sustainable development of tourism destinations.

In view of the above problems, although tourism management departments and tourism scholars at home and abroad attach great importance to the issue of tourism environmental capacity in tourism planning and give calculation formulas in theory, the application value is limited because researchers blindly pursue the fixed number of scenic spot tourism environmental capacity and simply apply various calculation formulas of tourism environmental capacity. In fact, tourism environmental capacity has certain dynamic characteristics [13]. Therefore, it is of more practical significance to explore the tools and methods of tourism environmental capacity management with practical application

value. With the development and application of emerging science and technology, weakening the calculation and research of theoretical capacity and paying attention to the research of capacity regulation mechanism will certainly become the direction of tourism environmental capacity research [14].

3. Research Methods

3.1. Calculation of Tourism Capacity

3.1.1. Peak Constraint Method

(1) *Peak Constraint Index*. At present, scholars have found that there is a certain proportion between the number of tourists received by the scenic spot and the maximum number of tourists during peak hours for scenic spots with certain regularity of daily passenger flow. Through the analysis of the data obtained from the field survey, it is found that there is also a certain proportional relationship between the number of daily tourists received by a park and the maximum number of tourists in peak hours (see Table 1). The correlation test is carried out by Spss20.0, and the result is $r = 0.9343 (>0.7)$. The results show that there is a significant correlation between the number of visitors received in a park and the maximum number of visitors in peak hours; that is, the proportional relationship between the number of visitors waiting in a park and the maximum number of visitors in peak hours is established. Therefore, this paper proposes that the peak constraint index g represents the ratio between the daily number of tourists m received by the scenic spot and the maximum number of tourists m during peak hours. If the peak constraint index g is stable, the total daily number of tourists received by the scenic spot can be determined by this value and the instantaneous spatial capacity of the scenic spot [15]. Due to the limited access to daily visitor volume data, this paper mainly theoretically verifies the stability of the peak constraint index G .

(2) *Theoretical Verification of Exponential Stability with Peak Constraint*. In this paper, the stability of peak constrained index g is theoretically verified by some assumptions and Bernoulli's law of large numbers in probability [16].

In this paper, the time when tourists enter the scenic spot is regarded as a random variable α , and the probability of tourists entering the scenic spot at time x is recorded as $f_1(x)$, that is, $f_1(x) = p(\alpha \leq x)$, where $f_1(x)$ is the distribution function of random variable α . Assuming that the time when m tourists enter the scenic spot in a day follows the same distribution function, and the time when each tourist enters the scenic spot is independent of each other, when m is infinite, according to Bernoulli's law of large numbers, the number of tourists entering the scenic spot before time x can be approximately $M \times f_1(x)$. In the same way, the time when tourists leave the scenic spot is regarded as a random variable β , and the probability of tourists leaving the scenic spot at time x is recorded as $f_2(x)$, that is, $f_2(x) = p(\beta \leq x)$,

where $f_2(x)$ is the distribution function of random variable β . Assuming that the time when m tourists leave the scenic spot in a day obey the same distribution, and the time when each tourist leaves the scenic spot is independent of each other, when m is infinite, the total number of tourists leaving before time x can be approximately $M \times f_2(x)$. Therefore, the number of tourists in the scenic spot at time x can be expressed by $M \times f_1(x) - M \times f_2(x)$, and the ratio G_x of the number of tourists in the scenic spot at time x to the total number of visitors received can also be obtained, that is, $G_x = M / [M \times f_1(x) - M \times f_2(x)] = 1 / [f_1(x) - f_2(x)]$. It can be seen from this that within a certain range of M , if the rules for tourists to enter and leave the scenic spot remain the same, and the peak time of tourists remains the same, it can be considered that the peak constraint index g is relatively stable.

At present, for a park, the time for tourists to enter and leave the scenic spot has a certain regularity, and the peak time of tourists also shows a certain regularity. In addition, as the development of the scenic spot is quite mature, the factors that may change the daily behavior of passenger flow, such as resource type, functional zoning, location traffic, tourist routes, and opening hours, are basically stable. Therefore, for a park, the peak constraint index g is relatively stable.

(3) *Peak Constraint Method*. In order to limit the number of tourists in the peak period to the instantaneous spatial capacity of the scenic spot, this paper improves the algorithm based on the previous spatial capacity based on the peak constraint index G and puts forward a new method: the peak constraint method, $C = C_0 \times G$ [17]. At present, the applicable algorithms for instantaneous space capacity include "area method," "trail method," and "bayonet method." In combination with the fact that the physical space that visitors can visit in a park is mainly planar, this paper uses "area method" to calculate the instantaneous space capacity of the scenic spot [18]. At the same time, according to previous experience, tourists' demands for basic space standards are different in different space places, but the existing "area method" usually takes the scenic spot as a class of space to calculate, without considering this factor. Therefore, this paper also needs to fully consider the impact of different types of space in a park on the calculation results of space capacity. The specific formula is as follows. The tourable physical space of a park can be divided into indoor architectural space of main scenic spots, indoor architectural space of other scenic spots, outdoor human landscape tourable space, and indoor natural landscape tourable space.

$$C = \sum_{i=1}^n \frac{S_i}{A_i}, \quad (1)$$

$$C = C \times G = \sum_{i=1}^n \frac{S_i}{A_i} \times \frac{M}{m}, \quad (2)$$

where M is the daily number of tourists received by the scenic spot; m is the maximum number of tourists in peak

TABLE 1: Daily total number of tourists and daily maximum number of tourists in the scenic spot at different times.

Date	11.23	11.24	11.25	11.26	11.27	11.28	11.29
Daily number of visitors M	14234 person	13542 person	15741 person	14281 person	17542 person	21563 person	21954 person
Maximum number of tourists m	8312 person	7601 person	9012 person	8114 person	8034 person	12841 person	13254 person
M/N	1.71	1.78	1.75	1.76	2.18	1.68	1.73

hours; n refers to the number of physical space types that different tourists can visit; S_i refers to the area of physical space that class i tourists can visit; A_i refers to the basic space standard of physical space that class i tourists can visit; and G refers to the peak constraint index, which is the ratio of the daily number of tourists m received by the scenic spot to the maximum number of tourists m during peak hours [19].

3.1.2. Calculation Method of Tourism Capacity

(1) *Calculation of Space Capacity.* Since there is no obvious regularity in the time when tourists go in and out of a place every day, and most of the time, especially on holidays, the number of tourists in the building will be in a relatively large state from the opening time to the closing time of the scenic spot. At the same time, considering that the accessible physical space in a certain place is planar, this paper mainly adopts the “area method” commonly used by scholars, combined with the daily average turnover rate of scenic spots, to calculate its instantaneous space capacity and daily space capacity. The specific formula is as follows.

$$C = \frac{A}{A_0}, \quad (3)$$

$$C = C \times Z = \frac{A}{A_0} \times \frac{T}{t}, \quad (4)$$

where A refers to the area of physical space that tourists can visit; A_0 refers to the basic space standard of tourists; T refers to the effective opening hours of the scenic spot every day; t refers to the average visiting time of each tourist in the scenic spot; and Z refers to the daily average turnover rate of the whole scenic spot, that is, the integer part value of T/t .

(2) *Measurement of Psychological Capacity.* Generally, scholars will use the “area method” to approximate the psychological capacity by taking the personal occupied area when the average satisfaction of tourists is the largest as the basic space standard [20]. However, since the psychological factors of tourists are considered to some extent when calculating the spatial capacity, it is not appropriate to use the spatial capacity algorithm to approximate the psychological capacity. According to previous studies, with the increase of the number of tourists, the sense of crowding of tourists will gradually increase, and after exceeding a certain number, the negative impact of the sense of crowding on the satisfaction of tourists will gradually become significant and enhanced [21]. Therefore, this paper can explore the impact of tourists’ perception of crowding on the tourist

experience, build a tourist satisfaction model, and determine the instantaneous psychological capacity. Daily psychological capacity is mainly calculated based on the instantaneous psychological capacity and daily turnover rate of the scenic spot. The specific formula is as follows.

$$C = C_b \times Z = C_b \times \frac{T}{t}, \quad (5)$$

where C_b refers to the instantaneous psychological capacity, which is mainly calculated by constructing the tourist satisfaction model; T refers to the effective opening hours of the scenic spot every day; t refers to the average travel time of each visitor in the scenic area; and Z refers to the daily average turnover rate of the whole scenic spot, that is, the integer part of T/t [22].

(3) *Determination of Final Capacity.* Since the tourism capacity of a certain place is only considered from the psychological capacity and spatial capacity, in order to ensure the tourist experience, according to the barrel theory, the minimum value of different capacity values should be taken as the actual tourism capacity of a certain place.

$$C = \min \{ C_{\text{Spatial capacity}} * C_{\text{Mental capacity}} \}. \quad (6)$$

3.2. *Sample Statistics.* The sample statistics of visitors to a park are shown in Table 2. It can be seen from the table that the number of male and female respondents is basically the same in terms of gender; in terms of age, the group aged 15-24 has the most respondents, followed by the group aged 25-44 and over; in terms of occupation, the number of students is the most because a park is implementing the free ticket policy, and students, especially college students, will have more free time to visit; in terms of educational background, the interviewees generally have high school education or above, and their overall quality is high, which is conducive to improving the accuracy of the questionnaire. In terms of income, the group with less than 2000 yuan has the largest number, followed by the group with 4001-6000 yuan.

Generally speaking, the different nature, place, and population density of the tourist destination will affect the tourists’ perception and satisfaction with the crowding of a certain space. At present, domestic scholars have achieved good results by using questionnaires to obtain basic spatial standards for different tourism spaces in tourism destinations. Therefore, according to the previous research results and the standard values of some standards and norms, this paper can obtain a reasonable basic space standard through a questionnaire survey of tourists.

TABLE 2: Demographic characteristics of tourists.

Features	Constitute	Frequency	Specific gravity (%)	Features	Constitute	Frequency	Specific gravity (%)
Gender	Male	261	52.52%	Occupation	Civil servant	51	10.26%
	Female	236	47.48%		Enterprises and institutions	43	8.65%
Age	Under 15	5	1.01%		Private enterprise	32	6.44%
	15-24 years old	207	41.65%		Liberal professions	42	8.45%
	25-44 years old	153	30.78%		Student	224	45.07%
	45-60 years old	55	11.07%		Retiree	64	12.88%
	Over 60 years old	77	15.49%	Other	41	8.25%	
Degree of education	Junior high school and below	26	5.23%	Monthly income	Below 2000	301	60.56%
	High school/technical secondary school	35	7.04%		2001-4000 yuan	131	26.36%
	Junior college	84	16.90%		4001-6000 yuan	32	6.44%
	Undergraduate	301	60.56%		6001-8000 yuan	21	4.23%
	Master degree or above	51	10.26%		Above 8000 yuan	12	2.41%

TABLE 3: Statistics of tourist survey standards.

	Below 0.25 m ²	0.25-1 m ²	1-2.25m ²	2.25-4 m ²	Above 4 m ²
Interior space of main scenic spot buildings					
Frequency	21	79	234	91	72
Proportion	4.23%	15.90%	47.08%	18.31%	14.49%
Interior space of buildings in other scenic spots					
Frequency	239	101	81	61	15
Proportion	48.09%	20.32%	16.30%	12.27%	3.02%
Outdoor natural landscape sightseeing space					
Frequency	139	197	91	58	12
Proportion	27.97%	39.64%	18.31%	11.67%	2.41%
Outdoor human landscape sightseeing space					
Frequency	8	196	213	61	19
Proportion	1.61%	39.44%	42.86%	12.27%	3.82%

From November 23 to 29, 2020, the author conducted a survey on the tourist space standards and collected 497 valid questionnaires. The survey results are shown in Table 3.

Statistical items can reflect tourists' subjective perception of per capita space. The minimum area interval takes the maximum value, the maximum area interval takes the minimum value, and other area intervals take the average value. Different space standards can be obtained based on the weight method: basic space standards for indoor building space of major scenic spots:

$$S_1 = 0.25 \times 4.23\% + 0.625 \times 15.90\% + 1.625 \times 47.08\% + 3.125 \times 18.31\% + 4 \times 14.49\% = 2.03 \text{ m}^2. \quad (7)$$

Basic space standards for interior space of buildings in other scenic spots:

$$S_2 = 0.25 \times 48.09\% + 0.625 \times 20.32\% + 1.625 \times 16.30\% + 3.125 \times 12.27\% + 4 \times 3.02\% = 1.02 \text{ m}^2. \quad (8)$$

Basic space standard of outdoor human landscape tourable space:

$$S_3 = 1 \times 1.61\% + 2.5 \times 39.44\% + 6.5 \times 42.86\% + 12.5 \times 12.27\% + 16 \times 3.82\% = 5.93 \text{ m}^2. \quad (9)$$

Basic space standards for outdoor natural landscape tourable space:

$$S_4 = 1 \times 27.97\% + 2.5 \times 39.64\% + 6.5 \times 18.31\% + 12.5 \times 11.67\% + 16 \times 2.41\% = 4.35 \text{ m}^2. \quad (10)$$

Therefore, the basic space standard for indoor space of buildings in major scenic spots is 2 m², that of buildings in other scenic spots is 1 m², that of outdoor human landscape is 6 m², and that of outdoor natural landscape is 4 m².

According to the data processing obtained from the survey, the indoor space area of the main scenic spot buildings is 2827 m², and the basic space standard is 2 m²; the area of

TABLE 4: Area statistics of different space types in the scenic spot.

Space type	Project	The measure of area (m ²)
Indoor architectural space of main scenic spots	Main attractions a	2132
	Main attractions B	695
	Total	2827
Indoor building space of other scenic spots	Other attractions a	1130
	Other attractions B	305
	Other attractions C	285
	Other attractions D	120
	Other attractions e	100
	Other attractions f	3112
	Total	5052
Outdoor human landscape sightseeing space	Outdoor cultural landscape a	6957
	Outdoor cultural landscape B	6620
	Outdoor cultural landscape C	5124
	Outdoor cultural landscape D	8025
	Total	29143
Indoor natural landscape sightseeing space	Indoor natural landscape a	280
	Indoor natural landscape B	325
	Indoor natural landscape C	230
	Indoor natural landscape D	1241
	Total	2076

TABLE 5: Statistical table of basic spatial standards of different spatial types in the scenic spot.

Space type	Indoor architectural space of main scenic spots	Indoor building space of other scenic spots	Outdoor human landscape sightseeing space	Indoor natural landscape sightseeing space
Basic space standards	2m ²	1m ²	6m ²	4m ²

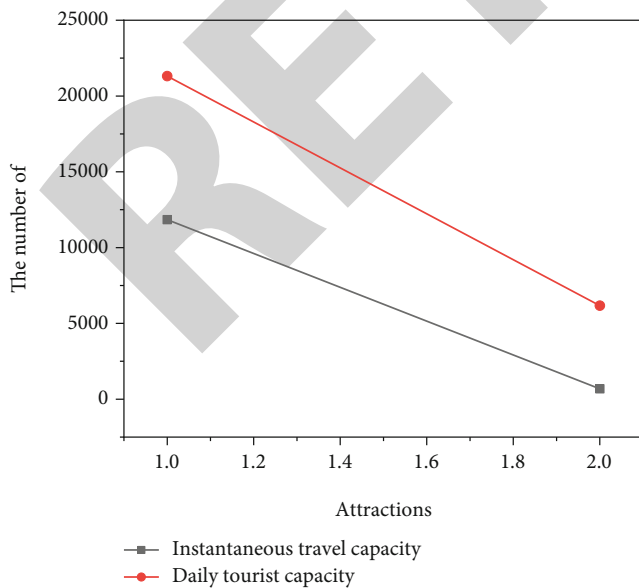


FIGURE 2: Tourism capacity calculation results.

indoor space of buildings in other scenic spots is 5052 m², and the basic space standard is 2 m²; the area of outdoor natural landscape sightseeing space is 29143 m², and the basic space standard is 2 m²; the area of outdoor human landscape sightseeing space is 2076m², and the basic space standard is 2 m² (see Tables 4 and 5). In order to accurately reflect the general trend of data changes, this paper takes the average value as the peak constraint index G, that is, the value of G is 1.80. By substituting the above data into formulas (1) and (2), the instantaneous space capacity of a park is 11841 person times/day, and the daily space capacity is 21313 person times/day.

3.3. Calculation of Tourism Capacity. The building area of a certain place is 3321 m². According to the field measurement, the actual area of accessible space is about 2132 m². At the same time, according to the investigation, the basic space standard in the building is 2 m², the per capita visiting time is about 1 hour, the daily opening time is 9.5 hours, and the turnover rate is about 9. According to formulas (3) and (4), the instantaneous space capacity of a certain place is

1066 person times/day, and the daily space capacity is 9594 person times/day.

Based on the impact of tourists' perception of crowding on the tourist experience, this paper constructs a satisfaction model to measure the psychological capacity of main scenic spot a . In order to ensure the tourists' experience, and in combination with the assignment of tourists' perception of crowding, it can be seen that 3 is the critical value of tourists' satisfaction, and the per capita tourists' satisfaction score cannot be lower than 3. When y is taken as 3, it is substituted into

$$y = -0.00001x^2 + 0.00711x + 2.82311. \quad (11)$$

Finally, X is 685, so the instantaneous psychological capacity of a place is 685 person times/day. At the same time, by substituting the instantaneous psychological capacity value into formula (5), the daily psychological capacity of a place can be calculated to be 6165 person times/day.

4. Result Analysis

According to the above calculation, the instantaneous space capacity of a certain place is 1066 person times/day, the daily space capacity is 9594 person times/day, the instantaneous psychological capacity is 685 person times/day, and the daily psychological capacity is 6165 person times/day. Based on formula (11), the instantaneous tourism capacity of a certain place is finally determined to be 1066 person times/day, and the daily tourism capacity is 9594 person times/day. Finally, the tourism capacity calculation results of scenic spot A and scenic spot B are shown in Figure 2.

Through the analysis of the characteristics of a park, it is considered that the spatial capacity can best reflect the actual tourism capacity of the scenic spot. At the same time, through the analysis of the general algorithm of spatial capacity, it is found that the existing methods cannot ensure that the number of tourists in a park can be maintained within the instantaneous spatial capacity during the peak period. Therefore, the peak constraint method is proposed to improve the daily spatial capacity algorithm of a park. Finally, the instantaneous tourism capacity of a park is 11841 person times/day, and the daily tourism capacity is 21313 person times/day. By analyzing the characteristics of a certain place, it is considered that the spatial capacity and psychological capacity can accurately reflect the actual tourism capacity of the scenic spot. Finally, combined with the barrel theory, it is determined that the instantaneous tourism capacity of a certain place is 1066 person times/day, and the daily tourism capacity is 9594 person times/day.

5. Conclusion

With the development of tourism informatization, the personalized demand of tourists has become increasingly strong, especially the research on the capacity early warning system of scenic spots. With the change of tourists' consumption behavior, tourists' demands for tourism information services have become increasingly strong. The capacity

early warning system of scenic spots will play an important role in the customized services of tourists, the innovation of scenic spot business processes, and the integration of tourism enterprise resources. This paper predicts and monitors the tourist quality, which provides a basis for the scenic spot to alleviate congestion and improve the tourist quality. The construction of tourism area early warning system can effectively solve the problems such as public tourism safety accidents caused by the problem of carrying capacity and will play an important role in the customized services of tourists, the innovation of scenic area business processes, and the integration of tourism enterprise resources.

Data Availability

The data used to support the findings of this study are available from the corresponding author upon request.

Conflicts of Interest

The author declares that they have no conflicts of interest.

Acknowledgments

The high-tech field project of Shanxi Science and Technology Department, "Research on the application of big data technology in patent analysis" (201903D121166), supports this study.

References

- [1] R. Millington, A. R. Giles, N. van Luijk, and L. M. C. Hayhurst, "Sport for sustainability? The extractives industry, sport, and sustainable development," *Journal of Sport & Social Issues*, vol. 46, no. 3, pp. 293–317, 2022.
- [2] S. Dong, "On the integration of computer application technology and information management," *Journal of Physics Conference Series*, vol. 1744, no. 3, article 032236, 2021.
- [3] I. Agustina and S. Basuni, "Supply optimization of objects and natural tourist attractions in situ Gunung, Gunung Gede Pangrango National Park," *Media Konservasi*, vol. 26, no. 1, pp. 36–43, 2021.
- [4] C. Wan and A. J. Onuike, "Illuminating opportunities for smart tourism innovation that foster sustainable tourist well-being using q methodology," *Sustainability*, vol. 13, no. 14, p. 7929, 2021.
- [5] J. N. D. Rivera, "VMS support: a mobile-based support to computerized visitor management system," *Software Impacts*, vol. 8, no. 1, article 100056, 2021.
- [6] C. Du, L. Liu, S. Shi, and J. An, "Prediction of traffic flow on highway ramp in scenic area," *Journal of Physics: Conference Series*, vol. 1646, no. 1, article 012057, 2020.
- [7] H. Hu and Y. Hou, "Study on spatial distribution and sustainable development of night tourism resources: take the central Guilin as an example," *IOP Conference Series: Earth and Environmental Science*, vol. 766, no. 1, article 012088, 2021.
- [8] A. Soroka and J. Wojciechowska-Solis, "Expectations of the Polish society related to recreational and tourist activities in the forest environment," *Sylvan*, vol. 164, no. 6, pp. 513–520, 2020.

Retraction

Retracted: Wearable Sensor and Its Application in Urban Landscape Design

Journal of Sensors

Received 3 October 2023; Accepted 3 October 2023; Published 4 October 2023

Copyright © 2023 Journal of Sensors. This is an open access article distributed under the Creative Commons Attribution License, which permits unrestricted use, distribution, and reproduction in any medium, provided the original work is properly cited.

This article has been retracted by Hindawi following an investigation undertaken by the publisher [1]. This investigation has uncovered evidence of one or more of the following indicators of systematic manipulation of the publication process:

- (1) Discrepancies in scope
- (2) Discrepancies in the description of the research reported
- (3) Discrepancies between the availability of data and the research described
- (4) Inappropriate citations
- (5) Incoherent, meaningless and/or irrelevant content included in the article
- (6) Peer-review manipulation

The presence of these indicators undermines our confidence in the integrity of the article's content and we cannot, therefore, vouch for its reliability. Please note that this notice is intended solely to alert readers that the content of this article is unreliable. We have not investigated whether authors were aware of or involved in the systematic manipulation of the publication process.

In addition, our investigation has also shown that one or more of the following human-subject reporting requirements has not been met in this article: ethical approval by an Institutional Review Board (IRB) committee or equivalent, patient/participant consent to participate, and/or agreement to publish patient/participant details (where relevant).

Wiley and Hindawi regrets that the usual quality checks did not identify these issues before publication and have since put additional measures in place to safeguard research integrity.

We wish to credit our own Research Integrity and Research Publishing teams and anonymous and named external researchers and research integrity experts for contributing to this investigation.

The corresponding author, as the representative of all authors, has been given the opportunity to register their agreement or disagreement to this retraction. We have kept a record of any response received.

References

- [1] D. Yao, "Wearable Sensor and Its Application in Urban Landscape Design," *Journal of Sensors*, vol. 2022, Article ID 7265038, 7 pages, 2022.

Research Article

Wearable Sensor and Its Application in Urban Landscape Design

Di Yao 

School of Design, Central Academy of Fine Arts, 100102 Beijing, China

Correspondence should be addressed to Di Yao; 11231411@stu.wxica.edu.cn

Received 29 June 2022; Revised 22 July 2022; Accepted 29 July 2022; Published 10 August 2022

Academic Editor: Haibin Lv

Copyright © 2022 Di Yao. This is an open access article distributed under the Creative Commons Attribution License, which permits unrestricted use, distribution, and reproduction in any medium, provided the original work is properly cited.

In order to meet the needs of people for the environment, physical, and psychological needs and to improve the characteristics of local areas, this paper proposes an urban environment measurement method based on wearable sensors. This method mainly relies on the previous questionnaire and tests the wearable sensor physiological data, subjective feelings, scoring tables, interviews, and other experimental methods in the psychological experimental environment. The recognition rate without adding association features was 93.3%, while the recognition rate of adding association features to individual test set verification reached 94.1%, an increase of about 1%. In this paper, naive Bayes and associated feature classification are used to effectively solve the influence of personal subjective factors and make up for the error of measurement data. The wearable sensor can achieve better results in the application of urban environmental measurement and can also be better applied in urban environmental landscape design, providing more effective data for urban landscape design.

1. Introduction

The rapid development of the socialization process has brought a series of problems, such as the deterioration of the ecological environment and urban pollution, people's health has also been threatened, and psychological diseases and chronic diseases threaten mankind. It has become an urgent need for urban construction to implement public health into the landscape design of colleges and universities. Different regions and climates have different effects on life comfort, mental health feeling, outdoor participation, and environmental accessibility. People's environmental feelings bring different audition feelings with climate change, temperature change, and seasonal change. Compared with other cities and regions, a certain region has higher latitude and cold climate [1].

The research shows that people in high-pressure environment are more likely to suffer from psychological diseases. The campus landscape should not only meet the physiological needs but also pay more attention to the psychological needs. With the improvement of the demand for the learning and living environment, the campus landscape design begins to pay more attention to the satisfaction of the space environment to the human spiritual needs.

Through the study of the campus landscape environment in a certain area, it is urgent to create a good campus landscape environment that combines the characteristics of a certain area, has a comfortable learning and living environment, has both campus culture, and adds luster to the city image. Starting from the feelings of campus landscape users, this paper studies the campus environment of colleges and universities in the area, analyzes the existing landscape problems of colleges and universities, and provides certain reference significance for the landscape design of colleges and universities in a certain area in the future [2]. The workflow of sensation, perception, and cognition system is shown in Figure 1.

2. Literature Review

According to this problem, Raj and others can monitor skin sweating, skin temperature sensor for skin temperature regulation, ECG sensor for cardiovascular activity, EEG sensor for brain activity, respiratory sensor for respiratory activity, etc. [3]. Regulated by the hypothalamus, sympathetic nerve, parasympathetic nerve, and other nervous systems, emotional experience will show a series of physiological reactions. These physiological responses can form millisecond

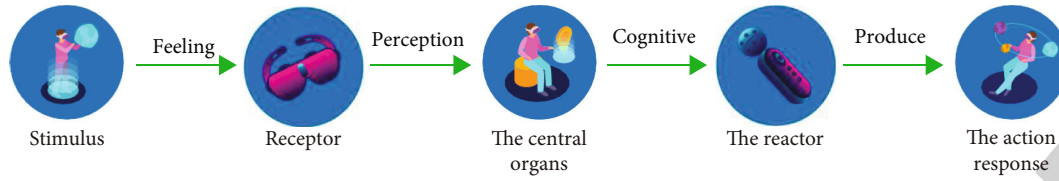


FIGURE 1: Workflow of sensation, perception, and cognition system.

responses to environmental stimuli, even including subdomain perception that is not fully conscious, and these physiological responses can be measured by biosensors more accurately and quickly. Ejaz-Ul-Haq and others used wearable devices to collect neurobioelectric reactions, so as to observe and record real-time environmental experience, which is a new technology for comprehensive environmental experience evaluation. Some pioneer scholars used skin and EEG technology to measure the experience during walking, identify emotional stressors, and analyze and evaluate the impact of the environment on people's emotional experience and cognitive function [4]. Li and others collected the skin electrical response of pedestrians during walking in the real environment to analyze and identify the potential pressure in the traveling space. The skin electricity or skin resistance records the conductive characteristics of the skin. Because the skin electricity is affected by the sweat secretion of the skin, it is a physiological indicator that better reflects the emotional pressure [5]. Liu and others used real-time picoelectric data to identify potential space environmental pressure sources through synchronous analysis with space GPS data [6]. Korolov and others found that when entering the natural environment with better greening from the urban block, pedestrians showed more calm mood, less frustration, anxiety, and active attention and showed more meditative thinking activities. This restorative receptivity caused by natural environment is in good agreement with the restorative nature theory of environmental psychologists [7]. Kpükü and others collected EEG data of walkers during real walking by using a portable EEG instrument with 14 electrodes and processed and analyzed their EEG data [8]. Compared with the EEG, the signal-to-noise ratio of EEG data is worse, but the data information that can be mined is much richer. In the experiment, the subjects wearing portable EEG walked through shopping blocks, green and natural areas, and busy commercial areas. The researcher used the EEG emotion analysis module based on machine learning developed by the instrument developer to analyze the collected EEG data and try to understand the pedestrian's environmental experience at that time. In the current research on sensor-based behavior recognition, there are many types of sensors used to obtain behavior data, and the motion information obtained by different types of sensors is obviously different. There is no unified standard, and everyone just verifies unilaterally, which cannot guarantee the scalability of the proposed method.

To solve the above problems, an effective association feature is proposed. At present, the features used in wearable sensor behavior recognition are mainly time-frequency domain features such as mean, variance, standard deviation,

and spectrum, which are commonly used in digital signal processing. Sensor-based behavior recognition is a new field, which is still in the stage of rapid development. Many theoretical knowledge is used in similar fields. Due to the lack of targeted features, the paper proposes the correlation feature experiment according to the correlation between sensor data at different positions during human movement [9, 10]. The results show that this feature can effectively improve the efficiency of behavior recognition and improve the scalability of the method.

3. Method

3.1. Landscape Applicable Population. The applicable groups of urban landscape around colleges and universities include students, faculty members, dormitories, and family members of faculty members. However, the behavior and activities of faculty members, dormitories, and family members of faculty members are relatively single, and the proportion of the number of people is relatively small compared with that of students, so they have little impact on the landscape design of colleges and universities [11, 12]. Therefore, the subjects of the study and test are mainly college students. The reasons are as follows: the campus landscape mainly serves the students, whose study, life, and daily activities are closely related to the campus landscape; college students have obvious aesthetic consciousness and communication needs; college students' behavior and environment interact with each other.

In this study, the preliminary questionnaire, E-Prime psychology experiment, wearable sensor physiological data measurement in real environment, subjective feeling rating scale, interview, and other experimental methods were used to analyze the measurement results, combined with the deviation distribution analysis method and the corresponding analysis and statistics method. Firstly, through the previous questionnaire survey, the landscape status and use preferences of three universities, namely, a technical university, a Forestry University, and a university, were determined, and the measured landscape spatial nodes of three universities were selected, respectively. Then, standardized tests are conducted through E-Prime psychological experiments to determine the physiological data under standard emotions. Then, wearable sensors are used for real-world measurement, and later landscape nodes are scored and interviewed. Finally, deviation distribution analysis and corresponding analysis statistics are used to analyze the real-world physiological data and subjective evaluation [12, 13]. Through the comparative analysis of objective physiological data measurement and subjective and objective evaluation of wearable

sensors in the whole stage, the emotional feelings under the campus landscape of colleges and universities, and the differences of individuals' feelings towards the landscape are obtained. Based on this, the optimization strategies for the built landscape of colleges and universities and the future campus construction are carried out.

3.2. Field Investigation. Preliminary field investigation through the preliminary field investigation of a technical university, a Forestry University, and a university, a preliminary understanding of the current situation of the built campus landscape to be studied has been formed, and the existing behavior and use preference of users have been mastered through field observation. Based on the theoretical basis of the interaction between environment and behavior, and based on the environmental feelings, detailed observation and investigation are carried out from two aspects: subjective factors and objective factors. Integrate and summarize and take photo records and field measurements as the preparation basis of the later questionnaire survey.

Based on the previous theoretical guidance and real scene investigation, this paper discusses the influencing factors of university landscape, designs a questionnaire, and finally, determines the content of the questionnaire after many comparisons, corrections, and adjustments.

The questionnaire is divided into four parts:

- (1) Research on the basic situation of university campus landscape users, including gender, age, major, grade, and other basic situations
- (2) The investigation of campus landscape space activities, needs, preferences, and initial evaluation
- (3) Investigation on the evaluation factors of landscape environment in colleges and universities
- (4) Expectations and suggestions for the campus

The questionnaire is distributed in paper form and collected on the spot to ensure the effectiveness of the questionnaire. Real-time communication and effective records are achieved during the survey. After the questionnaire is collected, a second check will be carried out to locate the incomplete questionnaires and those that do not meet the survey scope as invalid questionnaires, so as to ensure the authenticity and reliability of the questionnaire information. The preliminary investigation stage will be conducted in August 2020, and the questionnaire will be distributed in July 2020 and July 2021 [14, 15].

The number and recovery of questionnaires from the three schools are as follows: a total of 300 questionnaires were distributed by the three universities, and 293 were recovered, with a recovery rate of 97.67%. Except for invalid questionnaires, there were 289 valid questionnaires, with a total effective rate of 96.33%. The effective rates of the questionnaires were more than 75%, which was consistent with the scientificity of the questionnaire survey.

Since emotion is difficult to measure and no standard can be established, the psychological E-Prime program is

used to conduct the experiment of "arrangement and presentation of experimental stimuli," and the Chinese emotion system video is used to conduct the emotional stimulus experiment. At the same time, wearable sensors are used to record heart rate, skin electricity, blood oxygen, EEG, mental stress, fatigue index, cardiac compressive capacity, autonomic nerve balance, and other related physiological data. The measured standardized emotional physiological data are analyzed for similarity and correlation with the emotional physiological data in the real scene to determine the objective landscape evaluation of colleges and universities, as shown in Figure 2.

In the perceptual restorative scale in order to more accurately reflect the actual feeling of each campus space and facilitate the analysis and comparison with objective physiological data, a 1-5-level segmented quantitative description is set, 1 (none at all), 2 (relatively few), 3 (general), 4 (relatively many), and 5 (very many).

Corresponding to PRS question: I can have a good rest in this place. This place makes me feel interesting. I want to stay a little longer and have a look. There is some confusion here, which distracts me. I can do anything here. I enjoy it very much. I feel like I belong here to score. Combined with the real scene interview and evaluation score results, this paper summarizes the use evaluation and landscape preference of university campus landscape.

KMO (Kaiser-Meyer-Olkin) and Bartlett spherical tests were used in this experiment, and Table 1 was obtained through SPSS monitoring. It is concluded from the table that KMO statistic is $0.972 > 0.8$, $P < 0.05$. The closer the appropriate amount of KMO sampling is to 1, the stronger the validity of the questionnaire. KMO and Bartlett spherical tests are shown in Table 1.

3.3. Reliability Analysis. According to Table 2, Cronbach's $\alpha > 0.7$, showing a positive correlation, and the questionnaire has a strong correlation. The correlation statistics are shown in Table 2.

To sum up, the questionnaire in the experiment was input into SPSS for analysis and presented visually in the form of charts. The validity and reliability of the questionnaire are in line with the requirements of the questionnaire, indicating that the questionnaire has accuracy and relevance.

(1) Plant seasonal evaluation

At present, among the existing seasonal landscape of plants in colleges and universities, a university has the highest evaluation. The campus of a university has good greening and rich vegetation. Among the surveyed people, 56% think that a university has flowers in the seasons, the seasons are always green, and the seasonal landscape is good, 41% think that it is average, and the remaining 3% think that the seasonal change is not obvious. The university with the lowest evaluation is a technical university. Although the campus area of a technical university is large, the landscape environment space of the university is relatively small. 73% of the people think that the seasonal landscape is average, 19% of the people hold a good attitude towards the seasonal

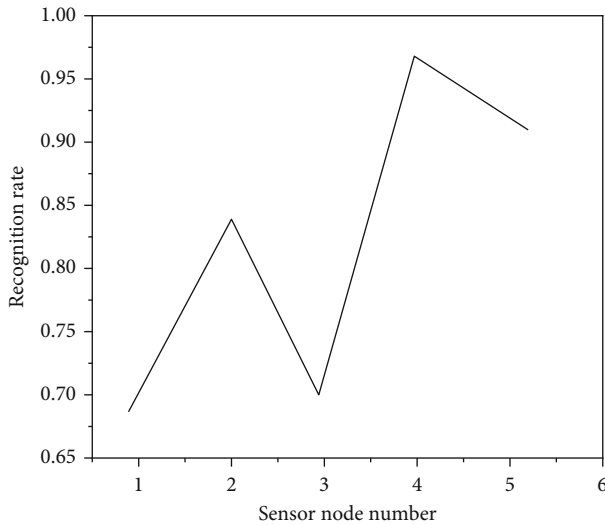


FIGURE 2: Recognition rate of different sensor node data for different behaviors.

landscape, and the remaining 8% think that the seasonal change is not obvious. In a forestry university, 41% of the respondents thought that the season was good, 54% thought that the season changed generally, and the remaining 5% thought that the change was not obvious. In the three schools as a whole, 55.67% of the respondents thought that the seasonal changes of their campus landscape were average, 39% thought highly of them, and the remaining 5.33% thought that the seasonal changes of campus landscape were not obvious. In the landscape design of colleges and universities, the creation of seasonal landscape can enrich the landscape changes, and the space created with seasonal landscape has more atmosphere.

(2) Evaluation of shade degree of plants

Among the three universities, only 5% of the respondents from a university think that the shading effect is very good, while the other two universities, a technical university and a forestry university, think that the shading effect is very good. On the whole, a university has a high degree of shading evaluation, and the school with the lowest degree of evaluation is a technical university. In general, 45% and 41.66% of the respondents, respectively, believe that the campus landscape has a small amount of shade and a part of shade. The shade degree of the campus landscape in summer affects the feeling of landscape use. In a certain area, the sun is strong in summer, and reasonable shade can meet the site activities of the landscape space, affecting the use preference, frequency, and frequency [16, 17].

There are many kinds of plants in a university; a technical university has the least plant species and the least richness. 43% of the respondents in a technical university think that a technical university has more plants and fewer species. Clove is the main tree species in the campus of a technical university, supplemented by other poplar and willow trees; 26% of the respondents of a forestry university think that a forestry university has a small number of plants

and a large number of species, which is deeply related to the fact that a forestry university is an agricultural and forestry university. There are several teaching and learning parks in the Donglin campus, which are rich in plant species for plant identification and investigation. In general, 43% of the respondents believed that the three universities had a large number of plants and a variety of species, and 26.67% of the respondents believed that there were a large number of plants and a few species. According to the comprehensive analysis of the three universities, the university with the best plant construction and the highest evaluation is a university. In terms of plant season, plant species, and shading degree, the existing plant landscape of a university is reasonably constructed and feels good.

After comprehensive consideration, 9 people were selected, including 4 boys, 5 girls, 5 design related majors, and 4 nondesign-related majors. From July 10, 2019, to August 12, 2019, real-life physiological data monitoring experiments of wearable sensors were carried out in the selected landscape spaces of a technical university, a forestry university, and a university. Through E-Prime in the early stage, subjective PRS scoring and real scene interview records in the later stage, the landscape environment of the university campus is comprehensively described.

3.4. E-Prime Standardization Experiment. As it is difficult to formulate the standardization of feelings and emotions, the E-Prime program of psychology is used to form a stimulation test. Physiological data are recorded when watching the standardized emotional video, and each experimental video is scored with a pleasure degree of 1-7 points. 1 means none at all, 4 means medium, and 7 means very strong, as shown in Figure 3. After the experiment, the similarity analysis between the measured data of the standardized experiment and the measured data in the real scene is carried out to determine the emotional state in the real scene environment. The final results of the landscape environment evaluation experiment are analyzed together with subjective evaluation and objective measurement. The pleasure level options are shown in Figure 3.

The deviation distribution between the actual measurement data collected in the whole experiment and the standard experiment measurement data is analyzed, and the resulting quartile bitmap compares the data information from two aspects: the smaller the median deviation is, the closer it is to the standard experiment; the more concentrated the distribution is, the closer it is to the standard experiment. Take the no. 1 experimenter as an example to draw the following conclusions. Next, take the no. 1 experimenter as an example to analyze the measurement process of his objective physiological data. In the five experimental spaces of a university, the Grove (space 2) is close to positive emotion, and the playground (space 1), library (space 5), small pool (space 3), and Yanyuan (space 4) are close to neutral emotion.

The wearable sensor experiment can analyze the university landscape space that is closest to the standard experimental mood in the real landscape environment. The experiment is carried out in the real landscape environment,

TABLE 1: KMO and Bartlett spherical test.

Appropriate amount of KMO sampling period		0.972
Bartlett ball test	Approximate chi square	7124.56
	Freedom	156
	Significance	<0.05

TABLE 2: Correlation statistics.

Cronbach's α	Cronbach's α based on standard items	Number of items
0.893	0.889	25

which is affected by uncertain factors, resulting in some errors in the measurement results. It needs to be analyzed in combination with subjective preferences to improve the accuracy of the evaluation of the university landscape environment space feeling.

3.5. Naive Bayesian Method. Naive Bayesian model is one of the most widely used classification models. The Bayesian theory proposed many years ago is the solid mathematical foundation of the model. Bayesian model has the advantages of stable classification efficiency, few parameters, insensitive to missing data, and simple and fast algorithm. The algorithm is based on probability and assumes that each attribute is independent. Its classification principle is to obtain the postexperiment probability by using Bayesian theorem according to the prior probability of the object and select the category with the largest postexperiment probability as the classification result. However, in practice, it is difficult to ensure that attributes are independent of each other. When the correlation between the attributes is large, the classification efficiency of the model is poor. Only when the attribute correlation is small, the model can perform well.

The working process of naive Bayesian classification is as follows:

- Let $X = \{x_1, x_2, \dots, x_n\}$ be an item to be classified, and each is a characteristic attribute of X
- There are m categories in total, forming a category set. $C = \{c_1, c_2, \dots, c_m\}$ gives an unknown data

Sample X : the classification method will predict the class with the highest a posteriori probability, that is, naive Bayes classification will assign the sample data without class label to the class if and only if

$$P(c_i|X) > P(c_j|X) \quad 1 \leq j \leq m, j \neq i. \quad (1)$$

Formula (2) can be obtained according to Bayesian theorem:

$$P(c_i|X) = \frac{P(X|c_i)P(c_i)}{P(X)}. \quad (2)$$

Given a dataset with many attributes, the calculation cost is large. In order to reduce the calculation cost, the attributes are assumed to be independent. Given the sample label, assuming that the attribute value conditions are independent of each other, that is, there is no dependency between attributes, formula (3) can be obtained:

$$P(X|c_i)P(c_i) = P(x_1|c_i)P(x_2|c_i) \cdots P(x_n|c_i) = P(c_i) \prod_{j=1}^n P(x_j|c_i). \quad (3)$$

Among them, $P(x_1|c_i)P(x_2|c_i) \cdots P(x_n|c_i)$ can be estimated by training samples.

Considering the advantages of naive Bayes classification method, such as easy implementation, stable classification efficiency, and fast execution speed, this method is added to the experimental performance evaluation.

4. Results and Analysis

This chapter conducts research in combination with the landscape environment, analyzes the existing problems through the questionnaire, and concludes that the existing urban university campus environment is a dynamic process. The quality of an environmental space is not a single evaluation, but a time-varying process determined by the influencing factors [18, 19]. Regional characteristics make the urban campus landscape inherit the historical foundation of local context. Using the test method in Section 3, each time, select volunteer data as the test set and other volunteers as the training set, and carry out individual independent leave one verification. As shown in Table 3, the behavior recognition rate is 94.1%, which is about 1% higher than the recognition rate of 93.3% without adding associated features, which verifies the effectiveness of this feature [20].

Generally, researchers prefer to make one-time feature selection for the stored data, that is, all the data used for recognition are stored in one feature quantity, but the feature selection method selects the features. Each feature has a feature weight value. A new feature vector is composed of N features with large sampling weight and finally transformed into multitask model logarithm, such as classification or recognition. However, this method has two important problems.

First, the direct difference of behavior indexing between sensor data at different locations is not fully considered, that is, the feature weights of feature vectors obtained from sensor node data at the same location are different; second, the traditional method needs to transmit the data of each sensor node to the background data mining processing

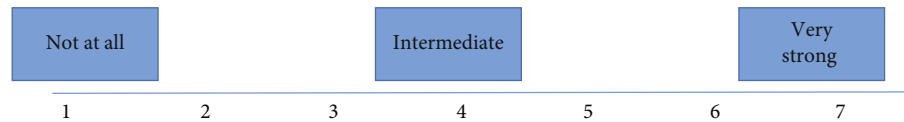


FIGURE 3: Pleasure level options.

TABLE 3: Analysis of objective feelings.

Test number	A forestry university	A technical university	A university
1	Spaces 1 and 3 > 4 > 2 and 5	Space 3 > 2, 4 > 1	Space 2 > 1, 3, 4, 4
2	Space 1 > space 2, space 4, space 5 > space 3	Space 2 > 1, 3 and 4	Spaces 2, 3, and 4 > spaces 1 and 5
3	Spaces 1 and 4 > 5, 3 > 2	Space 3 > space 2 > 4, space 1	Spaces 1, 2 and 4 > 3 > 5
4	Space 2 > 1, 3, 4 > 5	Spaces 1 and 3 > 4 > 2	Spaces 2 and 4 > 3 > 1 and 5
5	Space 1 > space 5 > space 2, 3 and 4	Space 3 > 2, 4 > 1	Space 3 > 1, 2 > 4 > 5
6	Spaces 3, 4 and 5 > 1 > 2	Spaces 2, 3 and 4 > 1	Spaces 1, 3 and 4 > spaces 2 and 5
7	Space 1 > 2, 4 > 3 > 5	Space 4 > 3 > 2 > 1	Spaces 2 and 3 > 5 > 1 and 4
8	Spaces 3 and 4 > 1 > 2 and 5	Space 1 > 2 > 3 > 4	Spaces 4 and 5 > 3 > 1 and 2
9	Spaces 1, 2, 4 and 5 > 3,	Space 4 > 2 > 3 > 1	Space 3 > space 2 > space 1, 4 and 5

center in advance. The data transmission volume of the log mining has not changed, which cannot effectively reduce the data transmission volume. However, the multitask feature selection mode can hoof select the data at the sensor points, to achieve the effect of reducing the data transmission volume. Considering the heterogeneous distribution of sensor nodes, we choose to select the features of each sensor node data. Each sensor node data corresponds to a feature weight vector. We select the features of each feature vector, and each feature vector selects the features with large weight. Finally, the feature vectors selected by each sensor node are transmitted to the background data processing center, and the behavior data are classified or identified.

5. Conclusion

In this paper, the author proposes a correlation method, which measures the changes of each person's psychological situation and personal feelings at individual different positions through sensors. Specifically, it is expressed by the change of heartbeat emotion and the questionnaire. According to the results of the observation questionnaire and the calculation of naive Bayes formula, we can draw a conclusion: the factors of urban environment have a great impact on individual psychology and physiological behavior. Therefore, we can use wearable sensors in urban landscape design to carry out portable measurement of the impact of the surrounding environment on us, so that we can timely transform the surrounding urban environment, meet our needs for learning and living environment, and meet the spiritual needs of human beings, and improve the different requirements of different regions, different climates, and different people for life comfort, mental health feelings, outdoor participation environment, etc.

Data Availability

The data used to support the findings of this study are available from the corresponding author upon request.

Conflicts of Interest

The author declares that there are no conflicts of interest.

References

- [1] T. Nguyen, T. Dinh, V. T. Dau, C. D. Tran, and D. V. Dao, "A wearable, bending-insensitive respiration sensor using highly oriented carbon nanotube film," *IEEE Sensors Journal*, vol. 99, pp. 1–1, 2020.
- [2] G. Dhiman, V. Kumar, A. Kaur, and A. Sharma, "Don: deep learning and optimization-based framework for detection of novel coronavirus disease using x-ray images," *Interdisciplinary Sciences Computational Life Sciences*, vol. 13, no. 2, pp. 260–272, 2021.
- [3] M. Raj, P. Manimegalai, P. Ajay, and J. Amose, "Lipid data acquisition for devices treatment of coronary diseases health stuff on the internet of medical things," *Journal of Physics: Conference Series*, vol. 1937, article 012038, 2021.
- [4] M. Ejaz-Ul-Haq, N. Hameed, M. Irfan-Ur, R. Khan, and I. Mohsin, "Temporal changes in physical signs of estrus and validation of fetal parameters for estimation of gestational stage through b-mode ultrasonography in beetal goats," *Pakistan Veterinary Journal*, vol. 40, no. 4, pp. 425–430, 2020.
- [5] L. Li, Y. Diao, and X. Liu, "Ce-Mn mixed oxides supported on glass-fiber for low-temperature selective catalytic reduction of NO with NH₃," *Journal of Rare earths*, vol. 32, no. 5, pp. 409–415, 2014.
- [6] W. Liu, L. Xing, L. Yao, Z. Zou, and Y. Zhang, "Design of portable eeg and blood oxygen synchronous acquisition system," *Zhongguo yi liao qi xie za zhi = Chinese Journal of Medical Instrumentation*, vol. 45, no. 3, pp. 280–283, 2021.

Retraction

Retracted: Development and Construction of Internet of Things Training Practice Platform for Employment Skills Assessment

Journal of Sensors

Received 13 September 2023; Accepted 13 September 2023; Published 14 September 2023

Copyright © 2023 Journal of Sensors. This is an open access article distributed under the Creative Commons Attribution License, which permits unrestricted use, distribution, and reproduction in any medium, provided the original work is properly cited.

This article has been retracted by Hindawi following an investigation undertaken by the publisher [1]. This investigation has uncovered evidence of one or more of the following indicators of systematic manipulation of the publication process:

- (1) Discrepancies in scope
- (2) Discrepancies in the description of the research reported
- (3) Discrepancies between the availability of data and the research described
- (4) Inappropriate citations
- (5) Incoherent, meaningless and/or irrelevant content included in the article
- (6) Peer-review manipulation

The presence of these indicators undermines our confidence in the integrity of the article's content and we cannot, therefore, vouch for its reliability. Please note that this notice is intended solely to alert readers that the content of this article is unreliable. We have not investigated whether authors were aware of or involved in the systematic manipulation of the publication process.

Wiley and Hindawi regrets that the usual quality checks did not identify these issues before publication and have since put additional measures in place to safeguard research integrity.

We wish to credit our own Research Integrity and Research Publishing teams and anonymous and named external researchers and research integrity experts for contributing to this investigation.

The corresponding author, as the representative of all authors, has been given the opportunity to register their agreement or disagreement to this retraction. We have kept a record of any response received.

References

- [1] X. Zhang, "Development and Construction of Internet of Things Training Practice Platform for Employment Skills Assessment," *Journal of Sensors*, vol. 2022, Article ID 3014565, 7 pages, 2022.

Research Article

Development and Construction of Internet of Things Training Practice Platform for Employment Skills Assessment

Xiaofeng Zhang 

Dongguan Polytechnic, Dongguan, Guangdong 523000, China

Correspondence should be addressed to Xiaofeng Zhang; 11231348@stu.wxlc.edu.cn

Received 28 June 2022; Revised 21 July 2022; Accepted 26 July 2022; Published 4 August 2022

Academic Editor: Haibin Lv

Copyright © 2022 Xiaofeng Zhang. This is an open access article distributed under the Creative Commons Attribution License, which permits unrestricted use, distribution, and reproduction in any medium, provided the original work is properly cited.

In order to solve the problem of employment skills assessment, a method using the Internet of Things training practice platform is proposed. The main content of this method is based on the research and analysis of the practical training platform of the Internet of Things. According to the data characteristics of the Internet of Things and through the construction of the practical platform, it is concluded that the development and construction of the practical training platform of the Internet of Things is highly feasible for the evaluation of employment skills. The experimental results show that the average RI value of data mining accuracy is 0.95, and the accuracy of data mining algorithm is high. *Conclusion.* It proves that the development and construction of the practical training platform of the Internet of things is feasible and accurate for the evaluation of employment skills.

1. Introduction

With the rapid development of China's science and technology level and production technology level, the demand for technical personnel has become increasingly urgent in recent years. Although the number of college graduates is gradually increasing every year, the inevitable contradiction between the single orientation of professional talent training and the diversity of human market demand makes some college graduates face severe employment problems. In view of the problem of difficult employment, many higher vocational colleges have carried out investigation and research and concluded that there is a huge difference between the actual needs of employing enterprises and the comprehensive level of college students' professional employment ability and adaptability. Lack of knowledge application ability and communication and cooperation ability, lack of sense of responsibility and professional ethics, lack of ability to grasp social needs and adapt to professional needs, and other personal conditions directly lead to the failure of students trained by schools to find jobs, while enterprises cannot recruit suitable talents [1].

In recent years, the employment of college students has been concerned by the society. The contradiction of higher education in China has been transferred from the entrance

to the exit, that is, from the difficulty of enrollment to the difficulty of employment [2]. Although China is a country with a large population, it faces a serious shortage of talents at the same time, and the total amount of college students cannot meet the needs of social development. The expansion of college enrollment has brought the proportion of the mainland's population in higher education to about 5%. Even so, compared with the proportion of the population receiving higher education in developed countries, China's higher education personnel training scale is far from meeting the needs of social development. On the other hand, the talent training of colleges and universities is disconnected from the market demand. What the market needs cannot be effectively supplied, and a lot of what the market does not need is cultivated. It is common that some people have nothing to do, and some people have nothing to do. At the same time, college students show an obvious imbalance in the choice of employment goals, and graduates flock to the central cities and hot fields in developed regions, while relatively backward second- and third-tier cities in central and western regions and unpopular industries at the grass-root level attract little attention.

Employability is a big problem facing the vast majority of people in today's society, and college students are a large

part of the majority of people. It is also an important premise of national economic development, and with the development of modern science and technology and knowledge economy, those traditional employment methods no longer adapt to the needs of the current market; thus, it can be seen how important it is to enhance the employment ability of college students to graduate to adapt to the development of the new era situation [3].

2. Literature Review

Employability refers to the ability of college graduates to realize the ideal of employment to meet social needs and realize their own value in social life through the study of knowledge and the development of comprehensive quality, including learning ability, ideological ability, practical ability, employment ability, and adaptability. After continuous development, the college students apply for a job as a process to deal with, and through the successful and unsuccessful student employment experience contrast, it was found that college students' employment ability can be divided into social psychological capital and professional identity of human capital four parts. Having the effect of the mutual promotion between the parts together constitutes the overall employment ability. As a result, today's college students no longer rely solely on their higher education qualifications, but must become flexible and adapt to changes in the labor market by developing and gaining position advantages over other graduates of similar academic and class status. To gain position advantage, college students need to develop and acquire skills, especially core skills (hard skills) and transferable skills (soft skills) [4]. It can be seen that college students' employability is a concept of dynamic development and a comprehensive framework of individual static basic quality and dynamic process characteristic. With the change of the social employment market environment, its content is constantly enriched and improved, from the initial focus on the employability of college students, to the basic ability to obtain and maintain the job, to the acquisition of subject knowledge, practical skills, and personal characteristics, and finally expanded to the overall focus on the key elements of college students' employability.

In view of the above problems, this paper proposes the development and construction of Internet of Things training practice platform for employment skills assessment. Start from the current situation of Internet of Things training practice teaching, combined with employment and professional certification. Through the development and construction of the practical training platform for the Internet of Things, the theoretical and practical teaching links of the Internet of Things can be served; the ultimate goal is to train outstanding talents in the field of the Internet of Things with the ability to solve complex engineering problems and to serve the regional economic development [5]. In order to improve the quantity and quality of students' employment, based on the analysis and summary of the existing practical teaching platform construction scheme, the development ideas and construction focus of Internet of Things practical training teaching platform suitable for this major are pro-

posed. Based on the guiding principle of a comprehensive platform, the software and hardware composition, the functions and characteristics of the system, and the feedback evaluation management system of the teaching platform are discussed. Through the construction of the practical teaching platform to serve the professional construction and professional certification, promote the reform, so that the practical and training courses can not only meet the training of students' practical and innovative skills. At the same time, reasonable feedback and evaluation can be carried out on the employment skills of students who participate in the training, which provides a strong and reasonable basis for students to find jobs and enterprises to choose the corresponding talents [6].

3. Research Method

3.1. Research on Practical Training Platform of Internet of Things

3.1.1. *Platform Status Analysis.* Internet of Things (IoT) is an emerging major that lays equal emphasis on multidisciplinary theory and practice, covering communication, computer network security, various sensors, and other knowledge. How to build a set of training and practice platform that can meet the needs of complex engineering problems and talents in the Internet of Things industry is an urgent problem to be solved in the construction of the Internet of Things specialty [7]. At present, the practical teaching of Internet of Things major has the following problems: Theoretical knowledge lags behind the development of social technology, leading to the practice of training content has been outdated or even eliminated. Students are not exposed to the latest developments in science and technology at school, leaving students facing unemployment when they graduate. The content of practical teaching is narrow and only involves the content of teaching materials, which is obviously divorced from the level of social development. Moreover, most of the practice content is based on the verification of basic experiments, which cannot cultivate students' innovation ability and the ability to solve complex engineering problems. The lack of practical equipment limits the progress of teachers' design and updating of teaching content, resulting in the fact that practical teaching lags behind theoretical teaching. Many experiments of the Internet of Things majorly involve many aspects of knowledge and are difficult to operate. In the absence of hardware equipment, students are forced to adopt virtual simulation experiments, which is not conducive to the establishment of system concepts and the cultivation of innovation ability [8].

The integrated practice teaching system of industrial research+on-campus training enterprise internship employment customization can fully cultivate students' employment ability in practice teaching and achieve the goal of classifying students. It is more suitable for colleges and universities aiming at cultivating application-oriented talents. The project-based practice teaching system adopts the way of joint training of schools and enterprises, which requires

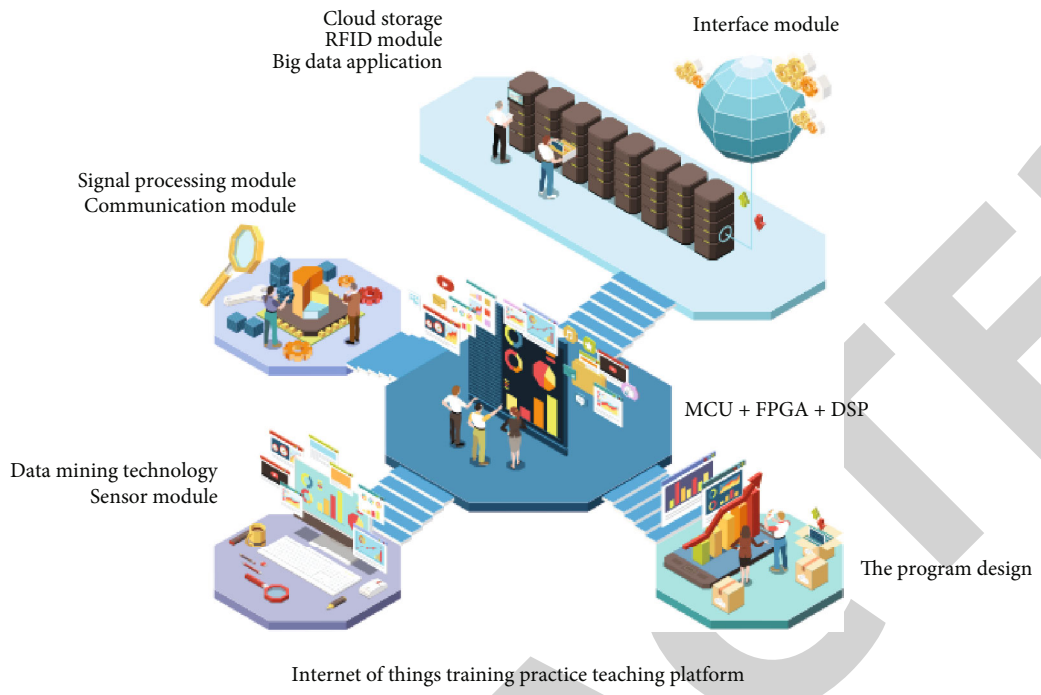


FIGURE 1: Block diagram of Internet of Things training practice teaching platform.

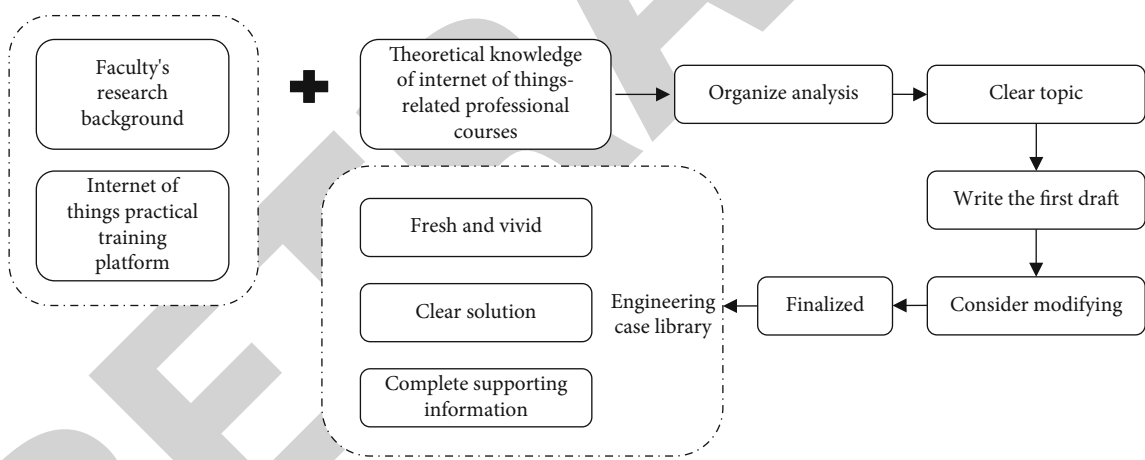


FIGURE 2: The characteristics and procedures of the Internet of Things experiment and teaching cases.

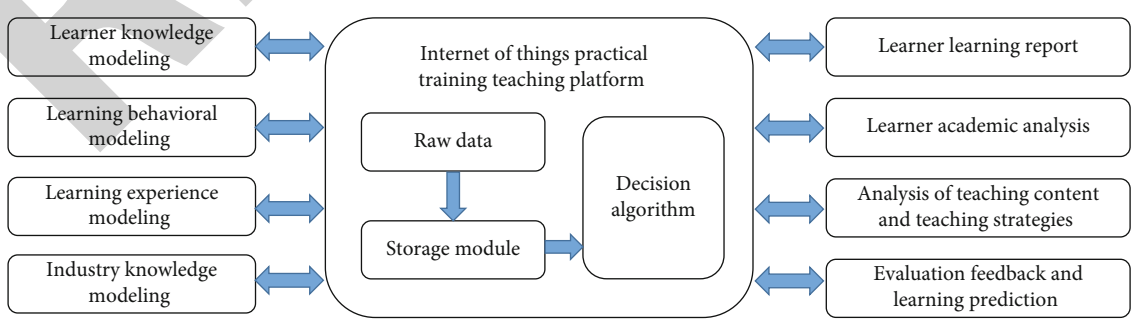


FIGURE 3: Big data application model of Internet of Things practice and training teaching platform.

high participation of enterprises, so it is difficult to implement. The disadvantages of this scheme are that it is not universal and has poor extension. Through a variety of teaching means or a variety of discipline competitions to promote practical teaching, the employment skills of college student targeted training, so as to achieve the purpose of improvement of the two methods, also have a certain one-sidedness, not fully consider the needs of enterprises [9].

3.1.2. Data Characteristics of Internet of Things. The data pattern tree obtained by the dimension comprehensive control mechanism can obtain the scope of data mining to a certain extent, but the specific results of data mining cannot be obtained because the calculation of model correlation degree is not accurate enough. Therefore, feature extraction method is adopted in this paper to detect feature data in Internet of Things big data. According to the attribute dimension of big data, the value dimension of information data is obtained, the data set to be mined is set as d , and the dimension of the data set is set as D , and the set W is obtained according to the value of data attribute. The subspace S required for data mining is contained in a collection of data attribute values, and the data objects OED in the subspace are for advices. According to the characteristics of outlier distribution, it can be concluded that the nearest neighbor domain (o, S) of data objects in subspace also presents nonuniform distribution. The outlier probability of a randomly selected data object in the subspace can be expressed as $l(o, S)$ in the data set. From the perspective of multidimensional data attributes, it can be found that the center point of the subspace is the data object [10]. Then, the probability calculation formula is as follows:

$$d_s = \frac{1}{I_d(o, S)}. \quad (1)$$

Distance is expressed as d . If the data object is still in the central position in all data sets to be mined, the standard distance σ between data s and data o can be obtained by the following formula:

$$\sigma(o, s) = \sqrt{\frac{\sum_{s \in S} d(o, s)^2}{|S|}}. \quad (2)$$

3.2. Internet of Things Training and Practice Platform Construction

3.2.1. An Integrated Platform. The platform can meet the dual teaching tasks of practice and training, that is, meet the needs of teaching links such as the independent experiment in the course of professional curriculum design and experiment in scientific research training and graduation design. It also needs to meet the requirements of comprehensive practical training projects such as discipline competition, simulation, and enterprise practice [11]. There are many factors that need to be considered in the development of a comprehensive platform, among which the teaching team is most concerned about the scalability and upgradabil-

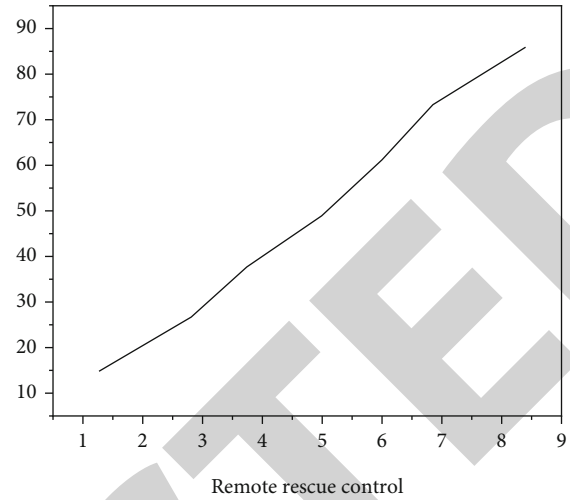


FIGURE 4: No employment services are currently available.

ity of the platform. Modular design is adopted in the design, and the functional richness of hardware products is considered in the selection of hardware products. It can not only ensure the diversity of practical teaching content of this major but also meet the diversified development requirements of students such as employment competition. It can also meet the needs of students of other majors for in-class and extracurricular experiments, as shown in Figures 1 and 2.

The hardware part of the integrated platform includes sensor technology-related practice module, RFID development and design-related practice module, SCM+FPGA +DSP-integrated embedded system development module, communication module, signal processing module, and interface module, which may be involved in the students' competition and employment training in the training program [12]. The software part includes JAVA, C++, and other related program design and development of data mining technology python, R and other language simulation and big data application technology, comprehensive application ability, and innovation ability training.

3.2.2. Two Innovative Developments. Considering the development trend of the Internet of Things, data mining and big data analysis-related technologies are introduced in the development process of the integrated platform for the first time. It can satisfy students' development of relevant experimental competitions and practical training based on professional core courses and help teachers obtain data models such as students' learning process detection, academic analysis and prediction, and final decision evaluation from the platform data [13]. The big data application model of the integrated platform is shown in Figure 3.

First of all, the integrated platform records the learning data of each link of learners and models the knowledge already possessed by learners through internal algorithms. Then, model the learning knowledge system and the behavior of the learning process of learners, analyze the internal relationship between their learning activities and teaching

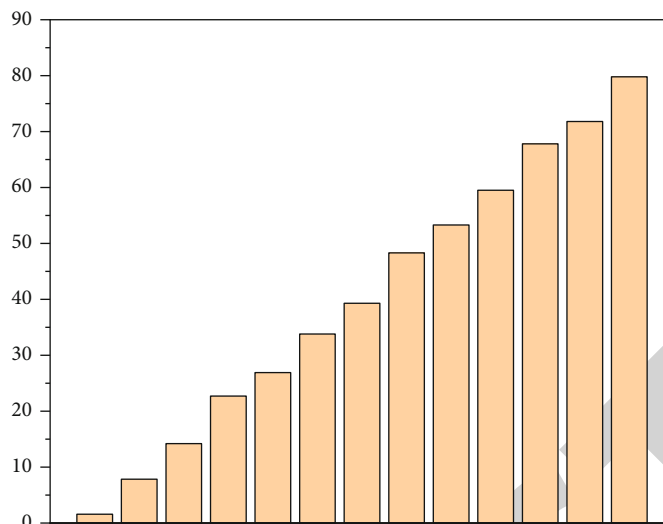


FIGURE 5: Employment services in the content, quality, and mode of problems.

TABLE 1: RI value's comparison.

	RI value
10%	0.96
20%	0.95
25%	0.95
50%	0.93
Mean value	0.95

objectives, and predict the learning effect of the course. Analyze the performance of learners' practice and training process and establish an experience model. Finally, the study data of each learner on the comprehensive platform are analyzed to obtain the study report, study analysis, and evaluation feedback, so as to help students find problems in time, motivate learning motivation, and improve learning efficiency [14]. At the same time, the comprehensive platform will also provide teachers with teaching analysis and strategies based on students' learning and other process data, helping teachers timely adjust course content and teaching methods, and providing basis for the next course reform. Teaching integration can also track students' academic performance on a platform and obtain abnormal report analysis, providing managers with risk intervention strategies in time and bringing great convenience to the quality of talent cultivation and professional certification of the whole profession [15].

The major of Internet of Things is a new major which involves a wide range, so the content of professional courses must keep pace with the development of science and technology. Therefore, the course content is required to be updated quickly, so the platform construction must also take into account discipline construction and professional course construction and update, and the expansibility and compatibility of the system should be fully considered in the development of software and hardware. With the help of the promotion of discipline competition, the competition con-

tent is integrated into the relevant curriculum knowledge points, which not only enriches the curriculum content but also enriches the construction of the curriculum teaching case base and stimulates students' learning motivation [11]. Subject competitions can also promote the innovative thinking of teaching teams, test teachers' mastery of professional knowledge and application ability, and promote the updating of curriculum content and continuous improvement of teaching ideas and methods. The participation of teachers or the guidance of students in the competition can help teachers understand and master the latest developments in the development of the Internet of Things industry. The teachers' ideas are conducive to the timely update of professional course content and experimental content, so that students' knowledge structure can keep up with the development of the industry and improve the employment competitiveness of Internet of Things student [16].

3.2.3. Employment Services. The survey shows that 97.12% of college students have carried out relevant employment services around the four aspects, and the most services in each aspect are the campus job fair organization service through the employment network to provide recruitment information services, career, and employment guidance lectures and employment contract management services [17]. However, only 17.81% of college students are satisfied with the scope of employment services provided by colleges and universities. Taking 50% of college students' choice as the threshold value, the questionnaire shows that the employment services that students need very much but universities do not carry out are employment information customization and intelligent push service (79.19%), campus job fair data analysis (73.62%), employer certification and integrity evaluation (69.15%), remote Job Search Service (64.37%), contract signing legal advice and assistance (62.42%), career and career orientation assessment (57.31%), peer employment guidance and mutual aid (52.33%), and career development and job search files (50.08%) (see Figure 4 [18]).

In terms of service content, the existing problems are mainly reflected in timeliness and pertinence, such as delayed updating of recruitment information (60.21%), false or incomplete recruitment information (58.71%), disconnection between employment guidance content and the market (55.30%), and outdated employment guidance cases (53.29%) [19]. In terms of service quality, the main problem is the lack of precision and professionalism of service. For example, the number of campus job fairs is insufficient (61.63%), and the number of recruitment information is insufficient (58.28%). The matching degree of campus job fairs is low (56.92%). The matching degree of recruitment information is low (55.31%), and the professional career guidance is not strong (50.00%). In the aspect of service mode, the existing problems are mainly reflected in the backward mode and low efficiency [20]. For example, the employment information service mode is single (77.29%), the employment contract process is complicated, the cycle is long (65.19%), the employment guidance service lacks interaction (53.36%), and the employment assistance effect is not obvious (52.91%), as shown in Figure 5 [21, 22].

4. Interpretation of Result

The accuracy of data mining is judged by RI value. RI value ranges from 0 to 1, so the closer the calculated result is to 1, the higher the similarity between the data mining result and the actual result is, and the accuracy of the data mining algorithm is higher [23, 24]. On the contrary, the closer the calculation result is to zero, the lower the accuracy of the data mining result is, and the algorithm performance is poor. The mean RI value is 0.95, and the accuracy of the data mining algorithm is higher, as shown in Table 1.

5. Conclusion

In order to solve the problem of employment skills assessment, a method using the Internet of Things training practice platform is proposed. The main content of this method is based on the research and analysis of the practical training platform of the Internet of Things. According to the data characteristics of the Internet of Things and through the construction of the practical platform, it is concluded that the development and construction of the practical training platform of the Internet of Things is highly feasible for the evaluation of employment skills. The practical teaching platform of Internet of Things training can not only meet the requirements of theoretical practice teaching but also adapt to the employment training of students in discipline competitions and also meet the requirements of data mining experiments for students of other majors. Therefore, our development and construction also integrates various forces, including discipline construction, professional course construction, teaching team construction, and industry-university-research construction, as well as resources from other universities and enterprises, so as to integrate the superior resources of all aspects and form a high-quality practical teaching platform.

Data Availability

The data used to support the findings of this study are available from the corresponding author upon request.

Conflicts of Interest

The author declares no conflicts of interest.

References

- [1] X. Ao and A. He, "Research on the comprehensive evaluation method of college students' achievements based on multi-view RSR," in *Journal of Physics: Conference Series, Volume 1821, International Conference on Mathematics: Pure, Applied and Computation (ICOMPAC)*, Kunming, China, July 2020no. 1.
- [2] Y. Zhang, "The influence of ideological and political education on employment quality of college students based on association rule analysis," *Journal of Physics Conference Series*, vol. 1744, no. 4, article 042169, 2021.
- [3] A. Rizwan, H. Alsulami, A. Shahzad, N. Elnahas, and H. Alshoabi, "Perception gap of employability skills between employers' and female engineering graduates in Saudi Arabia," *International Journal of Engineering Education*, vol. 37, no. 2, pp. 341–350, 2021.
- [4] S. Garcia-Esteban and S. Jahnke, "Skills in European higher education mobility programmes: outlining a conceptual framework," *Higher Education, Skills and Work-Based Learning*, vol. 10, no. 3, pp. 519–539, 2020.
- [5] W. Chen and Y. Yuan, "Design and development of mobile internet control system for embedded fitness training cycling device," *Microprocessors and Microsystems*, vol. 81, no. 4, p. 103668, 2021.
- [6] N. Ranabahu, S. Almeida, and E. Kyriazis, "University-led internships for innovative thinking: a theoretical framework," *Education + Training*, vol. 62, no. 3, pp. 235–254, 2020.
- [7] D. Zhao, H. Song, and H. Li, "Fuzzy integrated rough set theory situation feature extraction of network security," *Journal of Intelligent and Fuzzy Systems*, vol. 40, no. 4, pp. 8439–8450, 2021.
- [8] L. Su, Z. Liao, Y. Zhang, and T. Wang, "Production-oriented approach in localization teaching: a case study of interpretation practice teaching on the commentary of Baoding Military Academy," *Creative Education*, vol. 13, no. 3, pp. 1045–1066, 2022.
- [9] F. Esmaeeli and A. Ahmadi, "Three decades of research in language teaching and testing: a thematic categorization," *International Journal of Research Studies in Education*, vol. 10, no. 5, pp. 73–81, 2021.
- [10] J. Chen, "Kinetic foundation of the zero-inflated negative binomial model for single-cell RNA sequencing data," *SIAM Journal on Applied Mathematics*, vol. 80, no. 3, pp. 1336–1355, 2020.
- [11] M. M. Stephenson and S. Kllstrm, "Constructions of young migrants' situations in kinship care in a Swedish suburb by social workers in a non-governmental organisation mentoring programme," *Qualitative Social Work*, vol. 19, no. 5–6, pp. 901–916, 2020.
- [12] N. Pramesti, I. Mukhlash, and S. Nugroho, "Development of reuse module on stowage planning system using CBR for multiport route," in *Journal of Physics: Conference Series, Volume 1821, International Conference on Mathematics: Pure, Applied*

Retraction

Retracted: Design and Implementation of Multimedia Network Intelligent Control Robot Based on Software Definition

Journal of Sensors

Received 13 September 2023; Accepted 13 September 2023; Published 14 September 2023

Copyright © 2023 Journal of Sensors. This is an open access article distributed under the Creative Commons Attribution License, which permits unrestricted use, distribution, and reproduction in any medium, provided the original work is properly cited.

This article has been retracted by Hindawi following an investigation undertaken by the publisher [1]. This investigation has uncovered evidence of one or more of the following indicators of systematic manipulation of the publication process:

- (1) Discrepancies in scope
- (2) Discrepancies in the description of the research reported
- (3) Discrepancies between the availability of data and the research described
- (4) Inappropriate citations
- (5) Incoherent, meaningless and/or irrelevant content included in the article
- (6) Peer-review manipulation

The presence of these indicators undermines our confidence in the integrity of the article's content and we cannot, therefore, vouch for its reliability. Please note that this notice is intended solely to alert readers that the content of this article is unreliable. We have not investigated whether authors were aware of or involved in the systematic manipulation of the publication process.

Wiley and Hindawi regrets that the usual quality checks did not identify these issues before publication and have since put additional measures in place to safeguard research integrity.

We wish to credit our own Research Integrity and Research Publishing teams and anonymous and named external researchers and research integrity experts for contributing to this investigation.

The corresponding author, as the representative of all authors, has been given the opportunity to register their agreement or disagreement to this retraction. We have kept a record of any response received.

References

- [1] H. Zhang, "Design and Implementation of Multimedia Network Intelligent Control Robot Based on Software Definition," *Journal of Sensors*, vol. 2022, Article ID 4894714, 8 pages, 2022.

Research Article

Design and Implementation of Multimedia Network Intelligent Control Robot Based on Software Definition

Hui Zhang 

Yancheng Teachers University, Yancheng, Jiangsu 224002, China

Correspondence should be addressed to Hui Zhang; 2010551223@hbut.edu.cn

Received 5 June 2022; Revised 22 July 2022; Accepted 23 July 2022; Published 3 August 2022

Academic Editor: Haibin Lv

Copyright © 2022 Hui Zhang. This is an open access article distributed under the Creative Commons Attribution License, which permits unrestricted use, distribution, and reproduction in any medium, provided the original work is properly cited.

In order to solve the problem that the delay of wireless network and complex operating environment affects the stability and operating performance of teleoperation system, a method of intelligent control robot based on multimedia network defined by software is proposed in this paper. In the network environment established based on the software definition, the gain of the system control is increased according to the network delay to improve the operating performance of the system, and the output of parameters is dynamically adjusted to adapt to the stability of the system in complex environment. The experimental results show that the robot control system can obtain the best control stability by continuously adjusting the relevant parameters. After the simulation test, the final setting is $k_p = 0.8$, $k_i = 0.001$, $k_d = 0$. *Conclusion.* Based on the intelligence of gain scheduling control algorithm, the control effect of fuzzy control can be significantly improved when the network delay is large.

1. Introduction

Mobile robot technology is a field where digital information processing technology, computer science and technology, path planning, and navigation technology converge. Its research purpose is to be able to obtain all kinds of surrounding information in the whole movement process according to the predesigned map and other information, make path navigation planning, help the robot avoid obstacles, reach the destination safely, and complete the required operations. However, due to the influence of complex and changing working environment, there are great difficulties in the autonomous work of robots, and there are still many situations that require the intervention of operators [1]. At this time, it is an effective solution to this problem to guide the robot to work artificially through the teleoperation system. Robot teleoperation technology is a highly strategic top science and technology, which is predicted by scientists as the key development direction of science and technology in the future. Since its first appearance in 1960, robot has been regarded as an important reference for the progress of human scientific level. After 50 years of gradual development, it has been widely used in all aspects of life and pro-

duction [2]. The mobile robot teleoperation system is an important part of robot technology, and it is also a hot spot in the robot field. The mobile robot teleoperation system has a keen ability to perceive the external environment and its own state and a strong ability of self-organization and self-adaptive.

Robot teleoperation based on network refers to connecting the robot with the Internet, so that people can easily control the behavior of the robot at any place and at any time to meet specific services. With the growing development of mobile Internet, people's demand for information sharing is no longer limited to pictures, words, video, and audio. In the future, the development trend will be direct interaction with remote locations to obtain objective physical information and real-time feedback operation to achieve real interaction. Robot teleoperation based on Internet provides an effective means of interaction for this demand [3]. H. 264 is a new generation of digital video coding standard. As the most advanced video coding standard in the world, it has the characteristics of high compression rate, low coding rate, and low bandwidth requirements [4].

As the most basic industrial robot, the multidegree of freedom robot arm has multiple joints, generally composed

of the base, vertical arm, horizontal arm, and hand claw, which can complete a variety of complex movements in a specific space. Reasonable mechanical structure, including the driver, servo motor, sensors, and other hardware equipment, can achieve good human-computer interaction software, with an efficient, stable, and strong control algorithm. Mechanical arm system design needs to consider all aspects of things. In order to understand the dynamic characteristics of the system, dynamic analysis and simulation are needed to understand the movement trajectory, to develop the system software and meet the software requirements; to realize the data transmission between the software and the hardware, the communication is completed according to the communication protocol.

The multifunctional robot arm can be used for the experimental teaching of fully driven robot or for the experimental research of underdriven robot. The conversion between full drive and underdrive function is simple and convenient and can be easily realized by installing and unloading the drive. However, there is not many software developed about the robot system, so we need to develop the robot intelligent control system experimental platform software that can realize full drive/underdrive conversion. The solid-height multifunction four-degree of freedom robot arm is used as the experimental platform robot. The robot has four series joints, which can complete two motion modes: uniaxial point motion and multiaxis linkage. It is mainly used to study the influence of different control algorithms on the dynamic characteristics of the robot structure. After completing the requirement analysis, over all design and implementation of the software structure is also achieved. Besides, detailed design and implementation of the software test is conducted on the robot intelligent control system and the experiment platform.

Business requirements are the guide to action for the whole system, describing the purpose of developing the system and what goals to achieve from a macro perspective. For the software of the robot intelligent control experiment platform, it is the requirement of the robot intelligent control system for the software. As an important link of the robot intelligent control system, it is hoped to establish a bridge of information transmission for the operation users and the control system and realize the unity of control simulation and physical control. This is in the global level of the robot intelligent control experimental platform software put forward the target requirements.

User needs, that is, the needs established from the perspective of users, use the needs that the product has to provide to achieve the work objectives. For the robot intelligent control experimental platform software, the user demand is the task that users must achieve when using the software. Specifically, the software must be able to realize the performance parameters of each joint of the arm, the mechanism back to zero, and other operations and must be able to control the arm to complete various movements. Implement corresponding control and collect joint position information through the underlying hardware and perform data conversion. The component tech-

nology calls the simulation software to realize the control simulation of the mechanical arm and realize the transmission between the simulation experiment data and the physical experimental data, as well as the preservation of the experimental data and other related processing. This level of demand is extremely important. Since most requirements are recessive, incomplete, and variable, this raises high requirements for the needs of collecting users.

2. Literature Review

Mahboob and others adopted the Java Based Teleoperation mode to realize the image stream transmission of robot image based on JMF. The encoding method is based on MPEG4 standard, and the client needs to install plug-ins in advance, such as RealOne or Microsoft's media player [5]. Slawinski and others applied augmented reality technology in human robot communication. Since the operating environment of the remote robot is unstructured, and the computer is obtained through stereo vision, the use of augmented reality technology can greatly reduce the requirements of the system for video refresh rate [6]. The most typical application is the application of virtual reality in the Mars rover. Carvalho and others used the event-based intelligent control method to control the robot 1000 miles away from the Internet to grasp objects and avoid obstacles [7]. Carvalho and others directly control the car in unknown environment through Internet time-delay force feedback handle and VR helmet. A linear feedback observer with time delay is designed for Internet. Internet puts forward a network control model based on dissipative theory [7]. Assad UZ Zaman and others analyzed the transmission characteristics of robot image and control information according to the real-time requirements of robot teleoperation. The network protocol adopted RTP/RTCP/UDP to solve the problem. In addition, the transmission problem of low frequency and narrow bandwidth network is also a key research direction, which is also not limited to the application of robot teleoperation [8]. Solanes and others put forward several measures for fault tolerance and improving data reliability by analyzing the characteristics of video stream, which can be used as an effective means for robot image and other data transmission in robot teleoperation [9].

The wireless network time delay is sometimes variable and random, which not only reduces the control performance of the wireless network-based telerobot but also leads to the robot misoperation and inevitable losses. In order to solve the influence of wireless network delay on the controllability of telerobot, a gain scheduling control algorithm based on parameter model is proposed in this paper. According to the network delay, the gain of system control is increased to improve the operation performance of the system. At the same time, the output of parameters is dynamically adjusted by module control and the self-learning ability of neural network to adapt to the stability of system operation in complex environment.

3. Research Methods

3.1. Software Definition Network. Since the birth of the Internet, its technology and demand have been increasing day by day. The Internet is no longer satisfied with simple data forwarding. Higher and more intelligent services need to be supported by an intelligent network. These demands lead to the enhancement of network scale and carrying capacity, but limited by Moore's law, the update of hardware infrastructure is far from keeping up with the growth of demand. At present, the tens of thousands of demands of the Internet bring a large number of computing, storage, transmission, virtualization, and centralized control demands, which make the traditional network face great pressure [10].

Compared with the traditional network, the most prominent feature of SDN is the separation of data plane and control plane. The goal of SDN network is to simplify forwarding and centralize control. In the traditional network, because the network is transparent to users, users and service providers cannot obtain the internal information of the network, so the usual optimization methods are estimation and feedback. The former estimates the internal network traffic or packet loss rate by using windows or other means to count the relevant network information at the source end. The latter is to judge whether there is congestion in the network according to the feedback received from the user and then adjust the transmission bit rate from the source [11]. Although this indirect method can also solve the problem to some extent, it is ultimately limited by the network architecture. With the increasingly complex and intelligent application, some information observed at the terminal is completely insufficient to support the requirements of the entire application layer. In contrast, the centralized control layer of the SDN network can realize the comprehensive control of the data layer and can observe the network status in real time, providing sufficient information for the upper level decision-making.

As shown in Figure 1, SDN system architecture mainly includes infrastructure layer (i.e., data plane), control layer, and application layer. The infrastructure layer is mainly composed of programmable routers or switches, and OpenFlow switches are one of them. Deploying the routing and forwarding function through software can also save the hardware cost to a certain extent. The SDN network data plane follows the principle of simple forwarding. Each SDN router does not have the routing learning function, but guides the routing by accepting the "flow table" issued by the SDN controller to complete the data forwarding, replacing the forwarding based on the IP address in the traditional network, and the programmable feature enables the router to complete different functions. Compared with the simple data plane, the centralized control plane is responsible for the management and control of the entire network and the connecting task [12–14]. The SDN controller communicates with the switch through the "control data plane interface," and the flow table distribution and data upload are all realized through the South interface. On the other hand, the SDN controller provides a programmable interface API for the application layer, and the supply layer realizes various network applications.

After the establishment of the network system, the next problem to be solved is its implementation and deployment. Although there are mature and stable programmable switch equipment available to build the prototype system, considering the large network scale and experimental stability in the research problems in this paper, this paper will adopt the hardware in the loop simulation to realize the network architecture [15]. Network simulation has been a mature technology. There are many well-known network simulation tools, such as NS2, NS3, and Mininet. The network simulation tool used in this paper is Mininet. As a lightweight software development platform, it supports OpenFlow, supports user-defined topology, and provides external interfaces. Most importantly, the Mininet simulator has good hardware portability, so the experimental results obtained in the simulation environment created by Mininet are very convincing [16].

The control system of a typical type of pipeline detection robot has been studied. According to the working characteristics and use requirements of the robot, a three-layer structure model of the control system is established and designed from hardware, software, and communication aspects, respectively. Finally, the developed software completed the test and analysis of the control system functions and verified the feasibility and practicability of the pipeline detection robot control system. We study an indoor wheeled mobile robot based on differential drive control and develop control system software. According to the design and implementation of the robot control task deployment software, the transmission and receiving of the timing update instructions were completed through the CPU timing interrupt service program, and we communicated with the server driver through the ECAN module following the CANopen protocol standard. The designed robot control system has good navigation and control effect, and the positioning accuracy can reach within 1cm.

3.2. Design of Teleoperation Robot System Based on Wireless Network. The teleoperation robot system is a basic application of PID control. The teleoperation robot system is shown in Figure 2.

In Figure 2, the teleoperation robot system mainly includes the following parts: robot teleoperation console, remote operation computer, wireless AP, wireless network card, field control computer, and robot. As the communication medium between the remote control subsystem and the field control subsystem, the wireless network mainly carries the transmission of control signals and feedback signals. The control signals are transmitted from the remote control subsystem to the field control subsystem, and the feedback signals are fed back from the field control subsystem to the remote control subsystem [17]. The two transmission processes are carried out at the same time. If there is a delay in the signal transmission process, it is likely to lead to misoperation of the robot.

The communication efficiency of wireless communication network determines the working accuracy and precision of teleoperation robot. The wireless communication network consists of local area network, wireless AP, and wireless

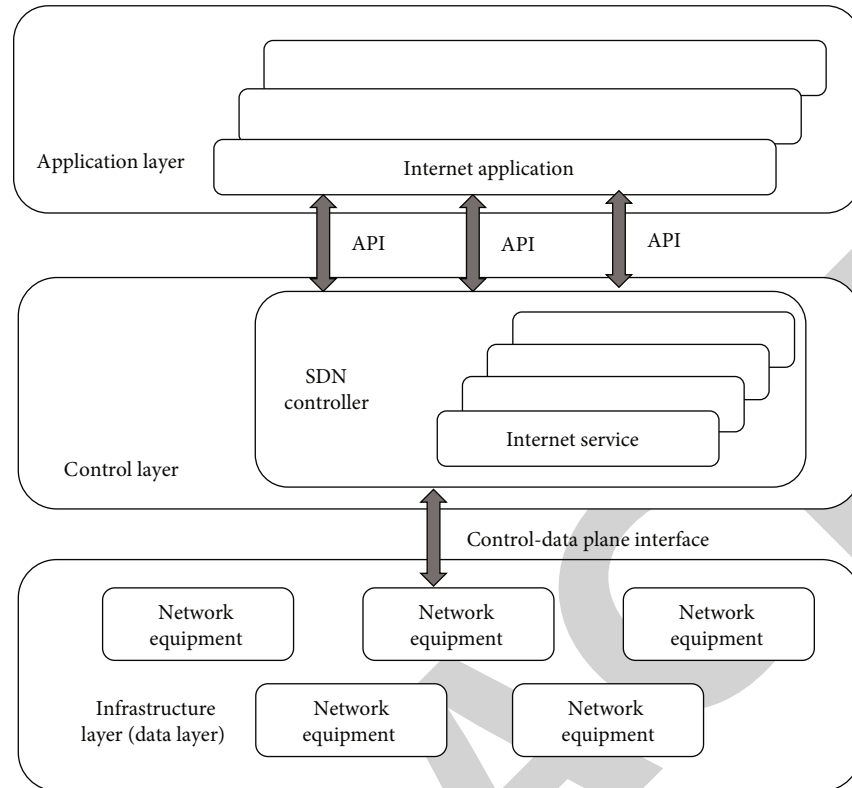


FIGURE 1: SDN system architecture.

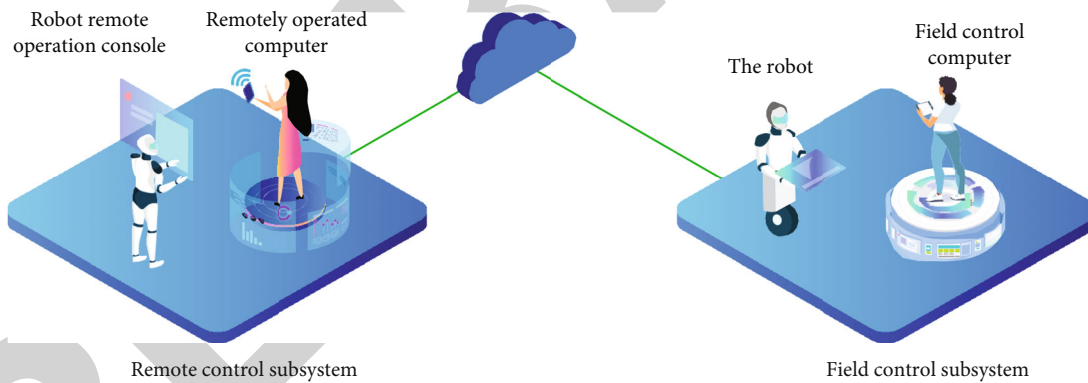


FIGURE 2: Structure diagram of teleoperation robot system.

network card deployed on the remote operation computer and field control computer. At the same time, wireless AP is used to connect the remote control subsystem and field control subsystem. After the system is started, the wireless AP deployed in the remote control terminal system within the working range of the field control subsystem is started, waiting for the connection of the field control subsystem. When the field control subsystem is connected to a specific wireless AP and logged in with the corresponding password, Figure 3 shows the workflow of the remote operation robot.

In the above workflow, it can be seen that most of the communication delay between the remote control subsystem and the field control subsystem will occur in the wireless communication node. For the robot, it is necessary to receive

the instructions from the remote control terminal in real time to complete the relevant work. For the remote operator, it is necessary to obtain the feedback of the robot in real time to adjust the subsequent operation. Once a large network delay occurs, it will bring inevitable losses to the system. Therefore, it is necessary to adopt a specific algorithm to deal with the delay problem of wireless network.

3.3. Gain Scheduling Control Algorithm Based on Parameter Model

3.3.1. Basic Principle of Gain Scheduling Control. Gain scheduling control is a nonlinear control algorithm. Its basic idea is to use an auxiliary variable to determine the change of

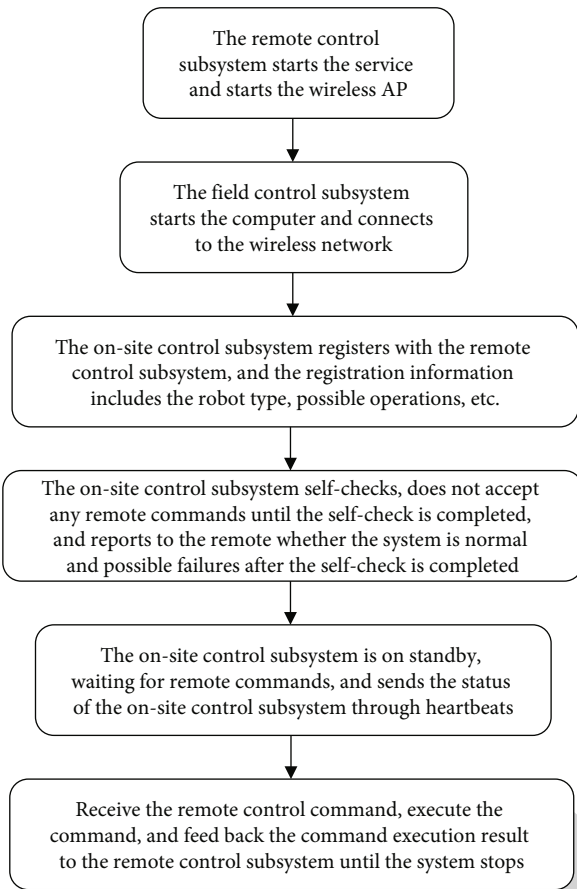


FIGURE 3: Workflow of teleoperation robot.

the auxiliary variable according to the change of the environment or the controlled object itself in the past period of time, that is, “gain,” and then use the change of the increase to adjust the output of the controller, so as to reduce the instability of the controlled object caused by some uncertain factors.

For the teleoperation robot system in this paper, because the wireless network is deployed in a relatively bad field environment, the direct consequence is that the network delay will cause a sudden change in the delay due to the change of the environment. For example, the obstruction of obstacles may bring a large delay, which is sudden and unpredictable. Therefore, the traditional PID control method cannot guarantee the stability and accuracy of the system control. The main idea of the gain scheduling control based on the parameter model is to add a gain α to the output of the conventional PID controller, which is dynamically adjusted for the network delay calculation of the monitoring wireless network [18].

The experimental platform software needs to record the position changes of the robotic arm at different times and collect the corner data of the robotic arm joint, while the periodic collection of the data requires a timer to achieve. In the process of windows message processing, the timing work is completed by processing the timer message requests in the message queue. Considering the priority of the message queue and the system clock fre-

quency, the timing accuracy may not be accurate, and the “second loss” phenomenon often occurs. There are many ways to solve this problem, but the simplest and most effective way is to use high-precision timing technology. General software provides a unified working framework, the same management ideas and modes, and completes the practical management process of real management according to the fixed business process. For customers without too many personalized needs, general software can fully provide functions to meet all customer expectations. Give customers a standardized and standardized mode for operation. For the customers who have urgent needs in terms of personalized needs, the software that does not take into account the personalized needs is easy to cause the phenomenon of “acclimation” in the process of use. Therefore, in order to meet individual needs, software systems are designed according to specific situations and requirements, and customized development providing corresponding personalized services is widely used.

The operation interface is the interface for users to interact with the experimental platform. Users complete various functions through the operation interface, such as the initialization of the card, back to zero operation, and calling the simulation module. The system modeling module completed the establishment of the dynamic model of 2R robot and the expression of MATLAB language, which lays for the subsequent construction of fuzzy PID control module. The fuzzy PID control simulation module completes the motion control simulation including full drive and underdrive. COM component module is used to make the modeling and simulation module written in MATLAB language into dll or exe components identified by VC to facilitate VC program calling, communication, and data management module to realize the communication between host and motion controller, data transmission, and management of various data files.

In the teleoperation robot system, the communication between the remote control subsystem and the field control subsystem requires a gain scheduling link, that is, gain α . In the actual operation process, gain α is not a specific value, but a proportion, which is calculated by a specific calculation function $\mu(k)$ to obtain a pure delay τ_k^{α} , where $\mu(k)$ is defined by the following formula:

$$\mu(k) = k_p \text{error}(k) + k_i \sum_{j=0}^k \text{error}(j) + k_d (\text{error}(k) - \text{error}(k-1)). \quad (1)$$

In order to control the precision of the teleoperation robot more accurately, theoretically, each pure delay τ_k^{α} should be used as the next feedback adjustment parameter of the next PID controller. However, because the delay adjustment is too frequent, it is necessary to sample the pure delay [19]. As can be seen from Figure 4, gain α is the key to gain scheduling control.

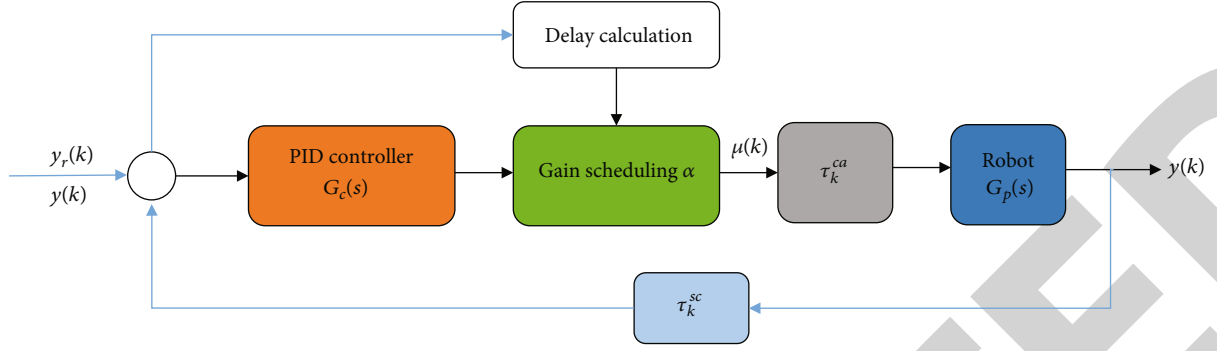


FIGURE 4: Gain scheduling control of teleoperation robot system.

3.3.2. *Determination of Gain.* As can be seen from Figure 4, the total network delay of each feedback adjustment is $\tau_k = \tau_k^{sc} + \tau_k^{ca}$. Suppose that during the first iteration is as follows:

$$G'_0(s) = G_c(s)\alpha\tau_k^{ca}G_p(s). \quad (2)$$

Therefore, the delay transfer function from the first closed loop $y_r(k)$ to $y(k)$ is as follows:

$$G(s) = \tau_k^{ca} \frac{G'_0(s)}{1 + G'_0(s)}. \quad (3)$$

The feedback delay from output to input can be expressed as the following equation:

$$G'(s) = \frac{G'_0(s)}{1 + G'_0(s)}. \quad (4)$$

It can be seen that the feedback delay can directly reflect the influence of the calculated delay on the system stability. Therefore, the influence of the system gain on the system stability can be determined by investigating the stability of the feedback delay $G(S)$, where τ_k^{ca} is the delay link. For simple calculation, Pade approximation method is used to express the following formula for the delay link:

$$\tau_k^{ca} = \frac{N_n(\tau_k s)}{D_n(\tau_k s)}. \quad (5)$$

In Pade approximation, the following equations are obtained:

$$N_n(\tau_k s) = \sum_{r=0}^n \frac{(2n-r)!}{r!(n-r)!} (-\tau_k s)^r, \quad (6)$$

$$D_n(\tau_k s) = \sum_{r=0}^n \frac{(2n-r)!}{r!(n-r)!} (\tau_k s)^r. \quad (7)$$

In order to avoid the influence of additional zeros on the approximation degree of the feedback curve and ensure that the root locus analysis completely approxi-

mates the whole locus within the value range, the rational fraction of the following formula is used for analysis in this paper.

$$\tau_k^{ca} = \frac{1}{(1 + (\tau_k s/n))^n}. \quad (8)$$

Therefore, the expression of $G'_0(s)$ is as follows:

$$G'_0(s) = \frac{\alpha G_c(s)G_p(s)}{(1 + (\tau_k s/n))^n}. \quad (9)$$

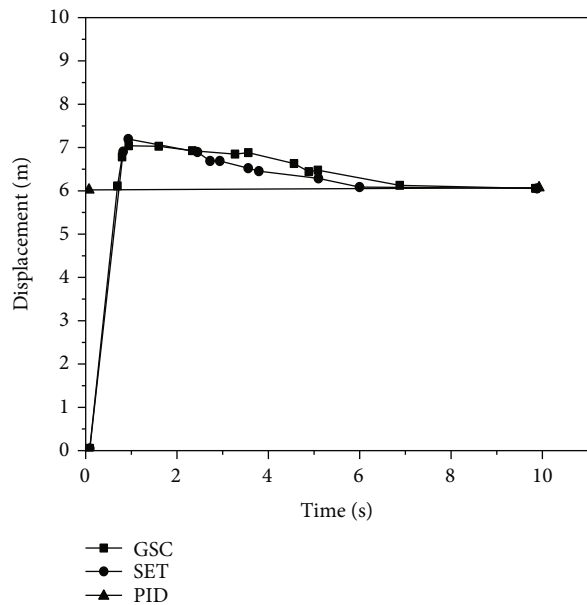
The delay transfer function of the system can be approximately expressed in the form of rational fraction, so the different network delays τ_k in the teleoperation machine system are the root locus with the gain α as the parameter [20].

According to equation (9), the method to obtain the maximum gain by using the root locus function can be obtained, that is, the method to obtain the maximum gain α_{\max} through the finally calculated delay space.

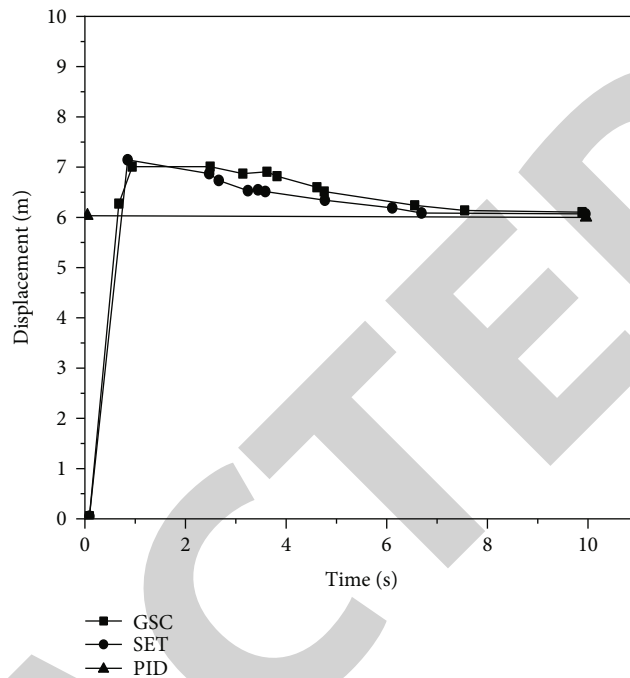
In order to determine the optimal gain, it is necessary to find the optimal gain in the spatial range of the gain. In this paper, a multilevel optimization strategy similar to the pruning algorithm is used to gradually reduce the spatial range of the optimal gain and finally determine the range space of the optimal gain. In order to determine the advantages and disadvantages of different gains, it is necessary to define a measurement standard, that is, the cost function, where the cost function is the following equation:

$$J_0 = \sum_{k=1}^M e(k)^2, \quad (10)$$

where $e(k) = y_r(k) - y(k)$ represents the error between the network delay sampling input and output, J_0 represents the sum of squares of errors at all sampling times, when the reference gain cost function is $\alpha = 1$, it is set as J_{0-k} , and J_0/J_{0-k} is used to measure the excellence of the gain. When $J > 1$, it represents that the gain is worse than the reference gain; otherwise, the gain is better than the reference gain [21].



(a)



(b)

FIGURE 5: Phase response test curve.

4. Result Analysis

In order to verify the effectiveness of the gain scheduling control algorithm in the teleoperation robot system, this paper applies the algorithm to the actual system. During the experiment, the delay sampling period of the teleoperation robot system is 20 ms. In this paper, PID control, gain scheduling control, and fixed parameter control are compared to compare their advantages and disadvantages [22]. During the experiment, the robot control system obtained the best control stability by continuously adjusting the relevant parameters. After the simulation experiment test, the final value obtained under the parameters of $k_p = 0.8$, $k_i = 0.001$, $k_d = 0$ was set as the best. This parameter will not be adjusted in the subsequent experiments. As mentioned above, all operation commands in the teleoperation robot system need to be transmitted between the two industrial control computers of the two remote control subsystems and the field control subsystem through the wireless network. The signal has a certain delay in the remote control process, and the impact of the delay alignment accuracy and accuracy must be overcome [23]. The experimental results are step response curves, as shown in Figures 5(a) and 5(b).

It can be seen from Figures 5(a) and 5(b) that the deviation amplitude of the two curves under the gain scheduling control is much smaller than the oscillation amplitude of the PID control curve. Therefore, it can be seen that the effect of gain scheduling control based on parameters is obviously better.

5. Conclusion

In order to meet the control accuracy and precision of tele-robot in wireless environment and avoid the damage to the system due to network delay, this paper introduces a parameter based incremental scheduling control algorithm. By analyzing the basic principle of gain scheduling control, this paper also analyzes how to determine the gain in the process of gain scheduling control, which can make the control accuracy meet the best state. Finally, the experiment verifies the improvement of the accuracy of the algorithm proposed in this paper compared with PID control.

Data Availability

The data used to support the findings of this study are available from the corresponding author upon request.

Conflicts of Interest

The author declares that they have no conflicts of interest.

References

- [1] F. Pasandideh, T. Silva, A. Silva, and E. Freitas, "Topology management for flying ad hoc networks based on particle swarm optimization and software-defined networking," *Wireless Networks*, vol. 28, no. 1, pp. 257–272, 2022.
- [2] F. Zeng, Y. Chen, L. Yao, and J. Wu, "A novel reputation incentive mechanism and game theory analysis for service caching in software-defined vehicle edge computing," *Peer-*

Retraction

Retracted: A Training Method for a Sensor-Based Exercise Rehabilitation Robot

Journal of Sensors

Received 3 October 2023; Accepted 3 October 2023; Published 4 October 2023

Copyright © 2023 Journal of Sensors. This is an open access article distributed under the Creative Commons Attribution License, which permits unrestricted use, distribution, and reproduction in any medium, provided the original work is properly cited.

This article has been retracted by Hindawi following an investigation undertaken by the publisher [1]. This investigation has uncovered evidence of one or more of the following indicators of systematic manipulation of the publication process:

- (1) Discrepancies in scope
- (2) Discrepancies in the description of the research reported
- (3) Discrepancies between the availability of data and the research described
- (4) Inappropriate citations
- (5) Incoherent, meaningless and/or irrelevant content included in the article
- (6) Peer-review manipulation

The presence of these indicators undermines our confidence in the integrity of the article's content and we cannot, therefore, vouch for its reliability. Please note that this notice is intended solely to alert readers that the content of this article is unreliable. We have not investigated whether authors were aware of or involved in the systematic manipulation of the publication process.

Wiley and Hindawi regrets that the usual quality checks did not identify these issues before publication and have since put additional measures in place to safeguard research integrity.

We wish to credit our own Research Integrity and Research Publishing teams and anonymous and named external researchers and research integrity experts for contributing to this investigation.

The corresponding author, as the representative of all authors, has been given the opportunity to register their agreement or disagreement to this retraction. We have kept a record of any response received.

References

- [1] P. Suo, X. Zhu, S. Wang et al., "A Training Method for a Sensor-Based Exercise Rehabilitation Robot," *Journal of Sensors*, vol. 2022, Article ID 4336664, 9 pages, 2022.

Research Article

A Training Method for a Sensor-Based Exercise Rehabilitation Robot

Peng Suo ¹, Xueqiang Zhu ¹, Shu Wang ², Mei Li ¹, Ting Yu ¹, Chunling Song ¹,
Haodi Ning ³ and Yi Xin ⁴

¹Shandong Sport University, Jinan, Shandong 250102, China

²Shandong Sports Rehabilitation Research Center, Jinan, Shandong 250102, China

³Shandong Taishan Football Club Co., Ltd, Jinan, Shandong 250102, China

⁴Shandong Sport Science Research Center, Jinan, Shandong 250102, China

Correspondence should be addressed to Yi Xin; 1710200415@hbut.edu.cn

Received 22 June 2022; Revised 14 July 2022; Accepted 23 July 2022; Published 2 August 2022

Academic Editor: Haibin Lv

Copyright © 2022 Peng Suo et al. This is an open access article distributed under the Creative Commons Attribution License, which permits unrestricted use, distribution, and reproduction in any medium, provided the original work is properly cited.

In order to solve the problem that the traditional mirror therapy did not take into account the real-time recovery of the affected limb and the training effect was limited, a training method of sports rehabilitation robot based on sensor was proposed. A mirror active rehabilitation training system was proposed, which was composed of four steps including trajectory acquisition of the limb inertial measurement unit (IMU), fuzzy adaptive proportion differentiation (PD) control in closed-loop variable domain, muscle force estimation of the surface electromyographic signal (sEMG) of the affected limb, and power compensation of the outer ring of the affected limb. The experimental results showed that the sagittal forward flexion angle of the healthy shoulder increased from 0° to 128° at a relatively uniform speed, and the sagittal forward flexion angle of the shoulder was basically consistent with that of the healthy limb after the adaptive power compensation of the affected limb. The calculated trajectory tracking error of the healthy limb controlled by the fuzzy adaptive PD controller in the variable domain was $0.21 \pm 1.35^\circ$. The horizontal backward extension angle of the healthy shoulder joint increased from 0° to 43°, and the following trajectory of the affected limb was roughly consistent with the movement trajectory of the healthy limb. The calculated tracking error of the healthy limb trajectory was $0.39 \pm 1.45^\circ$. It was concluded that the control system could provide the real-time power compensation according to the recovery of the affected limb, give full play to the training initiative of the affected limb, and make the affected limb achieve a better rehabilitation training effect.

1. Introduction

Sports injury refers to a variety of injuries that may occur when people are exercising. These sports injury reason mainly includes personal internal factors and external environment factors. The personal internal factors include exercise without warming up, lack of basic training, movement against science movement principle, incorrect movement posture, and a bad sports competitive state. The external environment factors include lack of scientific guidance of movement, without wearing special clothing, the improper organization of the training and competition, and the poor climate [1]. With the continuous pursuit of the quality of life, the public's health awareness has gradually improved. More and more people began to improve

their physical fitness through a variety of sports and exercise. But it is followed by a variety of sports injuries, bringing pain to people and affecting the normal work and study. At the same time, the proportion of sports injury in sports competition is higher. The survey found that national snowboarders had a 70% probability of some degree of sports injury during their career. In addition, once an athlete is injured, he or she cannot normally participate in the training and competition in a short period of time, and his or her psychology will also be affected. The double injury of physical and psychological will seriously affect the performance of the competition [2].

For different types of sports, the corresponding types and proportion of sports injuries are also different. The common types of sports injuries mainly include the acute injuries, such

as muscle strain, ligament injury, and fracture, or the chronic injuries such as tenosynovitis, bursitis, fatigue fracture, and muscle spasm. In the process of the injury rehabilitation, the sports treatment technology has played an important role. The exercise therapy technology is based on the biological mechanics, kinematics, and neurology, and blood circulation and metabolism of the body's tissues are improved in the form of the passive or active movement, so as to improve the damaged muscle strength and endurance and speed up the recovery of neural function, cardiopulmonary function, and the balance ability. Clinical practice has found that regular and periodic rehabilitation exercise can effectively accelerate the rehabilitation process, and the rehabilitation effect is better [3]. The scientific rehabilitation training can not only improve joint range of motion, improve muscle strength, and improve body coordination but also prevent muscle atrophy, osteoporosis, and other diseases, as shown in Figure 1.

2. Literature Review

Baothman and Edhah proposed the CPC model. Two parameters were added to the traditional D-H model, and the added parameters are used to realize the continuity of the robot kinematics model. The core was to define six parameters for each link of the robot to represent the rotation of the robot. This modeling method emphasized the integrity and continuity of parameters and solved the defects of traditional D-H models to a certain extent. This model was also improved in later experiments, and a new modeling method was proposed, called MCPC model [4]. Medghalchi et al. constructed POE model based on screw theory. In the model, only the inertial coordinate system and the tool coordinate system were determined during the system construction, which improved the modeling efficiency. In the calibration process, the modeling method did not need to identify the joint zero error separately, which simplified the calculation and improved the calibration efficiency. At the same time, the method also overcame the singularity problem in the traditional D-H model [5]. Yang et al. found that mirror therapy had a significant effect on patients with nerve injury and poor motor function [6]. Loflin et al. performed mirror therapy on stroke patients and found that the active range of motion and motor speed in the treated group were improved compared with those in the untreated group [7]. Tsoi et al. confirmed that mirror therapy had an obvious effect on weakening the pain sensation of the affected limb [8].

The traditional mirror rehabilitation training method has achieved a good effect in improving the motor ability of patients, but in the traditional therapy, the affected side does not get the actual rehabilitation training exercise. In order to avoid the disadvantages of traditional mirror therapy to a certain extent, a rehabilitation therapy was proposed, which integrated the mirror idea of the healthy limb movement into the robot system. Liu et al. used inertial measurement unit (IMU) to map the joint space motion trajectory of the healthy limb to the exoskeleton of the affected limb for synchronous mirror motion, which improved the rehabilitation effect of patients [9]. Vicharapu et al. developed a virtual reality mirror training system with Kinect and exoskeleton, which could detect the movement intention of rehabilitation robot. Experiments

showed that this system could be widely used as a therapeutic intervention method. Many researches showed that it had excellent therapeutic effects when the patients received the rehabilitation training on their healthy limbs at the same time [10].

The above mirror therapy realized the rehabilitation training of the affected limb through the synchronous mirror movement of the affected limb and the healthy limb assisted by the rehabilitation robot. However, it is just a simple passive following training, without considering the real-time recovery of the affected limb. So the training effect is limited. In order to solve the problem, an adaptive control method of mirror rehabilitation training is proposed. By constructing shoulder joint dynamics model and muscle force estimation model to calculate the compensation moment of the affected limb, the method can provide real-time power compensation for the affected limb to improve the initiative of the training of the affected limb, realizing the maximum training of muscle strength of the affected limb in the process of mirror training.

3. Research Methods

3.1. Structural Design of the Shoulder Rehabilitation Robot. According to the biomechanical characteristics of human shoulder joint, shoulder joint is composed of clavicle, humerus, and scapula, which is a typical ball and socket joint and can carry out multiaxial flexible movement. Shoulder joint motion can be specifically decomposed into three orthogonal motions: abduction or adduction in the coronal plane, flexion or extension in the sagittal plane, and internal rotation or external rotation in the horizontal plane [11].

According to the above biomechanical decomposition of human shoulder motion, an exoskeleton shoulder rehabilitation robot was developed in the research. Three orthogonal revolute joints J1, J2, and J3 in series were used to realize the ball joint motion of shoulder. At the same time, in order to meet the sitting height of different people, the robot was designed to be fixed on the lifting base. The whole structure could meet the needs of different body types.

3.2. Adaptive Adjustment Assisted Control Algorithm Design of Mirror Rehabilitation Training. In order to maximally train the muscle strength of the affected limb in the mirror rehabilitation training, the above exoskeleton-type shoulder rehabilitation robot was used as the experimental platform, and an adaptive adjustment assisted mirror rehabilitation training control method was proposed. It is mainly composed of four parts including the limb trajectory acquisition based on IMU, fuzzy adaptive proportion differentiation (PD) control in variable domain, muscle force estimation of affected limb based on surface electromyography, and adaptive power adjustment of the affected limb [12].

3.2.1. The Healthy Limb Trajectory Acquisition Based on IMU. In this system, IMU was used to capture the motion track of shoulder joint of healthy limb. Here, the original information provided by IMU needs to be converted to the shoulder coordinate system. The IMU was worn on the inner side of the

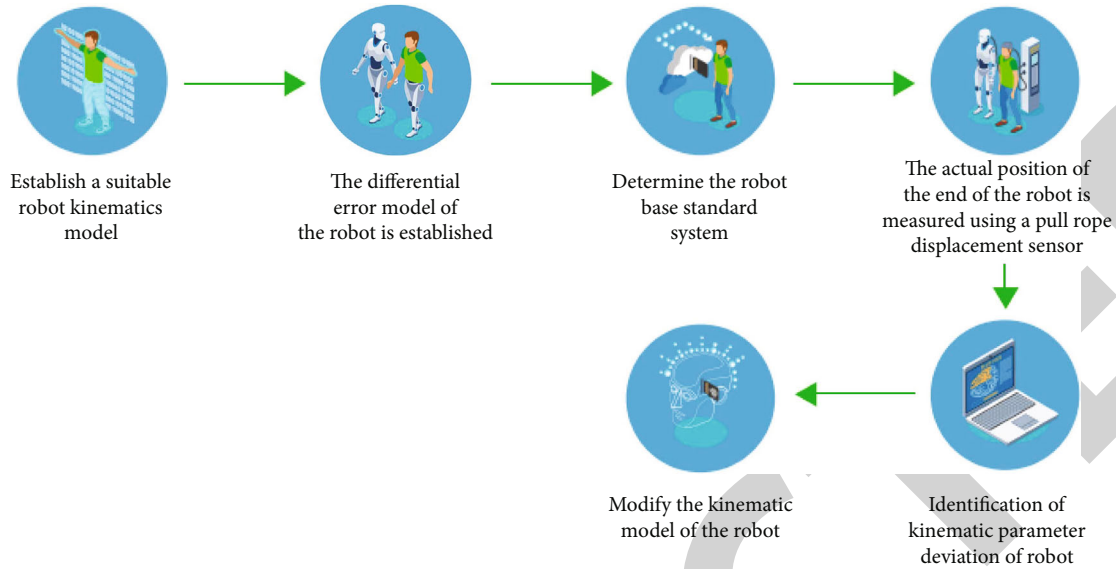


FIGURE 1: Sports rehabilitation robot training method.

upper arm, and the coordinates of IMU were set as O_{uvw} and shoulder joint as O_{xyz} .

All relevant original coordinate data joints can obtain new position vectors through rotation matrix R^T , which can be obtained as follows. Suppose that O_{xyz} has a fixed point M , and its position vectors at O_{uvw} and O_{xyz} are P_M^{uvw} and P_M^{xyz} , respectively, then Formulas (1) and (2) are as follows.

$$P_M^{uvw} = (u_M, v_M, w_M) = u_M i_u + v_M j_v + w_M k_w, \quad (1)$$

$$P_M^{xyz} = (x_M, y_M, z_M) = x_M i_x + y_M j_y + z_M k_z. \quad (2)$$

In Formulas (1) and (2), $i_u, j_v,$ and k_w are orthonormal basis of IMU base coordinate system. $i_x, j_y,$ and k_z are orthonormal bases of the shoulder coordinate system. The position vector of fixed point M in the shoulder coordinate system is always P_M^{xyz} , while the projection of position vector P_M^{uvw} of this point in the IMU coordinate system in the directions of $i_u, j_v,$ and k_w can be expressed as the following formula:

$$P_M^{uvw} = \& \begin{bmatrix} u_M \\ v_M \\ w_M \end{bmatrix} = \begin{bmatrix} i_u^T (u_M i_x + v_M j_y + w_M k_z) \\ i_v^T (u_M i_x + v_M j_y + w_M k_z) \\ i_w^T (u_M i_x + v_M j_y + w_M k_z) \end{bmatrix} \quad (3)$$

$$= \begin{bmatrix} i_u^T i_x & i_u^T j_y & i_u^T k_z \\ j_v^T i_x & j_v^T j_y & j_v^T k_z \\ k_w^T i_x & k_w^T j_y & k_w^T k_z \end{bmatrix} \begin{bmatrix} x_M \\ y_M \\ z_M \end{bmatrix} = R \begin{bmatrix} x_M \\ y_M \\ z_M \end{bmatrix}.$$

According to the properties of rotation transformation, R

is an orthogonal matrix; then, $R^{-1} = R^T$. R^T is the rotation transformation matrix.

The spatial position information of shoulder joint, namely, the relative relationship between shoulder coordinate system and IMU coordinate system, can be selected in the form of output data including Euler angle, quaternion, and rotation matrix. The attitude described by Euler angle is used in the research. Euler angles of IMU output are A_{roll} , A_{pitch} , and A_{yaw} , and its rotation matrix is the transformation matrix of shoulder coordinate system O_{xyz} and IMU coordinate system O_{uvw} [13]. By integrating the definition and IMU installation method, the real-time motion angle of healthy shoulder joint can be measured by IMU. The abduction and adduction angle of shoulder joint $\beta_1 = A_{pitch}$, the flexion and extension angle $\beta_2 = A_{roll}$, and the internal and external rotation angle $\beta_3 = A_{yaw}$.

3.2.2. Variable Domain Fuzzy Adaptive PD Control. Robot system is a complex nonlinear dynamic system with strong coupling. The traditional fuzzy proportional integral differential controller is only suitable for rough control occasions with fuzzy environment, and the fuzzy control effect is not ideal for high precision control problems. Therefore, variable domain fuzzy adaptive PD control is adopted in the system. On the premise that the rule form remains unchanged, the domain shrinks with the decrease of error, thus improving the control accuracy [14].

The input of the fuzzy adaptive PD controller in the variable domain adopted by the system is the change rate of the difference between the angle signal difference obtained from the trajectory of the shoulder joint of the limb and the difference. The initial fuzzy domain of the two values is divided into six levels, namely, $[-E3, -E2, -E1, -E0, E1, E2, E3]$ and $[-CE3, -CE2, -CE1, -CE0, CE1, CE2, CE3]$. The output of the fuzzy adaptive PD controller in the variable domain is the control moment of the robot τ_p . The domain of output torque can be expressed as $\tau_p = [-\tau_{p \min}, \tau_{p \max}]$. The fuzzy

producer is established through $\theta_e = [-E_{\min}, E_{\max}]$ and $d\theta_e/dt \in [CE_{\min}, CE_{\max}]$, as shown in the following formulas:

$$E = 6 \times \frac{(\theta_e - E_{\min})}{(E_{\max} - E_{\min})}, \quad (4)$$

$$CE = 6 \times \frac{(d\theta_e/dt - CE_{\min})}{(CE_{\max} - CE_{\min})}. \quad (5)$$

In Formulas (4) and (5), E_{\min} and E_{\max} , respectively, represent the minimum and maximum values of angle signal difference θ_e domain. CE_{\min} and CE_{\max} , respectively, represent the minimum and maximum values of angle signal difference change rate $d\theta_e/dt$ domain. E and CE are the output of fuzzy producer.

Fuzzy rules are designed according to the adaptive PD control rate as shown in the following formulas.

$$\tau_p = K_p E + K_d CE, \quad (6)$$

$$K_p = K_{p0} + \Delta K_p \times q_p, \quad (7)$$

$$K_d = K_{d0} + \Delta K_d \times q_d. \quad (8)$$

K_p and K_d are the final control parameters of PD controller. K_{p0} and K_{d0} are the initial setting parameters of PD controller. ΔK_p and ΔK_d are the output of fuzzy controller. And q_p and q_d are correction coefficients.

Fuzzy elimination of control is carried out through the membership maximum method, and the membership function peak value of the output fuzzy subset is directly selected as the determined value of the output. And the logical "union" of the output fuzzy subset τ_{pi} is $\tau_p = \bigvee_{i=1}^6 \tau_{pi}$, and the exact output of the control variable τ_p is inverted by taking the median value [15]. Then, the domain of angle signal difference θ_e and its change rate $d\theta_e/dt$ can be gradually reduced, and the domain of reduced θ_e , $d\theta_e/dt$, and output torque τ_p can be determined, which can be expressed as follows:

$$E(t) = [-\alpha_1(t)E_{\min}, \alpha_1(t)E_{\max}], \quad (9)$$

$$CE(t) = [-\alpha_2(t)CE_{\min}, \alpha_2(t)CE_{\max}], \quad (10)$$

$$\tau_p(t) = [-\beta(t)\tau_{p \min}, \beta(t)\tau_{p \max}]. \quad (11)$$

In Formulas (9)–(11), $\alpha_1(t)$, $\alpha_2(t)$, and $\beta(t)$ are expansion factors of corresponding domains.

3.2.3. Muscle Strength Estimation of Affected Limb Based on sEMG. The noninvasive sEMG was adopted by the Delsy surface myoelectrometer, which was simple in form and did no harm to the subjects. Flexion/extension, abduction/adduction, and internal rotation/external rotation were used as arm motion patterns in mirror rehabilitation training. Referring to the relevant muscle contraction during shoulder joint motion, combined with the human anatomical structure, the most relevant muscles, anterior deltoid muscle, posterior deltoid muscle, middle deltoid muscle, and trapezius muscle,

were selected, and the surface EMG sensor was worn at the corresponding muscle position.

In order to complete the muscle force estimation based on sEMG, force signals in the process of muscle force generation at the shoulder joint should be collected as reference data. In the research, ROBOTIQ FT300 six-dimensional force sensor was used for collection. In order to facilitate subsequent experiments, the force sensor used its own software for gravity compensation. During the experiment, the force sensor was placed on the part used to fix the affected limb in the robot component 3. During this process, sEMG (represented by X) and force signals (represented by F) of the four parts of the shoulder joint of the subject were collected in real time. For sEMG, the time-domain method for feature extraction was adopted to obtain the feature matrix X_F . And X_F and F were formed the sample S_m . The long short-term memory network (LSTM) performed the nonlinear mapping of the input network X_F to obtain the estimated value of the subject's shoulder joint force [16], as shown in the following formulas.

$$X = \begin{bmatrix} X_1 \\ X_2 \\ X_3 \\ X_4 \end{bmatrix} = \begin{bmatrix} x_{11} & x_{12} & \cdots & x_{1m} \\ x_{21} & x_{22} & \cdots & x_{2m} \\ x_{31} & x_{32} & \cdots & x_{3m} \\ x_{41} & x_{42} & \cdots & x_{4m} \end{bmatrix}, \quad (12)$$

$$F = \begin{bmatrix} F_x \\ F_y \\ F_z \end{bmatrix} = \begin{bmatrix} f_{x1} & f_{x2} & \cdots & f_{xm} \\ f_{y1} & f_{y2} & \cdots & f_{ym} \\ f_{z1} & f_{z2} & \cdots & f_{zm} \end{bmatrix}, \quad (13)$$

$$S_m = \begin{bmatrix} X_F \\ F \end{bmatrix}. \quad (14)$$

In Formulas (12)–(14), $X_1 \sim X_4$ are the four channels of sEMG collected by the first to the fourth EMG sensor. F_x , F_y , and F_z are the force signals detected by the force sensor in the x , y , and z directions, respectively, and m is the number of sampling points.

The sEMG and force signals were collected by EMG sensors and force sensors, and muscle force estimation of affected limbs was completed through recurrent neural network (RNN) training. Traditional RNN had a dependency problem, but LSTM was a recurrent neural network. It could effectively fit the time-varying characteristics of sEMG of human body. Therefore, the system substituted the collected sEMG eigenvalues and force signals into LSTM to identify the muscle force of the affected limb [17]. In LSTM network, the selection of output action mainly consists of three stages. The first is the forgetting stage, in which the calculated Z_f is used as the forgetting gate to control the state S_{t-1} that needs to be forgotten and remembered in the previous state C_{t-1} . The second is the selective memory stage, in which the input S_t is selectively remembered. If a higher reward value can be obtained, it will be recorded; otherwise, it will be remembered less. Since RNN is sequential, the current input content is the state of

the current moment, and Z_i is used as the gating signal to control the selection. The third is the output stage. Z_0 is used to control which will be regarded as the output action of the current state. Meanwhile, tanh activation function is used to scale the C_{t-1} obtained in the previous stage [18]. Here, force signals obtained synchronously in the process of force generation of shoulder joint muscles and sEMG characteristic values of shoulder muscles were input as training samples of LSTM to train LSTM. Then, the force signal of shoulder joint muscle in the process of force generation was used as LSTM training sample to test the established muscle force estimation model. The trained LSTM could estimate the joint force output by sEMG eigenvalue and obtain the torque according to the distance from the force sensor to the shoulder joint.

3.2.4. Assisted Adaptive Adjustment of Affected Limb. The motion trajectory of the healthy limb captured by IMU in Section 3.2.1 was used as the mirror expected trajectory followed by the affected limb in mirror training, and the shoulder dynamic model was established through the healthy arm with length l and mass m . The shoulder angle collected by IMU in real time is θ_d , so the kinetic energy E_1 and potential energy E_2 of this system could be obtained, which could be expressed as $E_1 = 1/2ml^2\dot{\theta}_d^2$ and $E_2 = mgl \sin \theta_d$, where g is the acceleration of gravity.

According to Lagrange equation, the following formula can be obtained.

$$\frac{d}{dt} \left(\frac{\partial L}{\partial \dot{\theta}_d} \right) - \frac{\partial L}{\partial \theta_d} = \tau_a, \quad (15)$$

In Formula (15), $L = E_1 - E_2$, and τ_a is the expected torque of shoulder joint movement following the healthy limb. The kinematic model of shoulder joint can be written in matrix form by Lagrange equation, which can be expressed as the following formula:

$$\tau_a = M(\theta_d)\ddot{\theta}_d + V(\theta_d, \dot{\theta}_d) + G(\theta_d). \quad (16)$$

In Formula (16), $M(\theta_d) = \begin{bmatrix} m & -ml \sin \theta_d \\ -ml \sin \theta_d & ml^2 \end{bmatrix}$ is inertial matrix. $V(\theta_d, \dot{\theta}_d) = \begin{bmatrix} 0 & -ml\dot{\theta}_d \cos \theta_d \\ 0 & 0 \end{bmatrix}$ $\dot{\theta}_d$ is centrifugal force and Coriolis force vector. $G(\theta_d) = \begin{bmatrix} 0 \\ mgl \cos \theta_d \end{bmatrix}$

is the gravity vector. The difference between the expected torque of the affected limb τ_a following the healthy limb and the force torque of the affected limb τ_s is defined as the torque τ_d that the rehabilitation robot needs to compensate for the affected limb. At the same time, a gravity compensation link is introduced, and the gravity compensation torque is τ_G . Finally, the total joint torque of the rehabilitation robot is the torque sum of fuzzy adaptive PD control in variable domain, power compensation, and gravity compensation of the affected limb, as shown in the following formula:

$$\tau = \tau_p + \tau_d + \tau_G. \quad (17)$$

4. Result Analysis

4.1. Shoulder Joint Force Estimation Experiment. In the shoulder joint force estimation experiment, the exoskeleton-type shoulder joint rehabilitation robot was taken as the experimental platform and a healthy subject was selected. The right upper limb of the subject was simulated to wear the rehabilitation robot. In the fixed mode, the six-dimensional force sensor is fixed to the robot, and the sEMG acquisition device was worn at the corresponding muscle position of the affected limb. The force signal and sEMG of shoulder muscle were obtained synchronously. The sampling frequency of sEMG acquisition device was set at 2,000 Hz, and the sampling time (the time for performing sagittal forward flexion or backward extension and horizontal forward flexion or backward extension, respectively) was set at 30 s to collect sEMG signals of shoulder joint motion-related muscles during the above two groups of force movements. The mean absolute value (MAV) was used to extract the EMG eigenvalues. Zero calibration was carried out before the force sensor was used to collect shoulder joint force signals [19].

The affected limb of the subject made force movements in four directions of sagittal flexion or extension and horizontal flexion or extension by means of the shoulder, respectively, in the positive or negative direction and the positive or negative direction of the stress sensing axis. The sEMG and force signals in the process of shoulder joint movement were collected, and these two signals were input as the training samples of LSTM. After the training, LSTM estimated the output of shoulder joint force through sEMG eigenvalues.

The subjects were instructed to extend the affected limb to the side of the body as the initial position. The rehabilitation robot assisted the affected limb to perform the force action of sagittal extension and then back to the initial position and sagittal flexion and then back to the initial position. Namely, the sagittal flexion or extension was completed. The subject was instructed to raise the affected limb at the straight side as the initial position, and the rehabilitation robot assisted the affected limb to perform the force action of horizontal forward flexion and then back to the initial position and horizontal backward extension and then back to the initial position. Namely, the horizontal forward flexion or backward extension was completed [20]. The sagittal front flexion or extension and horizontal front flexion or extension groups were repeated 20 times. 10 times were selected as the training samples, and the remaining 10 times were used as the test samples. Figures 2(a) and 2(b) show sEMG and force signals measured when subjects performed the above two sets of movements. Figures 3(a) and 3(b) show the experimental results of shoulder joint force estimation of the subjects.

The solid line in Figure 3 represents the muscle force of shoulder joint of affected limb measured by the six-dimensional force sensor, which is the actual value. The dashed line represents the muscle force estimated by sEMG characteristic information, which is the estimated value. In Figure 3(a), the subject was instructed to perform 6 and 20

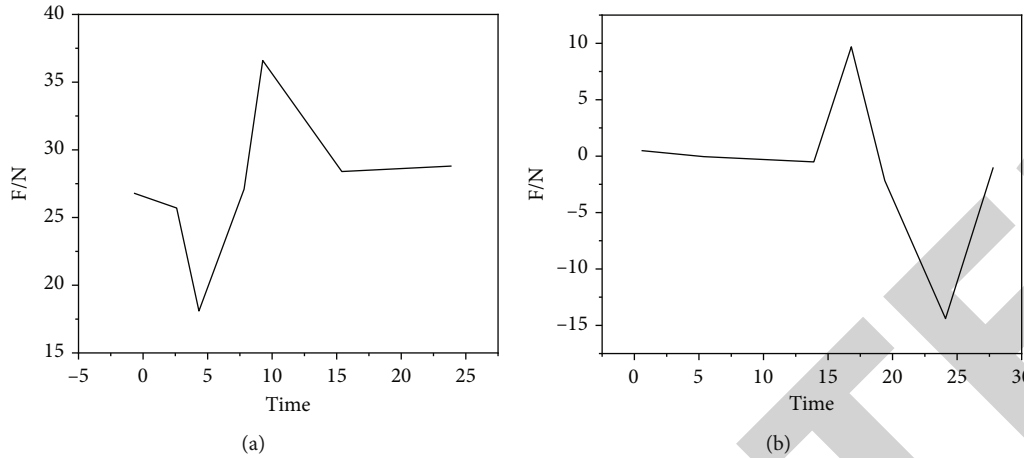


FIGURE 2: (a) sEMG and force signal of shoulder joint. (b) sEMG and force signal of shoulder joint.

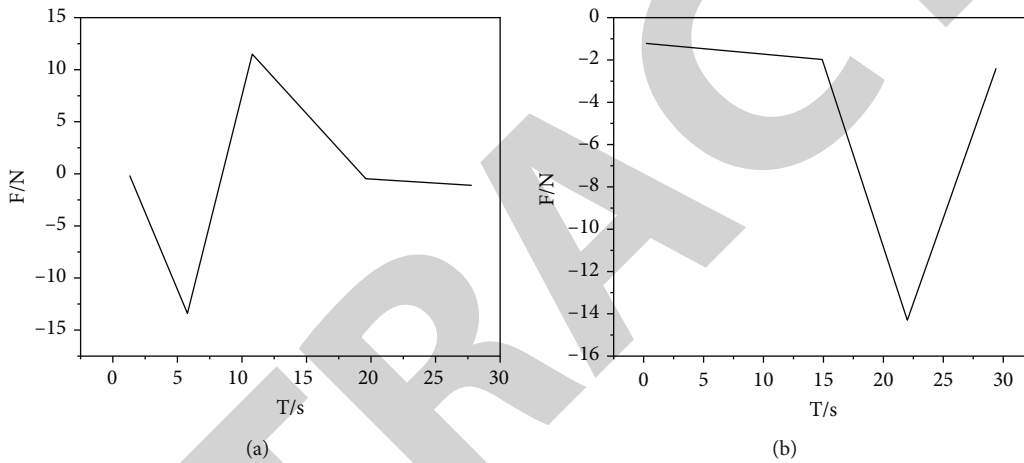


FIGURE 3: (a) Estimation of sagittal forward flexion or backward extension force of shoulder joint. (b) Estimation of sagittal forward flexion or backward extension force of shoulder joint.

sagittal forward flexion or backward extension movements of shoulder joint, respectively, for force estimation. Taking 20 repeated force movements as an example, it could be divided into four stages. (1) Initial position—sagittal backward extension. Within 2.9~4.8 s, the muscle strength of the affected limb increased in the opposite direction after sagittal backward extension from the initial position. (2) Sagittal backward extension—initial position. Within 4.8~7.5 s, the muscle strength of the affected limb decreased in the opposite direction when the subject underwent the force movement of sagittal backward extension back to the initial position. (3) Initial position—sagittal forward flexion. Within 7.5~11.4 s, the affected limb performed sagittal forward flexion from the initial position, and the muscle strength of the affected limb increased in the positive direction. (4) Sagittal forward flexion—initial position. Within 11.4~12.4 s, the positive direction of the muscle strength of the affected limb decreased when the subject underwent the force movement of sagittal backward extension back to the initial position. The root mean square (RMS) and mean absolute value of the error (MAVE) of the force measured in the sagittal flexion or extension direction of the shoulder joint during the four stages were calcu-

lated, with 0.76 N and 0.28 N, respectively. By comparing the error between the estimated value and the actual value of the specified force action performed for 6 times and 20 times, respectively, it could be seen that the error after 20 times of repeated test was significantly less than that after 6 times of repeated test, indicating that the trained LSTM network could accurately estimate the real distance of the affected limb [21]. Figure 3(b) shows that the subject was instructed to perform 6 and 20 sagittal forward flexion or backward extension movements of shoulder joint, respectively, for force estimation. Similarly, 20 repetitions of force movement were also taken as an example and divided into four stages. (1) Initial position—horizontal forward flexion. Within 14.2~16.3 s, the affected limb performed horizontal forward flexion from the initial position, and the muscle strength of the affected limb increased in the positive direction. (2) Horizontal forward flexion—initial position. Within 16.3~19.8 s, the affected limb returned to the initial position and the positive direction of muscle force decreased. (3) Initial position—horizontal backward extension. Within 19.8 to 22.6 s, the muscle strength of the affected limb increased in the opposite direction when the subject performed horizontal backward extension from

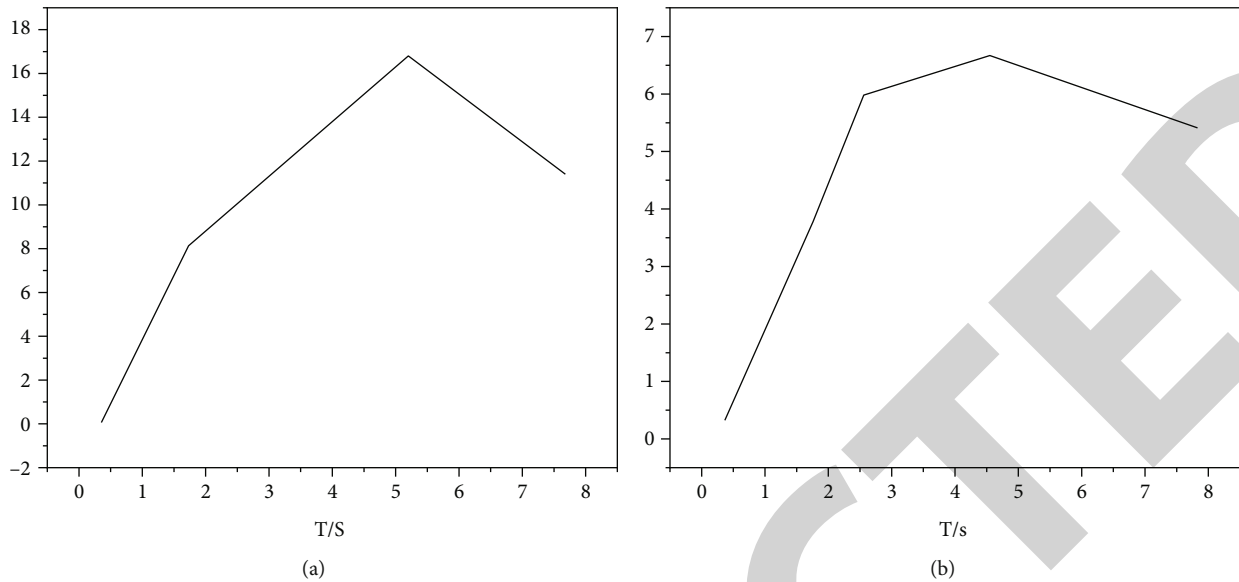


FIGURE 4: (a) Direction torque in sagittal forward flexion of shoulder joint. (b) Direction torque in sagittal backward extension of shoulder joint.

the initial position. (4) Horizontal backward extension—initial position. Within 22.6–24.9 s, the muscle strength of the affected limb decreased in the opposite direction when the subject performed the force movement of horizontal backward extension back to the initial position. In these four stages, RMS and MAVE of the measured force of shoulder joint in horizontal forward flexion or backward extension direction were 0.79 N and 0.41 N, respectively. By comparing the errors between the estimated values and the actual values of the 6 and 20 times force movements, respectively, it could also be seen that the errors after the 20 repeated tests were significantly less than the 6 repeated tests, indicating that the trained LSTM network could accurately estimate the real distance of the affected limb. The above results showed that the RMS and MAVE of the calculated force and measured value in the direction of sagittal forward flexion or backward extension and horizontal forward flexion or backward extension of shoulder joint were not greater than 1 N. Combined with the actual value and estimated value curves of Figures 3(a) and 3(b), it could be seen that the shoulder force output estimated by sEMG eigenvalue could better reflect the real shoulder muscle force measured by force sensor.

4.2. Mirror Rehabilitation Training Experiment. Similarly, in the mirror rehabilitation training experiment, the exoskeleton-type shoulder rehabilitation robot was used as the experimental platform and the six-dimensional force sensor was fixed on the robot. Subject wore IMU on the left upper limb as a healthy limb, a rehabilitation robot on the right upper limb as a simulated affected limb, and a sEMG acquisition device. During this process, the sampling frequency of the sEMG acquisition device was set at 2,000 Hz, and the sampling time was 8 s when performing sagittal forward flexion and 5 s when performing horizontal backward extension. The sEMG signals of the shoulder joint of the affected limb were collected, and their

characteristic values were extracted when performing sagittal forward flexion and horizontal backward extension. After the force sensor was zeroed, the force signal of shoulder joint of affected limb was collected. The subject was instructed to put his healthy limb and the affected limb straight to the side of the body as the starting position, and the healthy limb should keep as much speed as possible to do the sagittal forward flexion of the shoulder. The affected limb should follow the healthy limb to do the incomplete force in the mirror direction under the condition of no force or less force than the healthy limb, so as to complete the sagittal forward flexion of the healthy limbs. Similarly, the subject was instructed to raise the healthy limb and the affected limb flatly before unstretching as the starting position and the healthy limb as far as possible to do the force movement of horizontal backward extension of shoulder joint with the uniform speed. The affected limb followed the healthy limb to do incomplete force in the mirror direction under the condition of no force or less force than the healthy limb, so as to complete the horizontal backward extension experiment of the healthy limb [22].

In the process of the two groups of rehabilitation movements, IMU was used to collect the trajectory of the limb and substitute it into the shoulder dynamic model to obtain the torque of the limb τ_a . Then, the estimated moment of the affected limb τ_s could be obtained by synchronously collecting the sEMG and force signals of the affected limb and substituting them into the muscle force estimation model in Section 4.1. The difference between the two is the compensation moment τ_d that could be adjusted adaptively to the affected limb. Experimental results are shown in Figures 4(a) and 4(b) [23].

Figure 4(a) shows the variation curves of the healthy limb torque τ_a , the estimated torque of the affected limb τ_s , and compensated torque of the affected limb τ_d when the healthy limb performed sagittal forward flexion motion of shoulder

joint at the same time. It can be seen that the healthy limb torque τ_a is gradually enlarged to approach 9.8 N due to the need to overcome its own gravity. Because the affected limb follows the incomplete force in the mirror direction of the healthy limb, τ_s is the same as the direction of τ_a , but $|\tau_s| < |\tau_a|$, and τ_s increases gradually to 5.6 N. The compensation moment of the affected limb τ_d defined above varies with the change of τ_a and τ_s . τ_d gradually increases to 4.2 N. Figure 4(b) shows the variation curves of the healthy limb torque τ_a , the estimated torque of the affected limb τ_s , and compensated torque of the affected limb τ_d when the healthy limb performed horizontal backward extension motion of shoulder joint at the same time. Compared with the experiment results of the implementation of sagittal forward flexion of shoulder joint, the direction of the muscle force of the affected limb and the healthy limb is the same, but the torque is small. The experimental process of horizontal backward extension of shoulder joint can be divided into five stages. (1) Forward acceleration stage: Within 0~1.0 s, τ_a and τ_s increase in a positive direction. (2) Forward deceleration stage: Within 1.0~2.2 s, τ_a and τ_s decrease in a positive direction. (3) Constant velocity stage: Within 2.2~3.3 s, it remains constant. (4) Reverse acceleration stage: Within 3.3~4.0 s, τ_a and τ_s increase in an opposite direction. (5) Reverse deceleration stage: Within 4.0~5.0 s, τ_a and τ_s decrease in an opposite direction. In these five stages, the compensation moment of the affected limb τ_d remains within -1.9~1.8 N with the change of τ_a and τ_s .

Through the above experiments, the adaptive compensation moment of the affected limb was obtained when the subject performed the sagittal forward flexion and horizontal backward extension of the shoulder joint, and the data were fed back to the shoulder rehabilitation robot in real time, so as to assist the affected limb to follow the healthy limb to perform the force action in the mirror direction. In this experiment, the sagittal forward flexion and horizontal backward extension of shoulder joints were repeated for 10 times, respectively. Through the movement trajectory of the healthy limb collected by IMU, the following trajectory of the affected limb was obtained by the mirror mapping [24, 25].

5. Conclusions

Aiming at shoulder rehabilitation patients, a mirror rehabilitation training system with adaptive adjustment power and its control algorithm was designed in the research, realizing the synchronous mirror movement between the rehabilitation robot assisted the affected limb and the healthy limb. The selected rehabilitation actions were shoulder sagittal flexion and horizontal extension. IMU and sEMG data of the healthy limb were collected during the rehabilitation process. The following trajectory of the affected limb was roughly consistent with that of the healthy limb, indicating that the rehabilitation effect of the affected limb was better due to the mirror rehabilitation training. By adding fuzzy adaptive PD control in variable domain, the difference between the estimated torque of the healthy limb and the affected limb was taken as the compensation torque of the affected limb, so as to realize the adaptive power compensation of the affected limb. By considering the recovery of the

affected limb, the system gave full play to the training initiative of the affected limb and the rehabilitation training effect was better.

Data Availability

The data used to support the findings of this study are available from the corresponding author upon request.

Conflicts of Interest

The authors declare that they have no conflicts of interest.

References

- [1] L. Yao, R. Dimitrakopoulos, and M. Gamache, "Training image free high-order stochastic simulation based on aggregated kernel statistics," *Mathematical Geosciences*, vol. 53, no. 7, pp. 1469–1489, 2021.
- [2] Z. Zheng, Y. Liu, M. He, D. Chen, L. Sun, and F. Zhu, "Effective band selection of hyperspectral image by an attention mechanism-based convolutional network," *RSC Advances*, vol. 12, no. 14, pp. 8750–8759, 2022.
- [3] D. Karimi and S. E. Salcudean, "Reducing the Hausdorff distance in medical image segmentation with convolutional neural networks," *IEEE Transactions on Medical Imaging*, vol. 39, no. 2, pp. 499–513, 2020.
- [4] F. A. Baothman and B. S. Edhah, "Toward agent-based LSB image steganography system," *Journal of Intelligent Systems*, vol. 30, no. 1, pp. 903–919, 2021.
- [5] S. Medghalchi, C. F. Kusche, E. Karimi, U. Kerzel, and S. Korte-Kerzel, "Damage analysis in dual-phase steel using deep learning: transfer from uniaxial to biaxial straining conditions by image data augmentation," *JOM*, vol. 72, no. 12, pp. 4420–4430, 2020.
- [6] N. Yang, H. Tang, J. Yue, X. Yang, and Z. Xu, "Accelerating the training process of convolutional neural networks for image classification by dropping training samples out," *IEEE Access*, vol. 8, pp. 142393–142403, 2020.
- [7] B. Loflin, K. Cluff, J. Griffith, and N. Mohammed, "Identification of shoulder joint clearance in space suit using electromagnetic resonant spiral proximity sensor for injury prevention," *Acta Astronautica*, vol. 170, pp. 46–54, 2020.
- [8] C. Tsoi, C. Tsai, E. Law, R. Lee, and J. F. Griffith, "A comparison of ultrasound-guided rotator interval and posterior glenohumeral injection techniques for MR shoulder arthrography," *Clinical Imaging*, vol. 69, pp. 255–260, 2021.
- [9] F. J. Liu, Z. Y. Sun, Y. F. Tuo, Y. Ji, and Y. X. Bai, "Effect of shoulder geometry and clamping on microstructure evolution and mechanical properties of ultra-thin friction stir-welded Al6061-T6 plates," *The International Journal of Advanced Manufacturing Technology*, vol. 106, no. 3-4, pp. 1465–1476, 2020.
- [10] B. Vicharapu, H. Liu, H. Fujii, K. Narasaki, N. Ma, and A. De, "Probing residual stresses in stationary shoulder friction stir welding process," *International Journal of Advanced Manufacturing Technology*, vol. 106, no. 5-6, pp. 1573–1586, 2020.
- [11] Y. Liu, X. Li, A. Zhu, Z. Zheng, and H. Zhu, "Design and evaluation of a surface electromyography-controlled lightweight upper arm exoskeleton rehabilitation robot," *International Journal of Advanced Robotic Systems*, vol. 18, no. 3, pp. 172988142110034–172988142110232, 2021.

Retraction

Retracted: Artificial Intelligence Optimization Design Analysis of Robot Control System

Journal of Sensors

Received 13 September 2023; Accepted 13 September 2023; Published 14 September 2023

Copyright © 2023 Journal of Sensors. This is an open access article distributed under the Creative Commons Attribution License, which permits unrestricted use, distribution, and reproduction in any medium, provided the original work is properly cited.

This article has been retracted by Hindawi following an investigation undertaken by the publisher [1]. This investigation has uncovered evidence of one or more of the following indicators of systematic manipulation of the publication process:

- (1) Discrepancies in scope
- (2) Discrepancies in the description of the research reported
- (3) Discrepancies between the availability of data and the research described
- (4) Inappropriate citations
- (5) Incoherent, meaningless and/or irrelevant content included in the article
- (6) Peer-review manipulation

The presence of these indicators undermines our confidence in the integrity of the article's content and we cannot, therefore, vouch for its reliability. Please note that this notice is intended solely to alert readers that the content of this article is unreliable. We have not investigated whether authors were aware of or involved in the systematic manipulation of the publication process.

Wiley and Hindawi regrets that the usual quality checks did not identify these issues before publication and have since put additional measures in place to safeguard research integrity.

We wish to credit our own Research Integrity and Research Publishing teams and anonymous and named external researchers and research integrity experts for contributing to this investigation.

The corresponding author, as the representative of all authors, has been given the opportunity to register their agreement or disagreement to this retraction. We have kept a record of any response received.

References

- [1] H. Guo, Y. Wang, G. Wang, Z. Du, R. Chen, and H. Sun, "Artificial Intelligence Optimization Design Analysis of Robot Control System," *Journal of Sensors*, vol. 2022, Article ID 2235042, 6 pages, 2022.

Research Article

Artificial Intelligence Optimization Design Analysis of Robot Control System

Haifeng Guo , Yiyang Wang , Guangwei Wang , Zhongbo Du , Rui Chen ,
and He Sun 

College of Electrical and Information Engineering, Liaoning Institute of Science and Technology, Benxi, Liaoning 117004, China

Correspondence should be addressed to Haifeng Guo; 2013071431@stu.zjhu.edu.cn

Received 30 May 2022; Accepted 9 July 2022; Published 25 July 2022

Academic Editor: Haibin Lv

Copyright © 2022 Haifeng Guo et al. This is an open access article distributed under the Creative Commons Attribution License, which permits unrestricted use, distribution, and reproduction in any medium, provided the original work is properly cited.

In order to improve the accuracy of robot control system, a scheme based on artificial intelligence is proposed. On the basis of the software environment of reinforcement learning simulation platform, a kind of rounding scheme in dynamic environment is designed and simulated. The results show that when the inclination sensor is placed on an inclined plane of 300 and collected for ten times, the maximum error of measurement that can be seen from the experimental data is 0.40. The relative included angles were 30°, 45°, 60°, and 90°, respectively, by compass sensor. The measurement was carried out, and the average value of each angle was measured 5 times. It can be seen from the experimental data that the measurement error meets the requirements of the system. Therefore, it is feasible to use artificial intelligence algorithm to optimize the robot control system.

1. Introduction

Intelligent control is a control mode with intelligent information processing, intelligent feedback, and intelligent control decision, which is the advanced stage of the development of control theory. It is mainly used to solve the control problems of complex systems that are difficult to be solved by traditional methods. The main characteristics of intelligent control research object are highly nonlinear with uncertain mathematical models and complex task requirements. Now the practical control methods are: multi-level hierarchical intelligent control, knowledge-based intelligent control, fuzzy control, neural networks control, rule-based humanoid intelligent control, intelligent control and chaos control based on pattern recognition, etc. Fuzzy control and neural network control are the most widely used intelligent control methods in mobile service robot. The path planning of mobile robots can be divided into two types: one is global path planning based on environmental prior information, and the other is local collision avoidance planning based on sensor information in uncertain environment. Robot will develop into a highly automated intelligent tool with its progress and wide range of applications. This not

only frees one from the onerous and repetitive monotonous work but concentrates one on the work of intellect and creativity as well as interest. Beside, it also can serve as a servant of life and exploration and creation of nature, greatly improving and enriching human social life. Its technology development and wide application will bring social and life revolution. It can not only bring high productivity and huge economic benefits to social and economic construction but also contribute to the country's space development, ocean development, nuclear energy utilization, and other new fields. See Figure 1.

2. Literature Review

A large number of studies show that more and more roboticians and high-tech workers are willing to invest a lot of time and energy into the research of robots and further improve the quality of their products. The robot research technology is the integration of engineering, mechanical, and electronic basic knowledge, materials, artificial intelligence communication technology, and other aspects of advanced technology and research results, reflecting the highest comprehensive level and strength of the country. Common intelligent robots

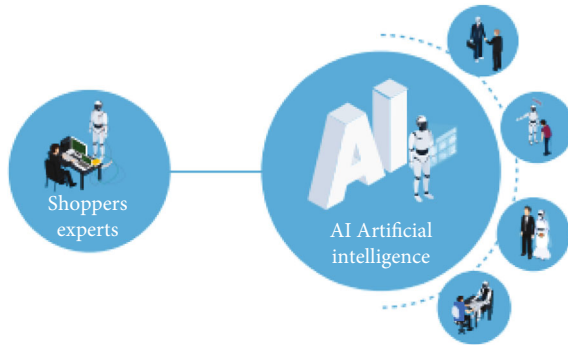


FIGURE 1: Robot control system.

mainly have foot walking robot, crawler walking robot and wheel walking robot. Wheeled and tracked robots are easy to walk stably, while bipedal robots (also known as two-legged humanoid robots) have more human characteristics and can operate in special environments and occasions, such as desert storms. In flood and other cases, it can take corresponding intelligent actions through the collection and perception of sensors to easily complete corresponding tasks through the road surface and the designated position, which brings convenience to human beings [1].

As early as in the 1970s, Cai and Zheng proposed the theoretical experiment and analysis of multirobot cooperative work [2]. Zheng and Cai and Qiu and Duan first proposed the concept of agent in their book *The Society of Mind* published in 1986. They believe that the basic idea of an agent is to simulate human cognition and social behavior, including cognitive thinking, problem-solving, evolution, mechanism, cooperation, and organization of human society. Its purpose is to enable agents to have the ability to recognize and understand the world environment, the ability to learn, the ability to adapt, and the ability to judge and reason [3, 4].

On the basis of the current research, the intelligent control technology of robot workers is proposed. **Autonomy:** autonomy refers to the ability of an agent to control its own behavior [5]. An agent has its own behavior control mechanism and limited computing resources. Without direct guidance or interference from other agents or human beings, the agent can run continuously and control its own behavior and state according to the perceived external environment information and internal state [6]. **Autonomy** is an important characteristic of agent, which can be distinguished from some other abstract concepts, such as interaction of object process. An agent can sense and influence the environment. In a certain way, the agent can monitor the surrounding environment and the service requests and interactive information sent by other agents and also communicate with other agents in the system in various forms, so as to complete tasks harmoniously [7]. **Initiative:** the behavior of an agent is the result of some kind of goal rather than simply reacting to events in the environment. The agent can take the initiative to complete the task according to its predetermined task. **Sociality:** agents can cooperate with other agents in the environment. There are mutual constraints and dependence among all intelligent agents. When conflicts occur, they can negotiate with each other to solve problems. An agent can

effectively perceive and act on its environment through sensors and effectors, respectively [8]. Therefore, at this time, the agent can be seen as an autonomous independent module. In the process of interacting with the environment, the agent needs to process and interpret the received information to achieve its own purpose [9]. See Figure 2.

3. Development History and Classification of Machine Intelligence Learning

3.1. Intelligent Control Theory. Intelligent control is the advanced stage of the development of traditional control theory. It is an interdisciplinary research field of control theory, operation research, artificial intelligence learning theory, and modern adaptive control. From the beginning of the 20th century to its 60s, traditional control theory has experienced the development from classical control theory to modern control theory. Its characteristic is that the research work should be based on the precise model of the control object [10]. However, most of the actual industrial production systems are complex control systems with complex objects, complex tasks, and complex environments. To solve the control problem of this kind of system, we must jump out of the framework of traditional control theory based on ideal mathematical model and start from decomposing complex tasks, perceiving complex environment, and analyzing control objects [11]. Intelligent control system is put forward in this context; it is the process of driving intelligent machines to achieve their goals autonomously and has such functions as learning to adapt to the organization. In the analysis and design of the system, it is not to establish accurate mathematical model but to carry on the symbol description of the nonmathematical model to develop and design the knowledge base and inference machine [12]. After the development of recent years, intelligent control theory has become the main way to solve the control problems of complex systems, and its further research will promote the development of intelligent robot field.

3.2. Bionics. Bionics is the application of biological methods and systematic knowledge to solve engineering problems. In the process of biological simulation, it is by no means simple bionics, but to innovate on the basis of bionics. The basic idea of multirobot system research is inspired by the cooperation within or between biological groups. This connection makes the combination of robot technology and bionic technology inevitable [13]. It is very beneficial to study the social characteristics of insects and animals and apply them to multirobot systems. The idea that interaction produces internal motion patterns has inspired current research methods for multirobot systems. Much of the current work in collaborative robotics uses biological systems as its inspiration or validation criteria, applying simple control rules derived from biological societies to develop similar behaviors in cooperative robotic systems. The purpose of this group bionics is to enhance individual intelligence through group behavior, improve the efficiency of the system as a whole, and reduce the influence of local faults on the whole [14]. Work in this area has shown the ability of robot groups to swarm foraging and track tracking. Put forward related topics include the following: in recent years by

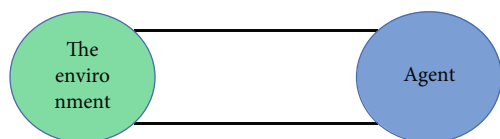


FIGURE 2: The abstract structure of an agent.

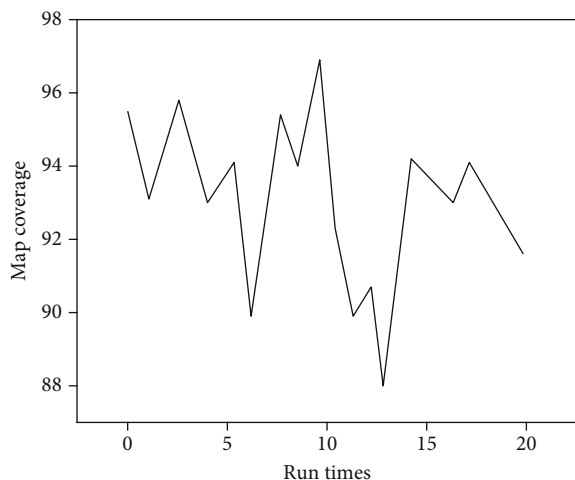


FIGURE 3: The improved algorithm has 20 search coverages.

imitation to learn new behavior, refer to the nature of competition behavior research robot soccer game, created by interaction of human machine system of group behavior, so as to show the swarm intelligence, through the research team to collect social insect food handling and cooperation behavior of the object and verify its social behavior which is the result of self-organization [15].

3.3. Multirobot Learning. Traditional robotics research is based on precise prior knowledge of the working environment. With the expansion of the application of robots from the early structured environment to the unstructured environment, multirobot systems have to face some new problems when completing complex tasks. It is difficult to establish an accurate model for dynamic uncertain environment, and incomplete information acquisition caused by sensor constraints leads to poor adaptability of the robot to the environment. The real-time requirements of the system require highly optimization of the robot strategy, etc. [16]. Obviously, it is unrealistic to solve the above problems through artificial design. An important goal of multirobot system development is to design a basic structure of distributed control, so that robots can perform tasks without supervision and have strong adaptive ability in unknown environment. Learning is a strategy to solve the above problems and enable the robot to adapt to the environment autonomously. By interacting with the external environment with the help of domain knowledge and sharing relevant information of other robots, the robot can understand the unknown state in the environment, realize the impact of its own behavior on the environment, and con-

TABLE 1: Software record used to build simulation platform environment.

Development tools	PyCharm
Operating system	Windows 10
Development language	Python 4.1
Robot learning platform	TensorFlow
Reinforcement learning platform	Gym

stantly adjust itself to better adapt to the environment [17]. For individual robots, this ability can improve the effectiveness of their own behavior and enhance their intelligence. For the multirobot system as a whole, it is helpful to improve the cooperation between individuals and improve the overall performance of the system.

3.4. Research Status and Existing Problems of Multirobot System. The development trend of today's robot technology mainly has the following outstanding characteristics. First, the application field of robot is expanding, and its types are increasing day by day. Second, the performance of robots is improving and gradually to the direction of intelligent development. Third, in order to improve the autonomy of robots, multirobot technology is developing from the traditional artificial intelligence method to the group robot technology and evolutionary robot technology [18]. Fourthly, the research of reconfigurable robot system makes multirobot system gradually develop towards modularization. This high degree of integration and reconfigurable characteristics can make it have higher robustness and various function. Therefore, driven by the dual needs of research and application, the research of multirobot system and its related technologies has become an important direction in robotics research [19].

4. Experimental Principles and Methods

4.1. Analysis of Simulation Result. Considering that the robot is always on the move, the coverage of the map is used as an evaluation index, and the coverage of the map is expressed as M_{occ} , as shown in

$$M_{occ} = 1 - \frac{U_{unexp} - U_{exp}}{U_{exp}} * 100\%. \quad (1)$$

When you have three robots that are basically done searching after 100 iterations, the method is proved to be effective for multirobot systems. Still, there are some areas that need to be improved. First, there is waste when the robot looks for the minimum parameter (cell value); that is, if there are more than two identical minimum values, the last one is chosen [20]. Second, when costs and benefits contain the same value, the robot can be stuck in one location in the search space, even if the other area has not been searched. It is therefore necessary to find solutions that enable robots to constantly seek out unknown areas. So we optimized the mapping process for a group of mobile robots. As an optimization technique, an improved GWO heuristic algorithm is used for sensor coverage task, which generates random

TABLE 2: Structural analysis.

	Conduct cooperation	Dynamic tasks	Complex task	The upper monitoring
Based on behavior	Ordinary	Excellent	Ordinary	Poor
Hybrid structure	Ordinary	Excellent	Excellent	Excellent

TABLE 3: Experimental data of inclination sensor.

The serial number of collection	1	2	3	4	5	6	7	8	9	10
Measurements	28.6	27.4	28.3	28.5	28.4	28.9	28.2	28.4	28.3	28.7
Deviation	0.2	0.5	0.1	0.4	0.3	0.6	0.5	0.6	0.4	0.3

TABLE 4: Compass sensor experimental data.

The data collected	29	44	59	89
Measurements	29.3	43.6	58.8	89.2
Deviation	0.3	0.3	0.2	0.2

parameters for the maximum position of changing order [21]. Therefore, the hierarchical optimizer has reformed the robot's position selection, which is a deterministic search method. In the case that it is impossible to optimize in the real-time process, random technique is adopted as one of the solutions of region coverage of mobile sensor system without environmental prior information. GWO was used to optimize the position of three robots in search, and different search effects were achieved according to different set parameters. In the case of one hundred iterations, the coverage results are shown in Figure 3.

4.2. Design of Roundup Scheme in Dynamic Environment. Bacterial chemotaxis is used to guide the robot towards the target it has found. Bacterial chemotaxis refers to the phenomenon that the bacteria follow the chemical concentration gradient around them to guide the robot towards [22], as shown in

$$C = A_0. \quad (2)$$

Initialize the robot's position and the concentration of each cell. A is the initial concentration. When each robot reaches all the grids in its cell, the robot is considered to have covered the cell. After initialization, robot i becomes A . The concentration of the base moves in the direction of the nearest grid. If the robot has multiple nearest targets to guide, the distance calculation method is used to calculate the direction S to guide the next target, as shown in

$$\frac{dN_i(t)}{dt} = b\delta + aD_i. \quad (3)$$

N is the position of robot i , s is the position of the target, and b is the velocity coefficient of the robot and is the constant coefficient of D . The collision between robots D is

the sum of the interactions between the i th robot and other robots, so as to avoid the problem as shown in

$$D_i = \sum_{j=1}^{b_i} D_i^j. \quad (4)$$

B is the number of neighbors around robot i , and D is the interaction force between them, which is determined by the relative distance between them compared to the absolute distance between them. The energy cost of a robot moving in a straight line is less than that of turning, so the robot will not change direction unless they are stuck in a local optimum [23]. In order to avoid local optimization, the orientation of the robot is determined as shown in

$$P(X = \delta) = P(V = 1)P(X = \delta, V = 1). \quad (5)$$

4.3. Construction of Software Environment of Reinforcement Learning Simulation Platform. Reinforcement learning agent in the environment needs to continue to try and learn, in order to avoid the consumption of real robots and improve the feasibility of reinforcement learning method. If the training and testing of the algorithm are transferred to the computer, carried out in the simulation environment, and the learned model is transplanted to the real robot, the learning cost will be greatly reduced. After the development of recent years, a variety of simulation platforms have emerged in deep reinforcement learning, but most of them are not convenient to modify the simulation environment according to their own needs, so a good experimental environment is very important. Considering that subsequent experimental models can interact with physical robots, we choose OpenAI Gym for environment construction. Gym is a toolbox for developing RL algorithm, combined with TensorFlow machine learning platform, which is convenient for improving development efficiency [24]. The simulation platform software is shown in Table 1.

4.4. Applicability Analysis of Hybrid Control Structure. The hybrid control structure is analyzed from the simulation results.

4.4.1. Conduct Cooperation. Hybrid control structure can make the movement of the robots much more regular than purely behavior-based movements, which makes a certain guarantee of behavioral cooperation.

4.4.2. Dynamic Environment. Hybrid control draws on the idea of behavior-based, and independent behavior processes directly process sensor information to ensure fast response to the environment.

4.4.3. Complex Task. Tasks are more constraints on the robot movement. Behavior management and behavior synthesis can better optimize the behavior of the robot and complete the upper monitoring of complex tasks. The upper monitoring ensures the combination of human control and autonomous command. When the robot cannot achieve autonomous planning, it often needs the participation of human thought [25]. To sum up, the comparative analysis of hybrid control structure and behavior-based structure is shown in Table 2.

4.5. Experimental Analysis of Inclination Sensor Acquisition. In the experiment, the inclination sensor was placed on an inclined plane of 300 and collected for ten times. It can be seen from the experimental data that the maximum error of measurement is 0.40, which can meet the requirements of the system, as shown in Table 3.

4.6. Experimental Analysis of Compass Sensor Acquisition. In the experiment, the compass sensor was used to measure the relative included angles of 30, 45, 60, and 90, respectively, and the average value of each angle was measured for 5 times. It can be seen from the experimental data that the measurement error meets the requirements of the system, as shown in Table 4.

5. Conclusion

Although with the development of robot technology, the ability of robot is constantly improved, and the field and scope of robot application are also constantly expanding, but for some complex tasks, a better solution is composed of multiple robots. Therefore, multirobot system has become an important field of robot research. Multirobot navigation technology is the core technology to realize intelligent system, and path planning is one of the key links. Based on the research of multi-robot-related technology, this paper conducts in-depth theoretical research and simulation analysis on multirobot path planning method. A series of theoretical research work should be done, the focus of the work lies in the innovation and feasibility of theoretical research to realize various methods, and the relevant verification has been done on the self-developed simulation platform. However, some related problems need to be further studied, the performance of the proposed algorithm needs to be further improved, and the effectiveness of each technology needs to be tested in a practical application environment. Therefore, there are still many problems and work to be studied, which will be gradually realized in the future research work. Aiming at the control system architecture of intelligent mobile robot, this paper analyzes the

function of robot system and control system control form, designs the control system, and realizes the scheme and principle block diagram.

Data Availability

The data used to support the findings of this study are available from the corresponding author upon request.

Conflicts of Interest

The authors declare that they have no conflicts of interest.

Acknowledgments

This work was supported by the Basic Scientific Research Project of Liaoning Provincial Department of Education, research on key technologies of health assessment of high safety equipment based on deep learning (Project No. LJKZ1061).

References

- [1] Z. Gao, D. Zhang, and Y. Ge, "Design optimization of a spatial six degree-of-freedom parallel manipulator based on artificial intelligence approaches," *Robotics and Computer-Integrated Manufacturing*, vol. 26, no. 2, pp. 180–189, 2010.
- [2] Z. Cai and X. Zheng, "A private and efficient mechanism for data uploading in smart cyber-physical systems," *IEEE Transactions on Network Science and Engineering (TNSE)*, vol. 7, no. 2, pp. 766–775, 2020.
- [3] X. Zheng and Z. Cai, "Privacy-preserved data sharing towards multiple parties in industrial IoTs," *IEEE Journal on Selected Areas in Communications (JSAC)*, vol. 38, no. 5, pp. 968–979, 2020.
- [4] H. Qiu and H. Duan, "Receding horizon control for multiple UAV formation flight based on modified brain storm optimization," *Nonlinear Dynamics*, vol. 78, no. 3, pp. 1973–1988, 2014.
- [5] A. Löffler, J. Klahold, M. Hußmann, and U. Rückert, "A visualization tool for the mini-robot khepera: behavior analysis and optimization," *Lecture Notes in Computer Science*, vol. 1674, no. 15, pp. 329–333, 1999.
- [6] B. Yang, B. Wu, Y. You, C. Guo, L. Qiao, and Z. Lv, *Edge Intelligence Based Digital Twins for Internet of Autonomous Unmanned Vehicles*, Software: Practice and Experience, 2022.
- [7] Z. Wan, Y. Dong, Y. Zengchen, H. Lv, and Z. Lv, "Semi-supervised support vector machine for digital twins based brain image fusion," *Frontiers in Neuroscience*, vol. 15, p. 802, 2021.
- [8] M. P. Aghababa, "Optimal design of fractional-order PID controller for five bar linkage robot using a new particle swarm optimization algorithm," *Soft Computing*, vol. 20, no. 10, pp. 4055–4067, 2016.
- [9] S. Li, "Structure optimization of e-commerce platform based on artificial intelligence and blockchain technology," *Wireless Communications and Mobile Computing*, vol. 2020, Article ID 8825825, 2020.
- [10] Z. Lu, F. Tao, and Z. Liu, "A multiobjective optimization algorithm based on discrete bacterial colony chemotaxis," *Mathematical Problems in Engineering*, vol. 2014, Article ID 569580, 8 pages, 2014.

Retraction

Retracted: Dynamic Path Planning Analysis of Warehouse Handling Robot

Journal of Sensors

Received 13 September 2023; Accepted 13 September 2023; Published 14 September 2023

Copyright © 2023 Journal of Sensors. This is an open access article distributed under the Creative Commons Attribution License, which permits unrestricted use, distribution, and reproduction in any medium, provided the original work is properly cited.

This article has been retracted by Hindawi following an investigation undertaken by the publisher [1]. This investigation has uncovered evidence of one or more of the following indicators of systematic manipulation of the publication process:

- (1) Discrepancies in scope
- (2) Discrepancies in the description of the research reported
- (3) Discrepancies between the availability of data and the research described
- (4) Inappropriate citations
- (5) Incoherent, meaningless and/or irrelevant content included in the article
- (6) Peer-review manipulation

The presence of these indicators undermines our confidence in the integrity of the article's content and we cannot, therefore, vouch for its reliability. Please note that this notice is intended solely to alert readers that the content of this article is unreliable. We have not investigated whether authors were aware of or involved in the systematic manipulation of the publication process.

Wiley and Hindawi regrets that the usual quality checks did not identify these issues before publication and have since put additional measures in place to safeguard research integrity.

We wish to credit our own Research Integrity and Research Publishing teams and anonymous and named external researchers and research integrity experts for contributing to this investigation.

The corresponding author, as the representative of all authors, has been given the opportunity to register their agreement or disagreement to this retraction. We have kept a record of any response received.

References

- [1] Y. Zhao, "Dynamic Path Planning Analysis of Warehouse Handling Robot," *Journal of Sensors*, vol. 2022, Article ID 4434971, 7 pages, 2022.

Research Article

Dynamic Path Planning Analysis of Warehouse Handling Robot

Yue Zhao 

School of Electrical and Computer Science, Jilin Jianzhu University, Jilin 130118, China

Correspondence should be addressed to Yue Zhao; 15095102210001@hainanu.edu.cn

Received 30 May 2022; Revised 1 July 2022; Accepted 14 July 2022; Published 25 July 2022

Academic Editor: Haibin Lv

Copyright © 2022 Yue Zhao. This is an open access article distributed under the Creative Commons Attribution License, which permits unrestricted use, distribution, and reproduction in any medium, provided the original work is properly cited.

In order to further improve the operational efficiency and the flexibility of automated warehouse, a path planning algorithm for a warehouse handling robot was evaluated. Under the background of determining the operation scene and environment of multihandling robot, a path planning algorithm with time window is proposed for multihandling robot, and a two-stage path planning method is also analyzed. The results show that the route planning using the improved Dijkstra algorithm saves 7.16 meters compared with the traditional algorithm, and the task is completed 3.17 seconds earlier. Comprehensively considering the heat of the various paths to turn to the required time, using the improved Dijkstra algorithm path, handling the robot's total running distance than the traditional algorithm saves 14.45 meters, the total run time saves 8.45 seconds, and whether in time or in the distance, crane robot handling efficiency compared with the traditional algorithm has an obvious increase, closer to reality.

1. Introduction

With the development of warehousing automation technology, handling robot technology is also developing rapidly and has become the focus of attention in the world today [1]. At present, the handling robot has completed the simple work such as palletizing, depalletizing, and handling, in-depth to more complex logistics operations such as sorting and picking [2].

With the acceleration and deepening of the aging process of China's population, the era of "demographic dividend" with abundant labor resources has gradually faded, and the problem of high labor cost of enterprises has gradually emerged. It has become an inevitable trend to replace manual operation with automatic equipment to improve the level of warehousing automation [3]. Undoubtedly, using the handling robot to replace manual picking operation of goods, for improving the level of automation and saving labor costs, improve the efficiency of the operation plays an important role [4].

The development of e-commerce and logistics industry has promoted the integrated application of intelligent handling robots in automated warehouses and promoted the transformation and upgrading of storage operation mode. However, a series of problems about intelligent and efficient task allocation, vehicle scheduling, path planning, and conflict handling restrict

the promotion and application of handling robots [5]. Therefore, it is necessary to increase the research on the handling robot, solve the technical difficulties affecting the integrated application of the handling robot, and realize the cooperative planning of multiple handling robots, so as to improve the operating efficiency, reduce labor costs, and maximize profits.

2. Literature Review

The handling robot is a new type of mobile robot which is used in storage operation field, by laying magnetic rails, navigation routes, positioning beacons, and other indicating devices in the warehouse, combined with motion control technology, task planning technology, sensor technology, and other technical methods. According to the information of indicating device, accurate positioning and path planning are needed. Smooth handling of mobile shelves and effective connection between shelves and staff are as shown in Figure 1 [6].

At present, there are mainly two kinds of robots used in warehouses, one of which is the logistics robot represented by Kiva used by Amazon, which is also used in most logistics warehouses in China [7]. This kind of robot subverted the traditional mode of looking for goods on the shelf through manual attack. Instead of picking goods by itself, the robot

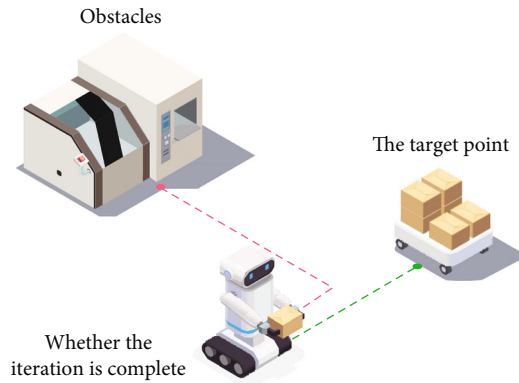


FIGURE 1: Transfer robot.

can directly carry the whole movable shelf to the picking platform for picking workers to pick goods, thus realizing the picking of goods to people mode [8]. The use of Kiva-like robots in the warehouse reduces the time for workers to walk in the warehouse to pick up goods. This greatly reduces the number of picking workers, greatly saves the labor cost, and improves the working efficiency of the storage system, and the robot delivers the work of picking goods to the picking workers. It also reduces the complexity, easy to operate, and is the main role in the future automated warehouse [9]. However, because the robot needs to move the whole shelf to the picking table at one time, the energy consumption is high and the goods category is less. Moreover, due to the limitation of the loading volume of the shelf, the handling robot cannot carry the goods with large volume and heavy weight, so there are certain restrictions on the types of goods and the promotion scope is narrow. Scheduling and path planning for multiple robots are also difficult and prone to conflict, which requires continuous improvement [10].

The other is the robot used by Tmall platform. This kind of robot can not only move to the shelf and use the mechanical arm to pick goods but also transport the picked goods to the packaging platform for direct packaging, without the need for picking workers to pick again [11]. Compared with Kiva, it can directly select goods according to the order information, with a higher degree of automation. However, it requires a robot for picking tasks and a robot for delivery tasks to cooperate to complete the task, which requires a large number of robots and a high cost. In addition, the technology of grasping goods with mechanical arm is not mature, and the grasping of goods with small volume is not very accurate and the efficiency is low, which needs to be improved gradually in the future [12, 13]. Facing the huge market demand, in order to win the time efficiency favored by customers, further improves the operational efficiency and enhances the flexibility of automated warehouse. Many enterprises such as Amazon, Tmall, Jingdong, and other e-commerce enterprises are actively carrying out the research of multi-handling robots, trying to use multihandling robots to carry goods, accelerate the layout of more intelligent automatic storage system, improve the quality of service, and increase the competitiveness of enterprises [14, 15].

On the basis of the current research, this paper takes the dynamic path planning problem of multiple porters as the

research object. This paper analyzes the research status at home and abroad and the existing problems in path planning of multihandling robots and designs a path planning model and its solving algorithm.

3. Research Methods

3.1. Path Planning Algorithm for Multiple Handling Robots with Time Windows. The time window algorithm was first proposed by Kim and Tanchoco and is often used for path optimization of multiple handling robots in bidirectional graphs [16]. The time window algorithm was first proposed by Kim and Tanchoco and is often used for path optimization of multiple handling robots in bidirectional graphs [17]. In the process of robot operation, the time occupied by each robot on each road section can be calculated [18]. When the time windows occupied by different robots do not overlap, it indicates that there is no collision [19]. If there is a potential collision, adjust the original time window to avoid collision [20]. The specific algorithm flow chart is shown in Figure 2. Therefore, as long as the start time, speed, start node, target node, and path information matrix of the robot are clear, the sequence of resources occupied by the robot can be prearranged through calculation to avoid conflicts and collisions.

3.2. Multihandling Robot Operation Description. In actual production, the picking mode of the person receiving the goods is that the handling robot moves the shelves of the items needed in the order to the picking table, and the picking workers only need to take out the SKU needed from the shelves at the picking station [21]. The use of the handling robot saves the time of manual walking and improves the operation efficiency. The operation process of the handling robot in the delivery and human picking mode is as follows:

- (1) According to the quantity of each SKU in the order: inventory and other information to select the matching task rack and will need to pick the shelves and picking platform to match (determined by the shelf location picking platform busy degree and other factors), determine the starting point and end point of picking
- (2) Assign tasks to moving robots: since a handling robot cannot execute multiple order tasks at the same time, the system needs to query the working status of the handling robot, assign the task to the idle handling robot nearest to the required handling shelf, and plan the optimal walking path from the starting point to the end point. If there is no free robot, wait until there is a free robot
- (3) After receiving the task, the state of the handling robot will be changed from idle to working state, drive to the task shelf according to the path planned by the system from the location, and lift the task shelf, and the robot will be changed from empty to load state

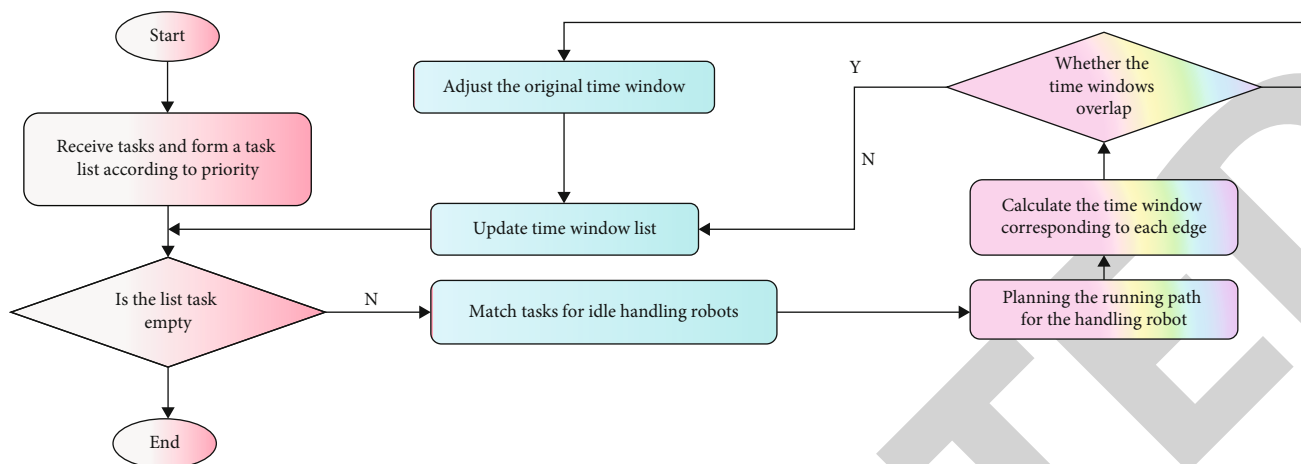


FIGURE 2: Flow chart of time window algorithm.

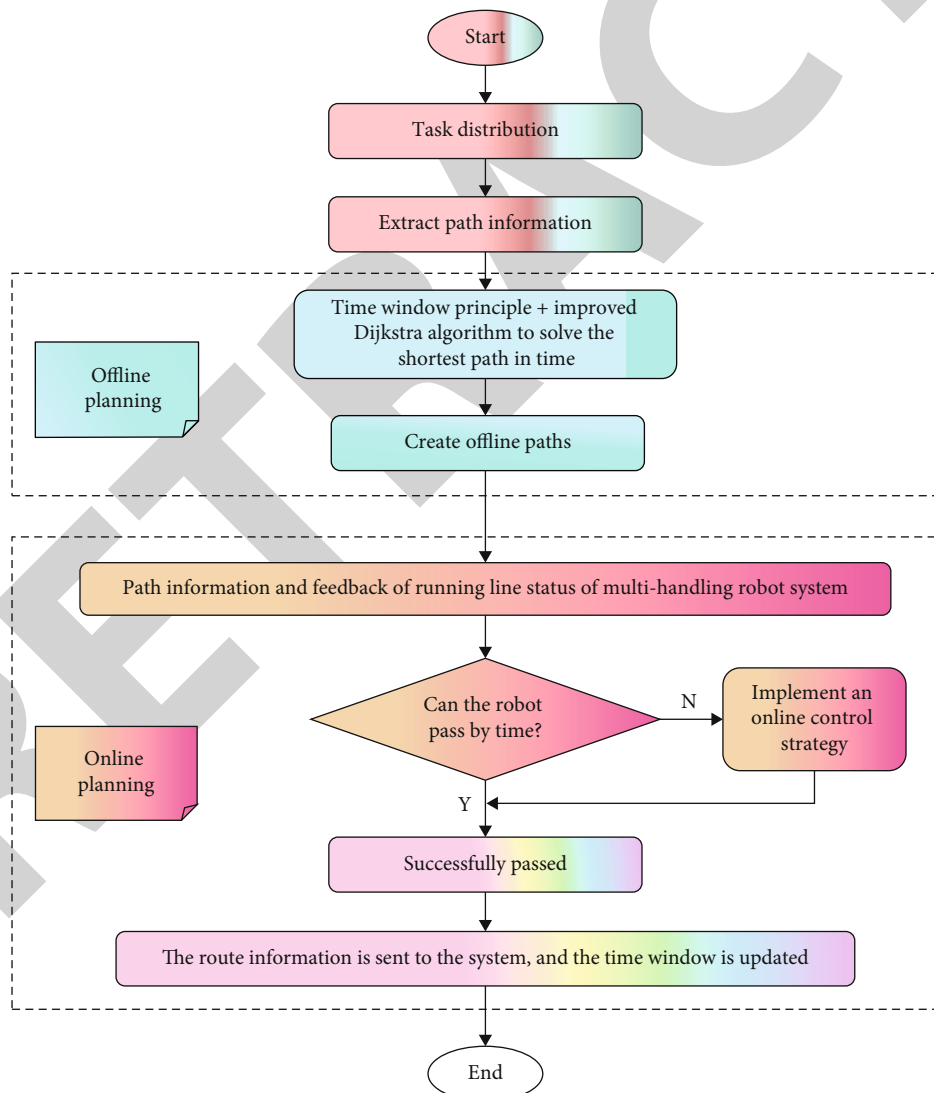


FIGURE 3: Flowchart of two-stage path planning method.

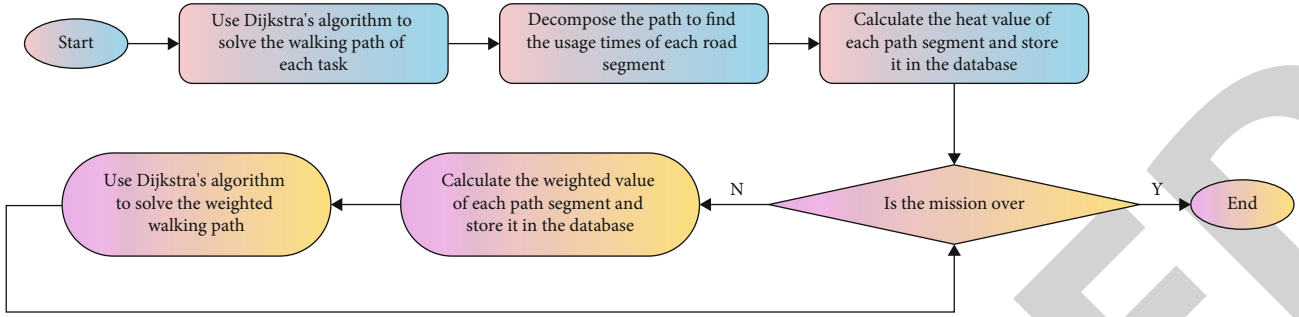


FIGURE 4: Improved Dijkstra algorithm flow chart.

TABLE 1: Computational results.

Algorithm	Distance (m)	Running time (seconds)
Traditional Dijkstra algorithm	268.96	273.96
Improved Dijkstra algorithm	261.80	270.7938

- (4) The handling robot with the task shelf drives to the target picking station and waits for picking. After the current picking task is completed, check whether there are other picking tasks. If so, move to the designated picking station and wait for picking. Otherwise, enter Step (5)
- (5) It requests the system to transport the task shelf back to the target location given by the system and designs the optimal return path for the carrying robot. The state of the carrying robot becomes empty
- (6) Determine whether the handling robot needs to be charged. If it needs to be charged, drive to the charging pile for charging, otherwise release the handling robot
- (7) Go to Step (2) and repeat until there are no picking tasks [22, 23]

3.3. *Environment Modeling.* Combined with the characteristics of different modeling methods and according to the actual warehouse operation environment, this paper adopts raster graph modeling method to create warehouse operation electronic environment map model [24].

The steps of warehouse operation environment modeling for handling robot are as follows:

- (1) Determine the number of grids

With the lower left corner of the warehouse as the origin of coordinates, the rectangular coordinate system is established. The axis of the coordinate system represents the length of the warehouse, and the axis represents the width of the warehouse. Assuming that the length of the warehouse is X , the width is Y , and the side length of the grid is z , the

number of grids of the axis x is the rounded value of the length of the warehouse divided by the length of the grid $\text{INT}(X/Z)$, and the number of grids of the axis y is the rounded value of the width of the warehouse divided by the width of the grid $\text{INT}(Y/Z)$ [25].

(2) Encoding

After the number of grids is determined, the grid data in the rectangular coordinate system is numbered. The grid's two-dimensional coordinates start at the origin (1, 1), and the grid's one-dimensional coordinates start at 1 and proceed from bottom to top, left, and right. Assuming that the two-dimensional numbering of the grid P is (x, y) , the corresponding formula of two-dimensional coordinates and one-dimensional coordinates is

$$\text{Coding} = (x - 1) * \text{INY} \left(\frac{X}{Z} \right) + y \quad (1)$$

(3) Barriers to assign a value

The obstacle grid on the international circle is divided into several grids on the international circle. Grids with impassable obstacles are marked with a 1, and grids with unpassable obstacles are marked with a 0.

3.4. *Two-Stage Path Planning Method.* The core idea of the two-stage path planning method is to generate N alternative paths for the handling robot in offline state and then plan the path of the robot in real time through online information. The algorithm has been widely used in the path planning of mobile robots because of its advantages such as low online computation burden. However, the optimal path generated by this method in the offline state is not the optimal path of the robot, which needs to be further planned online, making the overall efficiency of the system low. This paper optimizes the traditional two-stage path planning method.

Firstly, based on the weighted directed graph, Dijkstra algorithm with path heat evaluation index is used to generate global optimal path in the offline phase. Due to the static path planning for the handling robot, the route of each handling robot may be interfered by other robots as the tasks

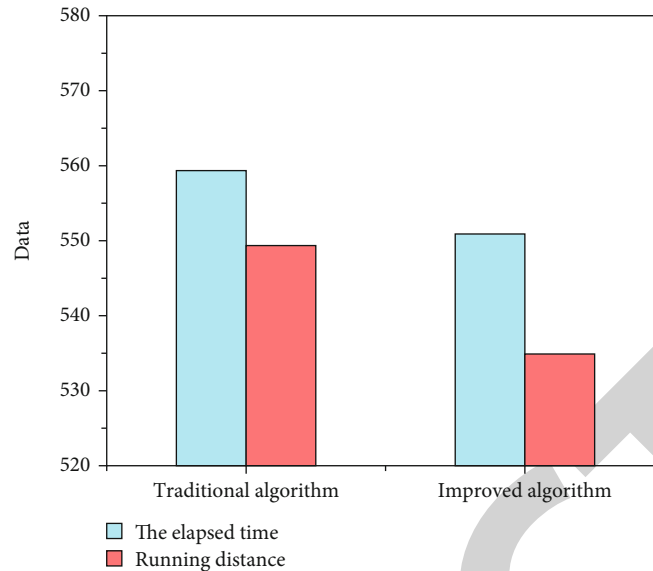


FIGURE 5: Comparison of calculation results before and after algorithm improvement.

continue to enter the system. Therefore, during the operation of the handling robot, the multihandling robot system needs to track and locate the route of the handling robot running in the system in real time. If there is no path interference, the static optimal solution is the global optimal solution. Once it is found that two or more handling robots have path interference and there is time window conflict, the traffic control strategy will be started. By adjusting the priority of vehicles, possible path conflicts can be prevented and avoided in advance. The structure of offline-online two-stage path planning algorithm is shown in Figure 3.

3.5. Improved Algorithm Dijkstra. In this paper, the traditional Dijkstra algorithm is improved by adding heat value into the path weight to make the route planning more reasonable. The heat of each path is defined $fb = \{fb_{12}, fb_{23}, \dots, fb_{mn}\}$ in the time cycle Δ , the real-time number of handling robots on each path during operation is $b_g = \{b_{12}, b_{23}, \dots, b_{mn}\}$, and E is the total number of paths. The specific calculation process is as follows:

- (1) The traditional Dijkstra algorithm is used to preliminarily plan the path of each carrying robot from the task starting point to the end point
- (2) The paths in step (1) are decomposed and the utilization frequency of each road section within the time cycle is counted
- (3) When the carrying robot passes through the current path, b_g automatically decreases by 1
- (4) The influence coefficient function of construction path busyness on path selection by Dijkstra algorithm is shown in

$$F(fb) = \frac{(b_g + 1)h_k}{\sum_{g=1}^p \sum_{k=1}^E b_g h_k} \quad (2)$$

Then, the path weight value after adding path heat is

$$w_{jk} = 1 + F(fb). \quad (3)$$

The improved Dijkstra algorithm flow is shown in Figure 4.

4. Interpretation of Result

4.1. Improved Dijkstra Algorithm Validation. In this paper, the proposed improved Dijkstra algorithm is verified by simulation experiments assuming that the moving speed of the robot is 1 m/s and the distance between grids is 5 m. The starting and ending coordinates of priority 1 are (10, 18), (8, 1), and the starting and ending coordinates of priority 2 are (21, 10), (16, 1). The results are shown in Table 1.

It can be seen from Table 1 that when the path heat value is added and the traditional algorithm and the improved algorithm are used to plan the path, the distance, and time of the carrying robot are different. Compared with the traditional algorithm, the route planning using the improved Dijkstra algorithm saves 7.16 meters and completes the task 3.17 seconds earlier. On the one hand, the improved algorithm coordinates the load balance of the path to avoid the congestion of the path; on the other hand, it also saves the running time and distance and improves the efficiency of the carrying robot.

4.2. Validation of Dynamic Path Planning Algorithm in Offline Phase of Multihandling Robot. On the basis of considering the busy degree of the path and turning time, four tasks were set for the carrying robot, and the total running distance and running time of the carrying robot were compared between the

traditional Dijkstra algorithm and the improved Dijkstra algorithm.

The starting point and ending point of priority 1 are (10, 18) and (8, 1), respectively. The starting point and ending point of priority 2 are (21, 10) and (16, 1), respectively. The starting point and ending point of priority 3 are (19, 23) and (24, 1), respectively. The starting and ending coordinates of priority 4 are (29, 8) and (32, 1), respectively.

The comparison of the total running time and total running distance of the four tasks before and after the algorithm was improved is shown in Figure 5. Experimental results show that when the heat of each path is considered comprehensively, the time required for turning is taken into account. Using the path solved by the improved Dijkstra algorithm, the total running distance and total running time of the robot are 14.45 meters and 8.45 seconds less than those of the traditional algorithm. Both in time and in distance, the handling efficiency of the handling robot has been significantly improved compared with the traditional algorithm and is closer to the reality.

5. Conclusion

Intelligent logistics is the development direction of the logistics industry in the future. By solving the key problems existing in intelligent logistics, it is conducive to promoting the transformation and development of the logistics industry and improving the overall level and efficiency of the logistics industry. The development of intelligent logistics technology has promoted the widespread application of handling robots in warehousing operations. How to carry out path planning for multiple handling robots has been widely concerned by the academic community and is summarized as follows:

- (1) According to the actual environment of logistics warehouse, the warehouse operation environment map model is established. According to the actual demand of e-commerce enterprises, the path planning mathematical model of multihandling robot with time window is established with the shortest total running time as the objective function
- (2) Based on the traditional two-stage path planning, a path planning algorithm for handling robot is designed which combines offline planning and dynamic scheduling. In the offline state, the path heat and turning time are considered, and the improved Dijkstra algorithm is used to plan the global optimal path. In the online state, real-time scheduling is carried out based on the priority of vehicles to avoid conflicts
- (3) The traditional Dijkstra algorithm is improved by adding the path heat value to the path weight, taking into account the congestion caused by busy paths and the time required by the transfer robot to turn. The improved algorithm makes the path load balance and saves the running time of the removal robot

Data Availability

The data used to support the findings of this study are available from the corresponding author upon request.

Conflicts of Interest

The author declares that he/she has no conflicts of interest.

References

- [1] B. Tang and L. Jiang, "Binocular stereovision omnidirectional motion handling robot," *International Journal of Advanced Robotic Systems*, vol. 17, no. 3, p. 172988142092685, 2020.
- [2] S. G. Gultekin and R. Taspinar, "Bicriteria scheduling of a material handling robot in an m-machine cell to minimize the energy consumption of the robot and the cycle time," *Robotics and Computer-Integrated Manufacturing*, vol. 72, no. 5, article 102207, 2021.
- [3] Z. Lv, Y. Han, A. K. Singh, G. Manogaran, and H. Lv, "Trustworthiness in industrial IoT systems based on artificial intelligence," *IEEE Transactions on Industrial Informatics*, vol. 17, no. 2, pp. 1496–1504, 2021.
- [4] Z. Lv, W. Kong, X. Zhang, D. Jiang, H. Lv, and X. Lu, "Intelligent security planning for regional distributed energy internet," *IEEE Transactions on Industrial Informatics*, vol. 16, no. 5, pp. 3540–3547, 2020.
- [5] G. Sawadwuthikul, T. Tothong, T. Lodkaew, P. Soisudarat, and N. Dilokthanakul, "Visual goal human-robot communication framework with few-shot learning: a case study in robot waiter system," *IEEE Transactions on Industrial Informatics*, vol. 18, no. 3, pp. 1883–1891, 2022.
- [6] V. A. Rosas-Cervantes, Q. D. Hoang, S. G. Lee, and J. H. Choi, "Multi-robot 2.5d localization and mapping using a Monte Carlo algorithm on a multi-level surface," *Sensors*, vol. 21, no. 13, p. 4588, 2021.
- [7] S. Alsamhi and B. Lee, "Blockchain for multi-robot collaboration to combat covid-19 and future pandemics. IEEE," *Access*, vol. PP (99), pp. 1–1, 2020.
- [8] K. Shen, C. Li, D. Xu, W. Wu, and H. Wan, "Sensor-network-based navigation of delivery robot for baggage handling in international airport," *International Journal of Advanced Robotic Systems*, vol. 17, no. 4, p. 172988142094473, 2020.
- [9] W. Shang, Z. Gao, D. Nicolo et al., "Benchmark analysis for robustness of multi-scale urban road networks under global disruptions," *IEEE Transactions on Intelligent Transportation Systems*, pp. 1–11, 2022.
- [10] H. Bi, W. Shang, K. Wang, and Y. Chen, "Joint optimization for pedestrian, information and energy flows in emergency response systems with energy harvesting and energy sharing," *IEEE Transactions on Intelligent Transportation Systems*, pp. 1–15, 2022.
- [11] J. Patel, P. Sonar, and C. Pinciroli, "On multi-human multi-robot remote interaction: a study of transparency, inter-human communication, and information loss in remote interaction," *Swarm Intelligence*, vol. 16, no. 2, pp. 107–142, 2022.
- [12] M. Jahanbakht, W. Xiang, L. Hanzo, and M. R. Azghadi, "Internet of underwater things and big marine data analytics—a comprehensive survey," *IEEE Communication Surveys*

Retraction

Retracted: Navigation and Positioning Analysis of Electric Inspection Robot Based on Improved SVM Algorithm

Journal of Sensors

Received 13 September 2023; Accepted 13 September 2023; Published 14 September 2023

Copyright © 2023 Journal of Sensors. This is an open access article distributed under the Creative Commons Attribution License, which permits unrestricted use, distribution, and reproduction in any medium, provided the original work is properly cited.

This article has been retracted by Hindawi following an investigation undertaken by the publisher [1]. This investigation has uncovered evidence of one or more of the following indicators of systematic manipulation of the publication process:

- (1) Discrepancies in scope
- (2) Discrepancies in the description of the research reported
- (3) Discrepancies between the availability of data and the research described
- (4) Inappropriate citations
- (5) Incoherent, meaningless and/or irrelevant content included in the article
- (6) Peer-review manipulation

The presence of these indicators undermines our confidence in the integrity of the article's content and we cannot, therefore, vouch for its reliability. Please note that this notice is intended solely to alert readers that the content of this article is unreliable. We have not investigated whether authors were aware of or involved in the systematic manipulation of the publication process.

Wiley and Hindawi regrets that the usual quality checks did not identify these issues before publication and have since put additional measures in place to safeguard research integrity.

We wish to credit our own Research Integrity and Research Publishing teams and anonymous and named external researchers and research integrity experts for contributing to this investigation.

The corresponding author, as the representative of all authors, has been given the opportunity to register their agreement or disagreement to this retraction. We have kept a record of any response received.

References

- [1] Y. Li, Y. Long, M. Du, X. Jiang, and X. Liu, "Navigation and Positioning Analysis of Electric Inspection Robot Based on Improved SVM Algorithm," *Journal of Sensors*, vol. 2022, Article ID 4613931, 6 pages, 2022.

Research Article

Navigation and Positioning Analysis of Electric Inspection Robot Based on Improved SVM Algorithm

Yongfu Li ¹, Yingkai Long ¹, Mingming Du ², Xiping Jiang ¹ and Xianfu Liu ³

¹State Grid Chongqing Electric Power Research Institute, Chongqing 401121, China

²State Grid Chongqing Electric Power Company, Chongqing 400013, China

³Nanjing Unitech Electric Power Co., Ltd, Nanjing 211100, China

Correspondence should be addressed to Yingkai Long; 31115307@njau.edu.cn

Received 30 May 2022; Revised 29 June 2022; Accepted 9 July 2022; Published 25 July 2022

Academic Editor: Haibin Lv

Copyright © 2022 Yongfu Li et al. This is an open access article distributed under the Creative Commons Attribution License, which permits unrestricted use, distribution, and reproduction in any medium, provided the original work is properly cited.

In order to improve the accuracy of electric inspection robot navigation and positioning, an improved SVM algorithm was proposed to improve the accuracy of inspection. The research focuses on sensor calibration technology, lane line detection and robot positioning technology, obstacle detection and tracking technology, and substation road scene understanding technology. The results show that the radar measurement results have great fluctuation and deviation due to the existence of noise, but the results are smoother after EKF estimation. Secondly, the accuracy of the improved SVM classifier in this paper is much higher than that of the traditional method, and the improvement effect is obvious.

1. Introduction

Operation and maintenance is the key measure to ensure the safe and reliable operation of the power system. As a power system, the substation undertakes the important responsibility of transmitting power, transforming voltage and distributing power, and power distribution in the power system. The substation is geographically distributed in a wide area, with a large number and a wide variety; the operation state changes rapidly and needs to withstand the test of various climatic conditions of the operation environment. Its operation and maintenance account for a large proportion in the technology and management of the power grid company [1, 2]. Therefore, adopting new technologies and methods to improve the operation and maintenance level and efficiency of substation has always been the focus of power grid companies. For a long time, substation patrol inspection has been mainly completed manually. With the rapid development of power system, power grid companies are facing great pressure on patrol inspection [3, 4]. Therefore, the introduction of new technologies and methods to improve the operation and maintenance level and efficiency of sub-

stations has always been in the focus of energy network companies. For a long time now, substation inspections have been carried out mainly by hand. At a time when the energy system is developing rapidly, power grid companies are facing a huge workload [5]. In recent ten years, China has carried out the research and application of inspection robot and achieved gratifying results [6]. However, from a practical point of view, the current control robot system is still difficult to perform on its own [7]. Because the robot does not have the ability to understand the sensor information, even if it obtains the road environment information, it is unable to judge the road environment. Usually, it can only drive blindly according to the map and guide wire but can not adjust according to the real-time road conditions. Manual intervention is often required in the event of a problem, and the ability to work independently in an emergency is insufficient [8, 9]. In conclusion, the study of more intelligent energy control robots is based on the need to develop power systems on the one hand and the development of new technologies on the other. It can be said that the rapid development of energy control robot technology is beginning in the spring. Figure 1 shows a study of the positioning

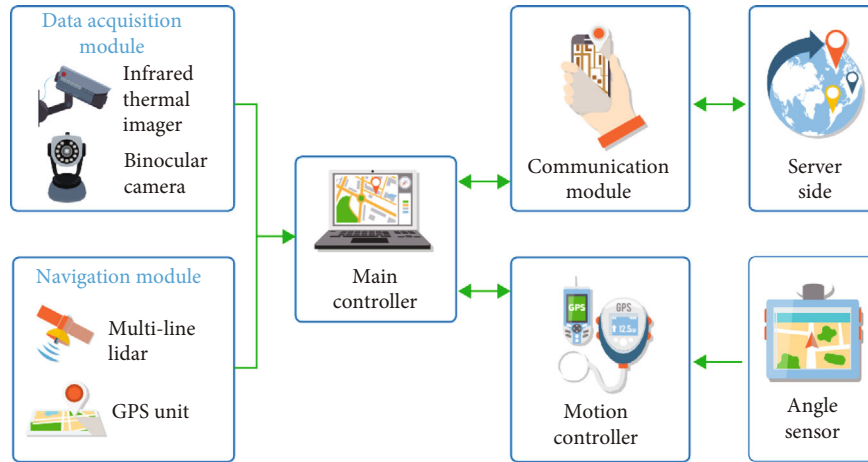


FIGURE 1: A positioning method of power inspection robot system based on improved PSO + SVM algorithm.

method of an electrically controlled robotic system based on an improved PSO + SVM algorithm.

2. Literature Review

The research on the operation and maintenance robot of power system started early. About 30 years ago, an intelligent robot for substation inspection and transmission line inspection was developed [10]. In 1984, Japan's Tokyo Electric Power Company and Mitsubishi group began to jointly study the intelligent robot. The company implanted the visual servo technology into the robot to enable it to carry out automatic positioning and automatic recognition of three-dimensional objects. The robot walks along the ground track and automatically obtains the data information in the station. So far, it has been developed to the third generation [11]. In 2003, Japanese experts put forward the idea of substation inspection robot and began to carry out simulation test [12]. In 2005, the first substation inspection robot was successfully developed by American experts. Its main task of inspection is to carry out infrared temperature measurement, and it has been put into production and use by power companies in the western United States [13]. In 2008, American scientists proposed a navigation system composed of inertial navigation and global positioning system, which can make the robot have continuous, real-time, and efficient navigation ability [14]. Muthugala et al. proposed a robot navigation method based on digital map and machine vision, and its effectiveness was proved by experiments. After that, experts and scholars from various countries began to study robot navigation methods, and many robot navigation methods have been proposed successively, such as RFID positioning method, computer vision-based navigation method, and depth learning-based navigation method. The proposal of these methods has gradually improved the autonomous navigation ability of substation inspection robot, which is of great significance to the practicability and popularization of substation inspection robot [15]. The research on inspection robot in China started relatively late compared with foreign countries, but many achievements have been made in recent years [16, 17].

Around 2004, with the support of the 863 project during the Tenth Five-Year Plan period, many units, including Shandong University, Tsinghua University, and Shandong electric power academy, carried out in-depth research on transmission line inspection robots and substation inspection robots [17, 18]. In the field of transmission line inspection robot, Professor Wu Gongping's team of Wuhan University has made great research achievements and important social impact. The inspection robot along the ground wire developed by the team can transform the shockproof hammer and suspension clamp on the ground wire into an unobstructed road structure, so as to realize the efficient and safe inspection of the inspection robot along the whole line [19]. The autonomous navigation technology of substation inspection robot can be divided into the following parts: sensor calibration technology, lane line detection technology, obstacle detection technology, road scene description, and understanding technology. The relationship between them and the system block diagram is shown in Figure 2. This paper will focus on these parts.

3. Research Methods

3.1. Lane Line Detection Based on Line Detection and Color Space Transformation. For the autonomous navigation of substation intelligent inspection robot, the most basic thing is to know its own local positioning [20]. Only by understanding the lane information can we obtain the position and direction of the robot relative to the lane. In the substation environment, most road scenes are structured roads. The so-called structured roads refer to standardized roads with clear lane signs, road boundaries, etc. [21]. The problem of how to extract accurate information from the outdoor environment, such as the amount of visual sensors, is often accompanied by a large amount of visual interference, which can not obtain accurate information from the outdoor environment.

The road detection method studied in this paper is applied in the substation environment. At present, most of the substation roads are structured roads, the lane lines are yellow and clear, and most of the roads are straight roads

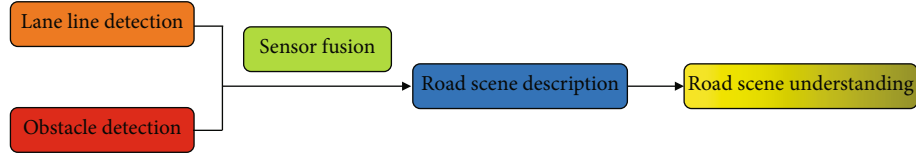


FIGURE 2: Block diagram of autonomous navigation system.

[22]. Even if there are a few curves, for the moving robot, the curvature radius of the lane line not far from the camera is very small, and the lane line can be approximated as a straight line [23]. Therefore, this paper will use the combination of Hough line detection and color space transformation to detect the lane line in the substation road. The processing flow is shown in Figure 3. Firstly, each frame image of the camera is obtained and converted into RGB format. On the one hand, the image is preprocessed by binarization and noise reduction; then, Canny edge detection is carried out, and then, Hough transform is used for line detection. Through the screening of line segments, the candidate road edge collection is obtained. On the other hand, the RGB image is transformed into HSV color space image. By limiting the threshold of three HSV channels, the yellow lane line area is extracted, and the lane line area is appropriately expanded by morphological operation. Finally, the detection results of the two parts are fused to obtain a straight line that can divide the road area and nonroad area, and the lane line extraction test is carried out on the substation road pictures under different lighting conditions and different pavement environments with MATLAB.

3.2. Obstacle Tracking Based on Extended Kalman Filter. Extended Kalman filtering is the usage form of Kalman filtering in nonlinear systems, and the main idea is to find the best balance between the system state estimates at the next moment and the measurements obtained for state estimation. The fusion of the two is to continuously adjust a changing weight and finally obtain an infinitely close to the accurate value of the system at this moment. When the system is a linear model, the Kalman filter can give the optimal estimation, but in practical application, because the motion trajectory of the obstacle relative to the radar is nonlinear, and the radar measurement system itself is also nonlinear, it is necessary to approximate linearize the nonlinear system first and then use the Kalman filter for the optimal estimation [24]. This method is the extended Kalman filter method (EKF). The process of optimal estimation using extended Kalman filter is as follows:

Firstly, the discrete process model is established, as shown in:

$$\hat{X}_k^- = f(x_{k-1}) + W, \quad (1)$$

where f is the nonlinear equation of the system and W is the process noise of the system. The update corresponds to the covariance matrix W of the system. The update formula is

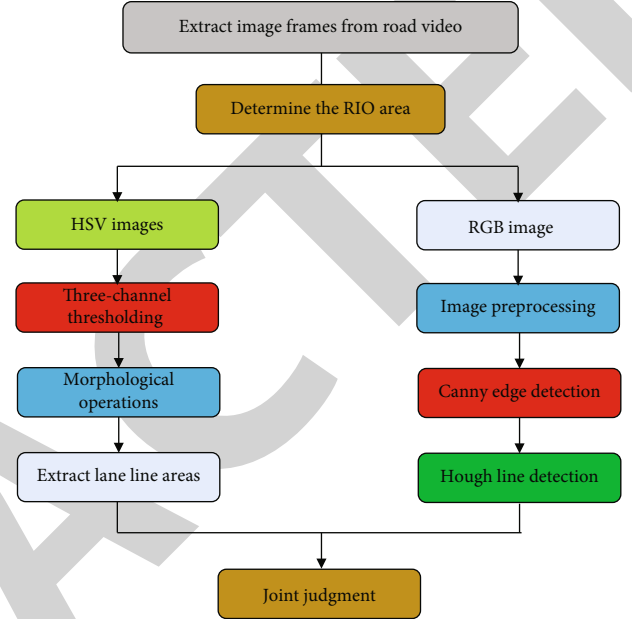


FIGURE 3: Flow chart of lane line detection based on Hough transform and HSV color space.

as follows:

$$P_k^- = F_{k-1} P_{k-1} F_{k-1}^T + Q, \quad (2)$$

where F is the Jacobian matrix form of the system and Q is the measurement noise of the observer. Then, calculate the Kalman gain, and the calculation formula is

$$K_k = P_k^- H_k^T (H_k P_k^- H_k^T + R)^{-1}, \quad (3)$$

where H is the measurement matrix of the system and R is the covariance matrix of the measurement noise. Then, the optimal estimation value of the current state is calculated through Kalman gain, and the calculation formula is

$$\hat{x}_k = \hat{x}_k^- + K_k (Z_k - h \hat{x}_k^-), \quad (4)$$

where Z_k is the measured value of the system at time k and h is the measured Jacobian matrix. The covariance matrix P in the current update state is

$$P_k = P_k^- - K_k H P_k^-. \quad (5)$$

3.3. Front Road Scene Recognition Based on SVM. After getting the schematic diagram of the road scene ahead, it needs to be transformed into road environment information that

can be understood by the robot. Firstly, the understanding method of the road scene ahead needs to be selected according to the application environment. The substation scene studied in this paper has the following characteristics:

- (1) The working environment of intelligent robot is fixed, which is only the substation environment, and there is no need to distinguish different scenes or perceive the similarity of scenes
- (2) The robot does not need to recognize the object in front. The obstacle in front is pedestrian or vehicle. For the robot, it can be attributed to the nonpassable area, and there is no need to know what the obstacle is. Therefore, the recognition of the road scene in front of the intelligent robot in the substation can be simplified to the state classification of the obstacles in front
- (3) Because the application scenario of intelligent robot in substation is substation environment, it is difficult to obtain samples, it is not easy to collect a large number of images for training templates, and in practical application, the conditions for increasing a large number of training samples are also difficult to meet. Therefore, the classification problem of road environment in front of substation environment belongs to the classification problem of small samples

Support vector machine is a classification algorithm in machine learning. It can obtain better statistical laws when the statistical samples are small. Around 2010, with the rapid improvement of computing power and the emergence of big data, neural network research rose rapidly and ushered in a climax of development. However, compared with neural network, SVM still has some advantages, such as the feature dimension is more than the number of samples. In this small sample learning problem, the use effect of neural network is poor, but support vector machine can still live up to expectations. The essence of classifying the input front scene schematic diagram is to classify the image features of these images. Therefore, we should first select the appropriate image features as the basis for classification. For the input front scene diagram, its main features are composed of two aspects: edge features and gray features. Therefore, the two features selected in this paper are directional gradient histogram (HOG) and gray level cooccurrence matrix (GLCM). The combination of the two forms the feature matrix of the complete front scene diagram. The definition of the HOG function consists of calculating the histogram of the radius in the region of the picture to form an image. The next step is to split the HOG function: make the image normal. The color of the image, then, makes the image's color space the gamma satellite, so that it can reduce the volume of light and noise. Calculate the gradient of the image. Rotate the image by a $[-1,0,1]$ gradient operator and its shift, and at the edge of each pixel, the gradient is full. In the vertical direction, you can figure out the gradient integrity and then use the following formula; the vertical and the horizontal

gradient of the current pixel is as follows:

$$\begin{aligned} G_x(x, y) &= H(x + 1, y) - H(x - 1, y), \\ G_y(x, y) &= H(x, y + 1) - H(x, y - 1), \\ G(x, y) &= \sqrt{G_x(x, y)^2 + G_y(x, y)^2}, \\ \alpha(x, y) &= \tan^{-1} \left(\frac{G_y(x, y)}{G_x(x, y)} \right). \end{aligned} \quad (6)$$

Of these, $G_x(x, y)$ represents the horizontal gradient of the pixel, $G_y(x, y)$ represents the vertical gradient, and $H(x, y)$ represents the value of the point pixel. $G(x, y)$ represents the size of the pixel point gradient, and $\alpha(x, y)$ represents the direction of the point gradient.

3.4. SVM Classification Experiment. The experimental process of classification is carried out on the schematic diagram of the road scene in front of the robot. The feature value extraction of the image, the training of the classifier, and the test of the training results are completed by MATLAB 2016b. The flow chart of the experiment is shown in Figure 4.

4. Result Analysis

4.1. Obstacle Tracking Experiment. MATLAB is used to simulate an obstacle with nonlinear motion relative to the robot. The effectiveness of extended Kalman filter in obstacle tracking is verified by comparing the errors between the measured value, estimated value, and real value before and after adding extended Kalman filter. Figure 5 shows the relationship between the actual value, observed value, and EKF estimated value of obstacle motion. In Figure 5, "*" represents the result of radar measurement, "+" represents the result after EKF estimation, and "-" represents the actual motion trajectory. It can be seen from the figure that due to the existence of noise, there are large fluctuations and deviations in the radar measurement result, and the result is smoother after EKF estimation.

4.2. SVM Classifier Test. The feature vector extracted from the training set and the corresponding sample label are used as the input of SVM, and LIBSVM is used to train the semantic classification of images. Because different kernel functions will lead to different classification results of support vector machine for nonlinear SVM classification problem, the selection of kernel function has an important impact on the performance of support vector machine. Considering that Gaussian radial basis function (RBF kernel) has fewer parameters and is easy to calculate and RBF kernel is a kernel function with strong locality, high flexibility, and accuracy, and it is also the most widely used kernel function. This paper uses Gaussian radial basis function (RBF kernel) to train radial basis function SVM classifier. The specific test results are shown in Figure 6.

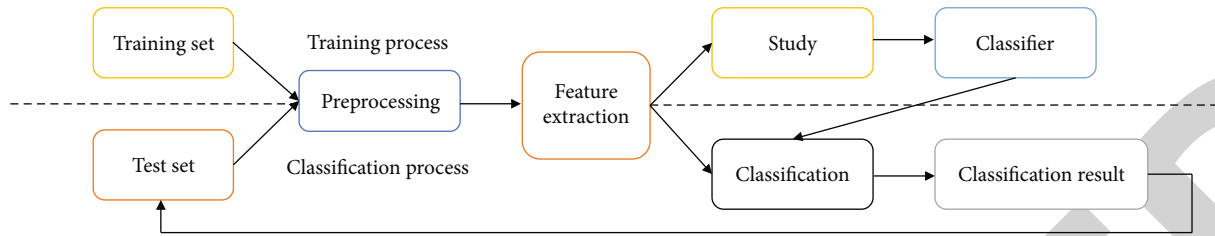


FIGURE 4: SVM experiment flow.

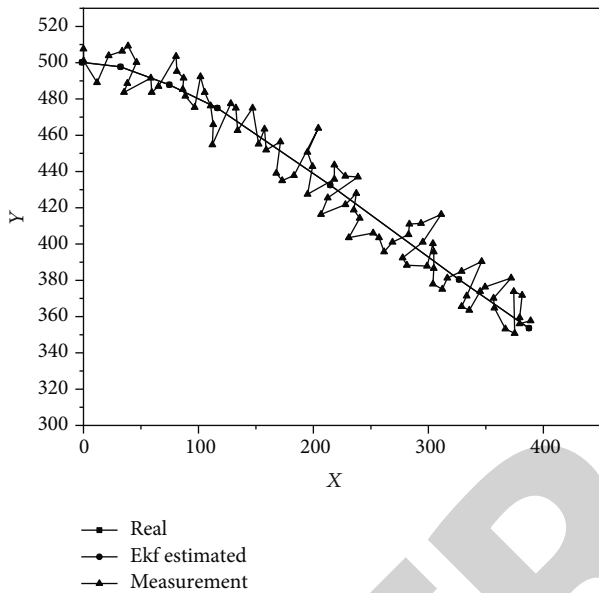


FIGURE 5: Relationship between actual value, observed value, and EKF estimated value of obstacle movement.

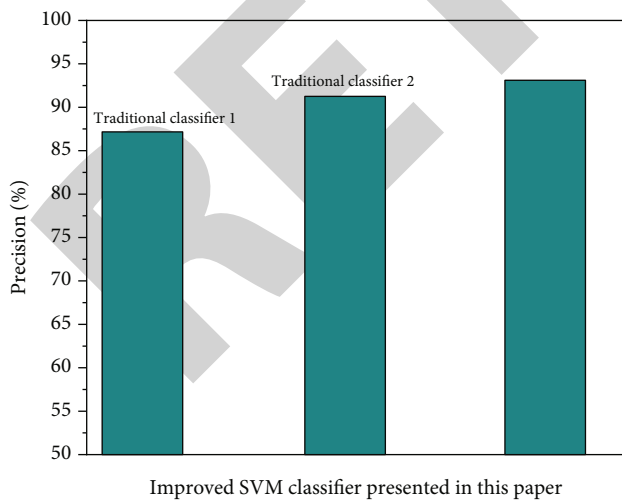


FIGURE 6: Comparison of classifier accuracy.

As shown in Figure 6, the accuracy of the improved SVM classifier in this article is much higher than that of the traditional method, and the effect of the improvement is obvious.

5. Conclusion

In order to realize substation intelligent inspection, it is imperative to develop substation inspection robot with autonomous navigation ability, and making the robot have the ability of environmental perception and intelligent information processing is the basis of autonomous navigation. Therefore, the research work of this paper mainly focuses on sensor calibration technology, lane line detection and robot positioning technology, obstacle detection and tracking technology, and substation road scene understanding technology. The detection of lane lines and obstacles is the basis of road scene understanding, and the calibration of sensors is a bridge to integrate the detection results of lane lines and obstacles. The innovation of this paper is as follows: combined with the environmental characteristics of substation, this paper explores and improves the methods of robot environment perception and scene understanding. The main research work of this paper includes the following:

- (1) A schematic diagram of the road ahead scene based on multisensor data fusion is proposed

For the macro description of the road scene in front of the robot, a geometric schematic diagram of the black-and-white road scene in front of the robot is proposed. Firstly, the results of lane line detection are used to distinguish road and nonroad areas. Through the processing of radar data, the characteristic information that can characterize the orientation and size of obstacles is extracted, and the results of sensor fusion are projected onto the image. The images of marked lane lines and obstacles are transformed into aerial view by inverse perspective transformation. Black represents the nonpassable area, and white represents the passable area. In black-and-white geometric form, the schematic diagram succinctly and intuitively shows whether a certain area is passable without redundant information, so as to highlight the characteristics of road obstacles and reduce the difficulty of robot scene understanding. Moreover, the schematic diagram is simple to obtain and can adapt to the changes of natural conditions such as lighting.

- (2) The front road scene recognition based on SVM is realized

To understand the front road map, an auxiliary vector machine (SVM) method is used to classify the front road map and define a schematic diagram. First, test the training

Retraction

Retracted: Automatic Modulation and Recognition of Robot Communication Signal Based on Deep Learning Neural Network

Journal of Sensors

Received 22 August 2023; Accepted 22 August 2023; Published 23 August 2023

Copyright © 2023 Journal of Sensors. This is an open access article distributed under the Creative Commons Attribution License, which permits unrestricted use, distribution, and reproduction in any medium, provided the original work is properly cited.

This article has been retracted by Hindawi following an investigation undertaken by the publisher [1]. This investigation has uncovered evidence of one or more of the following indicators of systematic manipulation of the publication process:

- (1) Discrepancies in scope
- (2) Discrepancies in the description of the research reported
- (3) Discrepancies between the availability of data and the research described
- (4) Inappropriate citations
- (5) Incoherent, meaningless and/or irrelevant content included in the article
- (6) Peer-review manipulation

The presence of these indicators undermines our confidence in the integrity of the article's content and we cannot, therefore, vouch for its reliability. Please note that this notice is intended solely to alert readers that the content of this article is unreliable. We have not investigated whether authors were aware of or involved in the systematic manipulation of the publication process.

Wiley and Hindawi regrets that the usual quality checks did not identify these issues before publication and have since put additional measures in place to safeguard research integrity.

We wish to credit our own Research Integrity and Research Publishing teams and anonymous and named external researchers and research integrity experts for contributing to this investigation.

The corresponding author, as the representative of all authors, has been given the opportunity to register their agreement or disagreement to this retraction. We have kept a record of any response received.

References

- [1] X. Zou and X. Zou, "Automatic Modulation and Recognition of Robot Communication Signal Based on Deep Learning Neural Network," *Journal of Sensors*, vol. 2022, Article ID 3519010, 7 pages, 2022.

Research Article

Automatic Modulation and Recognition of Robot Communication Signal Based on Deep Learning Neural Network

Xiaoguang Zou ¹ and Xiaoyong Zou ²

¹Zhejiang College, Shanghai University of Finance and Economics, Jinhua, Zhejiang 321013, China

²Jinhua Highway and Transportation Management Center, Jinhua, Zhejiang 321013, China

Correspondence should be addressed to Xiaoyong Zou; 201804307@stu.ncwu.edu.cn

Received 5 June 2022; Accepted 14 July 2022; Published 23 July 2022

Academic Editor: Haibin Lv

Copyright © 2022 Xiaoguang Zou and Xiaoyong Zou. This is an open access article distributed under the Creative Commons Attribution License, which permits unrestricted use, distribution, and reproduction in any medium, provided the original work is properly cited.

In order to solve the problem that the traditional method of manually extracting expert features for communication signal recognition has large limitations and low accuracy under low signal-to-noise ratio, this paper proposes an automatic modulation and recognition method of robot communication signal based on deep learning neural network. In this method, the received signal is preprocessed to obtain the complex baseband signal including in-phase component and quadrature component. The signal is used as the data set of the input convolution neural network model. The model structure and the super parameters such as convolution kernel, step size, characteristic graph, and activation function are adjusted through multiple training, and the trained model is used to extract and recognize the features of the communication signal. It realizes the identification and classification of seven types of digital communication signals: 2FSK, 4FSK, BPSK, 8PSK, QPSK, QAM16, and QAM64. The experimental results show that the average recognition accuracy of the seven signals has reached 94.61% when the signal-to-noise ratio is 0 dB. *Conclusion.* The algorithm is proved to be effective and has high accuracy under the condition of low signal-to-noise ratio.

1. Introduction

Recognition of communication signal modulation has a wide range of application requirements in modern wireless communication, and its typical application options are as follows: (1) In noncollaborative communication, the receiver cannot use the communication parameters effectively, especially the modulation mode, because the receiver does not know the sender's communication parameters. As tracking actions such as demodulation are performed, communication signal modulation recognition is widely used in noncollaborative communication options such as electronic countermeasures, communication intelligence, signal recognition, and electronic control. (2) In the cognitive radio system, it is hoped that the communication receiver will reach the universal level. The receiver will be able to receive the information sent by the sender accurately [1]. Recognition of signal modulation is a key technology in the general receiver model. Only by correctly defining the signal modulation mode can infor-

mation such as the signal bandwidth of the signal transmitter be calculated more accurately and thus facilitate subsequent operations. By signal demodulation and decoding. Therefore, studies to determine the modulation of communication signals are very important [2]. In today's increasingly complex environment of wireless communication, the space of electromagnetic signals is becoming more and more complex, the amount of information transmitted is increasing, and signal change is accelerating. Therefore, the study of automatic communication modulation signal recognition in high-speed modulation patterns is of great application [3].

In the noncooperative communication system and cognitive radio platform, the automatic modulation identifier of communication signal is a very key system component. The recognition performance of the modulation identifier is related to the normal and effective operation of the whole communication system. In this paper, it is a novel and ingenious method to realize communication signal modulation recognizer based on artificial neural network and graphics

processing unit (GPU) platform. It is an innovative idea to combine communication signal modulation recognition with the current hot artificial intelligence technology. Figure 1 shows a robot communication control device based on deep learning neural network.

2. Literature Review

Zhu et al. proposed a modulation recognition algorithm that can effectively recognize BPSK (binary phase shift keying) and QPSK (quadrature phase shift keying) signals from the perspective of average likelihood ratio for the first time. The algorithm estimates the carrier phase offset through ALRT and deduces the log likelihood ratio classification criteria to complete signal recognition [4]. Two years later, on this basis, they studied a quasi-optimized log likelihood ratio recognition algorithm, which further improved the recognition accuracy of BPSK and QPSK signals under the interference of additive white Gaussian noise (AWGN). Li et al. proposed a new PSK (phase shift keying) modulation classifier based on the maximum a posteriori probability criterion, which treats signal amplitude and noise variance as unknown deterministic variables and combines GLRT and ALRT to improve signal recognition performance [5]. Zeng et al. proposed a modulation recognition algorithm based on HLRT for multiple input multiple output (MIMO) scenarios. The algorithm first uses the channel estimation technique based on independent component analysis to estimate the relevant channel parameters, then uses the linear filter based on the minimum mean square error criterion to divide the MIMO channel into several subchannels, and uses the weighted sum rule to recombine the likelihood functions under each assumption to form a global likelihood function, so as to improve the algorithm performance [2]. Liu et al. studied the modulation recognition algorithm when the channel state information is unknown in the multicarrier scenario. First, the energy detector is used to confirm the working subcarriers, then the expectation maximization algorithm is used to estimate the channel state information, and finally, the HLRT function is constructed according to the estimated parameters to realize signal recognition [6]. Although the above modulation recognition algorithms can achieve high recognition rate, compared with the pattern recognition methods based on feature extraction, these algorithms have high computational complexity and are difficult to be applied in practical engineering projects. Therefore, how to reduce the computational complexity of these algorithms is also an important research direction of researchers. Arunkumar et al. studied an automatic modulation recognition algorithm based on normalized sixth-order cumulant. The algorithm simulates the channel propagation conditions in real scenarios. When the channel characteristic information is unknown, it successfully realizes the efficient recognition of BPSK, QPSK, 16QAM (quadrature amplitude modulation), and 64QAM [7].

Based on the above analysis, this paper studies a method of combining complex baseband signal with CNN and proposes a CNN model. This method can automatically learn the signal characteristics directly from the data. The model

first simulates and generates seven types of modulated signals under different signal-to-noise ratios and then processes the received signals into two channels of complex baseband IQ signals. After preprocessing the signals, the signals are used as the experimental data set. The data set is used to train the CNN model and adjust the super parameters. Finally, the trained CNN model is used to identify and classify the seven types of communication signals. Experiments show that the proposed method has better classification accuracy in the case of low signal-to-noise ratio, and the accuracy of classification and recognition method using convolution neural network after short-time Fourier transform is greatly improved.

3. Research Methods

3.1. Signal Modulation Model. There are three basic digital modulation modes: multiband frequency shift keying (MFSK), multiband amplitude shift keying (mask), and multiband phase shift keying (MPSK) [8, 9]. The three signals can be mathematically modeled as follows:

$$s_{\text{MFSK}}(t) = \sum_{i=0}^{N-1} A_0 \cos(2\pi f_c t + 2\pi f_i t + \theta_0) \cdot g_T(t - iT), \quad (1)$$

$$s_{\text{MPSK}}(t) = \sum_{i=0}^{N-1} A_0 \cos(2\pi f t + \theta_0 + \theta_i) \cdot g_T(t - iT), \quad (2)$$

$$s_{\text{MASK}}(t) = \sum_{i=0}^{N-1} A_i \cos(2\pi f_c t + \theta_0) \cdot g_T(t - iT), \quad (3)$$

where f_c is the initial carrier frequency, θ_0 is the initial phase, A_0 is the initial amplitude of the carrier, N is the number of observed symbols, T is the symbol period, $g_T(\cdot)$ is the waveform pulse formed in the symbol period, and $f_i \in \{f^{(1)}, f^{(2)}, \dots, f^{(M)}\}$ is the modulation frequency; $A_i \in \{A^{(1)}, A^{(2)}, \dots, A^{(M)}\}$ is the modulation amplitude; $\{2\pi/M(m-1), m=1, 2, \dots, M\}$ is the modulation phase.

On this basis, multiband quadrature amplitude modulation (MQAM) simultaneously uses the amplitude and phase of the carrier to modulate the transmission data [10]. The MQAM expression is as follows:

$$s_{\text{MQAM}}(t) = \sum_{i=0}^{N-1} A_i \cos(2\pi f_c t + \theta_0) \cdot g_T(t - iT). \quad (4)$$

The general expression of the modulated signal obtained from (1)–(4) is as follows:

$$s(t) = A(t) \cdot \cos[2\pi f_c t + 2\pi f(t)t + \theta(t) + \theta_0], \quad (5)$$

where $s(t)$ represents continuous time series signal. According to formula (5), seven modulation models are obtained by changing its frequency, phase, amplitude, or other parameters.

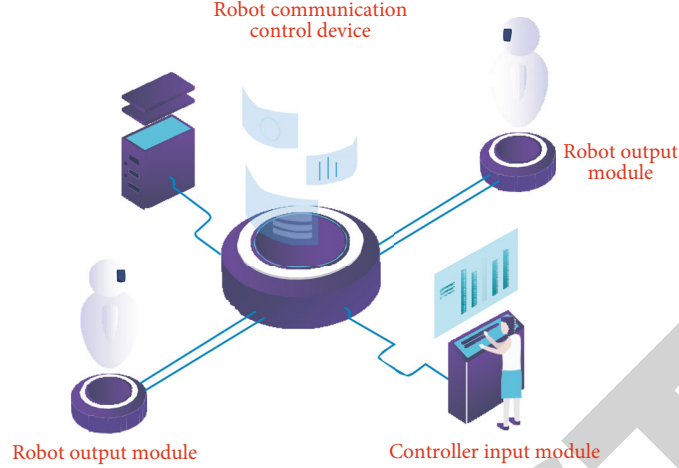


FIGURE 1: A robot communication control device based on deep learning neural network.

3.2. Data Set Generation and Preprocessing. Digital down converter (DDC) is used to process the signal obtained from formula (5) to obtain a complex baseband signal including in-phase component and quadrature component. The general expression is as follows:

$$\begin{aligned} I(n) &= A(n) \sin(\omega_0 n + n\omega(n) + \varphi(n) + \varphi_0), \\ Q(n) &= A(n) \cos(\omega_0 n + n\omega(n) + \varphi(n) + \varphi_0), \end{aligned} \quad (6)$$

where $I(n)$ represents the in-phase component of the modulated signal, and $Q(n)$ represents the quadrature component of the modulated signal. After passing through the channel, the received signal $y(n)$ can be described as the following equation:

$$y(n) = \sum_{i=1}^N C_i e^{-j2\pi f_i(n-k_i)} \cdot (I(n-k_i) + Q(n-k_i)) + v(n), \quad (7)$$

where C_i and k_i represent subpath gain and delay, f_i is Doppler frequency, and $v(n)$ represents additive white Gaussian noise (AWGN) [11].

In reality, in addition to channel noise, the accuracy of modulation signal identification is also affected by intersymbol interface (ISI) and frequency offset. Due to the existence of intersymbol crosstalk in the channel, in order to eliminate the impact of intersymbol crosstalk on the recognition accuracy, according to the Nyquist criterion, a raised cosine transmit filter (RCTF) is used to eliminate inter symbol crosstalk, so that each complex value signal passes through a raised cosine filter with a roll off coefficient of 0.4. The impulse response of the raised cosine filter is as follows:

$$h_{RC}(n) = \frac{\sin(\omega_0 n) \cdot \cos(\omega_0 \alpha n)}{\omega_0 n \cdot [1 - (2\alpha \omega_0 n / \pi)^2]}, \quad (8)$$

where α is the roll off coefficient of the raised cosine filter and f_0 is the bandwidth of the filter.

To sum up, this paper considers the pretreatment process of input data set under AWGN channel conditions as shown in Figure 2.

3.3. Working Principle of Modulation Recognition Method Based on Convolutional Neural Network

3.3.1. Structure of Convolutional Neural Network. The process of modulation recognition using convolutional neural network structure is as follows: Firstly, the preprocessed seven types of modulation signals are processed into training set and test set, respectively; then, the CNN model is trained through the training set, and the super parameters of the CNN model are fine tuned. After the training, the CNN model is tested by inputting the test set, and finally, the digital communication signals are recognized and classified [12].

Convolutional neural network is a multilayer neural network with forward feedback, which is composed of convolution layer, pooling layer, and full connection layer. The neurons of each layer in the convolutional neural network automatically extract features from the input data, so as to update the weights of neurons of each layer [13]. The working principle of the neuron is shown in Figure 3. The n input vectors $[x_1, x_2, \dots, x_n]$ and their corresponding weight vectors $[w_1, w_2, \dots, w_n]$ are used as the inner product, plus the bias b , and then, the output $f(x; w, b)$ is obtained through the nonlinear activation function $h(\sum_i w_i x_i + b)$. Convolutional neural network has the characteristics of local perception and weight sharing, which can reduce the number of training parameters and computational complexity [14].

- (1) Convolution layer is used to extract features from input data. The input data is generally the characteristic matrix. The convolution kernel size and moving step size of each convolution layer are manually set. Convolution operation is carried out through the convolution kernel and the characteristic matrix of the upper layer. After each data window is calculated, the convolution kernel shifts to the next

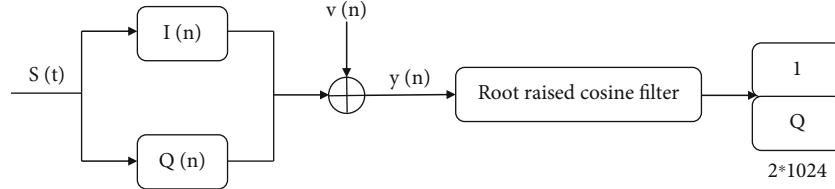


FIGURE 2: Schematic diagram of data set generation.

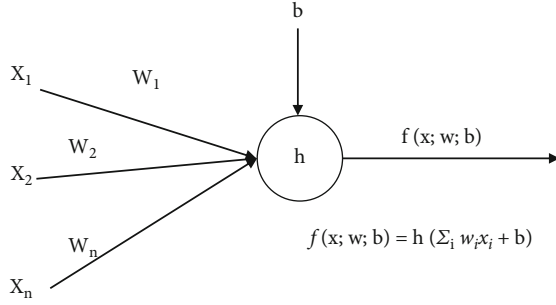


FIGURE 3: Working principle of neuron.

position, and the output characteristic matrix is obtained by activating the function. The calculation formula of convolution layer is as follows:

$$Y_j^l = f\left(\sum x_i^{l-1} * k_{ij}^l + b_j^l\right), \quad (9)$$

where l is the number of network layers, $f(\cdot)$ is the activation function, x is the input vector matrix, k is the convolution kernel matrix, b is the bias, Y is the output matrix, and j is the number of characteristic graphs [15].

- (2) The pooling layer can effectively reduce the matrix size and latitude and further reduce the parameters in the full connection layer. The forward propagation process of the pool layer is similar to that of the convolution layer, and the size and step length of the sliding window matrix need to be manually specified. In this paper, the pool layer takes the maximum value of each sliding window as the output, and the output is also in the form of a three-dimensional matrix, as shown in the following formula:

$$Y_j^l = f\left(\omega_j^l \max \left\{x_{N \times M}^l\right\} + b_j^l\right), \quad (10)$$

where x is the matrix of input characteristics in the pool layer, and $N \times M$ is the size of the pool sliding window.

- (3) The full connection layer connects all neurons with all neurons of the upper layer and outputs a two-dimensional matrix form of $1 \times N$. Since the output dimension after passing through the full connection layer is different from the original input dimension, it is finally necessary to connect with softmax. For

samples of specified categories, the probability of each category is finally calculated [16]. The probability that softmax regression marks sample $x^{(i)}$ as a category is as follows:

$$p\left(y^{(i)} = j \mid x^{(i)}; \theta\right) = \frac{e^{\theta_j^T x}}{\sum_{l=1}^k e^{\theta_l^T x}}. \quad (11)$$

Softmax cross entropy loss function is as follows:

$$L(\theta) = \frac{1}{M} \left[\sum_{i=1}^M \sum_{j=1}^k I\{y^{(i)} = j\} \log \frac{e^{\theta_j^T x}}{\sum_{l=1}^k e^{\theta_l^T x}} \right], \quad (12)$$

where $y^{(i)}$ is one hot code form, and if $y^{(i)} = j$ is true, then $I\{j\} = 1$; otherwise, $I\{j\} = 0$, k is the category, and M is the number of samples.

When training the neural network, in order to minimize the cross entropy loss function, the adaptive moment (Adam) optimization algorithm is used to update the weights [17]. Adam has the advantages of both momentum algorithm and root mean square propagation (rmsprop) algorithm. By calculating the adaptive learning rate of the first-order moment estimation and second-order moment estimation of the loss function, the global optimal solution can be quickly obtained. The specific steps are as follows.

Step 1. Initialize the first-order moment estimation of loss function gradient $m_w = 0$, the second-order moment estimation of loss function gradient $v_w = 0$, the number of iterations $t = 0$, and the training set $D = \{x^{(i)}, y^{(i)}\}, i = 1, 2, \dots, N$.

Step 2. Update iteration number $t \leftarrow t + 1$.

Step 3. Randomly take M subsets from training set D to obtain $D_m, D_m = \{x^{(i)}, y^{(i)}\}, i = 1, 2, \dots, M$. Carry out the feedforward operation of the neural network and calculate the output $\hat{y}^{(i)} = f(x^{(i)}; w)$.

Step 4. Calculate the gradient ∇L of the loss function.

$$\nabla L = \frac{\partial \left[\frac{1}{M} \sum_{i=1}^M L(y^{(i)}, \hat{y}^{(i)}) + \Omega(w) \right]}{\partial w}, \quad (13)$$

where $L(y^{(i)}, \hat{y}^{(i)})$ is called loss function, which measures the difference between the real output and the expected

output of the training sample, and $\Omega(w)$ is called L2 regularization term to prevent overfitting, as shown in the following formula.

$$\Omega(w) = \frac{1}{2} |\omega|^2. \quad (14)$$

Step 5. Update $m_w^{t+1} \leftarrow \beta_1 m_w^t + (1 - \beta_1) \nabla L^t$ and calculate its correction value as follows:

$$\bar{m}_w = \frac{m_w^{i+1}}{1 - \beta_1^{i+1}}. \quad (15)$$

Update $\bar{v}_w^{t+1} \leftarrow \beta_2 m_w^t + (1 - \beta_2) (\nabla L^t)^2$ and calculate its correction value as follows:

$$\bar{v}_w = \frac{v_w^{t+1}}{1 - \beta_2^{t+1}}. \quad (16)$$

Step 6. Update weight $w^{t+1} \leftarrow w^t - \eta \bar{m}_w / \sqrt{\bar{v}_w} + \varepsilon$, where β_1 is the weighted index, $\beta_1 = 0.9, \beta_2 = 0.999$, η is the learning rate to be fine tuned during training, and ε is the smoothing factor, $\varepsilon = 10^{-8}$ [18].

Step 7. Return to Step 2 and continue training until the stop condition is reached.

3.3.2. CNN-IQ Convolutional Neural Network Model. This paper presents a convolutional neural network model named CNN-IQ [19]. CNN's model framework consists of one input layer, two convolution layers (Conv), two Maxpool layers, one fully connected (Fc) layer, and one softmax classifier. Finally, the modulation types of seven signals are output (see Table 1 for model parameters).

The input layer inputs a 2-dimensional matrix with the size of 2×1024 ; Conv1 convolution kernel has a size of 1×2 , a depth of 256, and a step size of 1×1 . It is filled with all zeros. After convolution calculation, 256 2×1024 characteristic graphs are obtained. There are a total of $2 \times 512 \times 256 \times (1 \times 2 + 1) = 786432$ connections in this layer. Maxpool1 sliding window size is 1×2 , step size is 1×2 , and all zero filling is used to obtain 256 2×512 characteristic graphs [20]. In conv2, the convolution kernel size is 2×2 , the depth is 128, and the step size is 1×1 . All zero filling is not used. The two convolution layers use the rectified linear unit (Relu) as the activation function. The activation function makes the whole neural network model nonlinear. After convolution calculation, 256 1×511 characteristic graphs are obtained. There are $1 \times 511 \times 256 \times (2 \times 2 + 1) = 654080$ connections in this layer. The size of maxpool1 sliding window is 1×2 , the step size is 1×1 , and all zero padding is used to obtain 128 1×128 characteristic graphs. The full junction layer is composed of 256 neurons in total. The full junction layer has $1 \times 128 \times 128 \times 256 + 256 = 4184560$ connections. Finally, the number of softmax layer output nodes is 7 [21]. In order to avoid over fitting, a dropout with $P = 0.5$ is set at the full connection layer. The dropout method can randomly delete half of the neurons in the network while keep-

TABLE 1: Parameters of CNN-IQ model.

Layer	Convolution kernel	Step length	Characteristic diagram	Output
Input			1	$2 * 1024$
Conv1	$1 * 2$	$1 * 1$	256	$2 * 1024$
Maxpool1	$1 * 2$	$1 * 2$	256	$2 * 512$
Conv2	$2 * 2$	$1 * 1$	256	$1 * 511$
Maxpool2	$1 * 2$	$1 * 2$	128	$1 * 128$
Fc			256	$1 * 256$
Softmax			7	$1 * 7$

ing the input and output neurons unchanged, which can further improve the reliability of the model and prevent over fitting.

4. Result Analysis

4.1. Preparation of Experimental Data Set. In order to train convolutional neural network model, a large number of training set and test set sample data sets are required. In the experiment, Matlab is used to generate IQ data of seven digital signal models, including 2FSK, 4FSK, BPSK, 8PSK, QPSK, qam16, and QAM64. Each type of signal in the data set consists of 1024 sample points and is saved in a 2×1024 matrix format. The first row of the matrix is I-channel signal, and the second row is Q-channel signal. The specific division of the data set is shown in Table 1. The signal-to-noise ratio of the data set ranges from -10 dB to 18 dB with an interval of 2. Parameters for signal generation: the sampling frequency is 1000 Hz, the carrier frequency is 100 Hz, and the number of symbols is 256. The training set includes 49000 samples, and the test set includes 4200 samples. The signal sample label adopts one hot coding format [22].

The experimental environment is as follows: the graphics card is Titan x GPU, the processor is Intel (R) Xeon (R) CPU E5-2620v3@2.40 GHz, and the memory is 10 GB. Software environment: the data set is generated under Matlab2016b in Windows 10. The training of convolutional neural network is built under the framework of tensorflow1.12 in Ubuntu system. The development language is python3.6.

4.2. Analysis of Experimental Results. In the experiment, the learning rate starts from 0.001 to train the framework CNN-IQ. When the loss value of the test set during training is greater than the maximum loss value at this time, the learning rate at this time is multiplied by 0.02 to correct the learning rate. There are 100 rounds of training in the experiment, and each round takes about 23 seconds. Figure 4 is a graph of the training loss value, the validation loss value, and the training rounds. With the increase of rounds, the training loss and the validation loss both decrease rapidly, and the two curves gradually converge, indicating that there is no overfitting in the experimental model. After epochs = 38, the loss value is basically stable, and the two curves of training loss and validation loss converge. When epochs = 100, the validation loss value is 0.035, and the loss value at this

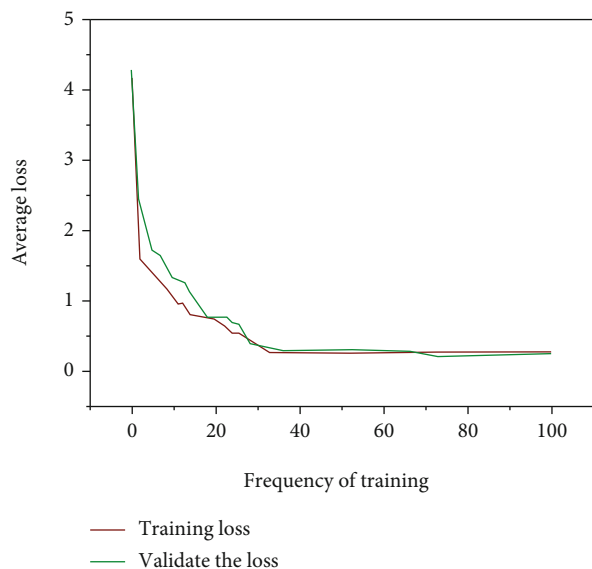


FIGURE 4: Variation of training loss and verification loss with training times.

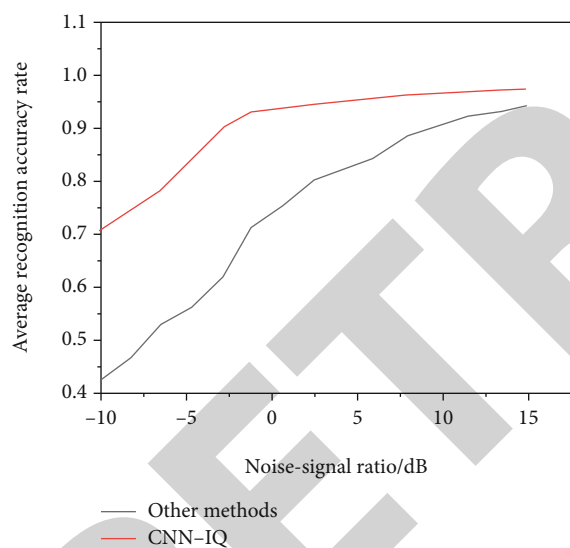


FIGURE 5: Average recognition accuracy of two methods under different signal-to-noise ratios.

time has reached the minimum value. A good convolutional neural network model framework and weights are saved to facilitate the transfer training of the CNN-IQ model [23].

In order to evaluate the range recognition performance of other methods under the same data set compared to our CNN-IQ method, we analyzed the effect of the two methods on the recognition accuracy as the signal-to-noise ratio increased. The analysis in Figure 5 shows that the accuracy of the method in this document is significantly improved compared to other methods when the signal-to-noise ratio is low. The results of the analysis shown in Figure 5 show that the method of this document improves the accuracy by approximately 25.41% when the signal-to-noise ratio is less than 0 dB. When the signal-to-noise ratio is equal to

0 dB, the average accuracy of this paper reaches 94.61%, while the average accuracy of other methods is 72.13%. When the signal-to-noise ratio is 18 dB, the accuracy level of the method in this document reaches 98.85%, while the accuracy level of other methods is 95.32%. Compared to other methods, the accuracy of CNN-IQ is significantly improved when the signal-to-noise ratio is low, and the accuracy is somewhat improved when the signal-to-noise ratio is high.

5. Conclusion

In order to determine digital communication signals, this paper proposes a method for determining modulation based on a complex backbone signal using a disruptive neural network. First, a method is developed to process the generated digital signal into a complex signal, and then, the data is preprocessed, and the disrupted neural network built on the generated data set is trained. The value loss is minimal and combined, offering the CNN-IQ model and finally using the CNN-IQ model to learn the transmission of seven types of digital communication signals. The simulation results show that the method in this document is effective in recognizing digital communication signals, and that the signal recognition accuracy is greatly improved when the signal-to-noise ratio is low. The next step is to consider a dual-channel neural network, to study how to reduce the structure and parameters of the circulatory neural network, and to further improve the speed of the entire recognition process, while maintaining a high degree of acceptance.

Data Availability

The data used to support the findings of this study are available from the corresponding author upon request.

Conflicts of Interest

The authors declare that they have no conflicts of interest.

References

- [1] W. Yan, L. C. Qian, D. Yj, and Z. Hao, "Communication modulation signal recognition based on the deep multi-hop neural network," *Journal of the Franklin Institute*, vol. 358, no. 12, pp. 6368–6384, 2021.
- [2] Q. Zeng, F. Xiao, Q. Ren, and S. Ai, "Modulation signal analysis and parameter selection for modular multi-level converters with harmonic injection method," *Journal of Power Electronics*, vol. 20, no. 2, pp. 455–465, 2020.
- [3] A. A. F. Júnior, J. Ribeiro, and D. H. Spadoti, "Large signal analysis on intensity-modulation direct-detection radio-over-fibre dispersive links," *Electronics Letters*, vol. 58, no. 3, pp. 112–114, 2022.
- [4] J. Zhu, P. Zhang, R. Yang, and Z. Wang, "Analyzing electrostatic modulation of signal transduction efficiency in MoS₂ nanoelectromechanical resonators with interferometric readout," *SCIENCE CHINA Information Sciences*, vol. 65, no. 2, pp. 1–7, 2022.

Retraction

Retracted: Mathematical Modeling Analysis of Data Attribute Encryption for Robot

Journal of Sensors

Received 22 August 2023; Accepted 22 August 2023; Published 23 August 2023

Copyright © 2023 Journal of Sensors. This is an open access article distributed under the Creative Commons Attribution License, which permits unrestricted use, distribution, and reproduction in any medium, provided the original work is properly cited.

This article has been retracted by Hindawi following an investigation undertaken by the publisher [1]. This investigation has uncovered evidence of one or more of the following indicators of systematic manipulation of the publication process:

- (1) Discrepancies in scope
- (2) Discrepancies in the description of the research reported
- (3) Discrepancies between the availability of data and the research described
- (4) Inappropriate citations
- (5) Incoherent, meaningless and/or irrelevant content included in the article
- (6) Peer-review manipulation

The presence of these indicators undermines our confidence in the integrity of the article's content and we cannot, therefore, vouch for its reliability. Please note that this notice is intended solely to alert readers that the content of this article is unreliable. We have not investigated whether authors were aware of or involved in the systematic manipulation of the publication process.

Wiley and Hindawi regrets that the usual quality checks did not identify these issues before publication and have since put additional measures in place to safeguard research integrity.

We wish to credit our own Research Integrity and Research Publishing teams and anonymous and named external researchers and research integrity experts for contributing to this investigation.

The corresponding author, as the representative of all authors, has been given the opportunity to register their agreement or disagreement to this retraction. We have kept a record of any response received.

References

- [1] J. Sun, J. Yan, and D. Yang, "Mathematical Modeling Analysis of Data Attribute Encryption for Robot," *Journal of Sensors*, vol. 2022, Article ID 3976806, 8 pages, 2022.

Research Article

Mathematical Modeling Analysis of Data Attribute Encryption for Robot

Jingyi Sun ¹, Jie Yan ² and Dingyi Yang ²

¹Department of Basic Education and Research, Changchun Finance College, Changchun, Jilin 130028, China

²School of Information Technology, Changchun Finance College, Changchun, Jilin 130028, China

Correspondence should be addressed to Jingyi Sun; 1333307202@post.usts.edu.cn

Received 24 May 2022; Revised 25 June 2022; Accepted 4 July 2022; Published 23 July 2022

Academic Editor: Haibin Lv

Copyright © 2022 Jingyi Sun et al. This is an open access article distributed under the Creative Commons Attribution License, which permits unrestricted use, distribution, and reproduction in any medium, provided the original work is properly cited.

Encrypting data based on the data attributes of robots is one of the effective methods to control access users in the data outsourcing environment. Therefore, a mathematical modeling method of robot data attribute encryption based on data redundancy elimination technology is proposed. The encryption algorithm structure is analyzed based on the Bloom filter. The Hamming distance is used to calculate the similarity of big data by the Bloom filter. Finally, a big data ellipse encryption algorithm is designed according to the calculation results. The results show that during the whole experiment, the approximate fluctuation range is 0.08%~0.14%, which is not only high but also has a large fluctuation range. In contrast, the probability of occurrence of redundant data is less than 0.05% under different byte rates of redundant data, which is far lower than the two traditional methods, indicating that the application performance of the proposed method is good.

1. Introduction

The mathematical modeling of big data attribute encryption uses mathematical methods to solve the problem of data encryption. Data encryption based on big data attributes is one of the effective methods to control data access users in the data outsourcing environment, but in the calculation process, it is impossible to realize the parallel application of multiple encryption methods. If the method is constantly updated, it will affect the execution efficiency of the overall algorithm and increase the time overhead [1]. In order to solve this problem, experts in relevant fields have obtained some good research results. According to the above situation, in the case of cloud computing data outsourcing environment, researchers propose a new method to expand data access and improve the security performance of encryption algorithm as a whole. For big data in multiauthority cloud, combined with improved attribute encryption, they propose a flexible and secure access control model, design a new policy update process based on improved proxy reencryption, and formulate an efficient policy update

scheme [2, 3]. However, this method has the problem of more redundant data in the process of big data encryption. Other scholars have proposed a full homomorphic encryption method of multisource information resources in cloud computing environment with short public key, adding a set of homomorphic encryption of perceptual resources with the same remainder pair, extracting the real resources from the ciphertext data after additive fusion, then using the Chinese remainder theorem to verify the integrity of resources, and finally fusing the new security parameters into the integrity verification parameters. After linear conversion, the number of public key elements is reduced and the size of public key is improved [4, 5]. This method still has the problem that the encryption algorithm takes a long time. To solve the problems of the above traditional methods, we offer a mathematical modeling method for encrypting large data properties based on information resource technology. The structure of the encryption algorithm is analyzed based on the Bloom filter. Use the Hamming space to calculate the similarity of large data through a Bloom filter. Finally, the big data elliptic encryption

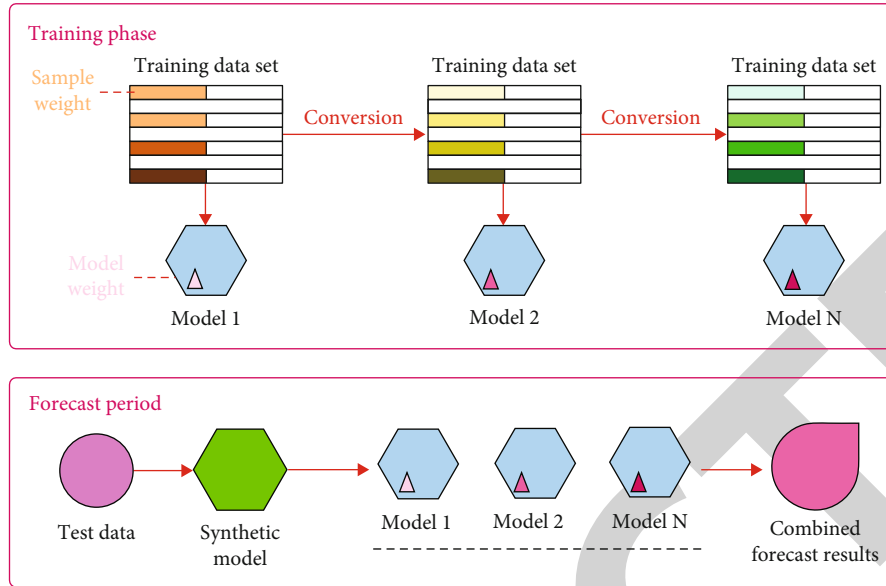


FIGURE 1: Common algorithms and redundancy elimination algorithms in encryption mathematical modeling teaching.

algorithm is designed according to the calculation results. Figure 1 shows the redundancy elimination algorithm commonly used in encryption mathematical modeling teaching.

2. Literature Review

The rapid development of technologies such as cloud computing, Internet of Things, and social networking has led to a rapid increase in network information flows from GB to TB, PB, EB, and even ZB [6]. The sheer size of the data, the rapid flow of data, the dynamic data system, the variety of data types, and the enormous value of big data have brought enormous impacts and challenges to the security and privacy of user information assets [7, 8]. Traditional data encryption storage and management methods have struggled to meet large data requirements in terms of encryption speed, storage capacity, and security [9, 10]. In addition, most data acquisition systems, such as satellite data signal acquisition, radar echo signal data acquisition, and digital video signal processing, require real-time and safe data transmission, which puts forward higher requirements for the transmission speed, storage speed, storage capacity, and security of the data acquisition and storage system [11, 12]. Secure storage of big data: the amount of data has increased from GB to EB and ZB and continues to grow explosively [13, 14]. According to IDC's report in March 2008, individual users just entered the TB era in 2006, and about 180 EB of data was generated worldwide: in 2007, the global new data volume was 281 EB, an increase of about 75% over the previous year, while the total capacity of all available storage media was 264 EB, and the new data volume has exceeded 6% of the capacity of all available storage media. The total amount of global data in 2011 was 10 times that in 2006, reaching 1.8 ZB [15]. In addition to the above typical examples, several other main sources of large-scale data are shown in Table 1:

In March 2009, a large number of Google users' data were stolen. In 2011, Nate, one of the three major portals in South Korea, and Saiwo, a social network, were attacked by hackers, resulting in the disclosure of 35 million user information: in April 2011, Sony's system vulnerability led to the theft of 77 million user data. On December 21, 2011, the data of 6 million users on CSDN, China's largest programmer community, was made public [16]. The files published by hackers contain a large number of user email accounts and password information. In August 2012, Shengda cloud enterprise lost a large amount of data of users due to virtual machine failure [17, 18]. Recently, Amazon has also constantly exposed various security incidents of big data in the cloud computing environment [19]. According to Gartner's 2012 survey report, more than 60% of enterprise CTOs believe that the main reason for not adopting cloud computing technology in the short term is that big data faces problems in security and privacy protection. From simple data to trade secrets to intellectual property rights, the disclosure of big data may lead to reputation damage, economic losses, and even legal sanctions [20].

In the process of big data security protection, potential threats may lead to some more basic threats. Common potential threats can be divided into the following four types: (1) eavesdropping, (2) traffic analysis, (3) information leakage caused by carelessness of operators, and (4) information leakage caused by media waste. Figure 2 shows some typical threats faced by big data and their relationship. The paths in the figure can be staggered. For example, counterfeiting attack can become the basis of all basic threats. At the same time, counterfeiting attack itself also has the potential threat of information disclosure.

The strength of big data security system is equal to that of its weakest link, and its security protection needs to combine different types of threat countermeasures. Therefore, the security protection technology of big data involves a very wide range of fields, including physical security, personnel security,

TABLE 1: Other sources of big data.

Serial number	Data category	Source
1	Sensor data	Sensor perception of environment
2	Click stream data	Click stream of users on the Internet
3	Mobile device data	Mobile phone, PDA, navigation, etc.
4	RFID data	Wide application of RFID

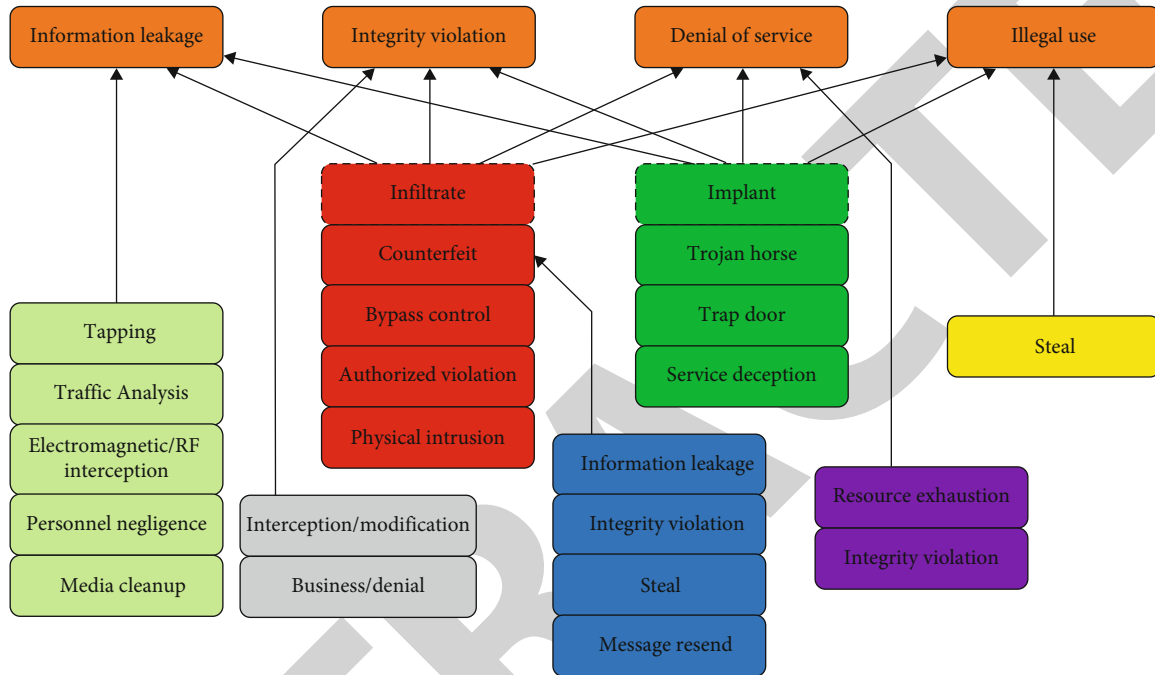


FIGURE 2: Typical threats and their relationships.

management security, media security, radiation security, and life cycle security (the process from the generation of big data to the demise of big data is called the life cycle of big data). No matter which link, big data encryption algorithm is the basis for the protection of big data. Limited to space, this paper only discusses the security problems related to big data encryption algorithms. Considering the existing powerful cryptographic analysis methods, such as differential cryptographic attack, linear cryptographic attack, integral attack, algebraic attack, man in the middle attack, and related key attack, we have to consider using more complex encryption algorithms and protective measures to protect the security of big data. To sum up, the amount of data in the era of big data increases nonlinearly. The increasing amount of data makes the traditional security and encryption tools no longer as effective as before. Modern cryptosystems are mostly designed for the needs of text data encryption and are not well combined with the characteristics of big data, so it is difficult to meet the actual application needs [21, 22]. The secure storage and data protection of big data are facing unprecedented pressure and challenges. Simply relying on increasing encryption, storage devices and bandwidth cannot fundamentally solve the problem, and new technical solutions must be sought. Based on this, this paper proposes a

scheme that can meet the symmetric cryptographic algorithm and asymmetric encryption algorithm of big data and makes a new attempt for attribute encryption of big data.

3. Research Methods

3.1. Big Data Redundancy Elimination Algorithm Based on Similarity Calculation. In the space of data structure Bloom filter, it has the advantages of high data compression efficiency. The eigenvalue of the algorithm is composed of the representation of the Bloom filter data structure [23]. Compared with the traditional data redundancy elimination algorithm, the Bloom filter algorithm has more advantages in query time and space efficiency and is more suitable for processing large data.

Assuming that a certain data is a shingle, the construction method of the Bloom filter can be formed according to the following points:

- (1) Construct BF data structure, where the structure is m bits and the initial value of all data is 0
- (2) Suppose that the mapping function is two hash functions, including hASH1 and hASH2 functions

- (3) Use the two functions in (2) to calculate the summary value in each shingle, and on this basis, set the bit value corresponding to BF as 1
- (4) The characteristic value of the file is BF of the output

According to the above research and analysis, in the process of calculating the similarity of big data, this paper uses the Hamming distance to determine the similarity through the Bloom filter. The Hamming solution method mainly calculates the corresponding different numbers in two binary sequences. In addition, there are four methods to solve the similarity, namely, cosine, overlap, dice, and Jaccard. The calculation method is shown in

$$\text{Cosine_sim}(x, y) = \frac{\bar{X} \cdot \bar{Y}}{\|\bar{X}\| \cdot \|\bar{Y}\|} = \frac{\sum_{i=1}^n X_i Y_i}{\sqrt{\sum_{i=1}^n X_i^2 \sum_{i=1}^n Y_i^2}}, \quad (1)$$

$$\text{Overlap_sim}(x, y) = \frac{\sum_{i=1}^n X_i Y_i}{\min(\sum_{i=1}^n X_i^2, \sum_{i=1}^n Y_i^2)}, \quad (2)$$

$$\text{Dice_sim}(x, y) = \frac{2 \sum_{i=1}^n X_i Y_i}{\sum_{i=1}^n X_i^2 + \sum_{i=1}^n Y_i^2}, \quad (3)$$

$$\text{Jaccard_sim}(x, y) = \frac{\sum_{i=1}^n X_i Y_i}{\sum_{i=1}^n X_i^2 + \sum_{i=1}^n Y_i^2 - \sum_{i=1}^n X_i Y_i}. \quad (4)$$

In formula, $\text{sim}(x, y)$ represents the similarity function. $\bar{X} \cdot \bar{Y} = \sum_{i=1}^n X_i Y_i$. According to the above process, the similarity between the two big data can be calculated.

Data redundancy elimination technology is also known as data compression technology [24–26]. The working principle of redundancy elimination technology is to delete two or more duplicate data in a data set to ensure that only the same data in the last data set is retained, so that the deleted redundant data will be replaced by data pointer. In this process, the data blocks in the data set will be shared by multiple data files at the same time, and the sharing relationship is shown in Figure 3.

According to Figure 3, in the data redundancy storage system, if a data block is damaged, multiple files may be unavailable at the same time. In the process of big data attribute encryption, the data storage space can be optimized through data redundancy elimination technology. Therefore, deleting the same data block in the data set in the processing process can reduce the workload of data encryption and improve the efficiency of data encryption. In addition, after deleting the redundant data in the data set, the data compression efficiency is improved and the number of transmitted data is reduced, so that the bandwidth of the transmission channel can be fundamentally alleviated.

When judging the reduction rate of data, it is mainly realized by the ratio of the number of bytes before the deletion of redundant data to the number of bytes processed. According to this result, the DER calculation formula is as follows:

$$\text{DER} = \frac{\text{Bytes In}}{\text{Bytes Out}}, \quad (5)$$

where data elimination ratio (DER) represents the discernible coding rule, bytes is the number of bytes, Bytes Out represents byte output, and Bytes In represents byte input. In general, the value of DER can be determined according to two conditional factors; that is, it does not strictly consider the overall cost of the original data. In order to better optimize the data overhead and optimize the calculation formula of data reduction rate, set DER as

$$\text{DER} = \frac{\text{DER}}{1 + f}, \quad (6)$$

In this way, according to the calculation results of the above formula, we can know that the cost of the original data is f , and its calculation method is shown in

$$f = \frac{\text{Metadata Size}}{\text{Average ChunkSize}}, \quad (7)$$

where Metadata Size represents the metadata size and Average ChunkSize represents the average block size.

3.2. Proposal of Big Data Encryption Algorithm. According to the above data similarity calculation results, this paper proposes an elliptic curve encryption algorithm (ECC) to realize the encryption of big data. The algorithm has the advantages of low computational overhead and high encryption security performance in the encryption process. The encryption principle security of the algorithm is based on the difficulty of curve discrete logarithm (ECDLP). Because ECC algorithm can use relatively short key to obtain the corresponding encryption security in practical application, it can fundamentally reduce part of the overhead in the overall calculation process.

The evaluation indexes of block cipher working mode mainly include the security performance of data encryption, the application performance after encryption, and the characteristic points in the calculation process, which are specifically expressed as follows:

- (1) Safety performance
 - (a) After encrypting the data, the data set can resist the attack
 - (b) Whether the overall security of the data set can be verified
 - (c) Whether the statistical characteristics of the output information of encrypted data are random
- (2) Application performance after encryption: this performance index mainly refers to the effectiveness in the calculation process, whether the storage space requirements are met, and the data preprocessing ability
- (3) Execution feature: this feature mainly refers to the password services that can be provided

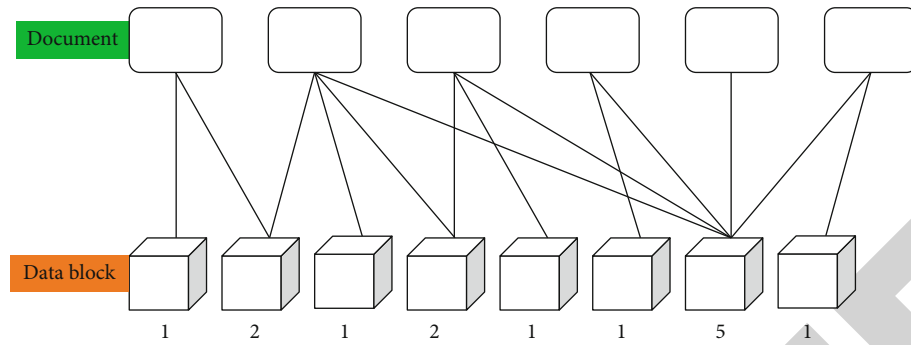


FIGURE 3: Relationship between file and data block.

The ECC offers an encryption scheme that combines the characteristics of an encryption algorithm and a block cipher algorithm to fully satisfy a combination of symmetric encryption algorithms and asymmetric encryption algorithms in a large data encryption process. The mathematical model of attribute encryption is presented in Figure 4.

3.3. Redundant Data Detection. Excess data detection is used to detect additional data that needs to be encrypted, and then the duplicate data in the data is deleted according to the detection results. The size of the data is described as the total number of files. The execution steps are as follows:

- (1) Initialize the contents in the hash function table, and on this basis, use the data file complete detection algorithm. In the process of detection and calculation, this paper will take the data file that needs to be encrypted separately as the granularity, preliminarily detect the duplicate data in the data file, and then get the hash function value according to the detection results
- (2) Compare the results of the values in the steps above with the results of the values stored in the hash function table. If the two values are the same or the error between them is within a reasonable, acceptable range, use the pointer to replace one of the files. If the matching values are different or the error is too large, it is two completely different data files, and the two data files need to be stored separately
- (3) In the complete document detection method, the data files that do not repeat each other are re-archived. In the process, this paper will use the CDC data block calculation method to archive them one by one from the source of the file
- (4) Input the data file after the archive partition into the data transmission stream in different areas again, and use the Bloom filter data structure to detect the data

3.4. Plaintext Encryption after Preprocessing. In the actual calculation process, the key length is 128192256 bits and the packet length is 128 bits. The calculation process is as follows:

(1) Numerical initialization

Here, the 128 bit message packet is divided into 16 bytes and marked as

$$\text{Inputblock} = m_0, m_1, \dots, m_{15}. \quad (8)$$

According to the calculation result of the above formula, the key grouping formula is expressed as

$$\text{InputKey} = m_0, m_1, \dots, m_{15}, \quad (9)$$

where Inputblock represents the input module, InputKey represents the input key, m represents the input byte, and the internal data structure is

$$\text{Inputblock} = \begin{pmatrix} m_0 & m_4 & m_8 & m_{12} \\ m_1 & m_5 & m_9 & m_{13} \\ m_2 & m_6 & m_{10} & m_{14} \\ m_3 & m_7 & m_{11} & m_{15} \end{pmatrix}, \quad (10)$$

$$\text{InputKey} = \begin{pmatrix} k_0 & k_4 & k_8 & k_{12} \\ k_1 & k_5 & k_9 & k_{13} \\ k_2 & k_6 & k_{10} & k_{14} \\ k_3 & k_7 & k_{11} & k_{15} \end{pmatrix}. \quad (11)$$

(2) Internal function (State) solution

In general, the internal function is described as any byte in State. Generally, x gives a nonlinear replacement byte, in which random non-0 byte $x \in F_{28}$ may be replaced by y :

$$y = \frac{A}{x} + b. \quad (12)$$

4. Result Analysis

4.1. Algorithm Performance Comparison. Simulations have been developed to further validate the practical effectiveness

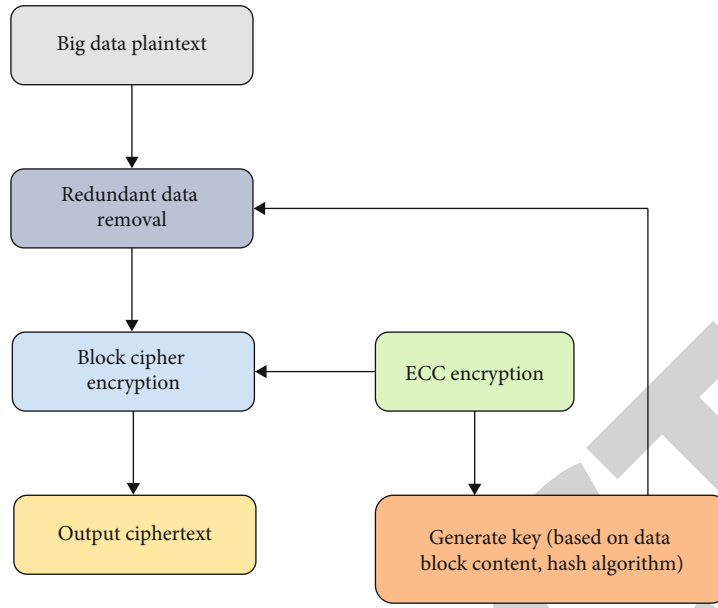


FIGURE 4: Model of large data encryption algorithm based on data resource technology.

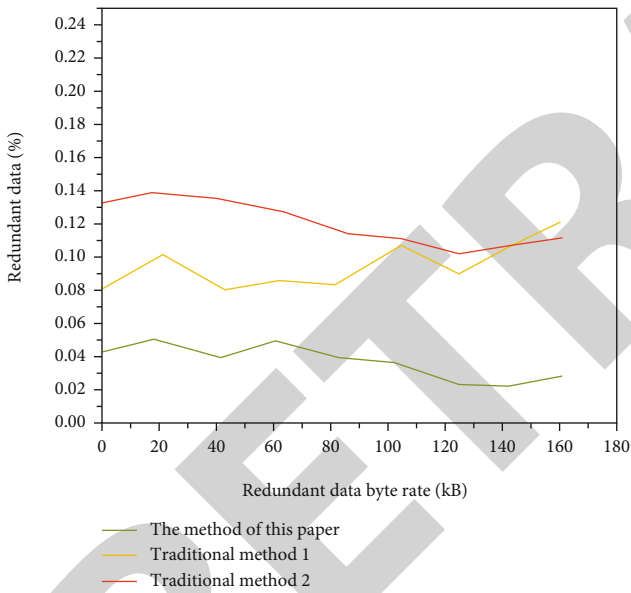


FIGURE 5: Comparison of different redundancy rate monitoring methods.

of the proposed method. Traditional method 1 and traditional method 2 are the control group of this experiment, and the experimental results of different methods are compared. The comparison index is redundant data detection rate and encryption time. The comparison results are shown in Figure 5.

As shown in Figure 5, the probability of redundant data in the traditional method is high. During the whole experiment, the approximate fluctuation range is 0.08%-0.14%, which is not only high but also large. In contrast, under the condition of different redundant data byte rate, the occurrence probability of redundant data is less than 0.05%, which is far lower than the two traditional methods; this suggests that the proposed method has good application performance.

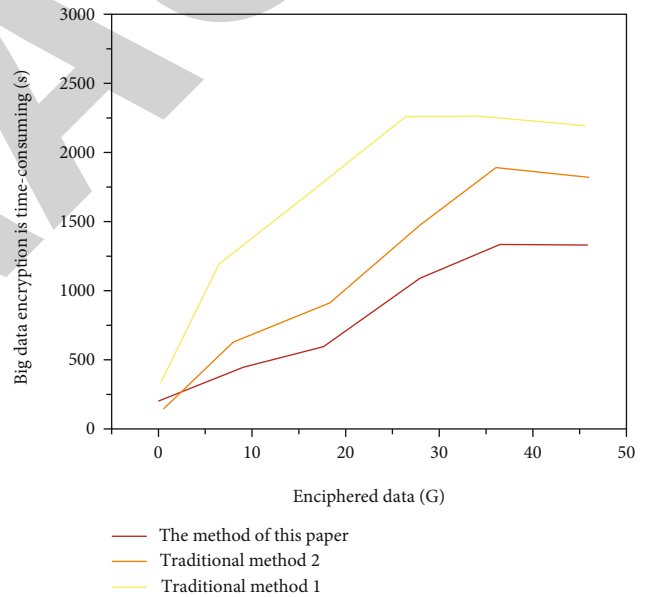


FIGURE 6: Comparison of encryption time of different methods.

In the process of encrypting data attributes, the actual simulation environment uses a PC with AMD Athlon (TM) IIX3, 3.10 GHz and 2 GB storage space, in which the programming language is C +. On this basis, three methods are used to compare the encryption time for files with file sizes of 1G, 5G, 10G, 30G, and 50G. The shorter the encryption time, the higher the efficiency of this method. The experimental comparison results are shown in Figure 6.

According to Figure 6, compared with the two traditional literature methods in terms of data encryption time, the algorithm in this paper takes less time to encrypt data of different sizes than the traditional method, and the encryption time does not increase due to the excessive amount of encrypted

data, while the literature method will increase the encryption time with the increase of encrypted data. In conclusion, the algorithm in this paper is more applicable.

5. Conclusion

At this stage, traditional large data character encryption methods do not meet the basic needs of the industry. Based on this, this paper proposes a new method of mathematical modeling of encryption of large data properties based on information resource technology. Based on the Bloom filter, a large data redundancy algorithm was developed, an elliptical encryption algorithm was proposed based on the data redundancy results, and a scheme and asymmetric encryption algorithm were developed that met the big data symmetric encryption algorithm. A mathematical model of encryption of large data properties was developed. The simulation results show that the method presented in this document has the advantage of low computation and encryption time and high efficiency in detecting redundant data. The results of the experiment show that the proposed method has good application value and is a reliable basis for in-depth study in this area.

Data Availability

The data used to support the findings of this study are available from the corresponding author upon request.

Conflicts of Interest

The authors declare that they have no conflicts of interest.

References

- [1] J. H. Lee and H. Y. Kwon, "Redundancy analysis and elimination on access patterns of the windows applications based on I/O log data," *IEEE Access*, vol. 8, pp. 40640–40655, 2020.
- [2] C.-L. Huang, Y. Jiang, and W.-C. Yeh, "Developing model of fuzzy constraints based on redundancy allocation problem by an improved swarm algorithm," *IEEE Access*, vol. 8, pp. 155235–155247, 2020.
- [3] L. Ye, Y. Yang, X. Jing, J. Ma, and H. Li, "Single-satellite integrated navigation algorithm based on broadband LEO constellation communication links," *Remote Sensing*, vol. 13, no. 4, p. 703, 2021.
- [4] D. Wang, W. Cui, and B. Qin, "Graph compression storage based on spatial cluster entity optimization," *IEEE Access*, vol. 8, pp. 29075–29088, 2020.
- [5] H. Bi, W.-L. Shang, Y. Chen, and K. Wang, "Joint optimization for pedestrian, information and energy flows in emergency response systems with energy harvesting and energy sharing," *IEEE Transactions on Intelligent Transportation Systems*, vol. 5, pp. 1–15, 2022.
- [6] X. Zhou, X. Xu, W. Liang et al., "Intelligent small object detection for digital twin in smart manufacturing with industrial cyber-physical systems," *IEEE Transactions on Industrial Informatics*, vol. 18, no. 2, pp. 1377–1386, 2022.
- [7] M. Selvi and B. Ramakrishnan, "Lion optimization algorithm (LOA)-based reliable emergency message broadcasting system in VANET," *Soft Computing*, vol. 24, no. 14, pp. 10415–10432, 2020.
- [8] J. Li, R. Zhang, Y. Liu, Z. Zhang, and W. Liu, "The method of static semantic map construction based on instance segmentation and dynamic point elimination," *Electronics*, vol. 10, no. 16, article 1883, 2021.
- [9] Z. Cai and X. Zheng, "A private and efficient mechanism for data uploading in smart cyber-physical systems," *IEEE Transactions on Network Science and Engineering*, vol. 7, no. 2, pp. 766–775, 2020.
- [10] X. Zheng and Z. Cai, "Privacy-preserved data sharing towards multiple parties in industrial IoTs," *IEEE Journal on Selected Areas in Communications*, vol. 38, no. 5, pp. 968–979, 2020.
- [11] S. Abdulateef, N. A. Khan, B. Chen, and X. Shang, "Multidocument Arabic text summarization based on clustering and Word2Vec to reduce redundancy," *Information*, vol. 11, no. 2, p. 59, 2020.
- [12] B. Yang, X. Li, Y. Hou et al., "Non-invasive (non-contact) measurements of human thermal physiology signals and thermal comfort/discomfort poses—a review," *Energy and Buildings*, vol. 224, article 110261, 2020.
- [13] X. Cheng, B. Yang, A. Hedman, T. Olofsson, H. Li, and L. Van Gool, "NIDL: a pilot study of contactless measurement of skin temperature for intelligent building," *Energy and Buildings*, vol. 198, pp. 340–352, 2019.
- [14] S. Kundu, A. D. Burman, S. K. Giri, S. Mukherjee, and S. Banerjee, "Selective harmonics elimination for three-phase seven-level CHB inverter using backtracking search algorithm," *International Journal of Power Electronics*, vol. 11, no. 1, pp. 1–19, 2020.
- [15] O. Abdel Wahab, A. Mourad, H. Otrok, and T. Taleb, "Federated machine learning: survey, multi-level classification, desirable criteria and future directions in communication and networking systems," *IEEE Communications Surveys & Tutorials*, vol. 23, no. 2, pp. 1342–1397, 2021.
- [16] H. Sami, A. Mourad, and W. El Haj, "Vehicular-OBUs-as-on-demand-fogs: resource and context aware deployment of containerized micro-services," *IEEE/ACM Transactions on Networking*, vol. 28, no. 2, pp. 778–790, 2020.
- [17] E. Y. Baagyere, A. N. Agbedemrab, Q. Zhen, M. I. Daabo, and Z. Qin, "A multi-layered data encryption and decryption scheme based on genetic algorithm and residual numbers," *IEEE Access*, vol. 8, pp. 100438–100447, 2020.
- [18] M. H. Saracevic, S. Z. Adamovic, V. A. Miskovic, M. Elhoseny, and K. Shankar, "Data encryption for internet of things applications based on catalan objects and two combinatorial structures," *IEEE Transactions on Reliability*, vol. 70, no. 2, pp. 819–830, 2021.
- [19] L. Teng, H. Li, S. Yin, and Y. Sun, "A modified advanced encryption standard for data security," *International Journal of Network Security*, vol. 22, no. 1, pp. 112–117, 2020.
- [20] P. Kumar and A. K. Bhatt, "Enhancing multi-tenancy security in the cloud computing using hybrid ECC-based data encryption approach," *IET Communications*, vol. 14, no. 18, pp. 3212–3222, 2020.
- [21] N. Nguyen, L. Pham, M. B. Nguyen, and G. Kaddoum, "A low power circuit design for chaos-key based data encryption," *IEEE Access*, vol. 8, pp. 104432–104444, 2020.
- [22] X. Yan, C. Yang, Q. Zhang, and J. Yu, "Revocable ciphertext-policy attribute-based encryption in data outsourcing systems

Retraction

Retracted: The Function of Remote Monitoring System of a Robot Inverter Based on PLC and Cloud Platform

Journal of Sensors

Received 13 September 2023; Accepted 13 September 2023; Published 14 September 2023

Copyright © 2023 Journal of Sensors. This is an open access article distributed under the Creative Commons Attribution License, which permits unrestricted use, distribution, and reproduction in any medium, provided the original work is properly cited.

This article has been retracted by Hindawi following an investigation undertaken by the publisher [1]. This investigation has uncovered evidence of one or more of the following indicators of systematic manipulation of the publication process:

- (1) Discrepancies in scope
- (2) Discrepancies in the description of the research reported
- (3) Discrepancies between the availability of data and the research described
- (4) Inappropriate citations
- (5) Incoherent, meaningless and/or irrelevant content included in the article
- (6) Peer-review manipulation

The presence of these indicators undermines our confidence in the integrity of the article's content and we cannot, therefore, vouch for its reliability. Please note that this notice is intended solely to alert readers that the content of this article is unreliable. We have not investigated whether authors were aware of or involved in the systematic manipulation of the publication process.

Wiley and Hindawi regrets that the usual quality checks did not identify these issues before publication and have since put additional measures in place to safeguard research integrity.

We wish to credit our own Research Integrity and Research Publishing teams and anonymous and named external researchers and research integrity experts for contributing to this investigation.

The corresponding author, as the representative of all authors, has been given the opportunity to register their agreement or disagreement to this retraction. We have kept a record of any response received.

References

- [1] M. Yu, "The Function of Remote Monitoring System of a Robot Inverter Based on PLC and Cloud Platform," *Journal of Sensors*, vol. 2022, Article ID 1178508, 8 pages, 2022.

Research Article

The Function of Remote Monitoring System of a Robot Inverter Based on PLC and Cloud Platform

Mengqi Yu 

Inner Mongolia Vocational College of Chemical Engineering, Hohhot, Inner Mongolia 010070, China

Correspondence should be addressed to Mengqi Yu; 202006000042@hceb.edu.cn

Received 5 June 2022; Accepted 13 July 2022; Published 23 July 2022

Academic Editor: Haibin Lv

Copyright © 2022 Mengqi Yu. This is an open access article distributed under the Creative Commons Attribution License, which permits unrestricted use, distribution, and reproduction in any medium, provided the original work is properly cited.

In order to improve the communication efficiency of the CAN bus application layer communication protocol of the inverter network monitoring system, this paper proposes a TTCAN scheduling optimization algorithm for the robot inverter remote monitoring system based on PLC and cloud platform. According to the analysis of the communication requirements of the frequency converter monitoring system, this paper designs the application layer protocol of the nodes in the system and establishes the system scheduling matrix. The time triggered can bus protocol (TTCAN) combines the event triggered mechanism with the time triggered mechanism. The hybrid scheduling strategy is used to optimize the system matrix of TTCAN; that is, the hybrid particle swarm optimization algorithm is used for periodic messages. For nonperiodic messages, uniform scheduling strategy and dynamic scheduling algorithm are adopted. The simulation is carried out by MATLAB tools. The simulation results show that the sum of partial minimum transmission time is 1928 and there are multiple optimal individuals through the hybrid particle swarm optimization algorithm. Compared with the traditional genetic algorithm and single particle swarm optimization algorithm, the hybrid algorithm is better than the traditional genetic algorithm and particle swarm optimization algorithm in terms of iteration times and average fitness value. In conclusion, the optimized TTCAN protocol improves the real-time performance, reliability, and bandwidth utilization of the communication network.

1. Introduction

In recent years, with the rapid development of modern industrial control technology, the scale of industrial monitoring system is growing, the speed of data exchange and the amount of communication of the monitoring system have become more demanding, and the real time and reliability of the network system have become more and more important. With the continuous development, popularization, and application of frequency converter, it is applied in metallurgy, petroleum, chemical industry, textile, electric power, building materials, coal, and other industries. At the same time, the demand for the development of frequency converter to information network is becoming stronger and stronger. More and more occasions require network communication and monitoring of frequency converter, as shown in Figure 1 [1]. Realizing message interconnection and standby switching between multiple frequency converters is the basic require-

ment of the frequency converter network monitoring system. Moreover, the electromagnetic interference on the application site of the frequency converter is large, and the distance between different frequency converters is nearly 100 meters. In order to meet the needs of the application, an industrial field bus with strong anti-interference is selected, which has the characteristics of reliable transmission and high real time, so as to ensure the reliable transmission of communication messages. In addition, because key messages are very sensitive to delay, it is necessary to study a scheduling strategy to ensure that a large number of messages are transmitted to obtain the minimum response delay [2]. The Internet of things is regarded as the application expansion of the Internet, and it is another technological revolution in the field of information technology after the computer and the Internet. It can connect any object to the Internet and exchange and communicate information and data, so as to realize the tracking, positioning, automatic identification, and remote monitoring of objects,

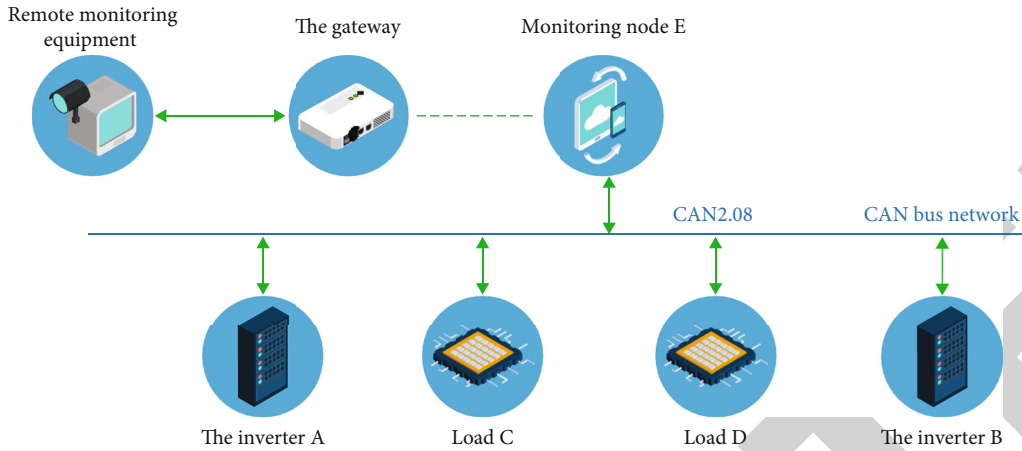


FIGURE 1: Monitoring system.

and allow information exchange between objects at any time [3]. Its main characteristics are comprehensive perception, reliable transmission, and intelligent processing.

2. Literature Review

Sundararajan and others designed a remote monitoring system for small and medium-sized coal mines based on arm. MMS information technology combined with relevant software and hardware was used to connect each module of the system for testing. The results showed that the development idea of the system was correct, the data transmission was correct, and it was suitable for promotion in small and medium-sized coal mines [4]. Brown and others designed a wireless and limited openable data communication network to meet the working conditions of the oil field. Finally, the function design, implementation method, and software development of the monitoring system are introduced. After the completion of the system, it was tested in the laboratory to prove that the data communication can be carried out normally [5]. Qian and others designed a frequency converter remote monitoring system based on a GPRS communication network in combination with oil field production. The system uses LabVIEW software to program the upper computer software. The system mainly focuses on frequency converter voltage, current and temperature data acquisition, GPRS wireless transmission, real-time display, and storage [6]. Gnanesikan and others described in detail the main functions of the system based on the monitoring of the scraper conveyor in the fully mechanized mining face. The fault diagnosis system is developed based on the monitoring data, and the technical indicators are defined. According to the system requirements, the hardware design is combined with software programming, and the fault diagnosis method is based on the D-S basic theory. The feasibility of the fault diagnosis method is verified by an example [7]. Okyem and others used PLC control technology and CAN communication technology and took KingSCADA KingView software as the development platform to design and implement PLC-based remote monitoring platform for air compressor [8]. The remote monitoring platform of the air compressor displays the operation status,

parameter information, sensor data information, and fault information of the frequency converter air compressor unit in real time. The models and application scope of PLC, frequency converter, air compressor, pressure sensor, and temperature sensor are given in detail. The experimental results show that the platform is safe, stable, and effective. As one of the most widely used field buses in the world, CAN bus is widely used in industrial control systems. At the same time, with the continuous development and application of frequency converter, the demand for its development towards informatization and networking becomes stronger. Therefore, the design of an efficient and reliable CAN bus application layer communication protocol is a necessary condition for its application in frequency converter network monitoring system [9]. This paper mainly studies the scheduling strategy and optimization design of TTCAN, designs the TTCAN application layer protocol according to the requirements of frequency converter system, and generates the message scheduling system matrix. According to the different characteristics of periodic messages and aperiodic messages, scheduling strategies are designed, respectively. Different hybrid particle swarm optimization algorithms and dynamic priority uniform scheduling are used to optimize the objective function, so as to minimize the response delay of messages and ensure the reliable transmission of hard real-time messages.

3. Research Methods

3.1. Design Method Based on TTCAN System. The core of TTCAN protocol is its unique system matrix period MC, which includes multiple basic periods BC. A BC starts with a reference message and is composed of multiple time windows, corresponding to one row of the matrix cycle. The time windows in the same column constitute the columns of the matrix cycle [10]. The time interval between the two reference messages of the matrix period is a basic period BC, and its length is the maximum common divisor of all task times in the task set. Refer to Figure 2.

Suppose there are n periodic messages in the network, the message instance set $M = \{M_1, M_2, \dots, M_{N-1}, M_N\}$, and each message has two attributes: transmission time t_{cm} and

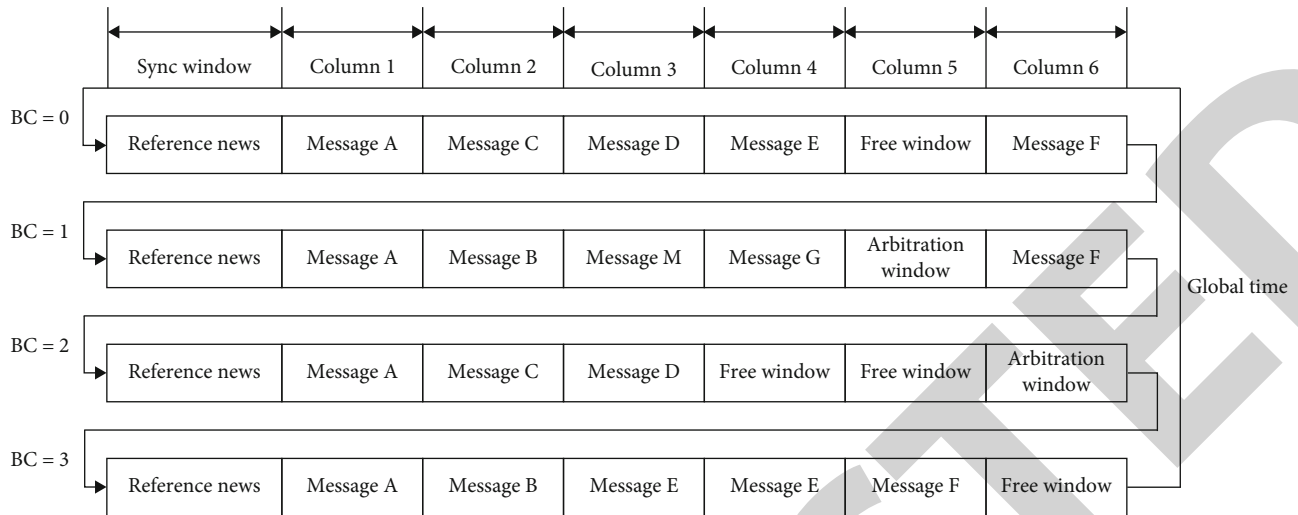


FIGURE 2: System matrix period MC of TTCAN.

period T_m . Determine the message sending period $T = \{T_1, T_2, \dots, T_{N-1}, T_N\}$ of each node, and take the maximum common divisor of all messages as the basic period BC_T [11]. Take the least common multiple of all message transmission cycles or its integer multiple as MC_T , and the multiple depends on whether the system cycle can complete the transmission of all messages.

The number of basic cycles is shown in

$$R = \frac{MC_T}{BC_T}. \quad (1)$$

The number of columns of matrix period

$$C = \left\lceil \frac{\sum_{i=1}^N MC_T/T_i}{MC_T/BC_T} \right\rceil, \quad (2)$$

where T_i is the transmission period of each node, BC_T is the basic cycle, and MC_T is the matrix period.

The essence of message scheduling table generation is to collect messages [12].

3.2. Scheduling Requirements and Problem Description

3.2.1. Overall Structure of Frequency Converter Monitoring System. For the application of frequency converter monitoring network, communication messages are divided into two categories: periodic and accidental. Periodic messages are mainly analog quantities and status quantities used for system control and monitoring, which must be triggered in strict accordance with the communication cycle to ensure the stability and rapidity of system control and the real-time monitoring of the system. Sporadic messages are mainly alarm signals and other signals sensitive to time delay. On the one hand, sporadic messages cannot affect the transmission of periodic messages. On the other hand, it is also necessary to minimize the response delay of sporadic messages to ensure the safe operation of the system [13]. Therefore, the TTCAN design method is used to

schedule the bus messages, corresponding to the specific time window and the competitive time window in the TTCAN scheduling matrix, respectively.

In order to illustrate the design method of TTCAN scheduling optimization algorithm in frequency converter monitoring system, the algorithm design is carried out with the simplified networking model as the object, as shown in Figure 3. The CAN network of the frequency converter monitoring system has five nodes, including frequency converter nodes A and B (master node), load nodes C and D (slave node) and monitoring node E. The scheduling of periodic messages and occasional messages among five nodes is the research object of TTCAN scheduling optimization algorithm in this paper.

Classify the messages, establish the scheduling time and transmission mechanism of the messages, and list the message attributes and communication task set shown in Table 1.

The bus message includes 14 periodic messages and 3 nonperiodic messages. $T = \{5, 5, 5, 10, 20, 10, 20, 10, 20, 10, 20, 20, 40\}$ is arranged in ascending order according to the sending cycle of periodic messages to determine $BC_T = 5$ ms and $MC_T = 40$ ms, and the number of matrix rows R is 8. The number of periodic message columns C of the basic cycle is 7, and the last column serves as an arbitration window for the scheduling of nonperiodic messages.

3.2.2. Establishment of Initial System Matrix. Part SM_0 and P_1 of the initialization matrix are exclusive windows with a message period equal to BC_T , including M_1, M_2, M_3 messages. Part P_2 is the exclusive window whose message period is greater than BC_T . Part 3 is the arbitration window for aperiodic messages [14]. The matrix is a matrix with 8 rows and 8 columns (the last column is the arbitration window). The window marked with f is a free window, and the window marked with ARB is an arbitration window, which is used to transmit event type trigger messages. According to the initial scheduling matrix SM_0 , the transmission time series of each column of messages $T_{c_0} = \{368, 484, 484, 444, 520, 520, 520, 1660\}$, in which

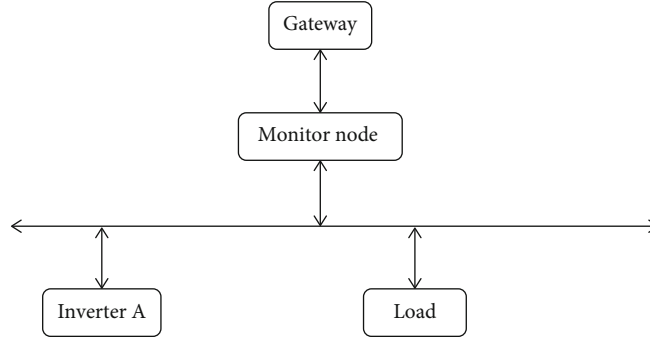


FIGURE 3: Network topology of frequency converter monitoring system.

TABLE 1: Communication task set of electrical system.

Message type	Message number	Trigger period (ms)	Deadline (ms)	Communication duration (μs)
Recurring messages	M_1	5	5	368
	M_2	5	5	484
	M_3	5	5	484
	M_4	10	10	444
	M_5	20	20	444
	M_6	10	10	444
	M_7	20	20	444
	M_8	10	10	520
	M_9	20	20	520
	M_{10}	10	10	520
	M_{11}	20	20	520
	M_{12}	20	20	404
	M_{13}	20	20	484
	M_{14}	40	40	520
Aperiodic message	M_{15}	Episodic	20	328
	M_{16}	Episodic	10	328
	M_{17}	Episodic	5	328

the occupation width of periodic messages is $3340 \mu s$ and the available width of the arbitration window is $1660 \mu s$.

3.2.3. Optimization Objectives of Message Scheduling. The protocol of TTCAN system matrix requires that the window width of the same column in each basic cycle should be consistent, which is determined by the message with the longest transmission time in this column. For Part P_2 , the optimization goal is how to arrange n messages into m columns, so that each column of Part P_2 occupies the minimum time, and the arbitration window can reach the maximum time in the same basic cycle [15]. In order to improve the real-time performance of messages, the system matrix needs to meet the following conditions to minimize the sum of the maximum transmission time of each column of messages, which means that the bus time occupied by periodic messages is the minimum, as shown in

the following equations.

$$\min \sum_{i=1}^m \left\{ \max [C_j x_{ij}]_{j=1, n} \right\} \quad (3)$$

$$\text{s.t.} \quad \sum_{j=1}^n w_j x_{ij} \leq W_i \quad i = 1, m \quad (4)$$

$$\sum_{i=1}^m x_{ij} = 1 \quad j = 1, n \quad \forall i, j \text{ make } x_{ij} \in \{0, 1\}, \quad (5)$$

$$w_j = \frac{MC_T}{T_j} \quad j = 1, n, \quad (6)$$

$$W_i = \frac{MC_T}{BC_T} i = 1, m, \quad (7)$$

where j is the message sequence number; i is the column number of time window SM; x_{ij} is the serial number of the corresponding j message; i whether the message of the time window column number exists, represented by 0 or 1; m is the number of columns of periodic trigger message; n is the number of messages; w_j is the number of the j -th message in the SM matrix; T_j is the period of the j -th message; C_j is the transmission time of the j -th message; and W_i is the total number of rows in the time window in column i of the SM matrix.

If the j -th message is placed in column i of SM, $x_{ij} = 1$; otherwise, $x_{ij} = 0$, and the same message can only be placed in one column; that is, there is at most one message in each row, and this message can only be stored in the current column.

The bus utilization of periodic messages is shown in the following equation:

$$U = \frac{\sum_{j=1}^N (MC_T \times C_j / T_j)}{\sum_{i=1}^R L_j m_i}, \quad (8)$$

where L_j is the window width of column j , m_i is the number of messages in column i , and the free window is not occupied by the bus during calculation.

The optimization problem of the frequency conversion monitoring system can be transformed into a multidimensional knapsack problem, that is, a NP (nondeterministic polynomial) problem; that is, each periodic message is reasonably placed in the system matrix to minimize the occupation time of the exclusive window, so as to increase the time of the arbitration window to ensure the timely response of nonperiodic messages [16].

3.3. Message Scheduling Optimization Algorithm

3.3.1. Periodic Message Scheduling Optimization Based on Hybrid Particle Swarm Optimization. For periodic messages, it is necessary to reasonably arrange the messages in the P2 time window to achieve effective scheduling.

The basic particle swarm optimization algorithm can be used to optimize the system matrix and determine the optimal value in the process of continuously tracking the extreme value, which is easy to realize and has fast convergence speed. However, due to the single optimization method, the optimal solution often cannot break through its own limitations [17, 18]. The hybrid particle swarm optimization algorithm proposed in this paper uses genetic algorithm for reference; that is, genetic algorithm is introduced into particle swarm optimization algorithm to make particles reach the optimal value in the cross mutation with individual extreme value and population extreme value, so as to solve the problem that particle similarity cannot jump out of the boundary of local optimal solution when the population converges.

(1) *Individual Code.* Firstly, the scheduling table is coded, and the particle individual coding adopts integer coding. Each particle represents the specific allocation of n messages

to a column. The Part B messages to be optimized are $M_4 \sim M_{14}$, a total of 11 messages. These 11 messages need to be reasonably allocated to 4 columns to minimize the total column width. The initial coding vector of individual particles is defined according to the initial system matrix, where the number of vector elements is 11, representing the 11 messages $M_4 \sim M_{14}$, and the vector value is the value of the column in which the message is located is 1, 2, 3, 4. A total of 4 columns need to be optimized, so the column numbers are allocated from 1 to 4. Therefore, in this numbering method, the initial vector is [1-4], representing that the 11 messages $M_4 \sim M_{14}$ are allocated to the first, third, first, and fourth columns, respectively. Use the same numbering method to generate any individual particle.

(2) *Design Fitness Function and Calculate Individual Fitness.* The fitness function is divided into two parts: one is the cost of the whole; the other part is the penalty function of illegal particles. The overall cost is calculated through the objective function, and the bus utilization is used as the evaluation standard. The overall cost of the k -th particle is as follows:

$$fk(v_k) = \sum_{i=1}^m \left\{ \max [C_j x_{ij}^k | j = 1, \dots, n] \right\}, \quad k = 1, 2, \dots, M, \quad (9)$$

where v_k is the position of the k -th particle, and x_{ij}^k is the corresponding decision variable, and the particle swarm size is M .

Since the total weight of each column of messages cannot exceed the current column capacity, in order to prevent the coding of some particles from exceeding this limit during the optimization process, a penalty function is introduced to deal with the problem that particles violate constraints. The penalty function factor p_k is shown in the following formulas:

$$p_k = \sum_{i=1}^m p_i k = 1, 2, \dots, M, \quad (10)$$

$$p_i = \begin{cases} 0, & \text{if } \sum_{i=1}^m x_{ij} = 1, j = 1, \dots, n, \\ \alpha_0 \left(\sum_{j=1}^n w_j x_{ij} - W_i \right), & \text{otherwise.} \end{cases}$$

If the formula $\sum_{i=1}^m x_{ij} = 1, j = 1, \dots, n$ is satisfied, then P_i is 0. Otherwise, a large positive number α_0 is introduced to reduce the fitness. The fitness formula consists of an evaluation function and a penalty function. The evaluation function is expressed in the following formula:

$$\text{eval}(v_k) = \frac{1}{fk(v_k) + p_k} k = 1, 2, \dots, M. \quad (11)$$

(3) *Crossover Operation.* Individuals are updated by crossing with individual extremum and group extremum, and the cross method is a certificate cross method. First, a crossover position

is randomly selected, and then individuals and individual extremum or individual and group extremum are crossed [19].

(4) *Mutation Operation.* The mutation method is to randomly select a mutation position for each individual and then randomly change the value of the position into other values within a range.

(5) *Judge Whether the Termination Conditions Are Met.* If the conditions are met, the optimal individual is selected and the number of iterations is given. If not, the particle swarm location is updated to continue the calculation.

3.3.2. *Nonperiodic Message Dynamic Scheduling Optimization Based on Uniform Strategy.* For nonperiodic messages, it is also necessary to ensure a certain real-time performance. They are transmitted in the arbitration window of the matrix cycle. The message transmission cannot be interrupted, which will affect the transmission of periodic messages [20]. The occurrence time of the message shall be recorded, and the arbitration window shall be dynamically allocated to the message according to the priority, transmission time, and waiting time of the message. Only when the nonperiodic message is reliably transmitted in the arbitration window can the stable transmission of periodic messages be guaranteed. The start sending time of acquiring bus right for aperiodic messages can be expressed as the following equation:

$$S_m = T_p + W_m, \quad (12)$$

where T_p is the time waiting for the transmission of periodic scheduling message to end and W_m is the waiting time from c competing with other aperiodic messages for the bus to obtaining the bus in the arbitration window.

It can be seen from equation (7) that S_m can be realized by reducing T_p and W_m . In order to achieve higher real-time performance of aperiodic messages, the following is to reduce the time for messages to wait for arbitration by reducing T_p through the uniform distribution algorithm. The dynamic identifier priority mechanism of delay priority is introduced to ensure the transmission of some nonperiodic messages with low priority.

(1) *Uniformly Distributed Scheduling Strategy.* Uniform distribution scheduling is to adopt the idea of uniform, distribute the arbitration time evenly according to the number of exclusive windows in the basic cycle of the system matrix, and add an equally distributed arbitration window after each exclusive window [21]. In addition, in order to prevent node identification confusion caused by the transmission of adjacent periodic messages, a time interval window t_{gap} shall be introduced between adjacent periodic messages. The length of uniformly distributed arbitration window is calculated as follows:

$$t_w = \frac{BC_T - T_{CP}}{N_w - t_{\text{gap}}}, \quad (13)$$

where t_w is the width of each arbitration window equally divided; BC_T is the basic cycle; T_{CP} is the time occupied by periodic messages in a basic cycle; N_w is the number of exclusive windows, which is consistent with the number of arbitration windows after equal distribution; and t_{gap} is the reasonable interval set between messages. For the convenience of analysis, $t_{\text{gap}} = 0$ is taken.

Of course, the average width of each arbitration window can guarantee the transmission of the longest non periodic message transmission time t_m . If $t_w < t_m$, it indicates that the uniform distribution time is insufficient. You can consider merging some uniformly distributed arbitration windows, so as to reduce the number of arbitration windows in the basic cycle to $t_w > t_m$.

After the design according to the above principles, the last arbitration window of the system optimization matrix is divided into four subwindows $Arb_1, Arb_2, Arb_3, Arb_4$, with window widths of [360, 360, 360, 656], respectively, to ensure the longest transmission time of nonperiodic messages of $328\mu\text{s}$, so as to reduce the response delay of nonperiodic messages.

(2) *Dynamic Priority Scheduling Policy.* Due to the arbitration mechanism of CAN bus, in order to avoid that messages with low priority cannot get the bus control right for a long time, a dynamic priority scheduling mechanism is introduced, and the delay priority is taken as an indicator of priority [22]. Delay priority is the number of message frames that have been transmitted during the waiting period of the arbitration window.

4. Result Analysis

For periodic messages, the hybrid particle swarm optimization algorithm is used in MATLAB to design the program and optimize the part of the system matrix. The parameters of the algorithm are set as follows: the population size is 20, the evolution times is 100, the penalty function factor is 1000, the number of message columns is 4, and the number of messages is 11. The simulation results of the algorithm are shown in Figure 4. Figure 4(a) shows the optimal individual fitness, and Figure 4(b) shows the total transmission time. The total transmission time of periodic messages is iterated from the initial 2080 to the 43rd generation to obtain a stable optimal value of 1928, and the fitness is optimized from 3.43×10^{-4} to 5.19×10^{-4} . The sum of the minimum transmission time of the four column windows is $1928\mu\text{s}$, and the corresponding optimal individual $M_4 \sim M_{14}$ is [1 3 3 3 2 2 4 4 1 2 4].

$T_{\text{Copt}} = \{368, 484, 484, 444, 520, 444, 520, 1736\}$ is the message scheduling sequence, in which the width occupied by periodic messages is $3264\mu\text{s}$, and the available width of the arbitration window is $1736\mu\text{s}$; $T_{C0} = \{368, 484, 484, 444, 520, 520, 520, 1660\}$ is the periodic message sequence of the initial matrix, where the occupied width of the periodic message is $3340\mu\text{s}$ and the available width of the arbitration window is $1660\mu\text{s}$. Compared with the initial state, the optimized message sequence of periodic messages saves $76\mu\text{s}$, and the arbitration window time is $76\mu\text{s}$ more, which improves the bus utilization

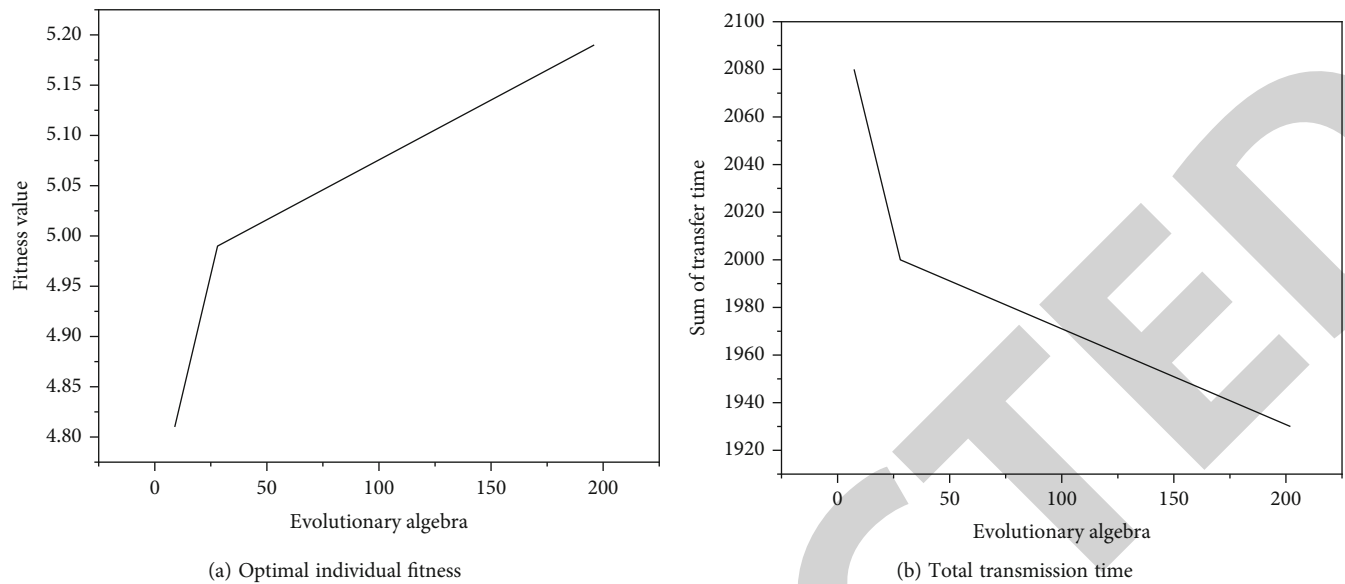


FIGURE 4: Hybrid algorithm generation results.

efficiency. When the number of nodes in the bus is more and the amount of message data is larger, the optimization effect is more prominent. The experimental results are as follows: according to the hybrid particle swarm optimization algorithm, the sum of partial minimum transmission time is 1928, and there are multiple optimal individuals. Compared with the traditional genetic algorithm and single particle swarm optimization algorithm, the hybrid algorithm is better than the traditional genetic algorithm and particle swarm optimization algorithm in terms of iteration times and average fitness value.

5. Conclusion

Based on the communication model of frequency converter monitoring system, this paper designs the TTCAN scheduling optimization algorithm. Aiming at the periodic messages of the system, the scheduling problem is transformed into a multidimensional knapsack problem, which is optimized by the combination of genetic algorithm and particle swarm optimization algorithm. The optimization matrix is obtained through MATLAB simulation experiments, which improves the bus utilization. For occasional messages, the uniform distribution strategy is adopted to arrange the arbitration window, and the delay priority is introduced as a part of the identifier to ensure the reliable transmission of event messages. In the more complex monitoring system with similar communication structure, the scheduling optimization algorithm can play a more obvious role in improving bus utilization and reducing communication delay.

Data Availability

The data used to support the findings of this study are available from the corresponding author upon request.

Conflicts of Interest

The authors declare that they have no conflicts of interest.

References

- [1] M. H. Sheffield, G. G. Schultz, D. Bassett, and D. L. Eggett, "Sensitivity analysis of the transit signal priority requesting threshold and the impact on bus performance and general traffic," *Transportation Research Record*, vol. 2675, no. 5, pp. 149–163, 2021.
- [2] C. Chu, C. Dong, M. Du, X. Zhou, and Z. Ouyang, "Aging monitoring of bond wires based on differential mode conducted interference spectrum for IGBT module," *IEEE Transactions on Electromagnetic Compatibility*, vol. 63, no. 4, pp. 1274–1283, 2021.
- [3] A. Silva, L. Bezerra, S. Juca, R. Pereira, and C. Medeiros, "Control and monitoring of a Flyback DC-DC converter for photovoltaic applications using embedded IoT system," *IEEE Latin America Transactions*, vol. 18, no. 11, pp. 1892–1899, 2020.
- [4] P. Sundararajan, M. Sathik, F. Sasongko et al., "Condition monitoring of DC-link capacitors using Goertzel algorithm for failure precursor parameter and temperature estimation," *IEEE Transactions on Power Electronics*, vol. 35, no. 6, pp. 6386–6396, 2020.
- [5] E. Brown, Y. Yan, and W. R. Marcum, "A novel method for predicting power transient CHF via the heterogeneous spontaneous nucleation trigger mechanism," *Nuclear Technology*, vol. 206, no. 9, pp. 1296–1307, 2020.
- [6] Y. Qian, Y. Xiao, T. Qin, F. Zhang, and B. Lin, "Investigating the formation mechanism of a nanoporous silver film electrode with enhanced catalytic activity for CO₂ electroreduction," *Chem Electro Chem*, vol. 7, no. 21, pp. 4354–4360, 2020.
- [7] A. Gnanadesikan, C. M. Speller, G. Ringlein, J. S. Soucie, and M. A. Pradal, "Feedbacks driving interdecadal variability in southern ocean convection in climate models: a coupled oscillator mechanism," *Journal of Physical Oceanography*, vol. 50, no. 8, pp. 2227–2249, 2020.

Retraction

Retracted: Motion Rehabilitation Robot Control Based on Human Posture Information

Journal of Sensors

Received 13 September 2023; Accepted 13 September 2023; Published 14 September 2023

Copyright © 2023 Journal of Sensors. This is an open access article distributed under the Creative Commons Attribution License, which permits unrestricted use, distribution, and reproduction in any medium, provided the original work is properly cited.

This article has been retracted by Hindawi following an investigation undertaken by the publisher [1]. This investigation has uncovered evidence of one or more of the following indicators of systematic manipulation of the publication process:

- (1) Discrepancies in scope
- (2) Discrepancies in the description of the research reported
- (3) Discrepancies between the availability of data and the research described
- (4) Inappropriate citations
- (5) Incoherent, meaningless and/or irrelevant content included in the article
- (6) Peer-review manipulation

The presence of these indicators undermines our confidence in the integrity of the article's content and we cannot, therefore, vouch for its reliability. Please note that this notice is intended solely to alert readers that the content of this article is unreliable. We have not investigated whether authors were aware of or involved in the systematic manipulation of the publication process.

Wiley and Hindawi regrets that the usual quality checks did not identify these issues before publication and have since put additional measures in place to safeguard research integrity.

We wish to credit our own Research Integrity and Research Publishing teams and anonymous and named external researchers and research integrity experts for contributing to this investigation.

The corresponding author, as the representative of all authors, has been given the opportunity to register their agreement or disagreement to this retraction. We have kept a record of any response received.

References

- [1] G. He, "Motion Rehabilitation Robot Control Based on Human Posture Information," *Journal of Sensors*, vol. 2022, Article ID 5067346, 7 pages, 2022.

Research Article

Motion Rehabilitation Robot Control Based on Human Posture Information

Guangfeng He 

Hainan Vocational College of Political Science and Law, Hainan, Haikou 571100, China

Correspondence should be addressed to Guangfeng He; 20160552@ayit.edu.cn

Received 5 June 2022; Accepted 11 July 2022; Published 21 July 2022

Academic Editor: Haibin Lv

Copyright © 2022 Guangfeng He. This is an open access article distributed under the Creative Commons Attribution License, which permits unrestricted use, distribution, and reproduction in any medium, provided the original work is properly cited.

In order to meet the needs of postoperative rehabilitation training of lower limbs, a motion rehabilitation robot control system based on human posture information is proposed in this paper. The functions of active/passive training mode control, movement posture and EMG signal acquisition, WiFi communication, safety protection, etc. of the lower limb rehabilitation robot are realized. The recognition and analysis of the training process are realized by using random forest machine learning algorithm and linear regression algorithm. The experimental results show that in the first row of the confusion matrix of the random forest algorithm, 7316 data are correctly identified as speed a and only one data is incorrectly identified as speed B , which is superior to other algorithms. In conclusion, the developed control and monitoring system of lower limb rehabilitation robot can be portable controlled by Android and can realize intelligent analysis of the training process through the monitoring signals in the training process. At the same time, the random forest algorithm has more advantages than the linear regression algorithm in motion recognition, which is of positive significance to the automatic monitoring and intelligent control of the training process.

1. Introduction

The ideal way for stroke patients to recover their motor ability is to use rehabilitation training to recover their motor function, while the traditional rehabilitation training is for doctors to hold the patient's affected limb and assist the patient to exercise by using simple instruments or various techniques. This training method has the following problems: first, the training process is boring, the patients receive the training passively, the active consciousness is not strong, and the effect is not good. Second, the labor intensity of rehabilitation doctors is very high, which affects the efficiency of rehabilitation training. Third, the effect of rehabilitation depends on the experience and level of rehabilitation doctors to a great extent. Fourth, the process of rehabilitation is based on qualitative observation, lacking objective monitoring basis, which is not conducive to the further determination of treatment plan. Fifth, there is no objective rehabilitation evaluation index, so it is impossible to conduct in-depth study on the neurorehabilitation law of patients [1]. Based on the above points, it is extremely urgent to find a

convenient and effective means of rehabilitation training to enable patients to recover their active sports ability, improve their quality of life, and reduce the burden on families and society. With the continuous progress of science and technology and the in-depth application of automated robots, the field of rehabilitation medicine is gradually using robots to train patients with motor dysfunction, which can significantly improve the loss of motor function caused by nervous system damage (such as stroke, trauma, and spinal injury), as shown in Figure 1 [2]. Using robot technology to evaluate, reconstruct, and improve the movement ability of patients' limbs has become a hot topic in domestic research. Therefore, the research on the control technology of medical rehabilitation robot is of great significance. Referring to the relevant technologies of industrial automation robots and combining the characteristics of medical robots, the medical rehabilitation robots first tried to commercialize robots that serve people with limb movement difficulties after the 1960s. After the test of practice, these attempts ended in failure [3]. The main reasons are as follows: first, the man-machine interface design is not ideal, and the installation and wearing

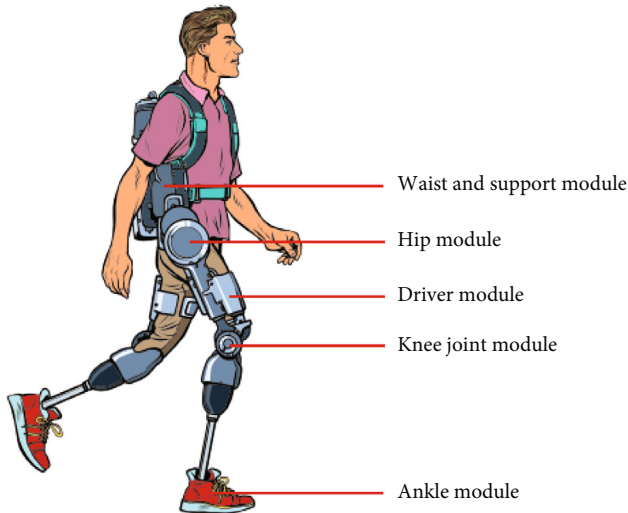


FIGURE 1: Rehabilitation robot.

cannot be completed by nonprofessionals. The second reason is the cost. At that time, the robot technology was not popularized, resulting in the high unit price of products, which patients could not afford.

2. Literature Review

Assad UZ Zaman and others found that there are nerve centers for coordinated movement of upper and lower limbs in the human body. Through scientific coordinated training of upper and lower limbs, the rehabilitation of injuries can be more effectively promoted [4]. Chen and others designed and completed the first upper limb rehabilitation robot. The robot is composed of two linkage mechanisms. Patients need to hold the end of the robot during training, and the robot drives them to complete rehabilitation training. The robot adopts the impedance control principle and can realize the smooth and compliant movement of the end point of the mechanism. The robot can collect and store the rehabilitation data of patients and provide help for the formulation of rehabilitation programs [5]. Yuvaraj and others designed a three degree of freedom arm guide for upper limb rehabilitation robot. The robot has a simple structure, can provide patients with multidirectional linear rehabilitation movement, and can also collect and store the rehabilitation movement information of patients. Because of its huge size and poor flexibility, it can only carry out limited training [6]. Li and others designed a prototype of a lower limb rehabilitation robot. In the aspect of mechanical design, the researchers designed the structure of the robot according to the different human body sizes of different patients, ensuring the coaxiality of human joints and robot joints during training [7]. Liu and others designed an active and passive rehabilitation robot for upper and lower limbs. The robot has a simple structure, and the upper and lower limb systems have two rotational degrees of freedom. The robot uses the single chip microcomputer as the main controller and adopts the double closed-loop PID control method of current loop and speed loop to control the motor speed and torque.

Finally, four training modes of passive, active, active assistance, and resistance are realized [8]. Raj and others designed a limb coordinated rehabilitation robot. The upper limb training system of the robot is a five-bar mechanism with end traction, which has two degrees of freedom. The lower limb is a bicycle mechanism with single degrees of freedom. The coordinated movement of the upper and lower limbs is realized through the coordinated control of the upper and lower limb systems. The robot has three postures: lying, sitting, and standing. It can realize adaptive passive training and impedance active training, but the training track is single [9]. Li and others designed an upper and lower limb rehabilitation robot. The robot has eight degrees of freedom including shoulder joint, hip joint, knee joint, and ankle joint. The passive linkage position control of the upper and lower limbs is realized by pole placement method. The robot has few degrees of freedom of upper limbs and cannot follow the patient well. Moreover, the rehabilitation mode is relatively simple, and the control system is simple [10]. In this paper, the monitoring technology of training mode control process of lower limb rehabilitation robot is studied, in order to realize the intelligent portable control of training process and the intelligent recognition analysis of training process and lay the foundation for the intelligent control of lower limb rehabilitation robot.

3. Research Methods

3.1. System Structure and Hardware Design

3.1.1. Lower Limb Rehabilitation Mechanical Structure. The lower limb rehabilitation robot serves patients with lower limb motor dysfunction. In order to avoid secondary injury to patients, the safety of the lower limb rehabilitation robot should be improved from all aspects of the control system [11]. The control system is divided into hardware system and software system. The hardware system is the bridge between the software system and the robot mechanical body. It is particularly important to build a reasonable hardware system. The software system should be designed with beautiful interface, convenient operation, and comprehensive functions, so as to better realize the value of the rehabilitation robot [12]. As a member of medical devices, rehabilitation robot must meet the requirements of electromagnetic compatibility. The lower limb rehabilitation robot actuator developed in this paper realizes the active and passive training functions of the lower limb according to the rehabilitation needs of the knee joint after operation. Each leg module has 3 degrees of freedom, corresponding to the hip, knee, and ankle on the sagittal plane of the human body. In order to meet the needs of patients with different heights, the thigh length and calf length in the leg module are designed to be adjustable. In order to meet the needs of different obese and thin patients, the width between the leg module and the seat is designed to be adjustable. In order to meet the needs of patients with different conditions, the angle of the seat back is designed to be adjustable, so that patients can train in lying posture and sitting posture. In order to facilitate patients' training, the seat is designed to be movable,

TABLE 1: Range of motion of knee joint.

Joint	Activity status	Maximum angle (°)	Maximum range (°)	Comfort range (°)
Knee joint	Flexion and extension	130	0~130	0~70
	Knee flexion pronation	30	0~30	0~8
	Knee flexion external rotation	45	0~45	0~8

and universal wheels are installed below. The seat can be separated from the lower limb rehabilitation robot. After the patient sits on the seat, push the seat into the robot and lock it [13]. All adjustment functions are realized by electric adjustment. The knee joint is mainly composed of the lower femur, the upper tibia and the patella. The maximum angle of motion of the knee joint in a normal human body is about 70°. The mechanical structure of the lower limb rehabilitation robot designed in this paper realizes the rotation movement by using the rotating pair. The range of motion of the knee joint is shown in Table 1.

Through the simulation of the motion range of the actuator of the lower limb rehabilitation robot with ADAMS software, the results show that the change range of the joint angle basically conforms to the range of human motion comfort, and the system structure basically conforms to the rehabilitation effect, which can help the user automatically complete the rehabilitation training process, as shown in Figure 2.

3.1.2. Design and Implementation of Training Control

(1) *Training Control Process.* In the passive training mode, the target speed of the motor is set first, and the user passively follows the training during the training. The intensity of the training process can be adjusted. After completing a rehabilitation training, the robot stops and saves the rehabilitation training data [14]. In the active training mode, the user is required to make active efforts. When the lower limb muscle strength of the user is insufficient to achieve the predetermined goal, the robot assists the patient to complete the corresponding training. After completing a rehabilitation training, the robot stops and saves the rehabilitation training data. The control flow is shown in Figure 3.

(2) *System Hardware Mechanism.* After the rehabilitation training control program is determined, the hardware part is selected and designed. For the normal operation of the equipment, the peripheral module circuit is used to meet the design requirements. The hardware control system structure of the system includes the single-chip microcomputer controller, power module, data communication module, upper computer industrial control host, data acquisition module, and execution module [15].

(3) *Control Circuit Design.* According to the requirements of training control process, power supply, clock, reset, signal acquisition, motor drive, communication and other circuits are designed.

STM32 is selected as the main control chip to realize the stable and accurate control of the lower limb rehabilitation

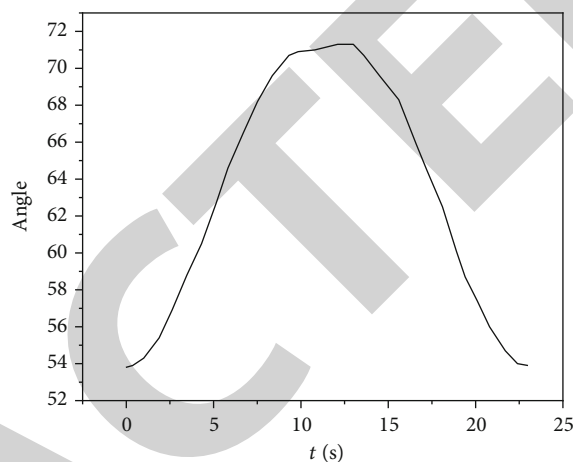


FIGURE 2: Adams motion range simulation.

robot [16]. The reset circuit is mainly used to restart the system and keep the system stable. The clock circuit can produce accurate oscillation circuit to ensure the accuracy of the system. At the same time, the system also designs a debugging interface, which can facilitate the single-step debugging of the control system program and facilitate the control, development, and debugging of the rehabilitation robot. The RS-485 serial bus communication is used to realize the information exchange between the upper computer and STM32 controller. Mc33931 chip produced by Freescale Semiconductor Co., Ltd. is used as the motor drive chip, which has the function of controlling inductive load. Its maximum current can reach 5 A. By default, the enable pin is set to high level, and three pins IN1, IN2, and FB are used to control the motor motion mode [17]. The specific control mode is shown in Table 2.

(4) *Design of Wireless Communication Circuit.* A WiFi module has the advantages of fast transmission speed, supporting multiperson connection, and long communication distance and can support web page and app configuration. Esp-m1 chip is selected in the system. The TXD pin of the chip is connected with the RX pin in the STM32 main controller, and the RXD pin of the ESP chip is connected with the TX pin of the STM32 main controller serial port. By default, the esp-m1 chip is enabled. The program initialization of the STM32 main controller determines the use of the module. The NRST pin of the chip is pulled up with 3.3 V voltage. When the pin level is pulled down, the chip resets.

3.2. *Software Design of Control System Based on Android.* The lower limb rehabilitation robot software system

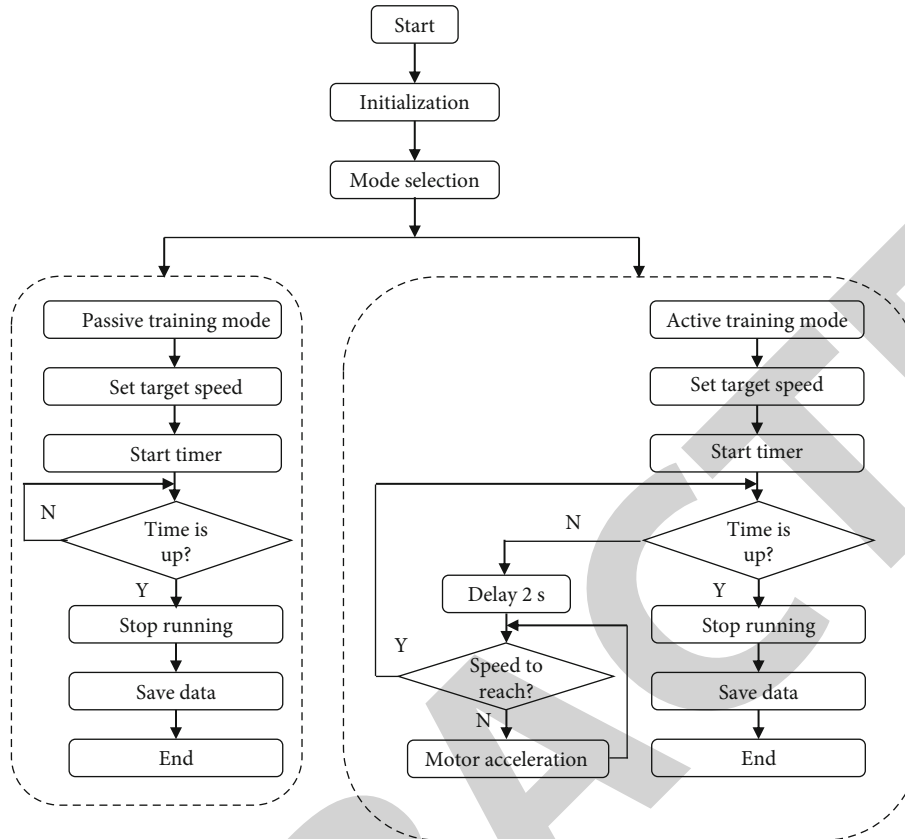


FIGURE 3: Control flow of lower limb rehabilitation robot.

TABLE 2: Motor control logic.

PC8_MC_IN1	PC9_MC_IN2	PC3_MC_FB	Motor status
1	0	PWM	Speed regulation forward rotation
0	1	PWM	Speed regulation reverse
0	0	PWM/0	Stall
1	1	PWM/0	Stop

developed on Android platform improves the controllability and practicability of the system. According to the overall scheme of the rehabilitation robot, the system realizes the functions of registration, training mode selection and control, monitoring data management, and so on. The operation interface is simple and improves the human-computer interaction ability [18]. The socket connection is made between the mobile phone and the esp-m1 chip on the control board. Based on the TCP/ip protocol, the request command can be sent through the remote control end of the Android mobile phone. When the controller receives the information sent by the mobile phone to the esp-m1 module, it sends the action command to drive the circuit to control the rehabilitation robot to perform the rehabilitation movement. Using Android control platform, the experiment of lower limb rehabilitation robot in passive training mode is carried out. By setting the joint training speed, the operation effect of the equipment is verified, and the training parameters and

training progress can be seen through the mobile phone interface. The acquisition card is used to collect the pulse signal fed back by the encoder, and the sampling frequency is 50 Hz, which preliminarily verifies the stability of the system. In the active training mode, when the patient's strength is not enough, the rehabilitation robot will judge for 2 s. When the patient does not reach the training speed, the rehabilitation robot will assist the patient in movement to meet the movement requirements [19].

3.3. Recognition of Training Process Based on Random Forest. Random forest is a strong classifier composed of multiple weak classifiers (decision trees) based on the bootstrap aggregation method. Firstly, the bootstrap method is used to sample and construct subtraining datasets. Each subtraining dataset constructs a decision tree, and then the characteristic parameters are randomly selected to train the decision tree. Each decision tree is irrelevant to each other. When making

a decision, the decision results of multiple decision tree classifiers are voted to obtain the final result [20]. The recognition performance of random forest is higher than that of single decision tree, and overcomes the over fitting problem of decision tree. At the same time, due to the use of random sampling, the training model has small variance and strong generalization ability and is robust to missing data and unbalanced data.

The random forest algorithm proposed in this paper adopts a feature selection method based on Gini coefficient and a classification and regression trees (CART) decision tree. Gini coefficient represents the chaos degree of the model. The smaller the Gini coefficient, the smaller the chaos degree. The feature with the smallest Gini coefficient is selected so that all samples of each child node belong to one classification as far as possible. The Gini coefficient of the probability distribution is as follows:

$$\text{Gini}(p) = 2p(1 - p). \quad (1)$$

For sample set D , after traversing all the segmentation points of feature parameter A , sample set D is divided into two parts by using the relationship between feature parameter and threshold (T_A) ($A > T_A$), that is, sample set D_1 satisfying $A > T_A$ and sample set D_2 not satisfying $A > T_A$. When $A > T_A$, the Gini index of sample set D is the following formula:

$$\text{Gini}(D, A) = \frac{|D_1|}{|D|} \text{Gini}(D_1) + \frac{|D_2|}{|D|} \text{Gini}(D_2), \quad (2)$$

where $\text{Gini}(D_1)$ and $\text{Gini}(D_2)$ represent the uncertainty of sample set D_1 and D_2 , respectively, and $\text{Gini}(D, A)$ represents the uncertainty of set d after $A > T_A$ division.

CART decision tree is a binary tree. According to the different numerical characteristics of dependent variables in the dataset, regression tree, and classification tree can be constructed, respectively. The construction method of classification tree is as follows.

- (1) The subdatasets are obtained through the self-help method, and the feature parameters are randomly selected as the division features of the classification tree nodes. For each feature parameter A selected, all possible thresholds T_A are taken, and the Gini coefficients of the subdatasets divided by $A > T_A$ are calculated. The feature parameters with the smallest Gini coefficients and their corresponding thresholds are selected as the feature division points of the node
- (2) If the number of samples in the node or the depth of the tree reaches the requirements, the construction of the classification tree ends and the CART decision tree that has been successfully constructed is returned. Otherwise, step 1 is recursively executed for the two child nodes

TABLE 3: SEMG signal characteristic values under different speed conditions.

Speed	Rectus femoris			Gastrocnemius muscle		
	MDF	MNF	PPV	MDF	MNF	PPV
A	413.8	454.5	0.04	415.0	455.2	0.045
B	454.1	484.0	0.03	460.3	489.6	0.038
C	486.8	501.9	0.03	485.7	498.4	0.036
D	510.3	518.5	0.02	514.2	520.1	0.017

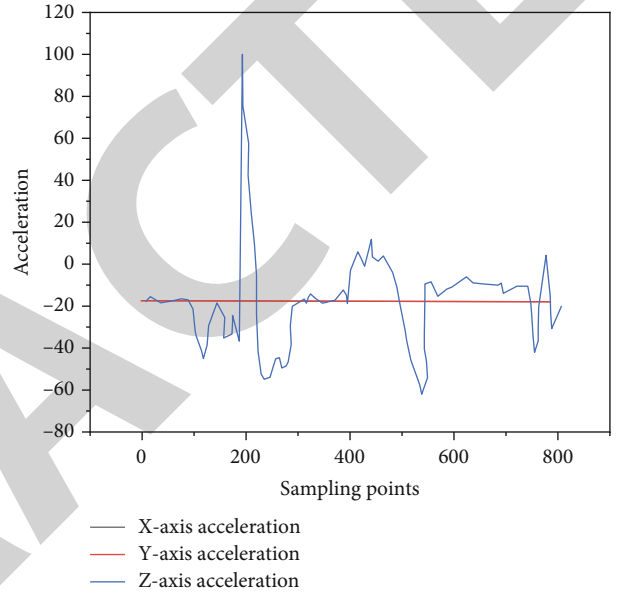


FIGURE 4: High acceleration change curve.

4. Result Analysis

Through experiments on a number of subjects with an average age of about 25 years, the measured original EMG signals are analyzed, and the signals of inertial measurement unit (IMU) are trained and recognized by four different machine learning methods, and the data are analyzed by machine learning algorithm. Preprocess the collected surface electromyography (sEMG) data and IMU data to eliminate the problems of missing data, uneven distribution, and abnormal data. Then, the data are divided into a training set and test set according to the ratio of 7:3, which are randomly disrupted. The training speed is recognized by four algorithms: decision tree, random forest, MLP (multi-layer perceptron) neural network, and linear regression.

Carry out passive training for users at four different speeds. By analyzing the characteristic values of EMG signals in a training cycle, it can be seen that the median frequency (MDF), mean frequency (MNF), and peak peak value (PPV) can better reflect the energy change, as shown in Table 3. It can be seen from Table 3 that under the four different training speeds, through the right shift of the median frequency, the muscle groups exert different forces and show regularity,

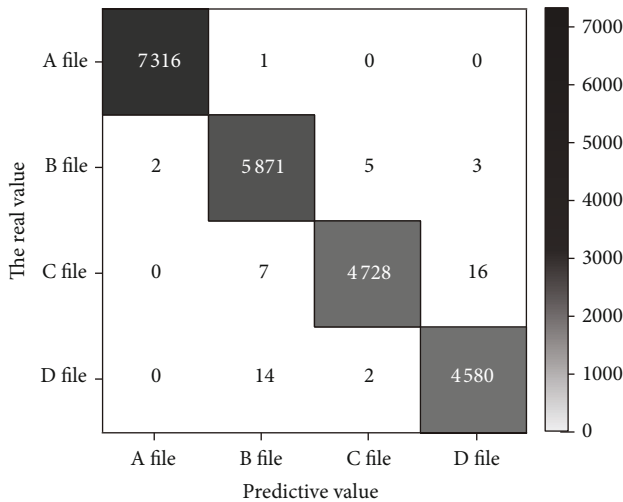


FIGURE 5: Confusion matrix based on the random forest algorithm.

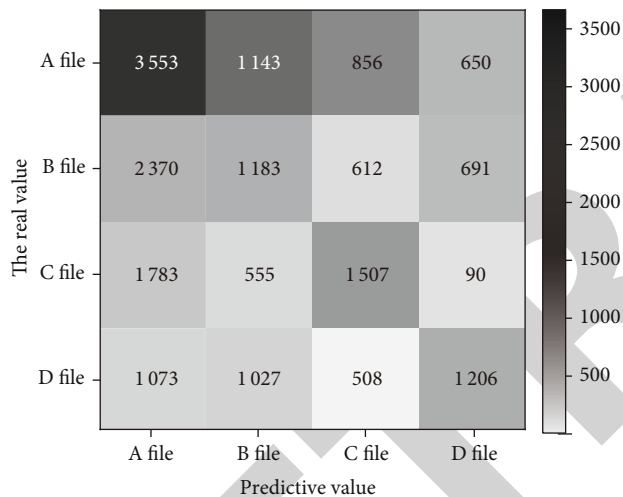


FIGURE 6: Confusion matrix based on the linear regression algorithm.

which is helpful for doctors to evaluate the effect of rehabilitation training.

Figure 4 shows the change curve of thigh IMU acceleration during training. Due to the structure of the lower limb rehabilitation robot, IMU can only detect the acceleration of the z-axis. It can be seen that the acceleration in the training process is variable and nonlinear.

Figure 5 shows the confusion matrix of the recognition effect of the random forest algorithm on the motion state, and Figure 6 shows the confusion matrix of the linear regression algorithm on the motion recognition effect. It can be seen that the recognition effect of the random forest algorithm is better. Taking the first behavior of random forest algorithm confusion matrix as an example, 7316 data were correctly identified as speed *a*, and only one data was incorrectly identified as speed *B*, which is superior to other algorithms.

5. Conclusion

In this paper, the hardware and software of the training control and monitoring system of the lower limb rehabilitation robot are designed for the passive training and active training of patients after lower limb surgery. The hardware design takes STM32F373RBT6 main control chip as the core, and the software system is developed based on an Android platform to realize the functions of registration, training mode selection and control, data monitoring, and management. At the same time, by analyzing the eigenvalues of EMG signals under different speed passive training, the difference of training effect under different speed is verified. Through the identification and classification of IMU signals, the superiority of random forest algorithm in motion state identification is verified, which lays a foundation for man-machine cooperative control. In the follow-up, the designed lower limb rehabilitation robot and its control and monitoring system should be applied to the actual rehabilitation process of patients, and the physiological signals of patients should be analyzed and studied.

Data Availability

The data used to support the findings of this study are available from the corresponding author upon request.

Conflicts of Interest

The author declares that there are no conflicts of interest.

References

- [1] Y. Liu, X. Li, A. Zhu, Z. Zheng, and H. Zhu, "Design and evaluation of a surface electromyography-controlled lightweight upper arm exoskeleton rehabilitation robot," *International Journal of Advanced Robotic Systems*, vol. 18, no. 3, pp. 172988142110034–172988142110232, 2021.
- [2] S. Biici and M. Zeybek, "Effectiveness of training sample and features for random forest on road extraction from unmanned aerial vehicle-based point cloud," *Transportation Research Record*, vol. 2675, no. 12, pp. 401–418, 2021.
- [3] X. Li, Z. Zhu, N. Shen, W. Dai, and Y. Hu, "Deeply feature learning by cmac network for manipulating rehabilitation robots," *Future Generation Computer Systems*, vol. 121, no. 1, pp. 19–24, 2021.
- [4] M. Assad-Uz-Zaman, M. R. Islam, M. H. Rahman, Y. C. Wang, and E. Mcgonigle, "Kinect controlled nao robot for telerehabilitation," *Journal of Intelligent Systems*, vol. 30, no. 1, pp. 224–239, 2021.
- [5] G. Chen, Z. Mao, H. Zhou, and P. Yang, "Design and control strategy of 3-prismatic-revolute-spherical ankle rehabilitation robot," *Australian Journal of Mechanical Engineering*, vol. 8, pp. 1–14, 2021.
- [6] N. Yuvaraj, K. Srihari, G. Dhiman, K. Somasundaram, and M. Masud, "Nature-inspired-based approach for automated cyberbullying classification on multimedia social networking," *Mathematical Problems in Engineering*, vol. 2021, Article ID 6644652, 12 pages, 2021.

Retraction

Retracted: Construction and Simulation of Deep Learning Algorithm for Robot Vision Tracking

Journal of Sensors

Received 17 October 2023; Accepted 17 October 2023; Published 18 October 2023

Copyright © 2023 Journal of Sensors. This is an open access article distributed under the Creative Commons Attribution License, which permits unrestricted use, distribution, and reproduction in any medium, provided the original work is properly cited.

This article has been retracted by Hindawi following an investigation undertaken by the publisher [1]. This investigation has uncovered evidence of one or more of the following indicators of systematic manipulation of the publication process:

- (1) Discrepancies in scope
- (2) Discrepancies in the description of the research reported
- (3) Discrepancies between the availability of data and the research described
- (4) Inappropriate citations
- (5) Incoherent, meaningless and/or irrelevant content included in the article
- (6) Peer-review manipulation

The presence of these indicators undermines our confidence in the integrity of the article's content and we cannot, therefore, vouch for its reliability. Please note that this notice is intended solely to alert readers that the content of this article is unreliable. We have not investigated whether authors were aware of or involved in the systematic manipulation of the publication process.

Wiley and Hindawi regrets that the usual quality checks did not identify these issues before publication and have since put additional measures in place to safeguard research integrity.

We wish to credit our own Research Integrity and Research Publishing teams and anonymous and named external researchers and research integrity experts for contributing to this investigation.

The corresponding author, as the representative of all authors, has been given the opportunity to register their agreement or disagreement to this retraction. We have kept a record of any response received.

References

- [1] S. Xu and L. Chen, "Construction and Simulation of Deep Learning Algorithm for Robot Vision Tracking," *Journal of Sensors*, vol. 2022, Article ID 1522657, 6 pages, 2022.

Research Article

Construction and Simulation of Deep Learning Algorithm for Robot Vision Tracking

Siping Xu ¹ and Lan Chen ²

¹College of Mathematics and Physics, Hubei Polytechnic University, Huangshi 435000, China

²Operation Department, Wuhan Jianxing Urban Resources Operation Management Co., Ltd., Wuhan 430000, China

Correspondence should be addressed to Siping Xu; 2010800405@hbut.edu.cn

Received 5 June 2022; Revised 30 June 2022; Accepted 11 July 2022; Published 20 July 2022

Academic Editor: Haibin Lv

Copyright © 2022 Siping Xu and Lan Chen. This is an open access article distributed under the Creative Commons Attribution License, which permits unrestricted use, distribution, and reproduction in any medium, provided the original work is properly cited.

As one of the indispensable basic branches of computer vision, visual object tracking has very important research value. Therefore, a deep learning based on robot vision tracking is evaluated. Based on the basic principles of target tracking and search principle, a deep learning algorithm for visual tracking is constructed, and finally, evaluated, and simulated. The results showed that the accuracy rate increased from 90.9% to 90.13% after the addition of channel attention mechanism module. Variance was reduced from 3.78% to 1.27%, with better stability. The EAO, accuracy, and robustness of the algorithm are better than those without significant region weighting strategy. The strategy of using the improved residual network SE-ResNet network to extract multiresolution features from the correlation filtering framework is effective and helpful to improve the tracking performance.

1. Introduction

As one of the indispensable basic branches of computer vision, visual object tracking has very important research value. The problem is specifically defined as that in a video sequence, an object of any category at any position in the initial frame is designated as the target, and the target tracking algorithm can frame the target quickly and accurately in the subsequent frames by means of image processing and machine learning. Target tracking technology, which can realize the above functions and has both real-time and robust performance, is the core of artificial intelligence-related applications. For example, in the autonomous driving system, target tracking can estimate and predict the position trajectory of pedestrians and vehicles in front of the vehicle, which can make decisions for the vehicles' next direction and speed. In the road navigation system, target tracking can avoid the dynamic obstacles on the road ahead. In the urban surveillance system, target tracking saves a lot of manpower for searching and tracking. Target tracking can also be embedded in the UAV equipment to achieve

autonomous obstacle avoidance and follow the designated target. Review the development of tracking algorithm, and its milestone innovation is usually established on the breakthrough of some theory or method, roughly experienced four stages: the machine learning methods represented by support vector machine Bayesian classifier sparse can realize simple and complete scene tracking. The discriminant model based on particle filter can distinguish the complex background well, but the sampling process is time consuming and random. The discriminant model based on particle filter can distinguish the complex background well, but the sampling process is time-consuming and random. Target tracking under the framework of correlation filtering mainly includes two aspects: cyclic shift sampling and ridge regression objective function optimization. With complete mathematical theory and high stability, it is the preferred method to try in landing applications. A lot of work is devoted to theoretical improvement and precision improvement of such algorithms, as well as tracking algorithms based on deep learning. Feature expression has good robustness and implicit nonlinear fitting ability. However, the exploration

time of such methods is short, and there is still a large space for development compared with mature algorithms in terms of accuracy and speed, as shown in Figure 1.

2. Literature Review

A large number of studies show that the target tracking algorithm has always been the breakthrough of machine vision learning, and new target tracking algorithms and ideas continue to emerge. However, it is difficult to have an algorithm to deal with all kinds of complex scenes, and the difficulties in improving the performance of target tracking are mainly as follows: structural changes to the nonrigid target itself, perspective transformation of rigid targets, similarity in scene and target characteristics, similarity between multiple objects, a change in illumination, occlusion of a target, a sudden change in its direction of motion, changes in target scale and resolution, and limitations in computational time and space complexity. Existing algorithms have solved one or more of these problems to a certain extent, but there is still a lot of room for performance improvement.

As early as in the 1960s, Ding et al. proposed a method to obtain three-dimensional shape information of objects from two-dimensional images [1]. This method based on computer theory requires physical photography to achieve [2]. At this point, the machine vision theory and practice research for the purpose of analyzing object 3D scene is like a fire like tea [3]. At the beginning of 1970, Sami et al. established a systematic computer vision theory, which laid the foundation for some researches on machine vision theory and was a milestone progress. Its core content was to recover three-dimensional geometric shapes of objects based on two-dimensional images [4]. Since the early 1980s, Zieliński and Markowska-Kaczmar's research on machine vision has been a hot research field in modern high-tech research and has become more and more mature in practical application [5]. Wu et al. first proposed the concept of mean-drift vector in 1975 [6]. Jahanbakt. applied the iterative procedure of calculating mean-drift vector to image segmentation and target tracking [7].

On the basis of current research, deep learning of the robot vision tracking algorithm is proposed, and most target tracking algorithms are based on candidate to find the target. Therefore, how to effectively generate screening candidate samples based on the location of the last frame is also a key link in target tracking. Most target tracking algorithms default that the movement of the object between consecutive frames is not too violent. Therefore, the motion model can be used to generate candidates around the location of the object in a frame. At present, there are mainly two ways to generate candidate frames: particle filter and sliding window particle filter, which use the predicted position of the above frame as the center to transform the radiation parameters of six candidate frames, so as to obtain a series of candidate samples [8]. The six parameters include horizontal displacement, vertical displacement, rotation angle, aspect ratio, stretch ratio, and dimension particle filter. Most of the methods use reconstruction error as the benchmark for target screening. However, this method also has its disadvan-

tages; that is, when generating candidate samples, there will be a lot of redundant calculation due to the overlap between samples [9]. In addition, the number of samples is also difficult to control: using too many samples will cause redundant calculation and tight computer memory, resulting in very slow tracking. If too few samples are used, the tracking speed will be improved to some extent, but the area where the real target is often cannot be proposed as a candidate, thus reducing the tracking accuracy. Therefore, many parameters of particle filter have many problems of manual adjustment in practical application. Sliding window is a method of exhaustive extraction in theory, which uses the horizontal and vertical displacement of the target frame to extract candidates [10]. Because a circular sample is put forward, and can be fast calculation, in fu, Dhiman et al. makes this method also has been widely used, but the nature of the edge effect, because of its circulation sample window need to add after the gauss window to calculate, led to the fast moving object is extremely easy to produce trace drift phenomenon. At present, there are many algorithms to solve this problem [11].

3. Appearance Modeling of Target Tracking

3.1. Basic Principles of Target Tracking. Although target tracking algorithms have different ideas based on point, line and plane, or generative and discriminant, they all revolve around the basic flow chart of target tracking based on four basic modules, including target feature extraction target construction model target search strategy and target model update. Firstly, it is necessary to initialize the tracking target and determine its initial position, then extract effective feature information in the target area to describe the target accurately, and then establish the target model [12]. Finally, according to the target model, an appropriate search strategy is designed to estimate the optimal target area according to the interference encountered in the target tracking process, and the target model is reasonably updated to adapt to the change of the target appearance [13], see Figure 2.

3.2. Search Strategy for Target Tracking. Target search strategy is to find the best method of similarity measure in the current image search which is most similar with the target area; usually by some distance to calculate the target tracking algorithm, the similarity measure reflects the similarity between the target template with the candidate; so, the selection of similarity measurement strategy is critical and has a direct effect on the result of the target tracking. Appropriate similarity measurement method can objectively reflect the relationship between candidate target and template [14].

Euclidean distance is the most common definition of distance, which represents the real distance between two points. The Euclidean distance formula between two points on a two-dimensional plane is shown in Formula (1).

$$\text{dist}_{ab} = \sqrt{(x_1 - x_2)^2 + (y_1 - y_2)^2}. \quad (1)$$

The Euclidean distance formula between two points in n

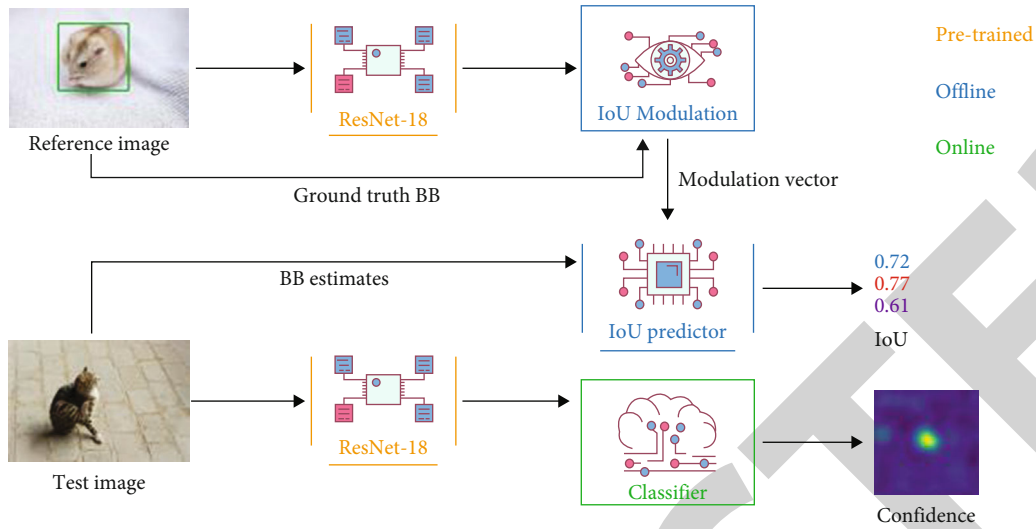


FIGURE 1: Deep learning robot vision tracking algorithm.

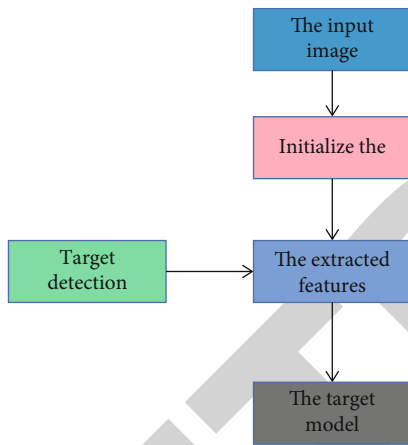


FIGURE 2: Robot target modeling diagram.

-dimensional space is shown in Formula (2):

$$\text{dist}_{ab} = \sqrt{(x_1 - y_2)^2 + (x_1 - y_2)^2 + (x_n - y_n)^2}. \quad (2)$$

3.3. Algorithm Framework. Offline training twin network of the two branches of learning in a 255×255 search area locates 127×127 goals, and it studied the estimation function, a similarity to the target and the search area of every position compared to predict a confidence figure; in the image, the target area high degree of confidence, confidence is low background area [15]. In particular, this algorithm proposes a crosscorrelation layer to calculate the similarity between each position and the target in the search area at one time, as shown in Formula (3).

$$F(z, x) = \varphi(z) * \varphi(x) + v. \quad (3)$$

The two branches of the network adopt the same structure and parameters and are composed of three parts,

namely, local pattern detection module background, modeling module, and integration module [16]. The details of these modules will be elaborated in the following sections. The last crosscorrelation operation is performed on the output of the integrated modules. The algorithm employs logical loss function to train the network, as shown in Formula (4).

$$L = \log(1 + e^{-\gamma v}). \quad (4)$$

In this paper, the target location task is described as a conditional probability modeling task; so, this paper first uses standard conditional probability learning to explain the algorithm [17]. Its purpose is to find a parameter matrix W for each video, which can minimize the loss of the prediction function F , where L is the average hundred of the loss of N target templates and sample pairs in the local search area, as shown in Formula (5).

$$\min_w \frac{1}{N} \sum_i L(F(x, Wz)). \quad (5)$$

3.4. Quantitative Analysis. Compared with THE FCT and ODFS algorithms, this algorithm has better performance on background anti-interference and occlusion problem, is not easy to lose and drift due to environmental interference and occlusion, and has strong robustness to the influence of background clutter scale change occlusion light. For David I and FaceocC2 sequences, although the tracking success rate of this algorithm is lower than that of the HCF algorithm, the real-time performance of this algorithm is very good on the basis of extracting image features with compressed sensing, while the real-time performance of the HCF algorithm is not ideal due to extracting image features with convolutional neural network [18]. Compared with the KCF algorithm, although the tracking success rate for David and FaceocC2 is slightly lower, it is

TABLE 1: Track success rate and frame rate.

	Shaking	David	Face	Sylvesier	Shaking	David	Faceooc	Sylvesier
Ours	89.5	93.4	88.1	91.2	27.8	29.1	28.3	29.5
FCT	84.3	91.1	84.2	86.1	31.7	38.3	38.6	36.1
ODFS	78.9	81.2	83.2	85.4	29.6	35.1	37.4	27.6
KCF	9.6	95.6	96.5	97.4	23.5		39.2	132.1
HCF	77.2	96.3	94.2	95.3	0.1	0.6	0.5	0.5

TABLE 2: Comparison of different models.

Method	Accuracy	Variance	F	G	A
MDNet	89.99	2.99	81.22	84.33	66.55
Ad channel attention module	90.33	1.28	83.22	86.99	65.77
The algorithm in this chapter	90.66	0.65	87.66	87.33	66.21

obviously much higher for shaking sequence tracking. The KCF algorithm does not build a robust apparent model, and the tracking success rate is very low when tracking difficult sequences such as chaotic background rotating motion and light influence [19]. For different sequences, each target is in a different environment, and the appearance of the target varies greatly as time goes by, leading to the difference in the processing speed of the same algorithm for different sequences. In addition, for the same sequence, different trackers have different processing speeds for the same sequence due to their different essential structure and performance [20]. The processing speed of this algorithm for image sequences of Shaking, David, Faceooc2, and S Bayvester is lower than that of the KCF algorithm and FCT algorithm, and it has better real-time performance than other algorithms, mainly because the algorithm in this chapter adopts the method of compressed sensing. Compared with the FCT algorithm, the real-time performance of this algorithm is poor. It mainly samples multiple instances and takes the weight of positive instances into consideration in the packet, which undoubtedly increases the computing load but is superior to the FCT algorithm in accuracy, see Table 1.

4. Experiments and Analysis

4.1. Comparison of Different Models. In the experiment, we first establish an independent MDNet vehicle tracking model and then add the channel attention mechanism module to see whether the tracking result is optimal. Finally, two attention mechanism modules are added, combined with case segmentation, to improve our tracking efficiency and solve the problems of vehicle occlusion in the tracking process [21]. We analyzed the differences between these models, calculated these indicators by the crossvalidation method, and evaluated the robustness of the algorithm, where FI represents the harmonic average of accuracy and recall rate, A. It can be seen from the comparison that the accuracy is improved from 90.9% to 90.13% after the addition of channel attention mechanism module. Variance was reduced from 3.78% to 1.27%, with better stability [22]. After the

addition of the two attention mechanisms, combined with the image segmentation algorithm, tracking accuracy is higher, and the algorithm is more stable, as shown in Table 2.

Furthermore, we explore the robustness and accuracy of different time series video data and truncate the test video in units with length ratios of 1, 2, 3, and 4 to form three groups of test data. We input these different data into the model to measure the tracking effect of the model on different video sequence lengths and compare the results. The results show that the shorter the video sequence is, the worse the tracking effect is, and the longer the video sequence is, the better the tracking effect is [23], see Table 3.

4.2. ResNet Network Model. Residual neural network, which for the first time, made it possible to train ultradeep neural networks. It is the first time to train neural network successfully and get good results in computer vision competition. Although the expression ability of convolutional neural network is enhanced with the deepening of layers, the performance degradation of neural network may occur. One reason for this is that the deeper the neural network, the greater the gradient disappearance or explosion. In order to solve the phenomenon of gradient disappearing after neural network deepening, a residual element is proposed, as shown in Figure 3.

4.3. Ablation Experiments. In order to verify the effectiveness of the significant regional weighting strategy in this chapter, ablation experiments were conducted in this chapter, and the algorithm in this chapter was compared with the algorithm without significant regional weighting strategy in VOT2016 and VOT2017. Ours represents no significant region weighting strategy; otherwise, it is the same as the algorithm in this chapter. It can be seen from the two tables that the algorithm in this chapter is superior to the algorithm without significant region weighting strategy in EAO accuracy and robustness. Experimental results show that significant region weighting strategy can improve tracking performance effectively. In addition, compared with ECO, the benchmark tracking algorithm in this chapter, the algorithm

TABLE 3: Comparison of results of different video sequences.

Video sequence	Accuracy	Variance	F	G	A
1	76.5	3.20	66.32	74.21	45.23
2	87.23	2.50	76.35	79.66	56.33
3	88.54	0.89	82.54	85.44	61.55
4	89.34	0.67	89.64	87.55	66.89

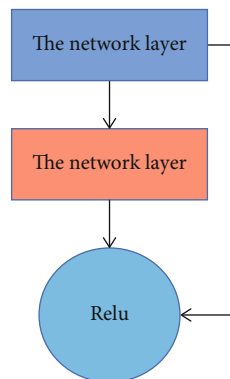


FIGURE 3: The imperfect unit.

TABLE 4: Comparison of ablation results on OVT2016.

	EAO	Accuracy	Robustness
Ours	0.3125	0.4458	0.235
Ours N	0.2586	0.5463	0.326
ECO	0.6482	0.6486	0.254

TABLE 5: Comparison of ablation results on OVT2016.

	EAO	Accuracy	Robustness
Ours	0.2403	0.6032	0.182
Ours N	0.2456	0.5423	0.324
ECO	0.2906	0.6542	0.364

in this chapter still outperforms ECO in the accuracy and robustness of EAO even without significant regional weighting strategy. The results show that the strategy of using the improved residual network SE-ResNet network to extract multiresolution features from the correlation filtering framework is effective and helpful to improve tracking performance, as shown in Tables 4 and 5.

4.4. Contrast Pooling of Ideas with Other Approaches. In order to extract appearance features from each 3D bounding box candidate constructed from the diagram, we propose a point-attention pooling method to abstract the interactions of internal points. In this part, ablation research is conducted on the use of point attention pooling, set abstraction layer, feature average, or feature maximum. Among them, SA layer is the same as the paper, feature averaging and fea-

ture maximization methods are connected behind MLP, and their outputs are one-dimensional features of the same size as our proposed method. We use these four methods to extract proposal capabilities and then use them as appearance features to build diagrams. We use these four methods to extract proposal capabilities and then use them as appearance features to build the diagram. Other settings of the framework we index are consistent with the original network. Below, a 3D bounding box candidate usually contains parts from different objects. Therefore, it is necessary to completely collect points on the surface of the same object and learn the semantic and geometric information associations between them when extracting index region features. We explore the effect of directional features on point-attention pooling, and we can see that it results in a gain of 0.3% compared to the learning index region features using only semantic features and 3D coordinates. Here is our interpretation: direction vector causes points belonging to the same object to attract each other, belonging to different objects mutually exclusive.

5. Conclusion

Aiming at the problem of unreliable spatial information association in complex scenes such as frequent occlusion of visual target interaction, this chapter focuses on the similarity of the same individual features rather than different individual features. The discriminant apparent information can be obtained by training two kinds of classification-based network and discriminant and generative learning network on large scale rerecognition data sets, which can provide reliable matching clues for subsequent data association in multitarget tracking. In this chapter, based on the extended multitarget tracking of spatial information association, the apparent information is transferred to the multitarget tracking process, and the apparent feature measurement method and the matching mechanism of multilayer cue association are constructed. Experiments verify that the multitarget tracking algorithm with the fusion of the apparent information reduces the number of mistaken identity transformation between the targets and improves the stability of the trajectory from the representation ability of the two apparent features, the statistical m -index tracking speed and other aspects. In addition, apparent features based on discriminant and generative learning networks are more reliable in association. There are still many challenges in practical application and popularization of multitarget tracking technology.

Data Availability

The data used to support the findings of this study are available from the corresponding author upon request.

Conflicts of Interest

The authors declare that they have no conflicts of interest.

Retraction

Retracted: Research on Intelligent Pick-Up Route Planning of a Logistics Cycle Automatic Robot

Journal of Sensors

Received 19 December 2023; Accepted 19 December 2023; Published 20 December 2023

Copyright © 2023 Journal of Sensors. This is an open access article distributed under the Creative Commons Attribution License, which permits unrestricted use, distribution, and reproduction in any medium, provided the original work is properly cited.

This article has been retracted by Hindawi following an investigation undertaken by the publisher [1]. This investigation has uncovered evidence of one or more of the following indicators of systematic manipulation of the publication process:

- (1) Discrepancies in scope
- (2) Discrepancies in the description of the research reported
- (3) Discrepancies between the availability of data and the research described
- (4) Inappropriate citations
- (5) Incoherent, meaningless and/or irrelevant content included in the article
- (6) Manipulated or compromised peer review

The presence of these indicators undermines our confidence in the integrity of the article's content and we cannot, therefore, vouch for its reliability. Please note that this notice is intended solely to alert readers that the content of this article is unreliable. We have not investigated whether authors were aware of or involved in the systematic manipulation of the publication process.

Wiley and Hindawi regrets that the usual quality checks did not identify these issues before publication and have since put additional measures in place to safeguard research integrity.

We wish to credit our own Research Integrity and Research Publishing teams and anonymous and named external researchers and research integrity experts for contributing to this investigation.

The corresponding author, as the representative of all authors, has been given the opportunity to register their agreement or disagreement to this retraction. We have kept a record of any response received.

References

- [1] Q. Hu and Y. Fan, "Research on Intelligent Pick-Up Route Planning of a Logistics Cycle Automatic Robot," *Journal of Sensors*, vol. 2022, Article ID 4268589, 8 pages, 2022.

Research Article

Research on Intelligent Pick-Up Route Planning of a Logistics Cycle Automatic Robot

Qinlong Hu  and Yimin Fan 

College of Management Science, Chengdu University of Technology, Chengdu, Sichuan 610059, China

Correspondence should be addressed to Yimin Fan; 20160765@ayit.edu.cn

Received 29 May 2022; Revised 28 June 2022; Accepted 7 July 2022; Published 19 July 2022

Academic Editor: Haibin Lv

Copyright © 2022 Qinlong Hu and Yimin Fan. This is an open access article distributed under the Creative Commons Attribution License, which permits unrestricted use, distribution, and reproduction in any medium, provided the original work is properly cited.

In order to improve the efficiency of a logistics cycle robot picking up goods, a path planning algorithm based on artificial intelligence was proposed. After analyzing the particle swarm optimization algorithm, the particle swarm optimization algorithm is optimized and improved and the path planning of a single robot is obtained. On this basis, a multipopulation particle swarm optimization (CMMPPSO) algorithm is proposed. The results show that the JMPOPSO algorithm is more accurate than the BPSO algorithm and the maximum fitness optimized by the BPSO algorithm is 1.59, while the maximum fitness optimized by the JMPOPSO algorithm is 1.98. The path optimized by the CMMPPSO algorithm based on JMPOPSO is better than that optimized by the CMMPPSO algorithm based on BPSO, shortening by about 25% and shortening the time by about 30. Simulation experiments verify the effectiveness of the CMMPPSO algorithm.

1. Introduction

Robots are widely used in industrial production and people's life. They can help people complete all kinds of hard, dangerous, and repetitive work, such as safety detection of nuclear equipment, complex medical diagnosis, glass exterior wall wiping, and assembly line operation [1]. The invention and popularization of robots have provided a strong driving force for the development of the world economy. Academician Zhao Lv once pointed out that "the birth of robots and the establishment and development of robotics are the most convincing achievements of automatic control in this century and the major achievements of human scientific and technological progress in the 20th century" [2]. The application of robots reflects the industrial automation level of a country to a certain extent [3]. With the continuous maturity and development of computer technology, intelligent control theory, VLSI, pattern recognition technology, sensor technology, and structure, robot technology has also entered a new development stage. Intellectualization and

humanization have become the main trend of the development of the robot industry in the future [4].

Based on the new herd intelligent optimization algorithm, particle swarm optimization (PSO) is a simple mathematical model, is easy to use, and requires no objective optimization function to distinguish, differentiate, and control. The algorithm can be used in most application fields that need optimization, among which the fields with great potential mainly include power system control, pattern recognition, signal processing, image classification, fuzzy controller design, and robot path planning. The improved algorithm can obtain a better path, as shown in Figure 1 for the control system of the logistics handling robot. However, the particle swarm optimization algorithm has the disadvantage of easy convergence to the local optimal solution, that is, it is prone to premature convergence. This problem has prompted scientists to optimize the animal algorithm and use it to plan the path of mobile robots. When using the particle optimization algorithm to solve the problem of mobile robot planning, in general, the best way is not the

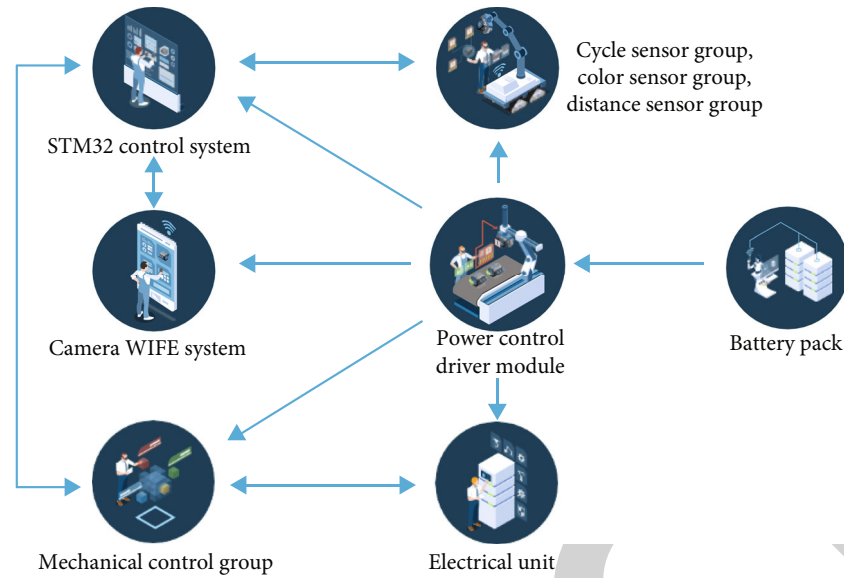


FIGURE 1: A manufacturing method of an intelligent logistics handling robot control system.

best way in the world, but the right way. Therefore, good planning is a very important part of research.

2. Literature Review

A mobile robot is a kind of robot with high intelligence, and it is also the focus and frontier field of intelligent robot research. As an important group in the robot family, mobile robots have made many remarkable achievements in the past decades [5]. Developed countries such as Europe, America, and Japan have studied mobile robot technology earlier, and the mobile robot technology of these countries represents the highest level in the world to a certain extent [6]. In 1966, the artificial intelligence center at the Stanford Research Center (ACSRC) successfully developed the world's first mobile machine—Shakey. It has certain observation ability to the environment and independent modeling ability, but it needs to use multiple large computers to control it [7]. Domestic scholars study mobile robot technology later than developed countries such as Europe and the United States, but after more than 40 years of unremitting efforts, they have also made many great achievements [8]. Zhao and others developed a new type of special robot—independent 4WD all-terrain explosive disposal robot. The independent 4WD all-terrain explosive disposal robot is mainly used in harsh environments such as wild mountains and can check, transport, and detonate suspected explosives [9]. Foroughi and others proposed the Voronoi diagram. At first, the Voronoi diagram was used to solve the proximity problem of plane points in mathematics but some scholars soon introduced it into robot path planning. In this method, the Voronoi diagram can be used to describe the networked structure of feasible areas in the robot working environment [10]. Cai and Zheng proposed robot path planning based on the grid method, which was proposed relatively early and widely used. They further tested and analyzed the reliability of applying the grid method to solve path planning problems

[11]. Zheng and Cai proposed a real-time robot path planning method based on the concept of the artificial potential field. This method can avoid collision with obstacles in real time in a complex environment. This method has been successfully applied to the cosmos system of a PUMA robot [12]. Sennan and others proved that Hopfield-type nonlinear simulation neurons are very effective for robot path planning and obstacle avoidance. From any starting position to any target position, the artificial neural network system can successfully avoid static and dynamic obstacles of arbitrary shape and quickly provide an appropriate path [13]. Kaya and others introduced the fuzzy control theory into mobile robot path planning and proposed a robot path planning method based on multiple motion instruction sets. This method uses fuzzy rules to guide the motion of the robot, avoids the disadvantage of poor real-time performance of mobile robot path planning due to large amount of calculation, and achieved good simulation results [14]. Pahnehkoei and others combined the improved genetic algorithm with the Dijkstra algorithm (DA) to optimize the robot path and designed a heuristic way to generate the initial population. As a swarm intelligence optimization algorithm, the ant colony algorithm is also widely used in robot path planning [15]. Wu and Song combined the ant colony algorithm with a probabilistic roadmap planner (PRM) to plan the robot path, which can reduce the path planning time to an acceptable range [16].

Robot navigation technology is one of the most important technologies in mobile robots. Robot navigation technology mainly includes the following three aspects: robot positioning, task planning, and path planning. Robot positioning is the key technology to realize autonomous navigation. This technology requires a mobile robot to determine its position and direction when its initial position is known or unknown. Task planning refers to the mobile robot completing some specific tasks in a specific time and space. Path planning requires the mobile robot to reach the

target position from the starting position at the least cost (such as the shortest walking path, the least walking time, and the lowest walking energy consumption). In this process, the collision between the robot and obstacles and between the robot and the robot should be avoided [17].

The research on robot path planning technology can reduce the working time of the robot, improve the working efficiency of the robot, and reduce some unnecessary wear and consumption of the robot, so as to achieve the purpose of saving resources and reducing costs [18]. In some special environments, a good robot path planning technology is particularly important, such as flood fighting and rescue, explosive disposal, rescue, and military reconnaissance. The use of good path planning technology can make the mobile robot quickly reach the designated target position. In order to save and ensure the safety of people's lives and property and win valuable time, the research on path planning technology can also reduce the uncertainty of the robot in the movement process and enhance the flexibility of the mobile robot, so as to enhance the intelligent level of the mobile robot and lay a solid foundation for the further wide use of the mobile robot in industrial production and people's life [19]. Robot path planning technology is the basis for the development of various high-performance mobile robots. Therefore, the research on robot path planning technology has very important theoretical and practical significance [20].

3. Research Methods

3.1. Particle Swarm Optimization Algorithm. The particle swarm optimization algorithm is a swarm intelligence evolutionary method proposed by Dr. Kennedy and Professor Eberhart [21, 22]. Like the genetic algorithm, evolutionary programming (EP), evolutionary strategies (ES), and other evolutionary algorithms, the algorithm is a direct search algorithm based on population evolution and does not need to rely on gradient, curvature, and other information.

In the particle swarm optimization algorithm, the calculation formula of $k + 1$ iteration of each particle i in the d dimension is as follows (1):

$$\begin{aligned} v_{id}^{(k+1)} &= v_{id}^{(k)} + c_1 \cdot \text{rand}() \cdot (p_{id}^{(k)} - x_{id}^{(k)}) + c_2 \cdot \text{rand}() \cdot (p_{gd}^{(k)} - x_{id}^{(k)}), \\ x_{id}^{(k+1)} &= x_{id}^{(k)} + v_{id}^{(k+1)}. \end{aligned} \quad (1)$$

Among them, c_1 and c_2 are called learning factors, which are used to adjust the step length of particles flying towards the optimal value of the individual position and the optimal value of the group position, respectively [2, 23]. $p_{id}^{(k)}$ represents the optimal value of individual position of the particle, $p_{gd}^{(k)}$ represents the optimal value of the group position, d ($1 \leq d \leq D$) represents the dimension of the position vector and velocity vector, and $\text{rand}()$ is a random number between (0,1).

When generating a new particle position, the constraint conditions of the particle velocity vector must also be met, as shown in formula (2):

$$\left| v_{id}^{(k+1)} \right| \leq V_{\max}. \quad (2)$$

In formula (2), V_{\max} represents the limiting constant of the velocity vector. The velocity vector constraint condition can also be expressed as equation (3):

$$\left| x_{id}^{(k+1)} - x_{id}^{(k)} \right| \leq V_{\max}. \quad (3)$$

This is also the Lipschitz condition of the dynamic system [3].

In the particle swarm optimization algorithm, the update function of the optimal value of the individual position of the particle is defined as equation (4):

$$p_{id}^{(k)} = \begin{cases} x_i^{(k)}, & f(x_i^{(k)}) \leq f(p_{id}^{(k-1)}), \\ p_{id}^{(k-1)}, & f(x_i^{(k)}) > f(p_{id}^{(k-1)}). \end{cases} \quad (4)$$

In the particle swarm optimization algorithm, the update function of the optimal position of the whole population is defined as equation (5):

$$\begin{aligned} p_{gd}^{(k)} &\in \{p_{1d}^{(k)}, p_{2d}^{(k)}, \dots, p_{md}^{(k)} \mid f(p_{id}^{(k)})\} \\ &= \min \{f(p_{1d}^{(k)}), f(p_{2d}^{(k)}), \dots, f(p_{md}^{(k)})\}, \end{aligned} \quad (5)$$

In formulas (4) and (5), $f()$ represents the fitness function value.

The steps of the particle swarm optimization algorithm are shown in Figure 2.

3.2. Path Planning of a Single Machine Robot Based on the Improved Particle Swarm Optimization (JMPOPSO) Algorithm. When using the particle optimization algorithm to improve the performance of the robot cell, the method can be estimated according to the physical function. Creating an outflow directly affects whether the algorithm can find a good way. The energy function is designed to improve the flow. For the optimization index method, the long road is the first index. Of course, other performance measures such as road safety and road smoothness should be determined. The performance force described in this paper includes three performance measures.

(1) Path length fit1

$$\begin{aligned} \text{Fit1} &= \sum_{j=0}^N |p_j p_{j+1}| = \sqrt{d + (y_s - y_1)^2} \\ &+ \sum_{j=1}^{N-1} \sqrt{d + (y_{j+1} - y_j)^2} + \sqrt{d + (y_g - y_N)^2}. \end{aligned} \quad (6)$$

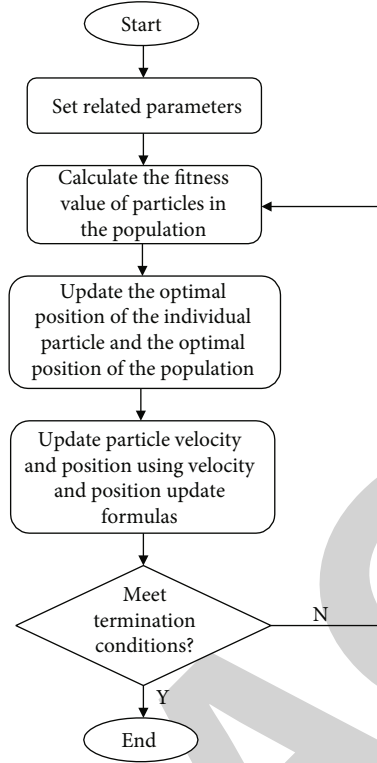


FIGURE 2: Flow chart of the particle swarm optimization algorithm.

In formula (6), $d = (x_s - x_g / N + 1)^2$ is the fixed value, which represents the length of each horizontal axis in the newly established coordinate system, $N + 1$ is the number of segments evenly divided by the vertical line, and (x_s, y_s) and (x_g, y_g) represent the coordinates of the starting point and target point in the robot path planning, respectively

(2) Path security fit2

The safety performance of the path can be expressed by the number of segments intersecting the obstacle in a complete path, as shown in equation (7).

$$\text{Fit1} = \begin{cases} n, & \text{number of sections where the path intersects the obstacle, the path is not feasible,} \\ 0, & \text{the path does not intersect with the obstacle, the path is feasible.} \end{cases} \quad (7)$$

(3) Smoothness of path fit3

The walking distance between mobile robots should be as small as possible and the walkway should be as smooth as possible. Only in this way can the wear and tear caused by the robot rotation be reduced. Therefore, as shown in equation (8), the design of the robot method must take into account the optimized method uniformity.

$$\text{Fit3} = \frac{\left(\sum_{j=0}^N \beta(l_j, l_{j+1}) \right)}{N}. \quad (8)$$

In formula (8), $\beta(l_j, l_{j+1})$ represents the included angle between two path segments l_j and l_{j+1} and N represents the

number of included angles. The greater the included angle between path segments, the smoother the optimized path.

Considering the performance indexes of the abovementioned three path optimizations, the fitness function $f_1(p)$ is designed as equation (9):

$$f_1(p) = \frac{N + 1 - \omega_2 \cdot \text{fit2} + \omega_3 \cdot \text{fit3}}{\omega_1 \cdot \text{fit1}}. \quad (9)$$

In formula (9), ω_1 , ω_2 , and ω_3 are the adjustment parameters of path length fit1, path security fit2, and path smoothness fit3, respectively, so that the three performance indexes can be unified in the order of magnitude. When

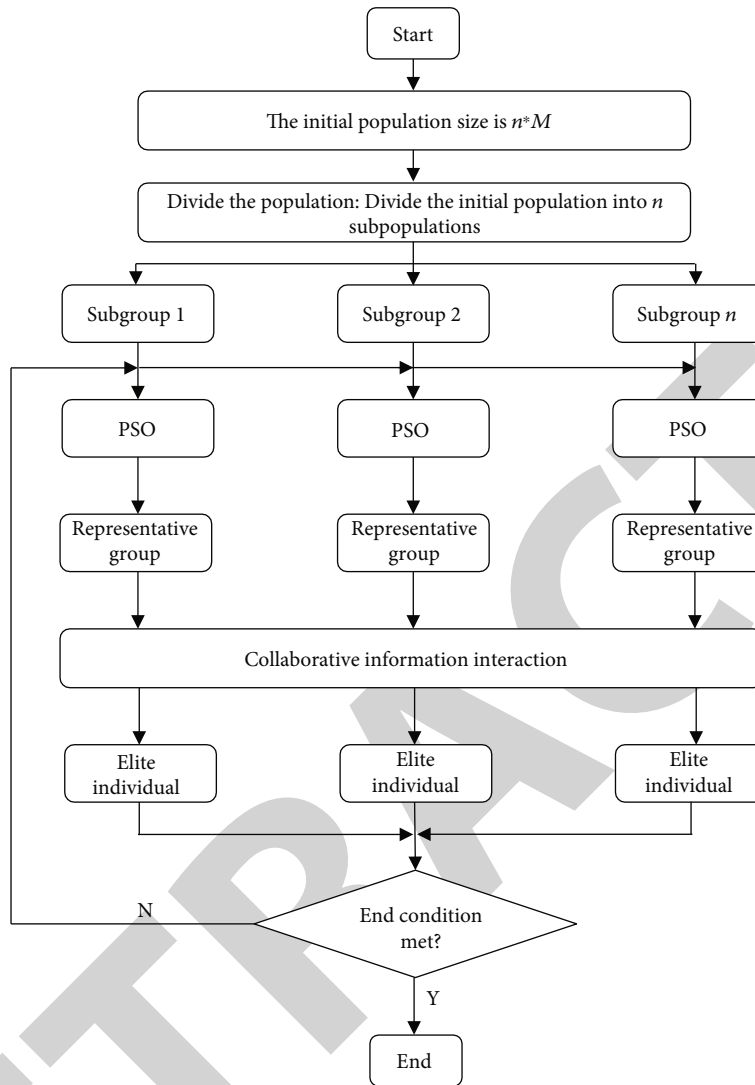


FIGURE 3: Flow chart of the CMMPPSO algorithm.

the fitness function value $f_1(p)$ is larger, the optimized solution is better, that is, the optimized path quality is better.

3.3. Multiswarm Particle Swarm Optimization (CMMPPSO) Algorithm Based on the Collaborative Mechanism. Previously, the use of single-robot planning based on particle optimization algorithms has been shown, but not the use of multirobot planning. To solve the problem of multiple robotic methods, a synergistic mechanism is integrated into the PSO algorithm and multiple public particle optimization based on the synergy (CMPPSO) algorithm is planned. Because multiple robots work in the same environment, there is a relationship of competition and cooperation between robots. Firstly, the multirobot path planning problem is decomposed into several subproblems for solution and the initial population is divided according to the number of robots. Each subpopulation corresponds to a robot's individual evolutionary optimization. Each robot is optimized separately by the corresponding subpopulation, and then, the representative individual group is selected according to the fitness evaluation function. The selected represen-

tative individual group is operated by collaborative information interaction, and the combination with the best fitness value is selected as the elite individual, so that each optimized path meets the objective constraints and outputs the final optimal combination. The flow of CMMPPSO algorithm is shown in Figure 3.

In the process of multirobot path planning, because there are multiple mobile robots in the same working environment and the starting point and target point of each robot are different, the path optimized by the algorithm may cross in the same space at the same time. When the robot moves along the optimized path, there will be a collision between the robot and the robot.

If there are two robots moving from the starting point to the starting point at the same speed, it can be judged whether there is a collision between the two robots at the same time:

$$d_{\text{cross}} = \text{cross} - \text{beg}. \quad (10)$$

In formula (10), cross represents the position of the intersection between the optimized two paths, beg is the starting

TABLE 1: Comparison of path planning performance based on the BPSO algorithm and JMPOPSO algorithm.

Algorithm	Maximum	Average value	Minimum value	Average time (S)
BPSO algorithm	1.59	1.43	1.17	7.56
JMPOPSO algorithm	1.98	1.76	1.34	9.39

point of the robot, and d_{cross} represents the distance from the starting point to the intersection of the two paths moving along the optimized path.

If the d_{cross} of the two robots are the same, it means that the two robots will collide when moving along the optimized path and the number of collisions between paths will be counted; otherwise, there will be no collision.

Here, a collision evaluation function fit4 is designed to evaluate the collision between each group of paths optimized in the multirobot system. The specific design is shown in formula (11):

$$\text{Fit4} = \begin{cases} 1, & \text{no collision between robots,} \\ 10 * \text{Num_cross}, & \text{collision between robots.} \end{cases} \quad (11)$$

In formula (11), Num_cross represents the number of collisions between each group of paths optimized in the multirobot system.

The construction of fitness function $f_1(p)$ is the same as the fitness function introduced in the previous article. The construction of fitness function $f_2(p)$ for collaborative information interaction is shown in formula (12):

$$f_2(p) = (f_{11}(p) + f_{12}(p) + \dots + f_{1i}(p) + \dots + f_{1n}(p)) \cdot \frac{1}{\text{fit4}}. \quad (12)$$

The fitness evaluation function $f_{1i}(p)$ is the same as the previously established fitness evaluation function $f_1(p)$, where $1 < i \leq n$, n is the number of robots, and fit4 is the collision evaluation function between paths of the multirobot system. In collaborative information interaction, the larger the value of fitness function $f_2(p)$, the better the representative individual of the combination and the best representative individual combination is set as the elite individual.

4. Result Analysis

4.1. Path Planning of a Single Machine Robot Based on the Improved Particle Swarm Optimization (JMPOPSO) Algorithm. In order to verify the performance of the JMPOPSO algorithm, this paper compares the JMPOPSO algorithm with the BPSO algorithm and makes 100 experiments on the two algorithms, respectively. Table 1 records the maximum, average, minimum, and average running time of the fitness optimized by the two particle swarm optimization algorithms.

As shown in Figure 4, from the comparison, we can see that the BPSO algorithm searches for a more accurate fitness value than the BPSO algorithm. The maximum fitness value

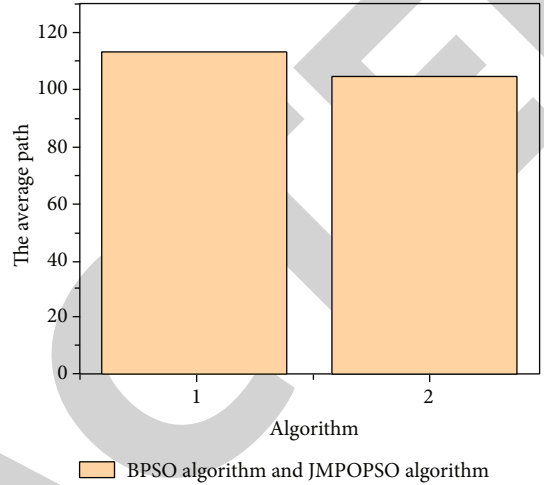


FIGURE 4: Average length of path planning based on the BPSO algorithm and JMPOPSO algorithm.

optimized by the BPSO algorithm is 1.59, while the maximum fitness value optimized by the JMPOPSO algorithm is 1.98. And in 100 experiments, the average value obtained by the JMPOPSO algorithm is higher than that of the BPSO algorithm. The average value obtained by the BPSO algorithm is 1.43, while the average value obtained by the JMPOPSO algorithm is 1.76, indicating that the JMPOPSO algorithm has stronger global search ability. The average path length of the JMPOPSO algorithm is about 7% shorter than that of the BPSO algorithm, and the running time is about 20%.

4.2. Multiswarm Particle Swarm Optimization (CMMPPSO) Algorithm Based on the Collaborative Mechanism. In order to verify the effectiveness of the algorithm, simulation experiments are carried out in this paper. Three mobile robots R1, R2, and R3 are set in the working environment, and five circular obstacles with radius $r = 2$ are set. In the simulation environment, the starting position and target position coordinates of the three mobile robots are set as shown in Table 2.

Figures 5 and 6 show the time and average path length of multirobot path planning based on the CMMPPSO algorithm based on BPSO and the CMMPPSO algorithm based on JMPOPSO, respectively.

The simulation results show that the path optimized by the CMMPPSO algorithm based on JMPOPSO is better than that optimized by the CMMPPSO algorithm based on BPSO, which is shortened by about 25% and the time is shortened by about 30%. Simulation experiments verify the effectiveness of the CMMPPSO algorithm.

TABLE 2: Setting of the starting point and target point of the mobile robot in the simulation environment.

	Robot	Starting point	Target point
Simulation environment settings	R1	S1(13,12)	T1(26,28)
	R2	S2(18,11)	T2(18,29)
	R3	S3(23,12)	T3(10,28)

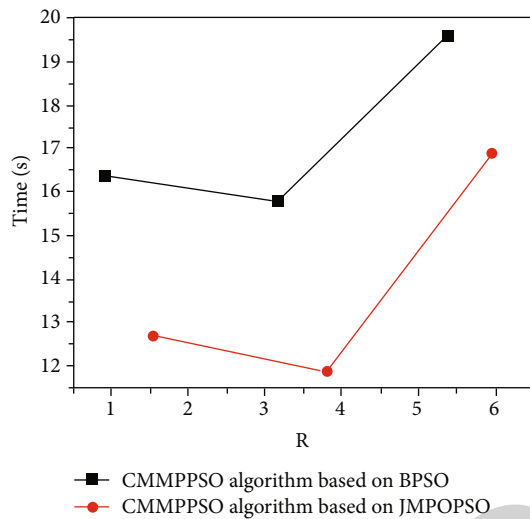


FIGURE 5: Algorithm time.

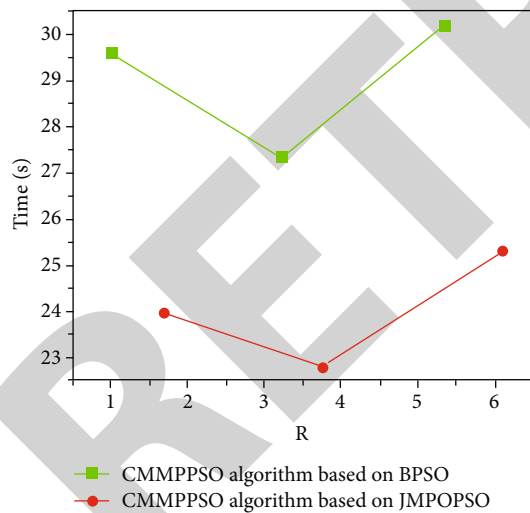


FIGURE 6: Average path length.

5. Conclusion

With in-depth study of herd intelligent technology, mobile robot planning technology has reached unprecedented heights. The particle herd optimization algorithm is a new bionic optimization algorithm. This line only focuses on improving the particle optimization algorithm, using optimization algorithms to improve the robotics process, and achieving positive results. This sentence focuses on the following issues.

First, we recommend the particle flock optimization (JMPOPSO) algorithm based on the jump mechanism and traction operation based BPSO algorithm. The JMPOPSO algorithm is more powerful in the world of search engine and integration faster.

The JMPOPSO algorithm was then used in the design of the same robotic method, with the disadvantage that it was difficult to improve the global process using the BPSO algorithm. First, the robot's office is modeled, and then, the fitness program is decided in order to improve the process. Finally, the method has been improved by the JMPOPSO algorithm based on the robust design. The simulation results show that the JMPOPSO algorithm is capable of better global research, more exploration, and better methods.

Finally, when studying the multirobot path planning problem, this paper proposes a multiswarm particle swarm optimization (CMMPPSO) algorithm based on the collaborative mechanism. In this algorithm, the multirobot path planning problem is decomposed into multiple single robot path planning problems and each subpopulation optimizes a robot separately. Select representative individuals from each subpopulation to coordinate information interaction, so as to select elite individuals as the path of multirobot system optimization. In the optimization process, not only the collision between robots and obstacles but also the collision between robots are considered and the collision evaluation function between paths is established. Simulation results show that the algorithm can better realize multirobot path planning.

Data Availability

The data used to support the findings of this study are available from the corresponding author upon request.

Conflicts of Interest

The authors declare that they have no conflicts of interest.

References

- [1] M. Shu, G. Chen, and Z. Zhang, "3d point cloud-based indoor mobile robot in 6-dof pose localization using a wi-fi-aided localization system," *Access*, vol. 9, pp. 38636–38648, 2021.
- [2] Z. Lv, Y. Han, A. K. Singh, G. Manogaran, and H. Lv, "Trustworthiness in industrial IoT systems based on artificial intelligence," *IEEE Transactions on Industrial Informatics*, vol. 17, no. 2, pp. 1496–1504, 2021.
- [3] Z. Lv, W. Kong, X. Zhang, D. Jiang, H. Lv, and X. Lu, "Intelligent security planning for regional distributed energy Internet," *IEEE Transactions on Industrial Informatics*, vol. 16, no. 5, pp. 3540–3547, 2020.
- [4] P. Singh, A. Nandanwar, L. Behera, N. K. Verma, and S. Nahavandi, "Uncertainty compensator and fault estimator-based exponential supertwisting sliding-mode controller for a mobile robot," *IEEE Transactions on Cybernetics*, vol. 99, pp. 1–14, 2021.
- [5] M. Ou, H. Sun, Z. Zhang, and S. Gu, "Fixed-time trajectory tracking control for nonholonomic mobile robot based on

Retraction

Retracted: Intelligent Optimization Design of Automatic Sorting Robot Process

Journal of Sensors

Received 13 September 2023; Accepted 13 September 2023; Published 14 September 2023

Copyright © 2023 Journal of Sensors. This is an open access article distributed under the Creative Commons Attribution License, which permits unrestricted use, distribution, and reproduction in any medium, provided the original work is properly cited.

This article has been retracted by Hindawi following an investigation undertaken by the publisher [1]. This investigation has uncovered evidence of one or more of the following indicators of systematic manipulation of the publication process:

- (1) Discrepancies in scope
- (2) Discrepancies in the description of the research reported
- (3) Discrepancies between the availability of data and the research described
- (4) Inappropriate citations
- (5) Incoherent, meaningless and/or irrelevant content included in the article
- (6) Peer-review manipulation

The presence of these indicators undermines our confidence in the integrity of the article's content and we cannot, therefore, vouch for its reliability. Please note that this notice is intended solely to alert readers that the content of this article is unreliable. We have not investigated whether authors were aware of or involved in the systematic manipulation of the publication process.

Wiley and Hindawi regrets that the usual quality checks did not identify these issues before publication and have since put additional measures in place to safeguard research integrity.

We wish to credit our own Research Integrity and Research Publishing teams and anonymous and named external researchers and research integrity experts for contributing to this investigation.

The corresponding author, as the representative of all authors, has been given the opportunity to register their agreement or disagreement to this retraction. We have kept a record of any response received.

References

- [1] J. Liu, J. Wang, and Y. Xu, "Intelligent Optimization Design of Automatic Sorting Robot Process," *Journal of Sensors*, vol. 2022, Article ID 4860006, 8 pages, 2022.

Research Article

Intelligent Optimization Design of Automatic Sorting Robot Process

Jia Liu , JunFeng Wang , and Yuequn Xu 

Shijiazhuang Institute of Railway Technology, Shijiazhuang, Hebei 050061, China

Correspondence should be addressed to JunFeng Wang; 20160939@ayit.edu.cn

Received 24 May 2022; Revised 24 June 2022; Accepted 5 July 2022; Published 18 July 2022

Academic Editor: Haibin Lv

Copyright © 2022 Jia Liu et al. This is an open access article distributed under the Creative Commons Attribution License, which permits unrestricted use, distribution, and reproduction in any medium, provided the original work is properly cited.

In order to further improve the efficiency of sorting robots, an algorithm based on artificial intelligence design is evaluated. On the basis of determining the design requirements of belt conveyor and motor selection, the reverse device and return device and camera bracket sorting car are redesigned, and the sorting car is further analyzed by finite element method. All programs are written based on PLC. The results show that the recognition and sorting rate of 100 express surface orders with the same specifications reaches 100% and the sorting rate reaches 94% by analyzing the data recorded in the database, and the average time consumed in each recognition process is 0.0493097 s and 0.047133 s, respectively, in basic and simulated recognition. The difference did not exceed 0.01 s, and the time was basically the same. Therefore, the scheme verifies the rationality of mechanical structure design, visual scheme design, and control system design.

1. Introduction

In March 2016, AlphaGo, a robot based on Google's Go software, beat Lee Se-dol in a game of Go. Many scientists and technologists thus believed that artificial intelligence had ushered in the third wave of its development, and we began to expect the progress of artificial intelligence to make human life better. Since the concept of artificial intelligence was put forward in 1956, it had entered the first stage of its development. By the 1960s, the programs of artificial intelligence had been able to prove many mathematical principles automatically [1]. Later, the introduction of knowledge made artificial intelligence enter the second period of rapid development. In this stage, the rapid inference of machines and the successful application of "expert system" caused another heat wave in the field of artificial intelligence. Until the 1990s, the emergence of machine learning enabled us to extract knowledge automatically from the data. Now, the third development heat wave of artificial intelligence has hit the world [2].

Machine learning is advancing rapidly as fields such as statistics, mathematics, computer science, and neuroscience

continue to improve. As a branch of artificial intelligence, the progress in machine learning will further promote the development of artificial intelligence [3]. Machine learning has been a crucial "catalyst" in the 60 years of development. Machine learning is to make the computer learn repeatedly to improve its performance and intelligently identify new samples through relevant algorithms, so that the computer can make correct responses and behaviors without explicit programming control [4]. In the past decade, machine learning has been widely applied in various fields such as autonomous driving, speech recognition, data mining, medical diagnosis, weather forecast, and industrial control. The manufacturing method of intelligent robot sorting system is shown in Figure 1.

Recently, the behavior of a group of robots that can organize themselves into a group to perform complex tasks has attracted extensive attention from the academic community [5]. More and more perfect intelligent algorithms are used to better control the robot population [6]. In the past few years, many learning methods have been developed, including supervised and unsupervised learning algorithms. Swarm intelligence algorithms were first proposed in the

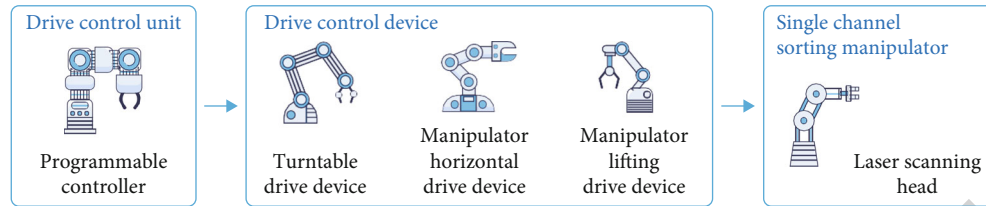


FIGURE 1: Manufacturing method of intelligent robot sorting system.

early 1990s in the research on a cellular robotic system. Since then, many kinds of swarm intelligence algorithms have been proposed. For example, ant optimization algorithm is inspired by the behavior of ants looking for the shortest distance between the nest and food. Particle swarm optimization algorithm simulates the flight of birds and the movement of searching for food, and artificial bee colony algorithm is inspired by the process of bees searching for food [7].

2. Literature Review

The diversity of unstructured environments and products requires new robotic solutions that combine intelligent machine design with advanced artificial intelligence techniques to address the challenges of object recognition, dexterous grasping, or path planning [8]. The essence of robot visual recognition is to capture images for detection and classification. Traditional target recognition technology is mainly divided into three stages: image preprocessing, feature representation, and region classification, which often requires the consistency of target scene structure. Irregular shape, color disunity, occlusion, and disorderly placement will bring great challenges to traditional visual recognition methods.

In 2006, the neural network as a visual recognition model was proposed for the visual recognition technology, which started a period of research upsurge. AlexNet network designed by Wu et al. won the championship in ImageNet image recognition competition with 10.9% lower test error rate than the second place, which promoted the development of deep neural network in the field of computer vision [9]. Soares et al. proposed r-CNN, the target detection algorithm. In the second year, fastR-CNN and FasterR-CNN detection algorithms were proposed, and the detection effect was constantly improved. In the ILSVRC and COCO2015 competition, a regional proposal network (RPN) was introduced. With detection speed of 7 FPS and detection accuracy of 73.2%, it ranked first [10].

At present, for target positioning methods, in order to better grasp objects, the application of depth camera was becoming more and more popular. Point cloud registration target estimation methods occupied the mainstream place. NDT algorithm was proposed by Z. Lv et al. This algorithm was used for point cloud registration when the initial value was not required, and it was relatively stable [11]. Z. Lv et al. designed the SUPER4PCS algorithm with fast operation speed but low registration [12]. Yang et al. proposed LINEMOD, a 6D pose estimation algorithm for objects in

a chaotic environment, on ACCV in 2012, and good results were achieved [13].

When the robot is sorting the goods placed on the shelf, the geometric constraints of the shelf and goods make the robot pass through the allowable pose change which is very small, so high requirements are put forward for the robot trajectory planning and control under multiple constraints. Yang et al. proposed the covariant Hamiltonian optimization (CHOMP) algorithm for motion planning, which was a parameter invariant trajectory optimization method and could be used to locally optimize the feasible trajectory of a 7-DOF manipulator [14]. Zhou et al. designed an accurate robust fuzzy control algorithm (PRFC) suitable for electric manipulator, adjusted the fuzzy rules for controlling tracking spatial origin, optimized the traditional fuzzy controller, and improved the robustness of robot system operation [15].

At present, most storage enterprises at home and abroad are doing more and more researches on mobile robots and scheduling algorithms, but a lot of labor is still needed for cargo picking. Therefore, in terms of the identification and positioning method of multitarget goods in the warehouse environment, the detection and positioning of shelf objects to improve the degree of automatic warehouse sorting were mainly investigated in the research.

3. Methods

3.1. Design Requirements of the Belt Conveyor. In the selection process of the belt conveyor, the main factors to consider were belt bandwidth and belt speed. For the belt design, the bandwidth was required to be greater than the width of the car base to ensure a good margin to avoid collisions between the car and the inner wall of the conveyor when turning. The adjustable range of the speed provided by the belt was required to be between 0.5 m/s and 1.5 m/s to ensure that the camera could still shoot clear and high-contrast images under the movement of the belt [16, 17].

3.2. Motor Selection. The maximum weight of express items was required to not exceed 5 kg in the research, and the requirement for the friction of the belt was not strict, so the flat belt with simple structure could meet the requirements. In addition, the transmission structure of flat belt was very simple, with high transmission efficiency, and the pulley was also very easy to manufacture, so flat belt was the ideal choice for the research [18].

T2.0 mm PVC belt was selected in the research. The simple choice of motor was as follows.

According to the requirements of the research, the total weight of the car and the object was not more than 10 kg, and the number of cars arranged on the whole ring belt machine was 6. In order to meet the requirements of the photo shooting, the belt speed was required to be between 0.5 m/s and 1.5 m/s.

The formulas were as follows.

$$F = \mu m_{\text{all}} g, \quad (1)$$

$$P = FV. \quad (2)$$

In the two formulas, F is the friction force, μ is the friction coefficient, m is the total weight of car and express, g is the gravitational acceleration, P is the output power of p -motor, and V is the velocity of belt running.

Then, the following could be obtained from formulas (1) and (2):

The minimum power of motor: $P = 0.5 \times 6 \times 10 \times 9.8 \times 0.5 = 147 \text{ W}$

The maximum power of motor: $P = 0.5 \times 6 \times 10 \times 98 \times 15 = 441 \text{ W}$

Based on the overall consideration, the motor model YB2-801-2 was selected here, with a rated power of 0.75 kW, which met the requirements.

3.3. Design of the Reversing Device and the Returning Device. In order to save space to the utmost extent, the design of the sorter should be in line with the requirements of not only completing the outer ring belt machine sorting but also completing the inner belt machine sorting. So it is a test for the car in the process of motion on the package action and reversing action. The reversing device and the returning device in the car were designed in the research.

Among them, the reversing device is installed between the first sorting mouth and the orbit of the visual scanning system. The cylinder of the reversing device could not move by default. When the visual system determined that the sorting port corresponding to the express loaded in the car was located inside the belt, the cylinder started to move. The cylinder jacked up the directional dial. In the process of the car passing through this section of curve path, its orientation would change from outward to inward, so that the express could be sorted out from the sorting mouth inside the belt machine. As for the returning device, its principle was the same as that of the reversing device, which was to reverse the carriage by changing its path [19]. Because the car circulated on the circular belt machine, the car carriage faced different directions before loading the bag. In order to facilitate loading, the car carriage faced the outside of the belt, and this action was completed by the returning device.

3.4. Design of Camera Bracket. Considering the spatial structure and convenient handling of the whole sorting machine, it was necessary to set up a camera bracket, which could not only maintain stability in the operation of the sorting machine but also made the height and angle of the camera and the light source convenient and adjustable, so as to

adapt to the movement of the sorting machine caused by some external factors [20].

The industrial camera and the light source are fixed on the horizontal profile above the bracket by bolts and nuts. The angle of the industrial camera and the light source could be controlled by adjusting the bolts and nuts. The upper horizontal profile was fixed to the vertical profile by angle code, so that the profile height could be adjusted and so as to ensure that the height of the industrial camera and the light source could be adjusted. At the same time, in order to ensure the stability of the whole camera bracket, a vertical profile was added under the bracket. According to the parameters of the camera and lens, the size of the car, and the width of the belt machine, the height of the whole camera bracket was 140 cm with the adjustable range of 30 cm in the height direction and the width was 80 cm that did not interfere with the movement of the car and cylinder and other components.

3.5. Structure Design of Sorting Car. For the design of the sorting car, high stability and reliability were required. During the movement of the main ring, it was necessary to keep the car running smoothly when it was not sorting, and the movement was timely and smooth when it was sorting [21, 22]. Sorting car was mainly composed of base, support, platform plate, door plate, spring rod, bevel gear, and so on.

Sorting car was the core mechanical structure of the sorting machine. Whether express could accurately fall in the corresponding sorting mouth completely depended on whether the car door could be accurately opened or not, and the completion of the action of the door opening mainly depended on the car transmission mechanism, so the design of the car transmission mechanism was particularly important.

3.5.1. Calculation of Gear Torque. In order to ensure that the rotation range of the lever was enough to open the door when the car lever was in contact with the pushing mechanism and avoid the express stuck in the door, according to the calculation of the maximum elongation of the reset spring constraining the door opening action and its elastic coefficient, the minimum torque of the input shaft required by the bevel gear was 5 N·m.

The weight of the object was set as 5 kg. The impact force of the car door was 100 N, The speed of shaft III was 15 r/min. The transmission efficiency of rolling bearing $\eta_1 = 0.985$, bevel gear $\eta_2 = 0.95$, and cylindrical gear $\eta_3 = 0.96$. Cylindrical gear transmission ratio $i_{\text{pillar}} = 2$, and bevel gear transmission ratio $i_{\text{awl}} = 1$.

$$\begin{aligned} n_{\text{II}} &= \frac{n_{\text{III}}}{i_{\text{pillar}}} = 7.5 \text{ r/min}, \\ n_{\text{I}} &= \frac{n_{\text{II}}}{i_{\text{awl}}} = 7.5 \text{ r/min}. \end{aligned} \quad (3)$$

In the formulas, n_{II} was the speed of axis II (r/min), and n_{I} was the speed of axis I (r/min).

The torque required by small spur gear was $T_{\text{mout}} = 3.9$ N/m, and then,

$$P_{\text{IIIout}} = \frac{T_{\text{IIIout}}^{\eta_{\text{III}}}}{9500}. \quad (4)$$

The data was taken into the following formulas.

$$\begin{aligned} P_{\text{IIIout}} &= 0.0061 \text{ km}, \\ P_{\text{IIIout}} &= P_{\text{IIenter}} \times \eta_1, \\ P_{\text{IIIenter}} &= P_{\text{Iout}} \times \eta_3, \\ P_{\text{Iout}} &= P_{\text{IIenter}} \times \eta_1, \\ P_{\text{IIenter}} &= P_{\text{Iout}} \times \eta_2, \\ P_{\text{Iout}} &= P_{\text{Ienter}} \times \eta_1. \end{aligned} \quad (5)$$

The above formulas could be calculated as follows:

$T_{\text{IIIenter}} = 3.918 \text{ N}\cdot\text{m}$, $T_{\text{Iout}} = 8.163 \text{ N}\cdot\text{m}$, $T_{\text{IIenter}} = 8.278 \text{ N}\cdot\text{m}$, $T_{\text{Iout}} = 8.723 \text{ N}\cdot\text{m}$, $T_{\text{Ienter}} = 8.856 \text{ N}\cdot\text{m}$, and then, $T_{\text{Ienter}} > 5 \text{ N}\cdot\text{m}$; then, it met the requirements of the transmission mechanism of the car.

3.5.2. Straight Bevel Gear Design. The gear type was standard straight bevel gear transmission, with 7-level gear precision and pressure angle of 20° . The material of two gears was 40Cr (quenching and tempering). The hardness of tooth surface was 280 HBS. The number of teeth of pinion $z_1 = 21$, $z_2 = 21$, and $u = 1$.

According to the calculation formula of circle diameter by pinion indexing,

$$d_{\text{It}} \geq \sqrt[3]{\frac{4K_{Ht} T_I}{\varphi_R (1 - 0.5\varphi_R)^2 u} \cdot \left(\frac{Z_H Z_E}{[\sigma_H]}\right)^2}. \quad (6)$$

The calculation formula of allowable stress of contact fatigue is as follows:

$$[\sigma_H] = \frac{K_{HN} \sigma_{Hlim}}{S}. \quad (7)$$

The calculation formula of gear modulus is as follows:

$$m_t \geq \sqrt{\frac{K_{Ft} T_1}{\varphi_R (1 - 0.5\varphi_R)^2 Z_1^2 \sqrt{\mu^2 + 1} \cdot (Y_{FtY_{sa}} / [\sigma_H])}}. \quad (8)$$

According to the design principle of gear contact fatigue strength and the design principle of tooth root bending fatigue strength, the following design conclusions could be obtained: tooth number $Z_1 = 41$ and $Z_2 = 42$, pressure angle $a = 20^\circ$, displacement coefficient $X_1 = 0$ and $X_2 = 0$, split cone angle $\delta = 45^\circ$ and $\delta_2 = 45^\circ$, and tooth width $b_1 = b_2 = 11 \text{ mm}$. 40Cr (quenching and tempering) was used by both gears. The gears were designed with 7-level precision.

3.5.3. Design of Spur Gear. Straight bevel gear transmission was selected, with the pressure angle of 20° and 7-level pre-

cision 7. The material of big gear was 45Cr (quenching and tempering). The hardness of tooth surface was 240 HBS. The material of small gear was 40Cr (quenching and tempering). The hardness of tooth surface was 280 HBS. The number of teeth of pinion $u = 0.5$ and $z = 61$.

From the formula $m = d/z$, $Z_2 = 30.5$ was obtained. Take z as 31, namely, $z = 31$. The calculation formula of the diameter of the indexing circle of the big gear was as follows.

$$d_{1t} \geq \sqrt[3]{\frac{2K_{Ht} T_1}{\varphi_d} \cdot \frac{\mu + 1}{\mu} \cdot \left(\frac{Z_H Z_E Z_\epsilon}{[\sigma_H]}\right)^2}. \quad (9)$$

For the allowable contact fatigue stress $[\sigma_H]$, take the failure probability as 1% and safety factor $S = 1$:

$$[\sigma_H] = \frac{K_{HN} \sigma_{Hlim}}{S}. \quad (10)$$

The calculation formula of gear modulus is as follows:

$$m \geq \sqrt[3]{\frac{2K_{Ft} T_1 Y_\epsilon}{\varphi_d Z_1^2} \cdot \left(\frac{Y_{Fa} Y_{sa}}{[\sigma_F]}\right)}. \quad (11)$$

According to the design principle of gear contact fatigue strength and the design principle of tooth root bending fatigue strength, the following design conclusions could be obtained: tooth number $Z_1 = 81$ and $Z_2 = 43$, modulus $m = 0.5$, pressure angle $a = 20^\circ$, displacement coefficient $X_1 = 0$ and $X_2 = 0$, center distance $a = 31 \text{ mm}$, tooth width $b_1 = 40.5 \text{ mm}$ and $b_2 = 21.5 \text{ mm}$. 40Cr (quenching and tempering) was used by small gear. 45Cr (quenching and tempering) was used by big gear. The gears were designed with 7-level precision.

3.6. Finite Element Analysis of the Sorting Car. Since the tilting car and the external cylinder worked through relative motion. The impact occurred when they contacted. So the finite element model was established to analyze the impact [23]. ANSYS software was used for display dynamics analysis. Firstly, the 3D model established with SOLIDWORKS was imported into the finite element analysis software ANSYS Workbench 18.1, and the push rod material was set as 45 steel and L-shaped rod material as stainless steel. Material properties were edited through EngineeringData module of Workbench. Through the size function, the grid size was defined and the total number of grids was 85557. Then, the analysis parameters were modified. The end time was set as 0.15 s. The fixed cylinder was added, then the speed limit was added, and the speed of the whole car was set as 1 m/s. Finally, the equivalent stress and equivalent strain were added into the solution, and the analysis was conducted by clicking solve.

By finite element calculation, when the equal effect of impact contact became 0.32 mm/mm, the equivalent stress of impact was 74.201 MPa, the yield strength of 45 steel was 355 MPa, and the yield strength of 304 stainless steel was 205 MPa. The experimental results were far less than the yield strength, and the strength check was safe.

TABLE 1: Table of I/O address allocation.

Input	Switch	Output	Element
X0	Start button	Y0	Cylinder 1
X1	Stop button	Y1	Cylinder 2
X2	Sensor 1	Y2	Cylinder 3
X3	Sensor 2	Y3	Cylinder 4
X4	Sensor 3	Y4	Cylinder 5
X5	Sensor 4	Y5	Cylinder 6
X6	Sensor 5		
X7	Sensor 6		
X10	Sensor 7		

3.7. PLC Programming. Before the preparation of PLC program, first of all, the functional requirements of the control system were analyzed. The tray sorting machine control system was required to meet the functional requirements. When each sorting port photoelectric was triggered, the number of photoelectric trigger and sorting number were judged to meet the trigger conditions in the counting principle. Solenoid valve was electrified for a second, so that the cylinder piston rod out of about a second and reset after a second. The belt motor could be controlled to start and stop [24]. The data registered from D1 to D7 would be reset when switched on. The sixth step was the motor start-stop procedure. X001 was responsible for starting, and X002 was responsible for disconnecting. X003 was the photoelectric switch, which was triggered once, the value of data register D1 plus 1 and to represent the value of the photoelectric switch. When the photoelectric switch was triggered, read the value of the corresponding register in PLC through the serial port (here was the value of D1). If the value of D1 and the sorting port number met the trigger conditions in the counting principle, then M0 was made forcibly closed through communication with PLC, so that the solenoid valve Y001 was energized for one second. That is, the cylinder was pushed out for about one second; the power was off and reset after one second. PLC I/O address allocation table is shown in Table 1.

3.7.1. PLC Communication. PLC communication refers to the data communication between PLC and PLC, between PLC and PC, and between PLC and other intelligent equipment. This function was conducive to PLC monitoring, and data reading and writing between PLC and PLC could be more convenient for control [25, 26].

PLC communication interface was mainly divided into RS232, RS485, and Ethernet. The RS232 interface was adopted in the research, which was connected to the touch screen serial port through the USB adapter, namely, serial communication. Here, there were two main types of serial port communication way. The first was that according to the communication between PLC and agreement, a small amount of code to do simple communication could be used through the SerialPort class provided by the NET, but when

TABLE 2: Enforcing ON to be set.

Start	Command	Address	Finish	Checksum
STX	CMD	ADDRESS	ETX	SUM
02 h	37 h	Address	03 h	Sum

TABLE 3: Enforcing OFF to be set.

Start	Command	Address	Finish	Checksum
STX	CMD	ADDRESS	ETX	SUM
02 h	38 h	Address	03 h	Sum

Note that the command (CMD) 37 represents enforcing ON and 38 represents enforcing OFF. Sum checksum: $SUM = CMD + ADDRESS + ETX$.

TABLE 4: Word element reading.

Start	Command	The first address	Digit	Finish	Checksum
STX	CMD	GROUPADDRESS	BYTES	ETX	Sum

Note that the command (CMD) 30 represents reading. First address algorithm: $Address = Address * 2 + 1000 h$ and then converted to hexadecimal.

the content of communication with PLC was large, the code needed to be done in a large number of data hexadecimal conversion and validation, etc., which seemed more complex. The second way was to use MXComponent software officially provided by Mitsubishi. By calling its dynamic link libraries ActUtilType.dll and ActUWzd.dll, data interaction with PLC could be carried out conveniently without considering problems such as base conversion verification, but the software must be downloaded, which was about 500 M in size. Through the analysis of PLC ladder diagram, the purpose of communication with PLC was just to control the forced closure of switch MO and read the value of data register D1. The content was very simple. The first way and communicating with PLC were chosen. The message format of setting and resetting of bit elements used in communication is shown in Tables 2 and 3. The message format read by word elements is shown in Table 4.

3.7.2. Design of the Software Running Interface. Before designing the interface, what functions the interface contain should be first analyzed. In the research, the interface included the following functions: serial port number detection, belt start and stop, serial port open and close, serial port parameter setting, displaying the number of sorted express, displaying the identified to be sorted express, and displaying the real-time update table in the database.

Sorting machine operation interface was mainly composed of three parts, which were the serial port debugging interface, the sorting interface, and the simulation experiment interface.

3.7.3. Design of the Serial Port Debugging Interface. As the lower machine in the research was PLC, so communication debugging with PLC was necessary. The serial port debugging interface mainly included the parameter configuration

TABLE 5: Physical prototype test records.

Test item	Test effect	Action time	Whether meets the requirements or not
The visual program	Information extraction	45 ms	Yes
Interface program	The interface runs smoothly	Fast	Yes
Belt conveyor	Synchronous start, consistent speed	Faster	Yes
Sorting car	The door can be opened and repositioned.	Slow	Yes
Pneumatic circuit	Stable operation	150 ms	

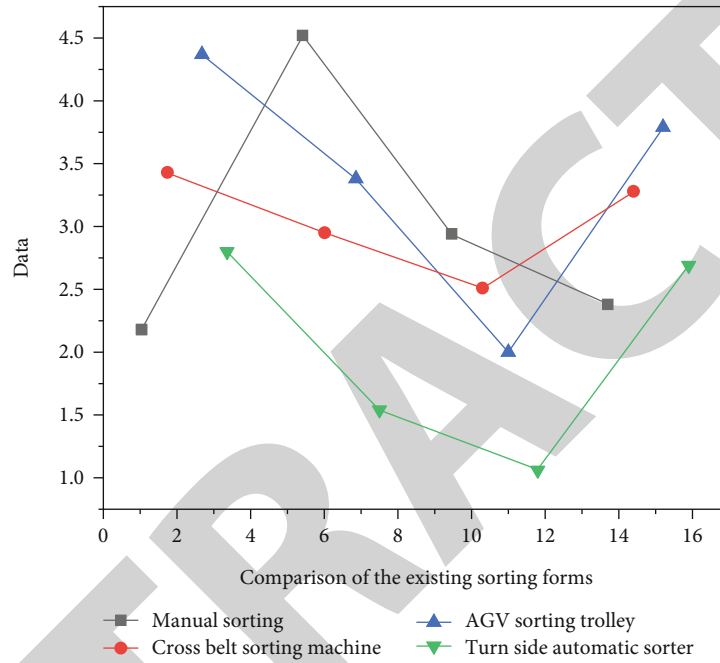


FIGURE 2: Comparison with existing sorting forms. Note: data from Huainan, Hefei, and Hangzhou logistics Park survey results.

area, the data receiving area, and the data sending area. The parameter configuration area was to ensure the serial port number, baud rate, data bit, stop bit, and parity bit of the parameter port to adjust. Due to the data receiving area and data sending area, the corresponding PLC soft components could be chosen according to the specified message format in the data receiving area to send relevant commands to PLC. The execution of this command by PLC also was displayed in the data receiving area in the format of messages. The design of the interface was beneficial to the debugging between the upper computer and the lower computer, which also provided a basis for troubleshooting.

3.7.4. Design of the Sorting Interface. The sorting interface was mainly composed of three control buttons and three parts of visual interface. The three control buttons were create template, start match, and stop match. Create template-supported manual interception of any area in the express order for modeling, which was convenient to change the template. The whole device and program would be run when the match started, and the whole device and program would

be stopped when the match stopped. The visual interface included the camera recognition interface, the data interface, and the chart interface. Among them, the camera recognition interface showed the image of each express order captured by the camera and the three-segment code area located. The data interface was used to display the number of fractional two-dimensional code matched by each express order template and the three-segment code identified. The chart interface mainly showed the sorting quantity of express order numbers at different addresses in the form of charts. The sorting interface made it easy to control the entire equipment and program, as well as visually observe the sorting process.

3.7.5. Design of the Simulation Experiment Interface. The simulation experiment interface was mainly to simulate the whole process of sorting machine and verified the sorting principle. After the sorting principle was changed, the simulation experiment interface could be verified at any time, and the feasibility of sorting principle could be guaranteed through the interface.

TABLE 6: Data analysis.

Item	Correct identification	Incorrect identification	Average time
Actual situation	94 pieces	6 pieces	0.0493097 s
Simulation	100 pieces	0 piece	0.0471338 s

4. Results and Discussions

On the basis of the testing through simulation system, the actual prototype was also needed to test the reliability and stability of the sorting machine. The test process was divided into the following parts.

4.1. Testing Capturing Pictures. Due to the limitations of the site and equipment, the design of the camera's support mechanism was relatively simple, which was easy to cause the camera position offset, leading to the failure to take the express delivery sheet. Before the sorting, the computer was used to connect to the camera to capture pictures. If the clear surface sheet could be captured, the next step was proceeded. Otherwise, the camera position was adjusted until the clear surface sheet was captured.

4.2. Turning on the Power. The whole ring belt machine was composed of two semicircular belt machines and two linear belt units. Through the change of the circuit, the four belt machine starting and stopping at the same time could be controlled.

4.3. Placing Package. After the power was turned on, the car moved circularly with the belt machine. The package was placed on the car manually under the condition of ensuring the smooth movement of the car. According to the counting principle described earlier in this research, the timing of placing package was not restricted, and package could be placed in the upper bag area at any time.

4.4. Sorting Package. The sorting process of package was a fully automatic process basically. In the whole process, on the one hand, the data changes of the control interface of the industrial computer needed to be detected. On the other hand, the running condition of the car on the belt should be observed, so as to turn off the power in case of accidents.

In order to combine the actual scene of package sorting to the maximum extent, the physical prototype was transported to Huainan Datong Logistics Park for further testing. The test results are shown in Table 5.

From the experimental records, the belt conveyor could realize synchronous start. The tilting car could realize the reservation function. The door and cylinder cooperated reliably, and the door could be opened normally. The car platform and the turning device cooperated reliably and could realize the turning of the platform in real time. The cylinder responded quickly, and the scheduled action with the car could be realized through the PLC program. HALCON software program ran stably after adjusting the parameters.

After adjusting the interface program parameters, the interface ran smoothly and responded quickly. PLC could normally complete the action information provided by the interface program. After the test was completed, the parameter comparison with the existing sorter is shown in Figure 2.

It could be seen from Figure 2 that on the premise of meeting the sorting efficiency, the tilting-pan automatic sorting machine could greatly save the cost of equipment and the floor area and could meet the sorting needs of the third and fourth tier cities.

The average time was calculated using the function-count_seconds (seconds) in HALCON, as shown in Table 6.

5. Conclusion

Based on the establishment of the experimental prototype in the research, the recognition scheme based on shape template matching was adopted to identify and sort 100 express surface sheets of the same specifications. By analyzing the data recorded in the database, the recognition rate reached 100% and the sorting rate reached 94%, and the average time consumed by each recognition process was 0.0493097 s and 0.0471338 s, respectively, and the difference was not more than 0.01 s. The time was basically the same, which verified the reasonableness of the mechanical structure design, visual scheme design, and control system design. Vision-based robot sorting system is a multidisciplinary field. Although the work of vision was mainly investigated in the research, there were still a lot of work to be further studied and explored.

Data Availability

The data used to support the findings of this study are available from the corresponding author upon request.

Conflicts of Interest

The authors declare that they have no conflicts of interest.

Acknowledgments

This study was supported by the Hebei Province "333 Talents Project" Funding Project (Project No. A202101033) and the Project of Hebei Provincial Department of Science and Technology (No. 22E50212D).

References

- [1] H. Jin, W. Fan, H. Chen, and Y. Wang, "Anti-corrosion wood automatic sorting robot system based on near-infrared imaging technology," *Journal of Mechanical Science and Technology*, vol. 34, no. 7, pp. 3049–3055, 2020.
- [2] Y. U. Zhi, X. Z. Shi, X. Chen, J. Zhou, and D. J. Rao, "Artificial intelligence model for studying unconfined compressive performance of fiber-reinforced cemented paste backfill," *Transactions of Nonferrous Metals Society of China*, vol. 31, no. 4, pp. 1087–1102, 2021.

Research Article

Construction of Robot Computer Image Segmentation Model Based on Partial Differential Equation

Quan Zhang 

The School of Science, Qiqihar University, Qiqihar, Heilongjiang 161006, China

Correspondence should be addressed to Quan Zhang; 202006000046@hceb.edu.cn

Received 5 June 2022; Revised 28 June 2022; Accepted 6 July 2022; Published 18 July 2022

Academic Editor: Haibin Lv

Copyright © 2022 Quan Zhang. This is an open access article distributed under the Creative Commons Attribution License, which permits unrestricted use, distribution, and reproduction in any medium, provided the original work is properly cited.

The application of partial differential equation in robot computer image smoothing and image segmentation based on curve evolution is studied to achieve the breakthrough and innovation of classical methods. First of all, the image is interpolated and enlarged, usually with double primary interpolation and double secondary interpolation. The robot computer image obtained by interpolation has a better effect on the smooth part of the image, but the edge becomes blurred. Then, the model is used to enhance the amplified image and remove the noise introduced during interpolation. In the process of PDE image segmentation, using the level set method, natural continuation cannot guarantee that the embedded function is always a signed distance function in the evolution process. The results show that compared with the classical fourth-order model, this model can well retain the details of the image, smooth bevels, and edges of the image. The proposed new model is better than the second-order model and the classical fourth-order model both in PSNR value and MAE value and in visual effect. Secondly, the model based on piecewise smooth Mumford-Shah not only expresses the original image better but also solves the problem of gradual image segmentation with gray value. Therefore, the robot computer image segmentation model based on partial differential equation can segment the image better.

1. Introduction

Image segmentation, as its name suggests, generally refers to the technology and process of extracting meaningful or interesting features from images. With the help of image segmentation and other technologies, the features in the image are extracted, which makes image analysis and understanding possible (Figure 1). It is a key step from image processing to image analysis. Using partial differential equation for image segmentation has strong theoretical support and is consistent with the classical image theory. Level set method is a method to solve the curve evolution. It implicitly expresses the closed curve of the plane; that is, the evolution curve is expressed as a partial differential equation with embedded function, which avoids the tracking and parameterization of the curve in the evolution process. Therefore, the level set method is relatively easy to deal with the

changes of curve topology, with high calculation accuracy and stable algorithm [1].

In the development of image processing, mathematics always plays an important role and permeates all branches of image processing. In the 1960s and 1970s, linear processing methods represented by Fourier analysis occupied the whole field of digital image processing. With the help of stochastic process theory, people have established image model. The frame of image coding is established by probability theory and information theory. Linear filter (Wiener filter, Kalman filter) provides a strong theoretical support for lower level image processing; FFT is widely used in all branches of image processing. These mathematical tools greatly promote the development and application of image processing. Since the 1980s, nonlinear science has gradually penetrated into image processing methods, and many novel mathematical tools have been introduced into the field of image

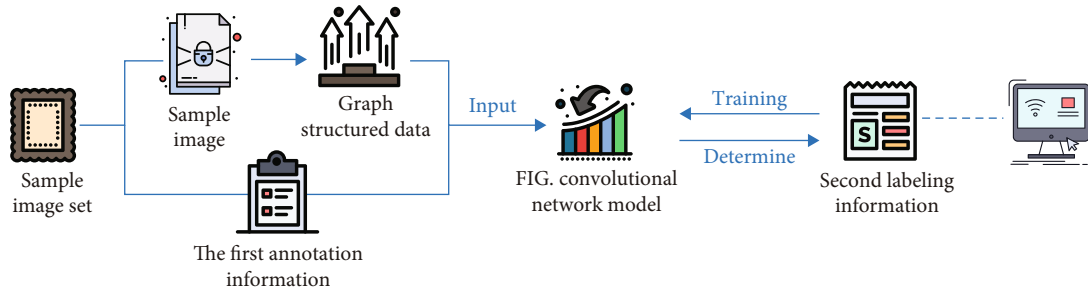


FIGURE 1: Image segmentation model.

processing, such as the application of wavelet and multiscale analysis in image segmentation, image filtering, edge detection, feature extraction, and analysis; the application of fractal in image coding and texture recognition [2]. In particular, image processing methods based on partial differential equations have become a continuous hotspot in recent years. Starting with the analysis of the mechanism of image noise reduction, combined with mathematical tools such as variational method, functional analysis, differential geometry, and projective geometry, it establishes an axiom system related to partial differential equations. It has been widely used in image segmentation, image smoothing, image reconstruction, image recognition, remote sensing image processing, image analysis, edge detection, image interpolation, medical image processing, motion analysis, and so on. In many directions of image processing, image segmentation is one of the important research hotspots.

This paper mainly studies the application of partial differential equation in image smoothing based on anisotropic diffusion and image segmentation based on curve evolution, trying to achieve a breakthrough and innovation of classical methods by deeply analyzing image features and using appropriate mathematical tools to obtain a more appropriate description of the image. Some new methods and ideas are proposed in this paper. Experiments and theoretical analysis have proved that the new method has obvious advantages over the classical method. It is an important supplement to the curve evolution and anisotropic diffusion theory and can be applied to all aspects of image processing engineering [3].

2. Literature Review

Nakamura and others believe that image segmentation is to segment the regions of interest in the image. Image segmentation is the basis of target recognition, tracking, and object-based coding. Therefore, image denoising has a very important application in the field of image processing. However, image segmentation is a very challenging task [4]. Zhao and others found that the storage and transmission of digital images are the main application direction of image compression. People's demand for high compression ratio of image and high quality of restored image is endless. The combination of partial differential equation and wavelet decomposition can effectively eliminate the Gibbs phenomenon at the edge in the process of wavelet decomposition, which provides a new idea for high-quality image compression [5].

Weng and others applied discrete wavelet, wavelet packet, and wavelet frame decomposition to texture analysis and proposed methods for multiscale texture feature extraction, texture classification, and texture segmentation in wavelet or wavelet packet transform domain [6]. Liu and others found that image segmentation algorithms based on partial differential equations are mainly divided into two categories: image edge-based segmentation model and image region-based segmentation model. Snake model, geodesic active contour (GAC) model, and gradient vector flow (GVF) model are edge-based segmentation models. Snake model is a variational model, which is divided into internal force and external force. Internal force is a contraction force, which minimizes the arc length of the contour and reduces the oscillation of the arc length. The external force is to control the contour on the edge of the image, so as to achieve the effect of segmentation [7]. Tu and others found that the representatives of region-based segmentation model are M-S model and C-V model, which approach the original image in the form of segmented plane, so as to achieve the purpose of segmentation [8]. Ren and others found that the storage and transmission of digital images are the main application direction of image compression. People's demand for high compression ratio of image and high quality of restored image is endless. The combination of partial differential equation and wavelet decomposition can effectively eliminate the Gibbs phenomenon at the edge in the process of wavelet decomposition, which provides a new idea for high-quality image compression [9]. Ma and others believe that for the numerical solution of the segmentation model, the commonly used methods are the level set method and the variational level set square, which represent the contour through the zero level set of an embedded function. The embedding distance of the gradient function should meet the requirements of 1. However, with the evolution of the embedded function, the gradient modulus will deviate from 1, so it is reinitialized during the evolution of the embedded function. Reinitialization not only reduces the computational efficiency but also destroys the evolution of embedded functions. Therefore, a distance regularized level set evolution (DRLSE) method is generated [10].

3. Research Methods

3.1. Generation of Fourth-Order Denoising Model. In essence, the second-order model will evolve the image towards the segmented plane, so most of the second-order

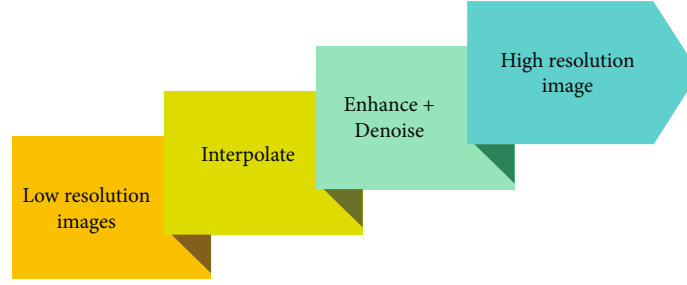


FIGURE 2: Image resolution enhancement algorithm flow.

models have the “ladder” effect; that is, the smooth region in the image produces false boundaries, which is visually unpleasant and may make the computer vision system mistakenly recognize some edges. The fourth-order partial differential equation denoising model can avoid the “ladder” effect [11].

The fourth-order partial differential equation denoising model can avoid the “ladder” effect because it approximates the original image through piecewise inclined plane. However, the classical fourth-order models start with variation. By improving the energy functional of the second-order model, the fourth-order partial differential equation is derived by using the gradient descent flow method.

3.2. A Kind of Fourth-Order Denoising Model Based on Image Features. Generally, an image can be divided into three types of regions: smooth region, edge region, and texture region. When the image is enlarged by the usual interpolation method, the edge of the image will be blurred [12]. The algorithm proposed in this section is as follows: firstly, the image is interpolated and enlarged to the desired size. Usually, double primary interpolation and double secondary interpolation are used. The smooth part of the image obtained by interpolation is better, but the edge becomes blurred. Then, use the model in this paper to enhance the enlarged image and remove the noise introduced during interpolation. The specific process is shown in Figure 2.

Based on the properties of the fourth-order partial differential equation and making full use of the characteristic information of the image, this paper selects the edge detection operator as the diffusion coefficient of the fourth-order equation [13] and directly constructs a new fourth-order partial differential equation. The constructed fourth-order partial differential equation is

$$\begin{cases} \frac{\partial u}{\partial t} = -\left(\Phi_1 \frac{u_{xx}}{|u_{xx}|}\right)_{xx} - \left(\Phi_2 \frac{u_{yy}}{|u_{yy}|}\right)_{yy}, & (x, y) \in \Omega, t \in (0, T), \\ \frac{\partial u}{\partial \vec{n}} = 0, \\ \left(\Phi_1 \frac{u_{xx}}{|u_{xx}|}\right)_x n_1 + \left(\Phi_2 \frac{u_{yy}}{|u_{yy}|}\right)_y n_2 = 0, & (x, y) \in \partial\Omega, t \in (0, T), \\ u(0, x, y) = f(x, y), & (x, y) \in \Omega. \end{cases} \quad (1)$$

Here, $\vec{n} = (n_1, n_2)$ represents the normal vector outside the unit on the boundary $\partial\Omega$ of the solution region, and the diffusion coefficient Φ_i , $i = 1, 2$, is a function related to $|\nabla u|$, u_x , and u_y , and $\Phi_i = \Phi_i(|\nabla u|, u_x, u_y)$ is the edge detection function. The boundary conditions are selected as zero derivative in the first-order external normal direction and zero derivative in the third-order external normal direction [14].

3.3. Level Set Method. In the process of PDE image segmentation, using level set method, natural continuation cannot ensure that the embedded function always remains a signed distance function in the evolution process. Therefore, the traditional approach is to reinitialize the embedded function into a signed distance function in the evolution process of the embedded function. This greatly reduces the efficiency of the segmentation algorithm. In order to avoid reinitialization, a regular term is added to the energy functional of the embedded function to keep the embedded function as a distance function as much as possible in the evolution process [15].

The geodesic active contour (GAC) model minimizes the following “weighted” arc length, as shown in

$$L_R(C) = \int_0^{L(C)} g(|\nabla u[C(s)]|) ds. \quad (2)$$

Minimize the gradient downflow corresponding to the above equation as

$$\frac{\partial C}{\partial t} = g(C)\kappa N - (\nabla g \cdot N)N. \quad (3)$$

N is the normal direction of curve evolution. Different from the previous parametric active contour model, the biggest feature of this kind of model is that it can automatically deal with the changes of topology.

The level set method transforms the original evolution of the curve into a partial differential equation of the level set function. In this way, the segmentation problem is transformed from the original differential geometry problem into the problem of solving partial differential equations. There are many existing results for the numerical solution of partial differential equations, and a better scheme can be selected for the discretization of the model [16].

TABLE 1: Experimental PSNR, MAE, and CPU time.

σ	PSNR			MAE			CPU time (s)		
	10	20	30	10	20	30	10	20	30
Segmented bevel image GZC01.bmp (128 × 128 pixels)									
Second-order model	28.20	22.13	18.70	7.86	15.94	23.67			
TV	41.42	37.63	34.05	1.48	2.61	3.46	0.77	1.34	2.32
Regularized PM	40.95	36.67	33.25	1.40	2.45	3.66	0.26	0.29	0.27
New model	47.63	42.23	37.56	0.71	1.30	2.00	4.38	4.84	8.83
lena.bmp (512 × 512 pixels)									
Second-order model	28.13	22.13	18.70	7.97	15.92	23.74			
LLT	34.28	31.03	29.25	3.67	5.08	6.18	20.05	55.60	97.76
Y-K	32.99	29.79	28.11	4.07	5.61	6.75	24.69	101.17	242.22
New model	34.42	31.40	29.64	3.53	4.76	5.72	41.63	109.33	191.08
pepper.bmp (256 × 256 pixels)									
Second-order model	28.18	22.16	18.76	7.94	15.84	23.45			
LLT	33.96	30.08	27.87	3.78	5.70	7.27	3.38	9.83	18.89
Y-K	32.49	28.62	26.32	4.24	6.37	8.50	5.94	19.15	42.47
New model	34.46	30.76	28.56	3.45	5.14	6.51	9.71	18.51	47.49

A curve is represented by the level set of high-dimensional function, as shown in

$$C(t) = \{(x, y) | \phi(x, y) = k\}. \quad (4)$$

The original curve evolution problem is replaced by the evolution problem of two-dimensional function. The time-varying curve C can be expressed as the level set of $\phi(x, y, t)$ in the time-varying function, that is,

$$C(t) = \{x, y | \phi(x, y, t) = k\}, \quad (5)$$

when curve $C(t)$ is as follows:

$$\frac{\partial C}{\partial t} = V. \quad (6)$$

During evolution, the embedded function $B(x, y)$ will evolve into

$$\frac{\partial \phi}{\partial t} = \beta |\nabla \phi|. \quad (7)$$

Here, $\beta = V * N$ is the normal component of the velocity of motion. The above formula is the basic equation of curve evolution level set method.

The choice of embedding function ϕ is not unique. The most commonly used is to let $\phi(x, y)$ represent the signed distance function from point (x, y) on the plane to curve C , that is,

$$\phi(x, y) = \begin{cases} d((x, y), C), & \forall (x, y) \in C^{\text{out}}, \\ -d((x, y), C), & \forall (x, y) \in C^{\text{in}}. \end{cases} \quad (8)$$

The distance function satisfies

$$|\nabla \phi| = 1. \quad (9)$$

This means that the change of embedded function is neither slow nor rapid, which meets the requirements of natural continuation. Assuming that the given curve motion equation is valid for all level sets of embedded functions, this natural continuation method is usually selected. However, with the evolution of the embedding function, the embedding function will gradually deviate from the distance function, and the deviation from the distance function will lead to the instability of numerical calculation [16, 17].

The level set method has the following advantages:

- (1) More than two edges can be detected, that is, with topological variability
- (2) It is easy to express curvature and unit normal vector N by embedded function
- (3) The numerical calculation can be carried out on the standard grid, which is a parameter-free method
- (4) It can be used in high-dimensional cases. For example, the surface can be expressed as a zero level set of volume function

If the level set method given above is applied, the evolution equation corresponding to the embedding function of GAC model is

$$\frac{\partial \phi}{\partial t} \& = (g\kappa - \nabla g \cdot N) |\nabla \phi| = |\nabla \phi| \operatorname{div} \left(g \frac{\nabla \phi}{|\nabla \phi|} \right). \quad (10)$$

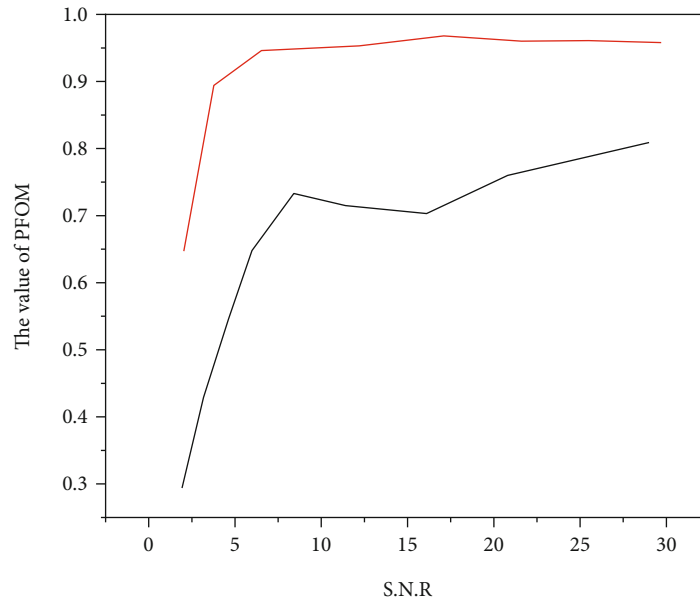


FIGURE 3: Comparison of image edge positioning accuracy of different detection methods.

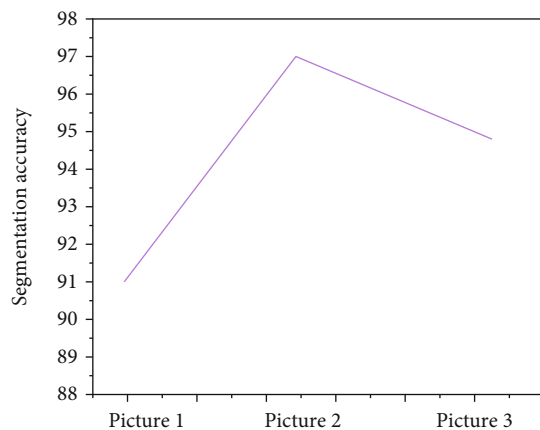


FIGURE 4: Segmentation accuracy.

This is a Hamilton-Jacobi equation, which needs to be solved by the upwind scheme. Zhao and Chan proposed a variational level set method in 1996. The variational level set directly starts from the energy functional and introduces the Heaviside function to replace the functional about the contour with the functional of the embedded function. The definition of Heaviside function is shown in

$$H(z) = \begin{cases} 1, & z \geq 0, \\ 0, & z < 0. \end{cases} \quad (11)$$

The derivative of Heaviside function H in the sense of distribution is Dirac function δ . In the actual calculation process, it is necessary to regularize the Heaviside function for numerical solution. $H_\varepsilon(z)$ is defined as the regularized Heaviside function, and it satisfies

$$H_\varepsilon(z) \xrightarrow{\varepsilon \rightarrow 0} H(z). \quad (12)$$

Two commonly used regularized Heaviside functions are given below, in the form of

$$H_\varepsilon(z) = \begin{cases} 1, & z > \varepsilon, \\ 0, & z < -\varepsilon, \\ \frac{1}{2} \left(1 + \frac{z}{\varepsilon} + \frac{1}{\pi} \sin \frac{\pi z}{\varepsilon} \right), & |z| \leq \varepsilon, \end{cases} \quad (13)$$

$$H_\varepsilon(z) = \frac{1}{2} \left(1 + \frac{2}{\pi} \arctan \frac{z}{\varepsilon} \right). \quad (14)$$

Both regularization functions are odd symmetric. $H_\varepsilon(z)$ is continuous and differentiable. Its derivative is defined as

$$\delta_\varepsilon(z) = \frac{dH_\varepsilon(z)}{dz}. \quad (15)$$

$\delta_\varepsilon(z)$ here can be regarded as the regularization of δ . For the corresponding derivative δ_ε , when the embedded function ϕ is used as the independent variable of function H , there is

$$\delta_\varepsilon(\phi) = \frac{dH_\varepsilon(\phi)}{d\phi}, \nabla H_\varepsilon(\phi) = \delta_\varepsilon(\phi) \nabla \phi. \quad (16)$$

By introducing the Heaviside function, the line integral is transformed into an area integral, as shown in

$$\oint_C g(C) ds = \iint_\Omega g |\nabla H_\varepsilon(\phi(x, y))| dx dy = \iint_\Omega \delta_\varepsilon(\phi) |\nabla \phi| g dx dy. \quad (17)$$

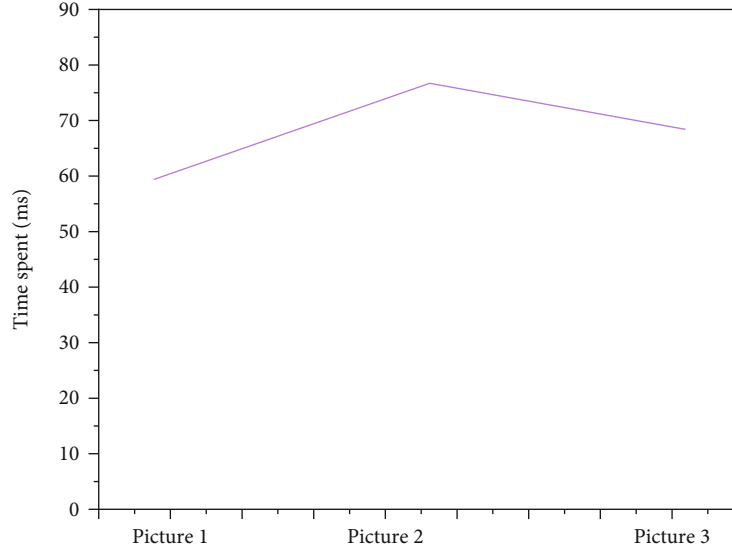


FIGURE 5: Time spent in segmentation.

The gradient downflow is obtained as

$$\frac{\partial \phi}{\partial t} = \delta_\varepsilon(\phi) \operatorname{div} \left(g \frac{\nabla \phi}{|\nabla \phi|} \right). \quad (18)$$

Through the above analysis and derivation, we can find that the type of PDE obtained by variational level set method is different from that obtained by level set method. The former is a parabolic equation and the latter is a hyperbolic equation. The difficulty in the process of numerical solution is different. Therefore, the variational level set method is a more widely used method [18, 19].

3.4. Numerical Scheme of Fourth-Order Regularized Level Set Method. In this paper, the numerical discretization of the fourth-order regularized level set method is given. The half-point center difference scheme is adopted. Based on the explicit scheme of the original segmentation model, the discretization of the fourth-order regular term is added. For the fourth-order regularization term f , the central difference explicit scheme is adopted, as shown in

$$F_{i,j}^n = - \left[D_{xx} \left(\Phi_1 \left(\varphi_{i,j}^n \right) \alpha_\varepsilon \left(\varphi_{i,j}^n \right) D_{xx} \varphi_{i,j}^n \right) + D_{yy} \left(\Phi_2 \left(\varphi_{i,j}^n \right) \beta_\varepsilon \left(\varphi_{i,j}^n \right) D_{yy} \varphi_{i,j}^n \right) \right]. \quad (19)$$

4. Result Analysis

4.1. Numerical Experiment and Result Analysis of Fourth-Order Denoising Model. This paper applies the algorithm proposed in this paper to denoise different noisy images and compares the experimental results with the classical second-order model (TV, regularized PM) and the classical fourth-order model (Y-K, LLT). Experiments were carried out on three different images: GZC01.bmp: segmented bevel image (128×128 pixels), lena.bmp (512×512 pixels), and pepper.bmp (256×256 pixels). The standard deviation is 10, 20, and 30. The numerical format pro-

posed above is realized by MATLAB, and the experimental results are shown in Table 1.

The denoising ratio of absolute noise to noise and the denoising ratio of absolute noise to noise (noise, noise, noise, noise) of smooth image are obtained.

For the noise-free smooth image u_0 and the smooth image u obtained by denoising, the indicators to measure the denoising effect are peak signal to noise ratio (PSNR) and mean absolute-deviation error (MAE).

Compared with the classical fourth-order model, it shows that this model can well retain the detailed information of the image, the smooth slope, and the edge of the image. The new model proposed in this paper is better than the second-order model and the classical fourth-order model in terms of PSNR value, MAE value, and visual effect [20].

From the data in the above table, it can be found that the PSNR value of the new model is much larger than that of other models, indicating that the fourth-order denoising model proposed in this paper can better retain the structure information of the image [21].

4.2. Segmentation Experiment of Fourth-Order Regularized Level Set Method. Figure 3 quantitatively analyzes and compares the edge positioning accuracy and noise resistance of the edge detection method, Canny edge detection method, and log edge detection method proposed in this paper for a synthetic image [22].

This paper presents the experimental results of several groups of segmentation models, as shown in Figures 4 and 5. The initial conditions are selected as binary functions [23].

The model is based on piecewise smooth Mumford-Shah, which not only better expresses the original image but also solves the problem of gray value progressive image segmentation. Secondly, the new method has the characteristics of global optimization and has no special requirements for the position of the initial contour line. Even if it is far away from the edge of the initial closed contour line, it can be segmented accurately. Third, this method does not rely

on edge information. For fuzzy or discrete edges, it can still obtain ideal segmentation effect [24, 25]. This experiment also reviews the typical methods of vector image segmentation based on active contour and extends the method in this paper to segment vector image. The new vector image segmentation method maintains many advantages of this method in gray image segmentation and can find some information that is difficult to obtain in single channel image from vector image.

5. Conclusion

Based on the modulus of directional curvature, this paper proposes a functional to describe the smoothness of image and deduces a fourth-order partial differential equation (PDE) image denoising model. The processing result is piecewise linear image (including linear image), and there is a step in the gradient at the edge. Taking advantage of this feature, this paper proposes a new geodesic active contour (new GAC) model, which improves the contour extraction performance of traditional GAC and is much faster. It is worth paying full attention to the new derivation of new GAC model. The region-based active contour model has certain robustness to noise, but the processing of strong noise image is still limited. The noise reduction model in this paper also greatly improves the segmentation effect of region based active contour model.

In short, variational methods and partial differential equations are widely used in image processing. They are a new and developing discipline. Many image processing problems can be expressed by variational models and differential equations. The research work can be deepened from two aspects: the improvement of model form and the efficiency and accuracy of algorithm implementation. We need to make more efforts to continuously improve the processing effect of model and improve the execution efficiency and accuracy of algorithm implementation.

Data Availability

The data used to support the findings of this study are available from the corresponding author upon request.

Conflicts of Interest

The author declares that there are no conflicts of interest.

Acknowledgments

The study was supported by the reliability modeling and analysis of aggregated stochastic dynamic systems based on ion channel theory, Project ID: 135509127.

References

- [1] H. Bi, W. L. Shang, Y. Chen, and K. Wang, "Joint optimisation for pedestrian, information and energy flows in emergency response systems with energy harvesting and energy sharing," *IEEE Transactions on Intelligent Transportation Systems*, vol. 4, 2022.
- [2] H. Jiang and D. Xu, "An efficient sinc-collocation method by the single exponential transformation for the nonlinear fourth-order partial integro-differential equation with multi-term kernels," *Mathematical Methods in the Applied Sciences*, vol. 45, no. 5, pp. 3166–3182, 2022.
- [3] B. Kumar, A. Halim, and R. Vijayakrishna, "Higher order pde based model for segmenting noisy image," *IET Image Processing*, vol. 14, no. 11, pp. 2597–2609, 2020.
- [4] X. Zhou, X. Xu, W. Liang et al., "Intelligent small object detection for digital twin in smart manufacturing with industrial cyber-physical systems," *IEEE Transactions on Industrial Informatics*, vol. 18, no. 2, pp. 1377–1386, 2022.
- [5] D. Zhao, B. Jiang, and H. Yang, "Backstepping-based decentralized fault-tolerant control of hypersonic vehicles in pde-ode form," *IEEE Transactions on Automatic Control*, vol. 99, pp. 1–1, 2021.
- [6] G. Weng, B. Dong, and Y. Lei, "A level set method based on additive bias correction for image segmentation," *Expert Systems with Applications*, vol. 185, no. 1–2, p. 115633, 2021.
- [7] A. Liu, D. Sun, B. Yu, J. Wei, and Z. Cao, "An adaptive coupled volume-of-fluid and level set method based on unstructured grids," *Physics of Fluids*, vol. 33, no. 1, article 012102, 2021.
- [8] B. Yang, B. Wu, Y. You, C. Guo, L. Qiao, and Z. Lv, "Edge intelligence based digital twins for Internet of autonomous unmanned vehicles," in *Software: Practice and Experience*, Wiley, 2022.
- [9] Z. Wan, Y. Dong, Z. Yu, H. Lv, and Z. Lv, "Semi-supervised support vector machine for digital twins based brain image fusion," *Frontiers in Neuroscience*, vol. 15, p. 802, 2021.
- [10] C. Ma, Q. Zheng, J. Wang, Q. Cai, and X. Tong, "A computational model of thrombus growth based on level set method," *IEEE Access*, vol. 9, pp. 100769–100780, 2021.
- [11] Z. Lv, Y. Han, A. K. Singh, G. Manogaran, and H. Lv, "Trustworthiness in industrial IoT systems based on artificial intelligence," *IEEE Transactions on Industrial Informatics*, vol. 17, no. 2, pp. 1496–1504, 2021.
- [12] Z. Lv, W. Kong, X. Zhang, D. Jiang, H. Lv, and X. Lu, "Intelligent security planning for regional distributed energy Internet," *IEEE Transactions on Industrial Informatics*, vol. 16, no. 5, pp. 3540–3547, 2020.
- [13] Y. Yao, E. Giner, J. Li, J. Toulouse, and C. J. Umrigar, "Almost exact energies for the Gaussian-2 set with the semistochastic heat-bath configuration interaction method," *The Journal of Chemical Physics*, vol. 153, no. 12, article 124117, 2020.
- [14] Z. Wang, W. Yao, C. Zuo, and X. Hu, "Solving phase change problems via a precise time-domain expanding boundary element method combined with the level set method," *Engineering Analysis with Boundary Elements*, vol. 126, no. 4b, pp. 1–12, 2021.
- [15] J. Li, P. Jiang, and H. Zhu, "A local region-based level set method with Markov random field for side-scan sonar image multi-level segmentation," *IEEE Sensors Journal*, vol. 21, no. 1, pp. 510–519, 2020.
- [16] O. Abdel Wahab, A. Mourad, H. Otrok, and T. Taleb, "Federated machine learning: survey, multi-level classification, desirable criteria and future directions in communication and networking systems," *IEEE Communications Surveys & Tutorials*, vol. 23, no. 2, pp. 1342–1397, 2021.
- [17] H. Sami, A. Mourad, and W. El Haj, "Vehicular-OBUs-as-on-demand-fogs: resource and context aware deployment of

- containerized micro-services,” *IEEE/ACM Transactions on Networking*, vol. 28, no. 2, pp. 778–790, 2020.
- [18] L. N. Larios-Cárdenas and F. Gibou, “A deep learning approach for the computation of curvature in the level-set method,” *SIAM Journal on Scientific Computing*, vol. 43, no. 3, pp. A1754–A1779, 2021.
- [19] J. Wang, P. Liu, F. Wen, R. Ying, and W. Wang, “Phase unwrapping for time-of-flight sensor based on image segmentation,” *IEEE Sensors Journal*, vol. 21, no. 19, pp. 21600–21611, 2021.
- [20] R. Sami, S. Soltane, and M. Helal, “Microscopic image segmentation and morphological characterization of novel chitosan/silica nanoparticle/nisin films using antimicrobial technique for blueberry preservation,” *Membranes*, vol. 11, no. 5, p. 303, 2021.
- [21] J. Qiu, Y. Chai, Z. Tian, X. Du, and M. Guizani, “Automatic concept extraction based on semantic graphs from big data in smart city,” *IEEE Transactions on Computational Social Systems*, vol. 7, no. 1, pp. 225–233, 2020.
- [22] M. Jahanbakht, W. Xiang, L. Hanzo, and M. R. Azghadi, “Internet of underwater things and big marine data analytics – a comprehensive survey,” *IEEE Communications Surveys & Tutorials*, vol. 23, no. 2, pp. 904–956, 2021.
- [23] J. Chen, J. Liu, X. Liu, X. Xu, and F. Zhong, “Decomposition of toluene with a combined plasma photolysis (cpp) reactor: influence of uv irradiation and byproduct analysis,” *Plasma Chemistry and Plasma Processing*, vol. 41, no. 1, pp. 409–420, 2021.
- [24] R. Huang, “Framework for a smart adult education environment,” *World Transactions on Engineering and Technology Education*, vol. 13, no. 4, pp. 637–641, 2015.
- [25] E. Guo, V. Jagota, M. Makhatha, and P. Kumar, “Study on fault identification of mechanical dynamic nonlinear transmission system,” *Nonlinear Engineering*, vol. 10, no. 1, pp. 518–525, 2021.

Retraction

Retracted: Motion Control Analysis of Tennis Robot Based on Ant Colony Algorithm

Journal of Sensors

Received 23 January 2024; Accepted 23 January 2024; Published 24 January 2024

Copyright © 2024 Journal of Sensors. This is an open access article distributed under the Creative Commons Attribution License, which permits unrestricted use, distribution, and reproduction in any medium, provided the original work is properly cited.

This article has been retracted by Hindawi following an investigation undertaken by the publisher [1]. This investigation has uncovered evidence of one or more of the following indicators of systematic manipulation of the publication process:

- (1) Discrepancies in scope
- (2) Discrepancies in the description of the research reported
- (3) Discrepancies between the availability of data and the research described
- (4) Inappropriate citations
- (5) Incoherent, meaningless and/or irrelevant content included in the article
- (6) Manipulated or compromised peer review

The presence of these indicators undermines our confidence in the integrity of the article's content and we cannot, therefore, vouch for its reliability. Please note that this notice is intended solely to alert readers that the content of this article is unreliable. We have not investigated whether authors were aware of or involved in the systematic manipulation of the publication process.

Wiley and Hindawi regrets that the usual quality checks did not identify these issues before publication and have since put additional measures in place to safeguard research integrity.

We wish to credit our own Research Integrity and Research Publishing teams and anonymous and named external researchers and research integrity experts for contributing to this investigation.

The corresponding author, as the representative of all authors, has been given the opportunity to register their agreement or disagreement to this retraction. We have kept a record of any response received.

References

- [1] F. Wang, Y. Dong, H. Gao, and L. Wu, "Motion Control Analysis of Tennis Robot Based on Ant Colony Algorithm," *Journal of Sensors*, vol. 2022, Article ID 6945310, 8 pages, 2022.

Research Article

Motion Control Analysis of Tennis Robot Based on Ant Colony Algorithm

Feng Wang , Yujie Dong , Haobo Gao , and Lin Wu 

Physical Education College of Xi'an Peihua University, Xi'an 710125, China

Correspondence should be addressed to Lin Wu; fl2041121@st.sandau.edu.cn

Received 29 May 2022; Revised 25 June 2022; Accepted 6 July 2022; Published 15 July 2022

Academic Editor: Haibin Lv

Copyright © 2022 Feng Wang et al. This is an open access article distributed under the Creative Commons Attribution License, which permits unrestricted use, distribution, and reproduction in any medium, provided the original work is properly cited.

Visual recognition and automatic control technology is an important way to realize robot automatic ball picking. Therefore, a tennis robot motion control method based on ant colony algorithm is evaluated. After the camera position was fixed, the motion control system software was designed, and the optimal path was solved by ant colony algorithm. The results show that the two adjacent positioning errors and the current total positioning errors fluctuate around -0.05 mm and -2.29 mm, respectively, and the fluctuation range is less than 3.50 mm. Ant colony algorithm is superior to greedy algorithm in path planning of collecting tennis balls. The number of iterations of ant colony algorithm for optimal path planning of 30 to 50 tennis balls is about 20 to 30 times, and the path length is reduced to reduce the time of collecting tennis balls, which meets the actual work requirements.

1. Introduction

With the development of society and promotion of all-people exercise, tennis has gradually become a fashion sport to get more people love. Especially after Li Na won the Grand Slam, the domestic tennis fever is set off, and more and more people participate in the sport of tennis [1]. According to statistics, China's tennis population has broken through 15 million, and tennis is becoming more and more common, for professional matches or professional athletes training, may be responsible for ball caddies [2]. But not all players and tennis fans have such conditions and benefits. With a standard tennis court measuring no less than 670 square meters, collecting the balls scattered on the court is no doubt a lot of physical work. At present, there are also some tennis picking machines on the market, most of which are pure mechanical or semiautomatic ball-picking machines with relatively economic manual operation [3]. Manual operation is both a waste of time and reduces the efficiency of training, and this manual operation is also subject to the danger of being hit by tennis balls [4]. To meet the market demand and solve these problems, it is necessary to develop a safe, efficient, stable, and economical intelligent

tennis collecting robot [5]. Machine vision technology is a new technology that has gradually developed in recent years. It can be applied in intelligent manufacturing and many intelligent living fields. Machine vision has become an important way of intelligent development, and its application has become more extensive [6, 7]. In this development background, this topic is proposed to achieve the identification of tennis ball positioning and pick up through machine vision technology and the improvement of existing equipment integration and innovation. This topic is to develop an intelligent tennis collecting robot, which can provide the possibility of convenience and better experience for tennis practitioners to practice alone. At the same time, it can also save physical strength for the practitioners, quickly and conveniently realize the tennis picking up, so that the practitioners can put more energy on physical and mental entertainment and technical improvement.

Therefore, the development of a tennis collecting robot with high intelligence and simple operation has better market demand and the possibility of intelligent development. This project integrates advanced visual technology into the research and development of tennis collecting robot, which is also a new attempt and practice. Therefore, this research

has great academic research significance and application value. Figure 1 shows the design and development of tennis robot.

2. Literature Review

After consulting a large number of relevant literature and market research, from the development of tennis picking robots, tennis picking institutions can be roughly divided into three categories.

(1) Simple tennis ball picker

Ball-picking basket and ball-picking Jane are the two most common ball-picking devices on the market. Because it is convenient and cheap to use and carry, it is a popular auxiliary ball-picking tool among most tennis trainers. This kind of ball-picking device mainly relies on artificial will pick up the ball basket or collection of Jane's goal port under pressure at the tennis ball, so that it enters the Jane; this kind of ball-picking device has the advantages of simple organization, low cost, but needs more people to participate in, and pick up tennis discontinuous, and its efficiency is very low.

(2) Sophisticated tennis ball picker

With the deepening of research and development of tennis ball-picking mechanism, the designed ball-picking mechanism is relatively complex and its functions are gradually improved, which overcomes some shortcomings of simple ball-picking device, but its intelligence degree is still not very high. In the aspect of picking up the ball, this topic uses the principle of rolling simple picking up the ball, carries on the modeling analysis to pick up the tennis ball process, carries on the design optimization to the mechanism, and through the prototype debugging finds that the experimental test data is basically consistent with the theoretical value. However, the overall size and weight of the device are too large. Although the body part of the car realizes the transformation from human drive to electric, it still needs human to control the direction and speed.

Some ball-picking institutions use electric drive, belt drive, or chain plate drive to pick up the ball for the wheel shaft drive belt baffle push tennis, and tennis collection is realized. The front end of the ball is added to collect the player and guide the tennis ball into the ball-picking device, and the degree of automation of the way of picking up the ball is obviously improved. However, this scheme reduces the continuity of ball picking and has a complex structure. With the use of multiple motors, its control becomes more complex, with an increase in cost and a decrease in efficiency. In addition, the control of walking mechanism is not flexible enough and has poor adaptability.

(3) A ball-picking robot with a high degree of intelligence

With the development of artificial intelligence and visual recognition technology, under the general trend of multidisciplinary integration, many researchers have applied

advanced visual technology to the ball-picking robot and put forward different ball-picking schemes. They have made breakthroughs in the research of tennis picking robot, and its intelligence degree has been improving, but only a small number of research teams have successfully developed a fully autonomous intelligent ball-picking robot.

In Li et al.'s project, the vision system uses ultrasonic ranging technology to find the landing tennis ball and adds infrared ranging sensors to the ultrasonic ranging system to guide the robot. Through the control system, the robot moves to the specified position and realizes the action of picking up the ball [8]. Ganser et al. proposed an embedded intelligent ball-picking car, and the scheme uses color and shape recognition algorithm, combined with PID control algorithm, respectively, using motor drive car body movement and steering gear control car ball-picking action, to achieve the function of picking up tennis balls [9, 10]. However, this scheme is only a theoretical solution, and the concrete realization remains to be practiced. According to the single-view imaging theory, the researchers made a panoramic camera with omnidirectional reflector [11]. Ba's designed ball-picking mechanism uses the friction force of the ball and the outer wall to pick up the ball and creatively combines the ball-picking device with the self-developed serving device. He designed a tennis car integrating ball picking and serving, realizing that the car drives the rolling machine to rotate to pick up the ball. However, manual movement of the car body and identification of the tennis balls are required in the process of picking up the ball, so the degree of automation of picking up the ball is not high [12]. The automatic tennis collecting robot designed by Tu and Chen uses infrared sensor to locate the tennis ball and grasp and recover the ball through the manipulator claw. This way of picking up the ball is more flexible and theoretical. It can pick up the net and the tennis ball near the corner, but the positioning of the tennis ball is higher. In addition, only one ball can be picked up each time, and each ball collection needs to be raised and released through alignment clamp, so the efficiency of ball picking is relatively low [13]. The ball-picking robot designed and developed by Shu et al. adopts a drum baffle type ball-picking mechanism. During the robot's progress, the impeller independently driven by the motor drives the baffle to rotate, and the tennis ball is involved and raised to the highest position and then falls into the collecting device by its own gravity. This way of picking up the ball is relatively efficient. However, due to the rigid contact between the baffle and the tennis ball, there is impact at the moment of contact between the baffle and the tennis ball in the process of picking up the ball [14]. Luo et al. use RFID radio frequency identification technology combined with LANDMARC algorithm, through the communication between the RFID tag installed on the sphere and the reference beacon arranged in the environment, to achieve the positioning of the sphere and the navigation of the ball-picking robot. This positioning scheme requires additional rf tags for tennis balls and the surrounding working environment, which is difficult to be applied in practice [15]. Li uses a global camera to collect the image information of the golf ball and the ball-picking robot in

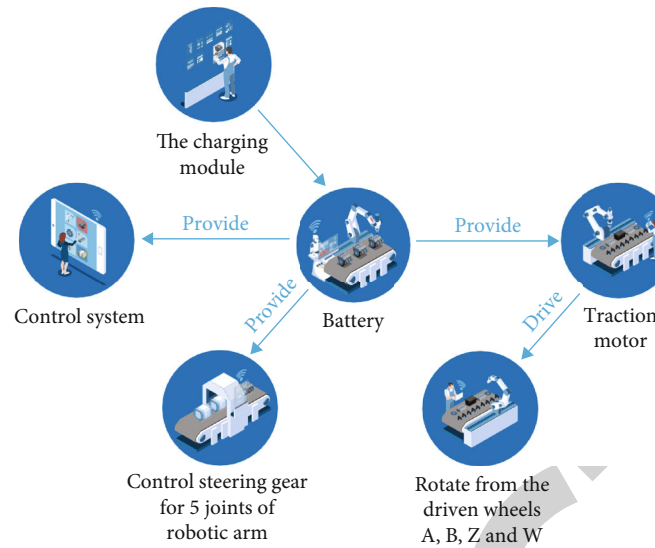


FIGURE 1: Design and development of tennis robot.

the field of vision and transmits it to the server in real time. He uses the image processing technology to identify the special artificial marks on the golf ball and the robot and realizes the autonomous positioning and navigation of the golf ball collecting robot [16]. The intelligent tennis ball-picking robot designed by Lv et al. uses binocular vision to realize the identification and positioning of tennis balls. Through BM (BlockMatching) algorithm, stereo matching is carried out on the imaging results of binocular vision system, and parallax matrix is obtained. The parallax matrix is mapped to the coordinate system of the ball-picking robot to complete the 3D reconstruction and relative positioning of the identified tennis balls in the robot coordinate system. In addition, the 2d plane positioning system is combined to determine its own orientation, and the autonomous ball picking under the visual guidance of the ball-picking robot is realized [17]. Visual recognition and automatic control technology is an important way to realize robot automatic ball picking. Many literatures have proposed the combination of multimodules such as visual recognition, motion control, and path planning to pick up the ball to realize intelligent tennis picking, but there is no specific implementation process, and many of these modules need to be further studied and optimized. Therefore, this topic can be studied and optimized in the module of visual recognition and target positioning, motion control, and path planning [18, 19].

3. Research Method

3.1. Camera Calibration. The purpose of camera calibration is to find the corresponding relationship between the pixel coordinates in the image and the world coordinates. Camera calibration is an essential step to obtain accurate position information of object in 3d space from 2d image taken by camera.

The camera imaging model mainly involves four coordinate systems:

World coordinate system: an artificial frame of reference that facilitates representation of the position of a target object in the real world.

Camera coordinate system: the Z axis is parallel to the optical axis of the camera.

Image frame X-Y: a coordinate system based on a photo taken by a camera with the focal point of the camera's optical axis and the imaging plane as the origin [20].

The pixel coordinate system takes the upper left corner of the image as the origin, and the coordinates and coordinates are the number of columns and rows of the pixel, respectively.

The transformations between partial coordinate systems are as follows:

Any coordinate (X, Y) in the image coordinate system has the following conversion relation with its corresponding pixel coordinate (u, v) , as shown in the following equation:

$$\begin{cases} u = \frac{x}{dx} + u_0, \\ v = \frac{y}{dy} + v_0. \end{cases} \quad (1)$$

dx and dy , respectively, represent the width of one pixel of the axis and the axis direction, (u_0, v_0) is called the main point of the image plane, equivalent to the discretization of the axis x and the axis y , and dx , dy , and (u_0, v_0) are the internal parameters of the camera. Write Equation (1) in matrix form, as in the following equation:

$$\begin{bmatrix} u \\ v \\ 1 \end{bmatrix} = \begin{bmatrix} 1/dx & 0 & u_0 \\ 0 & 1/dy & v_0 \\ 0 & 0 & 1 \end{bmatrix} \begin{bmatrix} x \\ y \\ 1 \end{bmatrix}. \quad (2)$$

Conversion of world coordinates to camera coordinates can be achieved by rigid body transformation.

The mathematical expression of rigid body changes between them is shown in the following equation:

$$\begin{bmatrix} X_c \\ Y_c \\ Z_c \end{bmatrix} = \begin{bmatrix} r_{00}r_{01}r_{02} \\ r_{10}r_{11}r_{12} \\ r_{20}r_{21}r_{22} \end{bmatrix} \begin{bmatrix} X_w \\ Y_w \\ Z_w \end{bmatrix} + \begin{bmatrix} T_x \\ T_y \\ T_z \end{bmatrix}. \quad (3)$$

Namely, in $X_c = RX + T$, X_c represents the camera coordinate system, X represents the world coordinate system, R represents rotation, T represents translation, and R, T are the external parameter of the camera.

3.2. Software Design of Motion Control System. The software design of motion control system mainly includes controlling motor speed and writing control algorithm suitable for motion as well as optimizing path to improve the efficiency of picking up tennis balls [21, 22].

In this study, PID algorithm is used to control the motor speed. PID controller measures the deviation between the actual value and the expected value of the controlled variable and corrects the system accordingly, so as to achieve the purpose of regulating the system. The control system schematic diagram is shown in Figure 2.

In PID control system, $r(t)$ is the target value set by the system, $y(t)$ is the actual value of the output and feedback of the system, $e(t)$ is the deviation, and it is the difference value between $r(t)$ and $y(t)$. PID control can be expressed as the following equation:

$$u(t) = K_p \left[e(t) + \frac{1}{T_i} \int_0^t e(t) dt + T_D \frac{de(t)}{dt} \right]. \quad (4)$$

K_p , T_i , and T_D are proportional coefficient, integral time, differential time, respectively. These three parts jointly affect the system. Formula (4) is a continuous PID algorithm calculation formula, most of the practical application of discrete digital controller, and digital controller algorithm is usually divided into position and incremental PID control algorithm [23].

Position PID is a kind of sampling control. It calculates the control quantity of the motor according to the deviation value at the moment. Therefore, Equation (4) must be discretized and approximated by using and replacing integral and difference to replace differential to get the following equation:

$$\begin{aligned} u(k) &= K_p \left[e(t) + \frac{1}{T_i} \int_0^t e(t) dt + T_D \frac{de(t)}{dt} \right] \\ &\approx K_p e_k + \frac{K_p T}{T_i} \sum_{j=0}^k e_j + \frac{K_p T_D}{T} (e_k - e_{k-1}). \end{aligned} \quad (5)$$

$e(k)$ and $u(k)$ are, respectively, the deviation value and the control quantity at the time of the first sampling. The incremental PID is to calculate the increment of control quantity of two adjacent samples $\Delta u(k) = u(k) - u(k-1)$. The incremental PID is used to control the motor speed.

The incremental PID control system is shown in Figure 3 below.

As can be seen from Equation (5), the location-based algorithm accumulates errors, occupies a large storage unit, and is difficult to write programs, so it is improved. The expression can be deduced from Equation (5) as the following equation.

$$u(k-1) = K_p e_{k-1} + \frac{K_p T}{T_i} \sum_{j=0}^{k-1} e_j + \frac{K_p T_D}{T} (e_{k-1} - e_{k-2}). \quad (6)$$

Then, the incremental PID control calculation formula is shown in Equation (7).

$$\Delta u(k) = K_p (e_k - e_{k-1}) + \frac{K_p T}{T_i} e_k + \frac{K_p T_D}{T} (e_k - 2e_{k-1} + e_{k-2}). \quad (7)$$

Compared with the position algorithm, the incremental algorithm does not need to do cumulative calculation, calculation error has less influence on the calculation of the control quantity, the cumulative error is small, the computer output controls quantity increment, and misoperation has less influence.

3.3. Ant Colony Algorithm to Solve the Optimal Path. For the randomly distributed tennis ball collection problem, this paper adopts ant colony algorithm to solve the multiobjective path planning problem. The algorithm is the ant colony algorithm proposed by Marco Dorigo inspired by the ant foraging process [24].

The algorithm mimics the way ants guide other ants by releasing secretions called pheromones during foraging. Because pheromones are volatile, the concentration of pheromones along the path of the ant colony decreases over time, and the shorter the distance, the more pheromones are retained [25]. Ants will forage along the path with high pheromone concentration, and the path with high pheromone concentration will accumulate more ants, showing a positive feedback. Two key steps in ant colony algorithm are the probability selection of target and pheromone updating method.

- (1) *Probabilistic Choice.* In the initial state, the pheromone quantity on each path is the same. Set the initial $\tau_{ij}(0) = C_0$, C_0 as a constant, and the ant $k(k = 1, 2, \dots, m)$ makes a judgment according to the visibility of the target point and the pheromone quantity on the path in the process of finding the path. The probability t that the ant k located at the tennis ball moves to the tennis ball j as in the following equation:

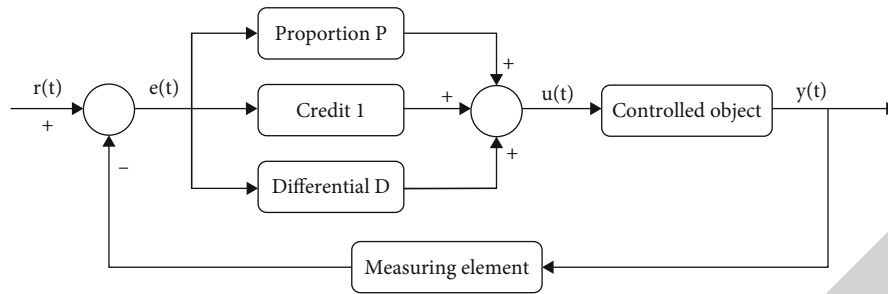


FIGURE 2: PID control system schematic diagram.

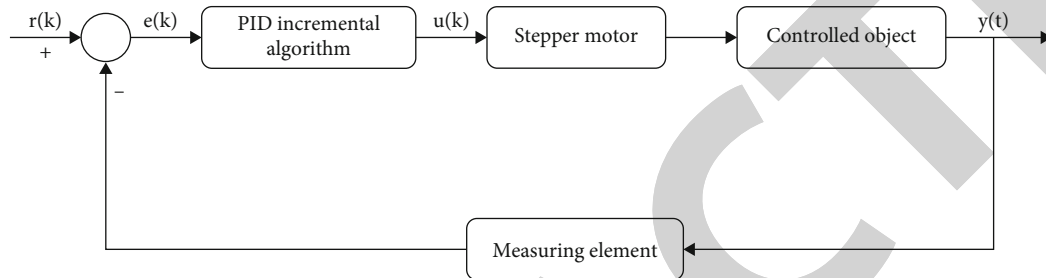


FIGURE 3: Schematic diagram of incremental PID control system.

$$P_{ij}^k(t) = \begin{cases} \frac{[\tau_{ij}(t)]^\alpha \times [\eta_{ij}(t)]^\beta}{\sum_{k \in \text{allowed}_k} [\tau_{ik}(t)]^\alpha \times [\eta_{ik}(t)]^\beta}, & \text{if } j \in \text{allowed}_k, \\ 0 & \text{others.} \end{cases} \quad (8)$$

$\tau_{ij}(t)$ is the pheromone intensity on the path of t time connection i and j . $\eta_{ik}(t) = 1/d_{ik}$, and it is the visibility of the ants at any moment. allowed_k is a collection of all tennis target points that have not yet passed. α, β are two constants and are the weighted values of pheromone intensity and visibility, respectively.

- (2) *Pheromone Update*. After searching all the tennis balls, update the pheromone on the path according to Equation (9).

$$\tau_{ij}(t) = (1 - \rho)\tau_{ij} + \sum_{k=1}^m \Delta\tau_{ij}^k. \quad (9)$$

m is the number of ants, ρ is pheromone volatilization coefficient, which represents the loss degree of information on the path, and $\Delta\tau_{ij}^k$ is the pheromone left by the first ant on the path in this cycle and is in the initial stage of search. The beginning of the search $\Delta\tau_{ij}^k = 0$.

$$\Delta\tau_{ij}^k = \begin{cases} \frac{Q}{L_K}, & \text{if the } k^{\text{th}} \text{ ant traverses } i \text{ to } j, \\ 0, & \text{others.} \end{cases} \quad (10)$$

$\Delta\tau_{ij}^k(t)$ represents the influence value of the first ant on

the amount of information on the path (i, j) in this search. Q denotes pheromone intensity, which affects the search speed of the algorithm: L_K denotes the path length acquired by the k^{th} ant in this search. Figure 4 shows the flow chart of ant colony algorithm. In order to verify the effectiveness and feasibility of ant colony algorithm for multiobjective path planning, Matlab was used for programming simulation, and the simulation results were compared with greedy algorithm.

4. Interpretation of Result

4.1. Tennis Ball Positioning Experiment. In order to verify the effect of this algorithm on tennis ball positioning, experimental verification is conducted. Due to the limited experimental conditions, the real three-dimensional coordinates of the tennis center cannot be measured accurately during the experiment, so the positioning error cannot be calculated accurately. Therefore, in this experiment, the movement of the binocular camera is precisely controlled by virtue of the precision movement of the six-axis mechanical arm, and the positioning error is calculated by using its precise relative displacement to verify the positioning effect of the tennis ball, as shown in Figures 5 and 6.

It can be seen from Figures 5 and 6 that the two adjacent positioning errors and the current total positioning errors fluctuate around -0.05 mm and -2.29 mm, respectively, and their fluctuation ranges are less than 3.50 mm, indicating that the positioning method can accurately position tennis balls and meet the positioning accuracy requirements of tennis balls.

4.2. Comparing Algorithm. In order to better compare the advantages of ant colony algorithm and greedy algorithm, a simulation experiment was conducted on the path

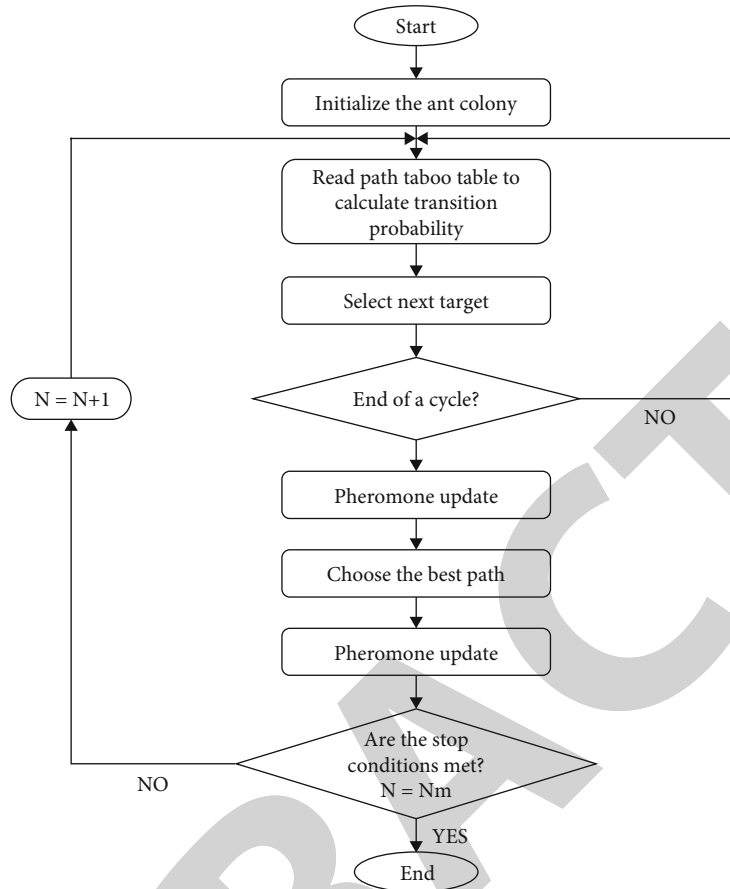


FIGURE 4: Flow chart of ant colony algorithm.

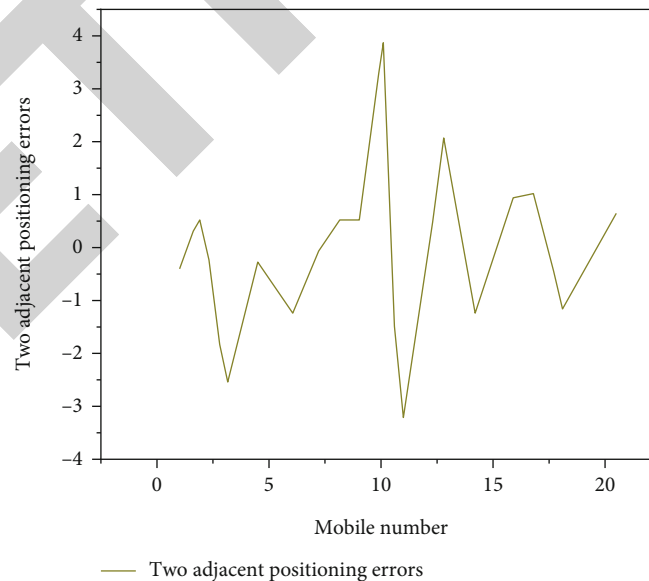


FIGURE 5: Analysis diagram of two adjacent positioning errors.

planning of 30, 35, 40, 45, and 50 tennis balls, respectively. Five experiments were conducted for each problem scale to calculate the average value as the experimental results for comparison, and the results are shown in Figure 7.

It can be seen from the experimental results that the ant colony algorithm is superior to the greedy algorithm in the path planning of collecting tennis balls. The number of iterations of the ant colony algorithm for the optimal path

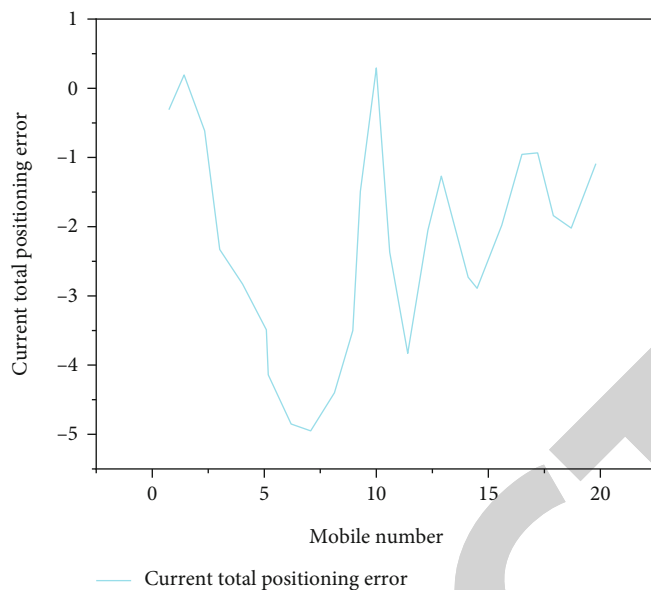


FIGURE 6: Current total positioning error analysis diagram.

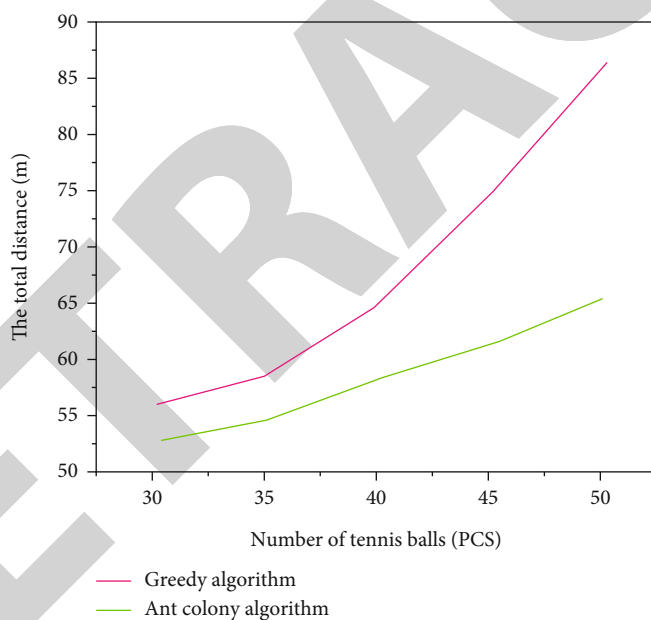


FIGURE 7: Comparison of algorithm data.

planning of 30 to 50 tennis balls is about 20 to 30 times. The path length is reduced to reduce the collection time of tennis balls to meet the actual work requirements.

5. Conclusion

At present, there are few intelligent tennis collecting robots on the market, and most of the existing equipment is simple auxiliary ball-picking device, which cannot achieve efficient and autonomous collection of tennis balls. For athletes and amateurs in training, picking up loose balls on the court can be a grueling, manual labor that can cost a lot to hire caddies. In view of the difficulty in picking up balls, this topic studies the key technology of tennis collecting robot

and tries to develop an intelligent tennis collecting robot based on vision to realize the autonomous collection of tennis balls instead of manual work. The main work and research results of this topic are as follows:

- (1) *Tennis Positioning*. A stereo matching algorithm is proposed, which takes the tennis ball recognition region as the basic element and the tennis ball center as the point to be matched. The matching of tennis target area is completed, and the coordinate of three-dimensional space is calculated by parallax, and the high-precision positioning of tennis ball is realized. The algorithm has short matching operation time and high accuracy

Research Article

Target Recognition, Localization, and Motion Control of Soccer Robot

Changsheng Zhu  and Min Gong 

College of General Education, Nanning University, Nanning, Guangxi 530200, China

Correspondence should be addressed to Changsheng Zhu; 19401012@masu.edu.cn

Received 29 May 2022; Revised 26 June 2022; Accepted 6 July 2022; Published 15 July 2022

Academic Editor: Haibin Lv

Copyright © 2022 Changsheng Zhu and Min Gong. This is an open access article distributed under the Creative Commons Attribution License, which permits unrestricted use, distribution, and reproduction in any medium, provided the original work is properly cited.

The realization of target tracking includes many technologies, among which the most critical and core element is the target tracking algorithm. Based on this, this paper first uses an omnidirectional vision image enhancement algorithm to identify the target and then designs an adaptive target recognition algorithm based on SVM to identify the actual target. The results show that, in the case of different illuminance, the fluctuation range of the four evaluation indexes after image enhancement is smaller than that of the original image, indicating that the brightness distribution of the image after enhancement is more uniform, which eliminates interference factors for the subsequent image recognition and tracking. The difference of recognition rate between the two algorithms is small when the illumination value is medium. When the illumination value is high or low, the recognition rate of the adaptive algorithm is much higher than that of the threshold method.

1. Introduction

The football robot vision module consists of two parts, the image acquisition part and the image processing part. The image acquisition is mainly completed by the camera. After the image is acquired, the most important thing is to extract the useful information contained in the image, which requires that further analysis and processing measures are taken for image information, which involves some algorithms for dedrying and feature extraction [1]. Therefore, whether useful information can be obtained depends largely on the performance of these algorithms. The performance evaluation indicators of image processing algorithms mainly include execution efficiency, robustness, and complexity. Background interference or chromatic aberration are often encountered in the game, which requires image processing algorithms to have strong anti-interference to these uncertain factors, so as to adapt to various complex environments [2, 3].

The research field of the football robot vision module mainly involves technologies such as target recognition and target tracking. Through the research and improvement of related technologies, on the one hand, the existing

theoretical system can be improved, and on the other hand, the application scope of recognition and tracking technology can be expanded [4]. In recent years, artificial intelligence has become more and more popular, and one of the most important aspects is image recognition and tracking, which plays an important role in realizing the autonomous operation of machines. Every year, a large number of scholars pour into this field [5]. With the continuous updating and improvement of algorithms, the application scope of this technology has also extended from the initial field of machine vision to many other fields such as industrial inspection, geological exploration, autonomous driving, and remote sensing images. Therefore, the research on image recognition and tracking technology has also played a positive role in promoting the progress of other research directions. Figure 1 shows the improvement of target positioning technology and tracking algorithm for humanoid soccer robots [6].

2. Literature Review

RoboCup has established the category of the mid-sized group since its inception, and the RoboCup Medium-Sized

League (MSL) has been held since 1997. The field of competition is set on an indoor football field with a size of 18 m * 12 m, which is appropriately reduced relative to the actual football field. Two teams, each team is allowed to have a maximum of six football robots, using orange balls to play. Human intervention is not allowed during the game, unless there is an unexpected situation such as a robot foul or a robot failure. For the shape of the robot, it is stipulated that the maximum diameter cannot exceed 50 cm, and each team can design hardware and software completely autonomously [7].

In the RoboCup competition, the competition of the medium group is more watchable and the competition is more intense than the competition of other groups. In these years of competition, there have also been many strong teams. In the first few years of the competition, the German team and the Japanese team performed relatively well. Later, Portugal and the Netherlands began to catch up slowly. In recent years, in the competition, the goal team is often the champion and runner-up. Some colleges and universities also participated. Although they started late, there were also teams that performed well. These teams have their own strengths [8].

At the beginning of the robot football competition, because the technical research of the participating teams was still in its infancy, in order to reduce the difficulty of the competition and allow the competition to proceed normally, the organizers set the competition rules relatively loosely. Compared with the past, there have been certain breakthroughs, and in order to make the robot adapt to a more complex environment, the organizer has revised the robot's competition rules, making the rules more and more similar to the rules of human competition. Therefore, the current competition environment is more complex; lighting changes, visual blind spots, and visual blur caused by movement are all key factors that affect the accuracy of the visual system's recognition of objects. Therefore, the main research purpose of the vision module of the football robot is to make the vision module recognize the target accurately in most cases, not just to complete the recognition task by precalibrating the color. In response to this robustness problem, domestic and foreign researchers have done a lot of research on it. Particularly in recent years, many new algorithms have been proposed in the field of machine vision, and the target features used in target recognition have gradually diversified, such as edge features, linear features, and HOG features, rather than just a single color feature to identify objects. Among the adopted recognition methods, the two most frequently used methods are the template matching method and the classifier method. Shruti and Deka proposed a target recognition algorithm based on optical flow field, which assumes that the gray gradient is basically constant or the brightness is constant. At this stage, the technology based on the first-order spatiotemporal gradient is still the mainstream of the optical flow recognition algorithm, and many new algorithms have also emerged [9]. Husari and Seshadrinath developed an optical flow field-based robot, which imitates the visual mechanism of bees and

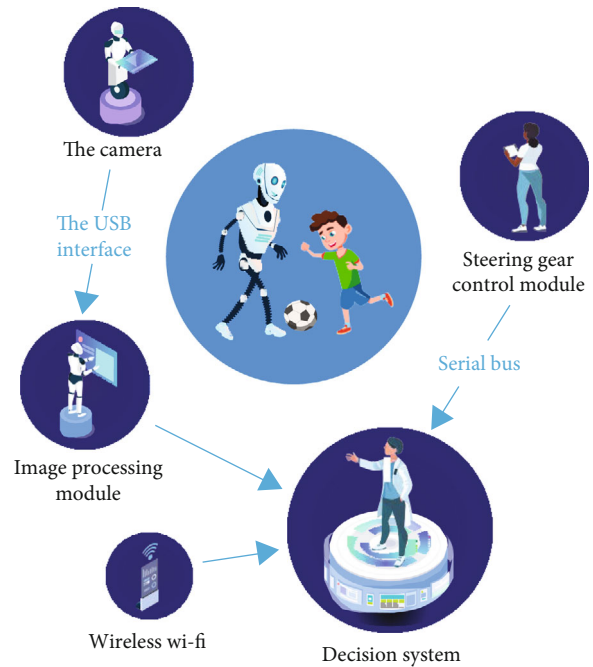


FIGURE 1: Improvement of target positioning technology and tracking algorithm of humanoid soccer robot.

can walk in corridors independently. However, the calculation algorithm of the optical flow field is complex and time-consuming, and when the distinction between the background and the target is small, or the image quality is not particularly high, the accuracy of the algorithm for the detection and recognition of the target will be greatly reduced [10]. The four-wheeled mobile robot introduced by Cai and Zheng is also a nonomnidirectional robot. Common omnidirectional mobile robots include one-wheel, three-wheel, and four-wheel. It can fully reflect the maneuverability of omnidirectional mobile robots in occasions where space is not very abundant. Omnidirectional robots generally use omnidirectional wheels. Compared with ordinary wheels, omnidirectional wheels can slide sideways, which determines that omnidirectional mobile robots have good maneuverability and can move at any speed and any angular velocity on the plane [11]. Xie et al. showed how to achieve the calibration of a parabolic reflection panorama system from the imaging of three lines in space or two sets of parallel lines in an omnidirectional view [12]. Wu et al. developed a new panoramic vision system, which improves the imaging shortcomings of the traditional omnidirectional vision system. It combines hyperbolic mirrors, vertical proportional mirrors, and horizontal proportional mirrors. The combination of mirrors improves the problem of severe image distortion in traditional imaging systems [13]. Zeng et al. proposed a recognition method based on the use of real-time adjustment of calibrated colors. This method adjusts color information in real time according to the principle of color drift and combined it with the degree of illumination change, so as to achieve robustness to changes in light intensity. Sexual purpose [14]. Li et al. proposed a method

of using the Gabor filter for target recognition of images based on the YUV color model. The two models used are the YUV color model fast and the Gabor filter model. Recognition accuracy [15]. Shen and Yan developed a classification-biased recognition method based on PCA and SIFT algorithms, which integrates traditional PCA and SIFT algorithms, thereby reducing the number of feature descriptors in the SIFT algorithm. And use the K-nearest neighbor classification algorithm for target feature matching, thereby improving the recognition accuracy, but the real-time performance needs to be improved [16]. Zhang et al. proposed an algorithm based on color lookup table and radial model matching, which is simple and fast and still has strong stability in complex environments [17].

The realization of target tracking includes many technologies, among which the most critical and core element is the target tracking algorithm. The algorithms that are often used at present are the frame difference method, mean shift algorithm, particle filter, multifeature fusion, etc. [18, 19]. These algorithms are mainly based on one of the basic algorithms such as detection, matching, filtering, etc., or the fusion of several different algorithms, so as to achieve the effect of complementary advantages [20].

Based on this, this paper first uses the omnidirectional vision image enhancement algorithm to identify the target and then designs the SVM-based adaptive target recognition algorithm to identify the actual target.

3. Research Methods

3.1. Homomorphic Filter Image Enhancement Algorithm Based on Mallat Wavelet Transform. Homomorphic filtering is generally performed in the frequency domain, so the omnidirectional image must first be converted from the spatial domain to the frequency domain, but the spatial resolution of the transformed image cannot reach the expected effect, because there is no local feature of the image optimization, which makes the image easily blurred, and the contrast improvement in the target area is not obvious [21]. Wavelet transform is a signal analysis theory based on Fourier transform, but Fourier transform does not have the ability of local analysis. Compared with the Fourier transform, the wavelet can analyze images from space and frequency. Local transformation can effectively extract local information. It solves the problem of local information extraction that is difficult to solve by Fourier transform. There are many kinds of wavelets. For the purpose of simplifying the algorithm, the Mallat wavelet is selected for wavelet table transformation, and it is applied to the homomorphic filtering algorithm [22, 23].

The specific implementation steps of the filtering enhancement algorithm based on the Marat wavelet transform are listed as follows:

- (1) Design the mask according to the characteristics of the omnidirectional image, and perform the bit AND operation on it with the initial image, so as to delete the noninformation area and reduce the size of the area that needs to be processed in the subsequent steps

- (2) Transform the trimmed image to the HSI color coordinate system, and list the luminance map I separately from it, let $I = f(x, y)$
- (3) Take the logarithm of the luminance function $f(x, y)$ to get $\ln f(x, y)$
- (4) Perform Marat frequency domain decomposition on $\ln f(x, y)$, the decomposition level is 3, and obtain the wavelet coefficients of the high-frequency part D_j^1 , D_j^2 , and D_j^3 ($j = 1, 2, 3$) and the low-frequency part A_3
- (5) Filter the frequency domain part after wavelet decomposition by using a filter
- (6) Reconstructing the filtered frequency domain components
- (7) Take the antilog of the restored image obtained after reconstruction, thereby generating an enhanced image $g(x, y)$

The flowchart of the homomorphic filtering image enhancement algorithm based on the Mallat wavelet is shown in Figure 2.

3.2. Adaptive Target Recognition Algorithm. In this paper, the orange football is selected as the recognition target of the football robot, and the color is used as the main target feature to recognize the ball [24]. The most traditional method is the threshold method. This method calibrates the limited colors in the field and establishes a look-up table. According to the table, the target of the specified color is identified. The main features are simple and short. The disadvantage is that the adaptability is poor, and the color drifts to a certain extent due to uneven lighting in the game. In this case, the stability of the traditional threshold method cannot be guaranteed. Although image enhancement can partially improve the color changes caused by factors such as lighting changes and textures, such changes still exist. The support vector machine (SVM) algorithm has strong adaptability and learning ability, so this algorithm is selected as the recognition model in this paper [25].

SVM, also called the support vector machine algorithm, is a classifier algorithm developed from the generalized portrait algorithm. SVM belongs to the category of supervised learning and is a generalized linear classifier for binary classification of data. The classifier calculates the empirical risk according to the loss function and applies regularization constraints to the classification model to optimize the structural risk. Compared with similar learning algorithms, this method requires a smaller sample size and higher learning efficiency. It is good at dealing with classifier problems and has been widely used in practice.

Since the IV color space is constructed for target recognition in this paper, the two feature quantities constitute a two-dimensional plane. Since the color composition in the scene is relatively simple, the samples in the two-

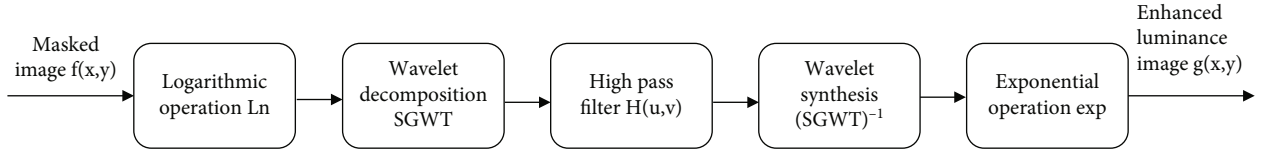


FIGURE 2: Flowchart of the homomorphic filtering image enhancement algorithm based on Mallat wavelet transform.

dimensional plane have a high probability of being linearly separable. Therefore, the classifier is mainly designed on the basis of linear separability, while the computational complexity is small when linearly inseparable. The specific algorithm is as follows:

(1) Suppose the known training set is as

$$T = \begin{bmatrix} I_1 & V_1 & y_1 \\ I_2 & V_2 & y_2 \\ \vdots & \vdots & \vdots \\ I_l & V_l & y_l \end{bmatrix}, \quad (1)$$

where $x_i = [I_i, V_i]$ is the training sample, that is, the pixel in the enhanced image, $y = [y_1, y_2, \dots, y_l]^T$ is the sample label, the positive sample is set to 1, and the negative sample is set to -1.

(2) The hyperplane equation is $(w * x) + b = 0$. In order for the classification surface to correctly classify all samples and have the largest classification interval, the minimum value of $1/2\|w\|^2$ must be obtained under the constraint of the condition $y_i[(w * x_i) + b] \geq 1 \{i = 1, 2, \dots, l\}$.

To this end, the following Lagrange function can be defined, where $a_i > 0$, as in

$$L(w, b, a) = \frac{1}{2}\|w\|^2 - \sum_{i=1}^l a_i y_i ((w * x_i) + b) + \sum_{i=1}^l a_i \quad a_i \geq 0, i = 1, \dots, n. \quad (2)$$

Taking w and b in the above formula as separate independent variables to obtain partial derivatives, and simplifying the obtained formula and making it equal to 0, formula (3) is obtained:

$$w = \sum_{i=1}^l a_i y_i x_i \quad \sum_{i=1}^l a_i y_i = 0. \quad (3)$$

Then, put formula (3) into formula (2), eliminate and simplify w and b to obtain the dual problem, and solve the

maximum value of the following formula as

$$\max Q(a) = \frac{1}{2} \sum_{i=1}^l \sum_{j=1}^l a_i a_j y_i y_j (x_i \cdot x_j) \quad (4)$$

$$\text{s.t. } \sum_{i=1}^l a_i y_i = 0, \quad a_i \geq 0, i = 1, \dots, n. \quad (5)$$

Get the optimal solution $a^* = [a_1^*, a_2^*, \dots, a_l^*]$.

(3) Substitute a^* into Equation (3) to get w^* to select a positive component a_i^* of a^* , and substitute into the following equation to obtain b^* as in

$$b^* = -\frac{1}{2} \left(\max_{ny_i=-1} (w^* \cdot x_i) + \min_{ny_i=1} (w^* \cdot x_i) \right). \quad (6)$$

(4) w^* and b^* are obtained in formulas (5) and (6), respectively, from which the classification hyperplane function $(w^* * x) + b^* = 0$ can be obtained, and thus, the decision function can be obtained as

$$f(x) = \text{sgn}((w^* \cdot x) + b^*) = \text{sgn} \left(\sum_{i=1}^l a_i^* y_i (x_i \cdot x) + b^* \right). \quad (7)$$

Among them, x_i is the support vector, and x is the sample to be classified.

(5) Target recognition

Step 1. Obtain the sample points to be tested in real time, that is, all the pixels on the scan line with the image center as the starting point and the site boundary as the end point, and take the pixels corresponding to the scan line as the samples to be classified.

Step 2. Use the sample points obtained in real time as the input of the trained SVM classifier to perform classification operations. Classify according to the output result of the decision function, that is, formula (7). When $f(x) = 1$, the pixel is classified as orange, and when $f(x) = -1$, the pixel is classified as nonorange. That is, the final target recognition result is the sample point of $f(x) = 1$. Figure 3 shows the flow chart of the target recognition algorithm in this paper.

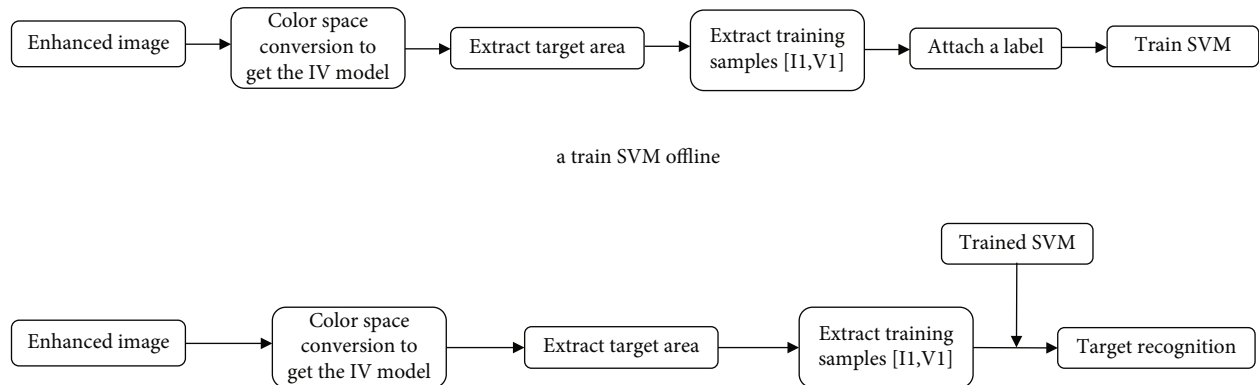


FIGURE 3: Flowchart of the adaptive target recognition algorithm.

4. Analysis of Results

4.1. Evaluation of Homomorphic Filter Image Enhancement Algorithm Based on Mallat Wavelet Transform

4.1.1. The Brightness Is Uniform.

$$\bar{L} = \frac{1}{M \times N} \sum_{x=1}^M \sum_{y=1}^N I(x, y). \quad (8)$$

Among them, M and N represent the size of the circle and direction, respectively.

4.1.2. Standard Deviation. The standard deviation is used to judge the contrast of the image. This metric is positively correlated with contrast.

$$S = \sqrt{\frac{1}{M \times N} \sum_{x=1}^M \sum_{y=1}^N (I(x, y) - \bar{L})^2}. \quad (9)$$

4.1.3. Entropy. Here, entropy is used to judge the richness of image details. The larger the value, the more details.

$$E = - \sum_{i=0}^{255} P_i \log P_i, \quad (10)$$

where P_i is the probability of the i th gray level.

4.1.4. Average Gradient. This indicator is used to evaluate local features such as contrast and texture. The larger the value, the higher the image definition.

$$G = \frac{1}{M \times N} \sum_{x=1}^M \sum_{y=1}^N \sqrt{\frac{((\partial I(x, y))/\partial x)^2 + ((\partial I(x, y))/\partial y)^2}{2}}. \quad (11)$$

By comparing the evaluation indicators in Tables 1 and 2, it can be seen that the fluctuation range of the four evaluation indicators after image enhancement is smaller than that of the original image under different illumination

conditions, indicating that the brightness of the image after enhancement processing is the distribution that is more uniform, and interference factors are eliminated for subsequent image recognition and tracking. When the illuminance is the same, the standard deviation and the mean brightness of the enhanced image are larger than the same index of the image without enhancement processing, reflecting the increase of contrast; moreover, the entropy and average gradient index of the enhanced image have a certain degree of increase. It reflects that the image contains more local features and more perfect details, which makes the image more recognizable.

4.2. Evaluation of Adaptive Object Recognition Algorithms. After adjusting the parameters of the football robot, start it, and adjust the brightness of the indoor fluorescent lamps and the degree of opening and closing of the curtains to change the illuminance. Then, turn on the camera and collect 100 omnidirectional pictures at various positions in the field, and take 30 of them as the test set and 70 as the sample set. Set the number of scan lines $N = 360$ and $M = 30$. First, the image is enhanced and preprocessed using the Marat-based homomorphic filtering algorithm mentioned above. Then, perform color model conversion on the obtained enhanced image to obtain an IV color model. In the offline state, the biSCAN scan line algorithm is used to extract the sample vector $[I_i, V_i]$ in the picture and input it into the SVM for training. When recognizing the target in a real-time state, the classification sample vector $[I_i, V_i]$ is extracted from the image by the biSCAN scan line method, and the trained SVM model is used to classify the sample, so as to obtain the recognition result of the target ball, as shown in Table 3.

By comparing the algorithm in this paper with the threshold method, the results in Figure 4 are obtained.

It can be seen from Figure 4 that the difference between the recognition rates of the two recognition algorithms is small under the condition of moderate illumination. When the illumination value is high or low, the recognition rate of the algorithm is much higher than that of the threshold method.

Overall, the target recognition algorithm proposed in this paper has a higher recognition rate than the threshold method. And it can maintain high stability under different conditions. The threshold method is less adaptable and only

TABLE 1: Evaluation indicators before image enhancement.

Illumination/ lux	Brightness mean	Standard deviation	Entropy	Average gradient
90	0.152	0.136	4.733	0.007
110	0.205	0.088	4.323	0.005
140	0.218	0.141	4.668	0.007

TABLE 2: Evaluation indicators after image enhancement.

Illumination/ lux	Brightness mean	Standard deviation	Entropy	Average gradient
90	0.423	0.147	4.958	0.015
110	0.457	0.118	4.749	0.014
140	0.470	0.151	4.938	0.015

TABLE 3: Target recognition rate based on biSCAN and SVM algorithms.

Illumination/lux	Recognition rate (%)
90	96.8
110	98.7
140	95.4

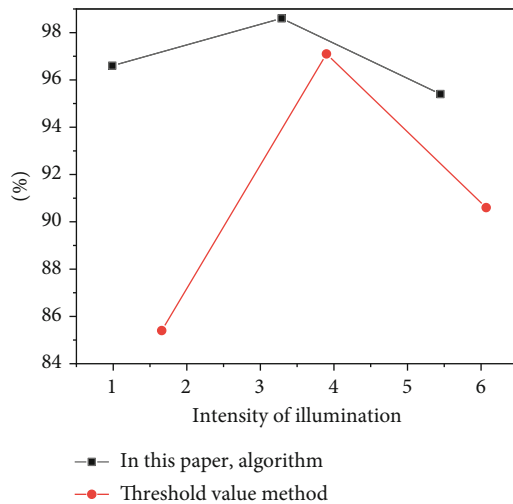


FIGURE 4: Comparison of the recognition rates of the two methods.

suitable for a specific situation. Therefore, the algorithm proposed in this paper is more adaptable and can meet the needs of target recognition.

5. Conclusion

Due to the particularity of imaging, the omnidirectional vision system has a large deformation of the obtained omnidirectional image, and these factors increase the difficulty of target recognition and tracking to a certain extent. However, most of the general target recognition and tracking algorithms are designed for images based on ordinary perspective imaging, so they can-

not be directly applied to omnidirectional vision systems. Moreover, in the soccer robot game scene, the color is highly coded and the target is often in a nonstationary state. Therefore, considering the characteristics of omnidirectional vision and the game environment, this paper studies the recognition and tracking of soccer balls in this application scene. The main research results of this paper are as follows:

- (1) A filtering algorithm based on Marat transform for image enhancement is proposed. This method combines the Mallat wavelet transform with the traditional homomorphic filtering to enhance the image. Then, use the Marat wavelet transform instead of the Fourier transform to transform it into the frequency domain and decompose it to obtain the wavelet coefficients of each high frequency and low frequency, and then, use the Butterworth type homomorphic filter function to filter each wavelet coefficient in the frequency domain. Then, the wavelet coefficients are reconstructed and inversely transformed to the spatial domain, and then, the transformed image is indexed to achieve the purpose of enhancement. According to the experimental results, it can be seen that the image enhancement method performs well in terms of robustness and adaptability and can meet the actual needs
- (2) The biSCAN algorithm and the SVM classifier are combined for target recognition. According to the intraclass scatter and interclass scatter matrix as the criterion, the traditional color space is improved, and an IV color model is designed for the football robot application scene. Based on this, the biSCAN scanning ray method is used to select the field. Then, the trained SVM model is used in an offline state to identify footballs under different light intensities and finally compared with the traditional threshold method. The experimental results show that the light adaptability and recognition rate of this method are greatly improved

Data Availability

The data used to support the findings of this study are available from the corresponding author upon request.

Conflicts of Interest

The authors declare that they have no conflicts of interest.

References

- [1] X. Liu, "RETRACTED: Research on decision-making strategy of soccer robot based on multi-agent reinforcement learning," *International Journal of Advanced Robotic Systems*, vol. 17, no. 3, p. 172988142091696, 2020.
- [2] R. Cao, L. Hao, Q. Gao, J. Deng, and J. Chen, "Modeling and decision-making methods for a class of cyber-physical systems based on modified hybrid stochastic timed petri net," *IEEE Systems Journal*, vol. 14, no. 4, pp. 4684–4693, 2020.

- [3] W. Shang, Z. Gao, D. Nicolo et al., "Benchmark analysis for robustness of multi-scale urban road networks under global disruptions," *IEEE Transactions on Intelligent Transportation Systems*, vol. 5, pp. 1–11, 2022.
- [4] H. Bi, W. Shang, K. Wang, and Y. Chen, "Joint optimization for pedestrian, information and energy flows in emergency response systems with energy harvesting and energy sharing," *IEEE Transactions on Intelligent Transportation Systems*, vol. 3, pp. 1–15, 2022.
- [5] L. Meng, Y. Li, and Q. L. Wang, "A calibration method for mobile omnidirectional vision based on structured light," *IEEE Sensors Journal*, vol. (99), pp. 1–1, 2020.
- [6] B. Tang and L. Jiang, "Binocular stereovision omnidirectional motion handling robot," *International Journal of Advanced Robotic Systems*, vol. 17, no. 3, p. 172988142092685, 2020.
- [7] J. Qiu, L. Du, D. Zhang, S. Su, and Z. Tian, "Nei-TTE: intelligent traffic time estimation based on fine-grained time derivation of road segments for smart city," *IEEE Transactions on Industrial Informatics*, vol. 16, no. 4, pp. 2659–2666, 2020.
- [8] J. Qiu, Y. Chai, Z. Tian, X. Du, and M. Guizani, "Automatic concept extraction based on semantic graphs from big data in smart city," *IEEE Transactions on Computational Social Systems*, vol. 7, no. 1, pp. 225–233, 2020.
- [9] K. S. Shruti and P. C. Deka, "Performance enhancement of svm model using discrete wavelet transform for daily stream-flow forecasting," *Environmental Earth Sciences*, vol. 80, no. 3, pp. 1–16, 2021.
- [10] F. Husari and J. Seshadrinath, "Incipient inter turn fault detection and severity evaluation in electric drive system using hybrid hcnn-svm based model," *IEEE Transactions on Industrial Informatics*, vol. (99), pp. 1–1, 2021.
- [11] Z. Cai and X. Zheng, "A private and efficient mechanism for data uploading in smart cyber-physical systems," *IEEE Transactions on Network Science and Engineering (TNSE)*, vol. 7, no. 2, pp. 766–775, 2020.
- [12] S. Xie, Z. Yu, and Z. Lv, "Multi-disease prediction based on deep learning: a survey," *Computer Modeling in Engineering & Sciences*, vol. 127, no. 3, 2021.
- [13] H. K. Wu, S. E. Chen, J. J. Liu, Y. Y. Ou, and M. T. Sun, "A self-relevant cnn-svm model for problem classification in k-12 question-driven Learning," *Access*, vol. 8, pp. 225822–225830, 2020.
- [14] J. Zeng, G. Z. Cao, Y. P. Peng, and S. D. Huang, "A weld joint type identification method for visual sensor based on image features and svm," *Sensors*, vol. 20, no. 2, p. 471, 2020.
- [15] J. Li, W. Wang, and Z. Han, "A variable weight combination model for prediction on landslide displacement using ar model, lstm model, and svm model: a case study of the Xinming landslide in China," *Environmental Earth Sciences*, vol. 80, no. 10, pp. 1–14, 2021.
- [16] F. Shen and R. Yan, "A new intermediate domain svm-based transfer model for rolling bearing rul prediction," *IEEE/ASME Transactions on Mechatronics*, vol. (99), pp. 1–1, 2021.
- [17] C. Zhang, S. Yuan, M. Shi, J. Yang, and H. Miao, "Fault location method based on svm and similarity model matching," *Mathematical Problems in Engineering*, vol. 2020, Article ID 2898479, 9 pages, 2020.
- [18] N. Borthakur and A. K. Dey, "Evaluation of group capacity of micropile in soft clayey soil from experimental analysis using svm-based prediction model," *International Journal of Geomechanics*, vol. 20, no. 3, pp. 04020008.1–04020008. 17, 2020.
- [19] Y. Cao, C. Zhou, and B. Ahmed, "Establishment of landslide groundwater level prediction model based on ga-svm and influencing factor analysis," *Sensors*, vol. 20, no. 3, p. 845, 2020.
- [20] C. Yan, L. Wang, W. Liu, J. Liu, and J. Liu, "Research on the ubi car insurance rate determination model based on the cnhsvm algorithm," *Access*, vol. 8, pp. 160762–160773, 2020.
- [21] Z. Lv, W. Kong, X. Zhang, D. Jiang, H. Lv, and X. Lu, "Intelligent security planning for regional distributed energy internet," *IEEE Transactions on Industrial Informatics*, vol. 16, no. 5, pp. 3540–3547, 2020.
- [22] Z. Lv, L. Qiao, J. Li, and H. Song, "Deep-learning-enabled security issues in the internet of things," *IEEE Internet of Things Journal*, vol. 8, no. 12, pp. 9531–9538, 2021.
- [23] R. Huang, S. Zhang, W. Zhang, and X. Yang, "Progress of zinc oxide-based nanocomposites in the textile industry," *IET Collaborative Intelligent Manufacturing*, vol. 3, no. 3, pp. 281–289, 2021.
- [24] X. Cheng, B. Yang, A. Hedman, T. Olofsson, H. Li, and L. Van Gool, "NIDL: a pilot study of contactless measurement of skin temperature for intelligent building," *Energy and Buildings*, vol. 198, pp. 340–352, 2019.
- [25] S. Yang, B. Deng, J. Wang et al., "Scalable digital neuromorphic architecture for large-scale biophysically meaningful neural network with multi-compartment neurons," *IEEE Transactions on Neural Networks and Learning Systems*, vol. 31, no. 1, pp. 148–162, 2020.

Retraction

Retracted: Data Encryption Technology Analysis of Robot Computer Network Information

Journal of Sensors

Received 13 September 2023; Accepted 13 September 2023; Published 14 September 2023

Copyright © 2023 Journal of Sensors. This is an open access article distributed under the Creative Commons Attribution License, which permits unrestricted use, distribution, and reproduction in any medium, provided the original work is properly cited.

This article has been retracted by Hindawi following an investigation undertaken by the publisher [1]. This investigation has uncovered evidence of one or more of the following indicators of systematic manipulation of the publication process:

- (1) Discrepancies in scope
- (2) Discrepancies in the description of the research reported
- (3) Discrepancies between the availability of data and the research described
- (4) Inappropriate citations
- (5) Incoherent, meaningless and/or irrelevant content included in the article
- (6) Peer-review manipulation

The presence of these indicators undermines our confidence in the integrity of the article's content and we cannot, therefore, vouch for its reliability. Please note that this notice is intended solely to alert readers that the content of this article is unreliable. We have not investigated whether authors were aware of or involved in the systematic manipulation of the publication process.

Wiley and Hindawi regrets that the usual quality checks did not identify these issues before publication and have since put additional measures in place to safeguard research integrity.

We wish to credit our own Research Integrity and Research Publishing teams and anonymous and named external researchers and research integrity experts for contributing to this investigation.

The corresponding author, as the representative of all authors, has been given the opportunity to register their agreement or disagreement to this retraction. We have kept a record of any response received.

References

- [1] Q. Shi and Y. Liu, "Data Encryption Technology Analysis of Robot Computer Network Information," *Journal of Sensors*, vol. 2022, Article ID 5127989, 7 pages, 2022.

Research Article

Data Encryption Technology Analysis of Robot Computer Network Information

Qiaolian Shi  and Yan Liu 

Xinxiang Medical University, Xinxiang, Henan 453003, China

Correspondence should be addressed to Qiaolian Shi; 201804331@stu.ncwu.edu.cn

Received 4 June 2022; Revised 28 June 2022; Accepted 6 July 2022; Published 15 July 2022

Academic Editor: Haibin Lv

Copyright © 2022 Qiaolian Shi and Yan Liu. This is an open access article distributed under the Creative Commons Attribution License, which permits unrestricted use, distribution, and reproduction in any medium, provided the original work is properly cited.

In order to ensure the security of robot computer network information, a data encryption technology is proposed. Through the comprehensive research of symmetric cryptography algorithm, open cryptography algorithm, hybrid encryption algorithm, AES algorithm, quantum cryptography technology, and ECC algorithm, a data encryption method suitable for robot computer network information is proposed. It is found that when analyzing the entanglement characteristics of the four-particle cluster state, the anomaly will inevitably disturb its state. In the eavesdropping detection, the communication parties can cooperate to detect the existence of abnormal conditions. In addition, in the formal communication stage, trial photons are introduced, whose confidentiality characteristics are guaranteed by the principle of quantum noncloning and the uncertainty principle. Therefore, this technology further ensures the confidentiality of communication.

1. Introduction

Today, with the widespread use of computer networks, more and more people are connected to this technology. The use of computers has been constantly improving and improving in all walks of life. With the advent of big data and cloud computing, data is emerging quickly and slowly in all areas of human life. However, with the widespread use of computers, information is still lost [1]. Therefore, the problem of computer network information security has become an urgent problem for relevant people to solve, and data encryption technology can prevent information leakage to a great extent (Figure 1). As a new network information protection measure, this technology has been recognized and accepted by more and more people in the shortest time after its emergence [2].

At present, all enterprises need to use computers to exchange information. In the process of using computers, data encryption technology plays an important role, which is related to the security of computer use. The continuous development of social economy has also expanded the application rate of electronic information technology and increased the challenges of technology application [3]. Because computer

networks are open and can share information with everyone, it is easy to divulge personal information and lose business. As science and technology continue to advance, people are increasingly using computer information, and people are paying more attention to the security of computer information. In terms of computer network information security, we need to use data encryption technology to create a secure network for people.

The use of information technology in various fields in China has led to the frequency of network exchange. In addition, China continues to improve the openness of the network, which further increases people's access to information, so it increases the risk of network information data. At present, people attach great importance to the security of network environment, so as to highlight the importance of data encryption technology. Through the analysis of this paper, this paper puts forward corresponding measures for the network security of robot computer [4].

2. Literature Review

The idea of publishing the key was first published in "New Cryptographic Concepts," which laid a solid foundation for



FIGURE 1: Data encryption technique.

the development of public cryptosystem information [5]. Several important public cryptosystems were then requested one by one. Several important public cryptosystems were then requested one by one, for example, the famous RSA public key cryptosystem, knapsack cryptosystem, Rabin cryptosystem, ElGamal cryptosystem, elliptic curve cryptosystem and so on. An oval curve cryptosystem (ECC) based on the theory of the oval curve can solve the problem of a very large key, and it is the same. Security level is according to RSA and ElGamal. The DCF mechanism in the MAC layer of the IEEE802.11 protocol has been studied, researched, and developed [6]. The improvements improve the use of the channel and make it more robust in two stages of “virtual racing.” The simplicity and exclusion of IEEE802.11 validation protocol service support have been well studied. Based on the 802.1x protocol framework and the EAP protocol, we offer a concept to improve password-based authentication. For some people, the input can meet the security requirements of WLAN authentication and improve 802.11i authentication. To improve the security of the IEEE802.1x protocol, the concept can improve process security by preventing the authentication of the IEEE802.1x protocol by authenticating the authentication mark. It also sets out the principles that easily oppose the 802.1x protocol—incompatibility, incompleteness, integrity, and precision protection of the latest systems true. An improved version of bilateral cooperation and offline evaluation was planned and implemented [7].

However, the security performance of a WLAN is not as stable as that of a wired network. Currently, the most widely used WLAN is the 802.11 series. Although 802.1x has some disadvantages of the 802.11 standard, it still has some disadvantages. The protocol explains why there are no authentication methods between the user and the authenticator and prevents the authentication message from being encrypted. Illegal users can use these issues to detect various attacks [8]. There are three main types of attacks: one is a false witness attack, the other is a conversation-stolen attack, and the third is a denial of service termination. To some extent, these security vulnerabilities have led to the development of wireless network-based robotic remote control technology. Improving the security of wireless network-based robot remote control technology will not only make WLAN more important for robot development, research, and application but also make wireless remote control technology safer and easier to use. This is essential for the development and improvement of robotic remote control technology, the

promotion and popularization of robots in various fields, and the robotics industry in China, especially the robotics industry. Therefore, how to ensure the security of data transmission during robotic wireless remote control is an important prerequisite to support the continuous expansion of robotic information. But so far, people have not seen the security of robotic remote control systems in wireless networks. Currently, the issues of wiretapping, forgery, and unauthorized surveillance are not given enough attention, like a remote-controlled bomb, and the remote control is in the hands of unauthorized people.

This paper mainly studies the security authentication access problem based on wireless network, that is, taking the wireless LAN security technology as the core, the improvement of IEEE802.1x/EAP-TLS protocol, and the research and application of quantum technology through symmetric cryptographic algorithm, public cryptographic algorithm, hybrid encryption algorithm, AES algorithm, quantum cryptographic technology, and ECC algorithm to improve the security performance of robot computer network [9].

3. Research Methods

3.1. Symmetric Cryptographic Algorithm. Symmetric encryption uses the same keys to encrypt and decrypt data. The algorithms used for symmetric encryption are simpler than for asymmetric encryption. Because these algorithms are simpler and use the same key to encrypt and decrypt data, symmetric encryption is faster than asymmetric encryption. Therefore, symmetric encryption is suitable for encrypting and decrypting large amounts of data. Figures 2 and 3 show the symmetric encryption process [10].

One disadvantage of multiple encryption is that it can encrypt and decrypt data using a single key. Therefore, all senders and recipients must know or have access to the encryption key. This requires organizations to consider the importance of environmental safety management and governance. The reason for the security management problem is that the organization must send this encryption key to any party that needs access to the encrypted data. Key management issues that an organization should consider include key indicators, allocation, resources, recovery, and life cycle. Symmetric encryption allows encrypted data [11]. For example, using symmetric encryption, you can be sure that only two parties with access to an organization’s shared

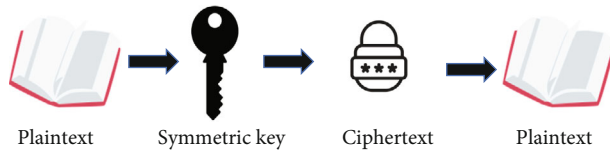


FIGURE 2: Symmetric encryption flow chart 1.

encryption key can decrypt the encrypted text. However, symmetric encryption does not provide authentication. For example, when many users access a shared encryption key, symmetric encryption cannot identify the sender of the file.

3.2. Public Cipher Algorithm. Traditional symmetric encryption algorithms face key management problems. If the key is lost during distribution and transmission, the entire security system will be damaged. Asymmetric encryption algorithms effectively avoid problems with partitions and control keys. Pair combinations of public and private keys are used in asymmetric cryptography [12]. Encrypted text encrypted with a public key can only be decrypted with a private key. Conversely, encrypted text encrypted with a private key can only be decrypted with a public key. As we work, we place the public key to the outside world to let outsiders know. We keep the key secret and only we can know. If you want to send a password, all you have to do is take the public key and then encrypt the password with the public key. This encrypted message can only be decrypted with a private key. Instead, you can use a public key to keep your information private. The file was sent by a third party, but could not be decrypted.

Encryption with public key is shown in

$$E_k(M) = C. \quad (1)$$

Although the public key and private key are different, decryption with the corresponding private key can be expressed as shown in

$$D_k(C) = M. \quad (2)$$

Sometimes, messages are encrypted with a private key and decrypted with a public key used for digital signing. Although confusion can occur, these actions can be expressed in equations (1) and (2), respectively.

Currently, public key cryptographic algorithms are based on complex mathematical problems. For example, the widely used RSA algorithm is based on the popular mathematical problem of large integers. The advantage of a public key cryptosystem is that it can meet network openness requirements, and the management key is simple and knows the function of digital signature and ID verification. It is the mainstay of today's e-commerce and other technologies [13]. The disadvantage is that the algorithm is complex and the speed and efficiency of data encryption is low. Therefore, in practice, symmetric encryption algorithms and asymmetric encryption algorithms are often used together. Symmetric encryption algorithms are used to encrypt large data files, while

symmetric encryption algorithms are used to replace the key used by the symmetric encryption algorithm. This method can increase the efficiency of encryption and simplify key management [14].

3.3. Hybrid Encryption Algorithm. Hybrid encryption is an encryption method that performs data encryption with a combination of symmetric and asymmetric encryption. The hybrid encryption method takes advantage of these two encryption methods to allow only the desired recipient to read the data [15].

In the concept of hybrid encryption, an organization provides symmetric encryption with a randomly generated key to encrypt the data. These steps take advantage of symmetric encryption speeds. The organization then encrypts the symmetric encryption key using the public key of the asymmetric key pair. These steps take advantage of the high security of asymmetric encryption. Encrypted data is sent to the recipient's data with an encrypted symmetry key [16].

To decrypt the data, the receiver first needs to decrypt the symmetric encryption key using the private key of the asymmetric key pair. The receiver then decrypts the data using the decrypted symmetric key.

3.4. AES Algorithm. The AES algorithm is an important symmetric teratonic block cipher algorithm. Its package length and key length are different. They can be listed as 128 items, 192 items, or 256 items. It contains plain text data files in the form of a two-dimensional byte array, called a state array. The array consists of 4 lines and Nb lines (Nb is equal to the length of the set divided by 32). Any changes to the AES algorithm are made on this state matrix. As an example, take AES-128 (key length 128 bits) and display the plain text input groups $a_0, a_1, a_2 \dots a_{15}$ in a state matrix between 4 lines and 4 lines. Many iterations are performed on this state matrix to achieve the goal of free data confusion, expansion, and data encryption. Each circular variable is called an environment and has a total $Nr + 1$ environment [17].

From the above four transformations, it can be seen that the decryption of AES algorithm process only converts the transformation of each round of function into the corresponding inverse transformation and transforms the state matrix obtained from ciphertext mapping in the opposite order.

3.5. Quantum Cryptography. Traditional cryptography is based on the difficulty of mathematical calculation, while quantum cryptography is based on quantum mechanics. In fact, quantum cryptography is an absolutely secure cryptosystem based on quantum properties. This is because if eavesdroppers want to steal communication information, they must measure the quantum system, which disrupts the balance of quantum channels and causes both sides of communication to give up communication [18].

December 21, 2011, was a painful day on the milestone of China's Internet. According to statistics, in less than ten days, major websites (or forums), including CSDN, Tianya,

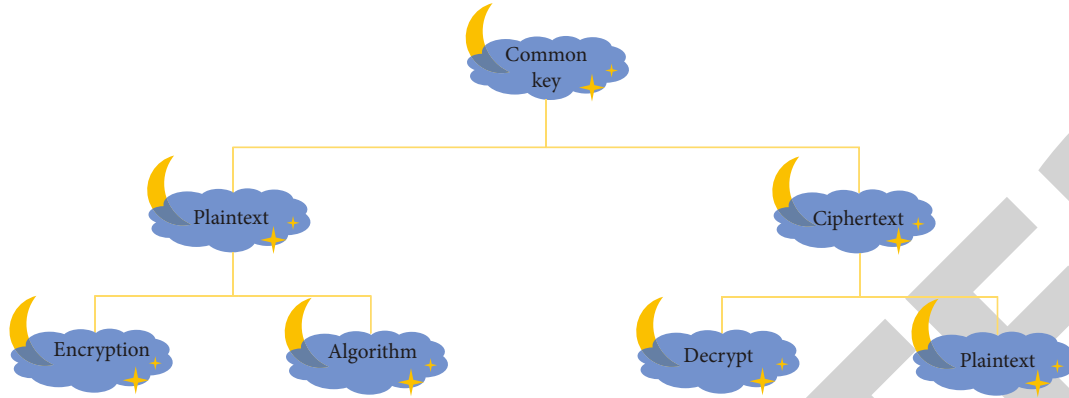


FIGURE 3: Symmetric encryption flow chart 2.

Renren, Netease, and Saipan, successively leaked important privacy information such as user account, password, and email. With the increasing number of Internet users, more and more people will suffer from the experience of password theft and website hacking.

The emergence of quantum cryptography will make this encounter disappear. The security of quantum cryptography depends on the physical laws based on quantum mechanics. Heisenberg uncertainty principle means that if a quantum state is measured, it will cause some interference to the original quantum state, and the measured quantum state will be different from the original state. Similarly, if a quantum system is measured, the measurement results obtained cannot include the complete information of the original system [19]. According to the uncertainty principle, both sides of communication can detect the existence of eavesdroppers at the first time. Because the eavesdropper cannot guarantee that the original state will not be disturbed when measuring the quantum state on the quantum channel, and once disturbed, the measurement results of both sides of the communication will change, and then, it is found that there is an eavesdropper. At present, the security of quantum state uncertainty principle has been proved, so even computers with supercomputing power are useless.

Data encryption/decryption technology is the basic premise and guarantee of information security. In recent years, quantum key distribution protocol has not only been improved and verified in theory but also made rapid progress in experiment. Although the classical information security technology is progressing day by day, the quantum information security technology has not stagnated. So far, researchers have made good achievements in the theoretical research and experimental research of quantum cryptography [20].

3.6. ECC Algorithm

3.6.1. Operation of Elliptic Curve

(1) *Definition of Point Addition Operation.* The point addition operation is defined as follows: let P and Q be any two points and l be the PQ connection. If P and Q coincide at

one point, that is, $P = Q$, then l degenerates to the tangent point of P . Let L and curve intersect at another point R , and W is the connecting line between R point and infinity point O ; that is, W is the parallel line of y axis through point R , and W and curve intersect at one point m , which is expressed as $M = P + Q$, that is, the result of point P and Q addition operation. The point addition operation of different points and the same points is shown in Figures 4 and 5.

In particular, if P and Q are symmetrical or coincident about the x axis, then the straight line PQ is perpendicular to the x axis, and L and the elliptic curve intersect at infinity O .

(2) *Group Operation Rules.* The points on the elliptic curve form an Abelian group under the defined addition operation. Let it be an elliptic curve given by the Weierstrass equation; then, under the addition rule of the addition of two points P and Q on E , for all $P, Q \in e$, there is

- (1) $O + P = P$, and $P + O = P$, then O is the infinity point
- (2) $-O = O$
- (3) $P + Q = Q + P$
- (4) $P(X, Y)$ then $-P = (X, -Y)$
- (5) if the coordinates of P and Q are the same (their Y coordinates are opposite), then $P + Q = O$

(3) *Point Addition on Elliptic Curve.* The following gives the different forms of the point addition operation of the elliptic curve in the form of equation (3) in affine coordinates and shadow coordinates.

$$E : Y^2 = X^3 + aX^2 + b. \quad (3)$$

- (1) Point addition in affine coordinates
 - (a) Point addition operation of different points

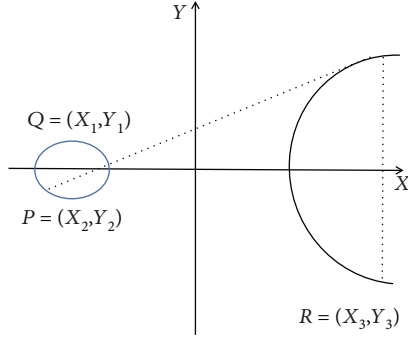


FIGURE 4: Generalized addition of points.

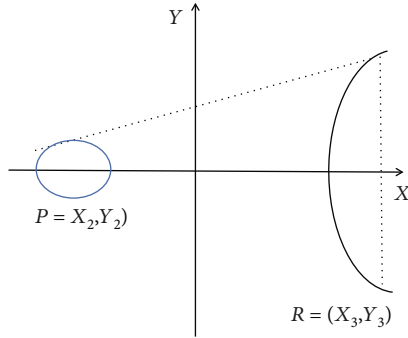


FIGURE 5: Point multiplication.

Set $P = (X_1, Y_1)$, $Q = (X_2, Y_2)$, $P \neq Q$, $P + Q = (X_3, Y_3)$; they are all points on an elliptic curve; the point plus formula is

$$\begin{aligned} X_3 &= \lambda^2 - X_1 - X_2, \\ Y_3 &= \lambda(X_1 - X_3) - Y_1, \end{aligned} \quad (4)$$

where $\lambda = (Y_1 - Y_2)/(X_1 - X_2)$.

(b) Point addition operation of the same point

Set $P = (X_1, Y_1)$, $P + P = 2P = (X_3, Y_3)$; they are all points on an elliptic curve; the formula of point addition is

$$\begin{aligned} X_3 &= \lambda^2 - 2X_1, \\ Y_3 &= \lambda(X_1 - X_3) - Y_1, \end{aligned} \quad (5)$$

where $\lambda = (3X_1^2 + a)/2Y_1$.

(2) Point addition operation in projective coordinates

The point addition operation in projective coordinates is also divided into (a) point addition operation at different points and (b) point addition operation at the same point.

(4) *Definition of Point Multiplication.* Point multiplication on elliptic curve is one of the core operations of elliptic curve cryptosystem. The point multiplication operation on an

elliptic curve is defined as follows: given an elliptic curve E and a point P on the curve, the point multiplication xP of point P on curve e is defined as the sum of the addition of point P and x itself, that is, $xP = p + p + \dots + p$, a total of xP are added. Point multiplication operation (including double point and point addition operation) is one of the most time-consuming arithmetic operations in elliptic curve cryptosystem.

4. Result Analysis

The security of the scheme in this paper is based on the safe transmission of P_A , P_B sequence and M_A , M_C sequence, so ensuring the safe transmission of message sequence can ensure the security of the scheme. Referring to the eavesdropping detection method in B92 protocol, Alice and Bob both use X-based or Z-based measurement to detect whether there are eavesdroppers, because B92 protocol is absolutely safe. Before the coding communication phase of the scheme in this paper starts, the message transmission method of B92 protocol is followed, and then Bob notifies Alice to code. Therefore, the security performance of this scheme is the same as that of B92 scheme [21]. If the eavesdropper Eve does not launch any eavesdropping behavior, he can only passively eavesdrop the amount of information he can obtain. After the eavesdropping detection of Alice and Bob, Alice performs $\sigma_0 = I$ or $\sigma_1 = \sigma_2$ transformation, respectively, according to the bit 0 or 1 of the transmitted message. For the convenience of analysis, here we assume that the probability of Alice sending secret message 0 or 1 is equal, both of which are 1/2. Since the encoding and decoding part of the communication process does not require the participation of classical messages, the eavesdropper Eve will not obtain relevant classical messages [22, 23]. It can be seen that Eve can only blindly guess the secret message sent by Alice. Obviously, the probability of his guess is 1/2. At this time, we calculate the mutual information of Alice and Eve, and we can get

$$I(A, E) = H(A) - H(A|E) = 1 - \frac{1}{2}H\left(\frac{1}{2}\right) - \frac{1}{2}H\left(\frac{1}{2}\right) = 0, \quad (6)$$

where H is entropy.

$$H(p) = -p \log_2 p - (1-p) \log_2 (1-p). \quad (7)$$

According to the famous Krull-Remak-Schmidt-Azumaya decomposition theorem, when Alice and Bob choose Z-basis for measurement, the error rate is 2FD. Similarly, when X-based measurement is selected, the error rate is 2FD.

To sum up, Eve will inevitably interfere with the entanglement characteristics of four particle cluster states when Alice and Bob analyze their entanglement characteristics [24, 25]. In eavesdropping detection, $2FD > 0$, as shown in Figure 6, the existence of Eve can be detected by the cooperation of both communication parties. In addition, in the formal communication stage, exploratory photons are

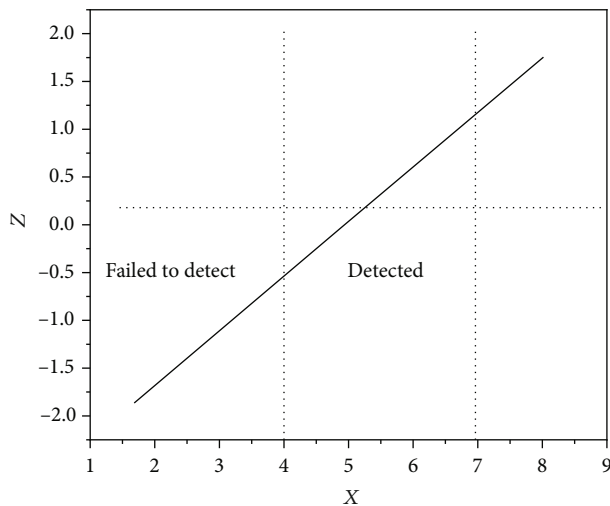


FIGURE 6: FD diagram of $Z-/X$ -base measurement error rate.

introduced, and their security characteristics are guaranteed by the quantum non cloning principle and uncertainty principle. Therefore, the existence of Eve eavesdropping will also be found, which further ensures the confidentiality of communication.

5. Conclusion

Through the above analysis of the security performance of the scheme, under the ideal channel, the scheme is secure against incoherent attacks, and the efficiency of quantum communication has been improved. Before officially entering the coded communication, exploratory photons are specially introduced to mainly detect the security of quantum communication channel, which improves the security defense ability of robot computer network communication protocol. The main conclusions of this paper are as follows:

- (1) The application of cryptography in network information security is deeply studied
- (2) It is concluded that secret information can be transmitted directly without transmitting password
- (3) It is concluded that using cluster state as information carrier, the entanglement degree is the largest, the correlation degree is the highest, and the communication efficiency is high

At present, the IEEE 802.11 family is very large, and the updating and improvement of its family protocol is also ongoing. In addition, many researchers outside IEEE organizations continue to study and improve the 802.11 protocol family. China has also put forward the WAPI Standard, but as long as it is announced, someone will find out the defects soon. Although this paper improves the IEEE802.1x/EAP-TLS authentication protocol, it still cannot completely solve the original security defects. Therefore, if we want to fundamentally solve the problem of information security, we must find an absolutely safe way. At present, quantum technology

has been proved to be unconditionally safe. If quantum technology can be as developed and mature as computer technology, our information will not be stolen by others.

Data Availability

The data used to support the findings of this study are available from the corresponding author upon request.

Conflicts of Interest

The authors declare that they have no conflicts of interest.

Acknowledgments

(1) This work was supported by the education and teaching research project of Xinxiang Medical University (Project No. 2019-XYJG-35). (2) This work was supported by the Henan Provincial Department of Education, Excellent grass-roots teaching organization construction project 2021. (3) This work was supported by the 2021 Higher Education Teaching Reform Research and Practice Project of Henan Province, Research on the construction of professional ideological and political three-dimensional model under CDIO engineering education mode, Project No. 2021SJGLX211.

References

- [1] N. Imansyah and W. Sri Handani, "The implementation of augmented reality-based learning in computer network system courses," *CCIT Journal*, vol. 14, no. 1, pp. 13–20, 2021.
- [2] R. Sendhil and A. Amuthan, "Contextual fully homomorphic encryption schemes-based privacy preserving framework for securing fog-assisted healthcare data exchanging applications," *International Journal of Information Technology*, vol. 13, no. 4, pp. 1545–1553, 2021.
- [3] Q. Cheng, J. Pang, D. Sun et al., "WSe22D p-type semiconductor-based electronic devices for information technology: Design, preparation, and applications," *Preparation and Applications*, vol. 2, no. 4, pp. 656–697, 2020.
- [4] Z. Lv, B. Hu, and H. Lv, "Infrastructure monitoring and operation for smart cities based on IoT system," *IEEE Transactions on Industrial Informatics*, vol. 16, no. 3, pp. 1957–1962, 2020.
- [5] Z. Lv and L. Qiao, "Deep belief network and linear perceptron based cognitive computing for collaborative robots," *Applied Soft Computing*, vol. 92, article 106300, 2020.
- [6] B. Yang, X. Li, Y. Hou et al., "Non-invasive (non-contact) measurements of human thermal physiology signals and thermal comfort/discomfort poses-a review," *Energy and Buildings*, vol. 224, article 110261, 2020.
- [7] X. Cheng, B. Yang, A. Hedman, T. Olofsson, H. Li, and L. Van Gool, "NIDL: a pilot study of contactless measurement of skin temperature for intelligent building," *Energy and Buildings*, vol. 198, pp. 340–352, 2019.
- [8] W. Shang, Z. Gao, D. Nicolo et al., "Benchmark analysis for robustness of multi-scale urban road networks under global disruptions," *IEEE Transactions on Intelligent Transportation Systems*, vol. 5, pp. 1–11, 2022.
- [9] H. Bi, W. Shang, K. Wang, and Y. Chen, "Joint optimisation for pedestrian, information and energy flows in emergency

Retraction

Retracted: Robot Target Localization and Visual Navigation Based on Neural Network

Journal of Sensors

Received 10 October 2023; Accepted 10 October 2023; Published 11 October 2023

Copyright © 2023 Journal of Sensors. This is an open access article distributed under the Creative Commons Attribution License, which permits unrestricted use, distribution, and reproduction in any medium, provided the original work is properly cited.

This article has been retracted by Hindawi following an investigation undertaken by the publisher [1]. This investigation has uncovered evidence of one or more of the following indicators of systematic manipulation of the publication process:

- (1) Discrepancies in scope
- (2) Discrepancies in the description of the research reported
- (3) Discrepancies between the availability of data and the research described
- (4) Inappropriate citations
- (5) Incoherent, meaningless and/or irrelevant content included in the article
- (6) Peer-review manipulation

The presence of these indicators undermines our confidence in the integrity of the article's content and we cannot, therefore, vouch for its reliability. Please note that this notice is intended solely to alert readers that the content of this article is unreliable. We have not investigated whether authors were aware of or involved in the systematic manipulation of the publication process.

Wiley and Hindawi regrets that the usual quality checks did not identify these issues before publication and have since put additional measures in place to safeguard research integrity.

We wish to credit our own Research Integrity and Research Publishing teams and anonymous and named external researchers and research integrity experts for contributing to this investigation.

The corresponding author, as the representative of all authors, has been given the opportunity to register their agreement or disagreement to this retraction. We have kept a record of any response received.

References

- [1] H. Guo, Y. Wang, G. Yu, X. Li, B. Yu, and W. Li, "Robot Target Localization and Visual Navigation Based on Neural Network," *Journal of Sensors*, vol. 2022, Article ID 6761879, 8 pages, 2022.

Research Article

Robot Target Localization and Visual Navigation Based on Neural Network

Haifeng Guo , Yiyang Wang , Guijun Yu , Xiang Li , Baoqi Yu , and Wenyi Li 

College of Electrical and Information Engineering, Liaoning Institute of Science and Technology, Benxi, Liaoning 117004, China

Correspondence should be addressed to Haifeng Guo; 2013071431@stu.zjhu.edu.cn

Received 29 May 2022; Revised 25 June 2022; Accepted 5 July 2022; Published 14 July 2022

Academic Editor: Haibin Lv

Copyright © 2022 Haifeng Guo et al. This is an open access article distributed under the Creative Commons Attribution License, which permits unrestricted use, distribution, and reproduction in any medium, provided the original work is properly cited.

Deep neural network has been widely used in image analysis, speech recognition, target detection, semantic segmentation, face recognition, automatic driving, and other fields due to its excellent algorithm performance. In this research, the neural network is mainly used to simulate robot target localization and visual navigation. Firstly, the data set based on ICP algorithm is constructed, and then, the navigation and positioning of robot are simulated by using neural network. The results show that the combination of ICP algorithm and direct method can effectively solve the problem of pose loss and expand the indoor range of data collection. The method using artificial neural network is effective and has better robustness and stability than the method based on frame matching. From the perspective of vision, positioning and navigation based on a single RGB image are feasible, and the processing time is relatively short, which can meet the requirements of real time and has higher practical value in general indoor scenes.

1. Introduction

In recent years, due to the efficiency of algorithms, deep neural networks have been widely used in image analysis, speech recognition, research purposes, semantic division, facial recognition, automatic navigation, etc. The reason why the deep neural network has become so successful is because its content is to simulate the training of the human brain. By increasing the number of layers, the machine can learn higher functions from the data. Currently, the depth of the network is hundreds or thousands of layers, and the design of network connections makes it difficult to implement in a timely manner. The development of deep neural network algorithms based on multiple capabilities in computer applications to reduce neural network training time has gradually become a hotspot in research [1].

The network architecture (redistribution algorithm) of BP neural network structure is multilayered, which is usually a way of optimizing the localization of gradient viruses and interfering with the treatment of latent errors in the network is heavy. The multilayered structure of the BP neural network leads to higher output standards, but the BP neural

network still has some shortcomings [2]. For nonspecific problems such as XOR, BP neural network may have the lowest local cost, which makes it difficult to find a solution globally, and MSE is too large for large data cooperation. The AdaBoost algorithm trained and calculated the error rate and weight of the first BP model and took the weight as the weight parameter of the next BP network and then carried out iterative calculation, in which a single hidden layer of the traditional BP network adopts a two-layer structure. When this method is applied to short-term sales forecast, the average prediction error is 18%. Compared with the 53.23% accuracy of the traditional BP network, the accuracy rate is significantly improved. However, this model has a large error in the case of a large time span of sample data and can effectively predict recent sales changes only with 5 days of sample data [3]. See Figure 1.

With the development of robot technology, the application fields of robots are also expanding, driving the transformation of all industries to intelligent technology for mobile intelligent robots; autonomous positioning and navigation is one of the keys to achieve intelligent. Without autonomous positioning and navigation, the robot

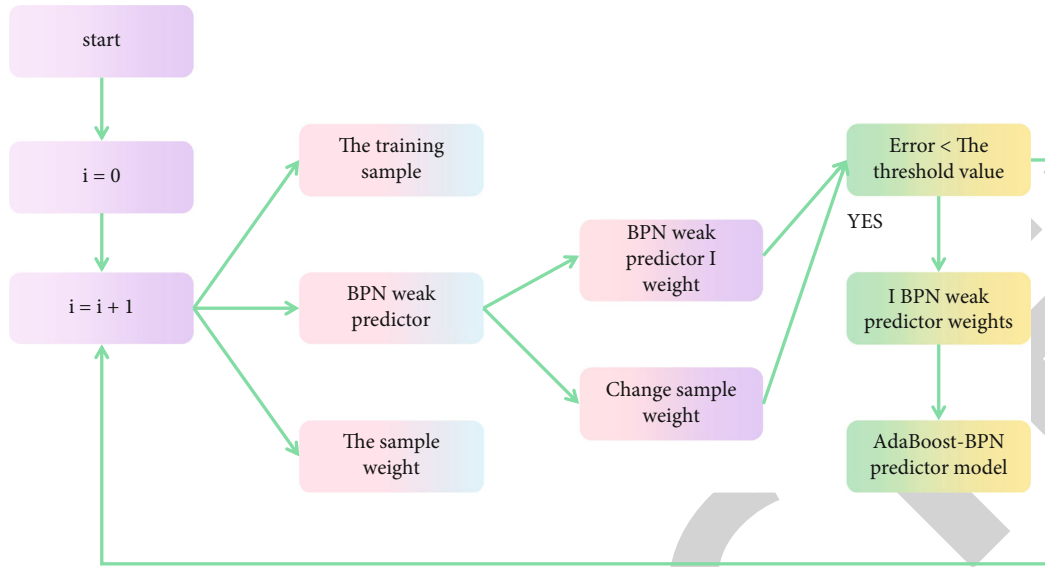


FIGURE 1: Flowchart of BP neural network model.

cannot perceive the surrounding environment and understand and analyze the scene information and move safely, and any interactive behavior based on this cannot be mentioned. Therefore, the realization of autonomous positioning and navigation of the robot is the core technology to achieve intelligence [4].

The development of computer vision technology has brought a new opportunity for the research of autonomous robot positioning and navigation technology, namely, visual positioning and navigation technology. Humans can quickly and accurately capture and integrate a large amount of element information in the target scene by using their eyes, which is a developed visual system. However, for robots, the target scene is rich in information due to the complexity of visual problems. Due to the complexity of computation, the present robot vision system is still difficult to achieve the cognitive recognition ability of human eyes [5, 6]. For a robot to the development of the intelligent visual perception system is an important part of the robot, which is one of the main sources of robot perception surrounding environment, whether the rapid and effective use of visual information will directly affect the interaction of the robot, in the environment of the variability, and randomness is particularly important.

As far as the current development of robot positioning and navigation technology is concerned, it is far from the established goal and lacks the ability to face diverse environments. No matter in theoretical or applied studies, most of them are aimed at small, simple, or even single indoor scenes with poor application effect, as shown in Figure 2. However, in practical applications, robots are faced with uncertain scenarios that are not predictable in scale or complexity. At the same time, in the pursuit of accuracy, real time, and stability, it is difficult to achieve by relying on a single method and sensor; therefore, multisensor fusion and multimethod coordination are the development trend to solve the robot function problems [7].

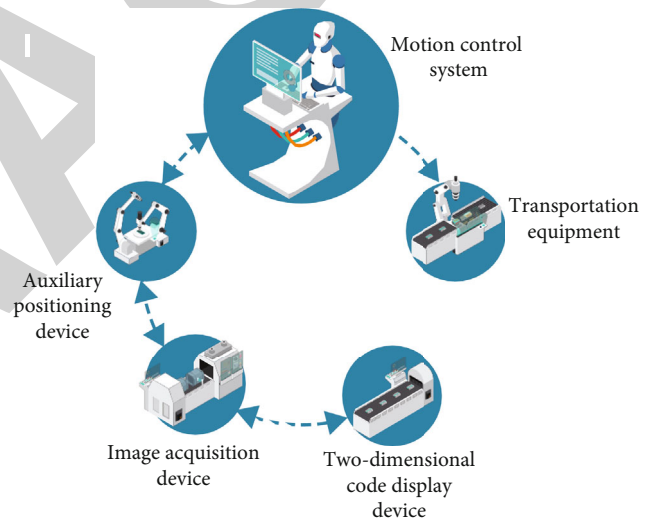


FIGURE 2: Robot target positioning method.

2. Literature Review

Robot positioning and navigation technology has been extensively computer-related for many years. The robot simply has to answer three questions: where am I, where am I going, and how am I going? Job is the answer to the question of where I live and especially where robots are the determinants of robotics in the world of governance office. The navigation process is often associated with the latter two, the main issues being the design, route planning, and vehicle management.

In recent years, with the rapid development of computer vision technology, vision-based positioning and navigation techniques have been widely studied and used. There are researches on positioning only from the perspective of images. An image retrieval and location method based on database is proposed [8]. In this method, the query image is matched with the image database annotated with location information (such

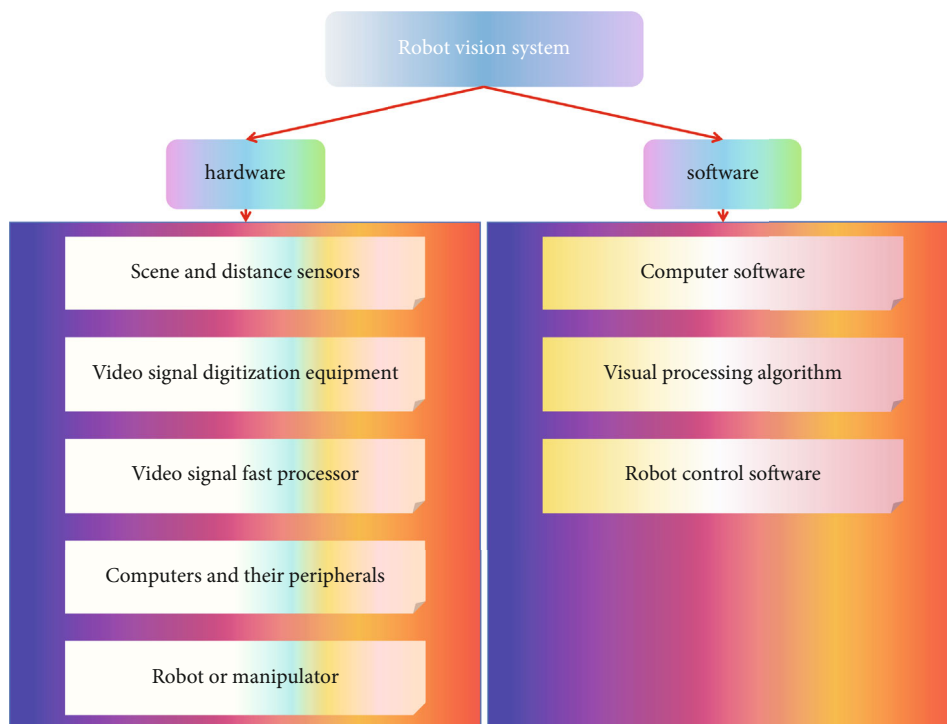


FIGURE 3: Visual composition of robot.

as geographic location) to obtain the location of the current query image. While these methods can scale to very large environments, they typically provide only rough estimates of camera positions and are highly database dependent.

The main idea of scene coordinate regression framework proposed by Tschernia is to map image blocks to corresponding points in 3D scene space, namely, scene coordinates [9]. This step can be learned from limited data because the local block appearance is relatively stable, and the random sampling consistency algorithm can be used to estimate the camera pose and align the image with the predicted scene coordinates. Based on the idea of this framework, Nakidkina proposes a differentiable RANSAC method for camera positioning in the network. The method is called DSAC (differentiable RANSAC). The main idea is to use a class VGG style convolutional neural network to find the mapping between image blocks and corresponding points in scene space, that is, to obtain the predicted scene coordinates [10]. Then, a random subset of scene coordinates was used to create a camera pose hypothesis pool, and then, a scoring CNN was used to score each hypothesis pose in the hypothesis pool, as shown in Figure 3.

Assuming that the principles behind neurons are found, the initial function has been taken as an important tool for counting neurons, reasoning needs to be expressed as computation, and neural networks and M-P models were planned, starting to create neural networks (ANN) [11]. Liu, in his book "Society of Behavior," reported on Hebb synapse and Hebb law education, which laid the theoretical basis for the development of neural network algorithms [12]. Mayandi developed the perceptron, the first body-building, science-capable neural network based on the JMP standard [13]. In Arya's Perceptrons:

An Introduction to Computational Geometry published, he proposed that Rosenblatt's single-layer perceptron could only learn linearly separable patterns, but could not deal with linear nonseparable problems such as XOR [14]. Hopfield's neural network (HNN) was introduced for the first time. Since then, Hopfield's understanding of neural network-based dynamic behavior has played a key role in data processing and engineering. The backpropagation neural network (BPNN) was later proposed to address multilayer neural network problems, but the BP network still had some shortcomings, such as poor local shrinkage, slow integration, and difficult to write large files [15]. According to the model network requested by Arutyunyan, the BP algorithm is used to train and design the lenet-5 model of the convolutional neural network (CNN) [16]. The DeepBelief Network (DBN) was developed by Guidara [17] approved. In recent years, neural devices have become a hot topic in many fields, with a wide range of achievements in imaging, medical biology, and more (Figure 4).

3. Method

3.1. Data Set Construction Based on ICP Algorithm. Perception of depth information is the premise of stereo vision. These depth data can obtain a group of discrete 3D points through reprojection, and a certain number of 3D points constitute the so-called point cloud. Although the depth data is very attractive, the depth information still has inherent noise, and the fluctuation of depth measurement often leads to the failure of reading information of some pixels, which is represented as holes in the depth image, indicating that there is no depth information. In order to make up the original shortages of depth transducer, as shown in KinectFusion algorithm, by

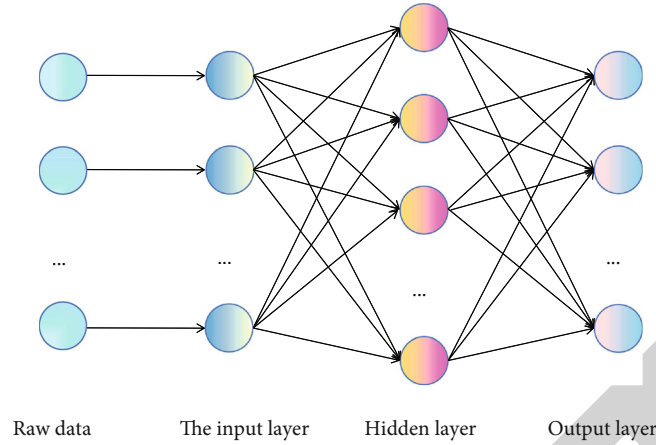


FIGURE 4: Basic neural network structure.

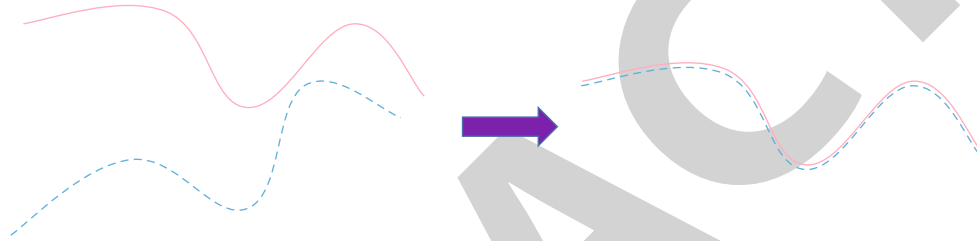


FIGURE 5: Basic idea of ICP algorithm.

obtaining a continuous depth image, the depth view merges with the new perspective to fill in the holes and fill in the missing depth information as much as possible [18]. Compared with other data representations, point cloud data achieves accurate topological structure and geometric structure of scene or object with lower storage cost, so it has certain advantages in 3D problem processing. Based on current technology, ICP algorithm is the most commonly used algorithm to process point cloud data, which has simple idea and high precision. ICP algorithm is also the main location method involved in the data set construction process in this paper, so this algorithm will be introduced in detail.

The basic idea of the ICP algorithm is for two point sets, the unique closed solution can be obtained by the relative transformation of the two point sets according to the constraints of a certain number of matching points on the corresponding relationship by searching for the correct corresponding matching points of the sampling points. Therefore, ICP algorithm is essentially a two-point set registration process for two three-dimensional data point sets from different coordinate systems. For example, this paper involves the world coordinate system and the camera coordinate system, by finding two 3D point set space, relative transformation relationship to the unified under the same coordinate system (usually refers to the world coordinate system); the purpose is to find in the global coordinate system to obtain the current view of the relative position of the camera and the direction, his appearance, makes the intersection area completely overlap between the two, the process said for registration. In the calculation process, registration is to find the 4 4 rigid transformation matrix T that makes the intersection area between the

two points converge completely coincide and to calculate the optimal rigid body transformation by repeatedly selecting the corresponding point pairs until the accuracy requirements of convergence are met [5, 6, 8]. The rigid transformation matrix T mainly includes the aforementioned translation vector T , rotation matrix R , perspective transformation vector V , and scale factor S , because point cloud data is obtained according to a certain number of continuous pictures. Therefore, there is only rotation and translation, but no deformation. Therefore, the perspective transformation vector V is set as zero vector, and the scale factor S is 1 [19]. See Figure 5.

As shown,

$$T = \begin{bmatrix} R_{11} & R_{12} & R_{13} & t_x \\ R_{21} & R_{22} & R_{23} & t_y \\ R_{31} & R_{32} & R_{33} & t_z \\ v_x & v_y & v_z & s \end{bmatrix} \rightarrow T = \begin{bmatrix} R & t \\ V & s \end{bmatrix} \rightarrow T = \begin{bmatrix} R & t \\ 0 & 1 \end{bmatrix}. \quad (1)$$

The matching of the ICP algorithm is a process of continuous iteration until convergence. Two continuous depth images are abstracted into two point sets as input. The iterative steps of the standard ICP algorithm are as follows:

- (1) According to the point sampling strategy, a certain number of sampling points are selected from the target point set P for matching. Common sampling strategies include uniform sampling, random sampling, and normal vector sampling

- (2) The point-to-point principle is used to find the corresponding matching point set in the source point set Q , find all matching point pairs in the two point sets, and form two new point sets
- (3) The above transformation matrix T is obtained by calculating the pose difference between the centers of gravity of two new point sets, which minimizes the error function, as shown in Equation (1)
- (4) The transformation matrix obtained in step 3 is used to carry out rotation and translation transformation for the target point set, and a new corresponding point set P' is obtained
- (5) Calculate the average distance d between the new point set P' and the source point set Q
- (6) When the distance d is less than the set threshold or the number of iterations exceeds the set maximum number of iterations, the iteration process is stopped. Otherwise, steps 2~6 are repeated until the requirements are met

Calculate the pixel coordinates of the new point set P obtained by the transformation matrix of the 3D point coordinate p_i in the target point set p' , where T represents the obtained transformation matrix and K represents the camera internal parameter matrix. (u_d, v_d) represents the coordinates of p_i in p' , n represents the scale of point set, p'_i represents pixels in point set P' , and q_i represents pixels in source point set Q .

As shown,

$$f(u_d, v_d, 1) = KTp_i. \quad (2)$$

As shown,

$$d = \frac{1}{n} \sum_{i=1}^n \|p'_i - q_i\|^2, \quad (3)$$

where p_i and q_i are the corresponding points of the two point sets found through the nearest neighbor principle, respectively, n represents the scale of the target point set, and $f(R, t)$ represents the conversion error between the two points, so the problem is transformed into a mathematical solution with the minimum error value R and t , as shown in Figures 6 and 7.

As shown,

$$f(R, t) = \frac{1}{n} \sum_{i=1}^n \|Rp_i + t - q_i\|^2. \quad (4)$$

In conclusion, the purpose of the ICP algorithm is to find the nearest point of the objective and the terms below certain constraints and to calculate the optimal agreement of the switching matrix and the switching vector does not work to minimize errors.

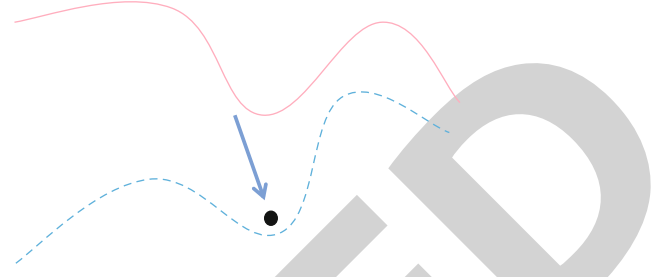


FIGURE 6: Nearest-neighbor heuristic.

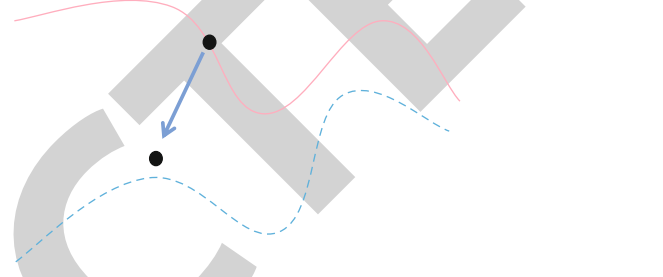


FIGURE 7: Nearest neighbor point method in normal vector direction.

As shown,

$$E = \sum_{i=1}^n ((Rp_i + t - q_i) \cdot n_i)^2. \quad (5)$$

Compared with the original classic ICP algorithm, the accuracy and speed of localization have been greatly improved by the above improvements. In particular, Kinect-Fusion algorithm uses frame-to-model registration form instead of image frame-to-frame, which reduces cumulative error to a certain extent. Meanwhile, the highly parallel processing on GPU improves the timeliness of the algorithm unprecedentedly [20].

As shown,

$$E = E_{icp} + W_{ite}E_{ite}. \quad (6)$$

E_{icp} is the error function value of ICP algorithm, E_{ite} is the error function value of direct method, and W_{ite} is the weight value of direct method. The combination of the two methods makes the result of each iteration optimization more accurate and the stability has been greatly improved [21].

3.2. Navigation and Positioning Based on Neural Network.

Neurons are the main functional components of neural network devices. Typically, it is an element with multiple inputs and one output and creates one type. x_i represents the input signal. j_{ij} represents the input signal thabi and the signal density of the neurons j , b_j represents the differentiation of the neuron, and y_j represents the output of the neuron. The relationship between signal input and output values is shown in the equation below.

As shown,

$$y_i = f\left(b_j + \sum_{i=1}^n (x_i \times w_{ij})\right). \quad (7)$$

$f(\cdot)$ is the activation function, generally available Sigmoid function, ReLU function, $\text{TANH}(X)$ function radial basis function, and other commonly used neural networks with multilayer perceptron limit Boltzmann machine radial basis neural network RBF, etc. [22]. See Figure 8.

Commonly used operating values in neural networks include square values, cross-entropy, and logarithmic probability function. The square value and the cross-entropy function are defined, where x is the model, n is the total model, y is the output value, and a is the output value. Compared with the quadratic function, the cross-entropy function combines fast and easy global optimization functions. When Softmax is used as a function of function, the logarithmic probability function is usually used as a function value, with a_k being the output value of the K -nerve cell and y_k being the value. Actual relative to K -nerve cell is 0 or 1 [23].

As shown,

$$C = \frac{1}{2n} \sum_x \|y(x) - a(x)\|^2. \quad (8)$$

As shown,

$$C = -\frac{1}{n} \sum_x [y \ln a + (1 - y) \ln (1 - a)]. \quad (9)$$

As shown,

$$C = -\sum_k y_k \log a_k. \quad (10)$$

Optimization algorithms are required to address operating costs in deep neural networks, and most commonly used algorithms include data gradient conjugate gradient methods such as LBGFS. Currently, the most commonly used optimization algorithm is the gradient loss algorithm, and the main goal of the simple process is to reduce operational goals. At each iteration, the value of the differential gradient of each variable is adjusted in the direction returned to the different gradient according to the working objective. Among these, parametric performance speed determines the number of iterations when a function reaches its minimum value. There are three differences in fall gradient: random light gradient drop and small gradient drop [24]. For BGD, this can ensure that the process converges to the best international or that the operations are not convex to the best local, but fast because all updates should be addressed on all records. This method is not available even with large files in memory, and the model cannot be modified online. It solves only one sample gradient in the file of each update, which makes it efficient and allows for online learning. However, compared to BGD, SGD tends to fall locally to a min-

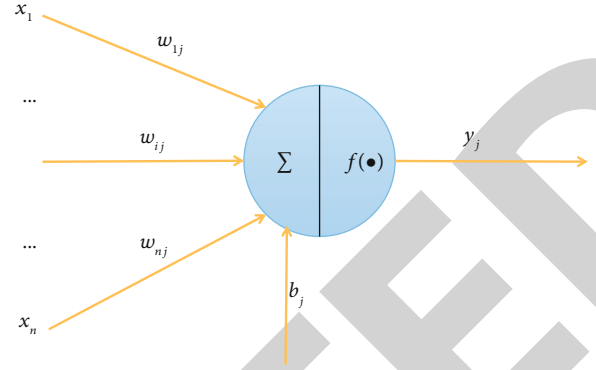


FIGURE 8: Neuronal model diagram.

imum, and the integration process is less stable. MBGD provides the advantages of two options for solving configuration problems including N models for each update, making the integration process more stable, which is usually the preferred algorithm for training neural networks [25].

4. Experimental Results and Discussion

The corresponding training test set was formed with the introduced data set to generate positioning model for each indoor scene. This section will introduce the loss change and accuracy in the training process from the perspective of three-stage training of scene coordinate initialization, reprojection error optimization, and end-to-end optimization.

It, respectively, represents the loss reduction of the data set corresponding to the multistation scene under strong light, the multistation scene under weak light, the half-room scene, and the unmanned supermarket scene in the training process. Similarly, the same test data set is used to test the training loss decline and accuracy information corresponding to mirror scene and window scene one by one for the three training stages, and the positioning accuracy is obtained within different error thresholds (5–10 cm means that the rotation angle error is 5°, and the translation error is within 10 cm). The maximum error threshold is about one-third of the radius of the robot base and gradually decreases with an interval of 1 cm.

As can be seen from the above, with the iteration update, the loss decreases continuously, and with the deepening of the training, the loss value remains stable and converges in the final end-to-end training. Accordingly, it can be concluded that for different indoor scenes, the positioning accuracy can reach more than 80% within the allowable error range of the robot. For the positioning target with smaller and more accurate error, the positioning accuracy can also be guaranteed by more than 60%. Among them, according to the average error value, it can be inferred that similar or repeated texture structure has a great influence on the positioning accuracy and has good robustness for other influence factors. Meanwhile, in all data set scenarios, positioning accuracy improved gradually with the deepening of training, proving that the three-stage training method is effective, as shown in Figure 9.

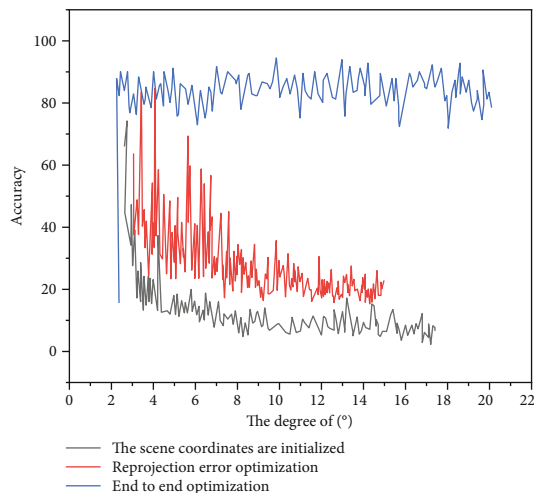


FIGURE 9: Loss visualization.

Firstly, the experimental environment of the robot positioning and navigation system based on visual positioning is introduced, including the hardware equipment, software kit and operating system used by each part, and the parameter settings of each module are explained. Then, from the experimental point of view, the positioning accuracy of each indoor scene in the data set was tested under different error thresholds. Finally, Tiago robot was used to conduct navigation tasks with the positioning results, and the feasibility and practicability of the system were verified.

The results of the experiment show that (1) the combination of ICP algorithm with direct method can solve the problem of loss and internal expansion of the data stored. (2) The process designed neural network positioning method is more efficient and robust and stable than the modification method. The operating time is shorter, which can meet the needs of the actual operation and be more cost-effective for all internal situations.

5. Conclusion

This paper proposes a robot visual navigation algorithm based on neural network and the target localization method from the visual angle, using the neural networks to locate, based on the idea of image frames to match a small amount of position and image information used to locate the initialization and training of neural network model, a small amount of data and information can effectively avoid posture loss and drift. Use of limited training data set information to generate an indoor scene of positioning model, based on the idea of scene coordinate regression, implementation does not depend on the depth information, by using a single RGB image positioning of the function of indoor positioning model can generate independent offline, so in the process of the system using the direct call the positioning model, without the calculation of a large number of real-time positioning letter to meet the task of system accuracy and real-time requirements.

Combined with the advantages of the current mainstream method, a positioning and navigation system with

high precision, high efficiency, and strong stability is realized by using a variety of sensors. Among them, the method based on neural network makes up for the shortcomings of the method based on image frame matching, which is easy to produce location failure, accumulation error, and even drift. Meanwhile, the method based on image frame matching creates conditions for the initialization of the location neural network model. By obtaining a large amount of environmental and structural information, the visual sensor makes up for the deficiency that the laser radar can only obtain the plane information of its own location. At the same time, the laser radar improves the accuracy of visual positioning and navigation, and the combination of the two can effectively expand the detection range and improve the accuracy of information.

Some limitations of the system need to be improved in the future: in the stage of data set construction, although the combination of ICP algorithm and direct method has expanded the scale of experimental scenes, there is still the problem of failure for the larger scene environment. The training time of neural network is long, and the training time of each scene is measured in hours, so the time cost is high. The navigation process does not take into account the use of semantic information, only using geometric methods, with lack of effective robot interaction function.

Data Availability

The data used to support the findings of this study are available from the corresponding author upon request.

Conflicts of Interest

The authors declare that they have no conflicts of interest.

Acknowledgments

This work was supported by the basic scientific research project of Department of Education of Liaoning Province, research on key technologies of health assessment of high safety equipment based on deep learning (Project No. LJKZ1061).

References

- [1] S. M. M. Kahaki, M. J. Nordin, N. S. Ahmad, M. Arzoky, and W. Ismail, "Deep convolutional neural network designed for age assessment based on orthopantomography data," *Neural Computing and Applications*, vol. 32, no. 13, pp. 9357–9368, 2020.
- [2] J. Tang, W. Zhu, and Y. Bi, "A computer vision-based navigation and localization method for station-moving aircraft transport platform with dual cameras," *Sensors*, vol. 20, no. 1, p. 279, 2020.
- [3] K. K. Pandey and D. R. Parhi, "Trajectory planning and the target search by the mobile robot in an environment using a behavior-based neural network approach," *Robotica*, vol. 38, no. 9, pp. 1–15, 2019.
- [4] J. Qiu, L. Du, D. Zhang, S. Su, and Z. Tian, "Nei-TTE: intelligent traffic time estimation based on fine-grained time

Retraction

Retracted: Path Planning of Storage and Logistics Mobile Robot Based on ACA-E Algorithm

Journal of Sensors

Received 22 August 2023; Accepted 22 August 2023; Published 23 August 2023

Copyright © 2023 Journal of Sensors. This is an open access article distributed under the Creative Commons Attribution License, which permits unrestricted use, distribution, and reproduction in any medium, provided the original work is properly cited.

This article has been retracted by Hindawi following an investigation undertaken by the publisher [1]. This investigation has uncovered evidence of one or more of the following indicators of systematic manipulation of the publication process:

- (1) Discrepancies in scope
- (2) Discrepancies in the description of the research reported
- (3) Discrepancies between the availability of data and the research described
- (4) Inappropriate citations
- (5) Incoherent, meaningless and/or irrelevant content included in the article
- (6) Peer-review manipulation

The presence of these indicators undermines our confidence in the integrity of the article's content and we cannot, therefore, vouch for its reliability. Please note that this notice is intended solely to alert readers that the content of this article is unreliable. We have not investigated whether authors were aware of or involved in the systematic manipulation of the publication process.

Wiley and Hindawi regrets that the usual quality checks did not identify these issues before publication and have since put additional measures in place to safeguard research integrity.

We wish to credit our own Research Integrity and Research Publishing teams and anonymous and named external researchers and research integrity experts for contributing to this investigation.

The corresponding author, as the representative of all authors, has been given the opportunity to register their agreement or disagreement to this retraction. We have kept a record of any response received.

References

- [1] Y. Zhao, "Path Planning of Storage and Logistics Mobile Robot Based on ACA-E Algorithm," *Journal of Sensors*, vol. 2022, Article ID 5757719, 7 pages, 2022.

Research Article

Path Planning of Storage and Logistics Mobile Robot Based on ACA-E Algorithm

Yue Zhao 

School of Electrical and Computer Science, Jilin Jianzhu University, Jilin 130118, China

Correspondence should be addressed to Yue Zhao; 15095102210001@hainanu.edu.cn

Received 29 May 2022; Revised 26 June 2022; Accepted 2 July 2022; Published 13 July 2022

Academic Editor: Haibin Lv

Copyright © 2022 Yue Zhao. This is an open access article distributed under the Creative Commons Attribution License, which permits unrestricted use, distribution, and reproduction in any medium, provided the original work is properly cited.

In this paper, warehouse logistics robot as the research object, starting from the reality of modern e-commerce logistics industry, proposed a warehousing logistics mobile robot path planning method. Ant colony algorithm is used to plan the forward path of mobile robot in static and dynamic environment of warehouse logistics. The results show that the elite-based strategy improves the global search capability of ACA and eliminates redundant nodes in the path, and the path length of the obtained plan is significantly better than that of traditional ACA, which is reduced by 3.46% and 5.90%, respectively, indicating that the elite-based strategy and the central-point-based smoothing method play their roles. The path length of the robot's final operation is larger than that of the global path planning, which increases by 1, accounting for 6.67% of the original path length. Therefore, the storage and logistics mobile robot based on ACA-E algorithm has short driving distance and superior obstacle avoidance ability.

1. Introduction

In recent years, major e-commerce websites have become popular, and the amount of online consumption has been refreshed repeatedly. In particular, the annual “Double 11 Shopping Festival” has created a miracle of online consumption. This reflects that people are more and more inclined to online consumption and logistics is an essential link. The quality of logistics services will have a direct impact on people's online consumption experience. Therefore, the efficiency and convenience of logistics is a difficult problem that must be solved [1].

However, the current logistics industry still has the disadvantages of low mechanization, high human demand, and low intelligence, which brings a series of problems such as high logistics cost and low operation efficiency, which seriously restrict the development of the logistics industry and even the progress of economy and society. In the modern logistics industry, the development of warehousing logistics, as one of the main forms of logistics, is undoubtedly the main factor affecting the above problems [2]. As the operation of warehousing logistics is inseparable from control, robotics, and other related disciplines, warehousing logistics has become more and more modern and intelligent with the progress and development of these disciplines [3].

The robot industry has a huge and bright future. With more and more robot application scenarios and the emergence of various advanced robots abroad, domestic manufacturers also see business opportunities and invest human and material resources in the robot industry. However, due to the characteristics of this industry, such as high development threshold, large amount of funds required, and it is difficult to obtain high returns in the short term; domestic robot enterprises cannot gain a foothold in the high-end robot industry and can only develop and produce some products with low technical content and low added value [4, 5]. However, for some domestic companies with strong R&D strength, they have invested a lot of human and financial resources in the R&D and application of mobile robot technology. Although they have also achieved corresponding results, they have not been used in large-scale distribution centers.

2. Literature Review

Foreign countries have carried out robot related research earlier. The world's first mobile robot Shakey was born in Stanford Research Institute in the United States in the 1970s. It completes various tasks through program control, which is generally divided into three types of programs: low level, medium

level, and high level. The functions of these three levels of programs are interrelated and influence each other to control the low-level movement and more complex movement and complete more advanced programmed tasks of the robot [6].

In today's world, the United States is one of the most developed countries, and its scientific and technological development is also in the forefront of the world. Robot technology also originated in the United States. At present, the performance of robots studied in the United States is still at the forefront of the industry [7]. Many soldiers in the United States are physically disabled and unable to walk normally due to their participation in the war, which seriously affects their daily life. In order to help these disabled soldiers and other disabled people, the U.S. military has developed a robot, which can act as the legs of the disabled and help people with legs to walk flexibly [8].

In Europe, robot research is also valued, and robot research in developed countries such as Germany, Britain, and France is also at the world advanced level [9]. In Europe, the proportion of empty nesters is more serious than that in China. Therefore, the German company has launched a companion robot, which can be used as a servant to complete housework, and it is also equipped with a camera as an observation response system [10]. In addition, it also has multiple sensors installed, which can be used as part of home intelligent services. For example, it knows whether the door of the refrigerator is open and when to turn on the coffee machine. It also has a motion detector to determine where people are in the room [11].

China's robot research began in 1986. Compared with other European and American developed countries, it started late and has a weak foundation [12]. However, China has always placed robot research in an important position and has always paid attention to robot projects in the national "863 project plan." It is gratifying that after more than 30 years of development, China has made great progress in the field of robots, trained a number of well-known robot experts and scholars at home and abroad, and developed many robots with outstanding performance [13]. The humanoid robot independently developed by the robot laboratory of the school of control of Zhejiang University is the only robot system in the world that can receive and play a rotating ball. Its higher degrees of freedom (more than 30) can realize more complex actions [14]. Jiaotong University has developed two kinds of Hexapod disaster relief robots. One has a variety of high-precision sensors, which can transmit the video and other information of the disaster area, and it is mainly responsible for the detection task. The other robot has the advantage of large load capacity, which can carry more than 600 kg of relief materials, and has strong passing capacity, which can make the post disaster relief materials even if they are transported to the disaster area [15]. The autonomous navigation system of micro nanorobot was researched and invented by researchers of Harbin Institute of technology and scholars at the University of California, San Diego. The robot can analyze the obstacles on the path in real time in the process of moving, adjust its moving route according to relevant algorithms, and realize the timely avoidance of obstacles. It can also plan its travel route in real time according to the complex environment and find the best route, so as to safely reach the target point in the shortest time [16, 17].

Based on the current research, this paper mainly takes the warehousing and logistics robot as the research object and puts forward a path planning method of warehousing and logistics mobile robot from the reality of e-commerce and modern logistics industry. In this paper, ant colony algorithm is used to plan the forward path of mobile robot in the static and dynamic environment of warehousing and logistics. Firstly, this paper expounds the development status and future development trend of the robot, studies and analyzes various optimization algorithms, and selects ACA to plan the path of the mobile robot. The information concentration in the transfer probability of the algorithm process is strengthened, and the improved algorithm is applied to the path planning of warehouse logistics mobile robot.

3. Research Methods

3.1. Environmental Modeling. Environmental model is a mathematical model describing the working area of mobile robot. Scholars at home and abroad have carried out a series of research on environmental model and put forward many modeling methods. The following introduces three classical modeling methods: grid method, geometric method, and topology method [18].

- (1) In order to reduce the complexity of obstacle boundary, the grid method divides the grid size according to the size of the real mobile robot and divides the robot operating environment into grids of the same size. There are both black grids representing obstacles and white grids representing free walking in the grid, which makes the robot operating environment from complex to simple, and the path planning problem is relatively simple. Therefore, for the grid method, the most important thing is to determine the size of the divided grid, which will directly affect the operation of the algorithm and the final planning effect [19]
- (2) Geometric method uses geometric features (such as points, lines, and surfaces) to represent objects in the scene; abstracts the environmental information collected by the sensors carried by the robot into common geometric features, such as vertices, lines, curves, and corners; and then describes and records them with coordinates [20]
- (3) The expression of topological graph method is more abstract. It uses graphs to represent the spatial relationship between objects in the environment, and the nodes of the graph represent the feature points in the environment [21]. This method can be used to build a large and simple environment. The topological model can usually be expressed by

$$G = (V, E), \quad (1)$$

where V represents the target object in the environment and E represents the connecting path between the target objects, which together constitute the topological map G .

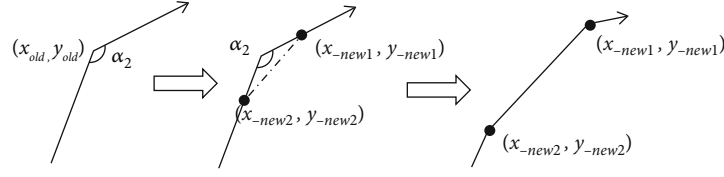


FIGURE 1: Schematic diagram of smoothing method.

3.2. *Basic Ant Colony Algorithm.* Step1. Variable initialization: The starting point S and target point E are fixed grid numbers, and the ant colony is placed at the starting point s . Initialize the number of ants m , the number of iterations N , the heuristic factor a , the expected heuristic factor β , and the tabu table (ants have walked the path) B_k to an empty set

Step 2. State transition probability p_{ij}^k : The state transition probability formula p_{ij}^k and j of ants transferring from grid point to grid point j are nodes that have not been visited. It can be expressed as

$$p_{ij}^k = \begin{cases} \frac{\tau_{ij}^\alpha(t) \eta_{ij}^\beta(t)}{\sum_{s \in \text{allowed}_k} \tau_{is}^\alpha(t) \eta_{is}^\beta(t)}, & j \in \text{allowed}_k \\ 0 & , \text{otherwise,} \end{cases} \quad (2)$$

where $\tau_{ij}(t)$ is the pheromone that the mobile robot transfers from point to point which is the trajectory intensity and $\eta_{ij}(t)$ is the heuristic degree of mobile robot transfer from point to point, and its formula is

$$\eta_{ij}(t) = \frac{1}{d_{ij}}, \quad (3)$$

where d_{ij} represents the distance between the grid i and j where the mobile robot is located.

allowed_k represents the grid points allowed to be selected by ant k in the next step, and its formula is

$$\text{allowed}_k = D - B_k, \quad (4)$$

where D represents the optional path node, $D = (0, 1, 2, \dots, n-1)$, and B_k represents the taboo table, that is, the grid point that ant k has passed

Step 3. Modify the tabu table B_k : Every time the ant k moves, add the moved node j to B_k , and clear the tabu table after this cycle

Step 4. Repeat Steps 2 and 3: Until each ant exits the cycle and reaches the end point, calculate the increment of pheromone according to the traversal quality (fitness) of each ant, calculate the path length traveled by each ant, and save it

Step 5. Update pheromone τ_{ij} , as shown in the following equation:

$$\tau_{ij}(t+1) = (1 - \rho)\tau_{ij}(t) + \Delta\tau_{ij}(t, t+1), \quad (5)$$

where,

$$\Delta\tau_{ij}(t, t+1) = \sum_{k=1}^m \Delta\tau_{ij}^k(t, t+1), \quad (6)$$

$$\Delta\tau_{ij}^k = \begin{cases} \frac{Q}{L_k}, & (i, j) \in l_k \\ 0 & , \text{Otherwise,} \end{cases} \quad (7)$$

where Q represents the information intensity element, which will affect the overall convergence speed of the algorithm and L_k is the total length of ant k 's path in this cycle

Step 6. Select and save the optimal path in this iteration and outputs the optimal obstacle avoidance path. Otherwise, repeat Steps 4 and 5 until the maximum number of iterations [22, 23]

3.3. *Improved Ant Colony Algorithm Based on Elite Strategy (ACA-E).* For the disadvantage that traditional ACA is easy to fall into local optimization, elite strategy is introduced to improve it. Elitist strategy means that after a cycle, each ant can find the optimal solution by using traditional ACA and elitist strategy gives additional compensation to its pheromone. The ant colony mainly relies on pheromone to transmit information, and the pheromone corresponding to the found optimal solution is enhanced. The purpose is that the optimal solution found in this cycle will be more attractive to the ants passing by after the pheromone enhancement operation in the next cycle of the ant, which solves the disadvantage that the ant colony algorithm is easy to enter the local optimization in the iterative process, resulting in unnecessary spikes in the path [24, 25]. The pheromone update formula is shown in the following equation:

$$\tau_{ij}(t+1) = \rho \cdot \tau_{ij}(t) + \Delta\tau_{ij} + \Delta\tau_{ij}^*, \quad (8)$$

where,

$$\Delta\tau_{ij}^* = \begin{cases} \alpha \frac{Q}{L^*}, & \text{If edge } (i, j) \text{ is part of the optimal solution} \\ 0, & \\ 0, & \text{Otherwise,} \end{cases} \quad (9)$$

where $\Delta\tau_{ij}^*$ represents the increase of pheromone of elite ants on path (i, j) ; α represents elite ants and their number; and L^* represents the total length of the path corresponding to the optimal solution found after the end of the cycle.

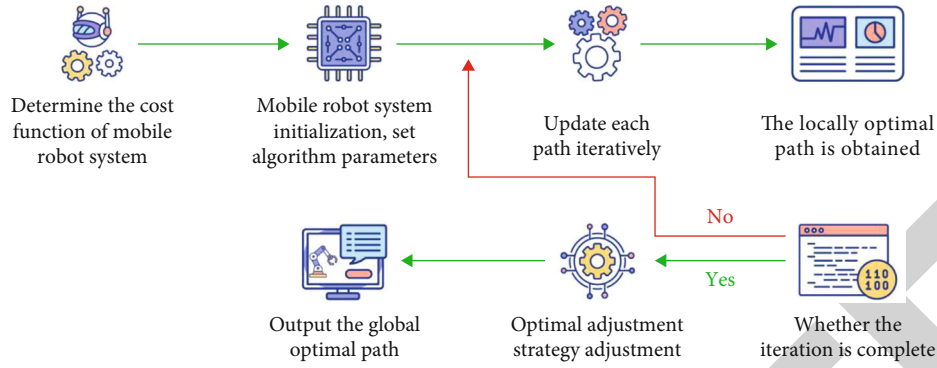


FIGURE 2: Improved algorithm flow.

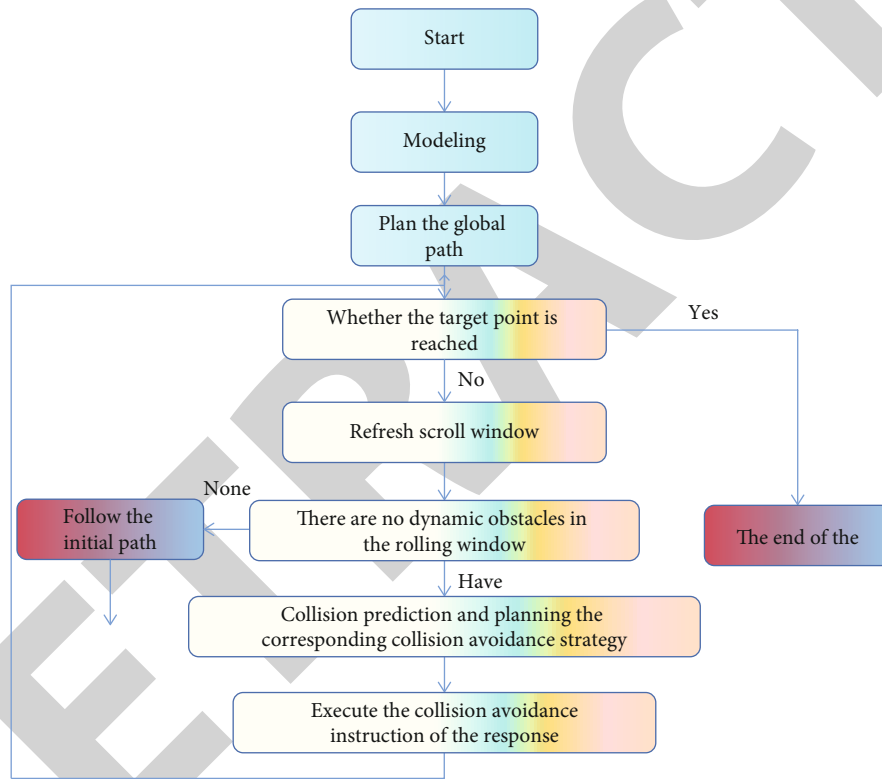


FIGURE 3: Flow chart of dynamic obstacle avoidance.

3.4. Improvement of Path Smoothing Machine Method for Mobile Robot (ACA-S). The improved ant colony algorithm (ACA-S) based on the center point smoothing method in this paper is realized by adding new nodes at the inflection point of the path. The new nodes replace the old nodes to complete the path smoothing. The selection and addition of new nodes have a direct impact on the improvement of path smoothness and the efficiency of overall path planning. Figure 1 is the operation diagram of the smoothing method based on the center point. The included angle of the original path segment is called α_2 . Selecting and adding new nodes and removing old nodes are related to the angle expected value α_1 of the two path corners set, and the angle expected value α_1 is set to 155° . If the actual corner α_2 of two adjacent lines is less than or equal

TABLE 1: Comparison of path length.

Algorithm name	Planning path length
Traditional ACA	33.8995
ACA-E	32.7279
ACA-ES	31.8995

to α_1 , take the midpoint (x_{-new1}, y_{-new1}) and (x_{-new2}, y_{-new2}) between the feasible regions of the two line segments, and then judge whether the corner angle formed by the new node and both sides meets or is greater than the expected angle α . If not, continue the above transformation to find new inflection points (x_{-new1}, y_{-new1}) and (x_{-new2}, y_{-new2}) . After meeting the

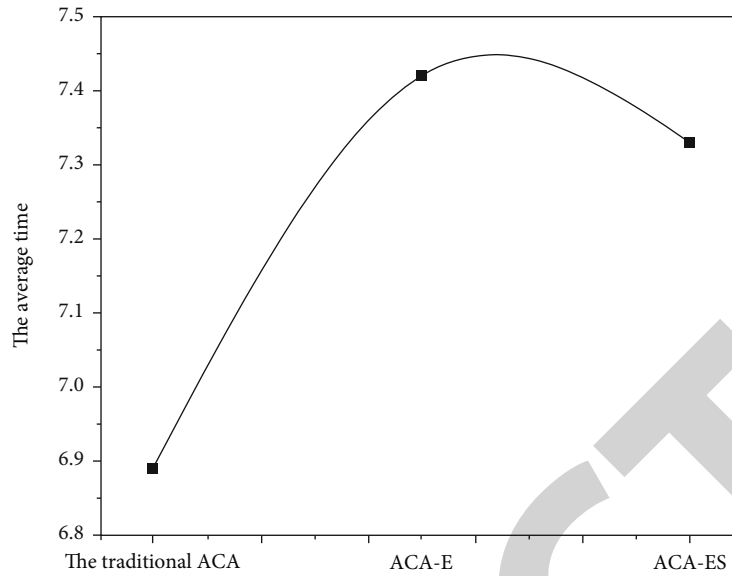


FIGURE 4: Comparison of average simulation time.

angle conditions, delete the old inflection point, and replace it with a new inflection point. Then, judge whether other inflection points in the path meet the conditions, and repeat them continuously so that the corners of the whole path are greater than the expected angle, as shown in the following equations:

$$\begin{cases} x_{-new1} = \frac{(x_{old1} + x_{old2})}{2} \\ y_{-new1} = \frac{(y_{old1} + y_{old2})}{2} \end{cases}, \quad (10)$$

$$\begin{cases} x_{-new2} = \frac{(x_{old2} + x_{old3})}{2} \\ y_{-new2} = \frac{(y_{old2} + y_{old3})}{2} \end{cases}$$

3.5. ACA-ES Algorithm. The steps of the improved ant colony algorithm (ACA-ES) based on the smoothing method of elite strategy and central point are shown in Figure 2.

3.6. Dynamic Path Planning Process. Step 1: Modeling. The grid method is used to model the information in the environment

Step 2: Using the improved ACA to carry out global static path planning without considering the dynamic and only considering the static obstacles

Step 3: Give priority to environmental prediction by using the rolling window. If there are no obstacles in the current rolling window, move to the next according to the path. If there are dynamic obstacles, collect and sort out the detected information, and make prediction judgment

Step 4: Analyze the predicted information, and judge and select the corresponding collision avoidance strategy according to the characteristics

Step 5: Under the theoretical guidance of the corresponding collision avoidance strategy, plan a local path to ensure that the robot does not collide with dynamic obstacles

Step 6: Continue to refresh the scrolling window, and repeat Steps 3 to 5 until the robot reaches the specified target point. The flow chart is shown in Figure 3.

4. Result Analysis

4.1. ACA-ES Application Test. In order to verify the feasibility and effectiveness of the improved algorithm (ACA-ES) applied to the path planning of mobile robot, the path planning simulation is carried out in the $17 * 17$ grid environment. The parameter settings are consistent with the $20 * 20$ grid. The coordinates of the starting point and the ending point of the robot are (0.5, 16.5) and (16.5, 0.5). Table 1 and Figure 4 summarize and compare the path length and simulation time.

The elite strategy improves the global search ability of ACA and eliminates redundant nodes in the path. As shown in Table 1, the path length is shortened from 33.8995 to 32.7279, 3.46%, and the number of iterations is reduced by half from 70 to 35. Secondly, the smoothing method based on the center point is introduced to further optimize the inflection point, making the path more smooth and in line with the motion characteristics of the solid robot. At the same time, the path length is shortened to 31.8995, 5.90%, and the number of iterations is reduced to 25.

The data in Table 1 and Figure 4 show that after the path planning passes the elite strategy (ACA-E) and adds the center point based smoothing method (ACA-ES), the planned path length is significantly better than the traditional ACA, reducing by 3.46% and 5.90%, respectively, indicating that the elite strategy and the center point based smoothing method have played their role. However, the shortening of the path is at the cost of time consumption. The improved ACA-E and ACA-ES increase the planning time by 5.48% and 4.51%, respectively.

TABLE 2: Final operation of mobile robot.

Starting point position	Target point location	Initial path length	Path length	Pause time
(0.5, 19.5)	(19.5, 0.5)	15.0208	16.0208	1

4.2. *Obstacle Avoidance Performance of ACA-ES.* In order to verify the performance comparison of the proposed improved method with dynamic obstacles moving in a straight line in the robot operating environment, this chapter uses Matlab2012a as the algorithm development platform to conduct simulation experiments under the environment of Windows 10 operating system.

The robot working environment is divided into $20 * 20$ grids for path planning simulation. The simulation parameters are set as follows: The number of ants M is 50, the number of iterations N is 200, the heuristic factor α is 1, the expected heuristic factor β is 7, the pheromone evaporation coefficient ρ is 0.7, and the pheromone increase intensity coefficient is 1. The coordinates of the starting point and the ending point of the robot are determined to be (0.5, 19.5) and (19.5, 0.5). In this experiment, it is assumed that the moving speed of dynamic obstacles in the environment is consistent with the forward speed of the robot. The results are shown in Table 2.

It can be seen from the table that the length of the planned path is 67.2% longer than that of the original path, which accounts for another 67.2% of the total path length. The results in the table fully show that in the environment with dynamic obstacles, the mobile robot increases the motion cost in the process of path planning, but the performance optimization is at the cost of path length.

5. Conclusion

In the research field of mobile robot technology, the path planning of mobile robot in the storage and logistics environment has become a hot research topic for researchers from all walks of life because of the rapid rise of e-commerce industry. This paper mainly analyzes and simulates the path planning method of mobile robot in the storage and logistics environment. The research work and results completed in this paper are summarized as follows:

- (1) In this paper, the existing ant colony path planning algorithm is improved, and an improved ACA with elite strategy is proposed. It is applied to the path planning of mobile robot in the storage and logistics environment, which enhances the pheromone concentration in the transfer probability of ants choosing the path in the process of moving forward. The addition of elite strategy solves the disadvantage that the traditional ACA is easy to fall into the local optimal solution, resulting in the stagnation of algorithm search, and improves the global understanding
- (2) On the basis of introducing the improved ACA of elite strategy, a smoothing method based on the center point is added. This method makes the small cor-

ner in the path more smooth, reduces the energy loss of the robot at the turn of the path, ensures the stability of the robot entity in the process of moving, and solves the practical problems that the mobile robot in warehousing and logistics will encounter in the process of moving forward

- (3) Aiming at the path planning of mobile robot with dynamic obstacles in the environment, the method of combining global static path planning with local dynamic collision avoidance planning is adopted, and the improved ACA is used to obtain a global optimal path

Data Availability

This study did not receive any funding in any form.

Conflicts of Interest

The authors declare that they have no conflicts of interest.

References

- [1] W. Yan, Z. Xu, X. F. Zhou, Q. Su, and H. Wu, "Fast object pose estimation using adaptive threshold for bin-picking," *Access*, vol. 8, pp. 63055–63064, 2020.
- [2] Z. Lv and L. Qiao, "Deep belief network and linear perceptron based cognitive computing for collaborative robots," *Applied Soft Computing*, vol. 92, article 106300, 2020.
- [3] L. Guo, L. Zhao, Y. Song, and J. Hu, "Design and control of a variable structure robot," *International Journal of Advanced Robotic Systems*, vol. 17, no. 1, 2020.
- [4] F. Rui, Y. Yamada, K. Mitsudome, K. Sano, and S. Warisawa, "Hangrawler: large-payload and high-speed ceiling mobile robot using crawler," *IEEE Transactions on Robotics*, vol. 36, no. 4, pp. 1053–1066, 2020.
- [5] Z. Lv, L. Qiao, J. Li, and H. Song, "Deep-learning-enabled security issues in the internet of things," *IEEE Internet of Things Journal*, vol. 8, no. 12, pp. 9531–9538, 2021.
- [6] N. Wang and H. Xu, "Dynamics-constrained global-local hybrid path planning of an autonomous surface vehicle," *IEEE Transactions on Vehicular Technology*, vol. 69, no. 7, pp. 6928–6942, 2020.
- [7] J. Zhang, J. Li, H. Yang, X. Feng, and G. Sun, "Complex environment path planning for unmanned aerial vehicles," *Sensors*, vol. 21, no. 15, p. 5250, 2021.
- [8] B. Yang, B. Wu, Y. You, C. Guo, L. Qiao, and Z. Lv, "Edge intelligence based digital twins for internet of autonomous unmanned vehicles," *Software: Practice and Experience*, vol. 1, 2022.
- [9] H. Zhang, Q. Zhao, Z. Cheng, L. Liu, and Y. Su, "Dynamic path optimization with real-time information for emergency evacuation," *Mathematical Problems in Engineering*, vol. 2021, Article ID 3017607, 9 pages, 2021.
- [10] Y. Chen, G. Bai, Y. Zhan, X. Hu, and J. Liu, "Path planning and obstacle avoiding of the usv based on improved aco-apf hybrid algorithm with adaptive early-warning," *Access*, vol. 9, pp. 40728–40742, 2021.
- [11] D. Zhao, H. Yu, X. Fang, L. Tian, and P. Han, "A path planning method based on multi-objective cauchy mutation cat swarm

Retraction

Retracted: New Energy Vehicle Electromagnetic Compatibility Test and Closed-Loop Simulation Analysis

Journal of Sensors

Received 19 December 2023; Accepted 19 December 2023; Published 20 December 2023

Copyright © 2023 Journal of Sensors. This is an open access article distributed under the Creative Commons Attribution License, which permits unrestricted use, distribution, and reproduction in any medium, provided the original work is properly cited.

This article has been retracted by Hindawi following an investigation undertaken by the publisher [1]. This investigation has uncovered evidence of one or more of the following indicators of systematic manipulation of the publication process:

- (1) Discrepancies in scope
- (2) Discrepancies in the description of the research reported
- (3) Discrepancies between the availability of data and the research described
- (4) Inappropriate citations
- (5) Incoherent, meaningless and/or irrelevant content included in the article
- (6) Manipulated or compromised peer review

The presence of these indicators undermines our confidence in the integrity of the article's content and we cannot, therefore, vouch for its reliability. Please note that this notice is intended solely to alert readers that the content of this article is unreliable. We have not investigated whether authors were aware of or involved in the systematic manipulation of the publication process.

Wiley and Hindawi regrets that the usual quality checks did not identify these issues before publication and have since put additional measures in place to safeguard research integrity.

We wish to credit our own Research Integrity and Research Publishing teams and anonymous and named external researchers and research integrity experts for contributing to this investigation.

The corresponding author, as the representative of all authors, has been given the opportunity to register their agreement or disagreement to this retraction. We have kept a record of any response received.

References

- [1] L. Ma and Y. Lu, "New Energy Vehicle Electromagnetic Compatibility Test and Closed-Loop Simulation Analysis," *Journal of Sensors*, vol. 2022, Article ID 3198944, 7 pages, 2022.

Research Article

New Energy Vehicle Electromagnetic Compatibility Test and Closed-Loop Simulation Analysis

Ling Ma ¹ and Yean Lu ²

¹College of Automobile and Rail, Anhui Technical College of Mechanical and Electrical Engineering, Wuhu 241000, China

²College of Electrical Engineering, Anhui Technical College of Mechanical and Electrical Engineering, Wuhu 241000, China

Correspondence should be addressed to Ling Ma; 201701350116@lzpcc.edu.cn

Received 24 May 2022; Accepted 29 June 2022; Published 12 July 2022

Academic Editor: Haibin Lv

Copyright © 2022 Ling Ma and Yean Lu. This is an open access article distributed under the Creative Commons Attribution License, which permits unrestricted use, distribution, and reproduction in any medium, provided the original work is properly cited.

With the rapid development of new energy vehicles, electromagnetic compatibility of new energy vehicles has been widely concerned. Therefore, based on the conducted electromagnetic interference theory of electric vehicle electric drive system, a kind of electromagnetic interference transmission path is proposed, and its closed-loop simulation is carried out. The results show that the key point that has great influence on the radiation emission of the electric drive system is whether there is a torque, essentially whether the motor controller has power output, and it has little relation with the motor speed and bus voltage. In addition to the influence of whether or not the torque has on radiation emission, the torque size is further compared, set 50 Nm, 100 Nm, and 200 Nm, respectively, for comparison, and it is found that the increase of torque has no obvious influence on radiation emission. Therefore, during the test, the appropriate torque can be selected according to the actual situation, rather than the maximum torque that the component can work.

1. Introduction

With the rapid development of new energy vehicles, especially the rapid popularity of new energy vehicles, their electromagnetic compatibility has been paid more and more attention. As an important part of new energy vehicles (Figure 1), electric drive system is one of the main interference sources of new energy vehicles with its high voltage, high current, complex structure, and multiple coupling paths [1]. Energy saving and environmental protection are the biggest advantages of electric vehicles, so governments are paying more and more attention to the research and development of electric vehicles. In recent years, electric vehicle technology has developed rapidly, and its functions are becoming more and more powerful. Accordingly, the integration degree of electric vehicle internal circuit is also gradually increased, and the electrical and electronic components used are also doubled and doubled [2]. Therefore, the development trend of electric vehicles must be highly inte-

grated electrical and electronic components. Highly integrated circuit system will inevitably have electromagnetic interference and heat problems, and this paper mainly studies electromagnetic interference. Because electric vehicle takes electric energy as the main energy source, its content electromagnetic field is extremely complex, and the deterioration of electromagnetic compatibility environment may affect its normal operation. In order to solve this problem, electromagnetic compatibility (EMC) technology is applied to electric vehicles.

Electromagnetic compatibility specifically refers to the coexistence of electrical and electronic equipment in a specific electromagnetic environment, which requires that in a completely consistent electromagnetic environment, all kinds of equipment can operate stably and do not interfere with each other, so as to achieve the “compatibility state.” But relative to the automobile, it refers to the internal module of the system, each system and the electromagnetic compatibility state existing between the system and the external

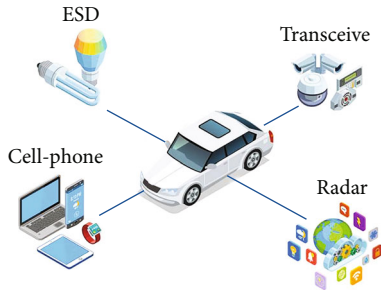


FIGURE 1: Electromagnetic compatibility test for new energy vehicles.

environment [3]. The International Electrotechnical Commission (IEC) points out that electromagnetic compatibility is essentially a capability. EC defines electromagnetic compatibility (EMC) as the ability of a device to operate stably in an electromagnetic environment without causing undue interference from other devices. The European Union (EU) standard states that automotive electromagnetic compatibility (EMC) is the ability of a vehicle or component to operate stably and reliably in a specific electromagnetic environment without causing electromagnetic disturbance to other things in this environment. The three factors of electromagnetic interference (EMI) are the main content of electromagnetic compatibility research. Interference source, propagation path, and sensitive equipment are the three elements of electromagnetic interference. Usually, the interference source is firstly analyzed, after finding the interference source to the specific in-depth study, to understand the cause of its emergence; then, according to the frequency band of the interference source, analyze whether the interference generated is conduction or radiation, and find out the specific propagation path; finally, how is the interference transmitted to the sensitive equipment, that is, how is the sensitive equipment affected by the interference [4].

This article proposes an electromagnetic compatibility closed-loop development technology for the electric drive system of new energy vehicles under load conditions, which mainly includes three key links: the development and improvement of test platform centering on test standards and test methods, which is a means to directly evaluate the electromagnetic compatibility performance of the electric drive system; the test equipment centers on the development of standardized and low-cost test bench, which is the hardware support for electromagnetic compatibility test of electric drive system. The simulation platform is a means of EMC performance control in the early design stage of electro-drive system products, which focuses on parameter design, prediction, and optimization of forward development. This paper focuses on the load test equipment and simulation platform of electric drive system [5].

2. Literature Review

EMC research of electric vehicle electric drive system is a part of EMC research of power electronics. In recent years, with the continuous innovation of science and technology, the energy loss of power converter continues to increase,

the volume continues to decrease, the frequency of switching on and off increases rapidly, and the output power is also increasing. Therefore, this kind of power electronic equipment will cause rapid changes of high voltage and high current in normal operation, which will cause additional electromagnetic interference to other circuits or components by using the parasitic inductance and parasitic capacitance of the circuit, thus affecting the normal operation of other electrical and electronic equipment. Electromagnetic compatibility of electric vehicle motor drive system has become a hot research topic.

As for the electromagnetic interference test method, Chen et al. mentioned the related content of conducted electromagnetic interference test of electric drive system and explained the general method. For impedance test methods [6], Wan et al. introduced the resonance method to measure the unknown impedance and proposed the insertion loss method to obtain the impedance value to be measured. For immunity tests [7], Zhou et al. introduced some good effects of conduction immunity and the advantages and disadvantages of transmission immunity testing methods [8]. According to Zheng and Cai, the defects of conducted immunity test and some practical examples are explained [9]. Cai and Zheng introduce some research on the specific application of iec61000-4-6, which is helpful to improve the automatic operation ability and test speed of the test [10]. Sami et al. focus on the comparison of some components in conducted immunity tests, such as electromagnetic forceps and high current injection forceps [11]. To sum up, although many scholars mentioned conducted electromagnetic interference test, they did not explain the test situation when the tested equipment was connected to load and did not analyze the advantages and disadvantages of voltage method and current method and how to select the two test methods. When the resonance method is used to measure unknown impedance, it is difficult and tedious to select the correct value of passive device and coordinate resonance. Especially at high frequency, the parasitic effect of passive devices is more obvious, which will affect the accuracy of measurement. To measure unknown impedance by insertion loss method, certain conditions must be met; for example, the insertion element impedance must be sufficiently large or sufficiently small. So once these conditions are not met, the method loses its accuracy. Although there are abundant literatures on conducted immunity testing, there are few researches on conducted immunity testing in industrial environment and its relationship with laboratory. Therefore, in view of these deficiencies, this paper carries out the corresponding research work [12].

3. Methods

3.1. Theoretical Basis of Conducted Electromagnetic Interference in Electric Vehicle Electric Drive System. Electromagnetic compatibility (EMC) refers to the normal operation of a device or system in its electromagnetic environment and is also a performance that does not cause unwanted electromagnetic interference (EMI) to other devices working in this environment. So, EMC is composed

of two parts: one part is the equipment in normal work to its electromagnetic environment caused by the electromagnetic interference (EM) in allowed range, and the other part is the equipment's ability to work properly under the influence of electromagnetic interference in its working environment, which is also called electromagnetic susceptibility (EMS).

Electromagnetic interference can be divided into two types, namely, conduction and radiation. Conducted electromagnetic interference refers to the interference signals transmitted to the connected circuits by conductors, while radiated interference refers to the interference signals transmitted to other circuits in space by electromagnetic fields [13]. This paper mainly studies conducted electromagnetic interference (EMI). Based on the definition of electromagnetic interference, it can be known that conducted electromagnetic interference mainly covers three elements, namely, interference source, coupling path, and sensitive equipment, and its formation mechanism is shown in Figure 2.

Because electromagnetic interference is abstract and invisible, it is necessary to use test equipment to show its size [14]. For conducting electromagnetic interference test, there are two commonly used voltage method and current method, and the specific content will be mentioned in the following chapters. Conducted EMI must be measured against the limits specified in the corresponding standards to see if it is within the permissible range. If it exceeds, rectification and debugging must be carried out to make it conform to relevant standards.

Electromagnetic compatibility (EMC) is a field that studies the coexistence of various electrical equipment in limited time, space, and spectrum [15]. The three elements of electromagnetic compatibility are time, space, and spectrum. Accordingly, the three elements that form electromagnetic interference are electromagnetic interference source, transmission path, and sensitive setting.

- (1) An electromagnetic interference source is an electrical device or a natural phenomenon that generates electromagnetic interference
- (2) Transmission path is also called coupling path, that is, electromagnetic energy through the medium coupling transmission process
- (3) Sensitive equipment, also known as interfered equipment, can be as small as circuit components or components and as large as systems or independent electrical equipment

3.2. Transmission Path of Electromagnetic Interference. In essence, the transmission of electromagnetic interference is the intentional or unintentional interaction between electromagnetic generation and receiving device or system. Corresponding to its formation mechanism, its transmission mode can be divided into conduction and radiation, namely, conduction coupling and radiation coupling. For conduction coupling, electromagnetic waves need to pass through a complete circuit to enable the electromagnetic energy of

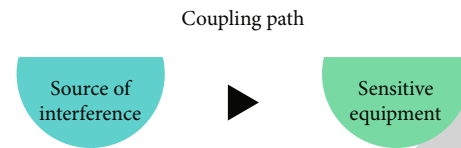


FIGURE 2: Formation process of conducted EMI.

the interference source to be coupled to the sensitive equipment or system. Conduction coupling can be divided into three types: resistive, capacitive, and inductive conduction coupling. For radiation coupling, electromagnetic wave can transmit electromagnetic energy to sensitive equipment or system in certain form and regularity without connecting circuit [16]. In general, the way of electromagnetic interference suffered by a system or equipment often includes many ways, which are not single, but play a dominant role in a certain coupling mode in different frequency range. This is also an important reason for the more complex and changeable electromagnetic environment.

Conduction coupling refers to the coupling interference caused by some connecting media (connecting wires, connecting capacitors, inductors, and other electronic components). Common conduction coupling is as follows.

3.2.1. Resistive Coupling. Coupling through nonreactance elements is resistive coupling. The most typical resistive coupling is the common impedance coupling, which can be divided into the common ground impedance and the common source impedance [17]. It often occurs in two circuits with a common current path. The effective way to reduce the common impedance coupling is to make the common impedance between the two zero or close to zero. In addition, leakage coupling (caused by breakdown or reduced insulation) is a more common resistive coupling mode.

The voltage U_L at both ends of the receiver load R_L is the coupling voltage, as shown in

$$U_L = \frac{R_L}{R + 2R_t + R_L} U_S. \quad (1)$$

3.2.2. Inductive Coupling. Inductive coupling, also known as electromagnetic coupling or electromagnetic induction, mainly occurs between transformers and parallel wires, so it often occurs between two closed loops. According to the knowledge of high school physics, the coil has relative cutting motion relative to the magnetic field line, which causes the change of the magnetic flux of the coil and produces the induced electromotive force. From the point of view of interference, the loop is disturbed by this wire, and the two closed loops are coupled by magnetic field lines, the degree of which can be expressed as mutual inductance [18].

Each wire forms a grounding loop, respectively, constituting the primary coil and secondary coil of the transformer. The expression of its inductive coupling is

$$V_2 = \frac{MdI_1}{d_t}, \quad (2)$$

TABLE 1: Standard working conditions of radiation test.

Controller operation	Motor controller power supply voltage/V	Dynamometer speed/(r*min ⁻¹)	The motor torque/Nm
Radiation speed 1	500	300	200
Radiation speed 2	500	80000	200
Radiation speed 3	500	1100	200

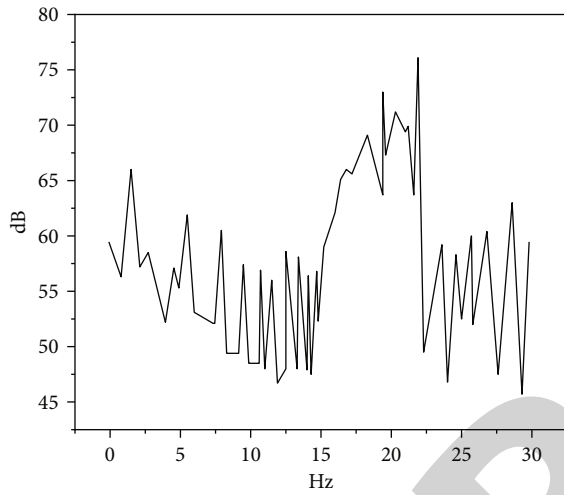


FIGURE 3: Comparison test results at different speeds.

where

$$M = \frac{\mu_0}{4\pi} \ln \left| \frac{(h_1 + h_2)^2 + d^2}{(h_1 - h_2)^2 + d^2} \right|. \quad (3)$$

According to the analysis of formula (1), the methods to reduce the inductive coupling are as follows: the distance between the power line and the power loop should be reduced as far as possible without affecting the performance. Keep power lines, signal lines, and control lines as far away as possible; if the signal cable is twisted-pair cable, it should be twisted tightly and close to the chassis for wiring. If the signal cable is shielded, it should be close to the chassis cloth under the condition that the grounding is good [19].

Capacitive coupling is the coupling caused by distributed capacitance, which often occurs in electric and electrostatic fields. The physical model is equivalent to inductive coupling. But capacitive coupling does not require primary and secondary loops, so the coupling principle is different. The coupling transmission expression is shown in

$$V_2 = \frac{R_2 V_1}{R_2 + X_C}. \quad (4)$$

Inductive coupling, also known as magnetic coupling, is the interaction of magnetic fields between two circuits that

TABLE 2: Test conditions of high-voltage power line with different torques.

Controller operation	Motor controller power supply voltage/V	Dynamometer speed/(r*min ⁻¹)	The motor torque/Nm
Radiation torque 1	500	800	0
Radiation torque 2	500	800	200

enables signals to be transmitted coupled. The physical nature of inductive coupling is similar to the principle of transformer: $0s = M0p$; a part of the magnetic flux OPp generated by the primary coil is crosslinked to the secondary coil, and a voltage is induced in it, and its size is

$$U_s = \frac{d\varphi_s}{dt} = M \frac{di_1}{dt}. \quad (5)$$

4. Experimental Analysis

4.1. EMI Simulation Platform of Electric Drive System under Load Condition Was Established. The parameters of the electric vehicle 3D model are basically from the actual vehicle parameters of a test vehicle. Considering that some real vehicle parameters are difficult to obtain, only general data parameters can be used, but it can basically guarantee that there is no significant influence on the simulation results. In addition, due to the compact connection structure of the actual car body, modeling of gaps and voids at the junction of lights, tires, windows, seats, electrical and electronic equipment, drives, and body joints is very complicated for electromagnetic simulation [20]. Therefore, the auxiliary devices and equipment of the vehicle that have no impact on the simulation results are deleted or simplified, and only the surface structure I0 of the vehicle model is established according to the actual structure of the test vehicle. The basic dimension parameters of the 3D model of the electric vehicle refer to a certain test vehicle, and the length \times width \times height are 4.9 m \times 2 m \times 1.5 m, respectively. In view of the actual circuit structure of the integrated electric drive system and in combination with the layout form of test standards, the conducted EMI simulation model of the electric drive system under load state should include IGBT power module model, high voltage LISN model, DC cable model, DC connector model, bus capacitance model, DC copper bar model, AC copper bar model, drive motor high frequency impedance model, motor torque control model, and motor load characteristic model. The EMI receiver mathematical model is used to convert the time domain simulation results to obtain the spectrum of peak value and average value [21]. The electromagnetic torque equation of the vehicle-mounted permanent magnet synchronous motor is shown in

$$T_{em} = p(\varphi_d i_q - \varphi_q i_d) = p[L_{md} i_q i_q + (L_d - L_q) i_d i_q], \quad (6)$$

where T_{em} is the electromagnetic torque, p is the polar logarithm of the motor, φ_d is the flux, i_d is the straight-axis

TABLE 3: Standard working conditions of radiation test.

Controller operation	Motor controller power supply voltage/V	Dynamometer speed/(r*min ⁻¹)	The motor torque/Nm
Radiation standard operating condition	500	800	200

current, i_q is the cross-axis current, L_u is the straight-axis inductance, and L_g is the cross-axis inductance.

In order to obtain the values of the above parameters, three-dimensional electromagnetic simulation was carried out. According to the main design parameters of the motor, the 3D electromagnetic model of the motor is established. After setting the boundary conditions, the simulation is carried out, and the characteristic parameter curves of the motor are output. The maximum torque/current control is required for the motor, so that the load characteristic parameters corresponding to the maximum torque under each working condition can be found and the motor load model under each working condition can be established [22].

There are many electromagnetic compatibility modeling methods, which depend on the type and nature of the problem, and have a great relationship with the complexity and precision of the system. It is generally divided into the following types:

- (1) Conducted interference and conducted anti-interference are analyzed by using circuit model and circuit principle
- (2) The lumped parameter equivalent circuit can be used to solve simple electromagnetic interference problems in the near field, such as cable crosstalk, distributed capacitance, and distributed inductance
- (3) The electromagnetic field theory under far field condition is used for analysis. It can solve the problems of antenna radiation and aperture radiation in far field
- (4) Using numerical software simulation analysis method, such as moment method and finite element method

The first three methods can only be used to solve a relatively simple, very limited number of physical processes. As the numerical software simulation analysis method introduces the powerful computing function of computer, it makes the numerical calculation of large complex model possible, so it can be used to solve many practical problems in engineering applications.

4.2. Analysis of Experimental Results. On the basis of the standard test conditions, change the motor speed, and the specific test conditions are as follows: power supply voltage of motor controller 500 V, motor torque 100 Nm, and dynamometer speed 300 r/min, 700 r/min, and 1000 r/min, as shown in Table 1. For the selection of motor speed, the test referred to the external characteristic curve of the driving motor and typical urban conditions and selected the most

representative driving motor speed as the test condition. The test results are shown in Figure 3. It can be seen from the comparison that in the band of 0.15 MHz~1 GHz, changing the driving motor speed has basically no effect on the radiation disturbance, and the peak test curve and average test curve basically coincide at different speeds [23].

On the basis of standard test conditions, the output torque of the motor is changed. The specific test conditions are as follows: the power supply voltage of the motor controller is 500 V, the speed of the dynamometer is 700 r/min, and the motor torque is 0 Nm and 100 Nm, as shown in Table 2. For the selection of motor output torque, the influence of torque on test results is mainly considered. By comparison, it can be seen that in the 0.15 MHz~1 GHz band, when the motor output torque is 100 Nm, both the peak value and average value are significantly higher than the test condition without torque of the driving motor, indicating that the torque has an obvious influence on radiation emission.

The radiation disturbance technique of the electric drive system was tested by dark fading method. The test frequency band was 0.15 MHz to 1 GHz, which was the same as the conduction test. The standard test conditions were first defined for comparative analysis as the reference data: the power supply voltage of the motor controller is 500 V, the speed of the dynamometer is 700 r/min, and the motor torque is 100 Nm, as shown in Table 3.

Through the above comparative tests, it can be preliminarily judged that the key point that has a great impact on the radiation emission of the electric drive system is whether there is a torque, essentially whether the motor controller has a power output, which has little relation with the motor speed and bus voltage [24]. In addition to the influence of whether or not the torque has on radiation emission, the torque size is further compared, and 50 Nm, 100 Nm, and 200 Nm are, respectively, set for comparison, which is found that the increase of torque has no obvious influence on radiation emission. Therefore, during the test, the appropriate torque can be selected according to the actual situation, rather than the maximum torque that the component can work.

5. Conclusion

The development of on-load test equipment and simulation platform for the electric drive system of new energy vehicles was studied. The EMC performance of on-load test equipment for the wall-through-wall electric drive system was evaluated through three-dimensional electromagnetic simulation, and a set of on-load test equipment for the wall-through-wall electric drive system was developed in accordance with the standard requirements. Among them, the simulation and test found that shaft material, wall hole,

shield cover, and grounding ring are the key parameters that affect the EMC performance of the equipment. In addition, the on-load simulation platform of the electric drive system was established by extracting the parameters of the motor on-load model through simulation. The accuracy of the model is verified by simulation and test, parametric analysis and EMI performance optimization are carried out, and a closed-loop electromagnetic compatibility performance control system is formed. The simulation results show that IGBT gate parasitic inductance, IGBT, and heat dissipation plate parasitic capacitance are the key parameters for conducting EMI performance optimization of electric drive system, which need to be controlled. Aiming at the electromagnetic compatibility bottleneck of the current electric drive system of new energy vehicles, simulation analysis and verification are carried out from the two aspects of test and verification equipment development and forward development platform establishment. It provides a basic way of verification design for improving EMC performance of electric drive system.

Electromagnetic compatibility has become the key problem of electric vehicle technology. In view of this problem, researchers at home and abroad have done a lot of research and obtained a lot of valuable research results, forming a relatively perfect research system of automotive electromagnetic compatibility. In addition, the establishment of professional electromagnetic compatibility testing and certification institutions, as well as the development of professional electromagnetic simulation software, provides convenience for electromagnetic compatibility research, reduces the cost of electric vehicles in the development stage, and promotes the research and development of electric vehicles more effectively.

Data Availability

The data used to support the findings of this study are available from the corresponding author upon request.

Conflicts of Interest

The authors declare that they have no conflicts of interest.

Acknowledgments

This work was funded by the Natural Science Research Project of Colleges and Universities in Anhui Province (project name: research on energy management of two gear pure electric vehicle based on condition prediction; project number: KJ2020A1098), the Anhui Quality Engineering Project (project name: ideological and political teaching team of new energy vehicle technology; project number: 2020kcszjxtd14), and the Support Program for Outstanding Young Talents in Colleges and Universities in Anhui Province (project name: outstanding young talents in colleges and universities in Anhui Province; project number: gxyqZD2020058).

References

- [1] W. Ma, M. Xu, Z. Zhong, X. Li, and Z. Huan, "Closed-loop control for trajectory tracking of a microparticle based on input-to-state stability through an electromagnetic manipulation system," *IEEE Access*, vol. 8, pp. 46537–46545, 2020.
- [2] H. H. Yu, K. H. Chang, H. W. Hsu, and R. Cuckler, "A Monte Carlo simulation-based decision support system for reliability analysis of Taiwan's power system: framework and empirical study," *Energy*, vol. 178, no. JUL.1, pp. 252–262, 2019.
- [3] Z. Lv, W. Kong, X. Zhang, D. Jiang, H. Lv, and X. Lu, "Intelligent security planning for regional distributed energy internet," *IEEE Transactions on Industrial Informatics*, vol. 16, no. 5, pp. 3540–3547, 2020.
- [4] Z. Lv, L. Qiao, J. Li, and H. Song, "Deep-learning-enabled security issues in the Internet of Things," *IEEE Internet of Things Journal*, vol. 8, no. 12, pp. 9531–9538, 2021.
- [5] B. Yang, B. Wu, Y. You, C. Guo, L. Qiao, and Z. Lv, *Edge Intelligence Based Digital Twins for Internet of Autonomous Unmanned Vehicles*, Software: Practice and Experience, 2022.
- [6] Z. Wan, Y. Dong, Y. Zengchen, H. Lv, and Z. Lv, "Semi-supervised support vector machine for digital twins based brain image fusion," *Frontiers in Neuroscience*, vol. 15, p. 802, 2021.
- [7] X. Zhou, Y. Li, and W. Liang, "CNN-RNN based intelligent recommendation for online medical pre-diagnosis support," *IEEE/ACM Transactions on Computational Biology and Bioinformatics*, vol. 18, no. 3, pp. 912–921, 2021.
- [8] X. Zhou, W. Liang, K. Wang, R. Huang, and Q. Jin, "Academic influence aware and multidimensional network analysis for research collaboration navigation based on scholarly big data," *IEEE Transactions on Emerging Topics in Computing*, vol. 9, no. 1, pp. 246–257, 2021.
- [9] X. Zheng and Z. Cai, "Privacy-preserved data sharing towards multiple parties in industrial IoTs," *IEEE Journal on Selected Areas in Communications (JSAC)*, vol. 38, no. 5, pp. 968–979, 2020.
- [10] Z. Cai and X. Zheng, "A private and efficient mechanism for data uploading in smart cyber-physical systems," *IEEE Transactions on Network Science and Engineering (TNSE)*, vol. 7, no. 2, pp. 766–775, 2020.
- [11] H. Sami, A. Mourad, and W. El Haj, "Vehicular-OBUs-as-on-demand-fogs: resource and context aware deployment of containerized micro-services," *IEEE/ACM transactions on networking*, vol. 28, no. 2, pp. 778–790, 2020.
- [12] A. Mourad, A. Srour, H. Harmanani, C. Jenainati, and M. Arafeh, "Critical impact of social networks infodemic on defeating coronavirus COVID-19 pandemic: Twitter-based study and research directions," *IEEE transactions on network and service management*, vol. 17, no. 4, pp. 2145–2155, 2020.
- [13] M. H. Chang and Y. C. Wu, "Speed control of electric vehicle by using type-2 fuzzy neural network," *International Journal of Machine Learning and Cybernetics*, vol. 13, no. 6, pp. 1647–1660, 2022.
- [14] G. Chen, H. Lin, H. Hu et al., "Research on the measurement of ship's tank capacity based on the Monte Carlo method," *Chemistry and Technology of Fuels and Oils*, vol. 58, no. 1, pp. 232–236, 2022.
- [15] N. Garcia-Hernandez, K. Huerta-Cervantes, I. Muoz-Pepi, and V. Parra-Vega, "Touch location and force sensing interactive system for upper limb motor rehabilitation," *Multimedia Tools and Applications*, vol. 81, no. 10, pp. 14133–14152, 2022.

Research Article

Research on Navigation and Positioning of Electric Inspection Robot Based on Improved CNN Algorithm

Yingkai Long ¹, Mingming Du ², Xiaoxiao Luo ¹, Siquan Li ¹ and Yuqiu Liu ³

¹State Grid Chongqing Electric Power Research Institute, Chongqing 401121, China

²State Grid Chongqing Electric Power Company, Chongqing 400013, China

³Nanjing Unitech Electric Power Co., Ltd., Nanjing 211100, China

Correspondence should be addressed to Yingkai Long; 31115307@njau.edu.cn

Received 29 May 2022; Revised 29 June 2022; Accepted 30 June 2022; Published 12 July 2022

Academic Editor: Haibin Lv

Copyright © 2022 Yingkai Long et al. This is an open access article distributed under the Creative Commons Attribution License, which permits unrestricted use, distribution, and reproduction in any medium, provided the original work is properly cited.

In order to improve the visual navigation performance in complex environment, a robust visual navigation method for substation inspection robot is proposed in this paper. Based on the robustness of hexagonal cone model to light changes, this method can solve the squeezing problem of navigation path in complex environment and reduce the interference caused by external light factors. Based on HM preprocessed images, semantic segmentation is carried out with deep convolutional neural network to obtain global features, local features, and multiscale information of images, so as to effectively improve the network recognition accuracy. The results show that the images after HM color space transformation and grayscale reconstruction can compress the color space while preserving the edge details, which is beneficial to the semantic segmentation network for further scene road recognition. Because the original structure of the network is not adjusted and the corresponding preprocessing layer is added, the size of the network model is relatively increased, but the reasoning speed of the original network is significantly improved, which is 16.4% on average.

1. Introduction

As a direction for the development of future energy networks, smart grids have been extended to existing power grid control networks [1]. Intelligent and efficient management technologies will be used to implement automation, integration, centralization, and intelligence in power grid management, such as power generation, transmission, distribution, and energy consumption [2]. As an important connection hub in the power supply network, the substation needs regular inspection in order to find potential problems in time and maintain them in time to ensure the safe operation of the power grid [3]. As an important carrier of automatic monitoring of substation operation, robot can be widely used in the automatic monitoring of substation environment [4]. The magnetic path navigation method is simple and reliable and has high navigation accuracy, but this method uses a magnetic path for navigation, which requires a change in the layout of the substation. There are cargo and potential safety hazards during actual work [5].

Inertial navigation and wireless positioning methods require the installation of wireless devices for signal transmission and reception in the work environment. Although the installation is convenient, the decentralized wireless devices lead to poor recognition stability and adaptability and are prone to cumulative errors [6, 7]. Although GPS navigation method can work without adjusting the working scene, it has poor accuracy and low accuracy. In particular, in the power system environment, electromagnetic interference is particularly strong, and the well cannot meet the accuracy requirements of substation patrol inspection [8]. Figure 1 shows a manufacturing technology of inspection robot based on improved LSTM+CNN algorithm.

2. Literature Review

The inspection system of electric power inspection robot is a scientific and technological achievement integrating multiple disciplines. In addition to the traditional and relatively perfect technologies such as machinery, electricians and

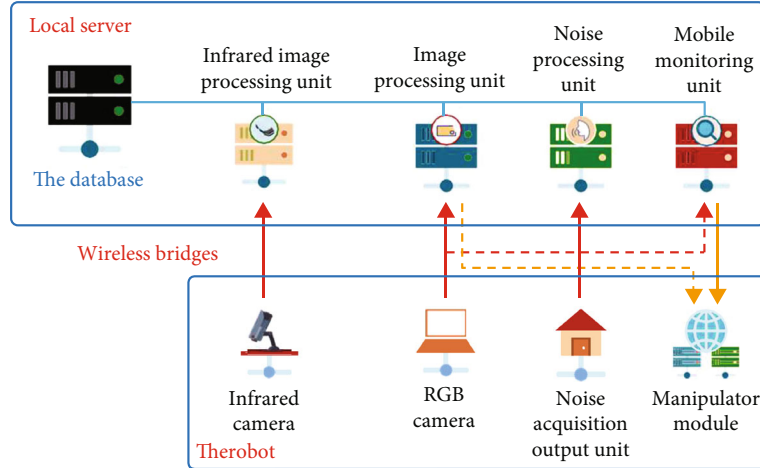


FIGURE 1: Manufacturing technology of inspection robot based on improved LSTM+CNN algorithm.

electronics, communication, automation, and sensors, it also adds deep learning neural network to improve the ability of system fault identification [9, 10]. The power inspection robot system is mainly composed of image detection and recognition unit, automatic obstacle avoidance unit, data monitoring unit, and data transmission and storage unit. The image detection system is a deep learning neural network based on PyTorch framework. It uses a neural network model similar to Yolov3 to dynamically collect image information, extract the characteristics of the image at any time, and judge whether there is fault information in the power system. Using this technology, the power inspection robot can directly warn the instrument panel, indicator lights, open fire, smoke, and other faults. At the same time, the video will be transmitted to the Alibaba cloud platform for backup, which can be retrieved by the inspectors at any time. It can also directly follow the real-time video and conduct video remote detection synchronously with the machine [11, 12]. Compared with the early inspection robot, the advantage of this power inspection robot is to increase the image detection function of convolutional neural network. Flexible neural networks are widely used in the field of visual target detection. Transient neural networks can automatically retrieve functional information from images, learn specific information from different lesion information, and continuously optimize their identification accuracy to effectively detect substations [13, 14]. The foreground vision device is used to capture the road image in real time, the image processing technology is used to identify the road surface to determine the position relationship between the inspection robot and the navigation line, and then the deep learning algorithm of the inspection robot walking and detection task is realized through the bottom motion control, which has attracted extensive attention in the existing visual path navigation methods [15]. Compared with other methods mentioned above, visual navigation method not only overcomes the disadvantages of low accuracy and poor adaptability of these methods in power system scene but also has the advantages of simplicity, reliability, accuracy, convenient transformation, and installation [16].

Based on this, we offer a reliable method of visual navigation for substation control robots to improve visual navigation performance in complex environments. This method uses the robustness of the gecko model (HM) to change the light, which solves the problem of compressing the navigation path in complex environments and reduces interference caused by external lighting factors. In order to effectively improve the accuracy of network recognition, semantic segmentation with a deep neural network (DCNN) based on a preprocessed image of HM is obtained, which provides information on global features, local features, and multiscale images.

3. Research Methods

3.1. Color Space Conversion. Good road recognition ability is the key to the self-adaptive navigation of the substation inspection robot. Only by controlling the inspection robot on the basis of identifying the effective road surface can the inspection robot effectively complete the inspection task and avoid entering the restricted area or areas that are not suitable for driving. Road recognition based on camera images needs to take into account various complex situations such as strong light, shadows, and rainy days. Define the maximum value of the three component values of R , G , and B of each pixel (i, j) as $\max(i, j)$ and the minimum value as $\min(i, j)$, and then, there are

$$\max(i, j) = \max(R(i, j), G(i, j), B(i, j)), \quad (1)$$

$$\min(i, j) = \min(R(i, j), G(i, j), B(i, j)). \quad (2)$$

For the three components in HM, V component represents color brightness, and $V(i, j)$ is expressed as

$$V(i, j) = \max(i, j). \quad (3)$$

S component represents color purity, and then, $S(i, j)$ represents

$$S(i, j) = \begin{cases} \frac{V(i, j) - \min(i, j)}{V(i, j)} V(i, j) \neq 0, \\ 0V(i, j) = 0. \end{cases} \quad (4)$$

3.2. Gray Image Reconstruction. Each component of the Hopfield Model (HM) has different characteristics. H , S , and V components of different weights are reassembled to restore the image to minimize the effect of lighting changes in the image [17, 18]. In terms of features, the navigation path properties on components H and V are essentially opposite; the normalization method is considered to enhance and preliminarily extract the navigation path feature information. First, inverse image processing is performed on the H component, as shown in

$$\bar{H}(i, j) = 255 - H(i, j). \quad (5)$$

Then, the inverse image \bar{H} is normalized, where the normalized range is $[a, b]$, where a is the minimum value of H and b is the maximum value of H , and then, the corresponding coefficient matrix H' is obtained, as shown in

$$H'(i, j) = \bar{H}(i, j) \times \frac{(b - a)}{255} + \frac{a}{255}. \quad (6)$$

This operation avoids the forced enlargement and reduction of the image in the normalization process. To recreate the gray image, add the components to the components and then multiply by a coefficient matrix according to

$$F(i, j) = (2 \times S(i, j) + V(i, j)) \times H'(i, j). \quad (7)$$

Analyze equation (7) and select the components of the reconstructed gray image and double the result. Consider effectively eliminating shadow interference in the image by increasing the weight of the components while restoring the gray image. This allows you to restore a gray image without the interference of external objects such as strong light, shadows, and surface water that highlight the road surface [19].

3.3. Image Acquisition under Dark Light Conditions. In the dark light environment, due to the light supplement defect of the point light source of the ordinary light source, the image acquisition of the inspection robot has light spots or concentrated light points, which brings the influence of image acquisition. Based on the HM, the image components are decomposed and used to detect the brightness of a simple light source, and the illumination of the collected image under the condition of dark light is appropriately adjusted. If the average brightness in the V component is defined as V_p , then equation (8) is shown.

$$V_p = \frac{\sum_{i=0}^{255} i \times v(i)}{\sum_{i=0}^{255} v(i)}, \quad (8)$$

where i is the saturation value of component s and $s(i)$ is the number of pixels in the saturation value. Define the average illuminance of the component as SP , followed by

$$S_p = \frac{\sum_{i=0}^{255} i \times s(i)}{\sum_{i=0}^{255} s(i)}, \quad (9)$$

where i is the saturation value in the S component and $s(i)$ is the pixel count in the saturation value. In combination with equations (8) and (9), the conditions for judging whether the image is too bright or too dark are (a) $V_p > 150$ and $S_p < 80$ and (b) $V_p < 75$ and $S_p > 60$.

According to the above results, the inspection robot analyzes the brightness information in the current image and determines whether the supplementary light intensity needs to be adjusted so that the light intensity can reach the same illuminance during path navigation in different road sections, so as to ensure the consistency and stability of the image collected by the camera [20, 21].

3.4. HM-DCNN. For a traditional CNN extension, the DCNN structure still consists of a circulation layer, a sampling layer, a consolidation layer, and a fully connected layer. Different from other conventional road semantic segmentation networks, HM-DCNN proposed in this paper performs semantic segmentation of the image through deep learning after image gray preprocessing, adding the adjustment of different light source intensity and supplementary preprocessing layer. In addition, because the preprocessed image is more concise and unified, the complexity of the network and the scale of target training parameters can be greatly reduced. The specific algorithm flow of the improved HM-DCNN is as follows. Based on the HM, complete the image acquisition and corresponding gray image reconstruction under the light conditions of different light sources, and adjust the fill light intensity appropriately. Through the first CNN, the global location is carried out to find the feature point region of continuous features and local features, and then, the maximum rectangular region of the target and surrounding objects is output. The convolutional layer is a key component of the HM-DCNN, and its primary function is to calculate the multiplication of the receiving field point and the rotation of the filter (or core) that can be studied. After the conversion operation, a nonlinear sample is performed in the aggregation layer to reduce the dimensionality of the data [22, 23]. The most common integration strategy is the most consolidated and average consolidation. Max pooling takes the maximum value from the candidates, while the average aggregation selects the average from the estimated candidates. Here, the maximum aggregation method is chosen to minimize the calculated average displacement due to the rotation layer parameter error in order to preserve the image structure information as much as possible. The function map obtained after the sample below is then sent to the activation function to process the nonlinear

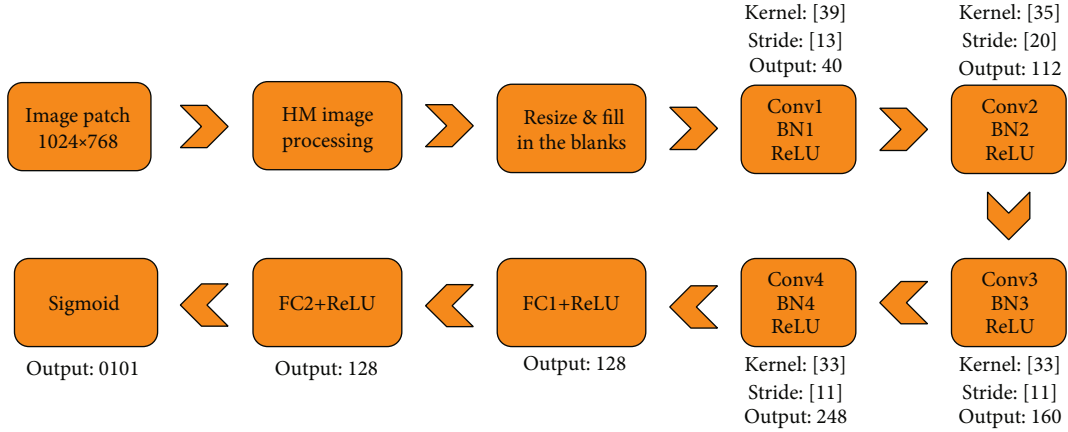


FIGURE 2: DCNN architecture.

TABLE 1: Network parameter settings.

Type	Convolution kernel parameters	Output
Convolution 1	Kernel: [3 9], stride: [1 3], output: 40	$46 \times 62 \times 40$
Max-pool 1	Kernel: [2 3], stride: 2	$23 \times 31 \times 40$
Convolution 2	Kernel: [3 9], stride: [1 3], output: 40	$25 \times 27 \times 112$
Max-pool 2	Kernel: [2 3], stride: 2	$13 \times 13 \times 112$
Convolution 3	Kernel: [3 3], stride: [1 1], output: 160	$13 \times 13 \times 160$
Convolution 4	Kernel: [3 3], stride: [1 1], output: 128	$13 \times 13 \times 128$
Max-pool 3	Kernel: [3 3], stride: 2	$6 \times 6 \times 128$
FC 1	Output: 128	128
FC 2	Output: 128	128

conversion. High-level grounding is done through fully connected layers. Nerve cells in this layer are involved in all the activations of the previous layer. The loss layer is usually the last layer of the DCNN and specifies how to punish the difference between the predicted and actual label during network training. Distribution points are strongly separated by a sigmoid layer. Here, a complete circulatory neural network based on the BVLC Caffe was selected to generate the HM-DCNN. The network structure is shown in Figure 2. There are a total of five circulation layers between the input and output layers. The network uses the Linear Unit (ReLU) as a function of nonlinear activation and finally identifies the distribution points of semantic segmentation through the sigmoid and builds the corresponding DCNN architecture. Table 1 shows the parameters for generating the corresponding circulation network according to the functional definition of the different layers of the DCNN [24].

Due to grayscale reconstruction preprocessing in the inspection robot, global gain normalization is applied to the processed images to further reduce the intensity changes in the images. This gain is calculated by aligning the calculated signal envelope using the median filter. To calculate the signal envelope, the image is filtered through a low-pass Gaussian core. DCNN is highly resistant to lighting effects, but the combination of image gray recovery and

TABLE 2: Lighting effect.

Scene	V_p	S_p	Effect
A	160.2	30.4	Normal
B	94.6	65	Suitable
C	60.2	103.5	Dark

normal processing makes the signal dynamic range more uniform, which can further improve processing accuracy and merging speed.

4. Result Analysis

4.1. HM Fill Light Experiment and Image Preprocessing. To test the effectiveness of the proposed HM-DCNN network application in combination with the gray reconstruction in the actual substation scene, the substation path map collected by the substation control robot was used to train the network and test the network recognition accuracy. The network was trained in stochastic gradient drop (SGD), and the learning speed was set to 0.01, the pulse parameter to 0.9, and the weight loss to 0.0005. In order to make the inspection robot still run well in the dark environment, it is particularly important to supplement the light

TABLE 3: Influence of different light intensity and light supplement on detection accuracy.

Algorithm	Average coverage accuracy of normal light	Average accuracy of dim light	Under fill light condition
VGG	0.863	0.832	0.846
HM-VGG	0.87	0.860	0.860
SCNN	0.940	0.886	0.910
HM-SCNN	0.941	0.910	0.915
BiseNet	0.935	0.900	0.920
HM-BiseNet	0.930	0.916	0.914
DCNN	0.950	0.878	0.900
HM-DCNN	0.952	0.942	0.948

appropriately. Scene A is the road condition during the day, scene B is the adaptive fill light condition, and scene C is the nonfill light condition. The calculation results of V_p and S_p are shown in Table 2.

From the results in Table 2, it can be seen that the differences between the V_p and S_p components are clear in different lighting conditions. According to different difference values, setting the corresponding threshold can achieve appropriate light compensation. In order to analyze the influence of HM on the network recognition effect in the scene, the traditional edge extraction processing alone has poor adaptability in the case of high illumination difference and scene feature brightness and will lose a lot of details. The image after HM color space conversion and gray reconstruction can compress the color space and greatly retain the edge detail features, which is conducive to further scene pavement recognition by semantic segmentation network.

4.2. HM-DCNN Semantic Segmentation Experiment. In the preparation process of HM-DCNN training samples, in order to avoid the overfitting of training, improve the robustness of the network, and better extract the core features, a series of adjustments are made to the sample data, including illumination, color saturation, rotation, and clipping.

As a user-defined layer of other reasoning network preprocessing, HM can be combined with a variety of semantic segmentation networks. The processed image is used for gray reconstruction, which is used as the input of each comparison network and compared with the network results trained with the original image directly as the input. The effects of different illumination conditions on the experimental results are shown in Table 3.

As shown in Figure 3, the recognition effects of several commonly used semantic segmentation networks are compared and analyzed through experiments. Under normal illumination, DCNN has high recognition effect, but under dim illumination and supplementary illumination, the recognition effect decreases significantly. Through the comparison of each network after adding HM treatment, although the improvement effect under normal light is not significant, the recognition rate of the dark environment of the original network has been greatly improved, especially when combined with DCNN.

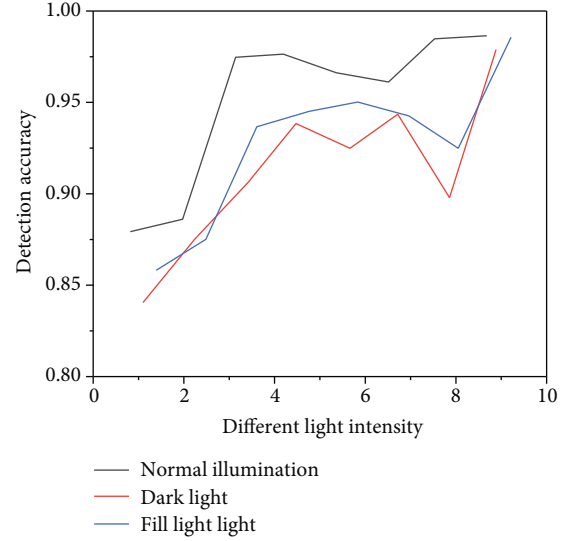


FIGURE 3: Influence of different light intensity and light supplement on detection accuracy.

TABLE 4: Comparison of model size and reasoning speed of different recognition networks.

Algorithm	Model size (MB)	Average error (%)	Embedded reasoning time (ms)
VGG	400	84.7	300
SCNN	157	91.2	160
HM-SCNN	158	92.2	120
BiseNet	55	91.8	110
HM-BiseNet	57	92.0	98
DCNN	45	90.9	90
HM-DCNN	47	94.7	78

As shown in Table 4, the original structure of the network is not adjusted and the corresponding preprocessing layer is added, which makes the size of the network model increase relatively, but the reasoning speed of the original network is significantly improved, with an average of 16.4%.

5. Conclusion

This document proposes a new method of reliable visual navigation of substation control robots in complex road environments, which has the advantages of strong anti-interference ability, simple operation, high precision, and good stability. This method fully considers the road characteristics and working conditions of the substation and uses the insensitivity of HM color space to light change, shadow, and interference to reconstruct the gray image of the collected image; therefore, the specifics of the navigation path are reflected in more detail. In addition, DCNN is used to train and recognize images processed on a grayscale to improve network recognition accuracy. Because the HM reduces the amount of color space, the first-ever DCNN

can be used in substation control robots with poor processing capabilities. The results of the experiment show that the network recognition results show a clear advantage in combination with the HM gray reconstruction compared to the existing pure training network. At the same time, the HM-DCNN method proposed in this paper can stabilize the average processing accuracy of DCNN from 91% to 93%, have the best effect on the entire network, and fully meet the actual needs of the substation situation.

Data Availability

The data used to support the findings of this study are available from the corresponding author upon request.

Conflicts of Interest

The authors declare that they have no conflicts of interest.

References

- [1] O. Abdel Wahab, A. Mourad, H. Otrok, and T. Taleb, “Federated machine learning: survey, multi-level classification, desirable criteria and future directions in communication and networking systems,” *IEEE Communications Surveys & Tutorials*, vol. 23, no. 2, 2021.
- [2] A. Mourad, A. Srour, H. Harmanani, C. Jenainati, and M. Arafah, “Critical impact of social networks infodemic on defeating coronavirus COVID-19 pandemic: twitter-based study and research directions,” *IEEE Transactions on Network and Service Management*, vol. 17, no. 4, 2020.
- [3] M. W. Kim, S. Lee, I. Dan, and S. Tak, “A deep convolutional neural network for estimating hemodynamic response function with reduction of motion artifacts in fmris,” *Journal of Neural Engineering*, vol. 19, no. 1, article 016017, 2022.
- [4] X. Zheng and Z. Cai, “Privacy-preserved data sharing towards multiple parties in industrial IoTs,” *IEEE Journal on Selected Areas in Communications (JSAC)*, vol. 38, no. 5, pp. 968–979, 2020.
- [5] J. Qiu, L. Du, D. Zhang, S. Su, and Z. Tian, “Nei-TTE: intelligent traffic time estimation based on fine-grained time derivation of road segments for smart city,” *IEEE Transactions on Industrial Informatics*, vol. 16, no. 4, pp. 2659–2666, 2020.
- [6] R. M. Churchill, B. Tobias, Y. Zhu, and DIII-D team, “Deep convolutional neural networks for multi-scale time-series classification and application to tokamak disruption prediction using raw, high temporal resolution diagnostic data,” *Physics of Plasmas*, vol. 27, no. 6, article 062510, 2020.
- [7] Z. Lv, W. Kong, X. Zhang, D. Jiang, H. Lv, and X. Lu, “Intelligent security planning for regional distributed energy internet,” *IEEE Transactions on Industrial Informatics*, vol. 16, no. 5, pp. 3540–3547, 2020.
- [8] Z. Lv, L. Qiao, J. Li, and H. Song, “Deep-learning-enabled security issues in the Internet of things,” *IEEE Internet of Things Journal*, vol. 8, no. 12, pp. 9531–9538, 2021.
- [9] S. Mekruksavanich and A. Jitpattanakul, “Deep convolutional neural network with rnn for complex activity recognition using wrist-worn wearable sensor data,” *Electronics*, vol. 10, no. 14, p. 1685, 2021.
- [10] F. Wu, B. Wu, M. Zhang, H. Zeng, and F. Tian, “Identification of crop type in crowdsourced road view photos with deep convolutional neural network,” *Sensors*, vol. 21, no. 4, p. 1165, 2021.
- [11] S. Kim and H. Kim, “Zero-centered fixed-point quantization with iterative retraining for deep convolutional neural network-based object detectors,” *IEEE Access*, vol. 9, pp. 20828–20839, 2021.
- [12] L. Song, H. Wang, and P. Chen, “Automatic patrol and inspection method for machinery diagnosis robot—sound signal-based fuzzy search approach,” *IEEE Sensors Journal*, vol. 20, no. 15, pp. 8276–8286, 2020.
- [13] V. Muthugala, P. Palanisamy, B. Samarakoon, S. Padmanabha, and D. N. Terntzer, “Raptor: a design of a drain inspection robot,” *Sensors*, vol. 21, no. 17, p. 5742, 2021.
- [14] X. Cheng, B. Yang, A. Hedman, T. Olofsson, H. Li, and L. Van Gool, “NIDL: a pilot study of contactless measurement of skin temperature for intelligent building,” *Energy and Buildings*, vol. 198, pp. 340–352, 2019.
- [15] S. Yang, B. Deng, J. Wang et al., “Scalable digital neuromorphic architecture for large-scale biophysically meaningful neural network with multi-compartment neurons,” *IEEE transactions on neural networks and learning systems*, vol. 31, no. 1, pp. 148–162, 2020.
- [16] B. Zhang, J. Wu, L. Wang, and Z. Yu, “Accurate dynamic modeling and control parameters design of an industrial hybrid spray-painting robot,” *Robotics and Computer-Integrated Manufacturing*, vol. 63, no. 1, article 101923, 2020.
- [17] M. Muthugala, K. Apuroop, S. Padmanabha, S. Samarakoon, and R. Wen, “Falcon: a false ceiling inspection robot,” *Sensors*, vol. 21, no. 16, p. 5281, 2021.
- [18] R. Parween, Y. W. Tan, and M. R. Elara, “Design and development of a vertical propagation robot for inspection of flat and curved surfaces,” *IEEE Access*, vol. 9, pp. 26168–26176, 2021.
- [19] R. G. Lins and S. N. Givigi, “Fpga-based design optimization in autonomous robot systems for inspection of civil infrastructure,” *IEEE Systems Journal*, vol. 14, no. 2, pp. 2961–2964, 2020.
- [20] T. Zhang, G. Han, C. Lin, N. Guizani, and L. Shu, “Integration of communication, positioning, navigation and timing for deep-sea vehicles,” *IEEE Network*, vol. 34, no. 2, pp. 121–127, 2020.
- [21] X. Zhou, X. Xu, W. Liang et al., “Intelligent small object detection for digital twin in smart manufacturing with industrial cyber-physical systems,” *IEEE Transactions on Industrial Informatics*, vol. 18, no. 2, pp. 1377–1386, 2022.
- [22] J. Wang, J. Liu, X. Xu, Z. Yu, and Z. Li, “A single foot-mounted pedestrian navigation algorithm based on the maximum gait displacement constraint in three-dimensional space,” *Measurement Science and Technology*, vol. 33, no. 5, p. 055113, 2022.
- [23] F. Potorti, F. Palumbo, and A. Crivello, “Sensors and sensing technologies for indoor positioning and indoor navigation,” *Sensors*, vol. 20, no. 20, p. 5924, 2020.
- [24] X. Zhou, W. Liang, K. Wang, R. Huang, and Q. Jin, “Academic influence aware and multidimensional network analysis for research collaboration navigation based on scholarly big data,” *IEEE Transactions on Emerging Topics in Computing*, vol. 9, no. 1, pp. 246–257, 2021.